Distribution Agreement

In presenting this thesis or dissertation as a partial fulfillment of the requirements for an advanced degree from Emory University, I hereby grant to Emory University and its agents the non-exclusive license to archive, make accessible, and display my thesis or dissertation in whole or in part in all forms of media, now or hereafter known, including display on the world wide web. I understand that I may select some access restrictions as part of the online submission of this thesis or dissertation. I retain all ownership rights to the copyright of the thesis or dissertation. I also retain the right to use in future works (such as articles or books) all or part of this thesis or dissertation.

Signature

_____ _____

Victor T. Adebomi **Date**

Developing Chemical Tools for Selective Peptide Modifications

By

Victor T. Adebomi

Doctor of Philosophy

Chemistry

_____

Monika Raj, PhD
Advisor

_____

William M. Wuest, PhD
Committee Member

_____

Vincent P. Conticello, PhD
Committee Member
Accepted:

_____

Kimberly J. Arriola, PhD
Dean of the James T. Laney School of Graduate Studies

_____

Date

Developing Chemical Tools for Selective Peptide Modification

By

Victor T. Adebomi

B.Sc., Osun State University, 2015

Advisor: Monika Raj, PhD

An abstract of

A dissertation submitted to the Faculty of the James T. Laney of Graduate Studies of Emory University in partial fulfillment of the requirements for the degree of Doctor of Philosophy in Chemistry

2022

Abstract

Developing Chemical Tools for Selective Peptide Modification

By: Victor T. Adebomi

Peptides represent an important class of biomolecules and have shown promise as efficient therapeutics for numerous disease states. However, the real time application of peptides as therapeutics is severely hampered by the low bioavailability, metabolic instability, and random conformations. Through selective peptide modification, we can provide useful tools to circumvent these limitations and improve physiochemical properties to enhance peptide applications in drug discovery. To this end, we have developed several strategies for peptide modifications. Peptide macrocyclization is a method highly touted for selective modification peptides due to their tendency to greatly improve the pharmacokinetic properties of peptides. A major limitation of most macrocyclization methods is that most techniques developed for peptide cyclization often result in the formation of dimers and oligomers at high concentrations. We have successfully developed the first exclusively intramolecular strategy for making cyclic peptides which we have used to make a wide range of cyclic peptides (12- to 23-membered rings) with varying amino acid compositions using mild reaction conditions. We termed this reaction CyClick because it works in an exclusively intramolecular fashion, exhibiting fast reaction kinetics, with high chemo selectivity and stereoselectivity (99% de). In addition, various NMR techniques and modeling studies have revealed that the 4-imidazolodinone moiety generated by the cyclization serves as an endocyclic control element to promote intramolecular hydrogen bonding, leading to the formation of a turn structure. This innovation is highly important as it bring about new ways of synthesizing cyclic peptides in high concentrations leading to higher efficacy of peptide synthesis. This CyClick technology developed in our lab is now being used as a new approach for making large libraries ($>10^6$) of pure cyclic peptides for screening against various biological targets. In tandem with the project above, I have developed a novel method for selective diversification of amides in polyamides. This has great importance to the scientific community because it incorporates various functional groups, moieties, and markers into peptides. The planarity and resonance character of secondary amides in polyamides lends to high stability making it difficult to selectively modify these locations. Although several advances have been made for the modification of secondary amides, the selective modification of a particular amide in a sea of other amides has never been done. Using Density Functional Theory (DFT) calculations as a guide, we have discovered a two-step approach for the selective modification of amides in a polyamide. The first step of the reaction involves the selective introduction of a carbonyl into peptides containing serine or cysteine. This results in the electronic activation of amide bonds thereby allowing new groups such as esters, amides, and other functional groups to be introduced into the peptide.

Developing Chemical Tools for Selective Peptide Modification

By

Victor T. Adebomi

B.Sc., Osun State University, 2015

Advisor: Monika Raj, PhD

A dissertation submitted to the Faculty of the James T. Laney of Graduate Studies of Emory University in partial fulfillment of the requirements for the degree of Doctor of Philosophy in Chemistry

2022

Acknowledgements

First, and most importantly, I would like to thank the Almighty God for all the successes I have had during my Ph.D. I am extremely grateful to God because I am fully convinced that without him, I am nothing. Without God, I will not be alive neither will I accomplish anything.

I am also extremely grateful to my family. I'll like to specially thank my wife for her support. I'll like to also appreciate my dad, mum and my siblings. They have been highly helpful, and God has used them to bring me to where I am today.

I'll appreciate my advisor, Dr. Monika Raj. Her mentorship, her patience, training and support has proved invaluable to me accomplishing this feat. She is a great teacher and if you can't understand Monika's explanation of a concept, then no one can ever get you to understand it. When I started in the Raj lab, she personally trained me on the use of many equipment, peptide synthesis and setting chemical reactions.

Other graduate students and post-doctoral researchers in the Raj group have also been highly helpful. Early in my Ph.D., Mahesh Sriram taught me about organic synthesis techniques and setting organic reactions. Together we have up to three publications on using nitroalkylation as a tool for modifying proteins and selective peptide modifications by twisting amide bonds.

As I continued to work in the Raj lab, I started to assume more of a leadership role and worked with other graduate students like Rachel who was very helpful for the development of CyClick Chemistry for making CyClick peptides. Over time, I also worked with Angele Bruce, and we together started to apply CyClick chemistry as an approach to generate high quality combinatorial libraries. I would like to thank Ashish Verma who I worked with for the project on applying CyClick Chemistry for making cyclic peptoids.

I interacted with many undergraduates such as Caroline Spancake, Holland Andrew Chavers and Patrick Czabala who were helpful in the development of the CyClick project. Undergraduates Yuwen Wang and Xavier Streety we're also very helpful for the development of the project on twisting amide bonds.

I would like to also appreciate other members of my lab Ogonna Nwajiobi, Kuei-Chein Tang, Benjamin Emenike, Patricia Rodriguez, Lyndsey Prosser, Samrat Sahu, and Rajendra Shirke for their great support both scientifically and emotionally.

I would like to acknowledge the efforts of collaborator Ryan Cohen and Gary Martin from Merck who helped with NMR analysis of CyClick peptide. I also appreciate Dr. Huiling and Professor Ken Houk from UCLA for shedding light on the mechanism of CyClick reaction.

The acknowledgement gives credence to the fact that science has and will always be a highly collaborative team effort and the work presented in this thesis is no exception.

Table of Contents

List of Illustrations

Figures

List of Abbreviations

Table of Contents

List of Illustrations

List of Figures **Page**

Chapter 1

List of Abbreviations

^{13}C NMR: Carbon-13 Nuclear Magnetic Resonance Spectroscopy

^{19}F NMR: Fluorine Nuclear Magnetic Resonance Spectroscopy

^{1}H NMR: Proton Nuclear Magnetic Resonance Spectroscopy

ACN: Acetonitrile

ADCs: Antibody-Drug Conjugates

Ala: Alanine

Arg: Arginine

Asn: Asparagine

Asp: Aspartate

Bn: Benzyl

Boc: tert-Butyloxycarbonyl

COESY: Correlation Spectroscopy

CREST: Conformer-Rotamer Ensemble Sampling Tool

CTP: Cyclic Tetrapeptide

$Cu(OTf)_3$: Copper(II) trifluoromethanesulfonate

Cys: Cysteine

DARs: Drug-to-Antibody ratio

DCM: Dichloromethane

DEPBT: 3-(diethoxyphosphoryloxy)-1,2,3-benzotriazin-4(3H)-one

DFT: Density Functional Theory

DIEA: N,N-Diisopropylethylamne

DMAP: 4-dimethylaminopyridine

DMF: dimethylformamide

DMSO: Dimethyl sufoxide

DSC: N,N'-Disuccinimidyl carbonate

Et: ethyl

Et_3N: Triethylamine

EtOAc: ethylacetate

Gln: Glutamine

Glu: Glutamate

Gly: Glycine

H_2O: Water

HATU: 1-[Bis(dimethylamino)methylene]-1H-1,2,3-triazolo[4,5-b]pyridinium 3-oxid hexafluorophosphate)

HMBC: Heteronuclear Multiple Bond Correlation

HOBt: hydroxybenzotriazole

HPLC: High Performance Liquid Chromatography

HPLC: high-performance liquid chromatography

HRMS: High-Resolution Mass Spectrometry

HSQC: Heteronuclear Single Quantum Coherence

iBu: isobutyl

Ile: Isoleucine

IMHB: Intramolecular Hydrogen Bonding

K_2CO_3: Potassium carbonate

LC-MS and LC-MS/MS: Liquid Chromatography with tandem mass spectrometry

Leu: Leucine

Lys: Lysine

Me: methyl

Me: Methyl

MeOH: methanol

Met: Methionine

MS/MS: Tandem mass spectrometry

MS: Mass Spectrometry

NMR: Nuclear Magnetic Resonance Spectroscopy

OMe: Methoxy

Pd-PEPPSI: Palladum - pyridine-enhanced precatalyst preparation stabilization and initiation

PEG: Polyethylene glycol

Ph: Phenyl

pH: potential of Hydrogen

Phe: Phenylalanine

PPIs: Protein-Protein Interaction

Pro: Proline

PTM: Post-Translational Modification

PyBOP: benzotriazol-1-yloxytripyrrolidinophosphonium hexafluorophosphate

ROESY: Rotating-framae nuclear overhauser effect correlation spectroscopy

Ser: Serine

TFA: Triflluroacetic acid

TfOH: Trifluoromethanesulfonic acid

THF: Tetrahydrofuran

thio-CDI: Thiocarbonyldiimidazole

Thr: Threonine

$TMS(OTf)_3$: Trimethylsilyl trifluoromethanesulfonate

TOCSY: Total Correlation Spectroscopy

Trp: Tryptophan

Ts: Tosyl

TS: Transition State

Tyr: Tyrosine

UV spectroscopy: Ultraviolet-visible spectroscopy

Val: Valine

Chapter 1: CyClick Chemistry for the Synthesis of Cyclic Molecules

Introduction

1.1.1 Introduction to Cyclic Peptides

Cyclic peptides are a class of biologically active organic compounds containing a circular sequence of amide bonds and are predominantly made up of amino acid residues.[1] Due to the pharmaceutical interest in cyclic peptides, there has been an abundance of methods developed for the synthesis of cyclic peptides. They can be formed by linking parts of a peptide sequence to form bonds such as amides, ether, thioether, oxime, disulfide, and so on. The many methods for peptide cyclization can be grouped into the following categories – head-to-tail cyclization (for example, an amide bond between the carboxyl and amino terminal), side-to-tail cyclization, head-to-side cyclization, and side-to-side cyclization (Figure 1).[2] Several cyclic peptides are currently being used as therapeutics for the treatment of various diseases.[2] Examples of pharmacologically active cyclic peptides include immunosuppressant cyclic peptide cyclosporin, gramicidin, tyrocidine, and vancomycin which saves as an antibiotic, octreotide used for the treatment of acromegaly.[2]

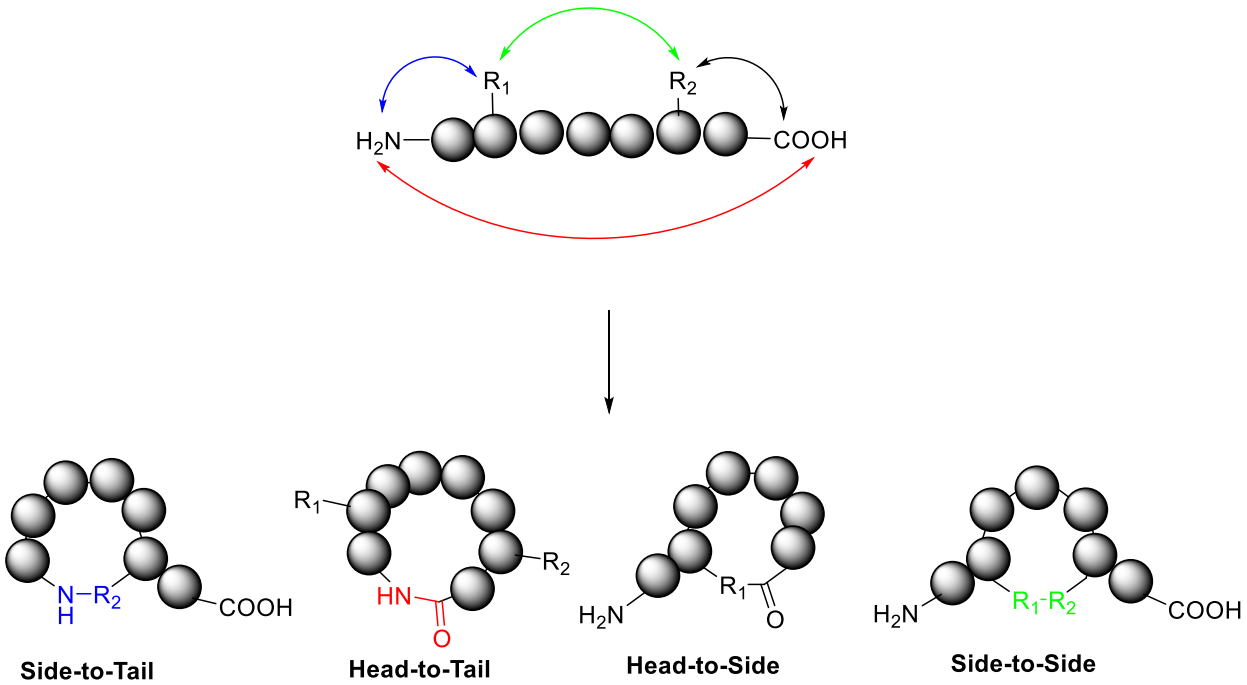

Figure 1. Current approaches for Peptide Cyclization

1.1.2 Why Cyclization of Linear Peptides is Important?

The interactions of linear peptides with their target are very specific as compared to small molecules.[3] They are generally less harmful as compared to small molecules because they are degraded rapidly by proteolytic enzymes, do not accumulate in organs and the degradation products are simply amino acids and would not have toxicity.[4] Some challenges with linear peptide drugs include the fact that they are not well absorbed in the gastrointestinal tract, they are rapidly metabolized, and do not cross the cell membrane as some small molecules do.[2] These limitations have hampered their use in the pharmaceutical industry.

In general, cyclic peptides show better biological activity as compared to their linear counterparts due to more conformational rigidity.[5] The rigidity in cyclic peptides decreases their entropy allowing them to bind more tightly to their targets and enhancing their selectivity. Also, because they mostly do not possess free N-termini or C-termini, they tend to be more resistant to proteolytic degradation as compared to linear peptides. Due to specific features in cyclic peptides such as increasing intramolecular hydrogen bonding, cyclic peptides tend to be sometimes more cell-permeable than linear peptides.[2]

1.1.2 Pitfalls of Common Methods for Cyclic Peptide Generation

Because cyclic peptides can combine useful properties of small molecules such as stability and large biologics such as specificity, they have received considerable attention in recent years. This has led to the development of several methodologies in recent years.[6] Despite the significance of cyclic peptides, laboratory synthesis of cyclic peptides can be challenging – particularly peptides containing less than seven amino acid residues.[7] Problems with many of the methods for peptide cyclization include a general lack of site selectivity, stereoselectivity, and very importantly their unsuitability for application on a large scale. At a large scale, intermolecular reactions often lead

to the formation of dimers and oligomers hampering the yields of desired cyclic peptides (Figure 2). Several cyclization methodologies can avoid dimerization by cyclization of peptides at very low concentrations increasing the intermolecular distance between reactive groups on the peptide. However, high dilution often results in long reaction times which can lead to peptide epimerization.[8] There is therefore great need to develop a cyclization methodology that can circumvent the challenges mentioned above and can also be applied to a large variety of unprotected linear peptides.

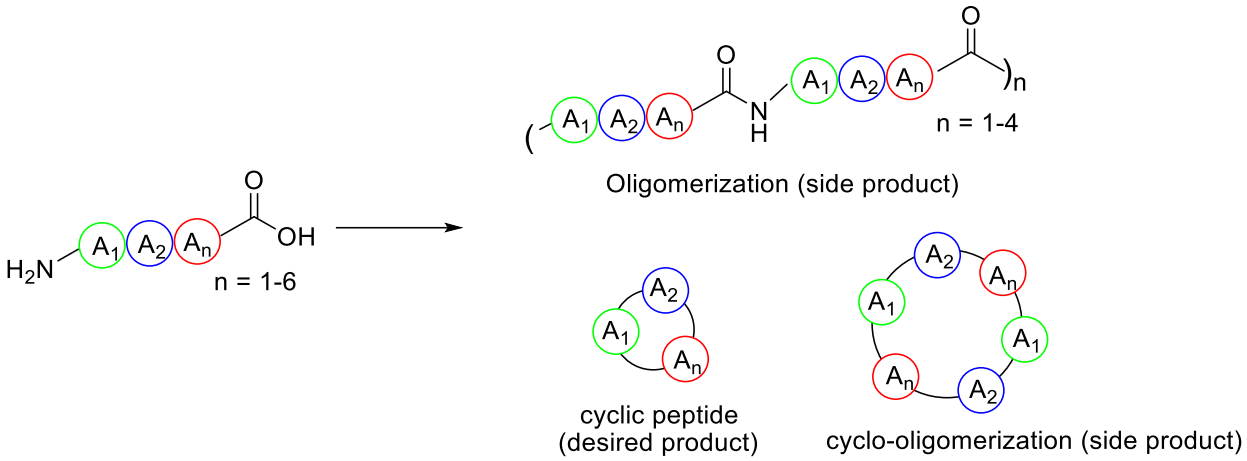

Figure 2. Limitations of Current Cyclization Methods

1.2 Result and Discussion

1.2.1 Experimental Design for New Cyclization Strategy: CyClick

To develop a reaction that would work in an exclusively intramolecular fashion we thought of using peptide aldehyde for macrocyclization. We hypothesized that the reaction between the aldehyde and amine would lead to a formation of an intramolecular imine. The conformational preorganization of this cyclic imine would bring the amide nitrogen of the second amino acid near to the electrophilic imine-carbon. This would then lead to a nucleophilic attack by the amide nitrogen to form a 5-membered imidazolidinone containing cyclic peptide. The linear imine formed by intermolecular reaction between two linear peptides is unable to activate the amide bond

and would not generate stable dimers. The reaction was called CyClick because it works in an exclusively intramolecular fashion even in the presence of reactive amino acids such as lysines, arginine, cysteines and precludes the formation of dimers or oligomers. This approach represents a rare example of conformationally induced amide bond activation that generates stable 4-imidazolinone-fused cyclic peptides. 4-imidazolidinone is an important structural motif in many biologically active compounds such as spiroimidazolidinone which is an anticonvulsant;[9] ML298, a selective inhibitor of phospholipase D (PLD)[10], Ro 64-6198, an agonist for the nociceptin/orphanin FQ opioid peptide (NOP) receptor[11] and *N,N'*-methyleno-didemnin A[12] (Figure 3).

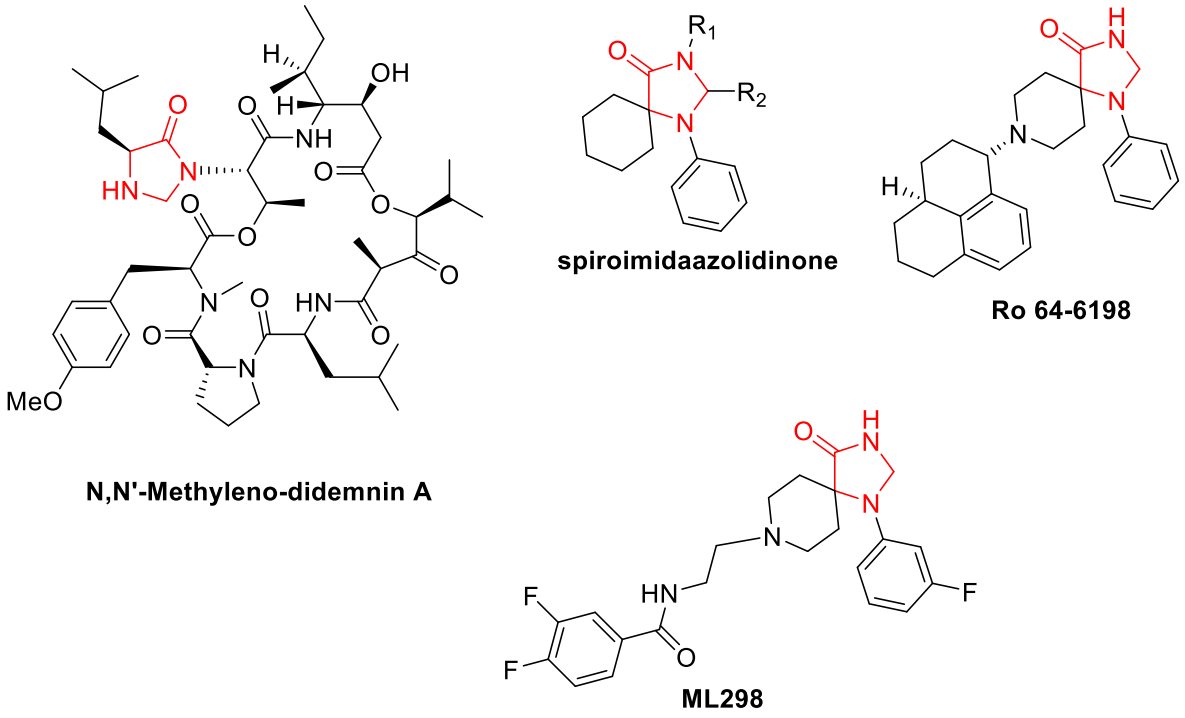

Figure 3. 4-Imidazolidinone containing bioactive compounds

We recognized that the CyClick strategy would:

1) Be triggered by the N-terminus and would not require coupling reagents and metals;

2) Be chemoselective for a reaction between the amino terminus and the peptide aldehyde without the interference of reactive amino acids such as lysine.
3) Utilize the cyclic imine as an internal directing group and thus would not require removable directing groups or external ligands.

In addition, this macrocyclization would lead to the generation of a new chiral center with high diastereoselectivity and introduce a non-peptidic scaffold into the cyclic peptide. This feature is generally known to improve the stability and pharmacokinetic property of the cyclic peptides while maintaining its biological activity.[9-13]

Herein, we report a successful execution of the above ideas and present a strategy for conformational activation of amide bonds applicable in the presence of completely unprotected peptides and across a wide range of peptide ring sizes. Very importantly, the reaction generates only cyclic peptides without the formation of side products such as linear dimers. Since the reaction works in an exclusively intramolecular fashion, reactions can be carried out at high concentrations enabling the reaction to occur at a faster rate. NMR investigation revealed the 4-imidazolidinone induces a turn structure in cyclic peptides which could make them useful for targeting specific motifs in proteins. This turn enables them to be more stable to proteolytic degradation.

1.2.2 CyClick Reaction for Peptide Cyclization

We started our investigation on a peptide with sequence AVGPFE(CHO)Y **1.1a,** where the side chain of Glu was modified to an aldehyde group (Figure 4). Optimization studies revealed that the macrocyclization between the N-terminus of the peptide and aldehyde occurs efficiently in aqueous medium (H_2O:DMF (1:1)) at room temperature with the addition of 4-(Dimethylamino)pyridine (DMAP, 7 equiv.) and resulted in the formation of a 4-imidazolidinine cyclic peptide **1.2a** with 99% conversion (Figure 4). Importantly, harsh conditions such as dry

conditions, metal catalysts and coupling reagents are not required for this reaction. The 4-imidazolidinone cyclic peptide **1.2a** was characterized by high-resolution mass spectrometry (HRMS) and NMR spectroscopy. The diagnostic aminal carbon chemical shift at 71.2 ppm for 4-imidazolidinone is much further downfield than any Cα carbon. Figure 4 ACD labs' (version 2015)[14] prediction for this chemical shift was 73.4 ppm. Using ^{1}H NMR, ^{13}C NMR, COESY, TOCSY, and HSQC, we confidently assigned all the protons and carbons of cyclic peptides. Also, heteronuclear multiple bond correlation (HMBC) NMR experiments confirmed the 4-imidazolidinone structure (Figure 4). It is noteworthy that linear and cyclic dimerization or oligomerization products were not observed either by HPLC or MS analysis.

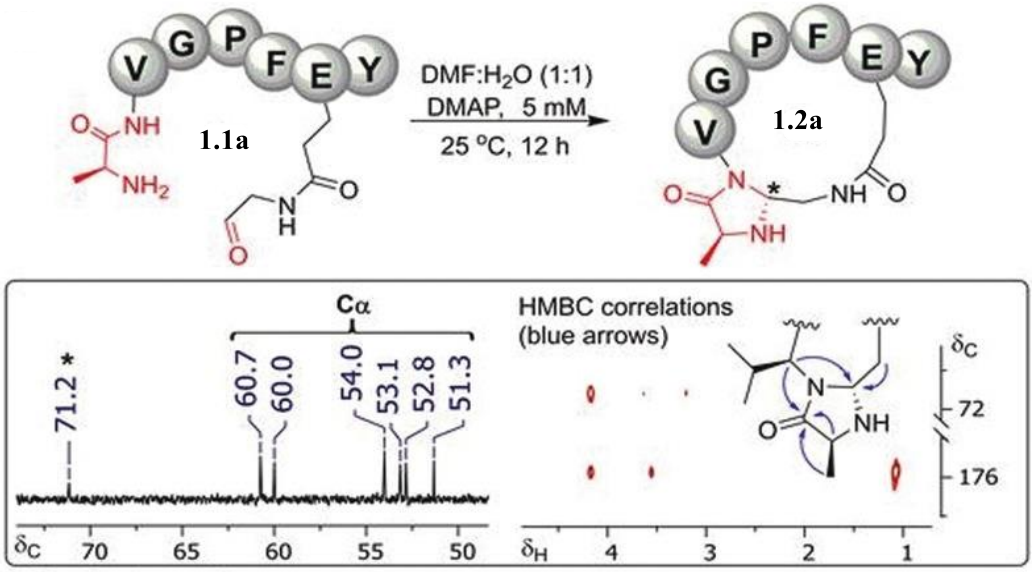

Figure 4: Structural characterization of cyclic peptide 1.2a by NMR spectroscopy. ^{13}C NMR spectrum with the diagnostic aminal chemical shift highlighted (*) and HMBC correlations confirming the 4-imidazolidinone ring structure of **1.2a.**

To further confirm that the second amide nitrogen was necessary for the cyclization reaction, the second amino acid residue in the peptide sequence was replaced with proline in the linear peptide aldehydes A**P**GAFE(CHO)Y **1.1A** and A**P**FA(CHO) (Figure 5). This substitution completely

abolished the macrocyclization showing that the amide proton is necessary for forming the 4-imidazolidinone containing cyclic peptide.

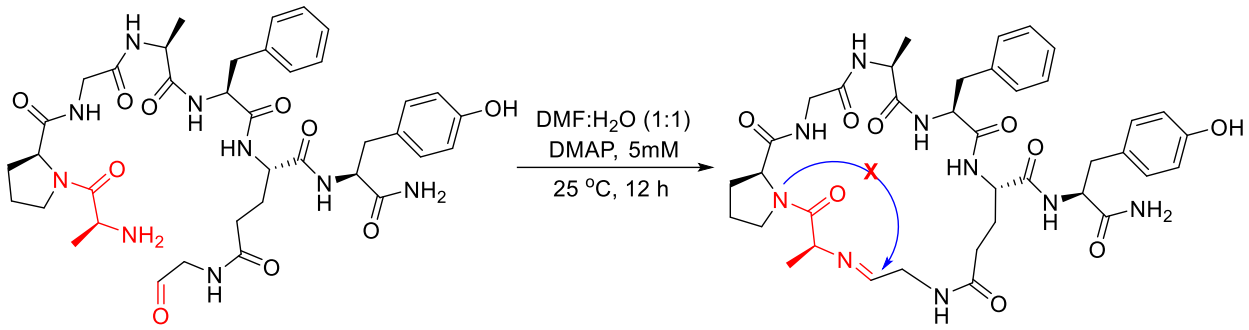

Figure 5: Control reaction using APGAFE(CHO)Y containing Pro in the second position validating that no macrocyclization occurs.

Most importantly, we attempted an intermolecular reaction between aldehyde pentanal and the N-terminus of linear peptide FVA. Intermolecular reaction forming 4-imidazolidinone was not observed between the aldehyde and N-terminus of the peptide. Although the intermolecular reaction led to the formation of a reversible imine, 4-imidazolidinone moiety was not detected. This was confirmed by the reduction of the linear imine with $NaCNBH_3$. We also attempted intermolecular reaction between highly reactive keto peptide aldehyde CHOVF and the N-terminus of the linear peptide ASVF under CyClick reaction condition; we did not observe the formation of any 4-imidazolidone-containing product under these conditions.

We hypothesize that this selectivity is based on the proximity of the amidic nitrogen to the cyclic imine. Taken together, this result confirms that the CyClick reaction takes place in an intramolecular fashion only.

1.2.3 Stereoselectivity of the CyClick Reaction

The cyclization technique also generates a new chiral center at the site of macrocyclization with a high diastereoselectivity (de >99%). This contrasts with many macrocyclization strategies leading to C-terminal epimerization.[15] The absolute configuration of the new chiral center in cyclic peptide

cyc(AVGPFEY) **1.2a** was determined to be *(R)* using correlations from ROESY NMR (Figure 6 and for additionally, see supplementary information for a full assessment). To determine the source of stereoselectivity, NMR analysis was done on a cyclized peptide cyc(**a**VGPFEY) where the first amino acid from the amino terminal was changed from configuration L to D. The stereochemistry of the new stereogenic center in 4-imidazolidinone containing cyclic peptide was *(R)* leading us to conclude that the configuration of the amino terminal is not responsible for directing the configuration of the new chiral center. Next, we synthesized cyclic peptide cyc(A**i**GPFEY) with D-Ile as the second amino acid residue. This led to a flip in stereochemistry with the new stereogenic center having a configuration of *(S)* in the cyclic peptide. This proved that the second amino acid's configuration, which most likely directs the amidic nitrogen's nucleophilic attack on the cyclic imine intermediate from the *Si* face, is what confers great stereoselectivity and the configuration of the new chiral center in cyclic peptides. The bulky Val residue would impede attacks from the *Re* face.

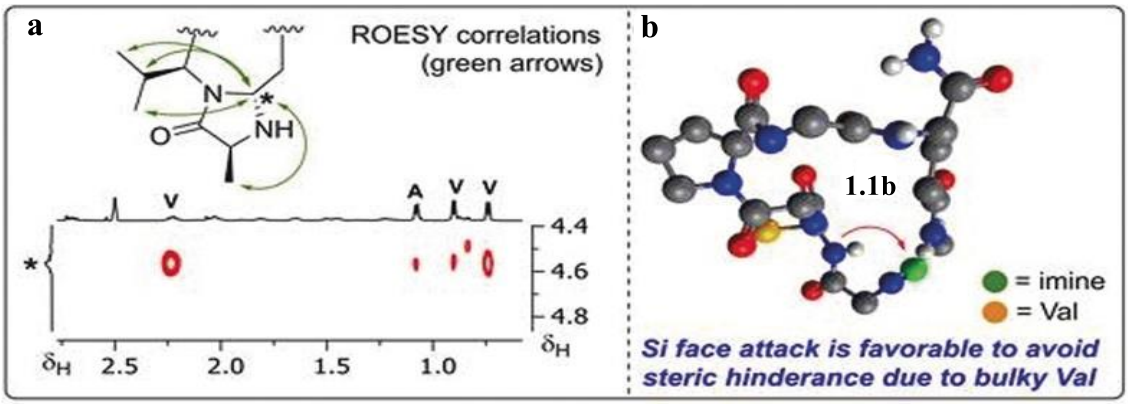

Figure 6: Stereoselectivity of CyClick Chemistry. a) Key ROEs used to assign **1.2a** the *(R)*-configuration of the new chiral center. Full-scale spectrum is included in the supporting information. b) proposed mechanistic pathway for the observed stereochemistry in the cyclic peptide.

1.2.4 Macrocyclization vs Oligomerization

One of the main drawbacks of the current peptide cyclization techniques is their propensity to form linear dimers, linear trimers, cyclic dimers, and cyclic trimers as a result of intermolecular processes.[16] To prevent the development of unwanted side products like dimers or oligomers, conventional macrocyclization operations are conducted at high dilutions of at least 0.004M.[16] High dilutions often result in slow reactions. Also, unwanted background processes like epimerization can be triggered by excessive dilution. Some methods for the synthesis of cyclic peptides in solution at high concentrations have been reported; however, they are constrained by their propensity to engage in intermolecular reactions, call for protected amino acids, like Lys or Glu/Asp, to prevent side reactions, and result in a mixture of diastereoisomers.[17]

The unique feature of our approach is that it shows high intramolecular selectivity. We therefore attempted macrocyclization of linear peptide AVGPFE(CHO)Y **1.1a** using high concentration (25mM, 25 times more than usually employed). We compared it to a conventional method of peptide macrocyclization (reductive amination). More about the impact of CyClick chemistry on macrocyclization can be shown with LC-MS analysis (Figure 7, top LC).

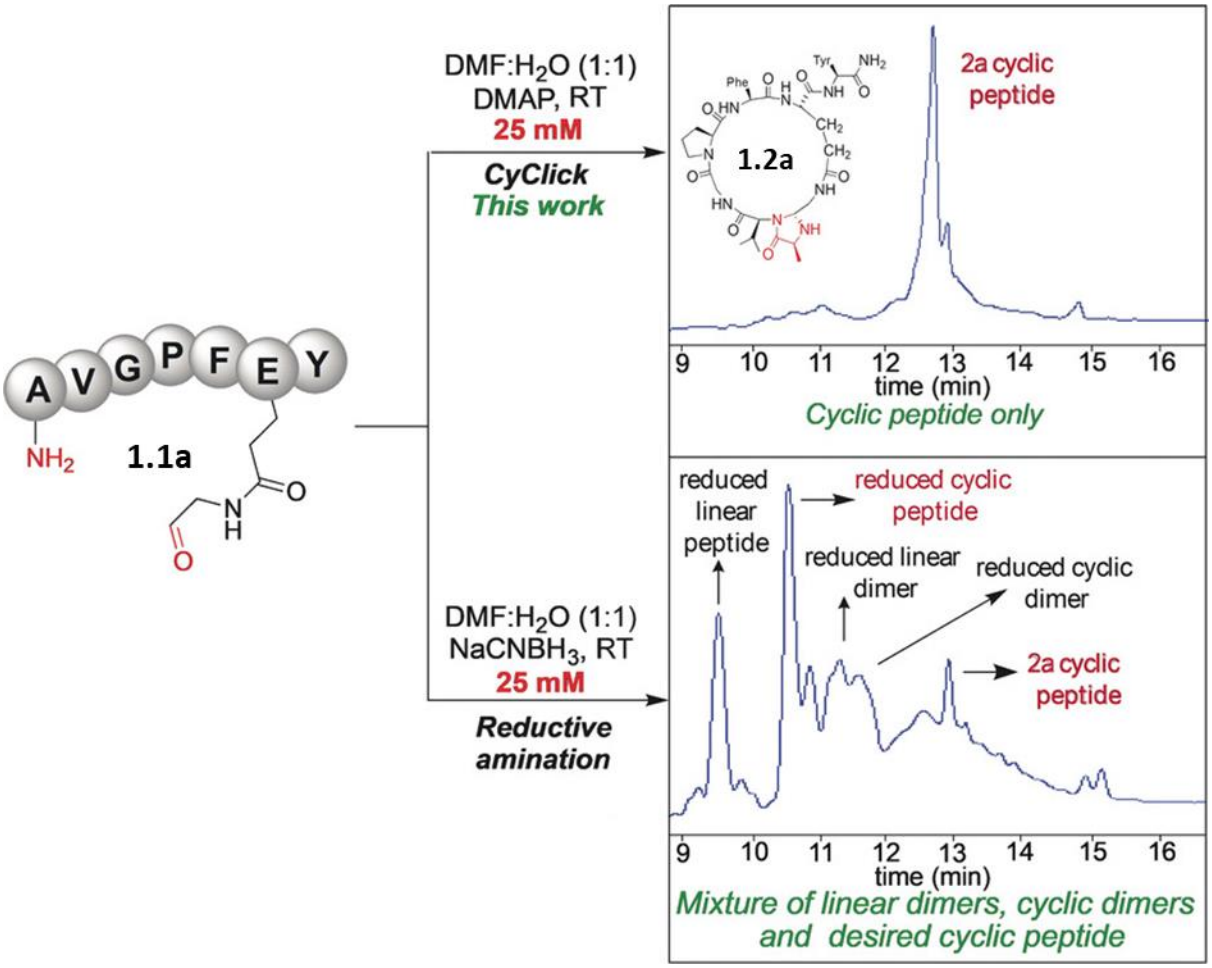

Figure 7: Macrocyclization vs. oligomerization. Direct comparison of CyClick reaction and reductive amination approach for the synthesis of cyclic peptide at high concentrations (25 mm). Chromatograms of the crude reaction mixtures.

Using the conventional reductive amination chemistry for making cyclic peptides,[18] we attempted reductive amination of linear peptide **1.1a** at high concentrations (25mM), significant amounts of dimers and cyclodimers were obtained (Figure 7, bottom LC). In contrast, cyclization of linear peptide **1.1a** by CyClick Chemistry proceeded efficiently with conversion (98%) without any appreciable amount of side products like dimers or cyclodimers (Figure 7, top LC). A significant improvement is thereby realized by macrocyclization using CyClick strategy. To challenge this CyClick approach, we attempted macrocyclization of linear peptide AVGPFE(CHO)Y **1.1a** at

100mM concentration with 21 equiv. of DMAP and stirring for 8 h at room temperature. We obtained majorly the desired cyclic peptide **1.2a** with high conversion (89%). We also did not observe any side products such as dimers or oligomers (HPLC trace of the reaction, See Supplementary Information).

For better understanding of the reaction rate, time-course studies on the rate of macrocyclization of linear peptide AVGPFE(CHO)Y **1.1a** were undertaken. For this studies, quantitative monitoring was carried out by injecting samples for HPLC analysis at fixed time intervals. The peptide AVGPFE(CHO)Y **1.1a** (0.67 mM) was subjected to CyClick macrocyclization and the conversion was monitored over a period of 4 h. From this data, we observed that most of the macrocyclization to generate the CyClick product occurs within the first 4 h with a conversion greater than 80%. (Figure 8). Taken together, these studies show that this reaction proceeds quickly gives high yields and does not generate side products such as linear or cyclic dimers and oligomers even at high concentrations.

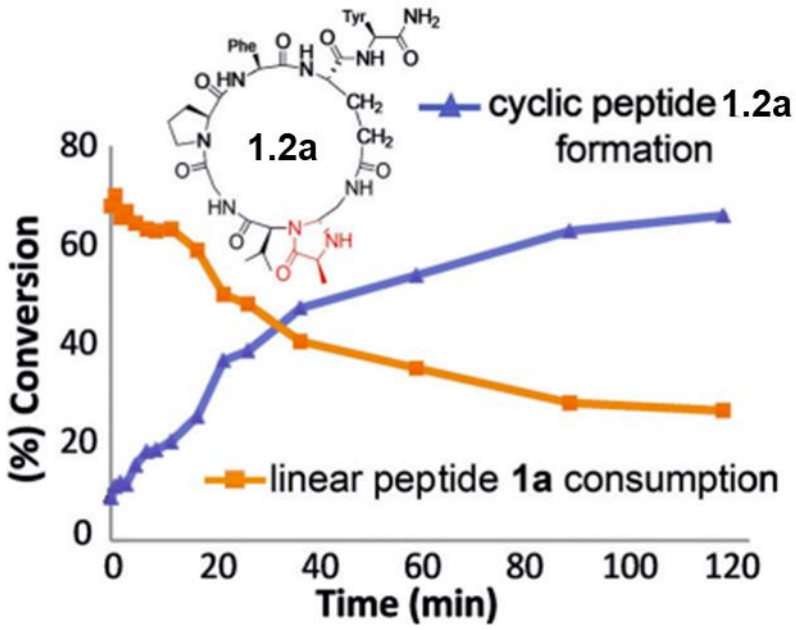

Figure 8: Rate studies for the synthesis of cyclic peptide 1.2a by CyClick chemistry. Peptides were quantified by HPLC.

1.2.5 Synthesis of Highly Diverse and Functionalized Cyclic Peptides by CyClick Chemistry

With the optimal conditions in hand, we proceeded to determine the versatility of this chemistry by carrying out cyclization of linear peptides with various amino acids at the *N*-terminus. As shown in Figure 9a, this approach adequately tolerated substrates having aromatic and aliphatic amino acids at the N-terminus, such as Trp, Tyr, and -branched Val (**1.1b-1.1d**), by producing the corresponding cyclic peptides (**1.2b-1.2d**) with good conversions (37-84 %). The cyclization process was not disrupted by reactions with N-terminal amino acids possessing reactive side chains, such as Gln, Asn, Asp, and Lys (**1.1e-1.1h**), and all these reactions produced the expected cyclic peptides (**1.2e-1.2h**) in excellent yields (64-94%). Surprisingly, under the reaction conditions (H_2O:DMF (1:1)), DMAP, cyclic peptide **1.2i'** with fused five-membered bicyclic imidazo[1,5-c]oxazol-7-one (40 % conversion) as well as the anticipated 4-imidazolidinone cyclic peptide 1.2i (60 % conversion) were produced (7 equiv.).

The thorough NMR and HRMS investigation of the imidazo[1,5-c]oxazol-7-one cyclic peptide **1.2i'** showed that the formyl group and the hydroxymethyl group of the side chain of serine were inserted late in the synthesis process.[19] The formaldehyde present in the undistilled DMF is most likely to be responsible for this. By performing the reaction in a different solvent with H_2O:ACN, we did not detect the production of fused five-membered bicyclic imidazo[1,5-c]oxazol-7-one cyclic peptide **1.2i'**, and the expected 4-imidazolidinone cyclic peptide **1.2i** was produced with an 70% conversion rate instead (Figure 9a).

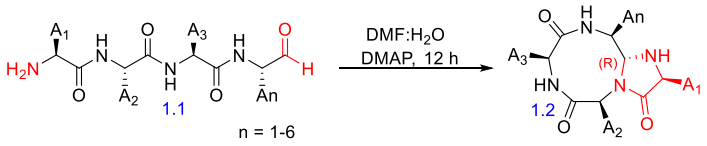

a.) Amino Terminus to Side-Chain Macrocyclization of Peptides

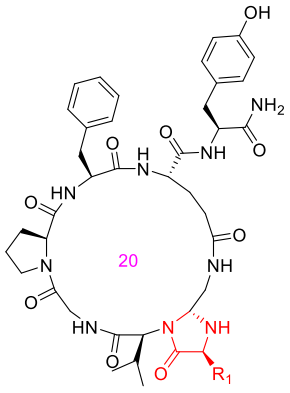

1.2a; R_1 = Ala, 99%; 1.2b; R_1 = Tyr, 40%
1.2c; R_1 = Val, 37%; 1.2d; R_1 = Trp, 84%
1.2e; R_1 = Gln, 94%; 1.2f; R_1 = Asn, 85%
1.2g; R_1 = Asp, 64%; 1.2h; R_1 = Lys, 84%
1.2i; R_1 = Ser, 48% (ACN = 70%)

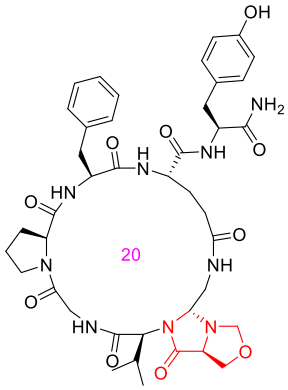

1.2i'; 32%
Imidazo[1,5-c]oxazolone late stage modification with formaldehyde

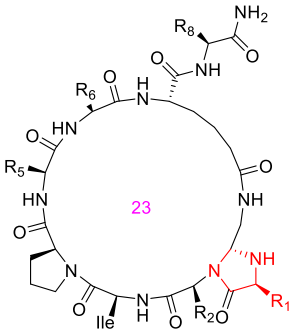

1.2j; R_1 = Asn; R_2 = Phe; R_5 = Cys; R_6 = Tyr, R_8 = His, 45%
1.2k; R_1 = Gln, R_2 = Asp, R_5 = Tyr, R_6 = Leu; R_8 = Ser, 61%

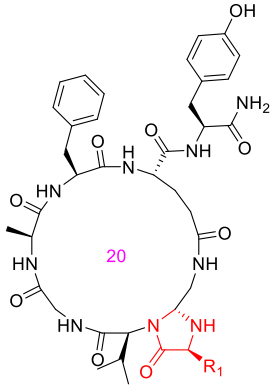

1.2l; R_1 = Gln, 53%
1.2m; R_1 = Asn, 65%

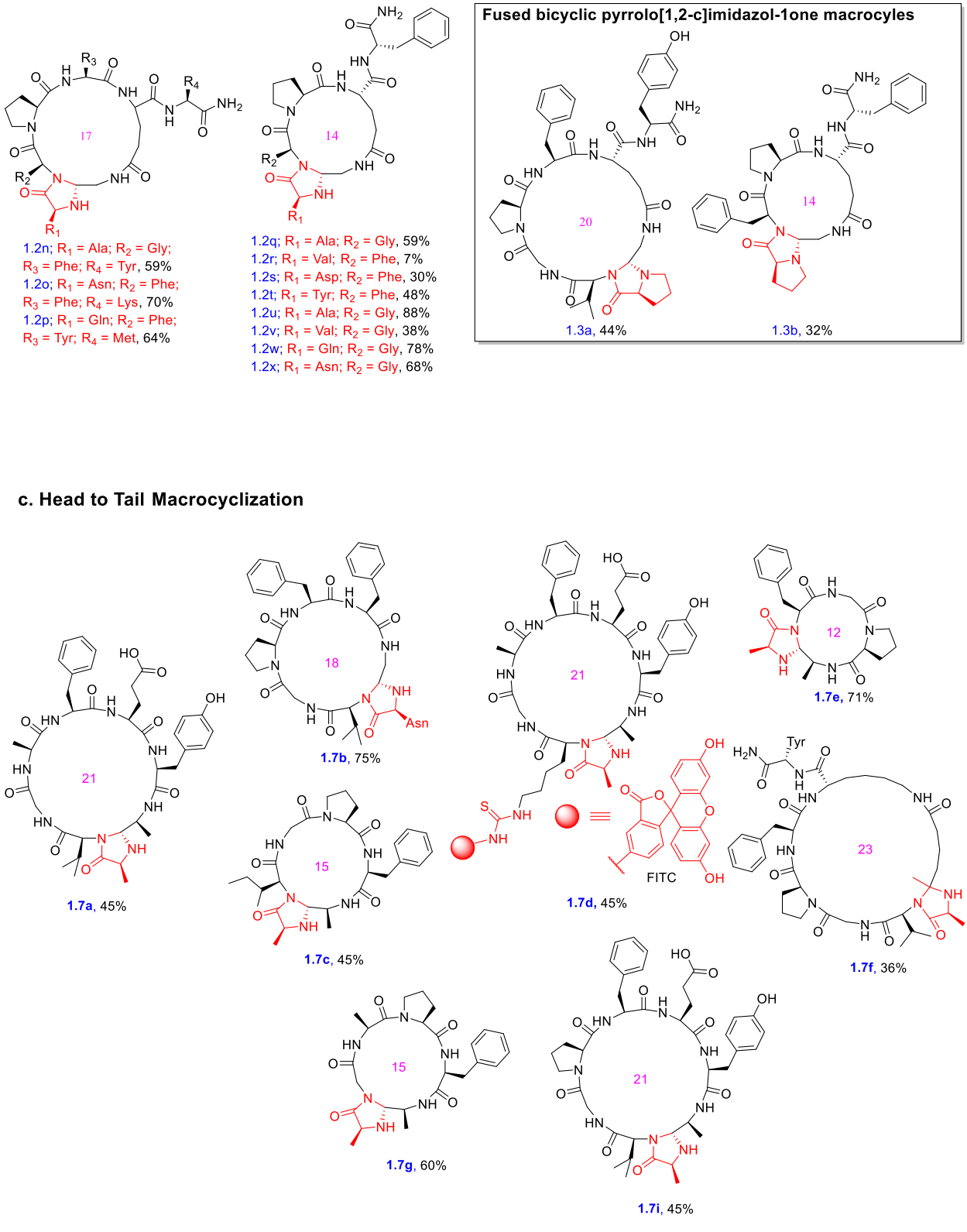

Figure 9: Substrate scope of CyClick chemistry. a) High conversions of cyclic peptides (12- to 23-membered) with various amino acid residues and lengths of peptide chains. b) Fused bicyclic

pyrrolo[1,2-c]imidazolone macrocycles at the site of macrocyclization. c) Head-to-tail macrocyclization of cyclic peptides by CyClick chemistry; number in the middle of the rings denotes ring size. Macrocyclic peptide **1.7f** with quaternary chiral center (*) was generated by reaction with peptide ketone.

The flexibility of the CyClick reaction was shown when unprotected linear peptides **1.1j** and **1.1k** with reactive amino acids including Asn, Asp, His, Tyr, Cys, Gln, and Ser afforded 23-membered cyclic peptides **1.2j** and **1.2k** with good conversions (45-61%, Figure 9a). The reaction was also used to cyclize challenging sequences, such as NVGAFE(CHO)Y **1l** and QVGAFE(CHO)Y **1m**, that had all L-amino acids with no turn inducers. High concentrations of DMAP (21 equiv.) enabled the linear peptides **1.1l-1.1m** to cyclize smoothly, yielding the corresponding cyclized products **1.2l-1.2m** (53–65%) (Figure 9a and Supplementary Information). Notably, neither linear nor cyclic oligomers were seen to form.

Most importantly, the -amino groups of lysine residues are inactive in such a pathway since there isn't a nearby amide group that can facilitate the CyClick cyclization. By preparing and cyclizing linear peptide aldehydes with unprotected Lys residues **1.1h** and **1.1o** under CyClick chemistry conditions, it was possible to examine the effects of interior lysine residues. With a good conversion rate (1.2h, 84%, and 1.2o, 70%, see Figure 9a), the processes produced the 4-imidazolidinone cyclic products **1.2h** and **1.2o**. Importantly, substantially identical yields of the cyclic products were produced in the absence of Lys (**1.2a**-**1.2g** Figure 9a), indicating that unprotected Lys does not affect the total yield of the CyClick products.

Encouraged by these outcomes, we continued to test the adaptability of this approach using peptides of various chain lengths, including pentapeptides and hexapeptides **1.1n**-**1.1x**. As shown in Figure 9a and Supplementary Information, all the substrates underwent efficient cyclization and

produced the matching 14- to 17-membered macrocycles **1.2n**-**1.2x** in good yields. This further demonstrates the versatility of our method for creating cyclic peptides.

Interestingly, the fused bicyclic 5-membered 1H-pyrrolo[1,2-c]imidazole-1-one cyclic peptides **1.3a** and **1.3b** were the major product of the cyclization of linear peptides containing proline at the N-terminus.[20] Similar to this, under the reaction circumstances, head-to-tail macrocyclization of octa-, hepta-, and hexa-peptides produced the corresponding 15-21 membered macrocycles **1.7a**-**1.7c** with good conversions (45-75%) (Figure 9c and Supplementary Information). In the absence of turn inducers, challenging linear peptides sequences like AVGAFEYA(CHO), underwent head-to-tail macrocyclization, producing the corresponding cyclized product **1.7a** with good conversion and no side-products as a result of linear and cyclic oligomerization (Figure 9c and Supplementary Information).

By creating a fluorescent-labeled 4-imidazolidinone-cyclic RGD peptide **1.7d** that can attach to breast cancer cells overexpressing v3 integrin,[21, 22] we further demonstrated the usefulness of this chemistry (Figure 9c and Supplementary Information). This data supports the efficacy of our strategy for creating bioactive peptidomimetics. We next put our methodology to the test by cyclizing a head-to-tail pentapeptide, which is very challenging to do with the current cyclization approaches due to their strong propensity to form oligomers.[7-15,17] To our delight, the 12-membered cyclic peptide, **1.7e**, was successfully synthesized with 71% yield (Figure 9c, Supplementary Information). We attempted the cyclization of a head-to-tail tetrapeptide, FGPA(CHO), utilizing a variety of reaction conditions, including high concentrations of DMAP, to further test our methodology. We were aware that a tetrapeptide aldehyde would produce a 9-membered ring which is not possible. We also did not observe any linear or cyclodimer production via CyClick chemistry (See Supplementary Information). By doing reduction with sodium cyanoborohydride,

we observed the formation of reduced linear tetrapeptide and reduced linear-dimer, which was confirmed by LC-MS. These results provided additional evidence that our approach only operates at the intramolecular level (See SI). Next, rather than peptide aldehydes, we looked at expanding the substrate range of CyClick Chemistry to less reactive peptide ketones. The cyclization proceeded efficiently resulting formation of 1.7f bearing a quaternary chiral center at the point of cyclization in 36% yield (Figure 9c). In addition, we were able to generate head-to-tail cyclic peptides **1.7g** and **1.7i** with 60% and 45% yields respectively.

More than 35 cyclic peptides of various ring sizes (12–24 members) and amino acid compositions have been created from the aforementioned reactions, demonstrating the effectiveness of CyClick as an intramolecular amide backbone activation method for the efficient synthesis of cyclic peptides.

1.2.6 Structural Impact of 4-imidazolidinone

To determine the secondary structure conferred by imidazolidinone on cyclic peptides, we performed detailed NMR investigation on head-to-tail cyclic peptide cyc (AVGAFEYA) **1.7a** in aqueous media. Using 2D COESY, HSQC, HMBC, TOCSY, and ROESY NMR we were able to confidently assign the ^{1}H and ^{13}C signals of **1.7a.** Using variable temperature NMR, we determined the presence of intramolecular hydrogen bonding within the cyclic peptide (Figure 10a). The presence of intramolecular hydrogen bonds in cyclic peptides is generally known to improve their cellular permeability. Variable temperature NMR revealed hydrogen bonding between Tyr amide Hydrogen and Ala carbonyl Oxygen. Using ROESY NMR, we were able to estimate intramolecular distances in the cyclic peptide. For peptide **1.7a**, long range ROEs between the residues Ala (ith) and Tyr (i + 3) were seen, indicating their proximity. Using ForceGen[22] with NMR constraints we were able to determine the secondary structure adopted by peptide **1.7a.**

These NMR investigations collectively offered the first direct experimental proof that 4-imidazolidinone truly is a turn inducer (Figure 10b).

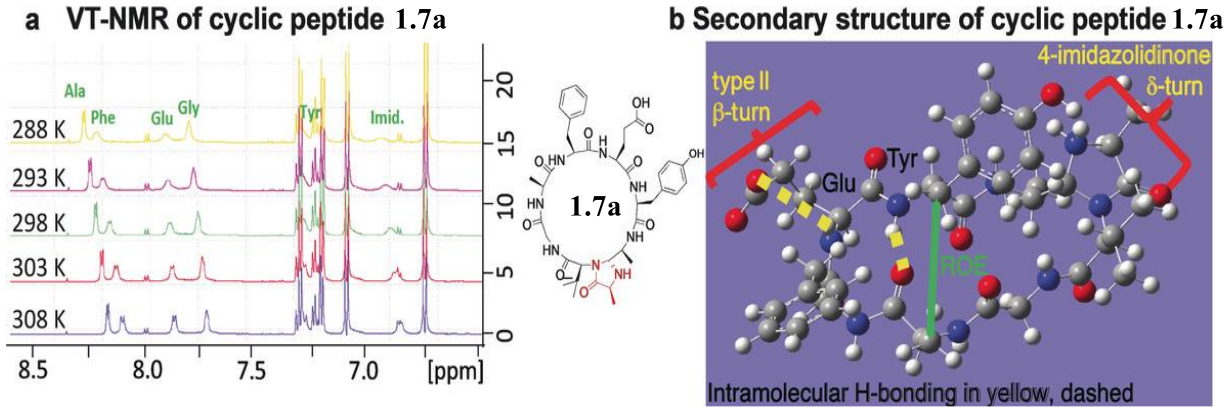

Figure 10: Impact of 4-imidazolidinone in cyclic peptides Structure: a) VT-NMR spectra of head-to-tail 4-imidazolidinone cyclic peptide **1.7a** in aqueous solutions. b) Turn structure of 4-imidazolidinone cyclic peptide **1.7a** obtained by running ForceGen with NMR constraints.

1.2.7 Biological Impact of 4-imidazolidinone in cyclic peptides

The stability of cyclic peptides in biological media is of great concern for pharmaceutical applications. Linear peptides are well known to degrade rapidly in the presence of digestive enzymes. We compared a cyclic peptide called cyc(AVGPFEY) **1.2a** against its linear equivalent, AVGPFEY, to determine which was more proteolytically stable. Chymotrypsin, a digestive enzyme that hydrolyzes peptide bonds at the C-terminal side of aromatic residues like Phe, was used to treat the linear peptide AVGPFEY and the cyclic peptide cyc(AVGPFEY) **1.2a**. Cyclic peptide **1.2a** exhibited only a 20% cleavage in the presence of chymotrypsin after 24 h. Its linear counterpart, AVGPFEY, however, degraded rapidly with a half-life of 20 min and was completely consumed in 90 min, according to HPLC and MS analysis (Figure 11). These findings showed that cyclization generated 4-imidazolidinone moiety considerably increased the stability of cyclic peptides against proteolytic degradations. Together, these findings show how the CyClick

chemistry can be used to create potentially bioactive cyclic peptidomimetics that can be used as molecular instruments to research biological systems.

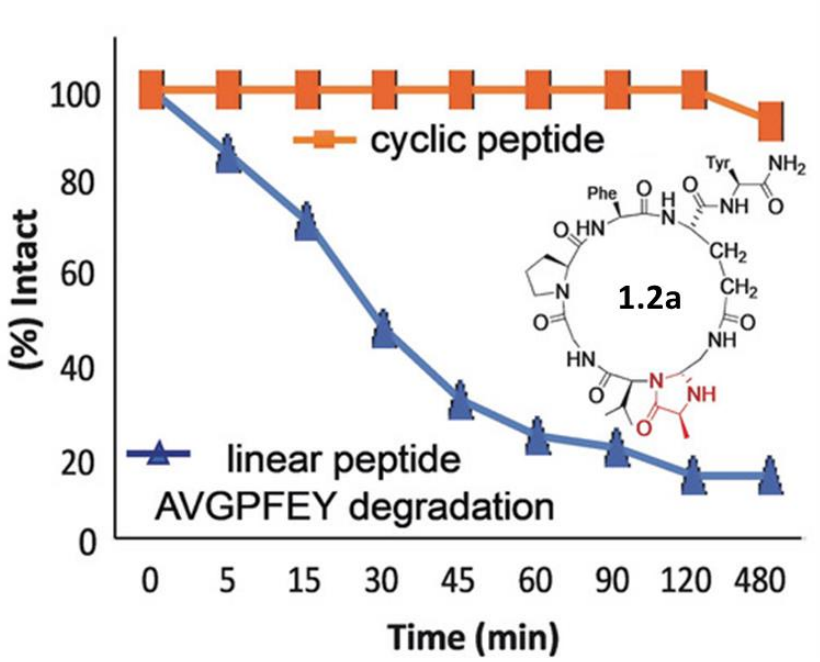

Figure 11: Proteolytic stability of 4-imidazolidinone cyclic peptide 1.2a as compared to its linear counterpart.

1.2.8 Reversibility of Cyclic Chemistry and MS/MS sequencing of cyclic peptides

Since CyClick Chemistry generates an aminal containing 4-imidazolidinone ring, we hypothesized that the imidazolidinone can respond to external stimuli by protonation leading to ring opening to generate the linear peptide. To test our hypothesis, we took cyclic peptide **1.7a** at pH 7.11, the M + 1 adduct of the cyclic peptide **1.7a** was seen in the HPLC (retention time, Rt = 14.632) and mass spectrometric analysis. Using Boc-Phe-OH as an internal standard, the conversion of the cyclic peptide to linear peptide was monitored by HPLC. After 24 h, we observed little degradation of 10% of the cyclic peptide to linear peptide. With heat at 37^{o}C, there was an increase in degradation (20%) to the linear peptide. The reaction was greatly catalyzed by heat and acidic pH as at a

temperature of 80 °C and pH 3.11 we observed ring opening of 80% after 1 h and complete ring opening after 8 h (Figure 12).

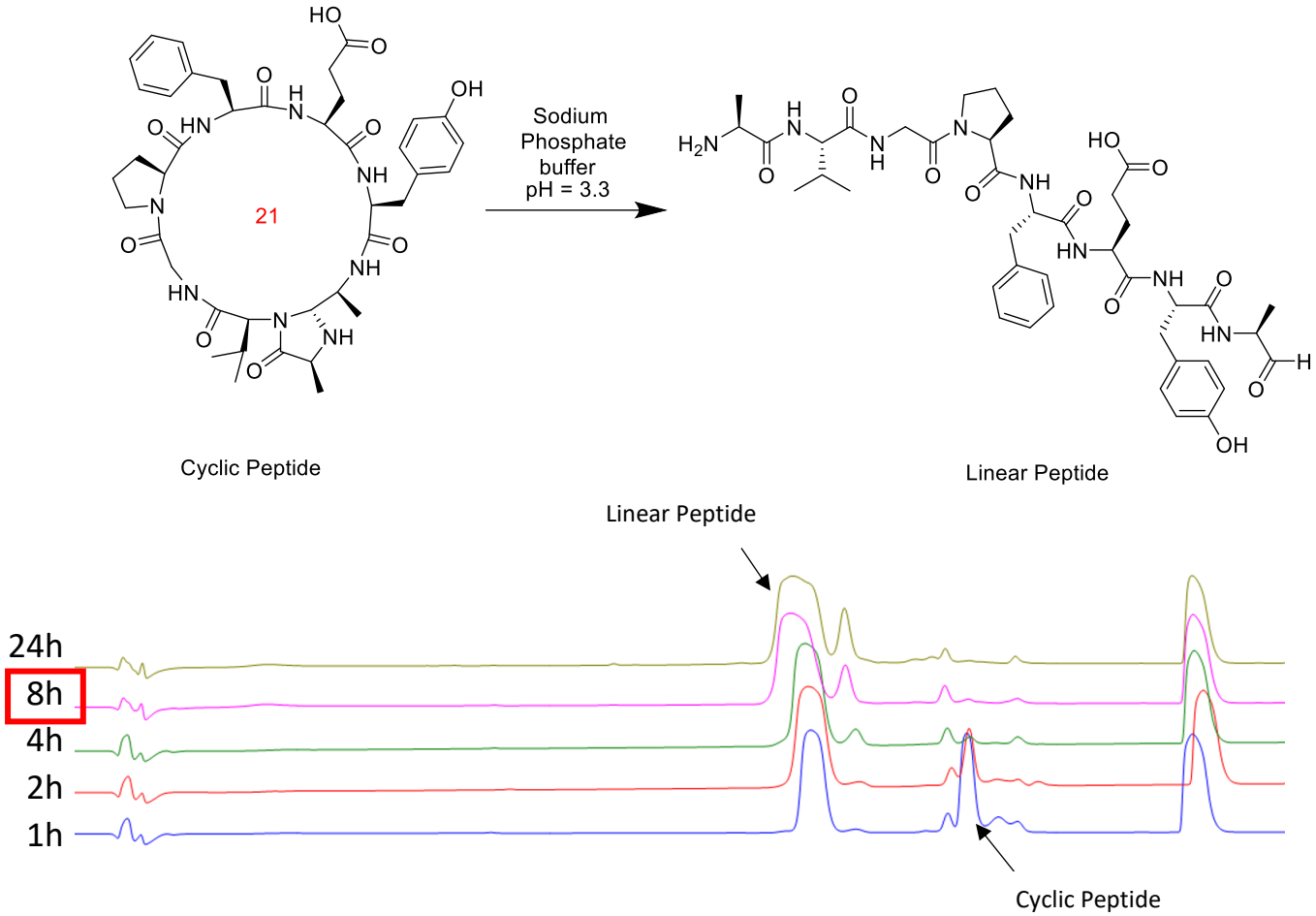

Figure 12: Optimization Data for Ring Opening of Cyclic Peptide.

The above experiment confirmed the unique feature of the CyClick Peptide responding to the change in pH, leading to opening of the ring by varying the pH conditions which is in contrast to the conventional methods of macrocyclization. This unique property of the imidazolidinone containing cyclic peptides could be utilized for sequencing of hit cyclic peptides obtained after library screening.

1.2.9 Mechanistic Investigation into CyClick Chemistry

Since neither a guiding group nor a catalyst is used in the "CyClick" chemistry, it is still unknown how the reaction takes place and where the high intramolecular selectivity comes from. We suggest that intramolecular hydrogen bonding (IMHB) may be responsible for promoting the "CyClick" intramolecular cyclization by stabilizing the cyclic imine intermediate over the linear imine intermediate in light of the significance of intramolecular hydrogen bonding in limiting the conformational flexibility of macrocyclic peptides. We, therefore, performed a detailed computational analysis to understand the reason for the high intramolecular selectivity, chemo- and stereoselectivity and the effect of peptide length on CyClick cyclization.

With the def2svp[23] basis set and the dispersion-corrected B3LYP-D3[24] functional, all geometry optimizations were carried out. The triple zeta def2tzvpp basis set and the M06-2X functional were used to calculate single point energies. By using the SMD[25] solvation model in water ($\varepsilon = 87.9$) for optimization and energy calculations, solvation effects were taken into account. On the UCLA Hoffman2 and XSEDE[26] supercomputers, Gaussian 16 was used for all calculations. In order to compare the outcomes of various density functionals, the reaction coordinate profile in Figure 13 at higher levels of theory was also analyzed (see SI for details).

To determine if the optimized structures are transition states (with imaginary frequency) or intermediates (no imaginary frequency), vibrational frequencies were estimated. Only one imaginary frequency was observed. In order to confirm the characteristics of each transition state, we have additionally undertaken intrinsic reaction coordinate calculations. Zero-point vibrational energies and thermal corrections at 298 K are included in the stated Gibbs free energies and enthalpies. We used the quasiharmonic approach from Grimme to compute the thermal

adjustments with a cut-off frequency of 50 cm-1 in order to achieve more precise Gibbs free energies and enthalpies. Using GoodVibes,[27] the quasiharmonic approximations were computed.

We used CREST to perform a thorough conformation sampling because macrocycles are known to have great structural flexibility. For each linear peptide aldehyde, the cyclic imine intermediates, and the imidazolidinone-cyclic peptides, we first performed CREST[28] calculations. Then, with a cut-off energy of 3.0 kcal/mol, we optimized all conformers using DFT calculations. As a result, we report the conformation with the lowest energy.

Using model substrate **1.4e**, we computed the reaction coordinate profile of the CyClick reaction of the linear peptide aldehyde **1.4e**. (Figure 13) Linear peptide aldehyde AFPGA selectively generates the 12-membered ring imidazolidinone cyclic peptide **1.7e-R**. To expedite computation, a Me group was substituted for the Bn substituent in **1.4e**. The formation of cyclic imine was exergonic by 12.1 kcal/mol. We presume that the creation of cyclic imine intermediate **1.5e** is not the rate-limiting step because it is reversible and can be experimentally verified (see SI for details).

The zwitterionic reaction pathway is the most favorable reaction pathway for the second cyclization process of **1.5e**. The intramolecular hydrogen transfer transition state TS1 has an energy barrier of 17.7 kcal/mol which is a relatively low energy barrier. The formation of the zwitterionic intermediate **1**.**6e** is endergonic requiring 16.0 kcal/mol with respect to the resting state **1.5e**. After the zwitterion (TS2-R) collapses, the imidazolidinone cyclic peptide product **1.7e-R** is formed.

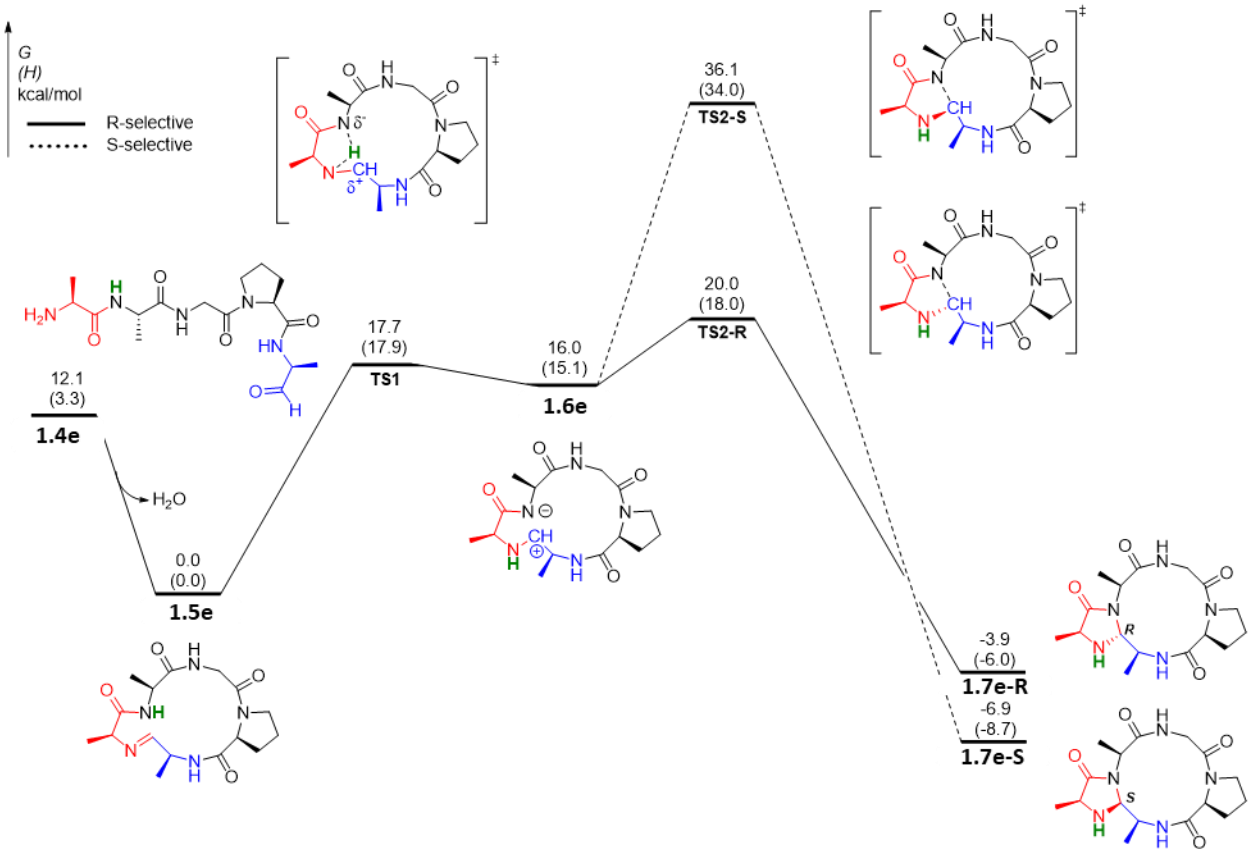

Figure 13: Reaction coordinate profile of intramolecular CyClick reaction of **1.4e**.

The C-N bond formation step (TS2-R), which has a total free energy barrier of 20.0 kcal/mol in relation to cyclic imine intermediate **1.5e**, is the rate-limiting transition state along the zwitterionic pathway. With respect to **1.5e**, the formation of the product **1.7e-R** is exergonic by 3.9 kcal/mol. A substantially higher free energy barrier of 36.1 kcal/mol is needed for the S-selective stereoisomeric pathway (dashed black pathway), which uses TS2-S. We also discovered that DMAP can further stabilize the imidazolidinone cyclic peptide product **1.7e-R**, increasing the exergonicity of the "CyClick" reaction and pushing the reaction equilibrium in the direction of the product, resulting in the greater conversion rate that was observed. DMAP is not a direct participant in any transition states or intermediates in the productive zwitterionic pathway.

Overall, we find that for the intramolecular CyClick of linear peptide aldehyde **1.4e**, the zwitterionic pathway is the most favorable reaction pathway. The rate-limiting transition state is the second cyclization TS2, and the resting state is the cyclic imine intermediate **1.5e**. Our experimental findings are consistent with the computed low free energy barrier and high R-stereoselectivity.

A more thorough analysis of the DFT-optimized intermediate and transition state geometries throughout the zwitterionic pathway demonstrated the crucial functions IMHB served in encouraging "CyClick" reaction (Figure 14). First, three IMHBs pre-organize the substrate by bringing the N-terminus near to the aldehyde C-terminus in the lowest energy conformation of **1.4e**, which should help the first cyclization step to generate cyclic imine **1.5e**. Second, a transannular IMHB in **1.5e** pre-organizes the macrocycle backbone into a rather stiff conformation, which endures through the subsequent hydrogen transfer transition state TS1, the rate-limiting TS2-R, the zwitterionic intermediate **1.6e**. Finally, the zwitterionic **1.6e** (1.83A) and the rate-limiting TS2-R (2.02A), is stabilized by a second transannular IMHB between the cationic iminium N-H and the backbone carbonyl group.

Our computational evaluation shows that the IMHB contributes greatly to the high diastereoselectivity observed experimentally. The estimated free energy barrier for TS2-S is 37.2 kcal/mol, which is much higher than the estimated free energy barrier for TS2-R (20.0 kcal/mol) (Figure 13). According to further analysis of the DFT optimized molecular geometries of the stereoselectivity-determining transition states, the low energy TS2-R adopts a less distorted conformation as the cyclic imine resting state **1.5e** (Edist = 2.1 kcal/mol), while the TS2-S adapts a more distorted macrocycle backbone conformation (Edist = 9.3 kcal/mol). Also, the second transannular IMHB between the cationic iminium N-H and the backbone carbonyl group (2.02),

significantly stabilizes TS2-R. In contrast, TS2-S lacks IMHB stabilization and has an iminium N-H that faces away from the macrocycle's backbone. In the lower energy TS2-R, the iminium cation also adopts a more stable trans shape.

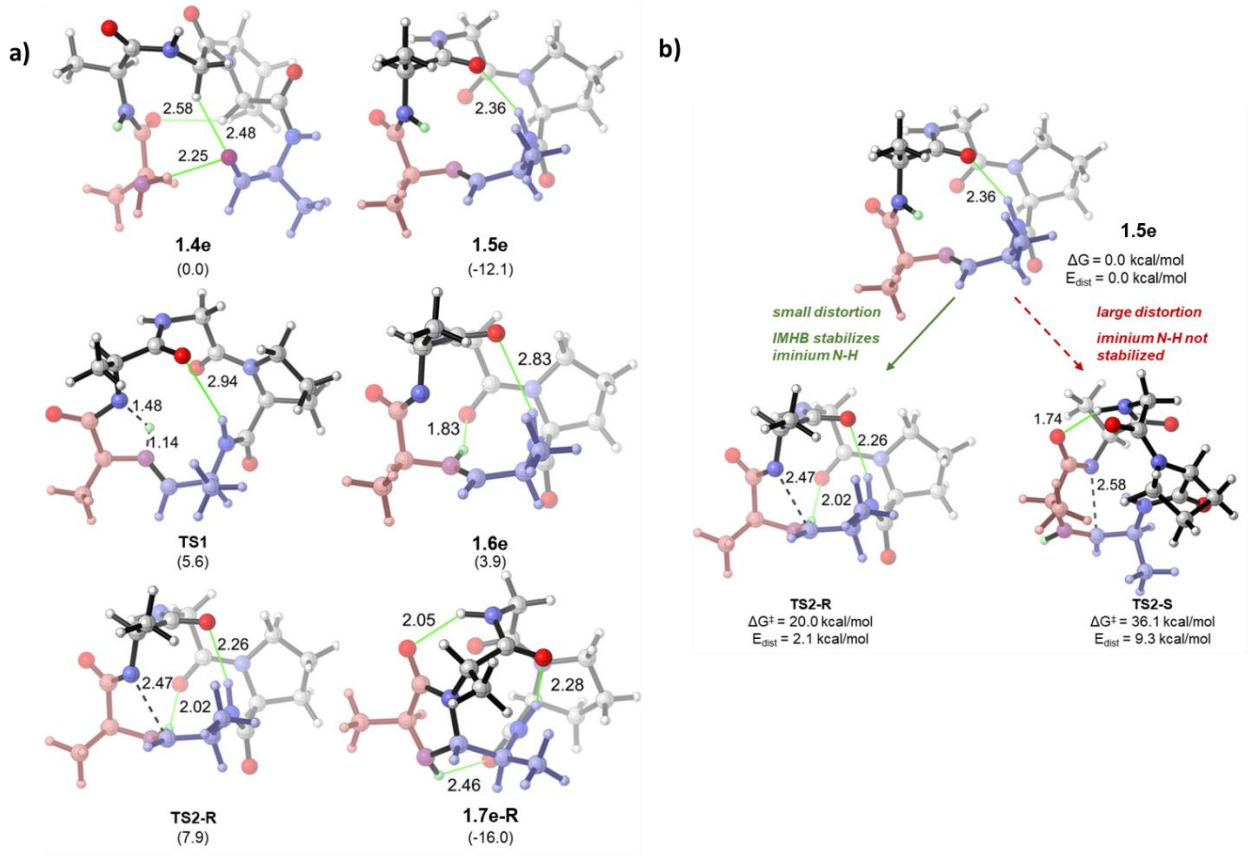

Figure 14: Geometries of Transition States and Intermediates for CyClick of 1.4e. a) intermediates and transition states along the zwitterionic pathway of intramolecular "CyClick" of **1.4e** (Computed Gibbs free energy ΔG in kcal/mol). b) Structure showing the origin of Stereoselectivity of **1.4e.**

To understand the reason for the intramolecular selectivity, the intermolecular CyClick reaction of **1.4e** was also investigated (Figure 15). We modeled the C-terminus of **1.4e** using a model substrate

1.8e to reduce computational time (Figure 15). The imine intermediate **1.9e** is only marginally exergonic by 2.1 kcal/mol, according to the estimated reaction coordinate profile. In comparison to the resting state **1.9e**, the hydrogen transfer transition state TS3 has a free energy barrier of 21.7 kcal/mol. Through intramolecular hydrogen atom transfer (TS3), the production of the zwitterionic intermediate **1.10e** is endergonic by 17.2 kcal/mol. The ensuing rate-limiting cyclization transition state TS4 exhibits a kinetic barrier that is relatively greater than that of the intramolecular cyclization, at 25.3 kcal/mol, or an increase of 5.3 kcal/mol.

In good agreement with the experimentally observed exclusive intramolecular chemoselectivity, this computed reaction coordinate profile predicts that the intermolecular CyClick reaction is significantly slower than the intramolecular CyClick reaction. As shown previously, our experimental observation demonstrated that even at very high peptide concentrations (100 mM), intramolecular cyclic product formation occurs. Although IMHB exists in both the rate-limiting TS4 and the resting state **1.9e**, analysis of the DFT optimized molecular geometries showed that the cationic iminium NH in TS4 points away from any hydrogen bond acceptors. Additionally, the intramolecular TS2-R peptide backbone's pre-organized macrocyclic peptide backbone (Edist = 2.1 kcal/mol) is somewhat less distorted than the peptide backbone of TS4 (Edist = 3.1 kcal/mol).

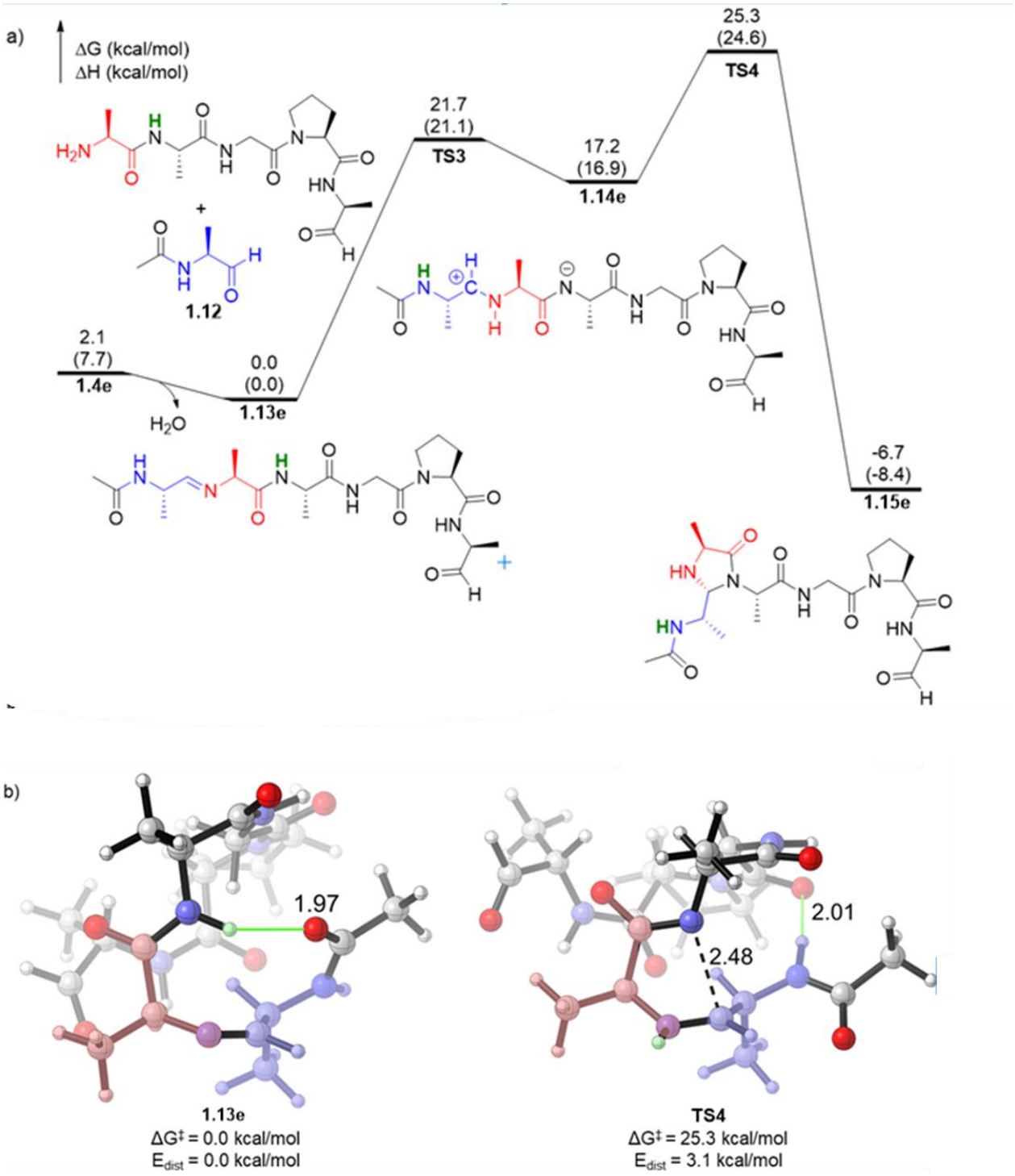

Figure 15. a) Computed reaction coordinate profile of intermolecular "CyClick" of **1.4e**; b) DFT optimized geometries of resting state **1.13e** and rate-limiting transition state **TS5-R.**

Overall, we conclude that IMHBs are essential in the “CyClick” cyclization of **1.4e** to a) pre-organize the linear substrate and promote the first cyclization to form the cyclic imine intermediate; b) stabilize cationic iminium N–H in the zwitterionic intermediate and the rate-limiting second cyclization transition state; c) promotes *R*-stereoselectivity and intramolecular chemoselectivity.

With a good understanding of the reaction mechanism of CyClick Chemistry, we used computation to determine the effect of length of linear peptide aldehyde on the CyClick reaction. We calculated the "CyClick" reactions of **1.4g** and **1.4h**, which result in the formation of the 15-membered and 9-membered ring imidazolidinone cyclic peptides, respectively (Figure 16). The reaction mechanism described in earlier parts is comparable to the "CyClick" of **1.4g** along the zwitterionic route. Exergonic by 12.4 kcal/mol, the cyclic imine intermediate **1.5g** is formed. The zwitterionic intermediate **1.6g** is created as a result of the succeeding hydrogen transfer transition state (G_{TS5} = 18.3 kcal/mol). The second cyclization TS6-R transition state, which has a free energy barrier of 20.6 kcal/mol, is the rate-limiting transition state. In comparison to the cyclic imine intermediate, the production of the product 15-membered ring imidazolidinone cyclic peptide **1.7g** is exergonic by 9.5 kcal/mol. The kinetic barrier for the S-selective TS6-S is 25.6 kcal/mol. All things considered, we anticipate that the CyClick reaction of **1.4g** will easily occur at room temperature to selectively generate **1.7g**, which is consistent with the experimental findings shown on Figure 9.

In addition, we modeled the linear peptide aldehyde substrate "CyClick" of **1.4h**, which has one less glycine than **1.4e**. The computed reaction coordinate profile suggests that the rate-limiting transition state for CyClick of **1.5h** is the hydrogen transfer transition state **TS7**. The reaction shouldn't occur at room temperature because the computed free energy barrier (GTS7 = 33.5

kcal/mol) is quite high and this is in accordance with the experimental observation. The formation of the 9-membered ring imidazolidinone cyclic peptide **1.7h** is only exergonic by 1.9 kcal/mol.

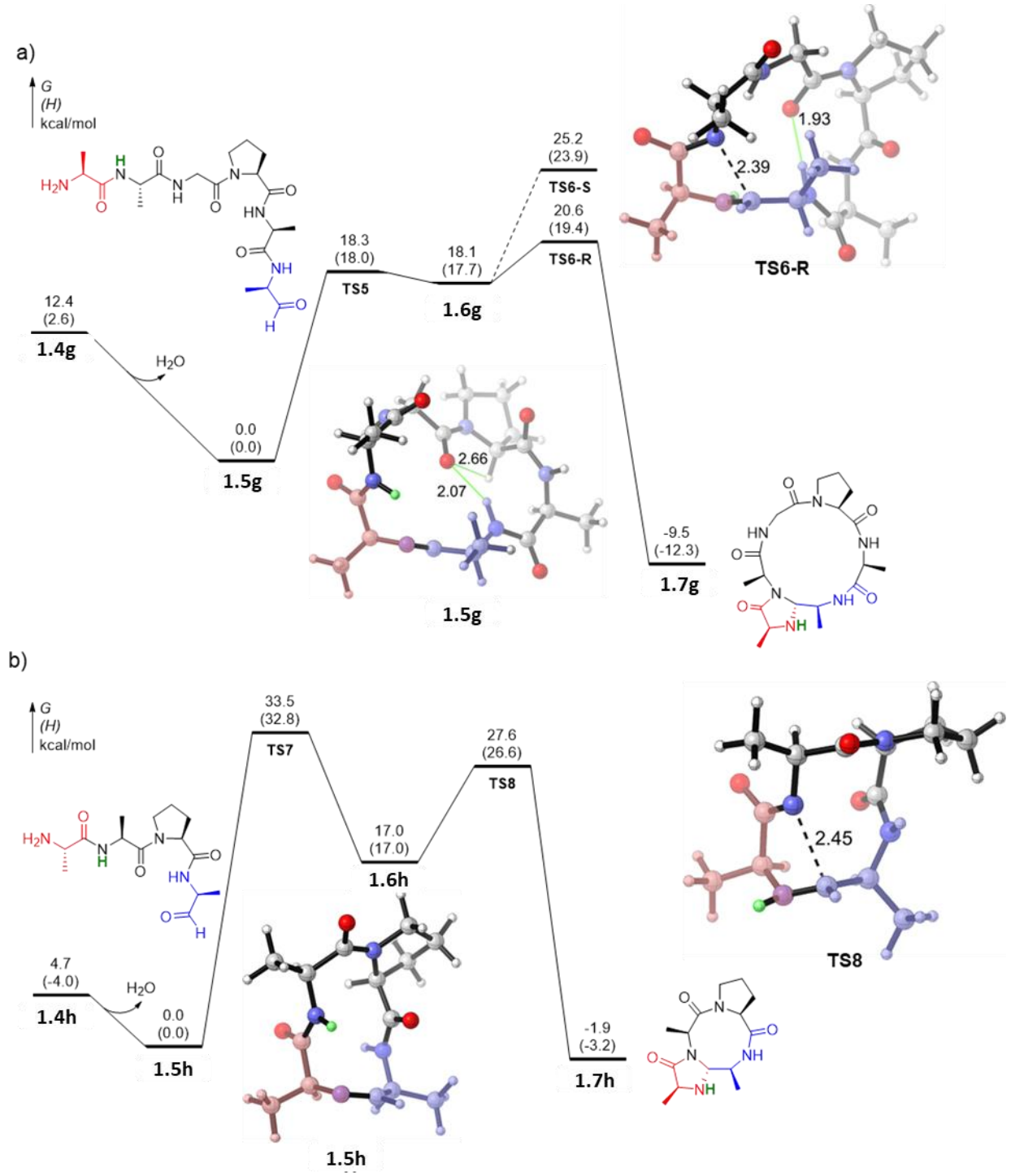

Figure 16. Reaction coordinate profile of CyClick reaction of **1.4g** and **1.4h**.

1.2.10 Application of CyClick Chemistry for Making Highly Stained Cyclic Peptides

Scientists working in a variety of fields, such as pharmaceutical chemistry and materials chemistry, find small cyclic peptides appealing due to their variety of biological characteristics and distinctive structural features.[29] Important members of this class called cyclic tetrapeptides (CTPs) are notoriously challenging to synthesize.[29] To make it easier to obtain many CTPs from natural products and their rationally designed equivalents many synthetic techniques have been devised recently to access these CTPs. These procedures also involve high dilution conditions and often high temperature.[29] The largest obstacle when attempting to synthesize cyclic tetrapeptides is the formation of side products such as oligomers or cyclo-oligomers.[30]

Since CyClick strategy can generate cyclic peptides with various ring sizes in moderate yields without dimerization, we proceeded to attempting Head-to-Tail cyclization of various linear peptides to generate corresponding cyclic tetrapeptide.[30] Only a very small quantity of the cyclic product was seen when the head-to-tail cyclization of the tetrapeptide was performed in the absence of a base, demonstrating the critical role that a base plays in this reaction. Using DMAP as a base at room temperature, we saw a (58%) conversion to the head-to-tail monocyclic 4-imidazolidinone product cyc-4-Imz-A(GPFA) **1.7e** (See SI for details). We increased the amount of DMAP to 21 equiv. in order to further improve the cyclization efficiency, and we observed a noticeable improvement in the conversion to the head-to-tail monocyclic product cyc-4-Imz-A(GPFA) **1.7e** (82%). The examination of the HPLC results was complicated by the use of excessive DMAP. Purification and analysis are difficult because the big DMAP peak in the HPLC chromatogram can obscure peptide peaks. Diisopropylethylamine (DIEA, pKa 10.98) - a volatile base that can be eliminated prior to HPLC analysis of a reaction mixture, was chosen to avoid this issue. The cyclization reaction of linear AGPFA **1.4e** with DIEA (21 equiv.) at 60 ^{o}C went

smoothly and produced the monocyclic product cyc-4-Imz-A(GPFA) **1.7e** with 89% conversion. DIEA and the solvent was removed in vacuo followed HPLC to obtain a clean chromatogram (Figure 17).[31]

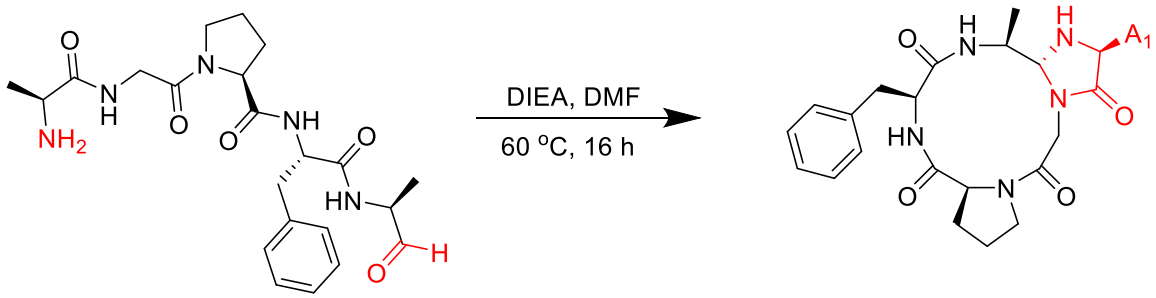

1.4e **1.7e**

Base (pKa)	Base (equiv.)	Temperature	Mono-CyClick 2b (%)
No Base	0 equiv.	RT	13.00
DMAP	7 equiv.	RT	58.00
DMAP	21 equiv.	RT	82.00
DIEA	21 equiv.	RT	73.00
DIEA	21 equiv.	60 °C	89.00

Figure 17: Optimization of linear peptides aldehyde cyclization using different bases

We proceeded by cyclizing random linear pentapeptide aldehydes XGPFA **1.8a-1.8g** (X = G, P, S, Y, D, N, R, H) with Ala at the C-terminus and different amino acid residues at the N-terminus. The peptide aldehydes were dissolved in a 1:1 molar solution of DMF:water, containing 3.3 mM of DIEA. Fortunately, within 16 hours, the linear peptide aldehydes XGPFA **1.8a-1.8g** cyclized smoothly to produce monocyclic tetrapeptides cyc-4-Imz-X(GPFA) (**1.9a-1.9g**). We realized that the significant strain associated with small ring cyclic peptides could potentially lead to the generation of cyclic dimers based on earlier cyclization techniques for making cyclic tetrapeptide. We carefully examined every reaction using LC-MS, and only the necessary monocyclic tetrapeptide products were found, in contrast to other methods of forming cyclic tetrapeptides,

which result in the synthesis of cyclodimers.[32,33,5] During the cyclization, unprotected amino acid residues such as Tyrosine, serine, asparagine, and aspartic acid did not have any undesirable side effects, demonstrating the chemoselective nature of the CyClick Chemistry (Figure 18).

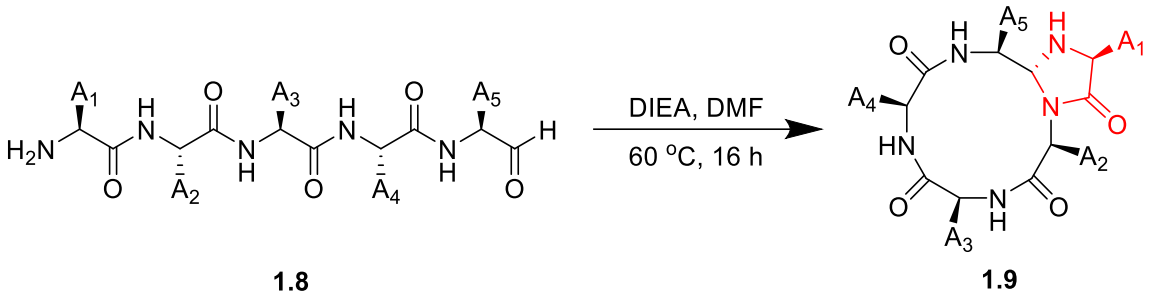

1.8 **1.9**

Linear Sequence 1.8	Mono-CyClick 1.9 (Conv. %)	m/z [Da]	monomer:dimer
GGPFA **1.8a**	Cyc-4-Imz-G(GPFA) **1.9a** (73%)	414.1883	>99:1
PDPFA **1.8b**	Cyc-4-Imz-P(GPFA) **1.9b** (57%)	454.2162	>99:1
SGPFA **1.8c**	Cyc-4-Imz-S(GPFA) **1.9c** (21%)	444.1983	>99:1
YGPFA **1.8d**	Cyc-4-Imz-Y(GPFA) **1.9d** (59%)	520.2243	>99:1
DGPFA **1.8e**	Cyc-4-Imz-D(GPFA) **1.9e** (17.7%)	472.2198	>99:1
NGPFA **1.8f**	Cyc-4-Imz-N(GPFA) **1.9f** (31%)	471.2367	>99:1
RGPFA **1.8g**	Cyc-4-Imz-R(GPFA) **1.9g** (50%)	513.2929	>99:1

Figure 18. Scope of peptide cyclization for the synthesis of strained head-to-tail cyclic tetrapeptides. Reaction conditions: 3.3 mM of peptides **1.8a-1.8g** in H_2O:DMF were treated with DIEA (21 equiv.) and reaction mixtures were left for stirring at 60 °C for 16 h and analysis by HPLC to determine the (%) conversion of cyclic tetrapeptides **1.9a-1.9g.**

It has been observed that traditional lactamization conditions (HATU, DIEA, DMF; DEPBT, DIEA, DMF; PyBOP, DIEA, DMF)[34] also produce linear dimers at high concentrations and alter the reactive side chains (Asp, Ser) of the amino acids.[34] We attempted head-to-tail cyclization of the linear peptide AGPFA **1.4e** at large concentrations (25 mM, 25 times of previous methods published in literature) under the optimal conditions because the CyClick approach only works

intramolecularly. With a high monoCyClick to cyclodimer ratio of >17:1, the reaction produced the monocyclic tetrapeptide cyc-4-Imz-A(GPFA) **1.7e** with a high conversion rate of 89.5 percent in 16 hours. These findings suggest that the CyClick strategy, which involves a two-step process that involves the formation of the cyclic imine with a pentapeptide (15 atoms, low energy barrier) and contraction of the ring by the amide backbone to produce highly strained monocyclic tetrapeptides (12 atoms), can make up for the high energy barrier in synthesizing head-to-tail cyclic tetrapeptides by conventional methods.

1.2.11 Application of CyClick chemistry for making Peptide-Peptoid Hybrid

In recent years, peptides, peptoids, and other peptidomimetics have received a lot of interest.[35] This is mostly because of their capacity to modulate different protein-protein interactions, which in turn can control a variety of biological processes.[35] Peptoids (poly-N-substituted glycine) in particular, are excellent peptidomimetics. They vary from peptides in that their R-groups are located right on the amide bonds, ensuring that their backbone is fully made up of tertiary amides.[36] This endows peptoids with a variety of unique physical and biological features.[37] Peptoids, for instance, are substantially more resistant to enzymatic degradation than peptides, which makes them appealing molecules for a variety of biological applications such as imaging probes, antimicrobials, antifungal, and anticancer medicines.[37] Additionally, because the backbone lacks an amide NH, hydrogen bonding cannot be used to support the creation of discretely folded secondary structures.[36] Due to their greater structural flexibility than peptides, it can be difficult to control the amide backbone's cis-trans isomer profile in peptoids.[37]

Combining amino acids and peptoid monomers generate peptide-peptoid hybrids that make them adopt unique structures which are able to combine the useful properties of peptides and peptoids.

Cyclization of peptide-peptoid hybrids presents a means of ensuring conformational rigidity in these peptidomimetics. This rigidity helps biomolecules have good binding affinities and good selectivity to their biological targets.

As with cyclization of many organic molecules and peptides, cyclization of linear peptoids and peptide-peptoid hybrids is often problematic due to the formation of unwanted side products like polymers, dimers and cyclic dimers due to competing intermolecular reactions.[38] Also, common methods for cyclizing peptoids are not easily amenable for certain functional groups such as propargyl groups.[38] This prompted us to apply CyClick strategy mentioned earlier in this thesis for exclusive intramolecular cyclization of linear peptide aldehydes for the cyclization for the cyclization of linear peptide-peptoid hybrids (Figure 19).

Herein, we report the preparation of a novel series of Cyclic peptide-peptoid scaffolds with various ring sizes.

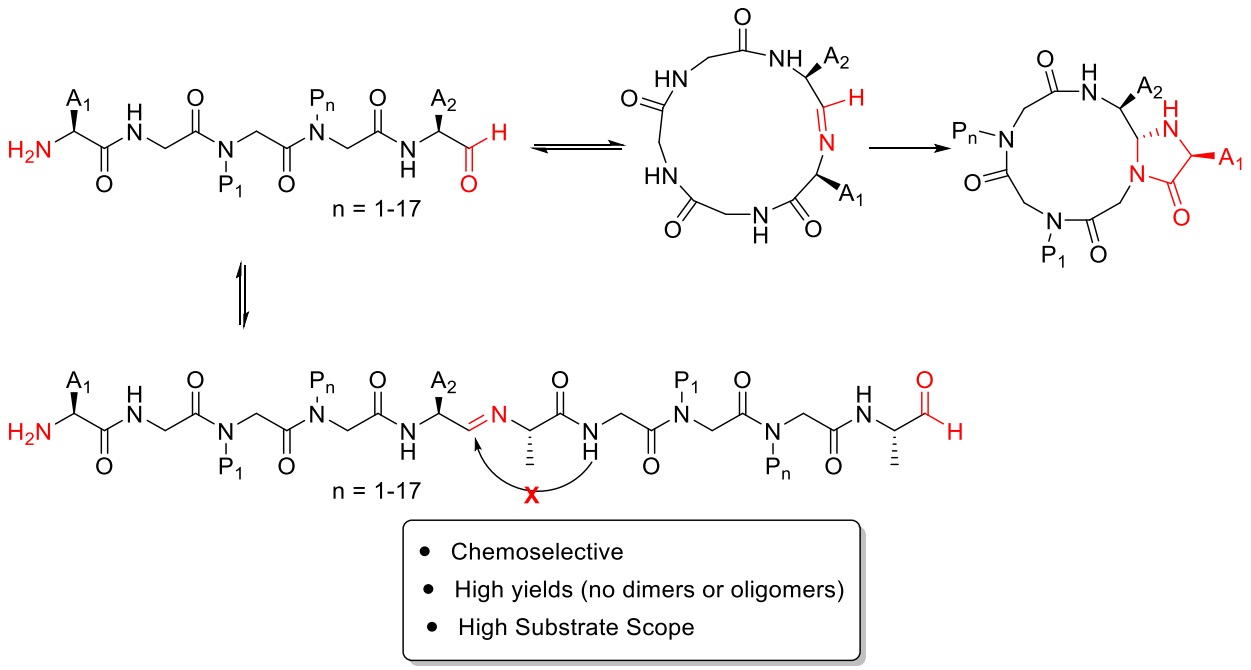

Figure 19. Application of CyClick Chemistry for cyclization of cyclic peptide-peptoid hybrid.

We started our studies with the synthesis of strained cyclic peptide-peptoid hybrid **1.11a** from linear peptide-peptoid hybrid aldehyde **1.10a** easily obtained from rink amide resin using solid phase synthesis (see SI for details). Cyclization of **1.10a** at 60 ^{o}C with 14 equivalence of DIEA generated cyclic product **1.11a** smoothly with complete conversion after 16 hours. Gratifyingly no dimer or cyclic dimer was observed due to intermolecular reactions. A linear imine intermediate formed between two peptide-peptoid hybrid molecules is not stable enough to activate the amide bond and lead to the formation of the 4-imidazolidinone moiety. The reaction proceeded smoothly without the requirement of harsh reaction conditions like coupling agents and transition metal catalysts. The formation of cyclic peptide-peptoid hybrid **1.11a** was characterized by high-performance liquid chromatography (HPLC) and high-resolution mass spectrometry (HRMS).

We proceeded to applying this chemistry for the synthesis of other strained 12-membered macrocycles of peptide-peptoid hybrid with various peptoid monomer side chains. Gratifyingly, all the linear peptide-peptoid aldehydes **1.10b-1.10d** cyclized smoothly with complete conversion to form the 12-membered ring cyclic products **1.11b-1.11d** (Figure 20).

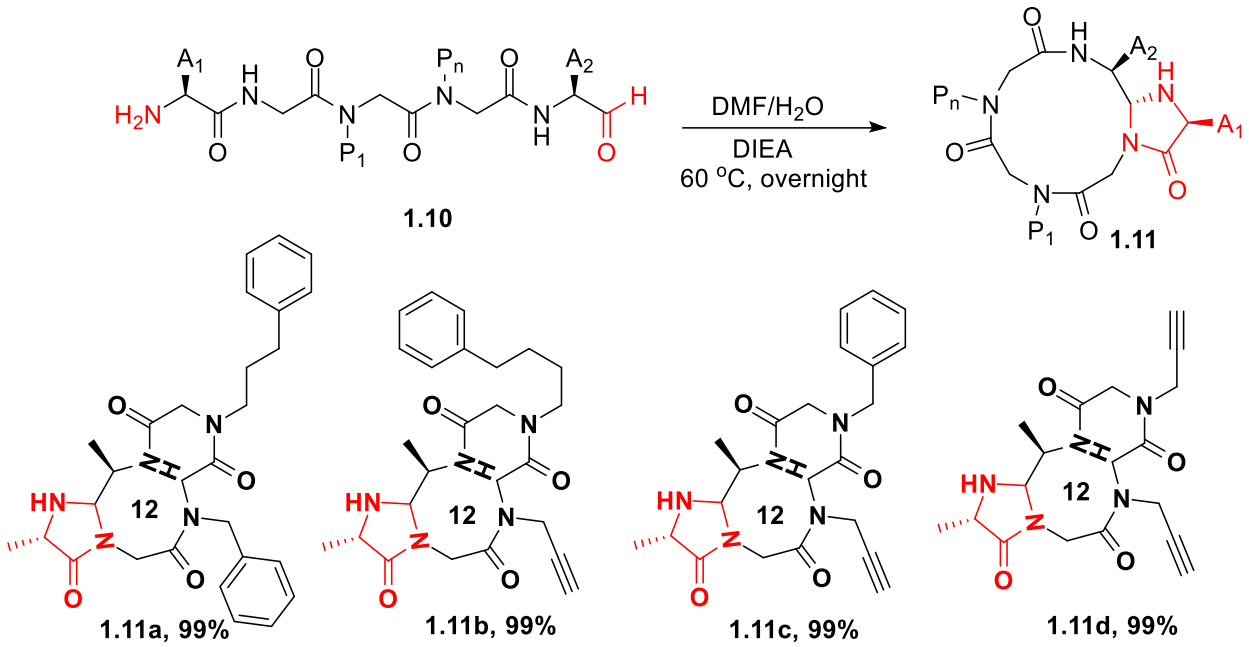

Figure 20: Synthesis of Cyclic tetrapeptide-peptoid Hybrid.

To further demonstrate the versatility of this chemistry, we cyclized of various other linear peptide-peptoid hybrids with variety of side chains and ring sizes. We generated cyclic peptide-peptoid containing 15-membered ring **1.11e-1.11f** from their linear counterparts **1.10e-1.10f**. Contrary to methods reported in literature stating that cyclization of linear peptide-peptoid hybrid containing multiple reactive groups such as allyl or propargyl groups is unamenable,[38] we show clean cyclization of peptide-peptiod hybrids containing numerous propargyl groups with the formation of 21-membered ring **1.11g-1.11j** from linear peptide-peptoid **1.10g-1.10j,** and 24-membered ring **1.11k** from linear peptide-peptoid **1.10k (**Figure 21**).**

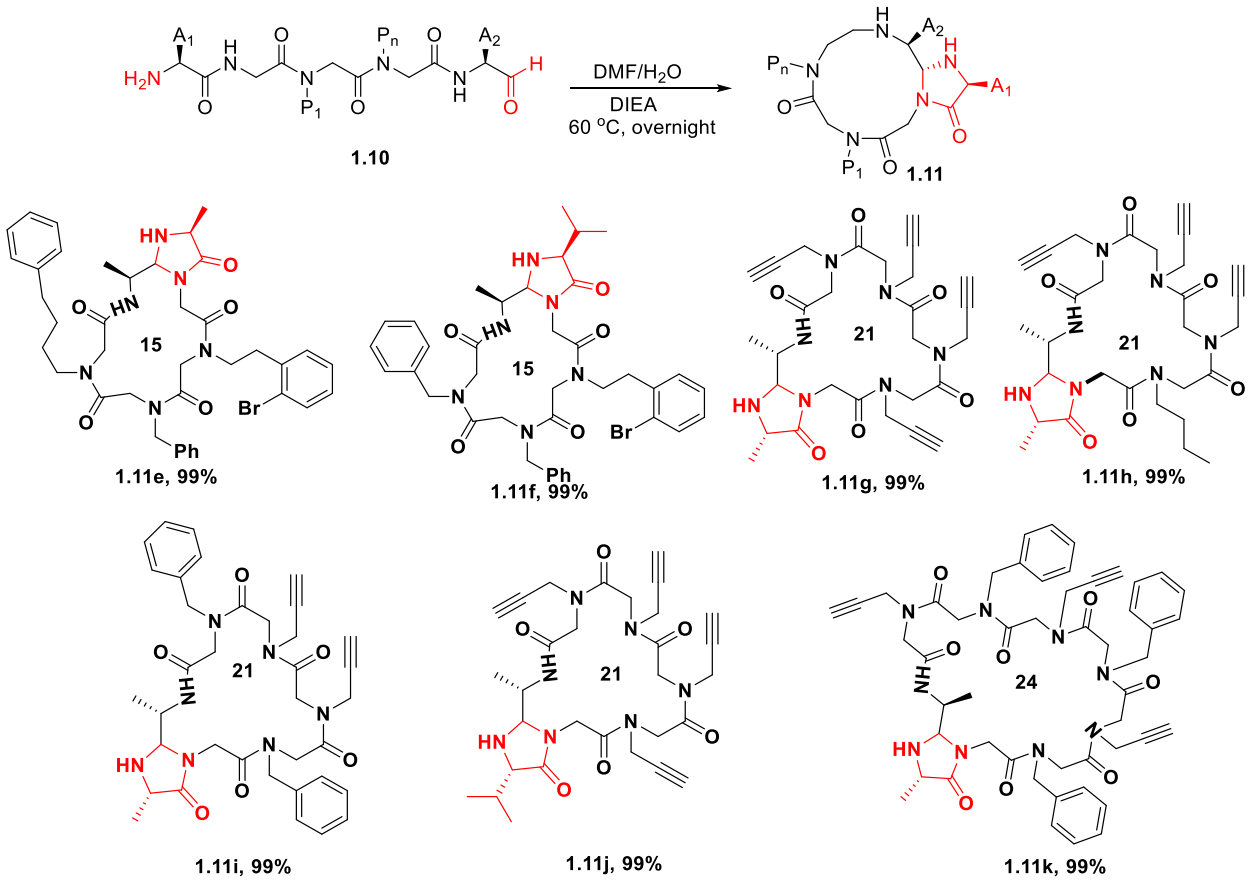

Figure 21: High HPLC conversions of cyclic peptide-peptoid (15- to 24-membered) with various R-groups and chain length.

Most interestingly, we were able to synthesize cyclic peptide-peptoid hybrid with very large ring sizes of 45-membered ring **1.11l** and 60-membered ring **1.11m** from linear peptide-peptoid **1.10l** and **1.10m** respectively (Figure 22). These large macrocycles are hard to synthesize due to the high intermolecular distance between the reactive moieties of the linear peptide-peptoid.

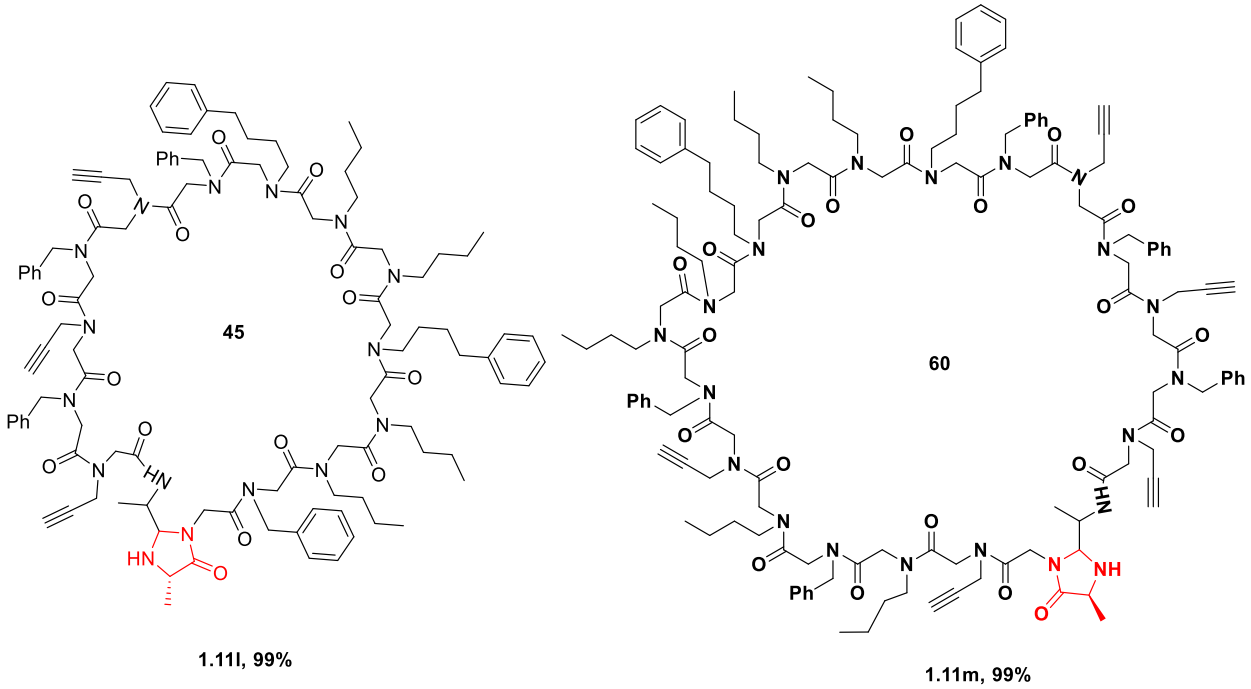

Figure 22: Cyclization of difficult sequences (45- to 60-membered macrocycles) with high conversions to the Cyclic peptide-peptoid hybrids.

To show the capability of CyClick Chemistry cyclic peptoids (containing all poly N-substituted glycines), we cyclized the linear peptoids **1.10n-1.10o** to generate cyclic peptides **1.11n-1.11o** **(**Figure 23**).**

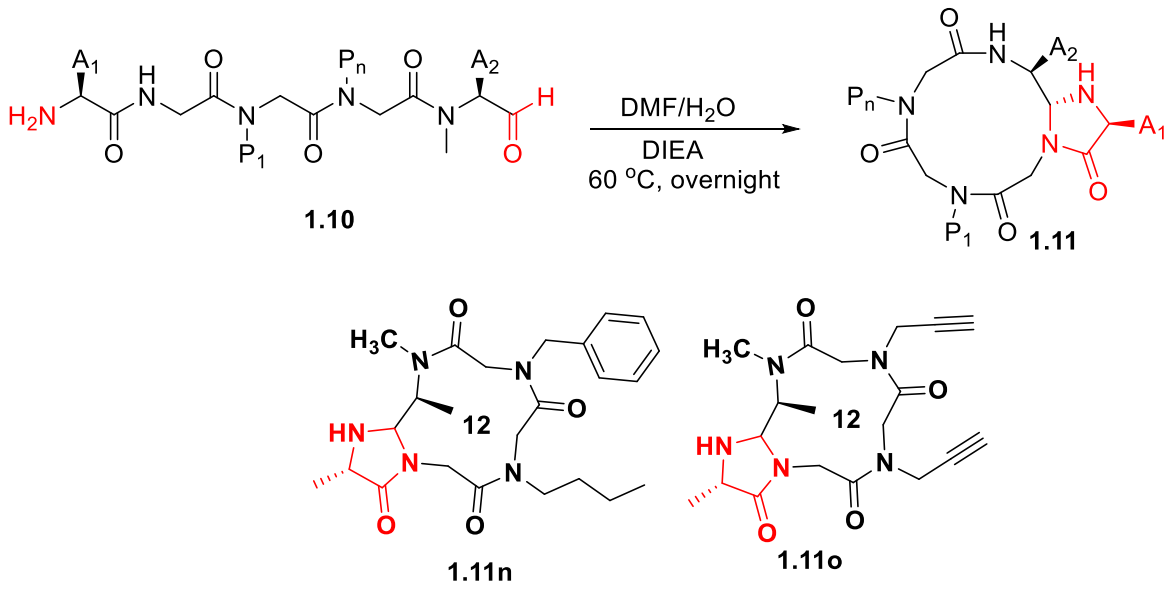

Figure 23: Extension of CyClick chemistry for cyclizing peptiods with high conversions.

Our attempt to generate cyclic peptide-peptoid hybrid **1.11p** with a ring size of 9 at 60 ^{o}C was unsuccessful from its linear counterpart **1.10p**. This has also been corroborated by many other publications unsuccessful in their attempts to make 9-membered ring cyclic molecules. At a very high temperature of 110 ^{o}C however, we observed the formation of 18-membered cyclic dimer **1.12p**. These are also interesting molecules which can be used for binding biological targets. To highlight the adaptability of this method to generate various bicyclic peptide-peptoid hybrids, we cyclized other linear tetra peptide-peptoid hybrids **1.10q-1.10r** and generated bicyclic hybrids **1.12q-1.12r (**Figure 24).

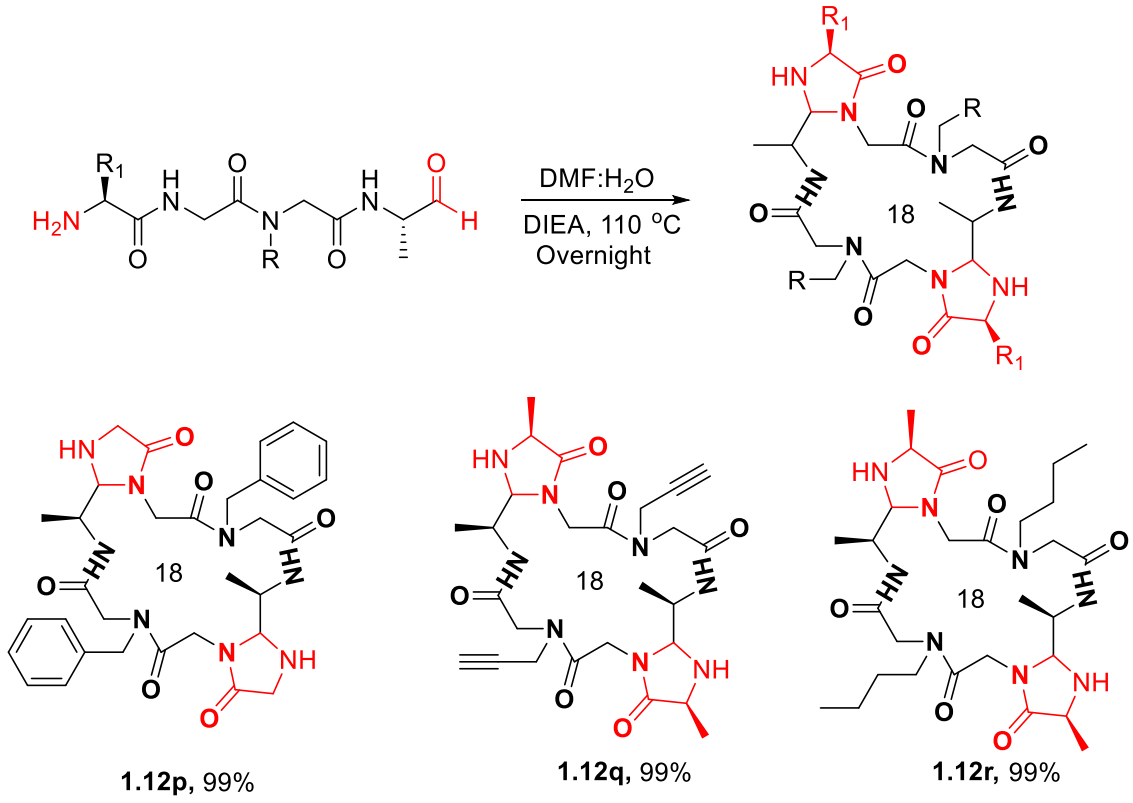

Figure 24. Synthesis of 18-membered ring bicyclic peptide-peptoid hybrid.

As mentioned earlier in this manuscript, cyclization of cyclic peptoids and molecules at high concentrations often lead to the formation of dimers. To determine the effectiveness of our macrocyclization strategy, we compared our method of cyclization of linear peptide-peptoid hybrid with lactamization method – a very common method for cyclizing peptoids. At a high concentration of 5mM cyclization via lactamization generated 75% conversion to undesired cyclic dimers. At the same concentration, we didn't observe any dimerization or cyclodimerization for CyClick chemistry. The demonstrate an improvement over previous method for cyclizing peptoids.

Chapter 2: Chemical Tools for Selective Modification and Diversification of Secondary Amides

2.1 Introduction

Some of the most prevalent functionalities in organic molecules are carbonyl groups, and techniques that allow for their selective functionalization while also facilitating an increase in molecular complexity are in constant demand.[39, 40] Historically, amides have been thought to be relatively non-reactive in comparison to acyl halides, anhydrides, ketones, and esters.[39] Increased stability of the electrophilic carbonyl carbon is caused by a unique delocalization of the lone pair of electrons at nitrogen on the π^* system,[39-41] also known as amidic resonance (Figure 1).[40, 41] The notion is that amides are substantially less useful functional handles than their ester and acyl halide counterparts is as a result of this difference in reactivity.[39] At various pH levels, Hansen *et al.* conducted rate investigations on the hydrolysis of amide bonds.[42] The rate constant showed that

the half-life of the amide bonds is 267 years and is similar to the value determined by Radzicka and Wolfenden.[43] This study provides further evidence for the high stability seen in amides.

Amides are however, one of the most frequently found moieties in functional molecules, including peptides, pharmaceuticals, bioactive natural products, and polymer materials.[40] Proteins and other biomolecules adopt three-dimensional (3D) structures due to the resonance of amide bonds, which creates a planar structure and prevents free rotation around the CO-N bond.[40] Biomolecules' 3D architectures are in charge of many crucial biological processes.[40]

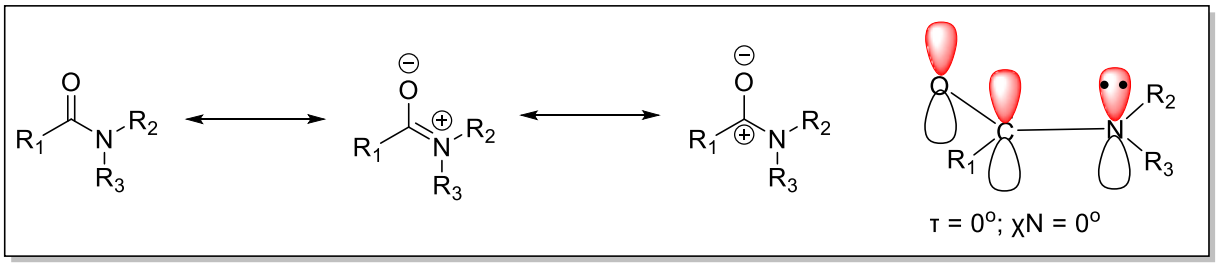

Figure 1: Typical Amide Bond Resonance[41]

2.1.1 Activation of Amide Bonds

As a valuable method for late-stage drug modification, highly selective amide activation can help with drug development and other areas of medicinal chemistry. As a result, since the 19th century, synthetic chemists have put a great deal of work into the selective activation of amides. The tendency for these processes to be highly selective towards carboxamide functionality, even when other, conventionally more reactive carbonyl moieties (such esters or ketones) are present, is particularly noteworthy.[41]

The employment of enzymes,[40] metal complexes,[44, 45, 46, 47-49] and non-metal-based techniques[50, 51] are among the techniques documented in the literature for selective amide bond reactions. It is common knowledge that planarity of amide causes the great majority of amides to have resonating properties.[52] According to Pauling's prediction from 1931, typical amides have planar bonds that

are around 40% partial double bonds ($n_N \rightarrow \pi^*_{C=O}$ conjugation; amidic resonance of 15−20 kcal/mol in planar amides) (Figure 1).[52, 53] However, deviations from planarity in the amide bond have a significant impact on each of the amides' key chemical characteristics which include[41, 52, 54, 55, 56] (i) Planarity of the amide bond's constituent atoms,[55] (ii) geometric alterations, including lengthening of the C=O bond and shortening of the N-C(O) bond geometric changes,[55] (iii) Nitrogen replaces oxygen as the thermodynamic protonation site,[56, 57] (iv) higher tendency for hydrolysis and nucleophilic acyl substitution, (v) cleavage of σ N−C bonds, and more recently, (vi) oxidative addition of the N−C(O) bond to transition metals.[41]

Luke postulated in 1938 that the characteristics of these twisted amides would be significantly affected by the limitation of the amide bond in a stiff bicyclic structure.[58] Investigations conducted by Woodward and Robinson in the 1940s on the structural prediction of β-lactam antibiotics provided yet another earliest illustration of how an amide bond strain may generate the primary driving force behind amides' reactivity.[58] In the years that followed, numerous research teams published extensive investigations on the structure and properties of nonplanar amides contained in stiff bridging scaffolds. One of the most elegant of these was the Stoltz group's 2006[59] creation of the now-classic 2-quinuclidonium tetrafluoroborate, while Kirby[60] and Greenberg's research on 1-aza-2-adamantanone and 1-azabicyclo[3.3.1]nonan2-one[57], respectively (Figure 2), has also greatly improved our understanding of the characteristics of geometrically nonplanar amide bonds.

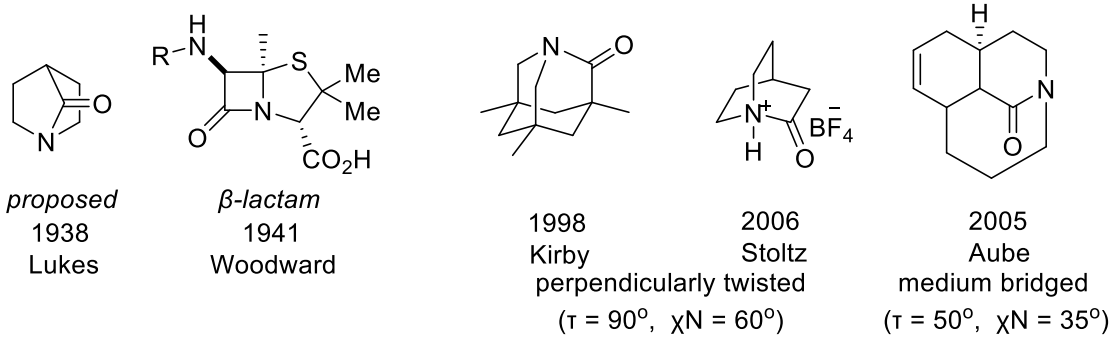

Figure 2: Evolution of classic twisted amides[58]

In addition to the classic twisted amide first known, many twisted amides have now recently been developed.[61-63] A number of highly desirable N-C amide bond cross-coupling and nucleophilic reactions with major synthetic significance have been made possible in the last 10 years thanks to the advancement of amide bond twist (distortion) into the general organic chemistry mainstream.[58, 61] These novel amides have acyclic non-planar amide bonds that can be systematically involved in potent reactions like nucleophilic additions and cross-coupling manifolds, as opposed to conformationally locked bridged lactams described in the previous paragraph.[41] As a preferred functional group in organic synthesis, the amide bond is already characterized by high stability, abundance, simplicity of synthesis, low cost, and absence of toxicity. Amides are among the most often used motifs in functional materials, agrochemicals, and medicines.[61, 64] A rationally engineered, chemo-selective reaction of ubiquitous amides by the strain-driven N-C bond cleavage is likely to occupy a central place in the organic chemistry toolkit given the prevalence of the amide bond in almost all subfields of chemistry.[52]

2.1.2 Nomenclatures used for Determination of Twisted Amide Reactivity:

Before proceeding to discussing the recent approaches for diversifying amide bonds, it is important to explain some specific terminologies employed in twisted amide chemistry. “As a logical consequence of the amide bond geometric changes, three types of non-planar amides can be distinguished: A) amides featuring perpendicularly twisted C(O)-N amide bonds and non-pyramidalized trigonal N atoms; B) amides featuring pyramidalized N atoms and planar C(O)-N bonds; C) amides featuring a combination of twisted C(O)-N bonds and pyramidalized N atoms. Hence, amides A), B), and C) are identified as non-planar amides. Amides A) and C) are referred

to as twisted amides, while amides B) as pyramidalized amides. All of these amides feature destabilized amide bonds."[58]

It is important to note that the phrase "non-planar amide" refers to an amide bond that has been geometrically destabilized either by i) steric distortion (such as with traditional bridging lactams), ii) electronic distortion, or iii) combination steric and electronic reasons (e.g., classic acyclic twisted amides). It makes no difference whether the distortion arises as a result of steric or electronic factors from the perspective of weakening the amide bond. To clearly pinpoint how steric substitution and electronic delocalization affect amide bond twisting, further study is needed.[61] The Yamada classification's three main categories of non-planar amides are summarized in Figure 3.

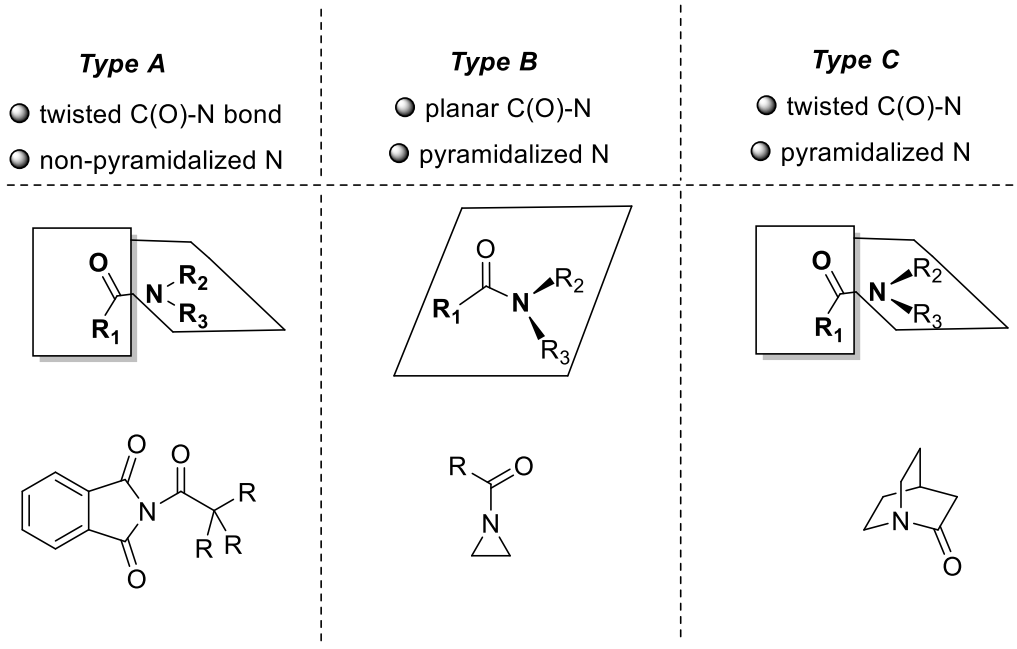

Figure 3: Yamada's classification of non-planar amides[58]

2.1.3 Recent Advances in Amide bond Distortion and Diversification

Moderately non-planar amides can undergo selective amide bond activation, as was previously mentioned in this chapter. The groundbreaking research on twisted amides showed how amidic resonance might be interrupted into amino-ketone-like reactivity using amide bond distortion. Three distinct, nearly simultaneous articles on the N-C cross-coupling were released in 2015.[44, 65, 66] It was immediately apparent that finding readily usable, acyclic twisted amides was essential for the amide bond activation hypothesis to be universally practical.[58] Fortunately, publications in the literature offer several examples of how moderate amide distortion (destabilization) can occur in a variety of typical acyclic amides.[61] I'll discuss some of the most popular twisted amides that have recently received a lot of attention.

2.1.3.1 N-Glutarimide Amides: Structure, Energetics and Reactions

The most reactive acyclic amides in a few specific N-C activation processes have been shown to be N-glutarimide amides. Computational and X-ray diffraction techniques have been used to investigate the structures of N-glutarimide and related amides.[67]

N-glutarimide contain highly distorted amide bonds (N-benzoylglutarimide: τ=91.48°, χ_N=6.68°, χ_C=0.88°, N-C=1.474 Å, C=O=1.200 Å. It is unexpected for simple acyclic amides like N-glutarimide to have such a big twist. The most twisted amide bond found in an acyclic amide to date is present in the N-glutarimide amide. The perpendicular twist seen in N-glutarimide is independent of the 1° and 2° substitution at the α-carbon atom of alkyl N-glutarimide. N-Glutarimide amide rotational profiles have been identified.[67] With a rotational barrier of 13.7 kcalmol^{-1} and dramatically inverted rotational profiles of the amide bond, N-glutarimide amides

show a predilection for the twisted conformation.[67, 68] This can be contrasted with the 19.5 kcal/mol rotational barrier of planar N,N-dimethylacetamide (Figure 4).

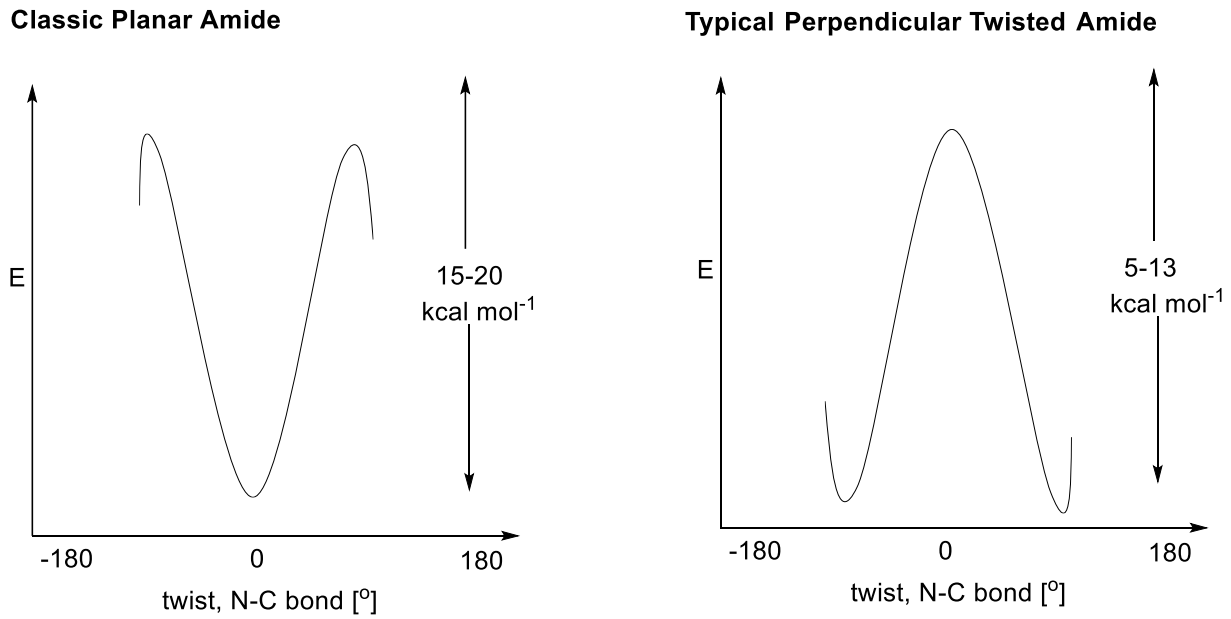

Figure 4: Rotational Energy Profile of the Most Twisted Amide (N-Acyl glutarimide in comparison to a Typical Planar Amide.[58]

Numerous new N-C reactions have been found as a result of the potent distortion of N-glutarimide amides. The following reaction manifolds have been successfully employed with N-glutarimide: i) nucleophilic addition reactions ii) acyl cross-coupling; iii) Decarbonylative cross-coupling reaction (Figure 5).[69] In all reported examples, N-glutarimides underwent N-C activation under milder conditions than other amide substrates under given conditions.[69]

The first Suzuki-Miyaura cross-coupling of boronic acids and N-glutarimide amide was reported in 2015.[66] The reaction took place under ambient circumstances and had a wide substrate range. The first Negishi acyl-aryl cross-coupling of N-glutarimide amides was reported by Szostak in 2016.[70] It has also been demonstrated that N-glutarimide amide is a highly efficient reagent for decarbonylative cross-coupling through N-C bond activation. In order to produce olefins and biaryl compounds, respectively, Szostak published the first decarbonylative cross-coupling in 2015 and 2016 using the Heck reaction[71] and the decarbonylative Suzuki cross coupling[68] of N-glutarimide amides respectively. Since then, up to 20 different articles on utilizing N-acyl glutarimide to create novel functional groups have been published (See Figure 5 for some popular reactions with N-acyl glutarimide)[69].

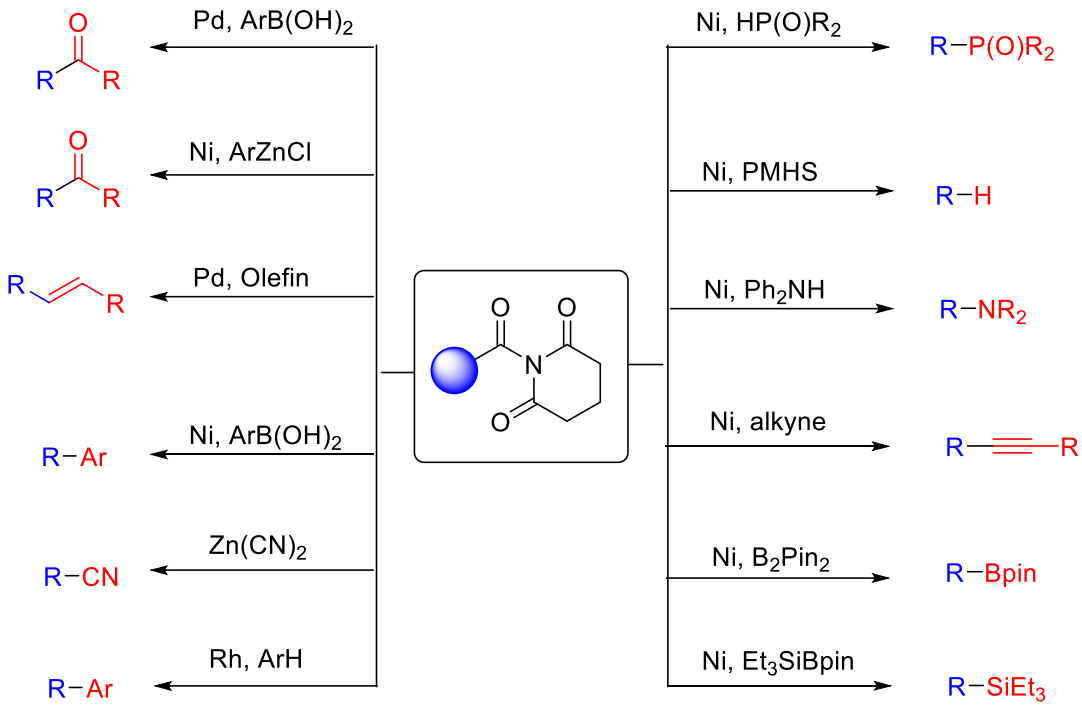

Figure 5: Reactions of N-Acyl glutarimide[69]

2.1.3.2 N-Acyl-tert-Butyl-Carbamates (Boc) and N-Acyl-Tosylamides (Ts)

A significant class of amides that readily participate in amide bond N-C cross-coupling has evolved, including N-acyl-tert-butyl-carbamates (Boc) and N-acyl-tosylamides (Ts). In N-acyl-tert-butyl-carbamates (Boc) and N-acyl-tosylamides (Ts), the amide bond distortion has been quantitatively assessed. These amides contain non-planar geometry. The most reactive aromatic N-Boc and N-Ts amides in N-C cross-coupling have amide bonds that are about one-third of their maximum distortion.[44, 65]

N-Acyl-tert-butyl-carbamates (Boc) and N-acyl-tosylamides (Ts) have emerged as the major class of amides that readily participate in amide bond N-C cross-coupling. The amide bond distortion in N-acyl-tert-butyl-carbamates (Boc) and N-acyl-tosylamides (Ts)[72] has been quantitatively

evaluated. These amides contain non-planar geometry. Aromatic N-Boc and N-Ts amides that demonstrate the highest reactivity in N-C cross-coupling feature amide bonds approaching one-third maximum distortion (Boc/Me: τ= 32.068°; χ_N=17.368°; Ts/Ph: τ=30.398°; χ_N=22.288°).[72] The distortion complies with the steric requirements of the N-substituent, however there were no strong connections with the -carbon substituent. Rotational profile investigations provide yet another cue to their high reactivity. There is free rotation around the N-C(O) axis of the synthetically significant N-Boc and N-Ts amides. It was found that the rotational barrier was 4.3 kcalmol-1 (N-Boc/Me) and 7.0 kcalmol-1 (N-Ts/Ph) for N-Boc and N-Ts amides respectively.[73] Evidently, the electronic activation and rotatable N-C bonds help to explain the rapid rate of oxidative insertion seen in experimental data.

In their pioneering research on the Ni-catalyzed esterification of amides from 2015, Garg and colleagues reported the first cross-coupling of N-Boc/alkyl and N-Ts/alkyl amides.[44] Additionally, the Zou group published the first N-Ts/Ph amide Suzuki cross-coupling with Pd as catalyst in 2015.[65] It's interesting to note that N-Boc amides were also tested, although a lower coupling yield was found. The first Ni-catalyzed Suzuki-cross-coupling of N-Boc/alkyl amides was created by the Garg group the same year[44]. Electron-withdrawing and donating groups are allowed in amides and boronate esters.[65] Aryl-alkyl Negishi cross-coupling reactions were carried out using N-Boc/alkyl amides and N-Ts/alkyl amides.[74]

Slow transmetallation and breakdown via β-hydride elimination is an important obstacle in the cross-coupling of alkyl nucleophiles by transition metals.[75] It's interesting that the authors discovered that N-Ts/alkyl amides produced the best outcomes, but that the amide electronics had a large impact as well.[76] As a result, amides containing arenes with low electron density conducted cross-coupling in higher yields utilizing N-Boc/alkyl substituents, demonstrating once again how

carefully adjusting the bonding characteristics of an amide can frequently enhance the yield of an N-C cross-coupling reaction.[76] Along with amidation and other reactions, the Garg group also documented up to 10 additional reactions involving N-Boc/alkyl and N-Ts/alkyl amides.[47, 48, 77]

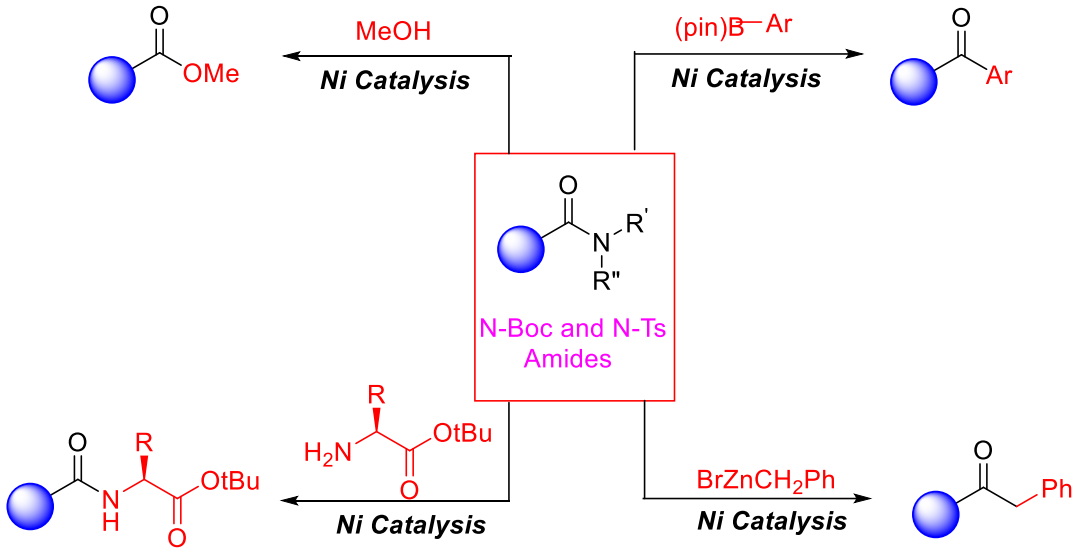

Figure 6: Reactions of N-Boc and N-Ts Amides. R' = Boc/Tosyl; R" = Aryl/Acyl

2.2 Limitations of the Current Approaches for Amide Bond Distortion and Diversification

Even though the current approaches for amide bond activation offer excellent chemo selectivity in the presence other functional groups and are effective for many different nucleophilic and impressive cross coupling reactions, many of the well-established methods are unable to activate unactivated amides for further diversifications. Another major limitation of all the current approaches for twisted amide activation is their inability to selectively activate a particular amide in a sea of other amides in polyamides such as peptides, natural products, and other pharmaceuticals (Figure 7).[58]

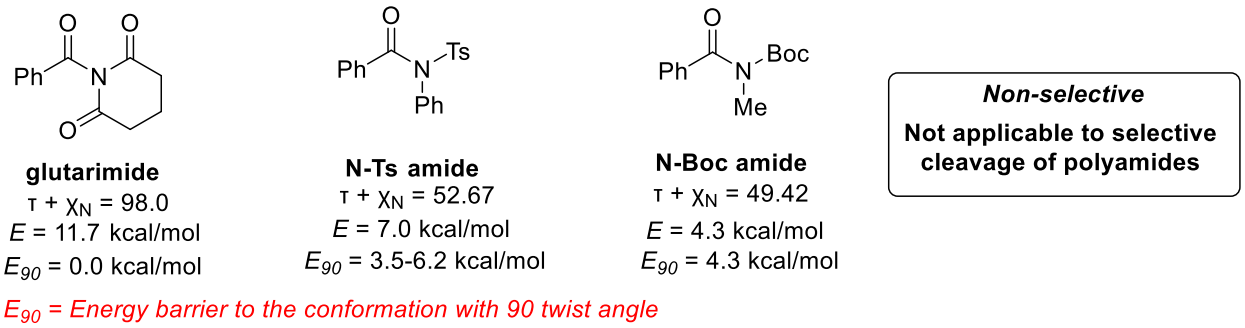

Figure 7: DFT Determination of Ground state Distortion for Conventional Twisted Amides.[58]

2.3 Metal-Free Selective Modification of Secondary Amides: Application in Late-Stage Diversification of Peptides

2.3.1 Selective Activation of Amides: Design

Here, we give evidence of the effectiveness of our two-step method for selectively transamidating and esterifying secondary amides in peptides. The process occurs at room temperature under mild reaction conditions, is metal-free, operationally straightforward, and does not require conditions that is sensitive to water or air. We hypothesized that the amide bond next to Ser/Thr or Cys could be weakened by the N-functionalization with the corresponding side chains of these residues through carbonyl or thiocarbonyl insertion based on our prior work on the synthesis of C-terminally modified peptides and acylation strategies for amide activation that are limited to C-terminal modification.[78, 79] By inserting a twist that changes the pi-pi overlap of the C-N bond, the resulting cyclic oxazolidinone or thiazolidinone molecule weakens the amide bond. The necessary transamidated and esterified products would be produced by intercepting these oxazolidinone or thiazolidinone intermediates with primary/secondary amines and alcohols. There are no known physical organic parameters previously known for the activation and modification of acylated amides. Here, we offer the rules and conditions for which we determine the reactivity of our acylated amides.

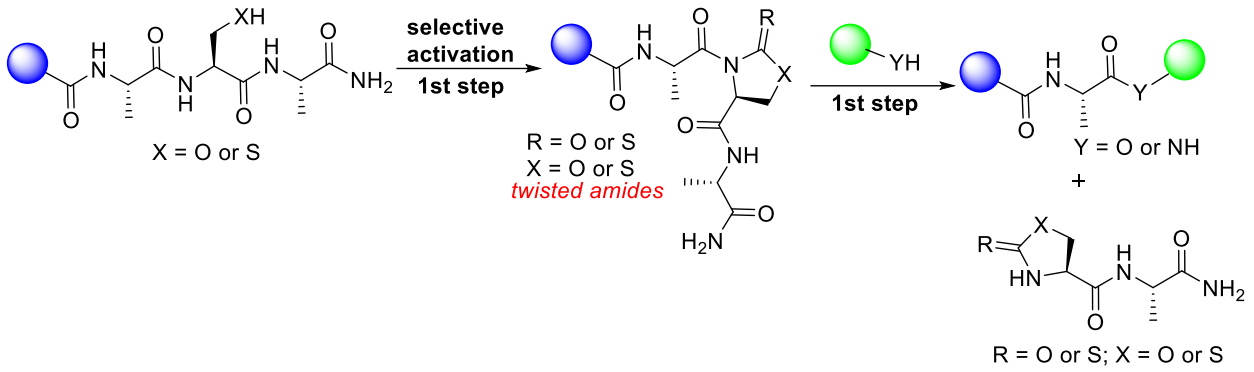

Figure 8: Our Work – Selective activation of the C-N amide in polyamides for transamidation and esterification.

We initiated our studies with the DFT calculations on carbonyl and thiocarbonyl acylated derivatives selective for cysteine and serine amides. Using the Winkler–Dunitz parameters of twist angles (τ) and pyramidization at nitrogen (χ_N), as well as N–C(O) and C=O bond lengths,[80] we calculated the amide bond distortion of B3LYP/6-311++G(d,p). We discovered that the addition of a carbonyl or thiocarbonyl group between the side chain of serine and the backbone CN amide bond resulted in the generation of the oxazolidinone **2.1a** (τ = 21.30°, χ_N = 9.1°) and oxazolidithione **2.1b** (τ = 24.0°, χ_N = 16.1°) respectively and caused the amide bond to twist in comparison to the unmodified analog E (twisted angle τ = 3.6°, χ_N = 0.5°) (Figure 9).[58] Similar to this, twisted thiazolidinone **2.1c** (τ = 28.65°, χ_N = 21.8°) and thiazolidithione **2.1d** (τ = 27.3°, χ_N = 13.7°) were produced by adding carbonyl and thiocarbonyl to cysteine. The most reactive of these twisted amides should be **2.1c**, which has the largest value of the Winkler-Dunitz parameters (τ + χ_N = 50.45°), but another aspect that affects the reactivity of twisted amides is their rotational energy profile.[58, 72] We calculated the rotational energy profile and barrier (E) of the twisted molecules **2.1a**–**2.1d** and the analog **2E** that was not modified/twisted. The computations of the rotational energy profile showed that the unmodified analog **2E**, has the lowest energy at a dihedral

angle of 3.6° and so prefers to remain in a planar state. Twisted amides **2.1a−2.1d** has the lowest energy at dihedral angles (21.3° −28.6°) and therefore clearly prefers to remain in its twisted conformation (Figure 1b). We compared the twisted amides **2.1a–2.1d** with well-known twisted amides such as N-Boc (τ = 32.06, χ_N = 17.36, E = 4.26 kcal/mol and E_{90} ~ 4.1 kcal/ mol), N-Ts amides (τ = 30.39, χ_N = 22.28, E = 7.00 kcal/mol and E_{90} ~ 3.5−6.2 kcal/mol) and N-acyl-glutarimides (τ = 91.4, χ_N = 6.6, E = 11.7 kcal/mol and E_{90} = 0 kcal/mol) in terms of twist angle and rotational energy barrier. Based on these calculations and results from previous twisted amides, we hypothesized that twisted amides **2.1b** and **2.1d** with lower E_{90} ~ 6 kcal/mol will be more reactive as compared to **2.1a** and **2.1c** with higher E_{90} (~9.5 kcal/mol).

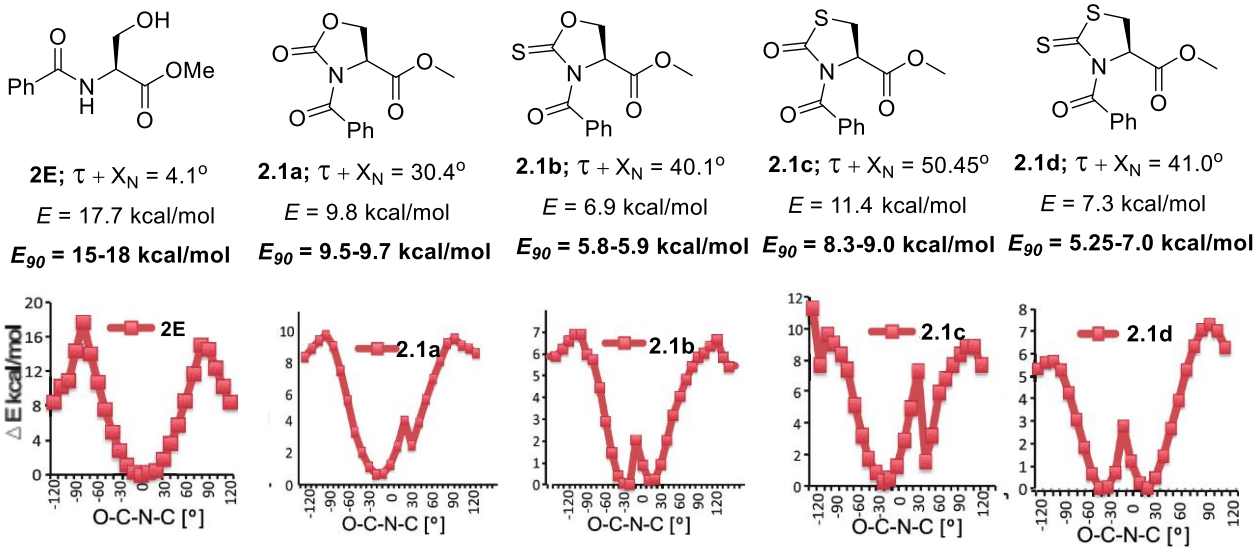

Figure 9: DFT Determination of Ground State Distortion and Rotational Energy of Amides **1a-1d** and **E.**

2.3.2 Key Experiments and Reaction Discovery for Transamidation

"To correlate twisted amide reactivity with the rotational energy profile, we carried out transamidation reactions on small twisted molecules **2.1a−2.1d** generated by incorporation of carbonyl or thiocarbonyl groups into the serine and cysteine methyl esters by using carbonyl donor (N,N′-disuccinimidyl carbonate DSC (1.3 equiv) or thiocarbonyl donor (1,1′-thiocarbonyldiimidazole (thio-CDI) (1.2 equiv) and Et_3N (1.1 equiv) in THF for 16h at room temperature.[78, 79] Optimization studies toward transamidation were carried out with benzylamine on thiazolidithione **2.1d** (lowest barrier E_{90} ~ 5.2 kcal/mol) using varying bases and solvents. We found that under mild reaction conditions **2.1d** (1 equiv), benzylamine (1.5 equiv), triethylamine (1.5 equiv) in DCM at room temperature for 2 h) the transamidation product **2.2a** was obtained in 96% yield. **2.1b** also generated transamidated product in high yield (94%). As predicted, twisted amides **2.1a** and **2.1c** with a higher energy barrier generated transamidation products with moderate yields (69−71%, Figure 10, Supplementary Figure 3). As expected, the attempted transamidation of unmodified analog **2.2E** with benzylamine failed, thus highlighting the unique ability of this approach to activate secondary amide bonds (Supplementary Figure 4).

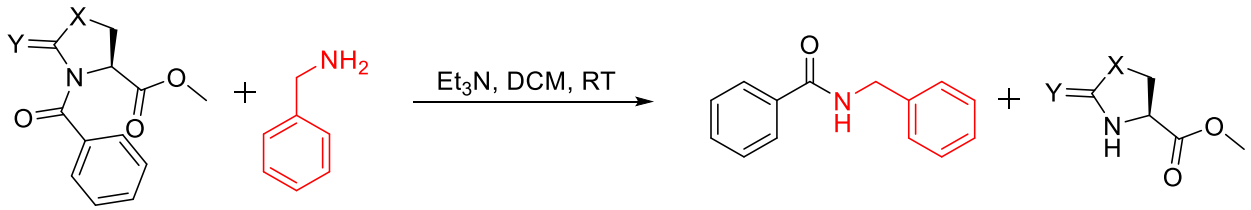

2.1a-2.1d **2.2a**

Probe	X	Y	Time (h)	Yield (%)
1a	O	O	16	71
1b	S	O	12	69
1c	O	S	2	94
1d	S	S	2	96

Figure 10: Metal-free transamidation reaction on 1a−1d (0.07 mm), amine (1.5 equiv), triethylamine (1.5 equiv), and DCM (5 mL) at RT.

2.3.3 Scope of the Transamidation

Examination of the scope of twisted amides **2.1b** and **2.1d** revealed that remarkably broad ranges of primary amines such as propargyl amine, dimethoxyethylamine, including sterically hindered isopropylamine and linear octylamine are suitable for this transamidation protocol and generated corresponding products **2.2b−2.2e** with high yields in 2 h under optimized reaction conditions (70−89%, Figure 11). Transamidation of **2.1b** and **2.1d** proceeded smoothly for the synthesis of tertiary amides **2.2f**−**2.2i** by the use of secondary amines such as N-Boc protected piperazine, piperidine, morpholine, pyrrolidine with yields 60−79% at room temperature in 2 h (Figure 11). The reaction generated transamidation product **2.2j** with 2- bromoethylamine in moderate yields (50%) without any functionalization of the bromo group (Figure 11). Finally, to test the scalability of this method, **2.2a** was synthesized by the reaction of **2.1d** with benzylamine on a gram scale reaction with 90% yield under the optimized reaction conditions (Supplementary Figure 5). Further, we performed the transamidation of **2.1b** and **2.1d** using a variety of chiral amino esters such as proline and phenylalanine methyl ester generated secondary amides **2.2k−2.2l** in high yields (60−70%, Figure 11).

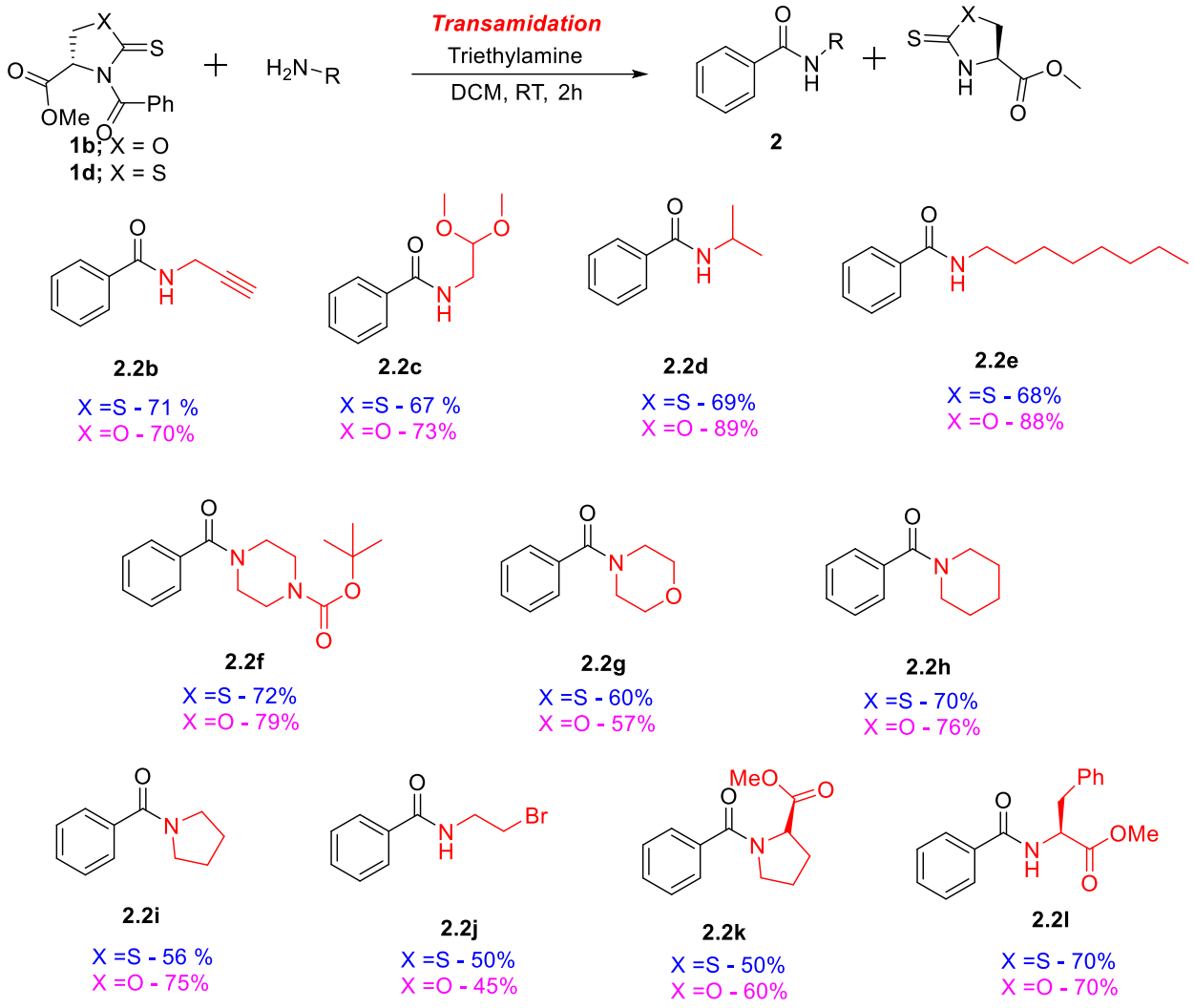

Figure 11: Scope of amine nucleophiles for transamidation of amide substrates **2.1b** and **2.1d**

2.3.4 Esterification of Amides

Next, we extended our strategy of the selective twist activation of secondary amides for esterification (Figure 12). Non-nucleophilic phenol with pKa of 10.0 was used for the optimization of esterification on twisted amides **2.1a**−**2.1d** (Supplementary Figure 6). K_3PO_4 (5 equiv.) in the presence of twisted amide **2.1b** or **2.1d**, and excess of phenol (1.5 equiv.) was found to be the optimized reaction condition for the generation of the ester product **3a** (Figure 12). Electronically diverse phenols with both electron-rich (p-bromo, p-methoxy), and electron-poor groups (m-

formyl, p-acetyl, p-trifluoromethyl, naphthyl) including sterically hindered bis-o-tolyl alcohol and benzylic alcohols such as 2-nitrobenzyl alcohol and benzyl alcohol were found to be excellent substrates and generated corresponding esters **2.3b−2.3j** in good to excellent yields with twisted amides **2.1b** and **2.1d** (58−99%, Figure 12, Supplementary Figure 7). The reaction with aliphatic alcohols such as methanol require high amounts of alcohol for the efficient modification.[79] Notably, the reaction tolerates substrates that are incompatible with metal-catalyzed and high-temperature protocols, including halides, aldehydes, ketones, highly electron-deficient arenes (e.g., p-trifluoromethyl and naphthyl); thus, this protocol would be widely applicable in the synthesis of biomolecules and pharmaceutically active compounds".

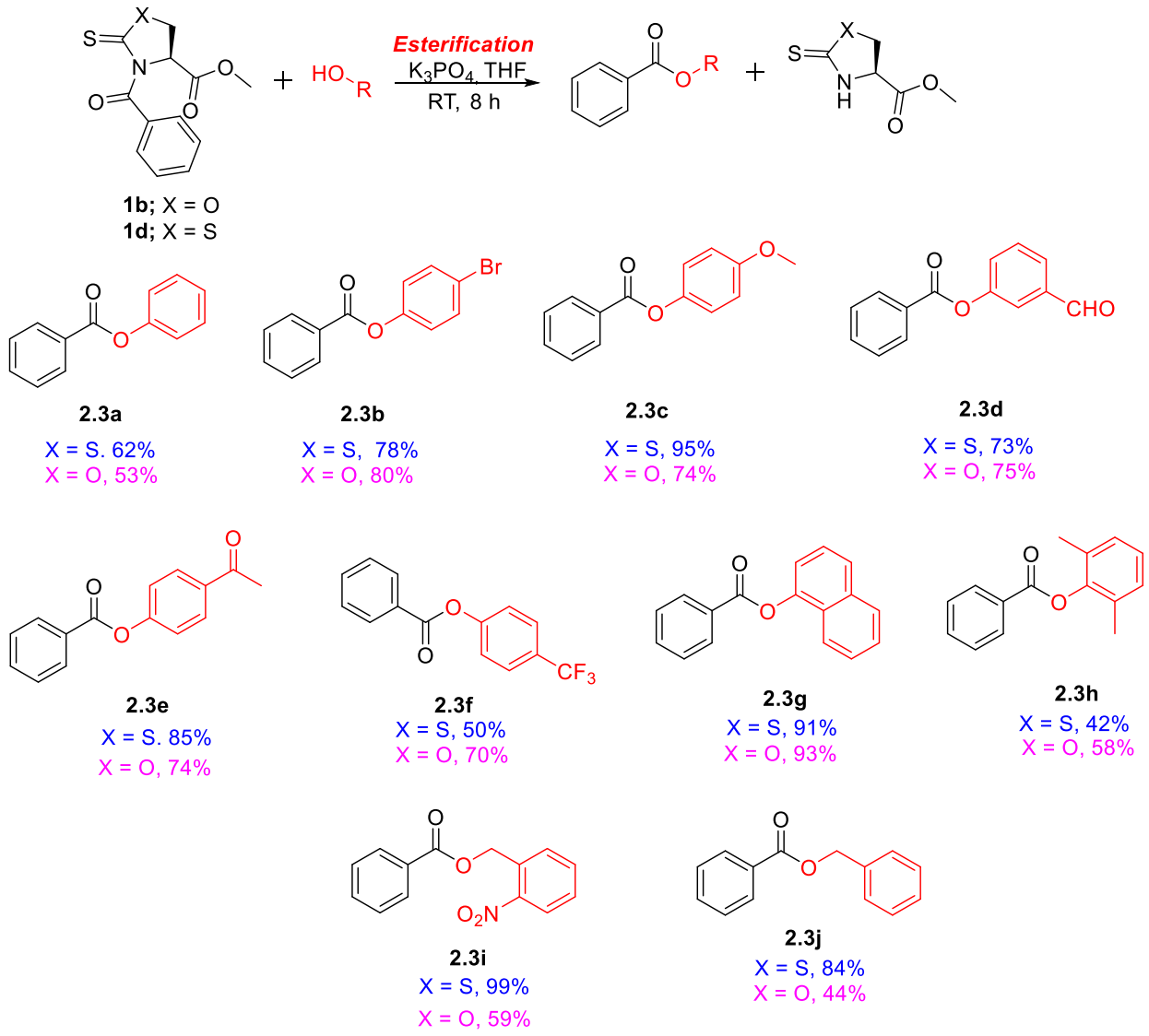

Figure 12: Scope of amine nucleophiles for transamidation of amide substrates **2.1b** and **2.1d**

2.3.5 Site-Selective Transamidation and Esterification of Peptides

The site-selective alteration of specific amides in peptides or polyamides containing related secondary and primary amides is a hallmark of this chemistry (Figure 13). We attempted selective insertions of thiocarbonyl at cysteine amide in tripeptides Boc-FCF-OMe and AcO-RFC-solid support by utilizing a variety of thiocarbonylating agents since **2.1b** and **2.1d**, according to the DFT calculations, had the lowest rotational energy barrier (See SI for details). The thiocarbonyl-

modified peptides were not produced by these processes. This could be as a result of the poor reactivity of an intermediate produced by the reaction of the side chain of serine/cysteine with thiocarbonylating reagent, which led to its quick hydrolysis/decomposition before the nucleophilic attack from the backbone amide bond. In order to create the corresponding oxazolidinone containing peptide AcO-FOxaF-NH2, we therefore site-selectively integrated carbonyl on a tripeptide AcO-FSF-NH2 by reaction with a carbonyl donor (DSC) utilizing DMAP as a base. "Exposure of twisted tripeptide **2.4** to optimized transamidation and esterification conditions with 4-phenylbutylamine, propargyl amine, and sterically hindered isopropylamine and both nucleophilic (2- nitrobenzyl alcohol) and nonnucleophilic alcohols (p-acetyl phenol) gave the corresponding secondary amides **2.5a−2.5c** (92−99%) and ester functionalized peptides **2.5d−2.5e** (45−65%) Figure 13a, Supplementary Figure 10). We did not observe any epimerization of chiral center on selective amidation on twisted tetrapeptides AcO-FA_LSF and AcO-FA_DSF under the reaction conditions (Supplementary Figure 11). In case of a nonapeptide AcO-FRWSFFSAF with two serines, double amide bond activation was observed at N-side of both serine residues to generate double twisted nonapeptide AcO-FRWOxaFFOxaAF **2.6** (Figure 13b). The treatment with 4- phenyl butylamine under optimized conditions generated two amidation products **2.7a** and **2.7b** in full conversions (Figure 13b)".

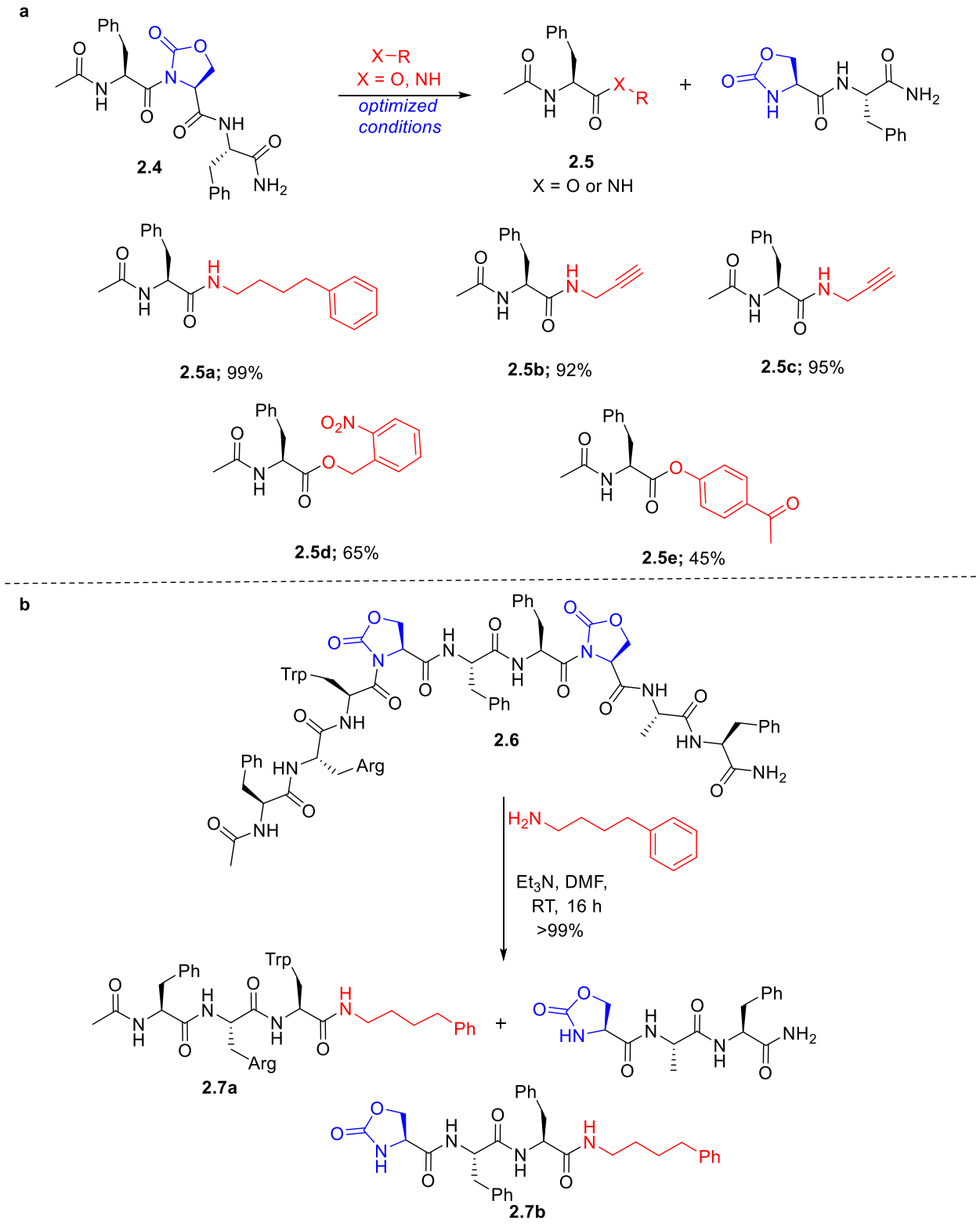

Figure 13: Selective modification of secondary amides in peptides a) 4 and b) 6 by transamidation and esterification

2.3.6 Conclusion on Selective Transamidation and Esterification of Secondary Amides

These experiments demonstrated the method's potential for adding novel functional groups to a variety of amide-containing biomolecules, synthetic compounds, and polymers. For the purpose of selective transamidation and esterification of secondary amides, we have created a mild, two-step, transition metal-free, and operationally straightforward method. By leveraging activation of Ser-, Cys-, and Thr to enable selective modification with different amines and alcohols, the methodology gets around the classic issue of selective activation of specific secondary amides in the presence of other similar amides.

The results of the transamidation and esterification experiments support our theory, which was based on DFT calculations, that the addition of the C = X bond reduces the amide double bond character and the twisted molecule with lowest energy barrier E_{90} to reach the most reactive twist conformation exhibits highest reactivity. The reaction had a wide use with amines, phenolic and benzylic alcohols, and it could be used to modify peptides in the late stages. We predict that selective amidation and esterification procedures will be of utmost importance in the fields of chemical biology, biotechnology, and material science due to the significance of numerous amide bonds in biomolecules, polymers, and materials.

2.4 Selective Conversion of Unactivated C-N Amide bond to C-C bond in the polyamide via Steric and Electronic Resonance Destabilization

Having developed a method for selective activation of unactivated amide bonds and applying it for various nucleophilic additions, we proceeded to using this strategy of resonance destabilization for the insertion of aryl ketones into organic compounds via cross-coupling reactions. In the last decade, several methods have been reported for the conversion of both primary and secondary C-N amide bonds to C-heteroatoms and C-C bonds using metal-catalyzed[44, 46, 48, 49] and metal-free

approaches (Figure 14a).[51, 58] Despite the elegance and power of these approaches for modification of C-N amide bonds, none of them are capable of selectively modifying a particular amide in polyamides. Enzymes are known to selectively hydrolyze C-N amide bonds in proteins but limited for the formation of C-C bonds. In this section, we report the first such method for the selective modification of a particular C-N amide bond to C-C bond in polyamides (Figure 14b). Most of the previous approaches activate amide bonds by either steric ground state distortion and/or electronics thus require highly twisted amides (close to the maximum twist angle ~ 90°) for the formation of C-C bond under metal-free conditions (Figure 14a).[10,17-22] To our knowledge, the direct metal-free formation of the C-C bond from less twisted amides is unknown. This is notable given that various twisted amides with much higher twist angles (twist angles = 26-65°) than those utilized in our approach (twists angles = 21.3-28.6°) do not lead to the formation of a C-C bond in the metal-free Friedel-Crafts acylation conditions.[17,20] This study develops a completely new concept of introducing both steric and electronic factors in one molecule to achieve the significant resonance destabilization of C-N amide bonds to generate C-C bonds (Figure 14b). This is the first approach where C-N amide bonds with small distortions (twist angles = 21.3-28.6°) can be successfully converted to C-C bonds under exceptionally mild, metal-free Friedel-Crafts acylation conditions (Figure 14b). Here we demonstrate both the metal-catalyzed Suzuki-Miyaura reaction and metal-free Friedel-Crafts acylation reaction for conversion of activated C-N amide bonds to C-C bonds in polyamides. In addition, we use density functional theory (DFT) calculations to predict the reactivity of the C-N amides towards C-C bond formation. We also applied the metal-free C-C bond formation approach for the selective late-stage direct modification of peptides with benzophenone fluorophore. These experimental and computational studies also lay the foundation

for further studies aimed at the strategic manipulation of selective amides in a variety of synthetic and biomolecules.

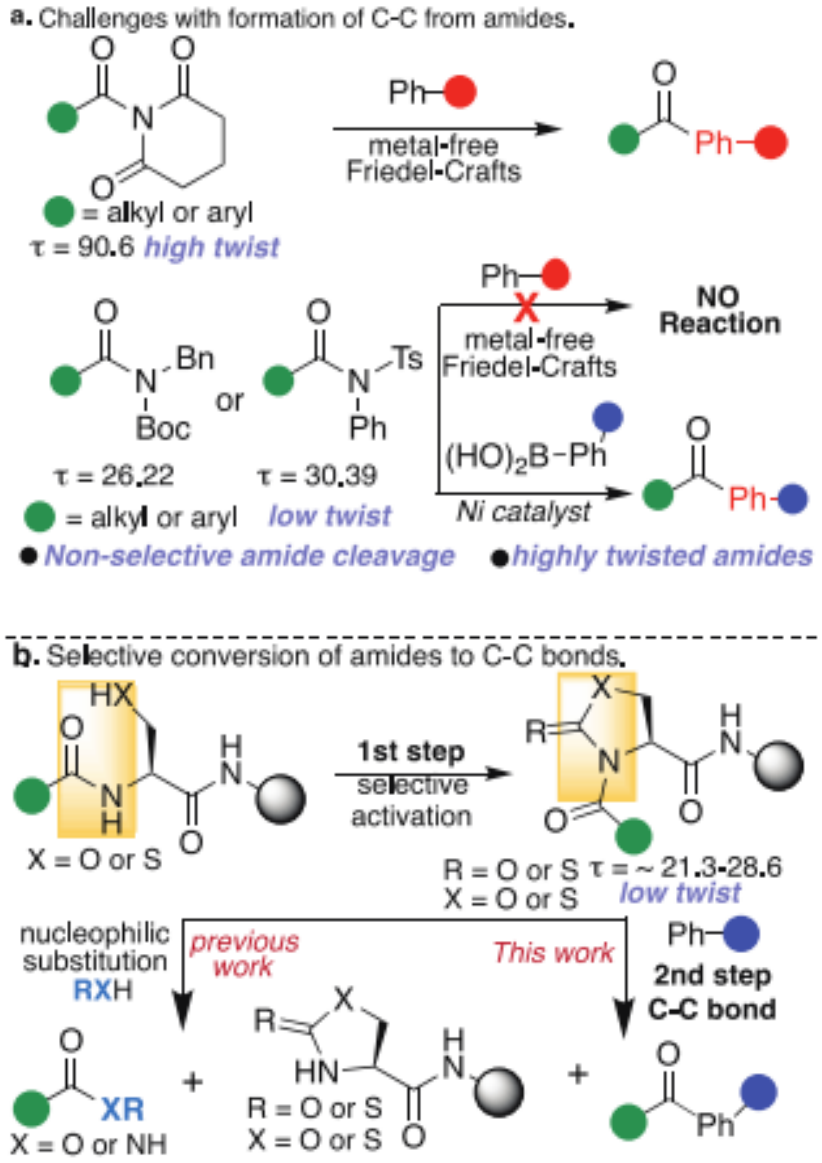

Figure 14. (a) Previous work: Activation of C−N amide bonds via metal-catalyzed and metal-free approaches, not applicable for the selective cleavage of a particular amide bond in polyamides. Requires high twist angle for metal-free C−C bond formation. (b) Our work: The selective activation of an amide in the presence of other amides; previously used for nucleophilic substitution with alcohols and amines to generate esters and amides. This work involves formation of C−C bond from activated amides to generate ketone under metal-free mild conditions.

2.4.1 Results and discussion. Discovery of site-selective activation of C-N amide bond for the formation of C-C bond.

Selective activation of amides: Design. We have previously shown via DFT calculations on these synthons **2.1a-2.1d** that the addition of carbonyl and thiocarbonyl groups leads to the resonance destabilization that weakens the C-N amide bond, greatly enhancing its reactivity and availability for further modification (Figure 15, Supplementary Figure 1). Using B3LYP/6-311++G(d,p), we determined their amide bond distortion using Winkler-Dunitz parameters: twist angles (τ), pyramidization at nitrogen (X_N) and N-C(O) and C=O bond lengths (Supplementary Figure 1).[80] We found that the addition of carbonyl or thiocarbonyl group between the side chain of serine and backbone C-N amide bond generated oxazolidinone **2.1a** (τ = 21.30, X_N = 9.1) and oxazolidithione **2.1b** (τ = 24.0, X_N = 16.1) and resulted in the twisting of the amide bond relative to the unmodified analog E (τ = 3.6, X_N = 0.5) (Figure 15, Supplementary Figure 1). Similarly, the addition of carbonyl and thiocarbonyl to cysteine generated twisted thiazolidinone 1c (τ = 28.65, X_N = 21.8) and thiazolidithione 1d (τ = 27.3, X_N = 13.7).

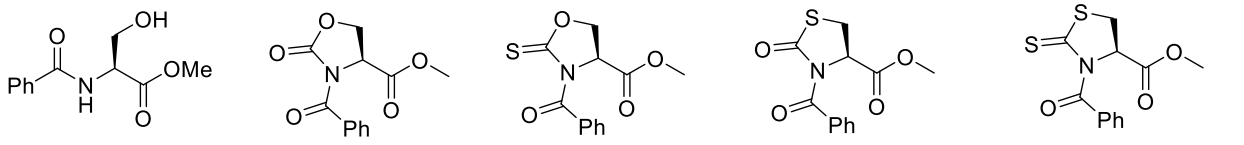

2E; τ + X_N = 4.1° | **2.1a;** τ + X_N = 30.4° | **2.1b;** τ + X_N = 40.1° | **2.1c;** τ + X_N = 50.45° | **2.1d;** τ + X_N = 41.0°

E = 17.7 kcal/mol | *E* = 9.8 kcal/mol | *E* = 6.9 kcal/mol | *E* = 11.4 kcal/mol | *E* = 7.3 kcal/mol

E_{90} = 15-18 kcal/mol | **E_{90} = 9.5-9.7 kcal/mol** | **E_{90} = 5.8-5.9 kcal/mol** | **E_{90} = 8.3-9.0 kcal/mol** | **E_{90} = 5.25-7.0 kcal/mol**

Figure 15: DFT calculations to determine the ground state distortion and activation of modified amides by insertion of carbonyl and thiocarbonyl group in C-N amide backbone and side chain of serine and cysteine

2.4.3 Metal-catalyzed C-C bond formation from C-N amide bonds.

2.4.3.1 Key Experiments and Reaction Optimization:

To correlate twist angle with amide reactivity, we initiated our studies by carrying out Suzuki-Miyaura reactions on these activated amides **2.1a-2.1d** (for synthesis, see SI) using p-methoxy phenylboronic acid **2.9a** and Pd-PEPPSI catalyst under different conditions (different bases, solvents and temperature) with several of our key results involving PEPPSI, K_2CO_3 and THF (Figure 16). Pd-PEPPSI was selected for the Suzuki-Miyaura reaction due to the ease of synthesis, broad accessibility, low price, and versatility of this class of Pd-NHC precatalysts.[81] Lower temperature only led to poor yields of the ketone product **2.10a** (0-20% Figure 16, entries 5-6). Although the cross-coupling of **2.1d** with boronic acid **2.9a** gave higher yields of the desired ketone **2.10a** (66%) under refluxing conditions, the formation of dehydroalanine was observed using toluene as a solvent (Figure 16, compare entries 4 and 7) and led us to utilize THF solvent for further studies. We also evaluated the reaction with another twisted amide **2.1b** under the optimized conditions leading to the formation of the ketone product **2.10a** in a good yield (70%, Figure 16, entry 2). Twisted amides **2.1a** and **2.1c**, were unstable and decomposed under the reaction conditions (Figure 16, entries 1 and 3). We were surprised that twisted amide **2.1c** with a relatively high twist angle ($\tau = 28.65$) and pyramidization at nitrogen ($\chi_N = 21.8$) decomposed and no product was observed as compared to **2.1b** ($\tau = 24.0$, $\chi_N = 16.1$) and **2.1d** ($\tau = 27.3$, $\chi_N = 13.7$) (entries 1-4, Figure 16). To understand the reason behind this anomaly, we proceeded with calculating rotational energy profile of the molecules **2.1a-2.1d** and the unmodified analog **2E**. Rotational energy barrier (*E*) has been shown to influence the reactivity of twisted amides.[15,19] Compound **2.1c** has higher rotational energy barrier (*E* = 11.4 kcal/mol) as compared to other reactive twisted amides **2.1b** and **2.1d** (*E* = 6.9 and 7.3 kcal/mol respectively) thus **2.1c** exhibited

lower reactivity for C-C bond formation (entry 3, Figure 16). The calculations revealed that all the twisted amides prefer to remain in a twisted conformation. The optimization studies showed the formation of the aryl ketone **2.10a** from activated amides **2.1b** and **2.1d** in good yields (66-70%, Figure 16, entries 2 and 4). As expected, the attempted Suzuki-Miyaura reaction of unmodified analog **2E** with p-methoxy phenylboronic acid **2.9a** under optimized reaction conditions failed to generate C-C bond, thus highlighting the unique ability of this approach to activate secondary amide bonds.

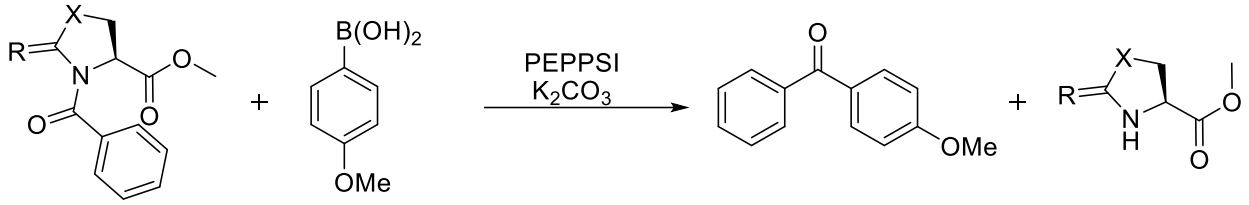

2.1a-2.1d **2.9a** **2.10a**

Entries	X	R	2.1a-2.1d	Temp (°C)	Solvent	PEPPSI (eq.)	Yield (%)
1	O	O	2.1a	Reflux	THF	0.4	Decomposed
2	O	S	2.1b	Reflux	THF	0.4	70
3	S	S	2.1c	Reflux	THF	0.4	Decomposed
4	S	S	2.1d	Reflux	THF	0.4	66
5	S	S	2.1d	40 °C	THF	0.1	20
6	S	S	2.1d	RT	THF	0.1	Decomposed
7	S	S	2.1d	Reflux	Toluene	0.1	Decomposed

Figure 16: Metal-catalyzed C-C bond formation on activated amides **1a-1d** obtained by selective chemical modification. Reaction conditions: activated amide **1a-1d** (0.07 mm, 1 eq.), arene boronic acid (2.0 eq.), Pd-Peppsi (0.1-0.4 equiv.), K_2CO_3 (3 eq.) in varying solvents (5 mL) at different temperatures for overnight.

2.4.3.2 Scope of the Reaction.

Examination of the scope revealed that a remarkably broad range of boronic acids are suitable for this Pd-catalyzed C-C bond formation reaction with twisted amides **2.1b** and **2.1d** (Figure 17). As shown, these conditions are compatible with diverse arylboronic acids, including neutral phenylboronic acid **2.9b** generating aryl ketone **2.10b** with 69-70% yield. Importantly,

electrophilic functional groups of phenylboronic acids, such as ketones **2.9c** are readily accommodated to generate aryl ketone **2.10c**. In contrast to acylpyrrole and pyrazole amide activation,[82] these reaction conditions are compatible with phenylboronic acids containing electron-withdrawing substituents at the conjugating 4-position of the aromatic ring including 4-cyanophenylboronic acid **2.9d** and 4-nitrophenylboronic acid **2.9e** to generate aryl ketones **2.10d** and **2.10e** (45-47%). We also obtained moderate yields (53-66%) of aryl ketones **2.10f-2.10g** from reactions conducted with the medicinally relevant F-containing phenylboronic acid **2.9f** and sterically hindered 2-formyl phenylboronic acid **2.9g** (Figure 17). Cross-coupling with 4-methoxy-carbonylphenyl boronic acid **2.9h** proceeds in unoptimized 29% yield of aryl ketone **2.10h**. In contrast, conjugated aromatic such as 4-vinyl phenylboronic acid **2.9i** is well tolerated, delivering the desired biaryl ketones **2.10i** in excellent yields (94%, Figure 17). The methodology was found to be tolerant of pharmaceutically important heterocyclic aryl boronates such as oxabenzindole boronic acid **2.9j**, and 3-thiopheneboronic acid **2.9k** and generated corresponding ketones **2.10j-2.10k** in good yields (65-76%, Figure 17). Interestingly, high efficiency is observed for polyaromatic substrates such as sterically demanding arene 1-naphthalene **2.9m** to generate corresponding ketones **2.10m** in high yields (74-91%, Figure 17).

Perhaps most notable is the capacity of the reaction to tolerate alkenylboronic acids such as 1-pentenylboronic acid **2.9p** and 1-octenyl boronic acid **2.9q** that are often problematic in the addition reactions to other secondary amides. We observed an efficient conversion of the starting materials to α,β-unsaturated ketones **2.10p-2.10q** with excellent yields of (69-80%, Figure 17). Noteworthy is the direct functionalization of secondary amides with styrylboronic acid **2.9r** to generate α,β-unsaturated ketone **2.10r** (pharmaceutical intermediate, Figure 17), highlighting the potential impact of this method.

We were also pleased to observe that sterically hindered fluorescent boronic acid such as fluorene-2-boronic acid **2.9n** could be employed for the synthesis of ketones using this methodology, as demonstrated by the formation of the corresponding ketone **2.10n** in high yield (88%, Figure 17). Collectively these examples demonstrate the broad scope of this reaction and provide a conceptually new method for the direct synthesis of ketones from secondary amides.

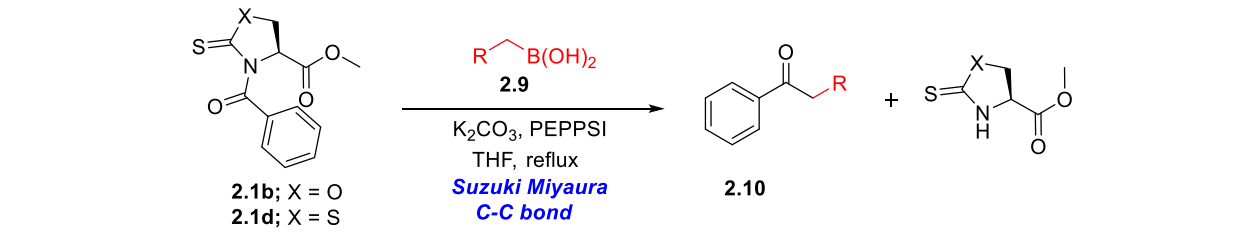

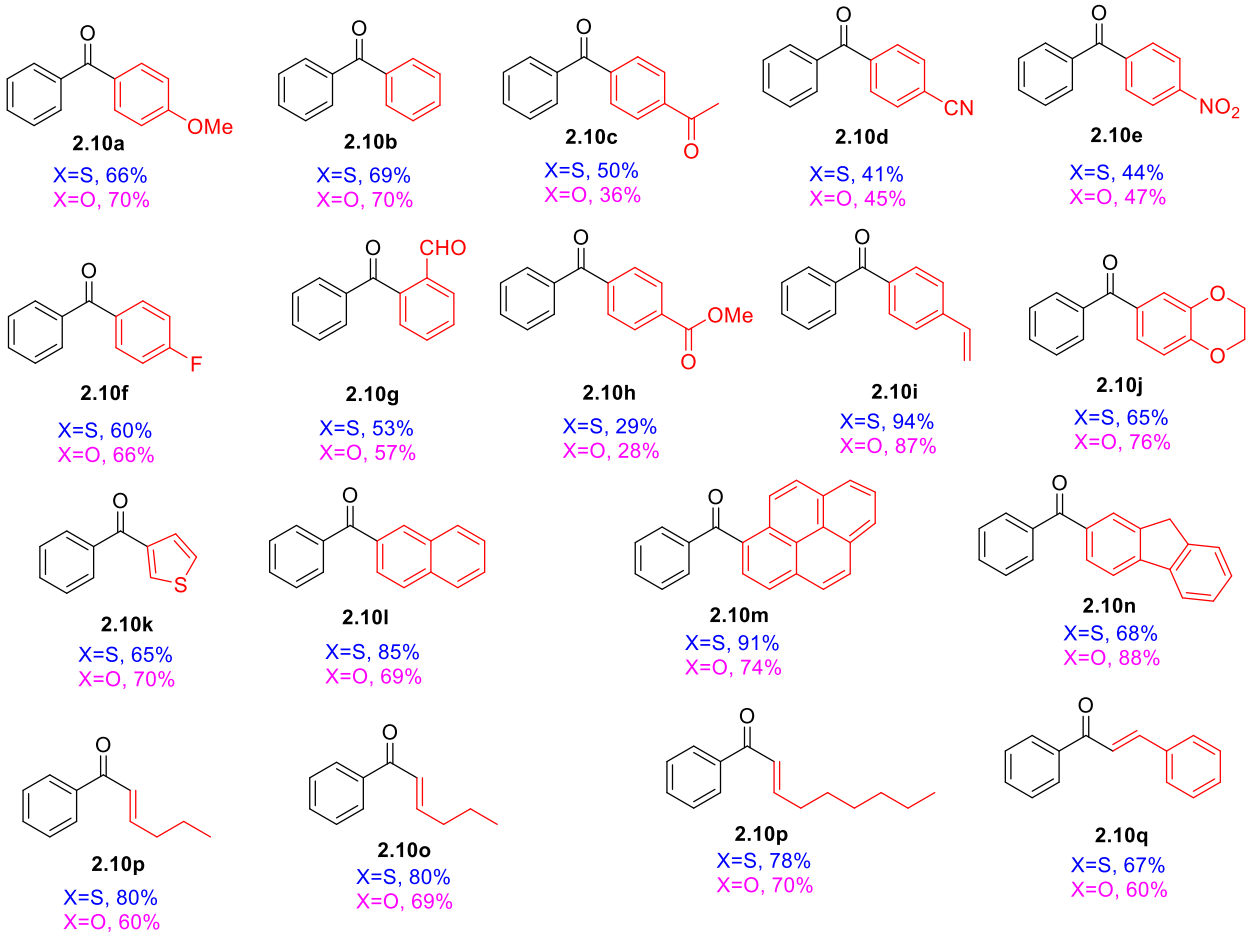

Figure 17: Scope of our methodology for metal-catalyzed C-C bond formation. The scope of C-C bond formation was evaluated with both amide substrates 1b and 1d, and with respect to varying arene boronic acids. Reaction conditions: activated amide 1b or 1d (0.07 mmol, 1 eq.), arene boronic acid (2.0 eq.), PEPPSI (0.4 eq.), K_2CO_3 (3 eq.) in THF (5 mL) under refluxing conditions for overnight.

2.4.4 Metal-free C-C bond formation by Friedel-Crafts reaction

Current metal-free approaches for making ketones by twist activation and subsequent Friedel-Crafts acylation is mainly limited to highly twisted amides such as glutarimides which contain the maximum twist angle of 90.6°.[63] Although the method widely used by the Garg group employs only moderately distorted N-Bz-,N-Boc-amides (twist angle = 26.22°) and N-Ph,N-Ts-amides (twist angle = 26.22°) for C-C bond formation, it ultimately resorts to undesirably harsh conditions and requires a metal catalyst for modification to occur.[49, 63] Herein we report for the first time the modification of C-N amide bonds with moderate twist angles (24.0° -27.3°) to C-C bonds under mild, metal-free mild conditions.

2.4.4.1 Key Experiments and Reaction Optimization

We extended our strategy of the selective "twist activation" of secondary amides for the formation of C-C bond by a metal-free approach (Figure 18). We initiated our studies on model twisted amides **2.1a-2.1d,** introduced by our laboratory, using anisole **2.11a** and trifluoromethanesulfonic acid (TfOH) as an acid catalyst in stoichiometric amounts based on the previous studies with highly twisted amides. We were pleased to see that twisted amide **2.1d** (twist angle - 27.3°) generated the ketone product **2.12a** in a high yield (90%, entry 4, Figure 18). The acylation occurred exclusively at the N–C amide bond, underscoring the heightened reactivity of the twisted amide bond. Figure 18 summarizes key optimization results with amide **2.1d** using various acid catalysts such as $Cu(OTf)_3$, $TMS(OTf)_3$ and TfOH (entries 1-4, Figure 18). The reaction with acid catalysts

$Cu(OTf)_3$ and $TMS(OTf)_3$ failed to generate any desired product even with the addition of stoichiometric amounts (entries 1-2, Figure 18). As anticipated, the use of a stoichiometric amount of TfOH was required (entry 4, Figure 18) due to amine protonation and/or the presence of dicationic intermediates (Figure 19).[26-27,41-42] The reaction failed to generate any desired product with other solvents such as DCM (Figure 18, entry 3). Anisole is used as a solvent for maximum efficiency of the reaction to generate ketone product **2.12a** with 90% yield (entry 4, Figure 18). With optimal conditions in hand, we used toluene **2.11b** for the formation of a C-C bond with all the activated amides **2.1a-2.1d**. As expected, **2.1d** with the Winkler-Dunitz parameters ($\tau + X_N$ = 41.0) and lower rotational energy barrier (E) (7.3 kcal/mol) gave the corresponding ketone product **2.10b** with highest yield using toluene as solvent (87%, entry 8, Figure 18).

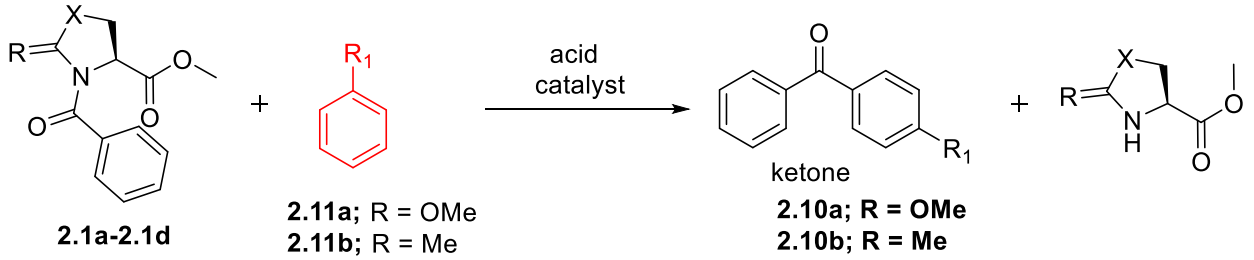

Entries	X	R	2.1a-2.1d	R_1	Solvent	Acid catalyst	Yield (%)
1	S	S	**2.1d**	OMe	-	$Cu(OTf)_3$	0%
2	S	S	**2.1d**	OMe	-	$TMS(OTf)_3$	0%
3	S	S	**2.1d**	OMe	DCM	TfOH	0%
4	**S**	**S**	**2.1d**	**OMe**	**-**	**TfOH**	**90%**
5	O	O	**2.1a**	Me	-	TfOH	62%
6	O	S	**2.1b**	Me	-	TfOH	50%
7	S	O	**2.1c**	Me	-	TfOH	73%
8	**S**	**S**	**2.1d**	**Me**	**-**	**TfOH**	**87%**

Figure 18: Key reactions and optimization for metal-free C−C bond formation from twisted amide.

All other twisted amides **2.1a, 2.1b** and **2.1c** (twist angles = 21.3-28.6) also generated corresponding ketone product **2.12b** with toluene in moderate yields (50-73%, entries 5-7, Figure 18) which is in contrast to the electronically activated amides N-Bz,-N-Boc-amide and N-Ph,-N-Ts-amide (twist angles = 26.22^{o} and 30.39^{o} respectively and rotational energy barrier (E) = 4.3-7.0 kcal/mol) generating 0% yields under the optimized metal-free conditions.[10,25] From these results, we anticipate that other factors in addition to the twist angle of the amide and rotational energy barrier play an important role in this C-C bond forming reaction. We hypothesize that in the presence of TfOH, the carbonyl and thiocarbonyl of the oxa- and thia-zolidinone rings undergo protonation that induces tautomerization between the keto and enol forms with the amidic nitrogen (proposed mechanistic pathway, Figure 19). This further decreases the tendency of the C-N amide bond to form a resonating structure leading to the weakening of the C-N amide bonds.[26] Moreover, the formation of the "dication" by these activated amides in the presence of TfOH favors the cleavage of the C-N amide bonds as this eliminates charge−charge repulsive interactions in "dication" (Figure 19).[53, 83] Such protonation of heteroatoms and formation of dications is not possible with activated amides N-Bz,-N-Boc-amide and N-Ph,-N-Ts-amide providing a rationale as to why the C-N bond remains unreactive under metal-free conditions. This study leads to the generation of a new concept for the first time regarding the modification of inert C-N amide bonds to C-C bonds by the combination of ground-state distortion and electronic destabilization under metal-free mild conditions.

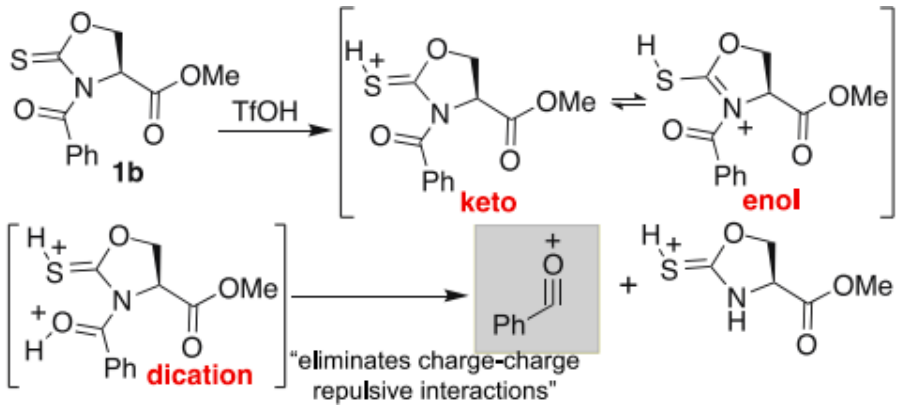

Figure 19: Proposed pathway for activation of amides for C−C bond formation by both ground-state steric distortion and electronic activation.

2.4.4.2 Scope of the Reaction

With optimal conditions in hand, the scope of the reaction was investigated on activated amides **2.1b** and **2.1d** with different arenes (Figure 20, See SI). The reaction readily accommodates electron-rich, neutral and multiple-substituents on the aromatic ring such as anisole, benzene, toluene, 1,3-dimethyl benzene and 3,5-dimethyl benzene. **2.11a-2.11e** to generate corresponding ketones **2.10a-2.10b** and **2.12a-2.12c** in good yields (71-95% Figure 20).

Our mild reaction conditions are compatible with a wide array of functional groups, including chlorides and even bromides **2.11f-2.11g** to generate corresponding ketones **2.12d-2.12e** in high yields (70-88%, Figure 5a, See SI). Notably, the reaction generated a high yield of the ketone product **2.12f** (72%) with sterically hindered ortho-functionalities arenes such as 1,3,5 trimethyl benzene **2.11h** providing versatile handles for synthetic manipulation. This study demonstrates that these twisted amides capable of undergoing protonation accommodate a wide range of functional groups on arenes under mild metal-free reaction conditions.

It is noteworthy that arenes without any functional groups and with varying substitutions can be directly utilized for the modification of the C-N amide bond that is unattainable by metal-catalyzed procedures.

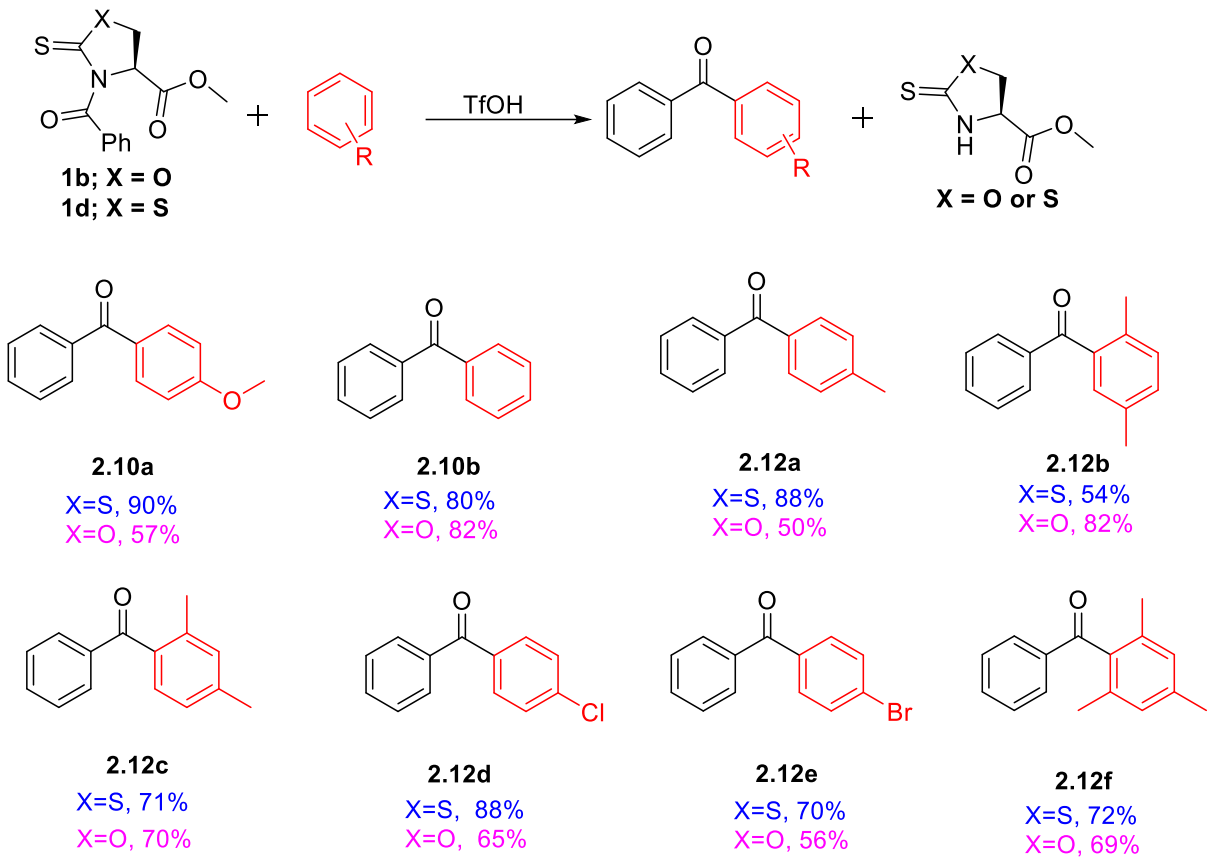

Figure 20: Scope of Metal-free C-C Bond formation in Twisted Amides.

2.4.4.3 Late-stage diversification of peptides via site-selective modification of C-N amide bond to C-C bond

The distinctive feature of this approach is the selective modification of a particular C-N amide bond to a C-C bond in the presence of other similar amides. Since **2.1b** and **2.1d** is twisted ($\tau+X_N$ = 40.1 and 41.0, respectively) and exhibited low rotational energy barrier (E = 6.9-7.3 kcal/mol) based on the DFT calculations on small molecules, we attempted selective insertions of thiocarbonyl at cysteine amide in tripeptides Boc-FCF-OMe and AcO-RFC-solid support by using

various thiocarbonylating agents. These reactions failed to generate thiocarbonyl-modified Ph-Cys-benzamide. This might be due to the low reactivity of an intermediate obtained by the reaction of the side chain of serine/cysteine with thiocarbonylating reagent resulting in its rapid decomposition/hydrolysis before the nucleophilic attack from the backbone amide bond. The addition of the thiocarbonyl was largely unsuccessful, with polyamides so we synthesized oxazolidinone **2.1a** analog, which also exhibited low rotational energy barrier (E = 9.8 Kcal/mol) and is twisted ($\tau+X_N = 30.4$), on polyamide, Ph-Ser-benzamide by reaction with a carbonyl donor (DSC) and using DMAP as a base to generate corresponding oxazolidinone Ph-Oxa-benzamide **2.13a** (Synthesis in SI). The other secondary amide present on Ph-Ser-benzamide remained completely unmodified and inert under the reaction conditions. Next, we attempted a metal-catalyzed Suzuki-Miyaura reaction on the twist activated tripeptides **2.13a** but found that the harsh conditions inherent to the method resulted in decomposition of the starting material.

With selectively activated polyamide Ph-Oxa-benzamide **2.13a** in hand, we carried out the metal-free reaction with arenes such as anisole and benzene and generated the benzophenone products in good yields (73% and Figure 5b, See SI). There are no other methods reported in the literature that can selectively activate particular C-N amide bonds of polyamide in the presence of other secondary and primary amides for the formation of C-C bonds under metal-free conditions. To determine the broad scope of this reaction, we selectively activated serine amide in polyamides Ph-Ser-phenylbutylamide and a dipeptide Ph-Ser-Phe-OMe to generate activated amides Ph-Oxa-phenylbutylamide **2.13b** and Ph-Ser-Phe-OMe **2.13c** (See SI for details) and carried out Friedel-Crafts reaction with varying arenes under metal-free conditions. The reactions resulted in selective formation of C-C bonds at the activated amides using varying arenes such as mesitylene and toluene and generated benzophenone analogs in good yields irrespective of the nature of

polyamides (Figure **2.13b**). It is noteworthy that the reaction on peptides for the formation of C-C bonds under mild metal-free reaction conditions overcomes one of the major limitations of nickel-catalyzed C-C bond formation requiring harsh conditions.[4, 43] Thus, provide a simple and general approach for introducing new benzophenone fluorophore functional groups and properties in various biomolecules, synthetic molecules and polymers.

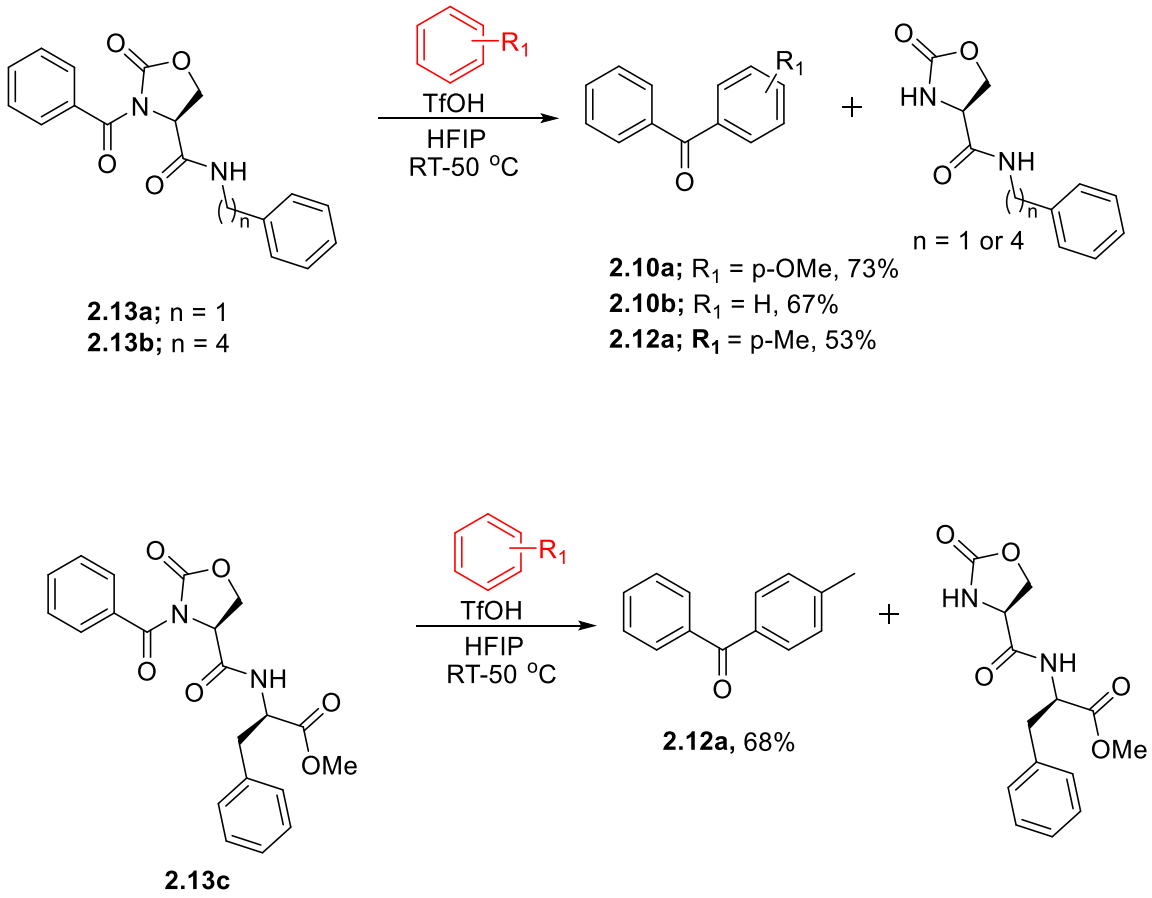

Figure 21: Selective modification of a particular C-N bond to C-C Bond in Polyamides.

2.4.4.4 Conclusion on Selective Conversion of Unactivated C-N Amide bond to C-C bond in the polyamide via Steric and Electronic Resonance Destabilization

In conclusion, we have developed the first approach for the site-selective conversion of C-N amide bonds in polyamides to C-C bonds. Our approach relies on the use of carbonyl and thiocarbonyl

reagents to first selectively activate the C-N amide bond by ground state distortion. This is followed by further activation with the protonation of the carbonyl group of oxa- and thio-zolidinone leading to transfer of electron density from the C-N amide bond to the oxazolidinone ring resulting in the resonance destabilization and weakening of the C-N amide bonds. Further, in situ reaction with unfunctionalized arenes furnishes ketone products via Friedel-Crafts reaction. The reaction is tolerant to a wide range of functional groups including chloride and bromide and exhibited mild, metal-free conditions thus obviating the requirement of toxic metal catalysts and harsh conditions. It is noteworthy, that this approach developed a new concept for the activation of C-N amide bonds with smaller twist angles (twist angles = 21.3-28.6) for the formation of C-C bonds by influencing their electronic factors that were earlier impossible to achieve with activated amides of moderate twist angles (twist angles = 26-65^{o}) thus avoiding the need of highly twisted amides for the mild metal-free modifications. With the future design, we expect that the scope of selective activation of amide bonds for multiple modifications will be broadened further. Collectively, these studies allow for the selective breakdown of inert amides under mild reaction conditions and render polyamides useful synthetic building blocks for the late-stage modification with varying functional groups.

Chapter 3: Bioinspired Nitroalkylation for Selective Protein Modification and Peptide Stapling

3.1 Introduction

Site-selective chemical modification of proteins is invaluable in the field of biochemistry and medicinal chemistry to study various biological processes such as post-translational modifications (PTMs)[84] and protein–protein interactions (PPIs).[85] Such methods are highly significant for generating therapeutic agents, such as antibody-drug conjugates (ADCs) with the specific drug to antibody ratios (DARs) and PEGylated biomolecules.[86] Although bioorthogonal methods using unnatural amino acids provide an elegant strategy for protein functionalization in complex biological mixtures,[87] a chemical means to prepare homogeneous proteins with defined modification in sufficient quantities are still required. One of the well-established methods installs aldehydes on proteins for modification by the addition of hydrazines and hydroxylamines to generate hydrazones[88] and oximes,[89] respectively. However, this approach has limitations, such as slow kinetics, high concentrations of harmful catalysts, cross-reactivity with metabolites, poor stability of the resulting conjugates due to reversibility, and the requirement of the acidic (pH 4–6) conditions.[90] The deviations from the physiological pH can have adverse effects on the structure of proteins, including disassembly of the histones and human hemoglobin,[91] and aggregation of antibodies and proteins associated with neurodegenerative diseases.[92] These limitations led to the development of more advanced aldehyde bioconjugations, which exhibit improved stability of conjugates, such as Pictet–Spengler,[93] indium-mediated allylation,[94] Wittig reaction,[95] and aldol chemistry.[96] Despite the recent advances, these aldehyde bioconjugations suffer from slow reaction rates, low conversions into desired bioconjugates (ca. 40–60 %), and low substrate scope.[97] Therefore alternative bioconjugation reagents that can overcome these limitations are highly desirable.

3.2 Results and Discussion

3.2.1 Design of Bioconjugation Reagents

Inspired by the observation of nitroalkane-modified proteins as an emerging PTM and its role in regulating enzyme functions, protein trafficking, and cell signaling, we sought to develop nitroalkane reagents for selective modification of proteins.[98] As a key design element, we postulated that the nucleophilic attack of nitroalkanes on aldehyde-containing proteins would lead to the formation of a stable C−C bond at the site of conjugation. This approach enables a rare example of nitroalkylation of proteins under physiological conditions and thus can be used to investigate the role of these PTMs in cellular signaling. Currently, there are no methods available to generate nitro-alkylated proteins in a selective manner. Henry bioconjugation offers a general method for efficient conjugation of proteins (Figure 1). Among a number of advantages, we recognized that this bioconjugation event would 1) be chemoselective for aldehydes over other reactive side chains of amino acids, without the need for coupling reagents and metals, 2) lead to the modification of proteins with a variety of different tags such as NMR tags, fluorophores, affinity tags, or clickable tags for example, terminal alkynes, 3) lead to the stapling of peptides (Figure 1 c), 4) introduce a nitroalkane group into the protein, a feature that is known to be responsible for modulating the functions of biologically active proteins, 5) introduce a handle for the site-selective fluorination of peptides for analysis by ^{19}F NMR spectroscopy (Figure 1 b). Unlike the ubiquitous hydrogen atom which is commonly used for ^{1}H NMR spectroscopy, fluorine is nearly absent in biological systems, making it a unique bioorthogonal atom for probing molecular interactions in biology.[99] This bioconjugation approach provides a simple and inexpensive approach for this kind of application. Moreover, nitroalkanes help in easy characterization of proteins due to their distinct finger pattern in mass spectrometry.[100] Herein, we

report the successful execution of these ideas and present a rapid, chemoselective bioconjugation approach for tagging a wide range of peptides and proteins and for making stapled peptides.

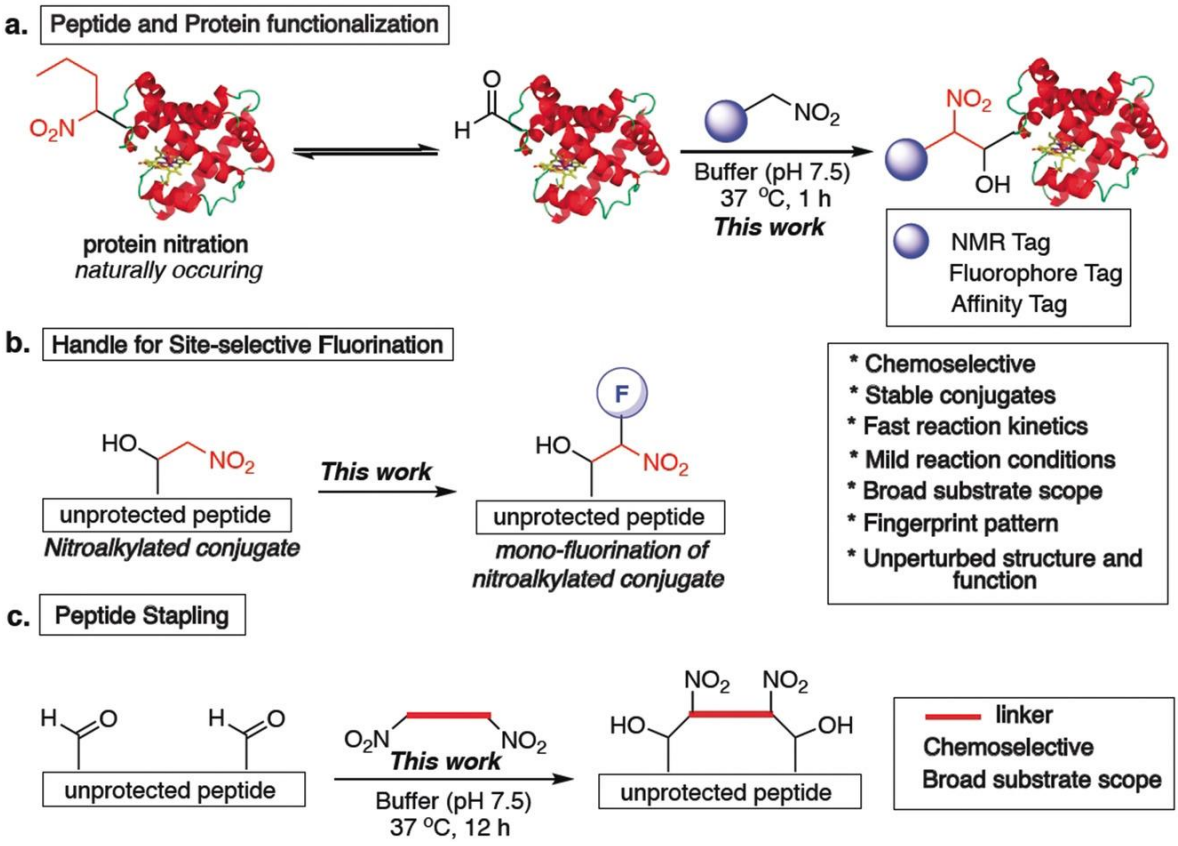

Figure 1: Nitroalkanes as bioconjugation reagents. a) Nitroalkanes for chemoselective peptide and protein functionalization. b) Nitro-alkylated peptides for site-selective fluorination. c) Dinitro-reagents for peptide stapling.

3.2.2 Nitroalkanes as Rapid and Aldehyde-Specific Bioconjugation Reagents

To initiate our investigation, we used nitromethane (**3.1a),** and sought to evaluate its potential for aldehyde bioconjugation (Figure 2). Incubation of **3.1a** (7.5 mm) with the aldehyde-tripeptide CHO-VF **2.2a** (1.5 mm) in 50 mm phosphate buffer at pH 7.5 led to rapid conversion into the nitro-peptide adduct **3.3a** in 20 minutes (80 % conversion, Figure 2a). High-performance liquid chromatography (HPLC) analysis showed that 75 % conversion of **3.2a** into **3.3a** was achieved

within 10 minutes, and full conversion was achieved after 20 minutes (Figure 2 a; see Figure S1 in the Supporting Information). The Henry bioconjugation between **3.2a** (0.625 mm) and **3.1a** (0.625 mm) at pH 7.5 follows a second-order rate constant (k=14.94 m−1 s−1; Figure 2 b; see Figure S1). This reaction undergoes complete conversion into the bioconjugate roughly 996 times faster compared to the oxime ligation (1 mm) at pH 7.0 without a catalyst (k=0.015 m−1 s−1) and 245 times faster compared to oxime ligation at pH 7.0 with 100 mm of the p-methoxyaniline catalyst (k=0.061 m−1 s−1).[101]

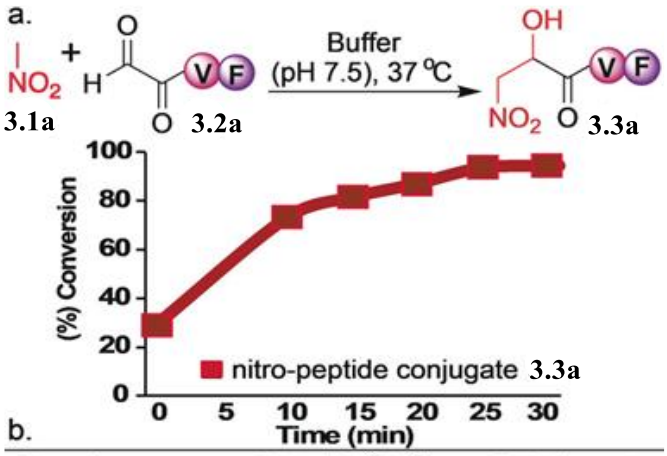

b.

Reaction	Rate ($M^{-1}S^{-1}$)	Relative rate
Henry	14.94	245
Oxime[18]	0.061 (100 mM catalyst)	1

Figure 2. a) Rate studies for synthesis of nitroalkane-peptide conjugate **3.3a**. b) The Henry bioconjugation between the aldehyde-tripeptide CHO-VF **3.2a** (0.625 mm) and nitromethane (**3.1a**; 0.625 mm) at pH 7.5 follows a second-order rate constant. Relative rate of this reaction (0.625 mm) is 245 times faster than oxime ligation (1 mm) at pH 7.0 in the presence of 100 mm p-methoxyaniline catalyst.

Next, we performed structural characterization of **3.3a** by NMR analysis, which indicated that the aldehyde is directly attached the carbon in alpha position of the nitroalkane (see Figure S2). This result suggests that the reaction proceeds by a Henry reaction, which involves a nucleophilic attack of an alpha carbon of the nitroalkane **3.1a** onto the electrophilic aldehyde on the peptide.[102]

Nitroalkanes with sterically hindered α-carbon atoms (e.g. 2-nitropropane) were shown to be unreactive towards aldehydes, supporting this reaction mechanism (see SI). Moreover, the reaction with the tripeptide SVF without any aldehyde group remained unreactive towards **3.1a** under the reaction conditions. This outcome further supports the chemoselective nature of the bioconjugation reaction (see SI)[103].

Henry bioconjugation leads to the formation of a new chiral center at the site of conjugation upon reaction between **3.2a** and **3.1a**. The stereochemical analysis of **3.3a** by ^{1}H NMR spectroscopy showed the formation of a newly generated chiral center with good diastereomeric ratio (d.r. 7:3), which could be of a great benefit in the derivatization of peptides and proteins involved in drug discovery.[103] The stability of protein conjugates is a major concern for bioconjugation reactions. Therefore, we evaluated the stability of the nitro-peptide conjugate **3.3b** in aqueous buffers at pH ranging from 3.5 to 10.5, for 24 hours at 37 °C. HPLC analysis showed high stability of **3.3b** at varying pH conditions (Figure 3; see SI). Together, this reaction exhibited fast reaction kinetics, high conversion, and synthesized stable conjugates under physiological conditions as compared to other aldehyde bioconjugations, offering an attractive alternative for aldehyde bioconjugation of proteins.

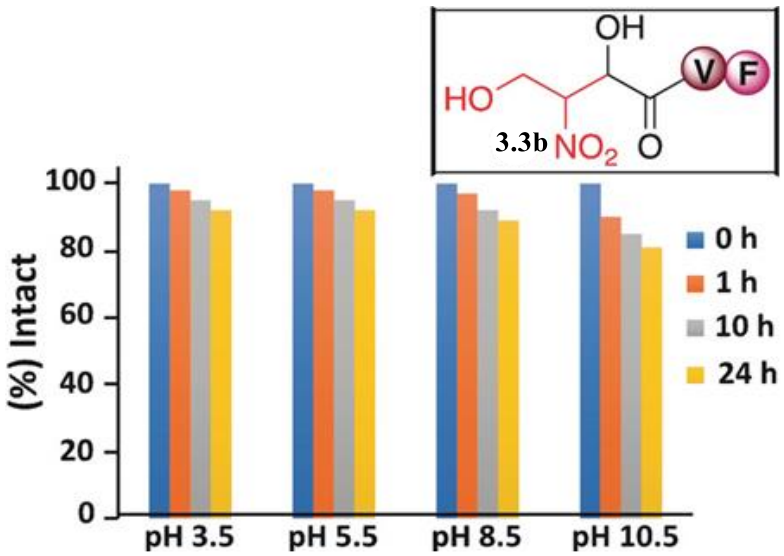

Figure 3. The pH stability of the nitro-peptide conjugate **3.3b**.

3.2.3 Fluorination of Nitro-Peptide Conjugates.

Another unique feature of this bioconjugation approach is that nitro-alkylated peptides provide a new handle for site-selective fluorination of peptides, thus providing a specific probe to study peptide–proteins interactions without background signals.[99] To achieve this, we carried out the reaction of **3.3a** with selectfluor for 16 hours under aqueous conditions (Figure 4). HPLC and MS analysis showed the formation of the monofluorinated nitro-alkylated peptide **3.4a** with 60% conversion. The site of the mono-fluorination on **4.4a** was confirmed by HSQC NMR and ^{19}F NMR spectroscopy (see SI). Fluorine is an extremely sensitive probe, making it easy to observe and is highly responsive to changes in its environment, therefore it can be used to understand the nature of peptide–protein interactions and quantify the strength of the interaction in cells using 19F MRI.[104]

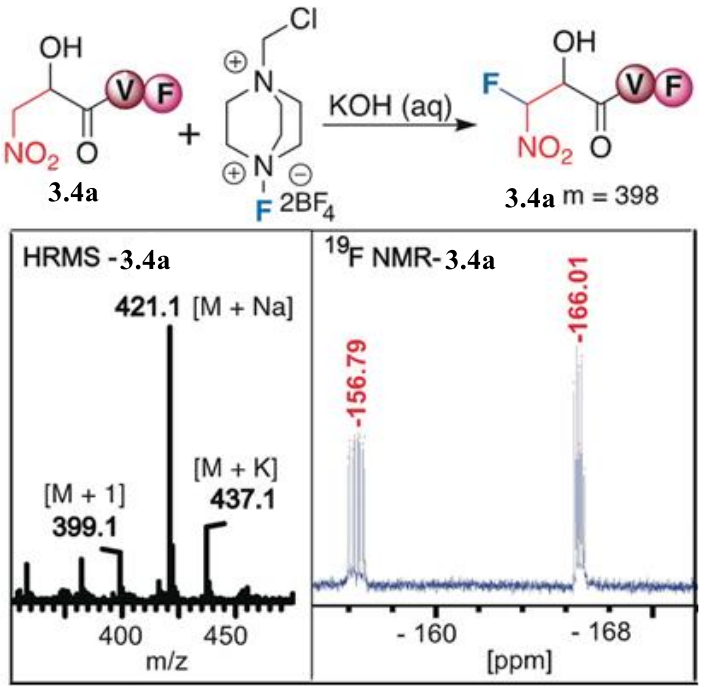

Figure 4. Site-selective fluorination of a nitro-alkylated peptide

3.2.4 Substrate Scope of Nitro-Reagents for Peptide Bioconjugation

Next, we evaluated the chemoselectivity of the nitroalkanes **3.1** with a variety of unprotected peptide aldehydes (**3.2**), having varying amino-acid residues and different lengths of peptide chains, under physiological conditions. The incubation of the peptide aldehydes **3.2** (7.1 mm) with the nitroalkanes **3.1** (35.5 mm) in 50 mm phosphate buffer at pH 7.5 yielded nitro-alkylated peptides (**3.3**) inaquantitative manner (Figure 5; see SI). The nitroalkanes **3.1** did not react with any reactive amino acids, including Tyr, Ser, Glu, Asp, Arg, and His, under neutral aqueous conditions, further establishing the aldehyde specificity of nitroalkanes (Figure 5a). High conversions into the bioconjugated products **3.3** were obtained in all the cases, independent of the nature of peptides and nitro-reagents, indicating the high substrate scope of this methodology and high chemo- and site-selectivity of this bioconjugation approach.

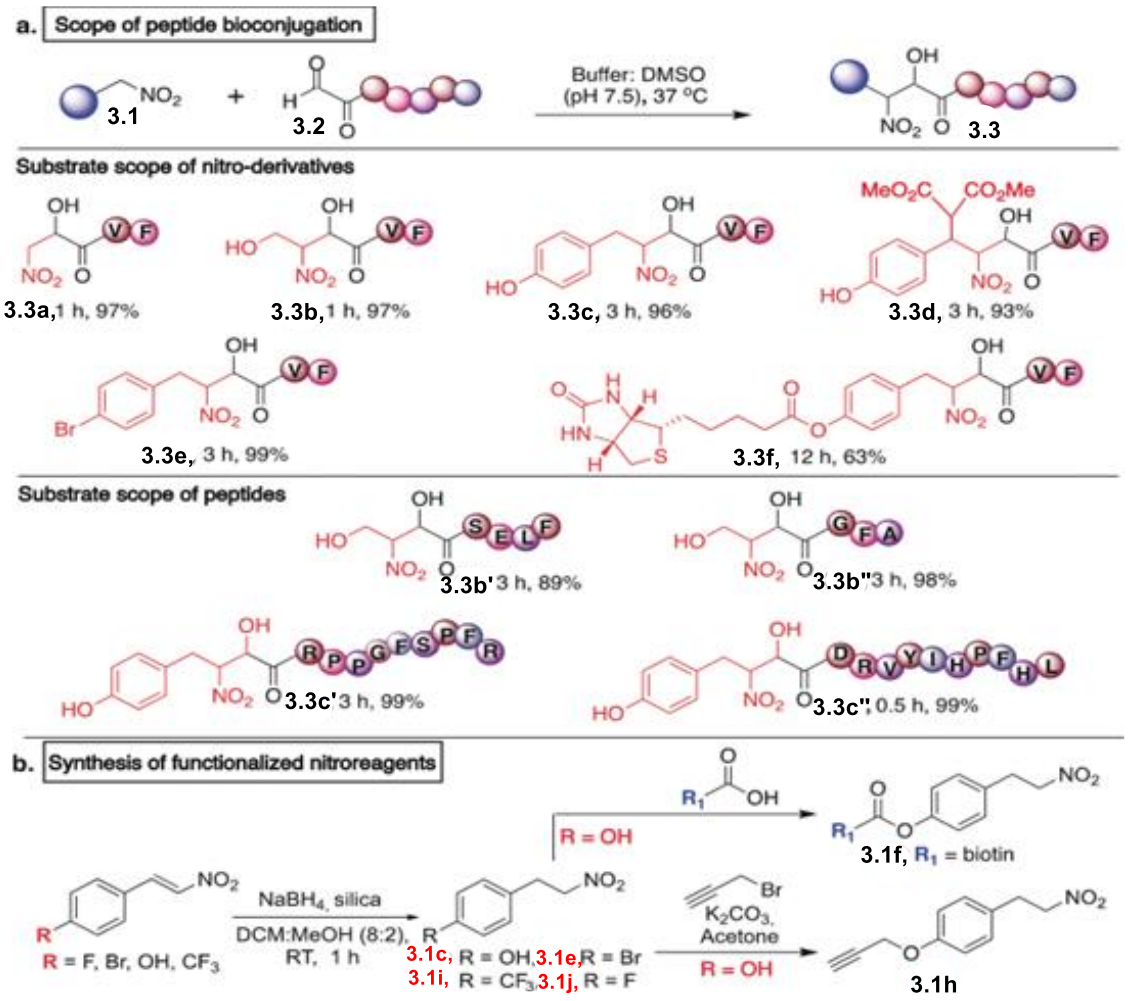

Figure 5 a) Scope of nitro-reagents for bioconjugation reaction. Reaction conditions. Aldehyde (7.1 mM) in buffer (pH 7.5, 50 mM): DMSO (9:1), 0.44 mL), and nitro-reagent (5 equiv) at 37 °C. % Conversions were determined by HPLC. b) Synthesis of functionalized nitro-reagents.

3.2.5 Synthesis of Functionalized Nitro-Reagents

An effective bioconjugation reaction should have the ability to attach various synthetic groups, thus a variety of functionalized nitro-reagents were synthesized. These nitroreagents were synthesized in two to four steps from nitrostyrenes for use as affinity tags, NMR tags, targeting agents, and fluorescence imaging dyes (1, Figure 5b; see SI). These reagents (**3.1c–f**) reacted with the peptide aldehydes **3.2** to afford the expected single-modification nitro-peptide conjugates (**3.3 c–f**) in good yields, as determined by LC-MS (Figure 5a; see SI). These results demonstrate that

this process could reliably be translated into the convenient site-specific attachment of many additional synthetic compounds to biomolecules.

3.2.6 Nitro-Reagents for Selective Modification of Proteins

Protein conjugates with different classes of functional tags, such as fluorophores, NMR tags, affinity tags, and targeting agents are valuable in the fields of biomaterials and chemical biology.[73, 105] To test the applicability of **3.1** in protein modification and their compatibility with diverse functional components, myoglobin was selected as a model protein. The N-terminus of myoglobin was converted into the aldehyde by using pyridoxal phosphate PLP[106] and it was expected that nitroalkanes could achieve aldehyde-specific labeling. Incubation of the myoglobin aldehyde **3.5** (0.13 mm) with different nitro-reagents (**3.1 a–j;** 200 equiv) for reaction times ranging from 30 minutes to 4 hours in 10 mm phosphate buffer at pH 7.5 resulted in the formation of a nitro-alkylated myoglobin (**3.6**) with high conversions as determined by LC-MS analysis (Figure 6; SI). The control reaction with myoglobin without the aldehyde group did not lead to the conjugation product (see SI). A large number of equivalents of the nitroalkanes were used to increase the rate of the process. With 200 equivalents of nitroalkanes, the reaction is completed in less than an hour with 99% conversion into the modified proteins. We also performed multiple reactions with 5 using five equivalents of different nitro-reagents. High conversions into the modified proteins were obtained but with longer reaction times (12–16 h; 60– 98%). Further, the reaction of **3.1a** with a protein ketone (a-lactalbumin ketone) did not lead to any conjugation, confirming the high chemoselectivity of nitroalkanes for aldehydes (see SI). The unique feature of this approach is that it generated nitro-alkylated proteins with very high conversions (99%) and excellent selectivities for a variety of nitro-reagents (Figure 6).

The bromo-derivative of the nitroalkane **3.1e** was synthesized for easy characterization of a modified protein since a bromine atom leads to a unique signature by MS analysis given the 1:1 abundance of the two bromine isotopes (^{79}Br:^{81}Br, Figure 6).[107] To confirm our hypothesis, nitro-bromomodified myoglobin was analyzed by MS and the two expected adducts of modified myoglobin bearing ^{79}Br and ^{81}Br were identified (see SI). To make nitro-reagents as a general approach to prepare diverse protein conjugates, we synthesized the alkyne-nitro-reagent **3.1h** and carried out reaction with **3.5** to generate the alkyne-nitro protein conjugate with high conversion (99%, Figure 6; see SI).

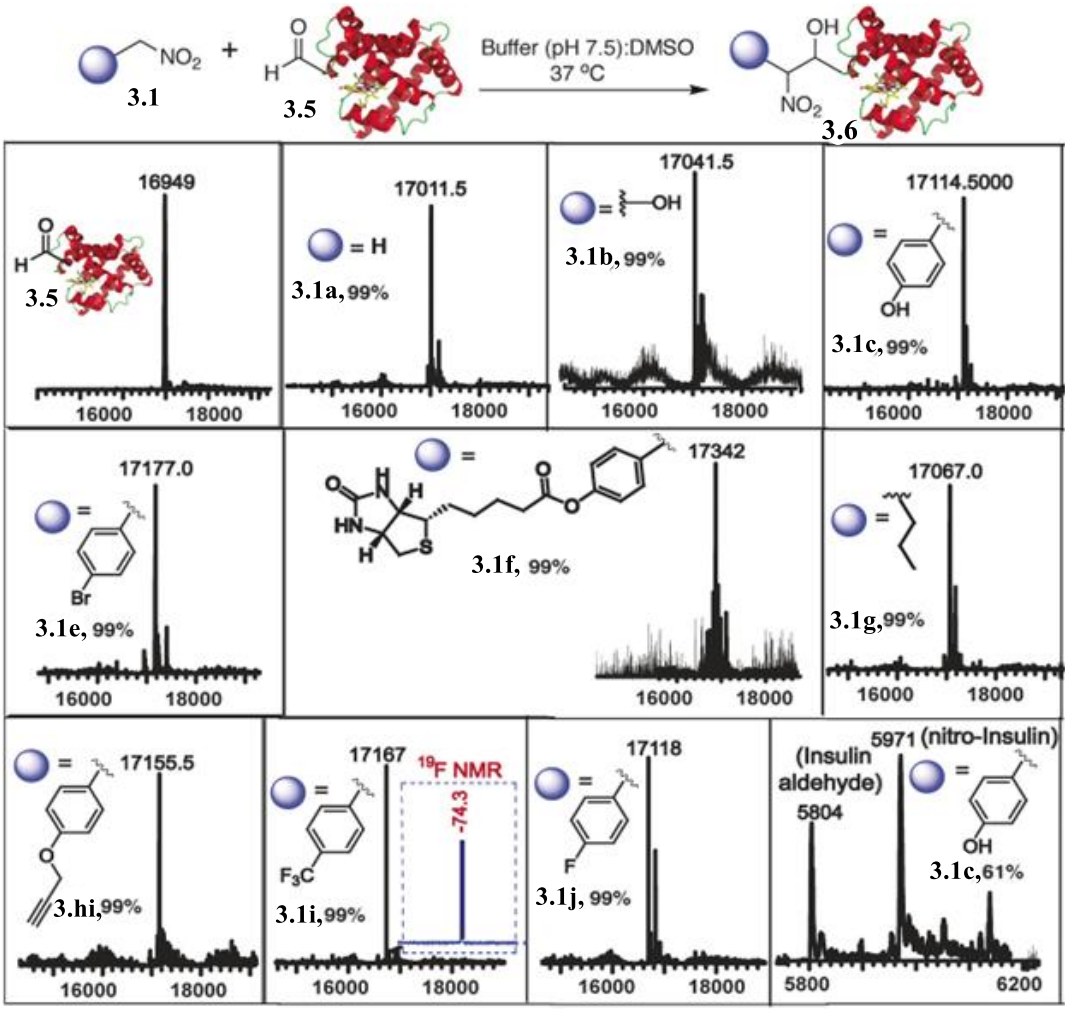

Figure 6. Nitro-reagents for site-selective modification of proteins. Reaction conditions. Protein aldehyde, myoglobin aldehyde or insulin aldehyde (0.13 mm) in buffer (pH 7.5):DMSO (9:1), 0.44 mL, and nitro-reagent (200 equiv) at 37 ^{o}C. % Conversions were determined by LC-MS.

The alkyne functionality can further be used for subsequent modification by click chemistry.[108] Fluorinated and trifluoromethylated nitro-reagents (**3.1i–l**) were synthesized for selective modification of proteins which were then analyzed using ^{19}F NMR spectroscopy (Figure 6 and Figure 7b; see SI). Notably, the mild reaction conditions of this bioconjugation reaction maintain the two structurally critical disulfide bonds in the insulin and generated nitro-alkylated insulin in good yield (Figure 6). Next, **3.5** was labeled with the biotin-nitro-reagent **3.1f** and 99% conversion into biotin modified myoglobin was observed under the reaction conditions (Figure 6; see SI).

To make water-soluble nitro-reagents, we developed a general approach for functionalizing nitro-reagents with a tertiary amine for increased water solubility (**3.1m, n** Figure 7a; see SI). The successful synthesis of water soluble nitro-reagents provides a facile method for aldehyde selective addition of various payloads to proteins of interest. HRMS analysis showed that myoglobin aldehyde was successfully labeled with the water-soluble Boc-nitro-reagent **3.1m** and the FITC-labeled dye-nitro-reagent **3.1n** with high conversions (99%, Figure 7b; see SI). The nitroderivative of metallocene analogue **3.1o** was synthesized for selective modification of a protein and was then analyzed by UV spectroscopy (Figure 7b; see SI). Together, these results demonstrate the high versatility of nitroreagents for bioconjugation of proteins.

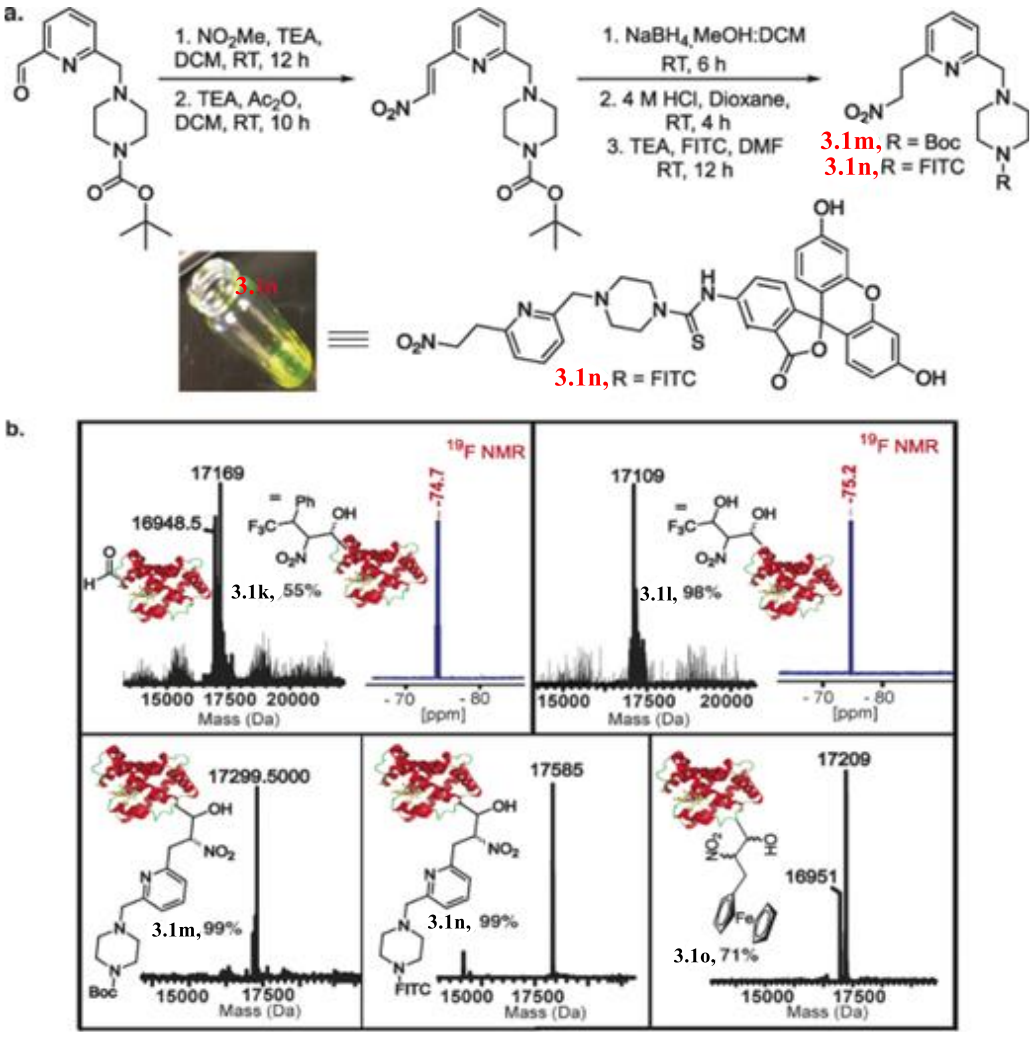

Figure 7. a) Synthesis of water-soluble nitro-reagents. b) Scope of nitro-reagents for bioconjugation of protein (Myoglobin aldehyde). ^{19}F NMR spectra of nitro-protein conjugates. Yields (%) were determined by LC-MS.

3.2.7 Fingerprint Pattern of Nitro-Alkylated Proteins

Nitroalkyl groups on proteins help in easy characterization of proteins since nitroalkanes give distinct signaling pattern by MS analysis.[100] Though the nitro group is not a charge-stabilizing moiety, a variety of fragmentation patterns are possible, for example, the loss of a NO_2 radical, loss of nitrous acid (M-HNO_2), decomposition of the resulting olefins, and McLafferty rearrangement followed by the subsequent decomposition of alkyl fragments.[109] The most interesting feature of the mass spectra of nitroalkanes is the occurrence of oxygen-free CHN fragments. This fragmentation pattern of nitroalkanes is sufficiently characteristic for fingerprint purposes. To confirm our hypothesis and to identify the modification site, the nitropentane-myoglobin conjugate was digested by trypsin, and subjected to LC-MS/ MS analysis. MS/MS data showed the formation of corresponding expected adducts bearing (M-HNO_2) and McLafferty rearrangement ions (M-117; see SI). The exogenous nature of nitroalkanes further enables detection of labeled peptides, regardless of whether or not they have been selected for MS/MS fragmentation by mass spectrometry (e.g., due to low abundance). The MS/MS data further confirms that modification occurs exclusively at the aldehyde N-terminus residue, and no lysine modification or any other modification was detected. Next, we carried out MS studies on the nitromethane myoglobin conjugate after digestion with cyanogen bromide CNBr and the MS data corresponding to the expected adduct bearing (M-NO) ion was identified (see SI). These results demonstrate that nitro-alkylated peptides can be directly identified in complex backgrounds without the need for pull-down or enrichment of the probebound peptides.

3.2.8 Protein Structure and Function is Retained After Modification

To obtain insight into whether the secondary and tertiary structure of the protein remained intact after the modification by nitro-reagents, we carried out UV studies on bromo-nitro- and dye-nitro-

modified myoglobin. Compared to the native protein, we did not observe any change in the UV absorbance pattern of the modified proteins. The absorbance at 408 nm is due to the heme group present inside the myoglobin (see SI). No change in the absorbance indicated that the heme group remained intact, further indicating that the secondary and tertiary structure of a protein is unaffected as a result of the modification under the reaction conditions.

3.2.9 Myoglobin Bioactivity Assay

We examined the activity of nitromethane-modified myoglobin through its ability to carry out the oxidation of o-phenylenediamine with hydrogen peroxide. The myoglobin binding to hydrogen peroxide and subsequent oxidation of o-phenylenediamine to 2,3-diaminophenazine provides a measure of its activity.[110] The formation of a 2,3-diaminophenazine was monitored at 426 nm by UV spectroscopy. The freshly prepared myoglobin, nitromethane-labeled myoglobin, o-phenylenediamine, and hydrogen peroxide (30%) solutions were used for the assay. The results confirmed that installation of a nitromethane does not alter the activity of myoglobin (see SI). Together, these results reaffirm that the nitro-reagents provide access to the single-site installation of a probe to a protein while conserving its structure and bioactivity.

3.2.10 Nitro-Reagents for Late-Stage Diversification of Peptides and Stapling of Peptides

Late-stage diversification of peptides (e.g., labeling, glycosylation, lipidation, etc.) and peptide stapling has a great potential as biological tools, and thus the development of such reagents is of high significance.[111] The capability of nitroalkanes for selective modification of aldehydes prompted us to explore their application in late-stage diversification of peptides and stapling of peptides. First, we introduced an aldehyde group on the side chain of the peptide **3.7** by modification of a side-chain of a glutamic acid[18] and then treated completely unprotected **3.7** with **3.1a** under physiological conditions (phosphate buffer 50 mm, pH 7.5). Higher conversion to the

modified peptide **3.8** was observed as analyzed by HPLC and MS (Figure 8 a; see SI). This study indicates that our methodology is independent of the nature and position of aldehydes (N-terminus and side-chain position). For peptide stapling, we synthesized the dinitrohexane **3.9** (see SI) and carried out reactions with the completely unprotected peptides **3.10**, containing two aldehyde groups at varying positions (i,i + 2 to i,i + 7), under neutral aqueous conditions (Figure 8b). High conversions into the peptide staples **3.11** were observed for all the dialdehyde peptides **3.10**, as determined by HPLC and MS analysis (see Figure S17). Our stapling method introduces two nitro groups in a peptide chain, which are considered to be a versatile and unique functional group in medicinal chemistry.[112, 113] These nitro-functionalized peptide staples can be used to investigate the target selectivity of stapled peptides for the development of new therapeutics.[112]

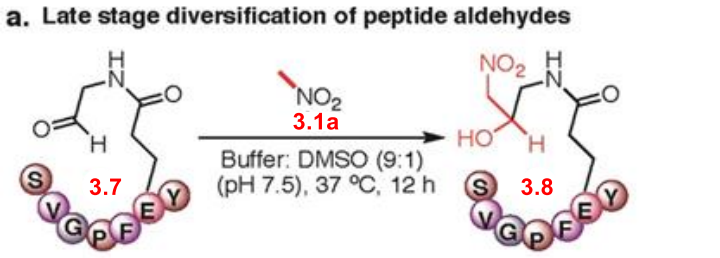

Position i, i +	Peptide sequence	Conversion (%)
i, i+2	NH_2-EGEPFY-$CONH_2$	98
i, i+3	NH_2-EGPEFY-$CONH_2$	93
i, i+7	NH_2-EADGPGFEY-$CONH_2$	87

Figure 8. a) Late-stage diversification of peptides. b) Nitroalkanes for peptide stapling.

3.3 Conclusion

In summary, we have demonstrated that nitroalkanes are highly efficient for bioconjugation reactions and exhibit excellent selectivities for a single functional group that can be easily installed by both chemical and biochemical approaches, in different proteins. Peptide and protein studies have shown that a diverse array of stable bioconjugates can be obtained rapidly under mild reaction conditions. Although some aldehyde bioconjugations often suffer from low conversion and slow reaction rate, no such effect was seen for this methodology. Very high conversions into protein bioconjugates were observed under the reaction conditions as shown in Figures 6 and 7. This approach leads to the nitroalkylation of proteins in a selective manner, and thus mimic a key PTM of proteins. Such nitro-alkylated proteins can be used to investigate the role of these PTMs in various cellular processes and enzyme functions. The nitro-alkylated proteins enable rapid detection of labeled peptides using MS/MS fragmentation, even if they are present in low abundance, because of the unique fingerprint pattern for the parent peptide resulting from the loss of the nitro species. This detection is significant because nitroalkane peptides can be identified in a complex mixture without the need for enrichment of the nitroalkane-bound peptides. Importantly, dinitroalkanes react exclusively with dialdehyde peptides to form peptide staples of different sizes. Considering the easy synthesis of a variety of nitroalkane derivatives (fluorescent tag, NMR tag, and an affinity tag) and their ability to carry out rapid and highly selective bioconjugation of proteins and peptide stapling with very high conversions (99%), we anticipate that this method will become a highly useful tool in many fields, including chemical biology and medicinal chemistry.

3.4 References

(1) Salehi, D.; Mozaffari, S.; Zoghebi, K.; Lohan, S.; Mandal, D.; Tiwari, R. K.; Parang, K. Amphiphilic Cell-Penetrating Peptides Containing Natural and Unnatural Amino Acids as Drug Delivery Agents. *Cells* **2022**, *11* (7). DOI: 10.3390/cells11071156 From NLM.
(2) Joo, S. H. Cyclic peptides as therapeutic agents and biochemical tools. *Biomol Ther (Seoul)* **2012**, *20* (1), 19-26. DOI: 10.4062/biomolther.2012.20.1.019 From NLM.
(3) Hummel, G.; Reineke, U.; Reimer, U. Translating peptides into small molecules. *Mol Biosyst* **2006**, *2* (10), 499-508. DOI: 10.1039/b611791k From NLM.
(4) Loffet, A. Peptides as Drugs: Is There a Market? *Journal of Peptide Science* **2002**, *8* (1), 1-7. DOI: https://doi.org/10.1002/psc.366.
(5) Horton, D. A.; Bourne, G. T.; Smythe, M. L. Exploring privileged structures: the combinatorial synthesis of cyclic peptides. *Journal of Computer-Aided Molecular Design* **2002**, *16* (5), 415-431. DOI: 10.1023/A:1020863921840.
(6) Wills, R.; Adebomi, V.; Raj, M. Site-Selective Peptide Macrocyclization. *ChemBioChem* **2021**, *22* (1), 52-62. DOI: https://doi.org/10.1002/cbic.202000398.
(7) White, C. J.; Yudin, A. K. Contemporary strategies for peptide macrocyclization. *Nature Chemistry* **2011**, *3* (7), 509-524. DOI: 10.1038/nchem.1062. Lambert, J. N.; Mitchell, J. P.; Roberts, K. D. The synthesis of cyclic peptides. *Journal of the Chemical Society, Perkin Transactions 1* **2001**, (5), 471-484, 10.1039/B001942I. DOI: 10.1039/B001942I. Le, D. N.; Riedel, J.; Kozlyuk, N.; Martin, R. W.; Dong, V. M. Cyclizing Pentapeptides: Mechanism and Application of Dehydrophenylalanine as a Traceless Turn-Inducer. *Organic Letters* **2017**, *19* (1), 114-117. DOI: 10.1021/acs.orglett.6b03308. Fairweather, K. A.; Sayyadi, N.; Luck, I. J.; Clegg, J. K.; Jolliffe, K. A. Synthesis of All-l Cyclic Tetrapeptides Using Pseudoprolines as Removable Turn Inducers. *Organic Letters* **2010**, *12* (14), 3136-3139. DOI: 10.1021/ol101018w. Wong, C. T. T.; Lam, H. Y.; Song, T.; Chen, G.; Li, X. Synthesis of Constrained Head-to-Tail Cyclic Tetrapeptides by an Imine-Induced Ring-Closing/Contraction Strategy. *Angewandte Chemie International Edition* **2013**, *52* (39), 10212-10215. DOI: https://doi.org/10.1002/anie.201304773.
(8) Tsukamoto, H.; Hanada, S.; Nomura, Y.; Doi, T. Total Synthesis of Spiromamakone A and Structure Revision of Spiropreussione A. *The Journal of Organic Chemistry* **2018**, *83* (16), 9430-9441. DOI: 10.1021/acs.joc.8b01075.
(9) Aboul-Enein, M. N.; El-Azzouny, A. A. S.; Saleh, O. A.; Amin, K. M.; Maklad, Y. A.; Hassan, R. M. Synthesis and Anticonvulsant Activity of Substituted-1,3-diazaspiro[4.5]decan-4-ones. *Archiv der Pharmazie* **2015**, *348* (8), 575-588. DOI: https://doi.org/10.1002/ardp.201500092.
(10) O'Reilly, M. C.; Scott, S. A.; Brown, K. A.; Oguin, T. H.; Thomas, P. G.; Daniels, J. S.; Morrison, R.; Brown, H. A.; Lindsley, C. W. Development of Dual PLD1/2 and PLD2 Selective Inhibitors from a Common 1,3,8-Triazaspiro[4.5]decane Core: Discovery of ML298 and ML299 That Decrease Invasive Migration in U87-MG Glioblastoma Cells. *Journal of Medicinal Chemistry* **2013**, *56* (6), 2695-2699. DOI: 10.1021/jm301782e.
(11) Chang, S. D.; Brieaddy, L. E.; Harvey, J. D.; Lewin, A. H.; Mascarella, S. W.; Seltzman, H. H.; Reddy, P. A.; Decker, A. M.; McElhinny, C. J.; Zhong, D.; et al. Novel Synthesis and Pharmacological Characterization of NOP Receptor Agonist 8-[(1S,3aS)-2,3,3a,4,5,6-Hexahydro-1H-phenalen-1-yl]-1-phenyl-1,3,8-triazaspiro[4.5]decan-4-one (Ro 64-6198). *ACS Chemical Neuroscience* **2015**, *6* (12), 1956-1964. DOI: 10.1021/acschemneuro.5b00208.
(12) Molinski, T. F.; Ko, J.; Reynolds, K. A.; Lievens, S. C.; Skarda, K. R. N,N′-Methyleno-didemnin A from the Ascidian Tridemnum solidum. Complete NMR Assignments and

Confirmation of the Imidazolidinone Ring by Strategic Analysis of 1JCH. *Journal of Natural Products* **2011**, *74* (4), 882-887. DOI: 10.1021/np100846s.
(13) Ji, D.; Sun, J. [3 + 2]-Cycloaddition of Azaoxyallyl Cations with Hexahydro-1,3,5-triazines: Access to 4-Imidazolidinones. *Organic Letters* **2018**, *20* (9), 2745-2748. DOI: 10.1021/acs.orglett.8b00951. Mach, R. H.; Jackson, J. R.; Luedtke, R. R.; Ivins, K. J.; Molinoff, P. B.; Ehrenkaufer, R. L. Effect of N-alkylation on the affinities of analogs of spiperone for dopamine D2 and serotonin 5-HT2 receptors. *Journal of Medicinal Chemistry* **1992**, *35* (3), 423-430. DOI: 10.1021/jm00081a002.
(14) Pagenkopf, B. ACD/HNMR Predictor and ACD/CNMR Predictor Advanced Chemistry Development, Inc. (ACD/Labs), 90 Adelaide Street West, Suite 600, Toronto, ON M5H 2V9, Canada. www.acdlabs.com. See Web site for pricing information. *Journal of the American Chemical Society* **2005**, *127* (9), 3232-3232. DOI: 10.1021/ja040946z.
(15) Bielawski, C. W.; Benitez, D.; Grubbs, R. H. An "Endless" Route to Cyclic Polymers. *Science* **2002**, *297* (5589), 2041-2044. DOI: doi:10.1126/science.1075401. Lawson, K. V.; Rose, T. E.; Harran, P. G. Template-constrained macrocyclic peptides prepared from native, unprotected precursors. *Proceedings of the National Academy of Sciences* **2013**, *110* (40), E3753-E3760. DOI: doi:10.1073/pnas.1311706110. Gracia, S. R.; Gaus, K.; Sewald, N. Synthesis of chemically modified bioactive peptides: recent advances, challenges and developments for medicinal chemistry. *Future Medicinal Chemistry* **2009**, *1* (7), 1289-1310. DOI: 10.4155/fmc.09.97. Skropeta, D.; Jolliffe, K. A.; Turner, P. Pseudoprolines as Removable Turn Inducers: Tools for the Cyclization of Small Peptides. *The Journal of Organic Chemistry* **2004**, *69* (25), 8804-8809. DOI: 10.1021/jo0484732. Ehrlich, A.; Heyne, H.-U.; Winter, R.; Beyermann, M.; Haber, H.; Carpino, L. A.; Bienert, M. Cyclization of all-l-Pentapeptides by Means of 1-Hydroxy-7-azabenzotriazole-Derived Uronium and Phosphonium Reagents. *The Journal of Organic Chemistry* **1996**, *61* (25), 8831-8838. DOI: 10.1021/jo951108d.
(16) Malesevic, M.; Strijowski, U.; Bächle, D.; Sewald, N. An improved method for the solution cyclization of peptides under pseudo-high dilution conditions. *Journal of Biotechnology* **2004**, *112* (1), 73-77. DOI: https://doi.org/10.1016/j.jbiotec.2004.03.015. Wessjohann, L. A.; Kreye, O.; Rivera, D. G. One-Pot Assembly of Amino Acid Bridged Hybrid Macromulticyclic Cages through Multiple Multicomponent Macrocyclizations. *Angewandte Chemie International Edition* **2017**, *56* (13), 3501-3505. DOI: https://doi.org/10.1002/anie.201610801. Martí-Centelles, V.; Pandey, M. D.; Burguete, M. I.; Luis, S. V. Macrocyclization Reactions: The Importance of Conformational, Configurational, and Template-Induced Preorganization. *Chemical Reviews* **2015**, *115* (16), 8736-8834. DOI: 10.1021/acs.chemrev.5b00056.
(17) Hili, R.; Rai, V.; Yudin, A. K. Macrocyclization of Linear Peptides Enabled by Amphoteric Molecules. *Journal of the American Chemical Society* **2010**, *132* (9), 2889-2891. DOI: 10.1021/ja910544p. Frost, J. R.; Scully, C. C. G.; Yudin, A. K. Oxadiazole grafts in peptide macrocycles. *Nature Chemistry* **2016**, *8* (12), 1105-1111. DOI: 10.1038/nchem.2636.
(18) Malins, L. R.; deGruyter, J. N.; Robbins, K. J.; Scola, P. M.; Eastgate, M. D.; Ghadiri, M. R.; Baran, P. S. Peptide Macrocyclization Inspired by Non-Ribosomal Imine Natural Products. *Journal of the American Chemical Society* **2017**, *139* (14), 5233-5241. DOI: 10.1021/jacs.7b01624.
(19) Davis, A. C.; Levy, A. L. 768. The interaction of α-amino-nitriles and aldehydes and ketones. *Journal of the Chemical Society (Resumed)* **1951**, (0), 3479-3489, 10.1039/JR9510003479. DOI: 10.1039/JR9510003479.

(20) Federsel, H. J.; Koenberg, E.; Lilljequist, L.; Swahn, B. M. Dichloromethane as reactant in synthesis: an expedient transformation of prolinamide to a novel pyrrolo[1,2-c]imidazolone. *The Journal of Organic Chemistry* **1990**, *55* (7), 2254-2256. DOI: 10.1021/jo00294a056.
(21) Kumagai, H.; Tajima, M.; Ueno, Y.; Giga-Hama, Y.; Ohba, M. Effect of cyclic RGD peptide on cell adhesion and tumor metastasis. *Biochemical and Biophysical Research Communications* **1991**, *177* (1), 74-82. DOI: https://doi.org/10.1016/0006-291X(91)91950-H. Dechantsreiter, M. A.; Planker, E.; Mathä, B.; Lohof, E.; Hölzemann, G.; Jonczyk, A.; Goodman, S. L.; Kessler, H. N-Methylated Cyclic RGD Peptides as Highly Active and Selective αVβ3 Integrin Antagonists. *Journal of Medicinal Chemistry* **1999**, *42* (16), 3033-3040. DOI: 10.1021/jm970832g.
(22) Jain, A. N.; Cleves, A. E.; Gao, Q.; Wang, X.; Liu, Y.; Sherer, E. C.; Reibarkh, M. Y. Complex macrocycle exploration: parallel, heuristic, and constraint-based conformer generation using ForceGen. *Journal of Computer-Aided Molecular Design* **2019**, *33* (6), 531-558. DOI: 10.1007/s10822-019-00203-1.
(23) Weigend, F.; Ahlrichs, R. Balanced basis sets of split valence, triple zeta valence and quadruple zeta valence quality for H to Rn: Design and assessment of accuracy. *Physical Chemistry Chemical Physics* **2005**, *7* (18), 3297-3305, 10.1039/B508541A. DOI: 10.1039/B508541A.
(24) Lee, C.; Yang, W.; Parr, R. G. Development of the Colle-Salvetti correlation-energy formula into a functional of the electron density. *Phys Rev B Condens Matter* **1988**, *37* (2), 785-789. DOI: 10.1103/physrevb.37.785 From NLM.
(25) Marenich, A. V.; Cramer, C. J.; Truhlar, D. G. Universal Solvation Model Based on Solute Electron Density and on a Continuum Model of the Solvent Defined by the Bulk Dielectric Constant and Atomic Surface Tensions. *The Journal of Physical Chemistry B* **2009**, *113* (18), 6378-6396. DOI: 10.1021/jp810292n.
(26) Towns, J.; Cockerill, T.; Dahan, M.; Foster, I.; Gaither, K.; Grimshaw, A.; Hazlewood, V.; Lathrop, S.; Lifka, D.; Peterson, G. D.; et al. XSEDE: Accelerating Scientific Discovery. *Computing in Science and Engineering* **2014**, *16*, 62-74. DOI: 10.1109/mcse.2014.80.
(27) Luchini, G.; Alegre-Requena, J.; Funes-Ardoiz, I.; Paton, R. GoodVibes: automated thermochemistry for heterogeneous computational chemistry data [version 1; peer review: 2 approved with reservations]. *F1000Research* **2020**, *9* (291). DOI: 10.12688/f1000research.22758.1.
(28) Pracht, P.; Bohle, F.; Grimme, S. Automated exploration of the low-energy chemical space with fast quantum chemical methods. *Physical Chemistry Chemical Physics* **2020**, *22* (14), 7169-7192, 10.1039/C9CP06869D. DOI: 10.1039/C9CP06869D.
(29) Sarojini, V.; Cameron, A. J.; Varnava, K. G.; Denny, W. A.; Sanjayan, G. Cyclic Tetrapeptides from Nature and Design: A Review of Synthetic Methodologies, Structure, and Function. *Chem Rev* **2019**, *119* (17), 10318-10359. DOI: 10.1021/acs.chemrev.8b00737 From NLM.
(30) Adebomi, V.; Cohen, R. D.; Wills, R.; Chavers, H. A. H.; Martin, G. E.; Raj, M. CyClick Chemistry for the Synthesis of Cyclic Peptides. *Angewandte Chemie International Edition* **2019**, *58* (52), 19073-19080. DOI: https://doi.org/10.1002/anie.201911900.
(31) Wills, R.; Adebomi, V.; Spancake, C.; Cohen, R. D.; Raj, M. Synthesis of L-cyclic tetrapeptides by backbone amide activation CyClick strategy. *Tetrahedron* **2022**, 133071. DOI: https://doi.org/10.1016/j.tet.2022.133071.

(32) Sarojini, V.; Cameron, A. J.; Varnava, K. G.; Denny, W. A.; Sanjayan, G. Cyclic Tetrapeptides from Nature and Design: A Review of Synthetic Methodologies, Structure, and Function. *Chemical Reviews* **2019**, *119* (17), 10318-10359. DOI: 10.1021/acs.chemrev.8b00737.
(33) El Haddadi, M.; Cavelier, F.; Vives, E.; Azmani, A.; Verducci, J.; Martinez, J. All-l-Leu-Pro-Leu-Pro: a challenging cyclization. *Journal of Peptide Science: An Official Publication of the European Peptide Society* **2000**, *6* (11), 560-570.
(34) Bechtler, C.; Lamers, C. Macrocyclization strategies for cyclic peptides and peptidomimetics. *RSC Medicinal Chemistry* **2021**, *12* (8), 1325-1351, 10.1039/D1MD00083G. DOI: 10.1039/D1MD00083G.
(35) Chongsiriwatana, N. P.; Patch, J. A.; Czyzewski, A. M.; Dohm, M. T.; Ivankin, A.; Gidalevitz, D.; Zuckermann, R. N.; Barron, A. E. Peptoids that mimic the structure, function, and mechanism of helical antimicrobial peptides. *Proceedings of the National Academy of Sciences* **2008**, *105* (8), 2794-2799. DOI: doi:10.1073/pnas.0708254105.
(36) Schwochert, J.; Turner, R.; Thang, M.; Berkeley, R. F.; Ponkey, A. R.; Rodriguez, K. M.; Leung, S. S. F.; Khunte, B.; Goetz, G.; Limberakis, C.; et al. Peptide to Peptoid Substitutions Increase Cell Permeability in Cyclic Hexapeptides. *Organic Letters* **2015**, *17* (12), 2928-2931. DOI: 10.1021/acs.orglett.5b01162.
(37) Molchanova, N.; Hansen, P. R.; Franzyk, H. Advances in Development of Antimicrobial Peptidomimetics as Potential Drugs. *Molecules* **2017**, *22* (9), 1430.
(38) Caumes, C.; Fernandes, C.; Roy, O.; Hjelmgaard, T.; Wenger, E.; Didierjean, C.; Taillefumier, C.; Faure, S. Cyclic α,β-Tetrapeptoids: Sequence-Dependent Cyclization and Conformational Preference. *Organic Letters* **2013**, *15* (14), 3626-3629. DOI: 10.1021/ol401478j.
(39) Feng, M.; Zhang, H.; Maulide, N. Challenges and and Breakthroughs in Selective Amide Activation. *Angew Chem Int Ed Engl* **2022**. DOI: 10.1002/anie.202212213 From NLM.
(40) Mahesh, S.; Tang, K.-C.; Raj, M. Amide Bond Activation of Biological Molecules. *Molecules* **2018**, *23* (10), 2615.
(41) Meng, G.; Zhang, J.; Szostak, M. Acyclic Twisted Amides. *Chemical Reviews* **2021**, *121* (20), 12746-12783. DOI: 10.1021/acs.chemrev.1c00225.
(42) Smith, R. M.; Hansen, D. E. The pH-Rate Profile for the Hydrolysis of a Peptide Bond. *Journal of the American Chemical Society* **1998**, *120* (35), 8910-8913. DOI: 10.1021/ja9804565.
(43) Radzicka, A.; Wolfenden, R. Rates of Uncatalyzed Peptide Bond Hydrolysis in Neutral Solution and the Transition State Affinities of Proteases. *Journal of the American Chemical Society* **1996**, *118* (26), 6105-6109. DOI: 10.1021/ja954077c.
(44) Hie, L.; Fine Nathel, N. F.; Shah, T. K.; Baker, E. L.; Hong, X.; Yang, Y. F.; Liu, P.; Houk, K. N.; Garg, N. K. Conversion of amides to esters by the nickel-catalysed activation of amide C-N bonds. *Nature* **2015**, *524* (7563), 79-83. DOI: 10.1038/nature14615 From NLM.
(45) Baker, E. L.; Yamano, M. M.; Zhou, Y.; Anthony, S. M.; Garg, N. K. A two-step approach to achieve secondary amide transamidation enabled by nickel catalysis. *Nat Commun* **2016**, *7*, 11554. DOI: 10.1038/ncomms11554 From NLM. Yu, S.; Shin, T.; Zhang, M.; Xia, Y.; Kim, H.; Lee, S. Nickel/Briphos-Catalyzed Direct Transamidation of Unactivated Secondary Amides Using Trimethylsilyl Chloride. *Organic Letters* **2018**, *20* (23), 7563-7566. DOI: 10.1021/acs.orglett.8b03304.
(46) Dander, J. E.; Baker, Emma L.; Garg, N. K. Nickel-catalyzed transamidation of aliphatic amide derivatives. *Chemical Science* **2017**, *8* (9), 6433-6438, 10.1039/C7SC01980G. DOI: 10.1039/C7SC01980G. Cheung, C. W.; Ploeger, M. L.; Hu, X. Nickel-Catalyzed Reductive

Transamidation of Secondary Amides with Nitroarenes. *ACS Catalysis* **2017**, *7* (10), 7092-7096. DOI: 10.1021/acscatal.7b02859.
(47) Boit, T. B.; Mehta, M. M.; Kim, J.; Baker, E. L.; Garg, N. K. Reductive Arylation of Amides via a Nickel-Catalyzed Suzuki-Miyaura-Coupling and Transfer-Hydrogenation Cascade. *Angew Chem Int Ed Engl* **2021**, *60* (5), 2472-2477. DOI: 10.1002/anie.202012048 From NLM.
(48) Boit, T. B.; Bulger, A. S.; Dander, J. E.; Garg, N. K. Activation of C–O and C–N Bonds Using Non-Precious-Metal Catalysis. *ACS Catalysis* **2020**, *10* (20), 12109-12126. DOI: 10.1021/acscatal.0c03334.
(49) Chaudhari, M. B.; Gnanaprakasam, B. Recent Advances in the Metal-Catalyzed Activation of Amide Bonds. *Chemistry – An Asian Journal* **2019**, *14* (1), 76-93. DOI: https://doi.org/10.1002/asia.201801317.
(50) Liu, Y.; Shi, S.; Achtenhagen, M.; Liu, R.; Szostak, M. Metal-Free Transamidation of Secondary Amides via Selective N-C Cleavage under Mild Conditions. *Org Lett* **2017**, *19* (7), 1614-1617. DOI: 10.1021/acs.orglett.7b00429 From NLM. Joseph, D.; Oh, M. S.; Jayaraman, A.; Lee, S. Amides Activation: Transition Metal-Free Coupling Between C□N Activated Amides and Enolizable Amides. *Bulletin of the Korean Chemical Society* **2021**, *42* (10), 1293-1295. DOI: https://doi.org/10.1002/bkcs.12371.
(51) Li, G.; Szostak, M. Highly selective transition-metal-free transamidation of amides and amidation of esters at room temperature. *Nature Communications* **2018**, *9* (1), 4165. DOI: 10.1038/s41467-018-06623-1.
(52) Szostak, M.; Aubé, J. Chemistry of Bridged Lactams and Related Heterocycles. *Chemical Reviews* **2013**, *113* (8), 5701-5765. DOI: 10.1021/cr4000144.
(53) Kemnitz, C. R.; Loewen, M. J. "Amide Resonance" Correlates with a Breadth of C−N Rotation Barriers. *Journal of the American Chemical Society* **2007**, *129* (9), 2521-2528. DOI: 10.1021/ja0663024.
(54) Clayden, J.; Moran, W. J. The Twisted Amide 2-Quinuclidone: 60 Years in the Making. *Angewandte Chemie International Edition* **2006**, *45* (43), 7118-7120. DOI: https://doi.org/10.1002/anie.200603016. Szostak, M.; Aubé, J. Medium-bridged lactams: a new class of non-planar amides. *Organic & Biomolecular Chemistry* **2011**, *9* (1), 27-35, 10.1039/C0OB00215A. DOI: 10.1039/C0OB00215A.
(55) Mujika, J. I.; Matxain, J. M.; Eriksson, L. A.; Lopez, X. Resonance Structures of the Amide Bond: The Advantages of Planarity. *Chemistry – A European Journal* **2006**, *12* (27), 7215-7224. DOI: https://doi.org/10.1002/chem.200600052.
(56) Mucsi, Z.; Tsai, A.; Szori, M.; Chass, G. A.; Viskolcz, B.; Csizmadia, I. G. A Quantitative Scale for the Extent of Conjugation of the Amide Bond. Amidity Percentage as a Chemical Driving Force. *The Journal of Physical Chemistry A* **2007**, *111* (50), 13245-13254. DOI: 10.1021/jp0759325.
(57) Morgan, J.; Greenberg, A. Novel bridgehead bicyclic lactams: (a) Molecules predicted to have O-protonated and N-protonated tautomers of comparable stability; (b) hyperstable lactams and their O-protonated tautomers. *The Journal of Chemical Thermodynamics* **2014**, *73*, 206-212. DOI: https://doi.org/10.1016/j.jct.2013.12.034.
(58) Liu, C.; Szostak, M. Twisted Amides: From Obscurity to Broadly Useful Transition-Metal-Catalyzed Reactions by N−C Amide Bond Activation. *Chemistry – A European Journal* **2017**, *23* (30), 7157-7173. DOI: https://doi.org/10.1002/chem.201605012.
(59) Tani, K.; Stoltz, B. M. Synthesis and structural analysis of 2-quinuclidonium tetrafluoroborate. *Nature* **2006**, *441* (7094), 731-734. DOI: 10.1038/nature04842 From NLM.

(60) Kirby, A. J.; Komarov, I. V.; Wothers, P. D.; Feeder, N. The Most Twisted Amide: Structure and Reactions. *Angew Chem Int Ed Engl* **1998**, *37* (6), 785-786. DOI: 10.1002/(sici)1521-3773(19980403)37:6<785::Aid-anie785>3.0.Co;2-j From NLM. Kirby, A. J.; Komarov, I. V.; Feeder, N. Synthesis, structure and reactions of the most twisted amide. *Journal of the Chemical Society, Perkin Transactions 2* **2001**, (4), 522-529, 10.1039/B008270H. DOI: 10.1039/B008270H.
(61) Liu, C.; Shi, S.; Liu, Y.; Liu, R.; Lalancette, R.; Szostak, R.; Szostak, M. The Most Twisted Acyclic Amides: Structures and Reactivity. *Organic Letters* **2018**, *20* (24), 7771-7774. DOI: 10.1021/acs.orglett.8b03175.
(62) Takezawa, H.; Shitozawa, K.; Fujita, M. Enhanced reactivity of twisted amides inside a molecular cage. *Nature Chemistry* **2020**, *12* (6), 574-578. DOI: 10.1038/s41557-020-0455-y.
(63) Liu, Y.; Meng, G.; Liu, R.; Szostak, M. Sterically-controlled intermolecular Friedel–Crafts acylation with twisted amides via selective N–C cleavage under mild conditions. *Chemical Communications* **2016**, *52* (41), 6841-6844, 10.1039/C6CC02324J. DOI: 10.1039/C6CC02324J.
(64) Meng, G.; Shi, S.; Lalancette, R.; Szostak, R.; Szostak, M. Reversible Twisting of Primary Amides via Ground State N–C(O) Destabilization: Highly Twisted Rotationally Inverted Acyclic Amides. *Journal of the American Chemical Society* **2018**, *140* (2), 727-734. DOI: 10.1021/jacs.7b11309.
(65) Li, X.; Zou, G. Acylative Suzuki coupling of amides: acyl-nitrogen activation via synergy of independently modifiable activating groups. *Chemical Communications* **2015**, *51* (24), 5089-5092, 10.1039/C5CC00430F. DOI: 10.1039/C5CC00430F.
(66) Meng, G.; Szostak, M. Sterically Controlled Pd-Catalyzed Chemoselective Ketone Synthesis via N–C Cleavage in Twisted Amides. *Organic Letters* **2015**, *17* (17), 4364-4367. DOI: 10.1021/acs.orglett.5b02209.
(67) Pace, V.; Holzer, W.; Meng, G.; Shi, S.; Lalancette, R.; Szostak, R.; Szostak, M. Structures of Highly Twisted Amides Relevant to Amide N−C Cross-Coupling: Evidence for Ground-State Amide Destabilization. *Chemistry – A European Journal* **2016**, *22* (41), 14494-14498. DOI: https://doi.org/10.1002/chem.201603543.
(68) Shi, S.; Meng, G.; Szostak, M. Synthesis of Biaryls through Nickel-Catalyzed Suzuki-Miyaura Coupling of Amides by Carbon-Nitrogen Bond Cleavage. *Angew Chem Int Ed Engl* **2016**, *55* (24), 6959-6963. DOI: 10.1002/anie.201601914 From NLM.
(69) Meng, G.; Szostak, M. N-Acyl-Glutarimides: Privileged Scaffolds in Amide N–C Bond Cross-Coupling. *European Journal of Organic Chemistry* **2018**, *2018* (20-21), 2352-2365. DOI: https://doi.org/10.1002/ejoc.201800109.
(70) Shi, S.; Szostak, M. Efficient Synthesis of Diaryl Ketones by Nickel-Catalyzed Negishi Cross-Coupling of Amides by Carbon–Nitrogen Bond Cleavage at Room Temperature Accelerated by a Solvent Effect. *Chemistry – A European Journal* **2016**, *22* (30), 10420-10424. DOI: https://doi.org/10.1002/chem.201602202.
(71) Meng, G.; Szostak, M. General Olefin Synthesis by the Palladium-Catalyzed Heck Reaction of Amides: Sterically Controlled Chemoselective N-C Activation. *Angew Chem Int Ed Engl* **2015**, *54* (48), 14518-14522. DOI: 10.1002/anie.201507776 From NLM.
(72) Szostak, R.; Shi, S.; Meng, G.; Lalancette, R.; Szostak, M. Ground-State Distortion in N-Acyl-tert-butyl-carbamates (Boc) and N-Acyl-tosylamides (Ts): Twisted Amides of Relevance to Amide N–C Cross-Coupling. *The Journal of Organic Chemistry* **2016**, *81* (17), 8091-8094. DOI: 10.1021/acs.joc.6b01560.

(73) Griffin, B. A.; Adams, S. R.; Tsien, R. Y. Specific covalent labeling of recombinant protein molecules inside live cells. *Science* **1998**, *281* (5374), 269-272.
(74) Simmons, B. J.; Weires, N. A.; Dander, J. E.; Garg, N. K. Nickel-Catalyzed Alkylation of Amide Derivatives. *ACS Catalysis* **2016**, *6* (5), 3176-3179. DOI: 10.1021/acscatal.6b00793.
(75) Jana, R.; Pathak, T. P.; Sigman, M. S. Advances in Transition Metal (Pd,Ni,Fe)-Catalyzed Cross-Coupling Reactions Using Alkyl-organometallics as Reaction Partners. *Chemical Reviews* **2011**, *111* (3), 1417-1492. DOI: 10.1021/cr100327p.
(76) Hu, J.; Zhao, Y.; Liu, J.; Zhang, Y.; Shi, Z. Nickel-Catalyzed Decarbonylative Borylation of Amides: Evidence for Acyl C−N Bond Activation. *Angewandte Chemie International Edition* **2016**, *55* (30), 8718-8722. DOI: https://doi.org/10.1002/anie.201603068.
(77) Boit, T. B.; Weires, N. A.; Kim, J.; Garg, N. K. Nickel-Catalyzed Suzuki–Miyaura Coupling of Aliphatic Amides. *ACS Catalysis* **2018**, *8* (2), 1003-1008. DOI: 10.1021/acscatal.7b03688. Knapp, R. R.; Bulger, A. S.; Garg, N. K. Nickel-Catalyzed Conversion of Amides to Carboxylic Acids. *Organic Letters* **2020**, *22* (7), 2833-2837. DOI: 10.1021/acs.orglett.0c00885.
(78) Elashal, H. E.; Cohen, R. D.; Elashal, H. E.; Zong, C.; Link, A. J.; Raj, M. Cyclic and Lasso Peptides: Sequence Determination, Topology Analysis, and Rotaxane Formation. *Angewandte Chemie International Edition* **2018**, *57* (21), 6150-6154, https://doi.org/10.1002/anie.201801299. DOI: https://doi.org/10.1002/anie.201801299 (acccessed 2022/10/07).
(79) Elashal, H. E.; Raj, M. Site-selective chemical cleavage of peptide bonds. *Chemical Communications* **2016**, *52* (37), 6304-6307, 10.1039/C6CC01509C. DOI: 10.1039/C6CC01509C.
(80) Winkler, F. K.; Dunitz, J. D. The non-planar amide group. *Journal of Molecular Biology* **1971**, *59* (1), 169-182. DOI: https://doi.org/10.1016/0022-2836(71)90419-0.
(81) Shi, S.; Nolan, S. P.; Szostak, M. Well-Defined Palladium(II)–NHC Precatalysts for Cross-Coupling Reactions of Amides and Esters by Selective N–C/O–C Cleavage. *Accounts of Chemical Research* **2018**, *51* (10), 2589-2599. DOI: 10.1021/acs.accounts.8b00410.
(82) Meng, G.; Szostak, R.; Szostak, M. Suzuki–Miyaura Cross-Coupling of N-Acylpyrroles and Pyrazoles: Planar, Electronically Activated Amides in Catalytic N–C Cleavage. *Organic Letters* **2017**, *19* (13), 3596-3599. DOI: 10.1021/acs.orglett.7b01575.
(83) Raja, E. K.; DeSchepper, D. J.; Lill, S. O. N.; Klumpp, D. A. Friedel-Crafts acylation with amides. *The Journal of organic chemistry* **2012**, *77* (13), 5788-5793. DOI: 10.1021/jo300922p PubMed. Anderson, K. W.; Tepe, J. J. The first intermolecular Friedel-Crafts acylation with beta-lactams. *Org Lett* **2002**, *4* (3), 459-461. DOI: 10.1021/ol010291w From NLM. Ohkubo, K.; Yoshida, T.; Tomiyoshi, K.; Okada, M. Electronic structures and configurational transformations of some protonated compounds. *Journal of Molecular Structure* **1976**, *34* (2), 273-281. DOI: https://doi.org/10.1016/0022-2860(76)82011-X.
(84) van Kasteren, S. I.; Kramer, H. B.; Jensen, H. H.; Campbell, S. J.; Kirkpatrick, J.; Oldham, N. J.; Anthony, D. C.; Davis, B. G. Expanding the diversity of chemical protein modification allows post-translational mimicry. *Nature* **2007**, *446* (7139), 1105-1109. DOI: 10.1038/nature05757 From NLM Medline. Zheng, M.; Zheng, L.; Zhang, P.; Li, J.; Zhang, Y. Development of Bioorthogonal Reactions and Their Applications in Bioconjugation. *Molecules* **2015**, *20* (2), 3190-3205.
(85) Krall, N.; da Cruz, F. P.; Boutureira, O.; Bernardes, G. J. L. Site-selective protein-modification chemistry for basic biology and drug development. *Nature Chemistry* **2016**, *8* (2), 103-113. DOI: 10.1038/nchem.2393.
(86) MacDonald, J. I.; Munch, H. K.; Moore, T.; Francis, M. B. One-step site-specific modification of native proteins with 2-pyridinecarboxyaldehydes. *Nature Chemical Biology* **2015**, *11* (5), 326-

331. DOI: 10.1038/nchembio.1792. Ducry, L.; Stump, B. Antibody−Drug Conjugates: Linking Cytotoxic Payloads to Monoclonal Antibodies. *Bioconjugate Chemistry* **2010**, *21* (1), 5-13. DOI: 10.1021/bc9002019.
(87) Chang, P. V.; Prescher, J. A.; Sletten, E. M.; Baskin, J. M.; Miller, I. A.; Agard, N. J.; Lo, A.; Bertozzi, C. R. Copper-free click chemistry in living animals. *Proceedings of the National Academy of Sciences* **2010**, *107* (5), 1821-1826. DOI: doi:10.1073/pnas.0911116107. McKay, Craig S.; Finn, M. G. Click Chemistry in Complex Mixtures: Bioorthogonal Bioconjugation. *Chemistry & Biology* **2014**, *21* (9), 1075-1101. DOI: https://doi.org/10.1016/j.chembiol.2014.09.002.
(88) Dirksen, A.; Dirksen, S.; Hackeng, T. M.; Dawson, P. E. Nucleophilic Catalysis of Hydrazone Formation and Transimination: Implications for Dynamic Covalent Chemistry. *Journal of the American Chemical Society* **2006**, *128* (49), 15602-15603. DOI: 10.1021/ja067189k.
(89) Dirksen, A.; Hackeng, T. M.; Dawson, P. E. Nucleophilic Catalysis of Oxime Ligation. *Angewandte Chemie International Edition* **2006**, *45* (45), 7581-7584. DOI: https://doi.org/10.1002/anie.200602877.
(90) Wendeler, M.; Grinberg, L.; Wang, X.; Dawson, P. E.; Baca, M. Enhanced Catalysis of Oxime-Based Bioconjugations by Substituted Anilines. *Bioconjugate Chemistry* **2014**, *25* (1), 93-101. DOI: 10.1021/bc400380f. Kalia, J.; Raines, R. T. Hydrolytic stability of hydrazones and oximes. *Angewandte Chemie International Edition* **2008**, *47* (39), 7523-7526.
(91) Eickbush, T. H.; Moudrianakis, E. N. The histone core complex: an octamer assembled by two sets of protein-protein interactions. *Biochemistry* **1978**, *17* (23), 4955-4964. Huang, Y.-X.; Wu, Z.-J.; Huang, B.-T.; Luo, M. Pathway and mechanism of pH dependent human hemoglobin tetramer-dimer-monomer dissociations. *PLoS One* **2013**, *8* (11), e81708.
(92) Tipping, K. W.; Karamanos, T. K.; Jakhria, T.; Iadanza, M. G.; Goodchild, S. C.; Tuma, R.; Ranson, N. A.; Hewitt, E. W.; Radford, S. E. pH-induced molecular shedding drives the formation of amyloid fibril-derived oligomers. *Proceedings of the National Academy of Sciences* **2015**, *112* (18), 5691-5696. Swietnicki, W.; Petersen, R.; Gambetti, P.; Surewicz, W. K. pH-dependent stability and conformation of the recombinant human prion protein PrP (90–231). *Journal of Biological Chemistry* **1997**, *272* (44), 27517-27520.
(93) Sasaki, T.; Kodama, K.; Suzuki, H.; Fukuzawa, S.; Tachibana, K. N-terminal labeling of proteins by the Pictet–Spengler reaction. *Bioorganic & medicinal chemistry letters* **2008**, *18* (16), 4550-4553.
(94) Alam, J.; Keller, T. H.; Loh, T.-P. Indium mediated allylation in peptide and protein functionalization. *Chemical Communications* **2011**, *47* (32), 9066-9068.
(95) Han, M.-J.; Xiong, D.-C.; Ye, X.-S. Enabling Wittig reaction on site-specific protein modification. *Chemical Communications* **2012**, *48* (90), 11079-11081.
(96) Howard, T. S.; Cohen, R. D.; Nwajiobi, O.; Muneeswaran, Z. P.; Sim, Y. E.; Lahankar, N. N.; Yeh, J. T.-H.; Raj, M. Amino-Acid-Catalyzed Direct Aldol Bioconjugation. *Organic letters* **2018**, *20* (17), 5344-5347.
(97) Alam, J.; Keller, T. H.; Loh, T.-P. Functionalization of peptides and proteins by Mukaiyama aldol reaction. *Journal of the American Chemical Society* **2010**, *132* (28), 9546-9548. Wang, P.; Zhang, S.; Meng, Q.; Liu, Y.; Shang, L.; Yin, Z. Site-specific chemical modification of peptide and protein by thiazolidinediones. *Organic letters* **2015**, *17* (6), 1361-1364.
(98) Freeman, R. H. D.-U. V. BA Nitric oxide regulation of tissue free radical injury Chem Res Toxicol 9809820 1996. 201. Rubbo H, Darley-Usmar V, and Freeman BA. *Nitric oxide regulation of tissue free radical injury. Chem Res Toxicol* **1996**, *9*, 809-820. Schopfer, F. J.; Baker, P. R.;

Giles, G.; Chumley, P.; Batthyany, C.; Crawford, J.; Patel, R. P.; Hogg, N.; Branchaud, B. P.; Lancaster, J. R. Fatty acid transduction of nitric oxide signaling: nitrolinoleic acid is a hydrophobically stabilized nitric oxide donor. *Journal of Biological Chemistry* **2005**, *280* (19), 19289-19297.
(99) Chen, H.; Viel, S.; Ziarelli, F.; Peng, L. 19F NMR: a valuable tool for studying biological events. *Chemical Society Reviews* **2013**, *42* (20), 7971-7982.
(100) Melo, T.; Montero-Bullón, J.-F.; Domingues, P.; Domingues, M. R. Discovery of bioactive nitrated lipids and nitro-lipid-protein adducts using mass spectrometry-based approaches. *Redox biology* **2019**, *23*, 101106.
(101) Spears, R. J.; Fascione, M. A. Site-selective incorporation and ligation of protein aldehydes. *Organic & Biomolecular Chemistry* **2016**, *14* (32), 7622-7638.
(102) Luzzio, F. A. The Henry reaction: recent examples. *Tetrahedron* **2001**, *57* (6), 915-945. Bora, P. P.; Bez, G. Henry Reaction in Aqueous Media at Neutral pH. *European Journal of Organic Chemistry* **2013**, *2013* (14), 2922-2929. DOI: https://doi.org/10.1002/ejoc.201201682.
(103) Nguyen, L. A.; He, H.; Pham-Huy, C. Chiral drugs: an overview. *International journal of biomedical science: IJBS* **2006**, *2* (2), 85.
(104) Srinivas, M.; Heerschap, A.; Ahrens, E. T.; Figdor, C. G.; de Vries, I. J. M. 19F MRI for quantitative in vivo cell tracking. *Trends in biotechnology* **2010**, *28* (7), 363-370.
(105) O'Hare, H. M.; Johnsson, K.; Gautier, A. Chemical probes shed light on protein function. *Current Opinion in Structural Biology* **2007**, *17* (4), 488-494. DOI: https://doi.org/10.1016/j.sbi.2007.07.005. Witus, L. S.; Francis, M. B. Using synthetically modified proteins to make new materials. *Accounts of chemical research* **2011**, *44* (9), 774-783.
(106) Witus, L. S.; Francis, M. Site-Specific Protein Bioconjugation via a Pyridoxal 5′-Phosphate-Mediated N-Terminal Transamination Reaction. *Current Protocols in Chemical Biology* **2010**, *2* (2), 125-134. DOI: https://doi.org/10.1002/9780470559277.ch100018.
(107) Castro-Falcón, G.; Hahn, D.; Reimer, D.; Hughes, C. C. Thiol Probes To Detect Electrophilic Natural Products Based on Their Mechanism of Action. *ACS Chemical Biology* **2016**, *11* (8), 2328-2336. DOI: 10.1021/acschembio.5b00924. Chavas, T. E. J.; Fuchter, M. J.; DiMaggio, P. A. Unbiased Mass Spectrometry Elucidation of the Targets and Mechanisms of Activity-Based Probes: A Case Study Involving Sulfonyl Fluorides. *ACS Chemical Biology* **2018**, *13* (10), 2897-2907. DOI: 10.1021/acschembio.8b00530.
(108) Himo, F.; Lovell, T.; Hilgraf, R.; Rostovtsev, V. V.; Noodleman, L.; Sharpless, K. B.; Fokin, V. V. Copper(I)-Catalyzed Synthesis of Azoles. DFT Study Predicts Unprecedented Reactivity and Intermediates. *Journal of the American Chemical Society* **2005**, *127* (1), 210-216. DOI: 10.1021/ja0471525.
(109) Gross, M. L. Focus in honor of Fred McLafferty, 2003 Distinguished Contribution Awardee, for the discovery of the "McLafferty Rearrangement". *Journal of the American Society for Mass Spectrometry* **2004**, *15* (7), 951-955. DOI: 10.1016/j.jasms.2004.05.009. McLafferty, F. W. Mass Spectrometric Analysis. Molecular Rearrangements. *Analytical Chemistry* **1959**, *31* (1), 82-87. DOI: 10.1021/ac60145a015.
(110) Adusumalli, S. R.; Rawale, D. G.; Singh, U.; Tripathi, P.; Paul, R.; Kalra, N.; Mishra, R. K.; Shukla, S.; Rai, V. Single-Site Labeling of Native Proteins Enabled by a Chemoselective and Site-Selective Chemical Technology. *Journal of the American Chemical Society* **2018**, *140* (44), 15114-15123. DOI: 10.1021/jacs.8b10490.
(111) Ricardo, M. G.; Llanes, D.; Wessjohann, L. A.; Rivera, D. G. Introducing the Petasis Reaction for Late-Stage Multicomponent Diversification, Labeling, and Stapling of Peptides.

Angewandte Chemie International Edition **2019**, *58* (9), 2700-2704. DOI: https://doi.org/10.1002/anie.201812620. Tang, J.; Chen, H.; He, Y.; Sheng, W.; Bai, Q.; Wang, H. Peptide-guided functionalization and macrocyclization of bioactive peptidosulfonamides by Pd(II)-catalyzed late-stage C–H activation. *Nature Communications* **2018**, *9* (1), 3383. DOI: 10.1038/s41467-018-05440-w. Verdine, G. L.; Hilinski, G. J. Chapter one - Stapled Peptides for Intracellular Drug Targets. In *Methods in Enzymology*, Wittrup, K. D., Verdine, G. L. Eds.; Vol. 503; Academic Press, 2012; pp 3-33.
(112) Strauss, M. J. The Nitroaromatic Group in Drug Design. Pharmacology and Toxicology (for Nonpharmacologists). *Industrial & Engineering Chemistry Product Research and Development* **1979**, *18* (3), 158-166. DOI: 10.1021/i360071a002.
(113) Nepali, K.; Lee, H.-Y.; Liou, J.-P. Nitro-Group-Containing Drugs. *Journal of Medicinal Chemistry* **2019**, *62* (6), 2851-2893. DOI: 10.1021/acs.jmedchem.8b00147.

Chapter 4. Supplementary Information

Experimental Details for Chapter One

General. All commercial materials (Sigma-Aldrich, Fluka, and Novabiochem) were used without further purification. All solvents were reagent or HPLC (Fisher) grade. All reactions were performed under air in glass vials. Yields refer to chromatographically pure compounds; % yields were obtained by comparison of HPLC peak areas of products and starting materials. HPLC was used to monitor reaction progress.

Materials. Fmoc-amino acids, Rink amide resin, 3-[bis(dimethylamino)methyliumyl]-3Hbenzotriazol-1-oxide hexafluorophosphate (HBTU), 1-hydroxy-7-azabenzotriazole (HOAt), N,N′-iisopropylcarbodiimide (DIC), and N,N-diisopropylethylamine (DIEA) were obtained from CreoSalus (Louisville, Kentucky). 4-dimethylaminopyridine (DMAP), piperidine, trifluoroacetic acid (TFA), ditert-butyl dicarbonate (BOC_2O), 4-methyl morpholine (NMM) and hydrazine monohydrate were obtained from Alfa Aesar (Ward Hill, Massachusetts). N,N-dimethylformamide (DMF), dichloromethane (DCM), methanol (MeOH), acetonitrile (ACN), sodium cyanoborohydride, tetrahydrofuran (THF), and Fmoc-Ala-aldehyde were obtained from VWR (100 Matsonford Road Radnor, Pennsylvania). sodium dimethyldithiocarbamate dihydrate (DTC) and aminoacetylaldehyde dimethyl acetal were obtained from Sigma-Aldrich (St. Louis, Missouri). benzotriazol-1-yloxytripyrrolidinophosphonium hexafluorophosphate (PyBOP), phenysilane, palladium(triphenylphosphine)tetrakis, and levulinic acid were obtained from TCI (Portland, OR). Water was purified using a Millipore Milli-Q water purification system.

Purification. **HPLC:** Purification was performed using high performance liquid chromatography (HPLC) on an Agilent 1100/1200 series HPLC equipped with a 5 μm particle size, C-18 reversedphase column. All separations involved a mobile phase of 0.1% formic acid (v/v) in water (solvent A) and 0.1% formic acid (v/v) in acetonitrile (solvent B). The HPLC method employed a

linear gradient of 0–80% solvent B over 30 minutes at ambient temperature with a flow rate of 1.0 mL min^{-1}. The separation was monitored by UV absorbance at both 220 nm unless otherwise noted.

Analytical Methods.

LC-MS: Mass spectrometry to check reaction mixtures was performed using an Agilent 1100 Series HPLC with MSD VL mass spectrometer using positive polarity electrospray ionization (+ESI).

High resolution LC-MS conditions for all purified peptides: Analyses were performed on an ultra-performance LC system (ACQUITY, Waters Corp., USA) coupled with a quadrupole time-offlight mass spectrometer (Q-ToF Premier, Waters) with electrospray ionization (ESI) in positive mode using Mass lynx software (V4.1). Unless otherwise mentioned a sample was injected either onto a C4 column (Phenomenex Aeris™ 3.6 µm WIDEPORE C4 200 Å, LC Column 50 x 2.1 mm) with a 300 µL/min flow rate of mobile phase of solution A (95 % H_2O, 5% acetonitrile and 0.1% formic acid) and solution B (95% acetonitrile, 5% H_2O, and 0.1% formic acid) beginning gradient- Time- 0 min 10% B; 5 min 28% B; 20 min 38% B; 22 min 90% B; C18 column (ACQUITY UPLC BEH 1.7 µm 1x 50 mm) with a 200 µL/min flow rate of mobile phase of solution A (95 % H_2O, 5% acetonitrile and 0.1% formic acid) and solution B (95% acetonitrile, 5% H_2O, and 0.1% formic acid) beginning gradient- Time- 1 min 0% B; 1-10 min 100% B for chromatography analysis (or) directly injected with mobile phase 50% H_2O: 50% ACN, 0.1% formic acid at 200 µL/min flow rate in ESI positive mode.

Fmoc Solid-Phase Peptide Synthesis (Fmoc-SPPS). Peptides were synthesized manually on a 0.25 mm scale using Rink amide resin. Resin was swollen with DCM for 1 h at room temperature. Fmoc was deprotected using 20% piperidine–DMF for 5 min to obtain a deprotected peptide-resin. First Fmoc-protected amino acid (1.25 mm/5 equiv.) was coupled using HOAt (1.25 mm/5 equiv.)

and DIC (1.25 mm/5 equiv.) in DMF for 15 min at room temperature. Fmoc-protected amino acids (0.75 mm/3 equiv.) were sequentially coupled on the resin using HBTU (0.75 mm/3 equiv.) and DIEA (1.5 mm/6 equiv.) in DMF for 5 min at room temperature. Peptides were synthesized using standard protocols.1 Any Fmoc-protected amino acid added after Fmoc-proline was subjected to the conditions of the first amino acid coupling. Peptides were cleaved from the resin using a cocktail of 95:5, trifluoroacetic acid: water for 2 h. The resin was removed by filtration and the resulting solution was concentrated. The residue was diluted with ACN/water mixture. The resulting solution was purified by HPLC.

General Procedure for synthesis of peptide aldehydes. Peptide aldehydes were necessary to facilitate macrocyclization. An aldehyde was added on either the side chain of the peptide or the C terminus.

Procedure for synthesis of side chain peptide aldehydes. Peptides with Fmoc-Glu(Oall)-OH were synthesized by Fmoc solid phase peptide synthesis protocol. Fmoc-glutamic acid is commercially available with an O-allyl protected side chain. The selective deprotection of the O allyl group from the side chain of the Glu on a peptide (0.5 mm/g) was achieved on solid support through the addition of palladium(triphenylphosphine)tetrakis (0.05 equiv.) and phenylsilane (24 equiv.) in DCM (6 mL/6.9 mM) and shake for 40 min. This process was repeated, and the resulting resin was washed with DCM (5x). Extra washings with 0.5% DIEA in DMF (2x), 0.5% mass/vol DTC in DMF (2X), and DMF (5x) were carried out to remove the palladium from the resin. Cleavage of the small amount of resin followed by LCMS evaluation confirmed the deprotection. Next, the deprotected peptide (0.075 mm) on solid support was treated with a solution of PyBOP (0.75 mm/10 equiv.), DIEA (1.5 mm/20 equiv.), and amino acetyl aldehyde dimethyl acetal (0.75 mm/10 equiv.) and resin was shaken for 4 h at room temperature. The resulting resin was washed

with three times with DMF, DCM and MeOH. This was followed by the cleavage of the peptide from solid support using cleavage cocktail TFA:H2O (95:5) for 2 h at room temperature. The resulting peptide aldehyde was analyzed by LCMS and purified by HPLC followed by lypholization to obtain pure peptide aldehyde.

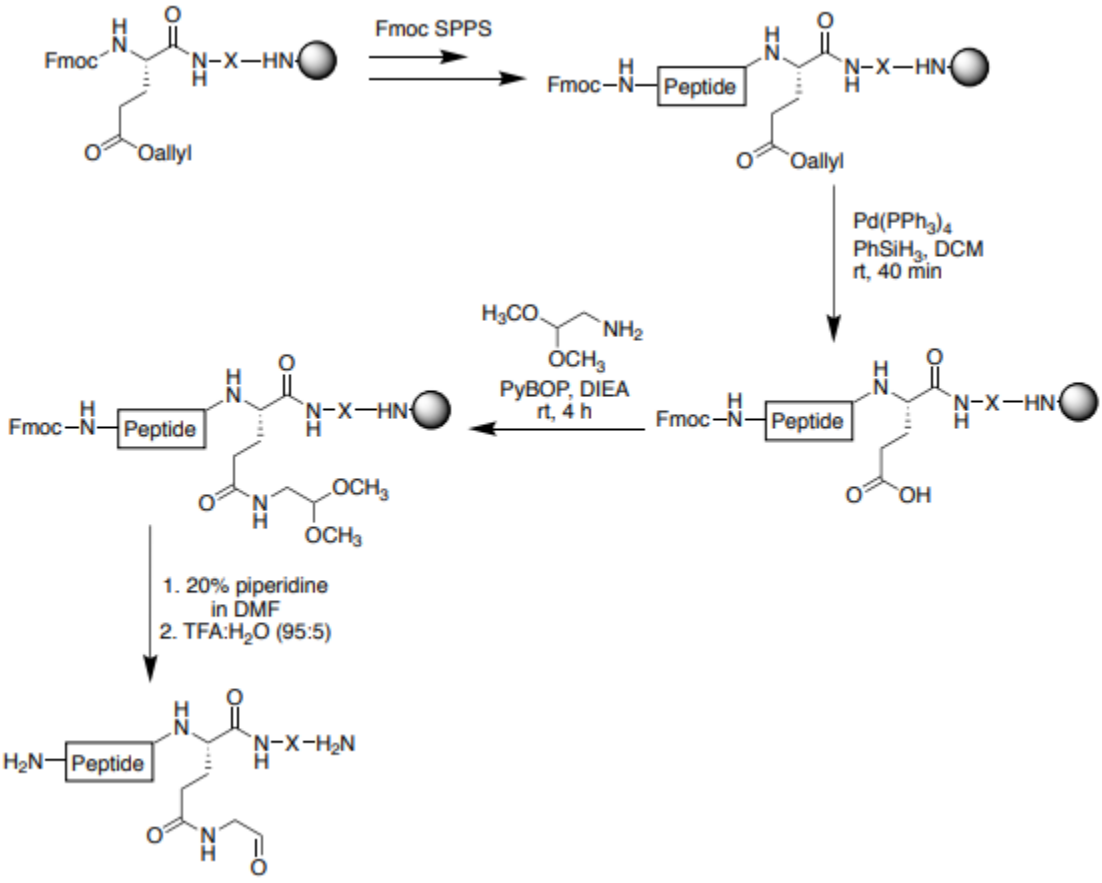

Procedure for synthesis of C-terminal peptide aldehydes. Fmoc-Gly-OH and Fmoc-Thr-OH were coupled with the general peptide synthesis procedure to swollen Rink resin (0.5 mm/g). Following Fmoc deprotection, the resin (500 mg) was added to a solution of Fmoc-Ala-CHO (alanine aldehyde) (1 mm/4 equiv.) in 1% DIEA v/v in MeOH (2.5 mL/final conc. 0.1 M) and

rocked for 5 h at 60 °C. The resin was washed with MeOH (5 x 3 mL), DMF (5 x 3 mL), DCM (5 x 3 mL), and THF (5 x 3 mL). The resin was then rocked for 5 h at 50°C in a solution of Boc anhydride BOC_2O (1.25 mm/5 equiv.), NMM (1.25 mm/5 equiv.) in THF (2.5 mL/final conc. 0.1 M). The resin was washed with THF (5 x 3 mL), DCM (5 x 3), and DMF (5 x 3 mL) followed by the coupling of rest of Fmoc-amino acid residues using Fmoc SPPS. After Fmoc-SPPS, the resulting resin was washed three times with DMF, DCM and MeOH. This was followed by the cleavage of the peptide from the solid support using cleavage cocktail TFA:H_2O (95:5) for 2 h at room temperature. The resulting C-terminal peptide aldehyde was analyzed by LCMS and purified by HPLC followed by lyophilization to obtain pure peptide aldehyde.

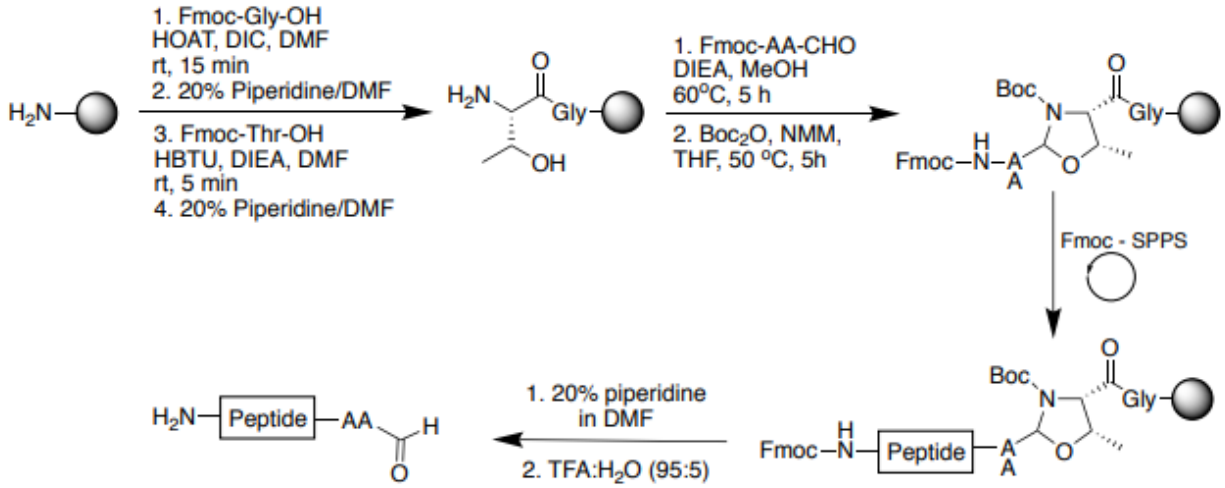

Procedure for synthesis of N-terminal peptide aldehydes. Fmoc-Phe-OH, Fmoc-Val-OH, and Fmoc Ser(trt)-OH were sequentially coupled to Rink amide resin (0.5 mm/g) using standard SPPS protocol. The peptide was cleaved with TFA:TES:H_2O (95:2.5:2.5) and purified with HPLC. Lyophilized peptide (10 mg) was shaken with sodium periodate (5 equiv.) in 50 mM phosphate buffer (1 mL, 31 mM) at room temperature for 3 h in the dark. The sample was analyzed by HPLC and MS.

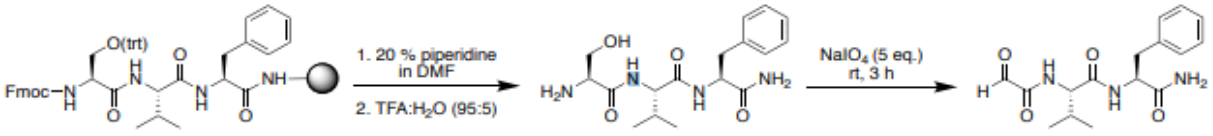

General procedure for synthesis of peptide ketones. Peptide containing lysine with Dde as a protecting group on resin (0.5 mm/g) was first selectively deprotected from resin using 2% hydrazine monohydrate in DMF (260 µL) for 3 min at room temperature (3x) and washed with DMF (3x). Next, 0.05 mm of lys-deprotected resin was treated with levulinic acid (0.5 mm/10 equiv.), PyBOP (0.5 mm/10 equiv.), DIEA (1 mm/20 equiv.), in DMF (6 mL, final conc. 0.01 M) and rocked for 4 h at room temperature. The resulting resin was washed three times with DMF, DCM and MeOH. This was followed by the cleavage of the peptide ketone from solid support using cleavage cocktail TFA:H2O (95:5) for 2 h at room temperature. The peptide ketone was analyzed by LCMS and purified by HPLC followed by lyophilization to obtain pure peptide ketone.

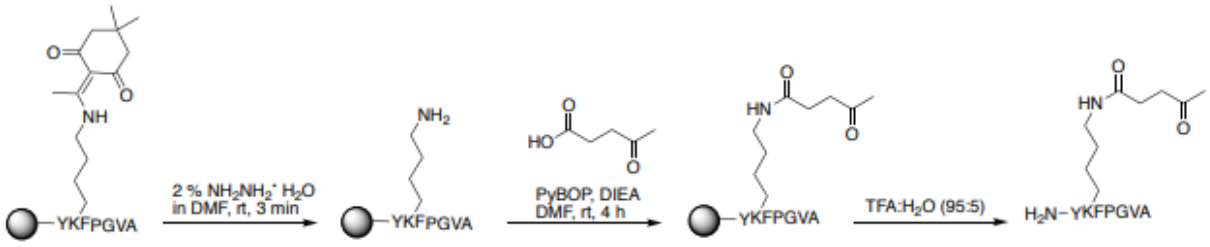

General procedure for CyClick reaction. Lyophilized peptide aldehyde (2 mg) was mixed with 7 equiv. DMAP in a 1:1 DMF:H_2O solution (final conc. 5 mM). The reaction was shaken at room temperature for 8-16 h. The product was analyzed with HPLC, NMR, and MS. Confirmation of cyclic product by MS. The cyclic imine intermediate exhibits mass equivalent to the cyclic product. In an effort to determine the cyclic product, sodium cyanoborohydride (50 equiv.) was added to reduce the cyclic imine intermediate.

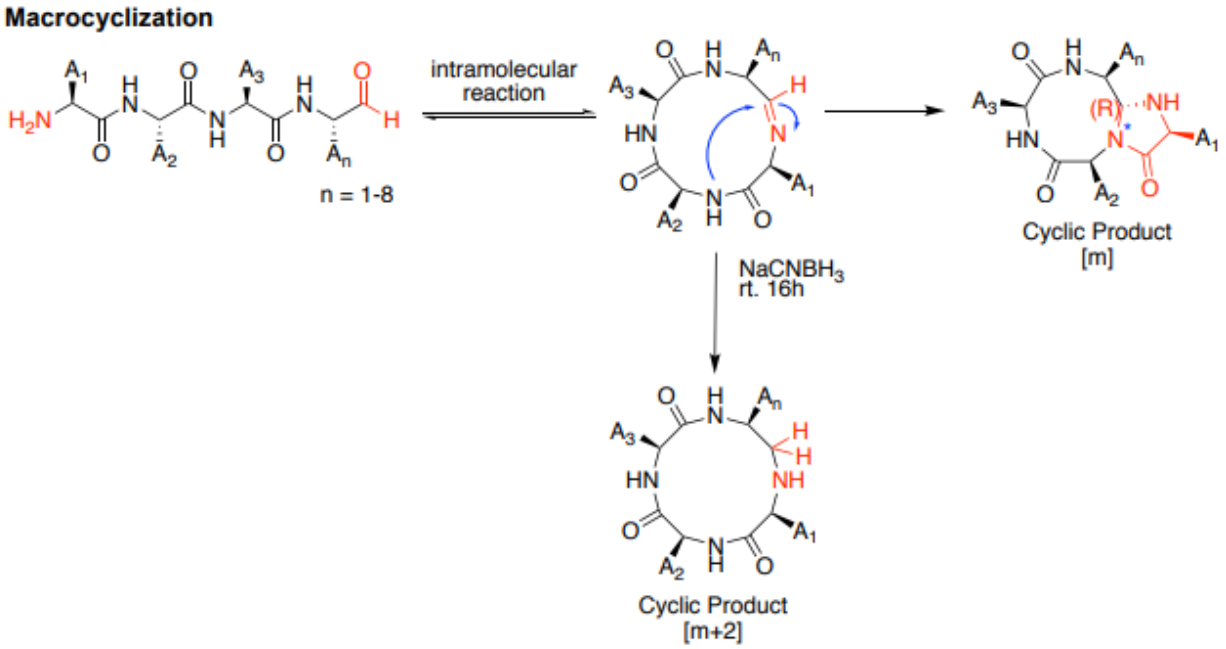

CyClick reaction optimization. Linear peptide aldehydes AVGPFE(CHO)Y **1.1a** and NVGPFE(CHO)Y **1.1f** were selected for optimization and CyClick reaction was carried out in H_2O:DMF (1:1) under following different conditions.

CyClick Reaction Optimization				
Linear peptide sequence **1**	DMAP	Time	Concentration	Conversion to cyclic peptide **2**
AVGPFE(CHO)Y **1.1a**	No DMAP	16 h	5 mM	**1.2a**, 11 %
AVGPFE(CHO)Y 1.1a	**7 equiv.**	**8 h**	**5 mM**	**1.2a, 99 %**
NVGPFE(CHO)Y **1.1f**	No DMAP	16 h	5 mM	**1.2f**, 10 %
NVGPFE(CHO)Y 1.1f	**7 equiv.**	**16 h**	**5 mM**	**1.2f, 85 %**

Bold entries represent optimized reaction conditions.

Structure Elucidation via NMR. An approximately 1 mg sample was dissolved in 0.15 mL of DMSO-d_6, and the solution was then transferred to a 3-mm NMR tube. ^{1}H, ^{13}C, COSY, TOCSY, HSQC, HMBC, and ROESY spectra were acquired at ambient temperature (298 K) using a 3-mm

triple resonance (HCN) helium cryoprobe on a 600 MHz Agilent DD2 NMR spectrometer. Proton chemical shifts were referenced to residual DMSO-d_5 at 2.50 ppm, and carbon chemical shifts were referenced to DMSO-d_6 at 39.52 ppm. Spectra were processed using Mnova ver. 12.0.4. A gradient COSY spectrum was acquired using 2048 x 400 increments, and 0% sine squared II apodizations were applied in both dimensions. A TOCSY spectrum was acquired using a 60 ms mixing time and 2048 x 512 increments; the spectrum was then linear predicted to 1048 points in the f1 dimension. An adiabatic gradient multiplicity-edited HSQC spectrum was acquired using 2048 x 512 increments. An adiabatic gradient HMBC spectrum was acquired using a J-optimization of 8 Hz and 2048 x 512 increments, and then a 0% sine squared II apodization was applied in the direct dimension. An adiabatic gradient ROESY spectrum was acquired using a 200 ms mixing time and 2048 x 400 increments, and 90° sine squared apodizations were applied in both dimensions.

NMR Data of compound cyc(AVGPFE(CHO)Y) 1.2a from Linear Peptide 1.1a

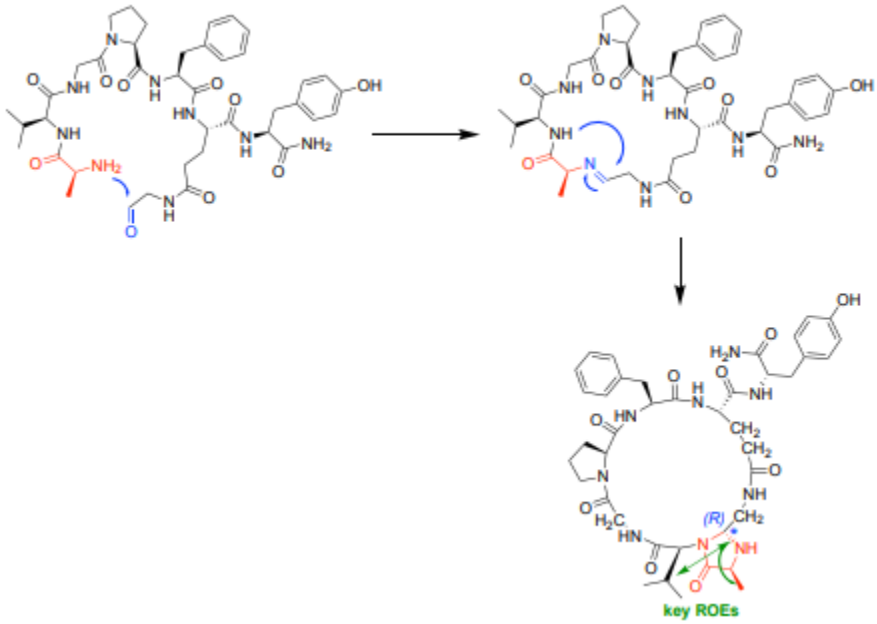

^{13}C NMR chemical shift for validation of 4-imidazolidinone structure of cyclic peptide 1.2a

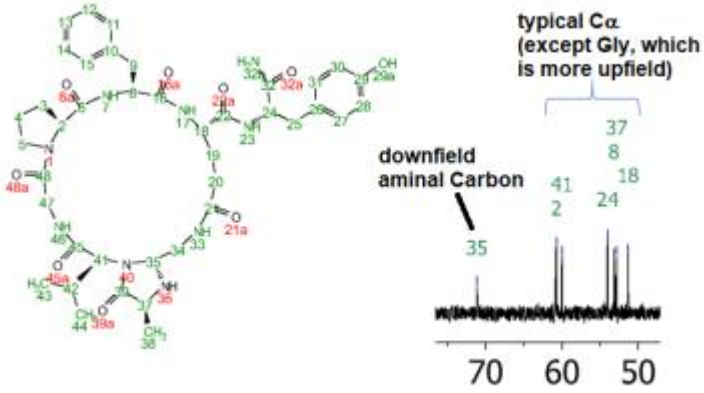

Downfield aminal carbon chemical shift at 71.15 ppm (below), which is much further downfield than any Cα carbon. This downfield aminal chemical shift shows up in all cyclized structures in the paper (i.e., 71.2, 71.6, 71.7, 72.4, 78.4 for bicyclic, and 74.7 ppm), and thus it is diagnostic for the imidazolidinone moiety. ACD labs' (ver 2015) predictions for this carbon chemical shift were between 68 to 78 ppm.

HMBC correlations for validation of 4-imidazolidinone structure of cyclic peptide 1.2a

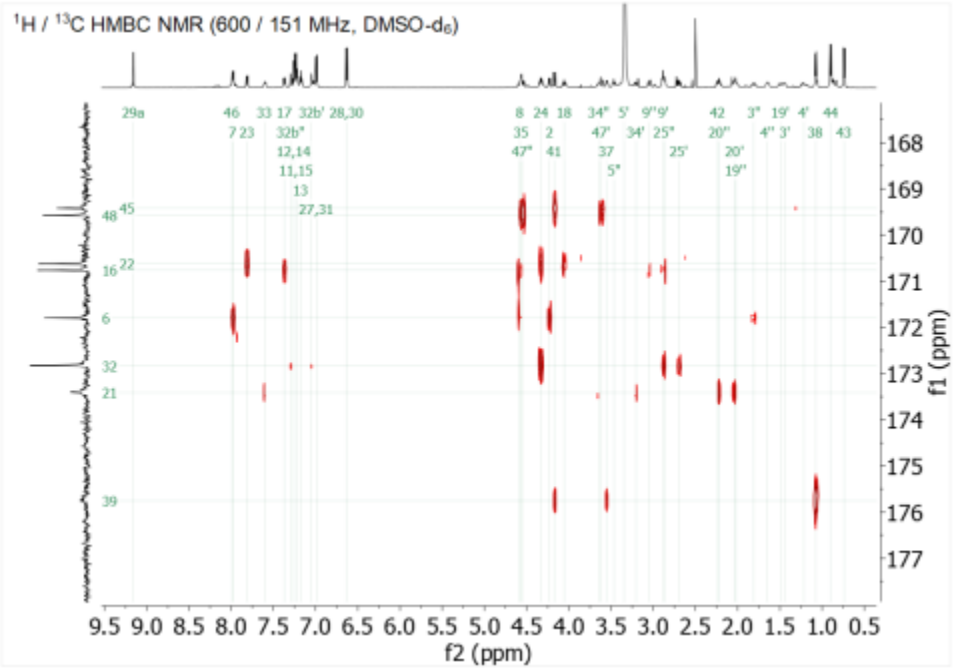

HMBC correlations from Val (41), 37, and 38 to the carbonyl carbon C39

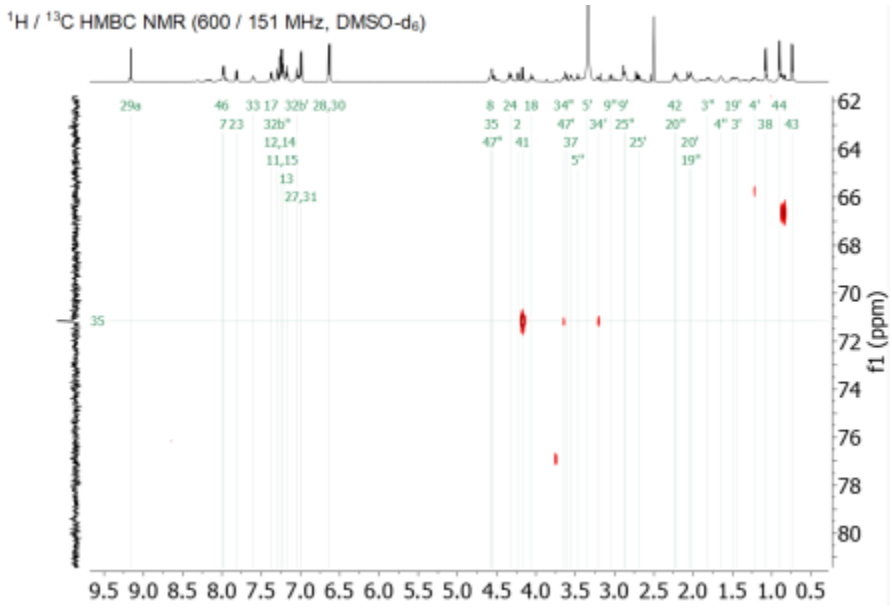

HMBC correlations from Val (proton 41) and Glu (protons 34' and 34'') to the C35 carbon.

It is also worth noting that there 2JCH correlations from H34' and H34" are weaker than the

correlation from H41 to C35, which is consistent with 2JCH coupling from the 34 methylene protons to C35 being smaller than the optimization of the HMBC, which was set for 8 Hz. Overall, the data are completely consistent with the imidazolidinone moiety.

NMR data for cyc(AVGPFE(CHO)Y) 1.2a

Residue	Atom Name	Numbering	d_H (ppm), multiplicity	d_C (ppm)
Pro	N	1	--	--
	C_aH	2	4.23, d (*J* = 9.0, 2.2 Hz)	60.75
	C_bH_2	3	1.45, m; 1.81, m	28.86
	C_gH_2	4	1.22, m; 1.65, m	23.41
	C_dH_2	5	3.35, m; 3.46, t (*J* = 9.3 Hz)	46.15
	CO	6	--	171.80
Phe	NH	7	7.98, d (*J* = 8.5 Hz)	--
	C_aH	8	4.58, m	53.14
	C_bH_2	9	2.88, m; 3.05, dd (*J* = 14.5, 4.6 Hz)	34.63
	C_1	10	--	138.16
	C_2H, C_6H	11, 15	7.23, m	129.02
	C_3H, C_5H	12, 14	7.26, m	128.06
	C_4	13	7.18, t (*J* = 7.1 Hz)	126.17
	CO	16	--	170.76
Glu	NH	17	7.37, d (*J* = 8.5 Hz)	--
	C_aH	18	4.06, ddd (*J* = 11.1, 8.4, 3.0 Hz)	51.32
	C_bH_2	19	1.49, m; 2.03, m	26.86
	C_gH_2	20	2.04, m; 2.22, m	29.45
	C_dO	21	--	173.41
	CO	22	--	170.62
Tyr	NH	23	7.81, d (*J* = 8.4 Hz)	--
	C_aH	24	4.33, td (*J* = 8.6, 4.9 Hz)	54.01
	C_bH_2	25	2.70, dd (*J* = 13.9, 9.0 Hz); 2.87, m	36.72
	C_1	26	--	127.86
	C_2H, C_6H	27, 31	6.99, d (*J* = 8.3 Hz)	130.11
	C_3H, C_5H	28, 30	6.63, d (*J* = 8.4 Hz)	114.81
	C_4OH	29	9.16, s	155.74
	$CONH_2$	32	7.05, s; 7.30, s	172.83
Linker	NH	33	7.60, dd (*J* = 8.1, 4.7 Hz)	--
	C_aH_2	34	3.21, dd (*J* = 13.5, 4.4 Hz); 3.65, m	41.64
	C_bH	35	4.57, m	71.15
Ala	NH	36	--	--
	C_aH	37	3.55, q (*J* = 7.0 Hz)	52.84
	C_bH_3	38	1.08, d (*J* = 6.9 Hz)	19.62
	CO	39	--	175.75
Val	N	40	--	--
	C_aH	41	4.17, d (*J* = 11.3 Hz)	59.99
	C_bH	42	2.23, m	25.25
	$C_{g1}H_3$, $C_{g2}H_3$	43, 44	0.74, d (*J* = 6.5 Hz); 0.90, d (*J* = 6.4 Hz)	18.30, 19.74
	CO	45	--	169.42
Gly	NH	46	7.99, m	--
	C_aH_2	47	3.62, dd (*J* = 16.6, 3.1 Hz); 4.55, m	40.74
	CO	48	--	169.57

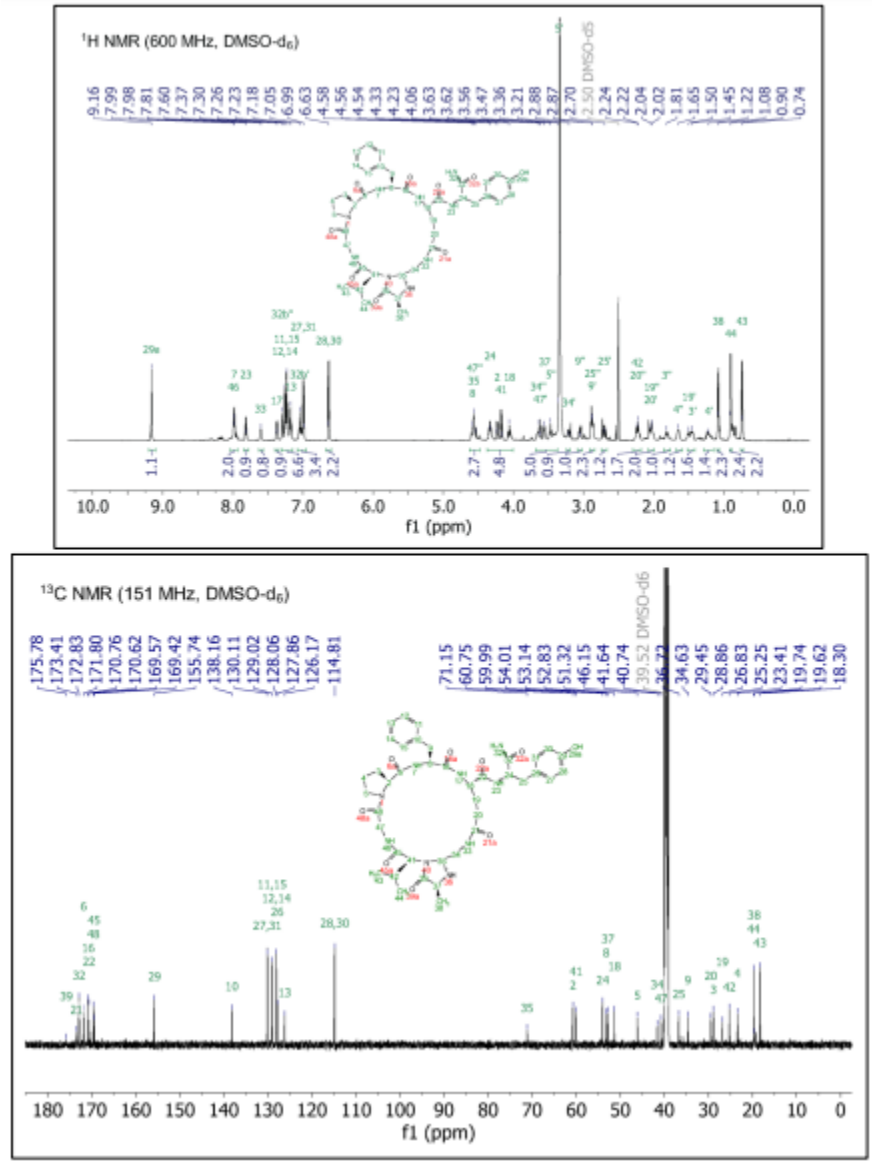
^{1}H NMR (600 MHz, DMSO-d$_6$)
^{13}C NMR (151 MHz, DMSO-d$_6$)
DMSO-d5
DMSO-d6
f1 (ppm)

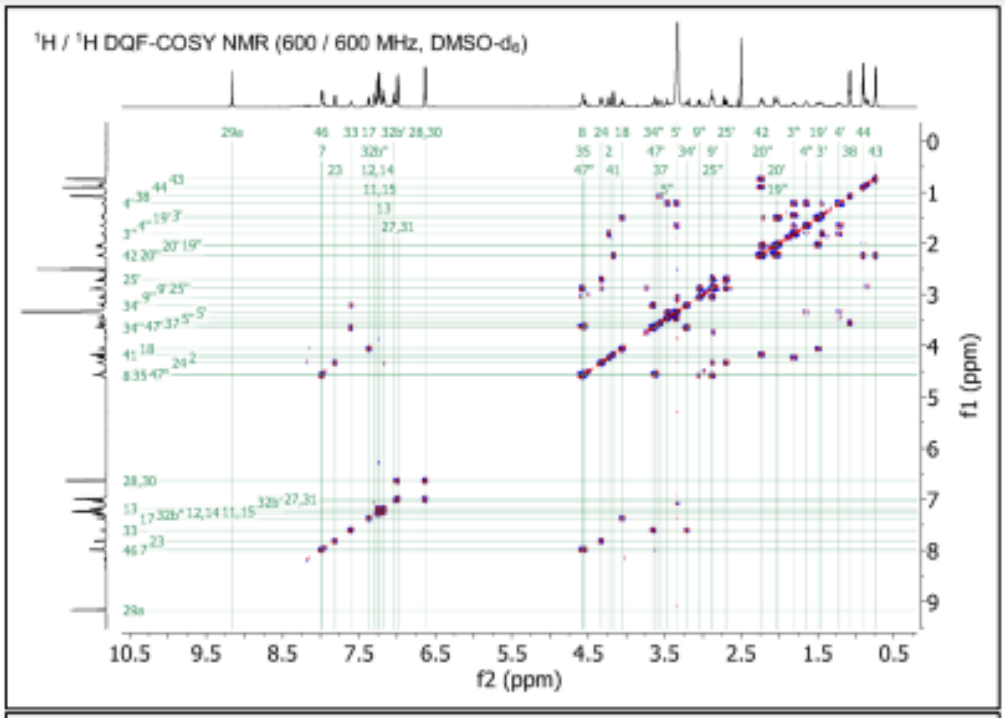
^{1}H / ^{1}H DQF-COSY NMR (600 / 600 MHz, DMSO-d$_6$)
f2 (ppm)
f1 (ppm)

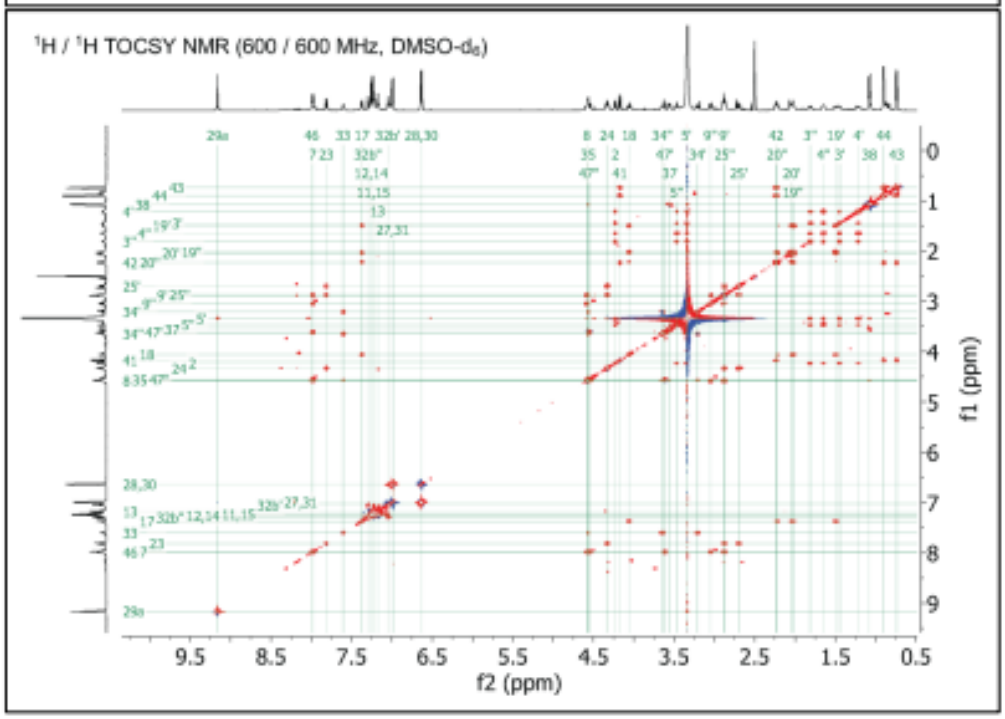
^{1}H / ^{1}H TOCSY NMR (600 / 600 MHz, DMSO-d$_6$)
f2 (ppm)
f1 (ppm)

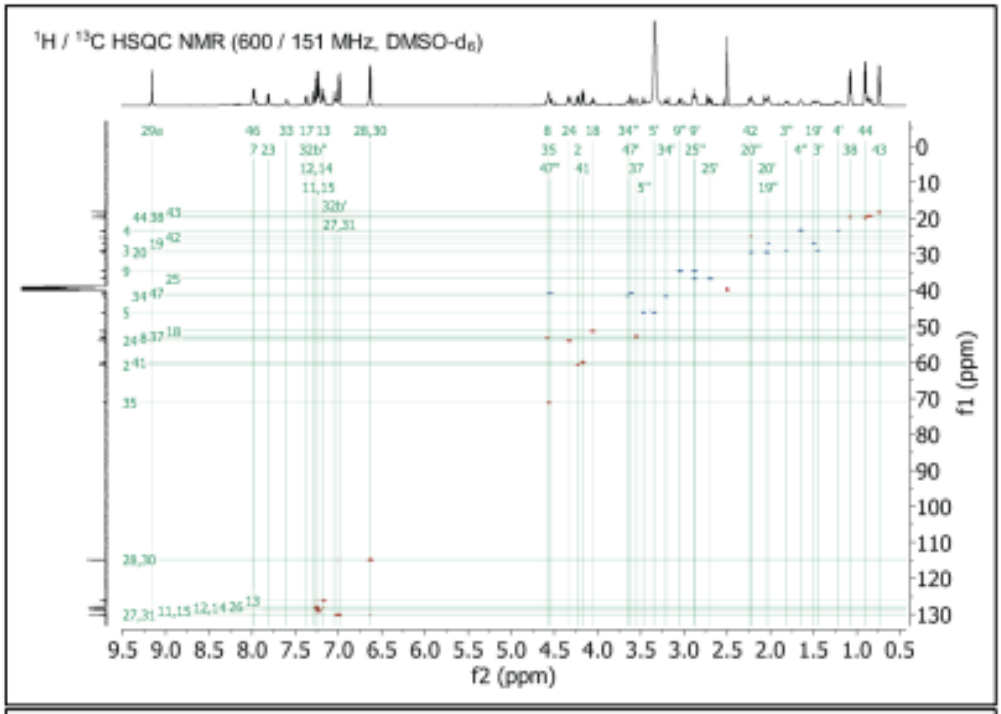
^{1}H / ^{13}C HSQC NMR (600 / 151 MHz, DMSO-d$_6$)
f2 (ppm)
f1 (ppm)

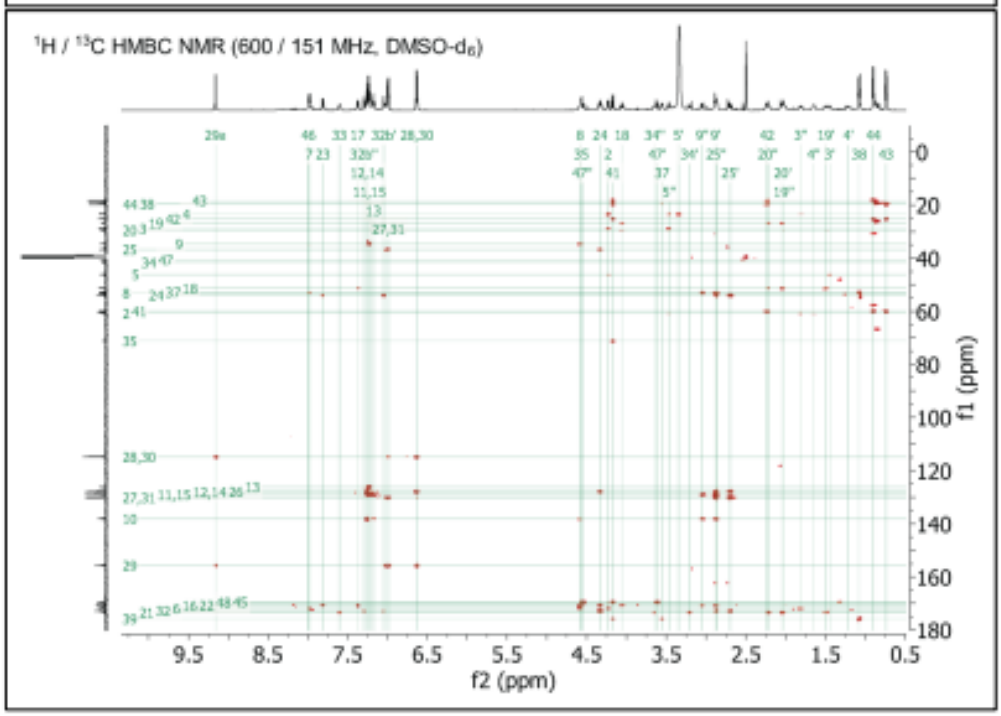
^{1}H / ^{13}C HMBC NMR (600 / 151 MHz, DMSO-d$_6$)
f2 (ppm)
f1 (ppm)

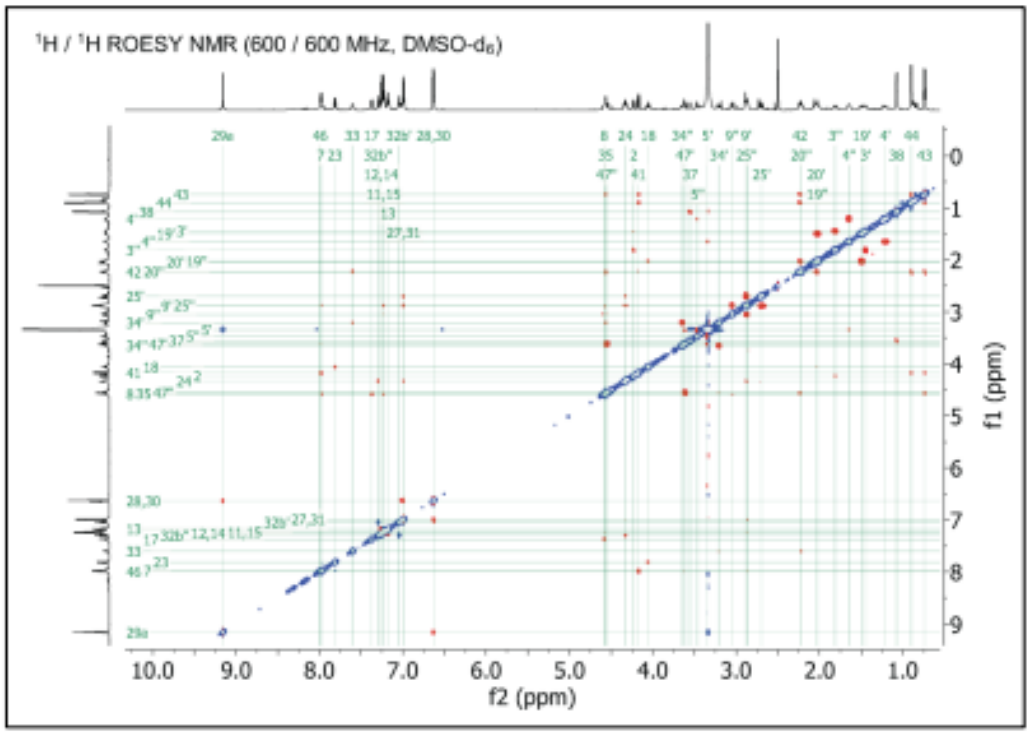

NMR Data of compound cyc(QVGPFE(CHO)Y) 1.2e

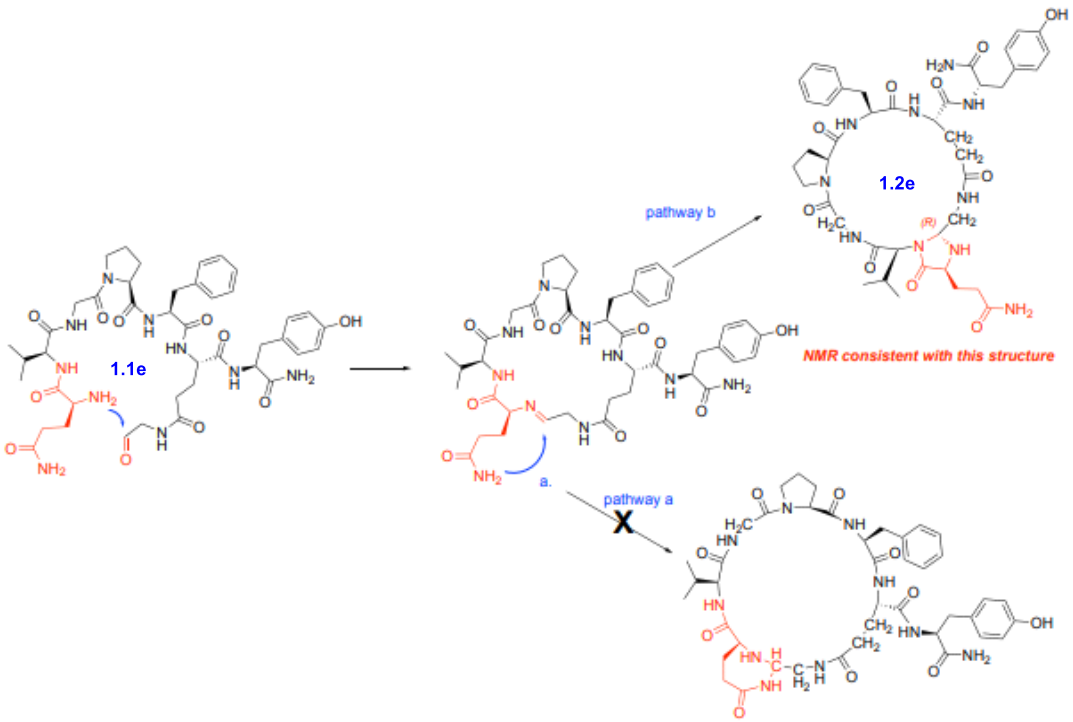

ACD Labs (ver. 2015) ^{13}C Chemical shift Predictions

From the below ACD Labs predictions (ver. 2015) of carbon chemical shifts, the aminal carbon (i.e., newly formed stereocenter) was predicted to be 62.39 ppm in the 7-membered ring structure and 73.44 ppm in the 5-membered ring structure. The observed chemical shift was 71.58 ppm, which fits the 5- membered ring structure. Furthermore, both sets of NH_2 protons on the terminal amide were observed in the ^{15}N HSQC spectrum.

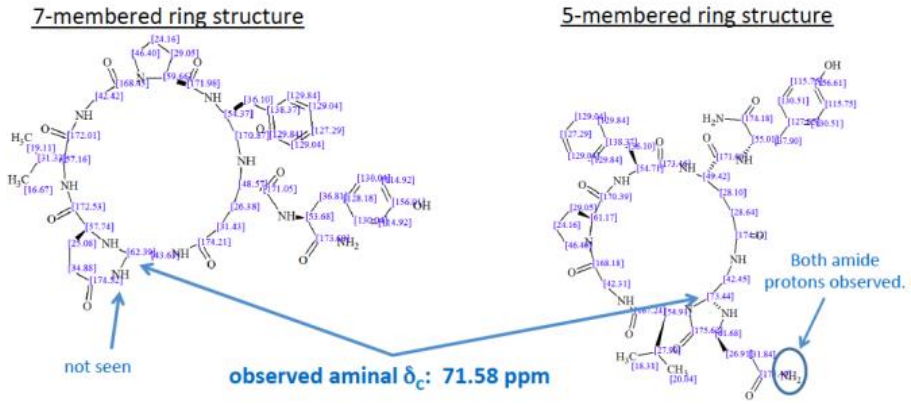

NMR of cyclic peptide cyc(QVGPFE(CHO)Y) 1.2e

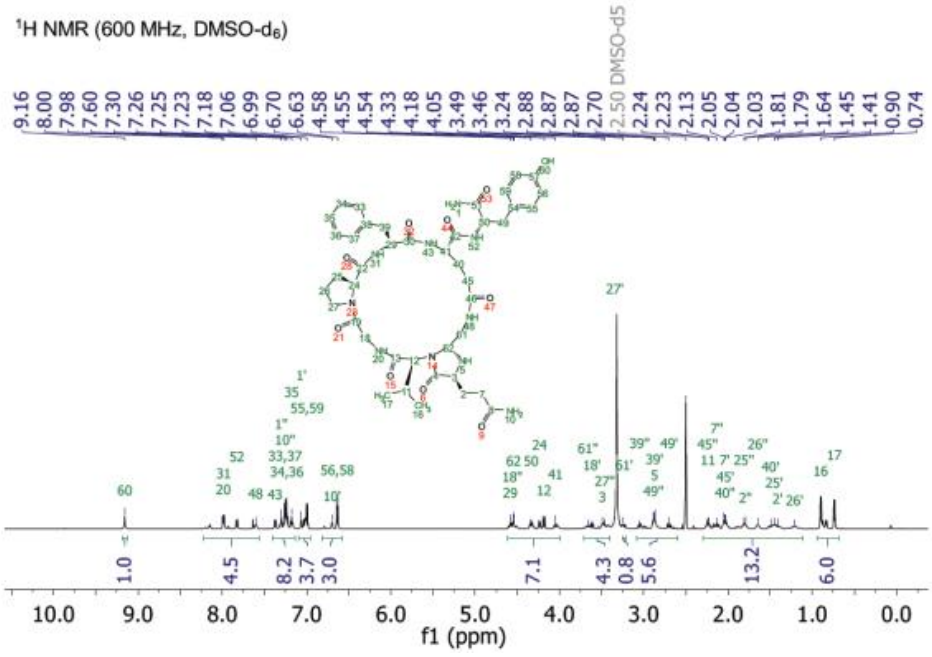

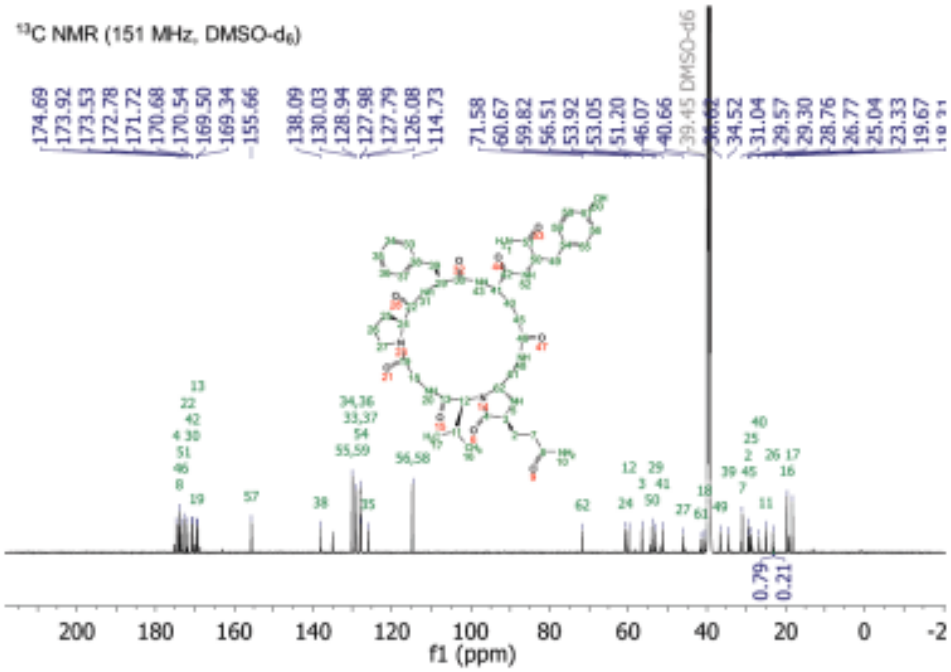
13C NMR (151 MHz, DMSO-d6)
174.69
173.92
173.53
172.78
171.72
170.68
170.54
169.50
169.34
155.66
138.09
130.03
128.94
127.98
127.79
126.08
114.73
71.58
60.67
59.82
56.51
53.92
53.05
51.20
46.07
40.66
39.45 DMSO-d6
34.52
31.04
29.57
29.30
28.76
26.77
25.04
23.33
19.67
0.79
0.21
200
180
160
140
120
100
80
60
40
20
0
-2
f1 (ppm)

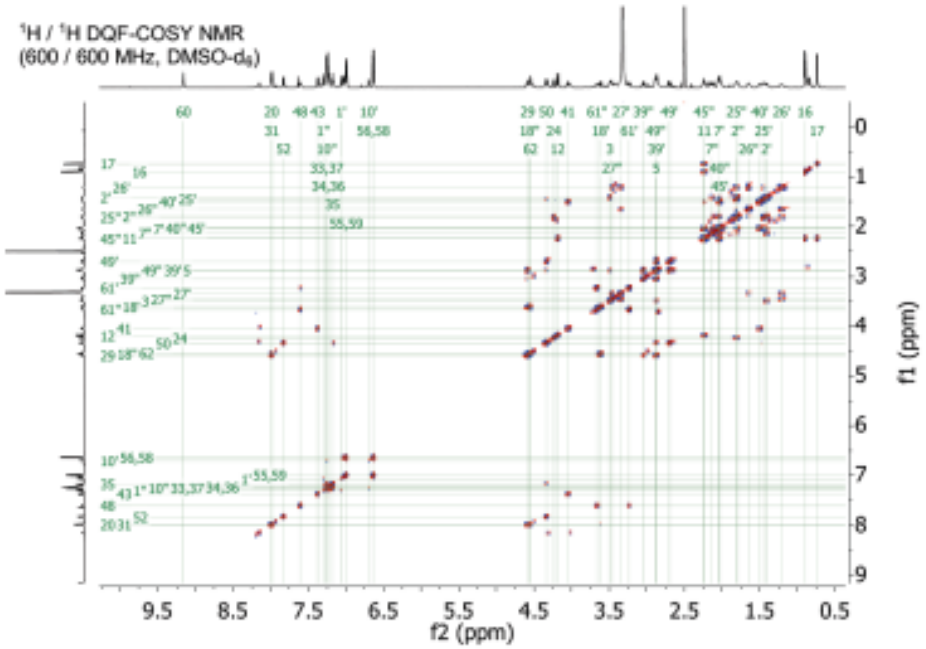
1H / 1H DQF-COSY NMR
(600 / 600 MHz, DMSO-d6)
9.5
8.5
7.5
6.5
5.5
4.5
3.5
2.5
1.5
0.5
f2 (ppm)
f1 (ppm)

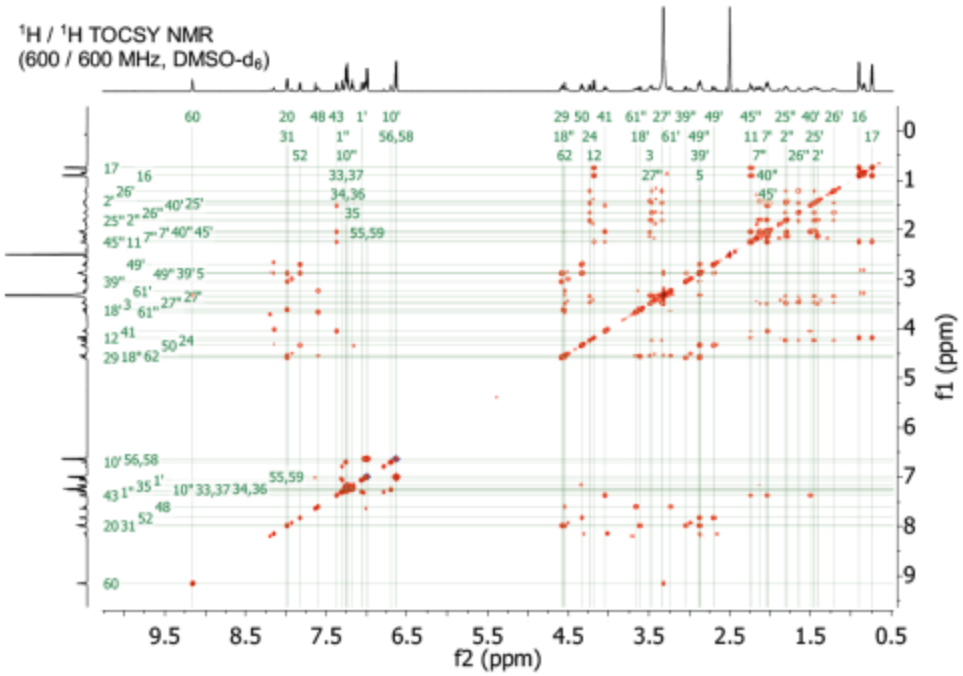
^{1}H / ^{1}H TOCSY NMR
(600 / 600 MHz, DMSO-d$_6$)
f2 (ppm)
f1 (ppm)

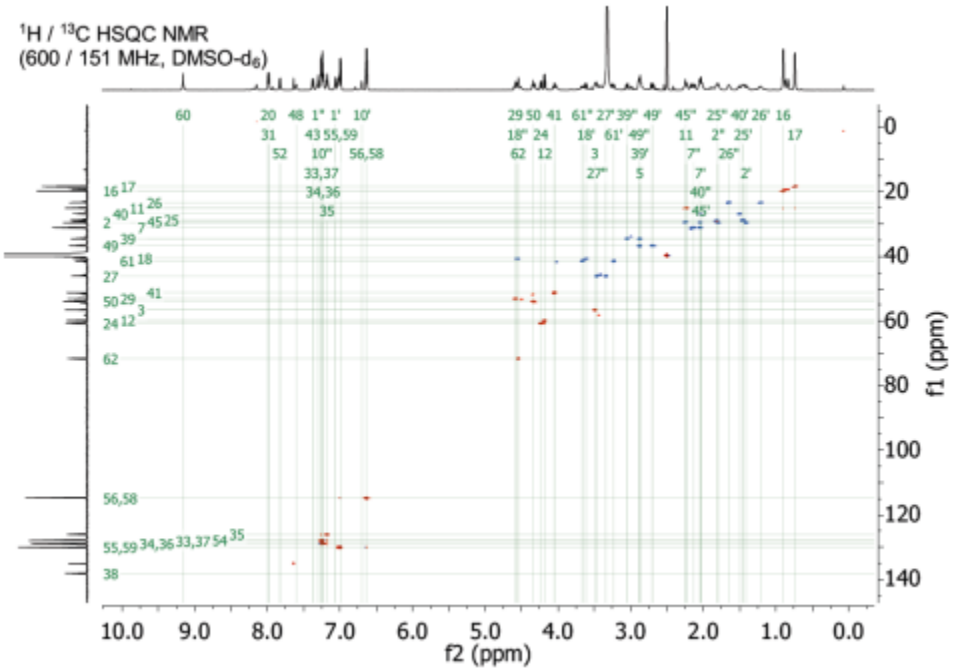
^{1}H / ^{13}C HSQC NMR
(600 / 151 MHz, DMSO-d$_6$)
f2 (ppm)
f1 (ppm)

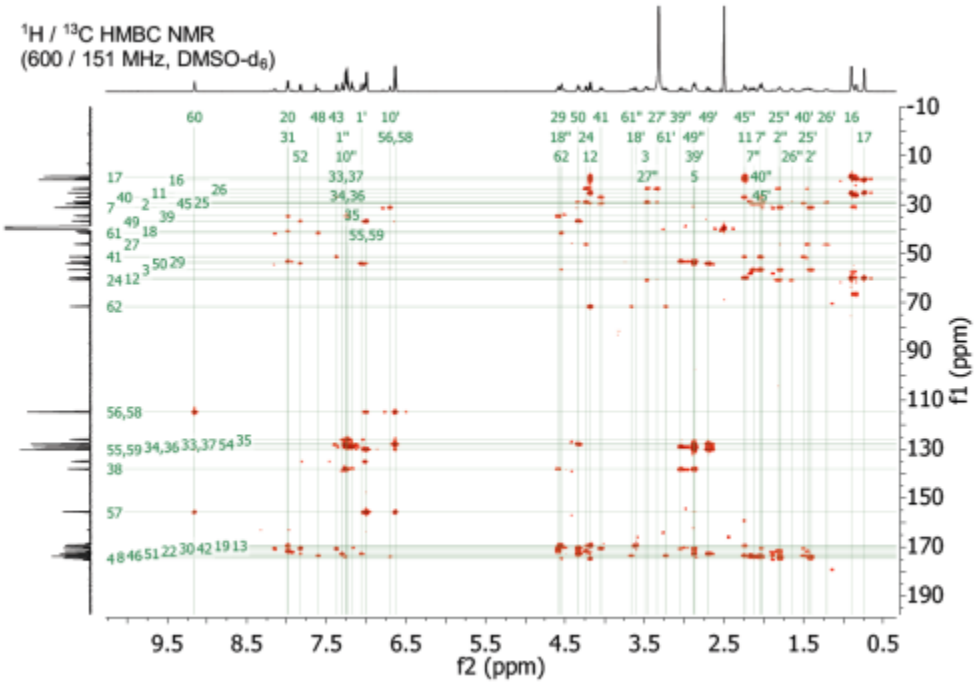
^{1}H / ^{13}C HMBC NMR
(600 / 151 MHz, DMSO-d$_6$)
f2 (ppm)
f1 (ppm)

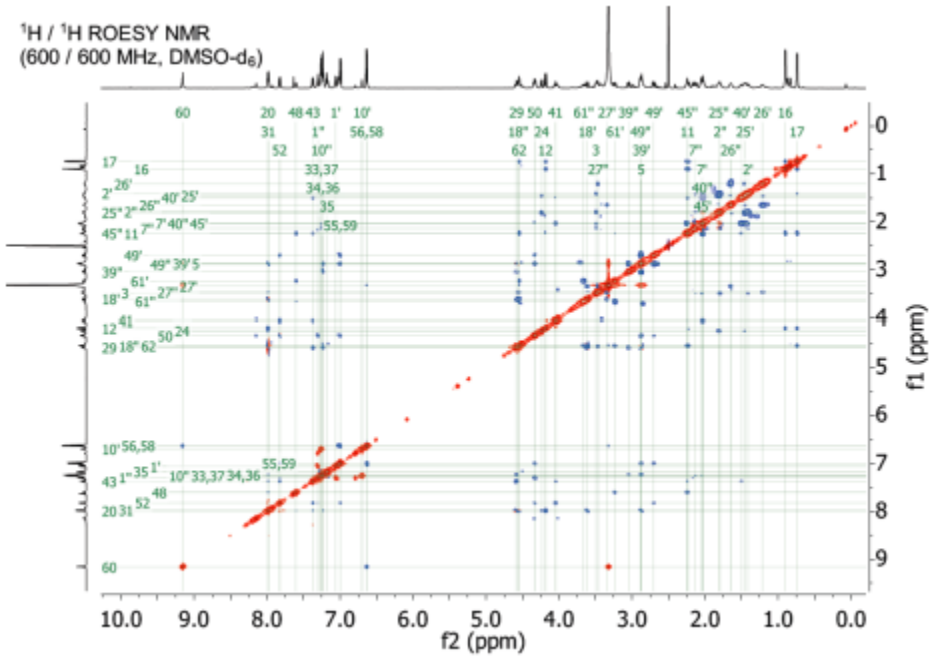
^{1}H / ^{1}H ROESY NMR
(600 / 600 MHz, DMSO-d$_6$)
f2 (ppm)
f1 (ppm)

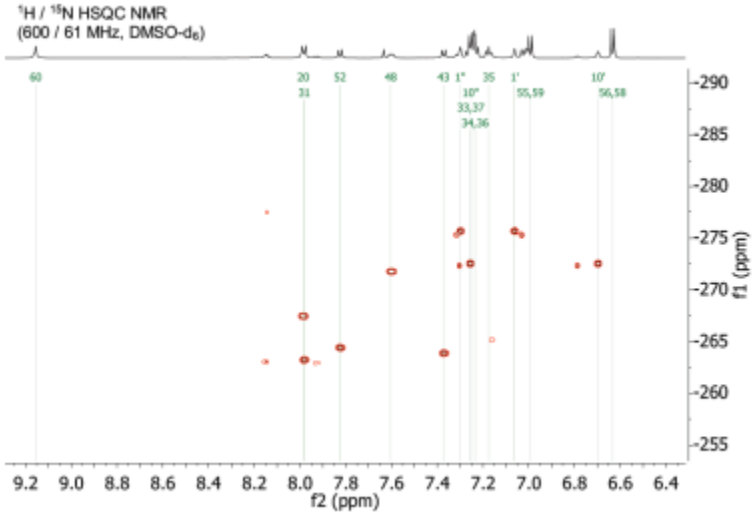

NMR Data of compound cyc(NVGPFE(CHO)Y) 1.2f

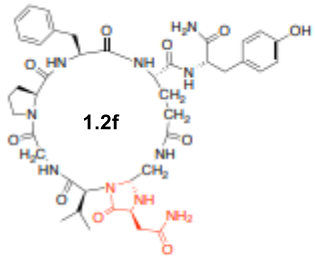

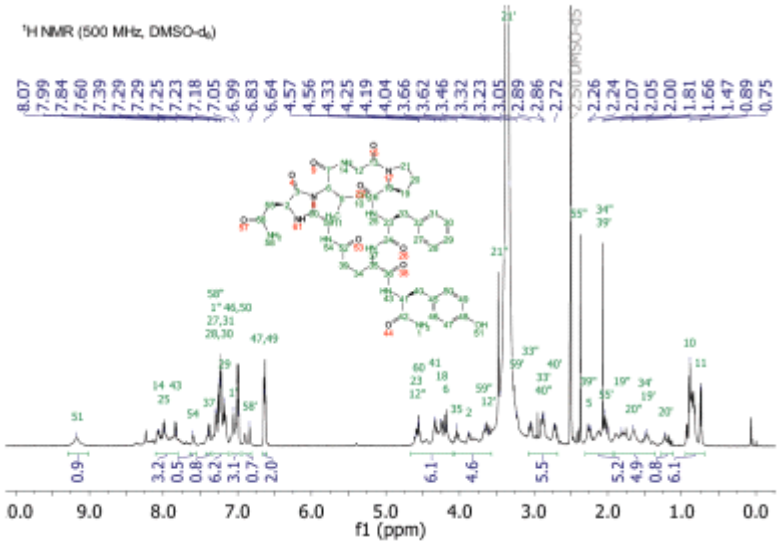

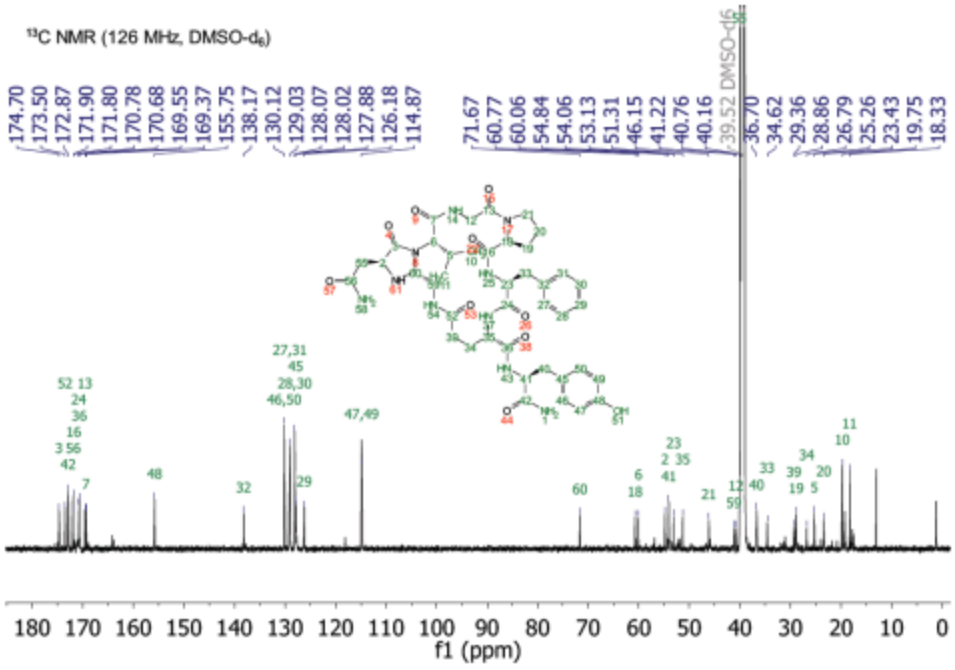
13C NMR (126 MHz, DMSO-d6)
174.70
173.50
172.87
171.90
171.80
170.78
170.68
169.55
169.37
155.75
138.17
130.12
129.03
128.07
128.02
127.88
126.18
114.87
71.67
60.77
60.06
54.84
54.06
53.13
51.31
46.15
41.22
40.76
40.16
39.52 DMSO-d6
36.70
34.62
29.36
28.86
26.79
25.26
23.43
19.75
18.33
f1 (ppm)

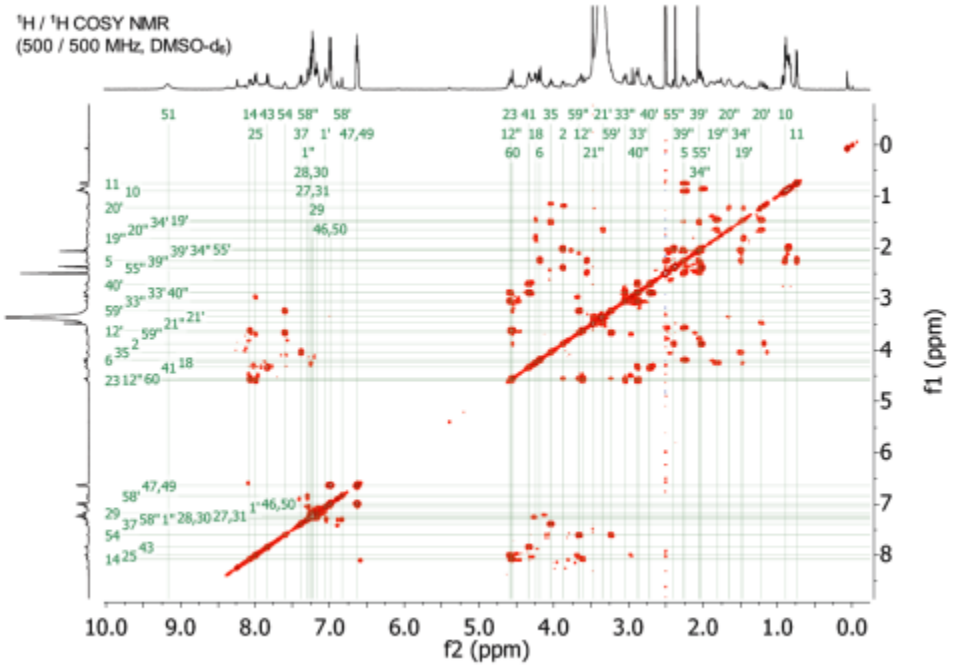
1H / 1H COSY NMR
(500 / 500 MHz, DMSO-d6)
f2 (ppm)
f1 (ppm)

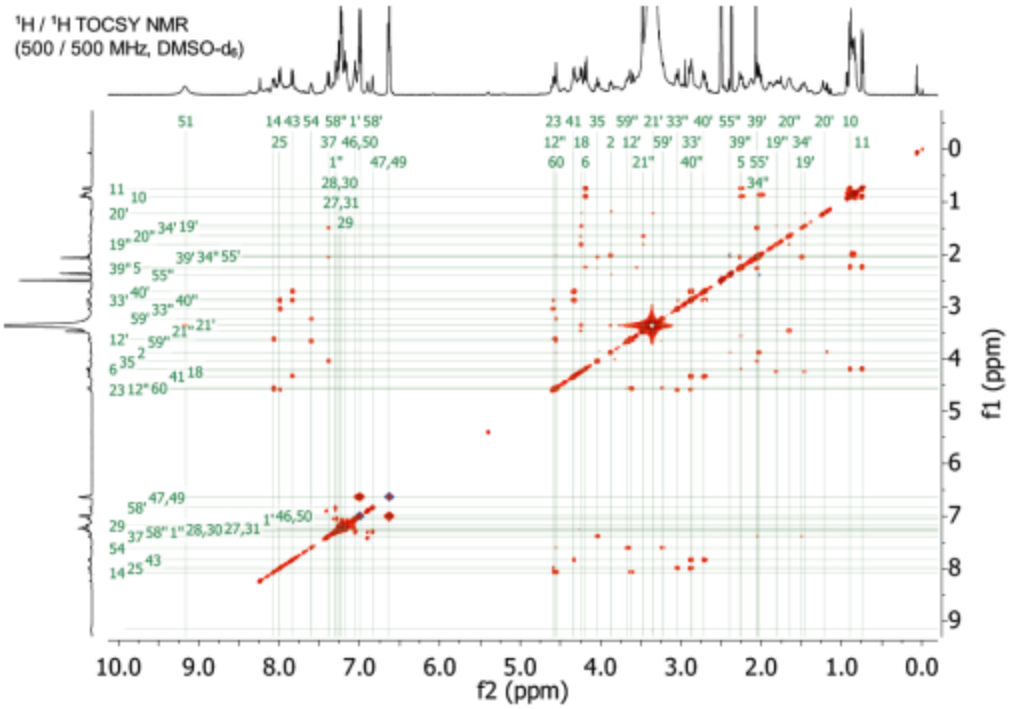
¹H / ¹H TOCSY NMR
(500 / 500 MHz, DMSO-d₆)
f2 (ppm)
f1 (ppm)

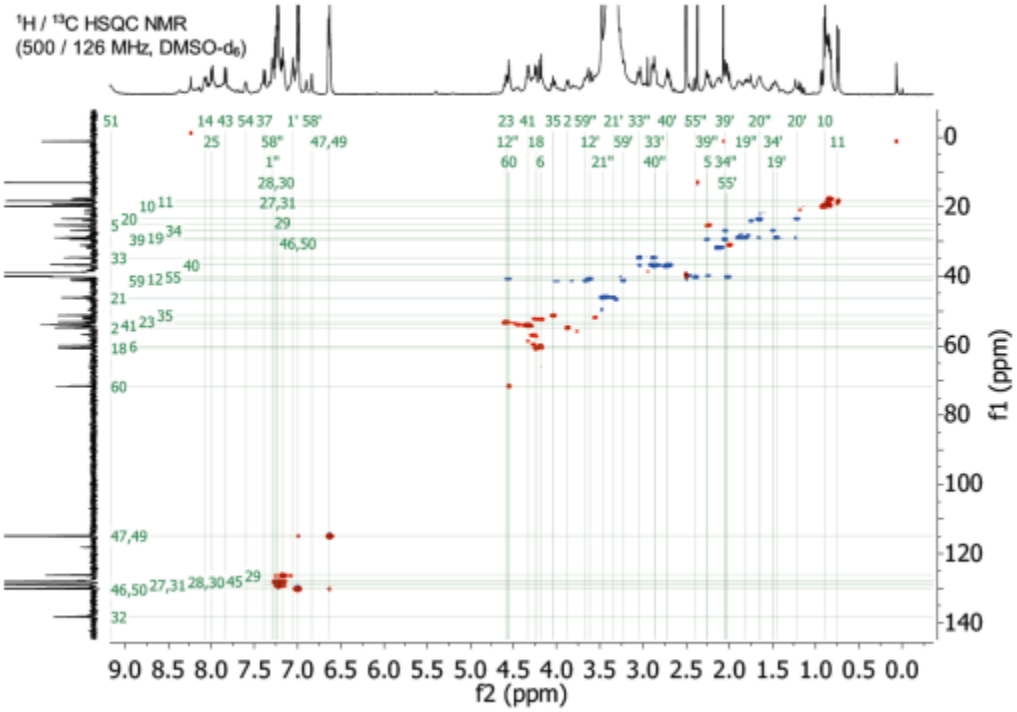
¹H / ¹³C HSQC NMR
(500 / 126 MHz, DMSO-d₆)
f2 (ppm)
f1 (ppm)

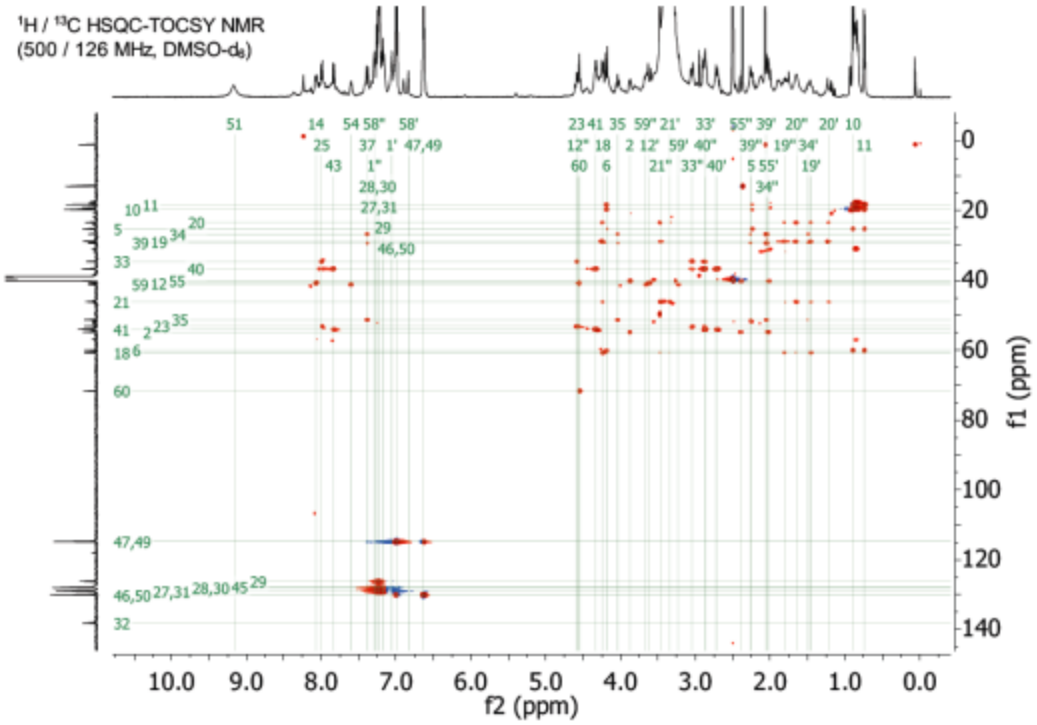
^{1}H / ^{13}C HSQC-TOCSY NMR
(500 / 126 MHz, DMSO-d$_6$)
f2 (ppm)
f1 (ppm)

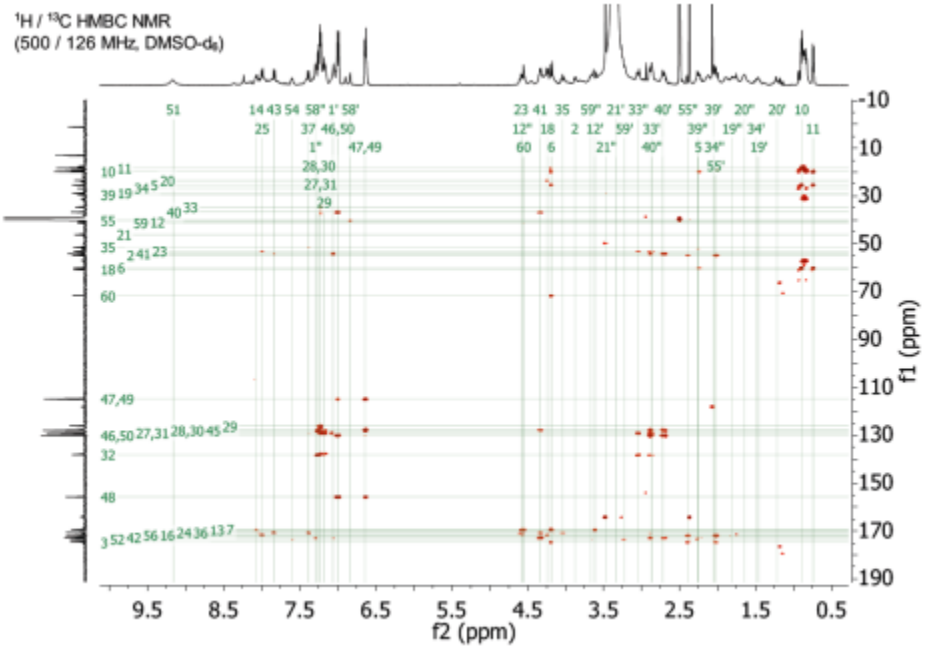
^{1}H / ^{13}C HMBC NMR
(500 / 126 MHz, DMSO-d$_6$)
f2 (ppm)
f1 (ppm)

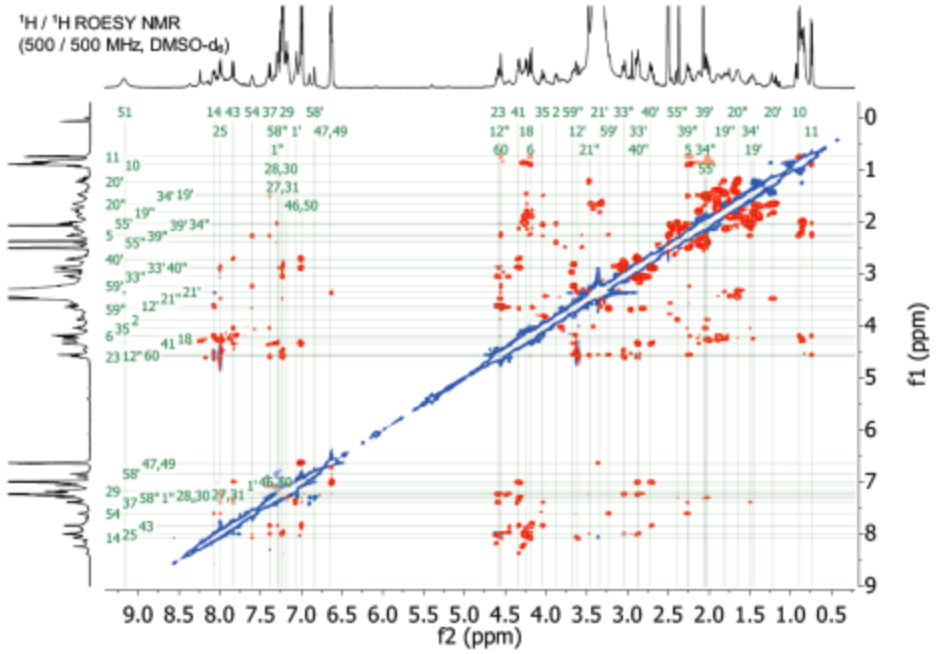
¹H / ¹H ROESY NMR
(500 / 500 MHz, DMSO-d₆)
f2 (ppm)
f1 (ppm)

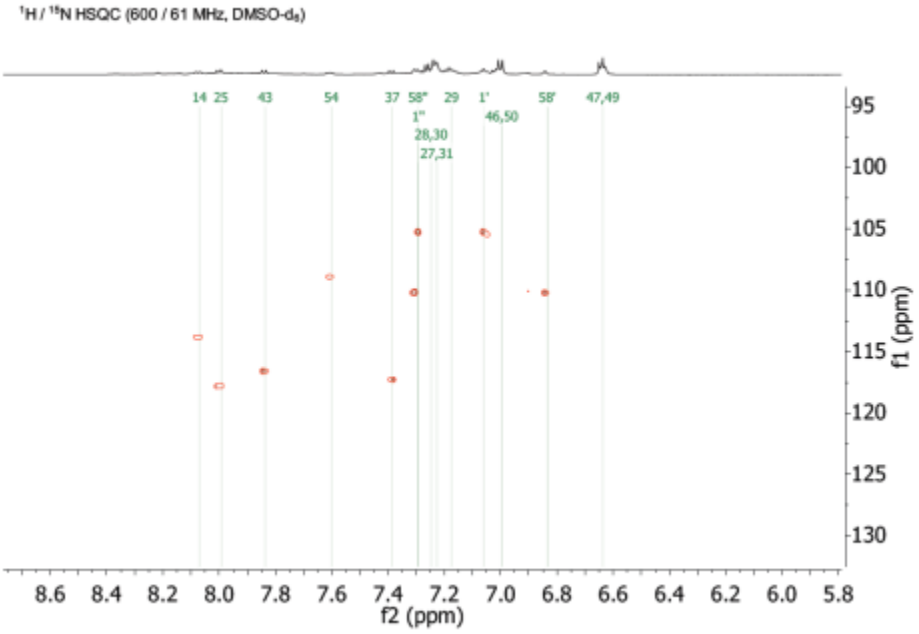
¹H / ¹⁵N HSQC (600 / 61 MHz, DMSO-d₆)
f2 (ppm)
f1 (ppm)

Control reactions to determine the role of backbone amide bond at second position in macrocyclization: Two peptide aldehydes, NH_2-A**P**CA-CHO and NH_2- A**P**GAFE(CHO)Y with proline amino acid at the second position were subjected to optimized CyClick chemistry. No product was observed under the reaction conditions.

Head-to-Side chain cyclization of peptide NH2-APGAFE(CHO)Y

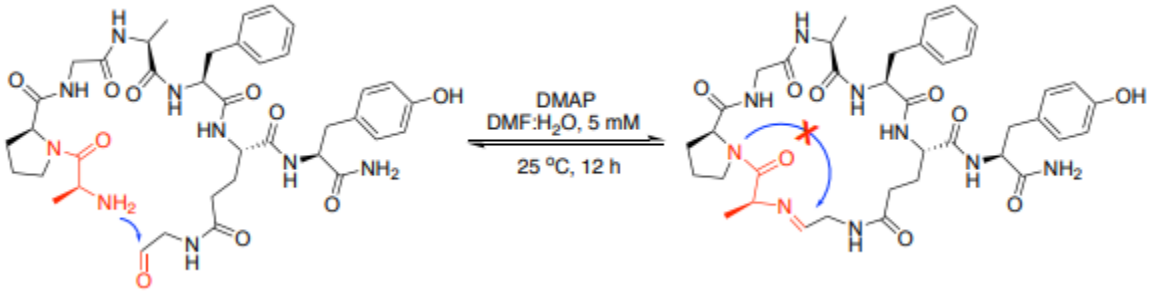

Head-to-Tail cyclization of peptide NH_2-APCA-CHO

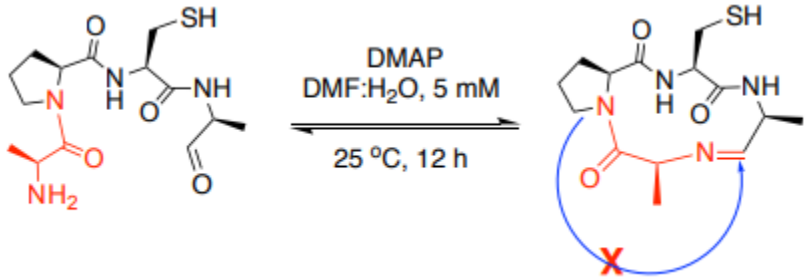

Reaction 1: Comparison of Intermolecular vs Intramolecular reaction. Intramolecular macrocylization was completed with various peptide examples reported in the paper. Intermolecular reaction was attempted with FVA and pentanal.

Lypholized peptide FVA (4 mg, 60 mM) was mixed with aldehyde pentanal (5 equiv., 300 mM) and DMAP (30 equiv., 1800 mM) in a 1:1 DMF:H2O solution (200 µL). The reaction was shaken at room temperature for 24 h. 4-imidazolidinone product vs linear imine intermediate. The linear

imine intermediate exhibits mass equivalent to the desired 4-imidazolidinone products. In an effort to determine the nature of the product of intermolecular reaction, sodium cyanoborohydride (50 equiv.) was added which can reduce the linear imine intermediate and reaction was stirred for additional 16 h. The resulting product was analyzed with LC-MS. The results indicated the formation of reduced linear imine. We do not observe the formation of any 4-imidazolidinone product.

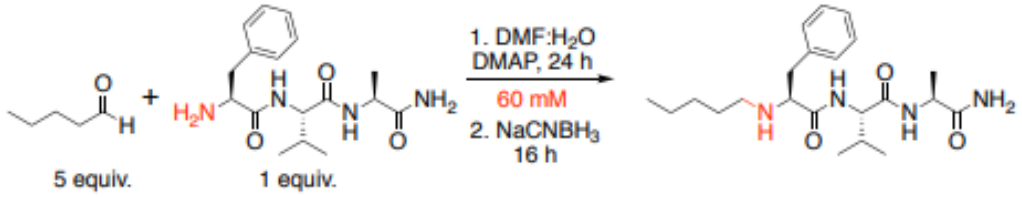

Comparison of Intermolecular vs Intramolecular reaction. Intermolecular reaction was attempted with ASVF and keto aldehyde CHOVF **1.1B.** ASVF (1 equiv.) was combined with the CHOVF **1.1B** (1 equiv.) and DMAP (7 equiv.) in 1:1 DMF:H_2O mixture (200 µL, final conc. 12 mM) and shaken at room temperature for 19 h. No product was observed under the reaction conditions.

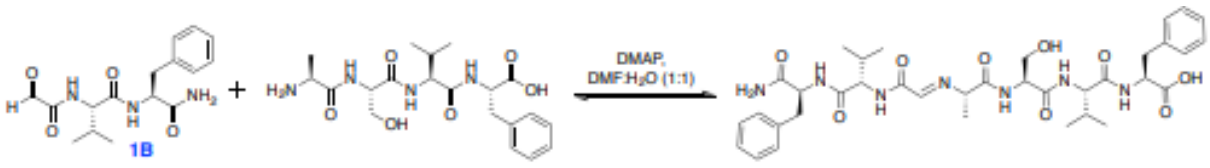

Stereo-configuration of cyclic peptide cyc(AVGPFE(CHO)Y) 1.2a via NMR

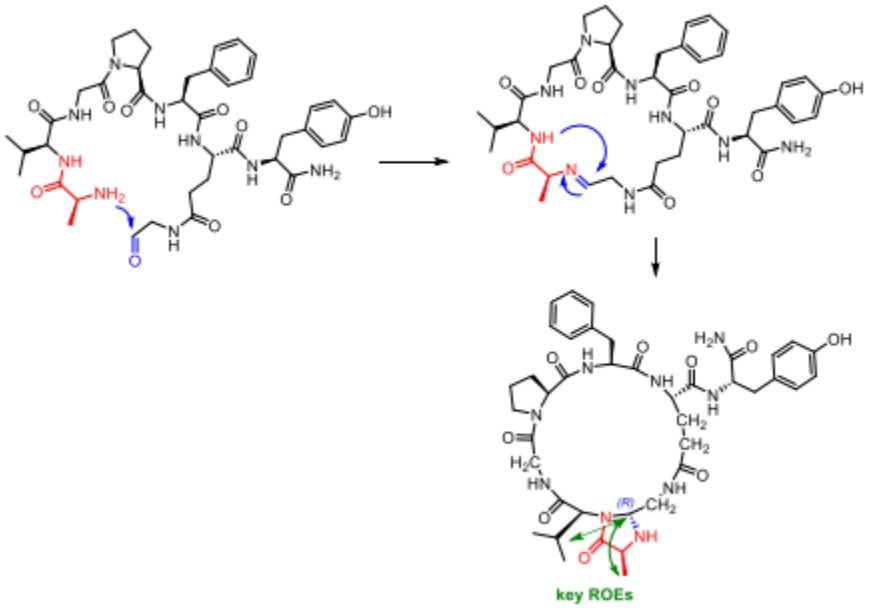

ROEs from 35 to 42, 43, 44, and 38 (weak ROE that determines stereoconfiguration

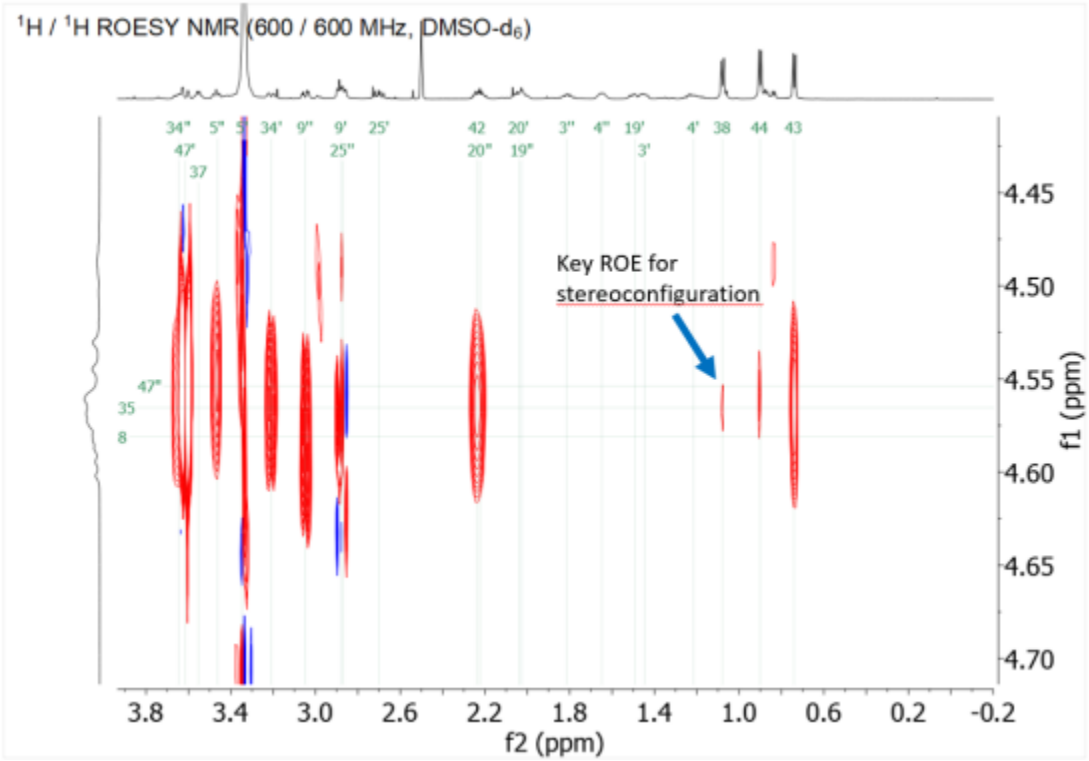

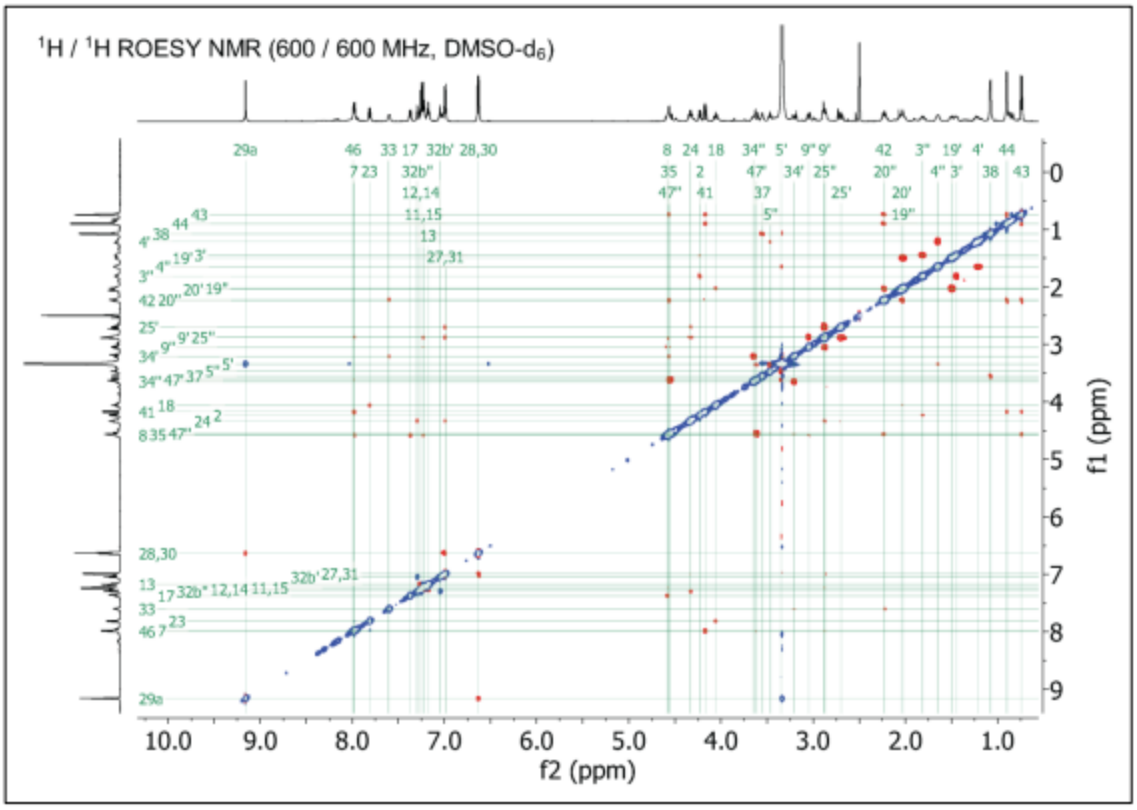

Mechanistic determination of the reason for high stereoselectivity of new chiral center.

In an effort to determine the reason for the high stereoselectivity of new chiral center in cyclic peptide **1.2a** cyc(AVGPFEY) with *R* configuration two linear peptide aldehydes, **a**VGPFE(CHO)Y and A**i**GPFE(CHO)Y were synthesized with D-configured amino acids. The peptide aldehydes had D-amino acids strategically placed in either the first or the second position. This is followed by the macrocyclization of linear peptide aldehydes **a**VGPFE(CHO)Y and A**i**GPFE(CHO)Y under optimized CyClick reaction conditions and a new chiral center in resulting cyclic peptides cyc(**a**VGPFEY) and cyc(A**i**GPFEY) were analyzed by NMR (see below).

Cyclic peptide **cyc(aVGPFEY) 1.2a'**.

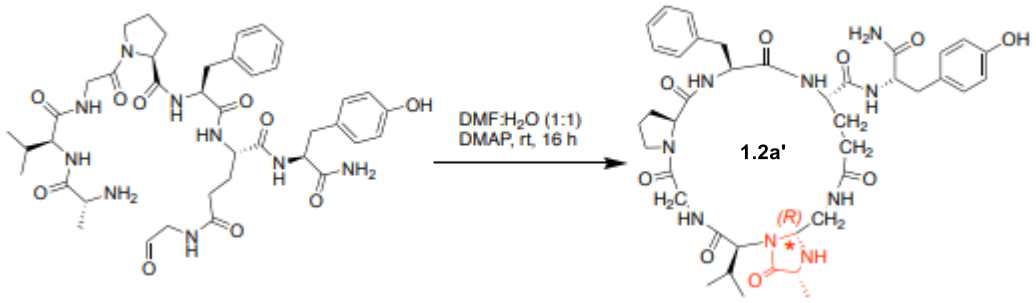

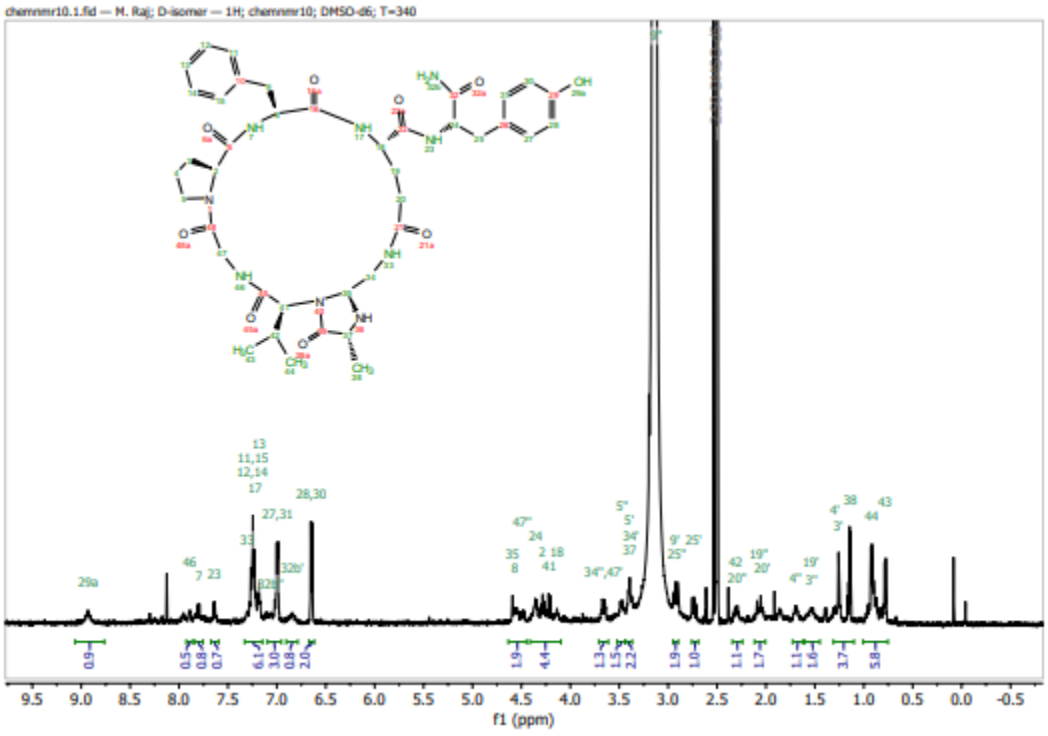

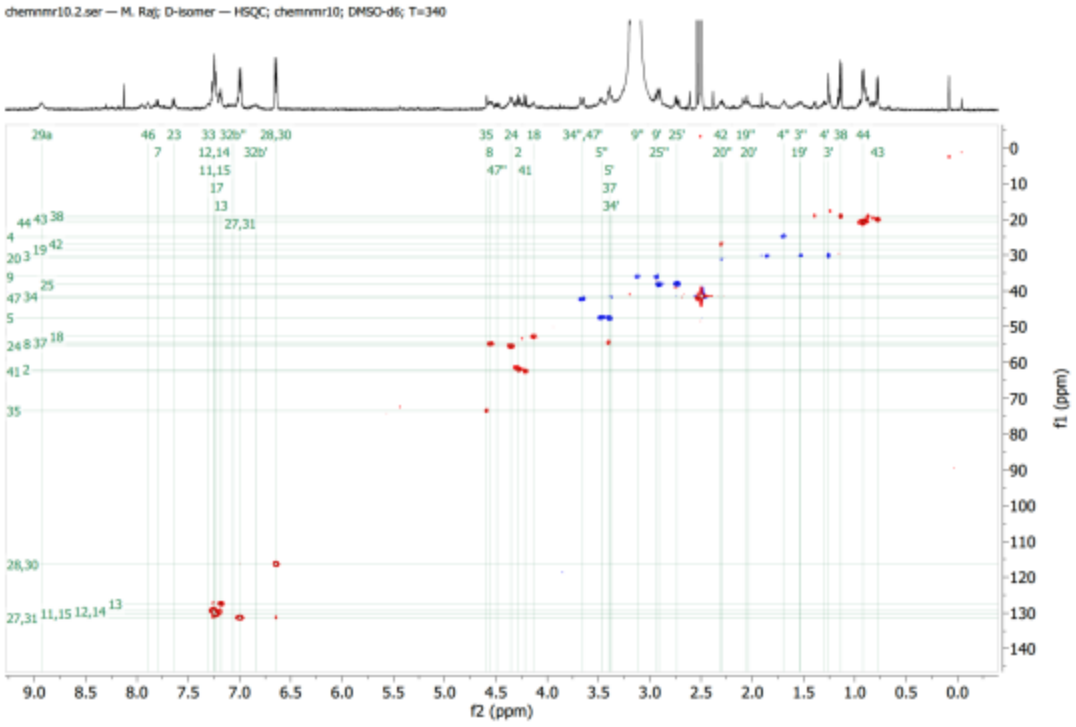
chemnmr10.2.ser — M. Raj; D-isomer — HSQC; chemnmr10; DMSO-d6; T=340
f2 (ppm)
f1 (ppm)

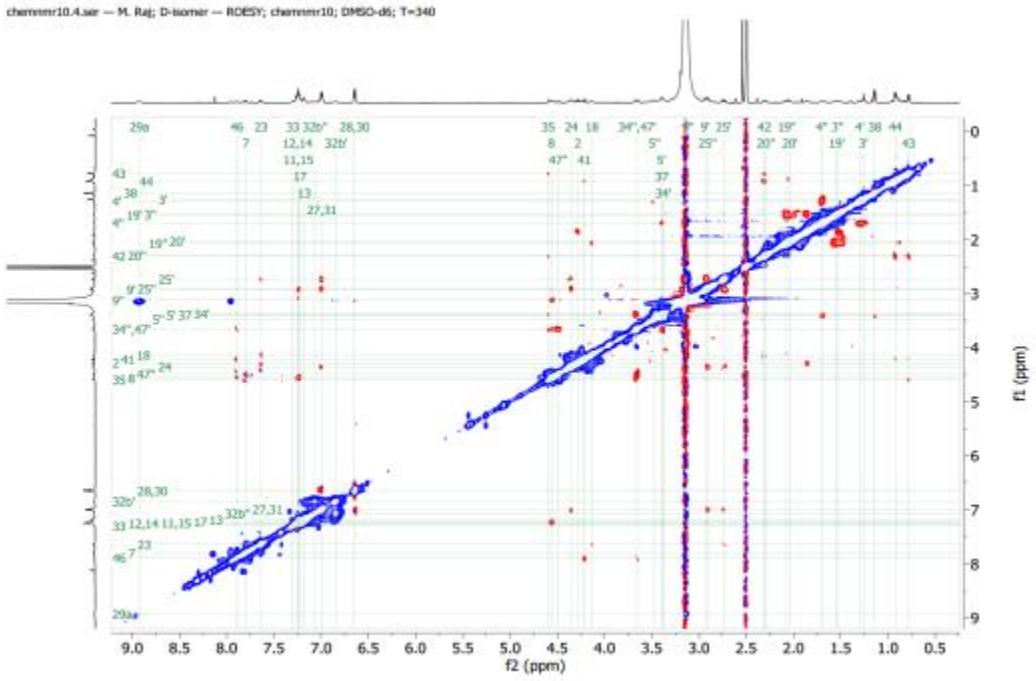
chemnmr10.4.ser — M. Raj; D-isomer — ROESY; chemnmr10; DMSO-d6; T=340
f2 (ppm)
f1 (ppm)

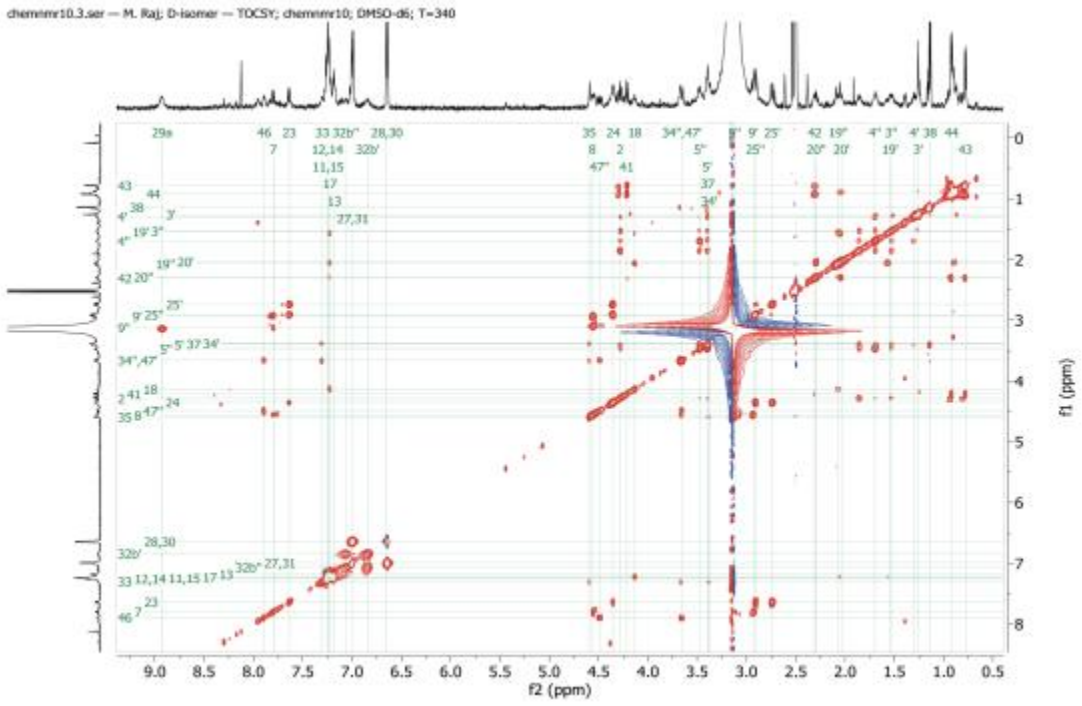
chemmr10.3.ser — M. Raj; D-isomer — TOCSY; chemmr10; DMSO-d6; T=340
f2 (ppm)
f1 (ppm)

cyclic peptide **cyc(AiGPFEY).**

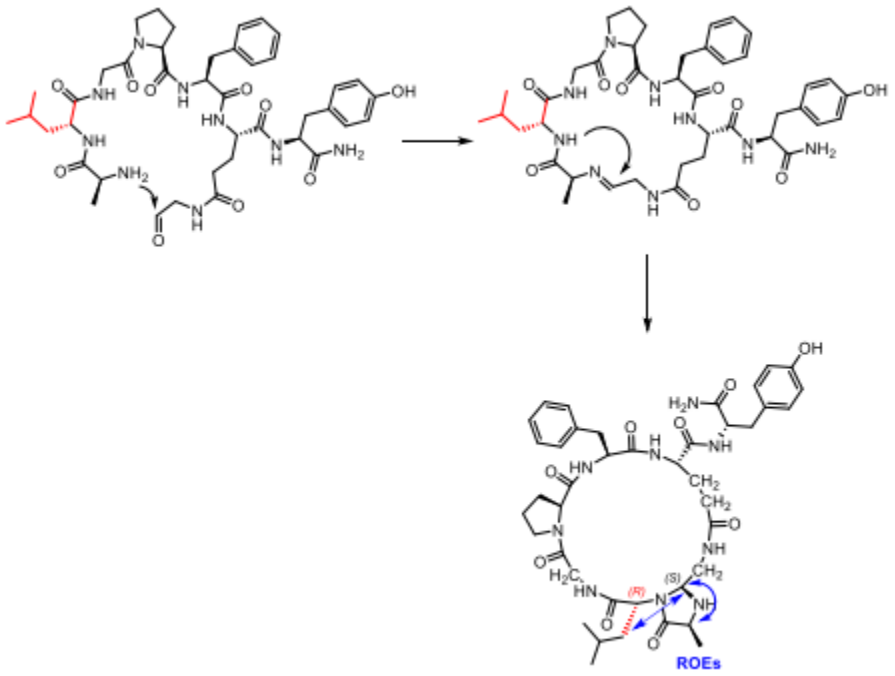

NMR experiments:

An approximately 1 mg sample was dissolved in 0.15 mL of DMSO-d_6, and the solution was then transferred to a 3-mm NMR tube. ^{1}H, ^{13}C, COSY, TOCSY, HSQC, HMBC, and ROESY spectra were acquired at ambient temperature (298 K) using a 3-mm triple resonance (HCN) helium cryoprobe on a 600 MHz Agilent DD2 NMR spectrometer. Proton chemical shifts were referenced to residual DMSO-d_5 at 2.50 ppm, and carbon chemical shifts were referenced to DMSO-d_6 at 39.52 ppm. Spectra were processed using Mnova ver. 12.0.4. A gradient COSY spectrum was acquired using 2048 x 400 increments, and 0% sine squared II apodizations were applied in both dimensions. A TOCSY spectrum was acquired using a 60 ms mixing time and 2048 x 512 increments; the spectrum was then linear predicted to 1048 points in the f1 dimension. An adiabatic gradient multiplicity-edited HSQC spectrum was acquired using 2048 x 512 increments. An adiabatic gradient HMBC spectrum was acquired using a J-optimization of 8 Hz and 2048 x 512

increments, and then a 0% sine squared II apodization was applied in the direct dimension. An adiabatic gradient ROESY spectrum was acquired using a 200 ms mixing time and 2048 x 512 increments, and 90° sine squared apodizations were applied in both dimensions.

NMR data for cyc(AiGPFE(CHO)Y)

Residue	Atom Name	Numbering	δ_H (ppm), multiplicity	δ_C (ppm)
Pro	N	1	--	--
	$C_\alpha H$	2	4.18, d (J = 9.1 Hz)	60.86
	$C_\beta H_2$	3	1.44, m; 1.95, m	29.10
	$C_\gamma H_2$	4	1.40, m; 1.73, m	23.66
	$C_\delta H_2$	5	3.42, q (J = 8.5 Hz); 3.52, t (J = 8.1 Hz)	46.13
	CO	6	--	171.93
Phe	NH	7	7.93, d (J = 8.2 Hz)	--
	$C_\alpha H$	8	4.46, ddd (J = 13.5, 8.3, 4.9 Hz)	53.50
	$C_\beta H_2$	9	2.97, m; 3.04, dd (J = 14.3, 4.5 Hz)	34.09
	C_γ	10	--	138.27
	C_2H, C_6H	11, 15	7.21, d (J = 7.2 Hz)	129.00
	C_3H, C_5H	12, 14	7.25, t (J = 7.2 Hz)	128.06
	C_4	13	7.18, t (J = 6.5 Hz)	126.19
	CO	16	--	170.35
Glu	NH	17	7.18, d (J = 7.4 Hz)	--
	$C_\alpha H$	18	4.24, td (J = 8.3, 3.0 Hz)	51.92
	$C_\beta H_2$	19	1.50, m; 1.95, m	28.86
	$C_\gamma H_2$	20	2.00, m; 2.05, m	31.21
	$C_\delta O$	21	--	174.68
	CO	22	--	170.35
Tyr	NH	23	8.00, d (J = 8.4 Hz)	--
	$C_\alpha H$	24	4.29, td (J = 8.8, 4.9 Hz)	54.39
	$C_\beta H_2$	25	2.65, dd (J = 13.8, 9.4 Hz); 2.89, dd (J = 13.9, 5.0 Hz)	36.70
	C_γ	26	--	127.93
	C_2H, C_6H	27, 31	7.02, d (J = 8.1 Hz)	130.07
	C_3H, C_5H	28, 30	6.62, d (J = 7.9 Hz)	114.86
	C_4OH	29	9.15, s	155.79
	$CONH_2$	32	7.05, s; 7.24, s	172.81
Linker	NH	33	8.41, t (J = 6.0 Hz)	--
	$C_\alpha H_2$	34	3.00, m; 3.64, dd (J = 14.8, 7.6 Hz)	39.74
	$C_\alpha H$	35	4.51, s	72.39
Ala	NH	36	--	--
	$C_\alpha H$	37	3.31, m	53.48
	$C_\beta H_3$	38	1.12, d (J = 6.8 Hz)	17.65
	CO	39	--	176.43
Ile	N	40	--	--
	$C_\alpha H$	41	4.67, dd (J = 9.2, 6.6 Hz)	51.92
	$C_\beta H_2$	42	1.58, m	35.39
	$C\gamma H$	43	1.31, p (J = 6.6 Hz)	24.16
	$C_\gamma H_3$, $C_\beta H_3$	44, 45	0.83, d (J = 6.5 Hz); 0.89, d (J = 6.6 Hz)	21.78, 22.64
	CO	46		170.46
Gly	NH	47	7.96, dd (J = 5.6 Hz)	--
	$C_\alpha H_2$	48	3.83, dd (J = 16.6, 5.9 Hz); 4.08, dd (J = 16.9, 5.3 Hz)	42.16
	CO	49	--	168.95

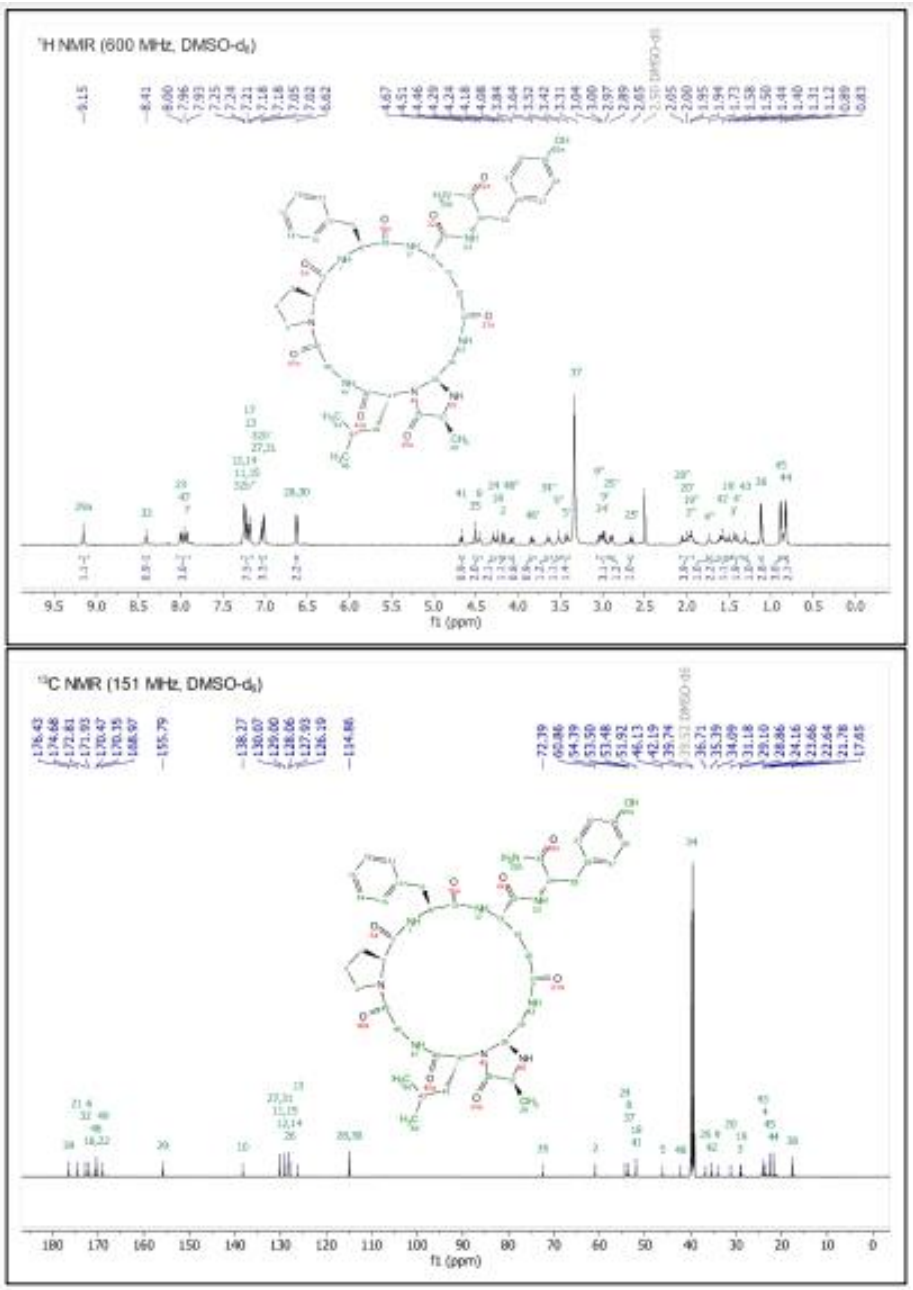
^{1}H NMR (600 MHz, DMSO-d_6)
f1 (ppm)
^{13}C NMR (151 MHz, DMSO-d_6)
f1 (ppm)

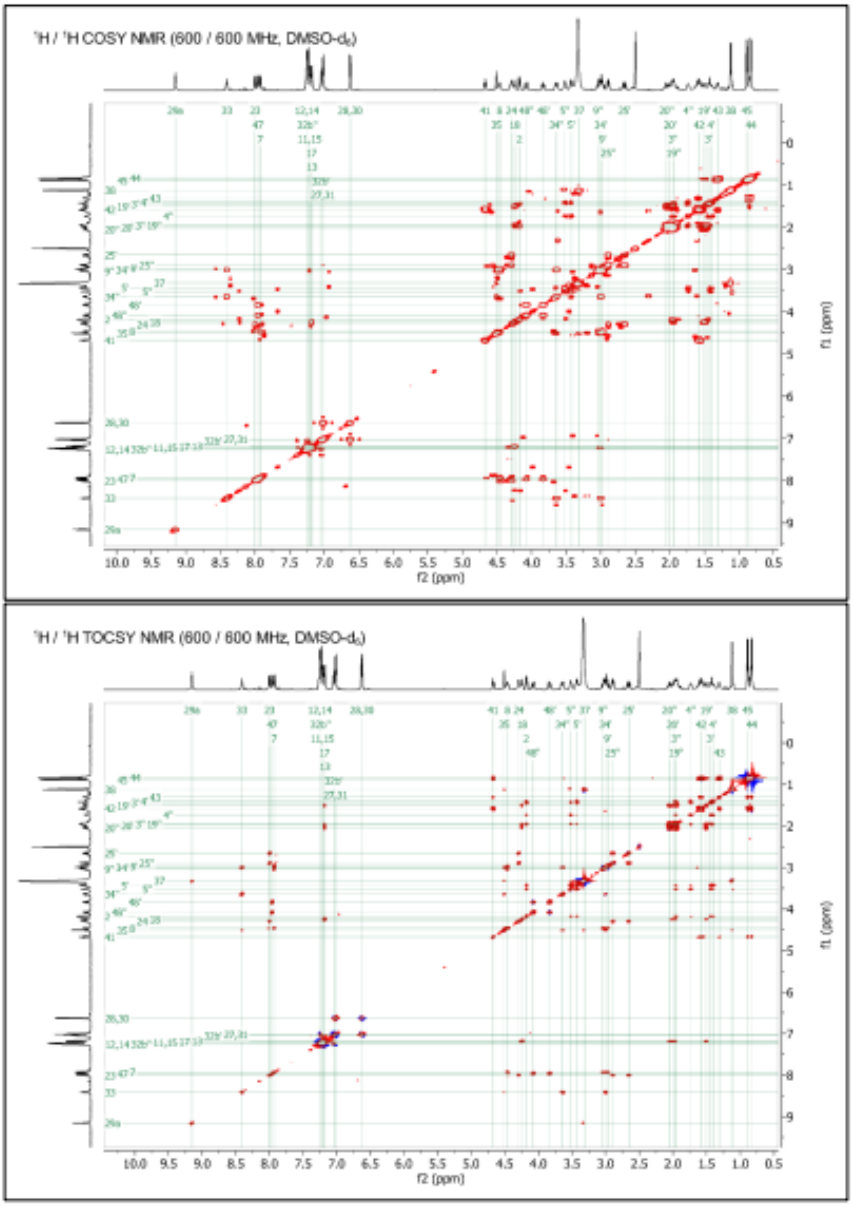
^{1}H / ^{1}H COSY NMR (600 / 600 MHz, DMSO-d_6)
f2 (ppm)
f1 (ppm)
^{1}H / ^{1}H TOCSY NMR (600 / 600 MHz, DMSO-d_6)
f2 (ppm)
f1 (ppm)

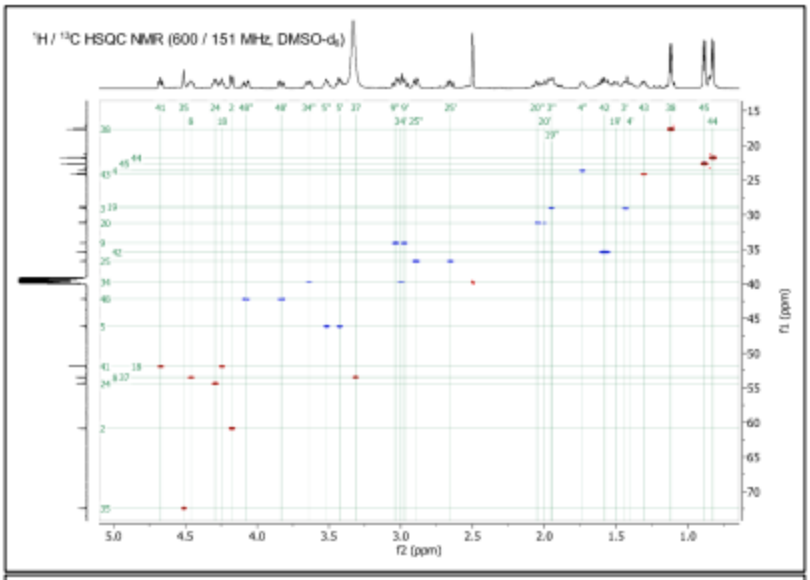
^{1}H / ^{13}C HSQC NMR (600 / 151 MHz, DMSO-d_6)
f2 (ppm)
f1 (ppm)

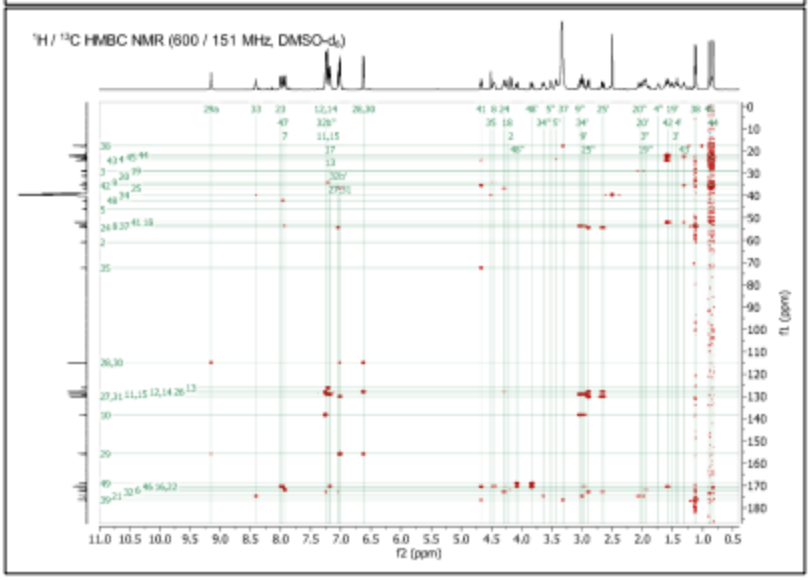
^{1}H / ^{13}C HMBC NMR (600 / 151 MHz, DMSO-d_6)
f2 (ppm)
f1 (ppm)

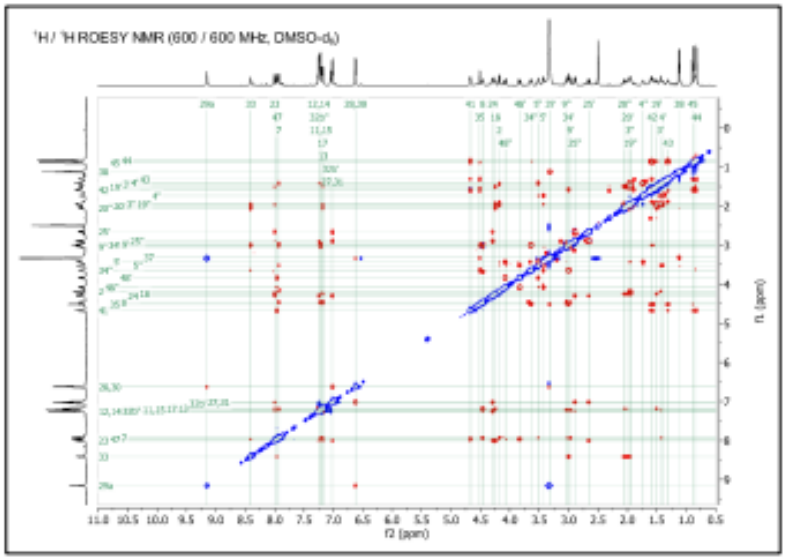
¹H / ¹H ROESY NMR (600 / 600 MHz, DMSO-d₆)
f2 (ppm)
f1 (ppm)

HRMS of cyc(AiGPFE(CHO)Y): (from Agilent 6560 Q-TOF) Observed m/z: 818.4208 Theoretical m/z: 818.4196; Mass accuracy: 1.5 ppm

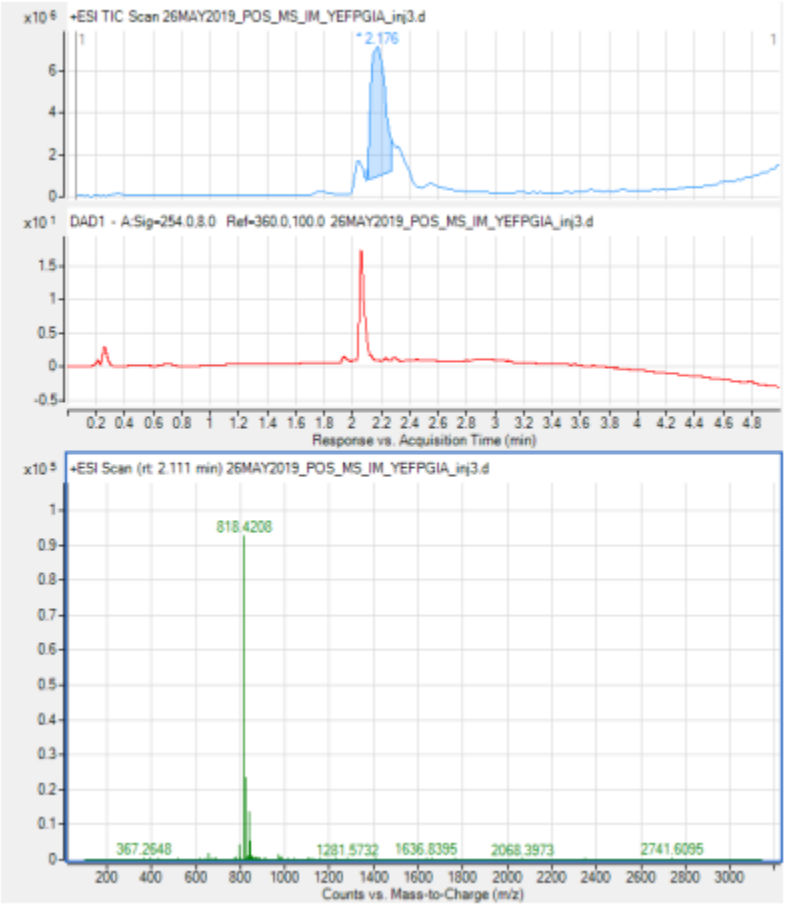

Procedure for High Concentration Studies. Linear peptide AVGPFE(CHO)Y 1a was cyclized at high concentrations (25 mM) with two different methods, our CyClick procedure and conventional reductive animation procedure and results were compared.

CyClick method: Linear peptide AVGPFE(CHO)Y **1.1a** (4 mg, 0.005 mmol) was dissolved in 1:1 DMF/H2O solution (200 µL, final conc. 25 mM) and DMAP (21 equiv.) was added. The resulting solution was stirred at room temperature for 19 h. The reaction was analyzed by HPLC, which showed the formation of only desired cyclic peptide **1.2a.** The formation of any dimers or polymers was not observed under the reaction conditions.

Conventional reductive animation method.[2] Linear peptide AVGPFE(CHO)Y **1.1a** (4 mg, 0.005 mmol) was dissolved in 1:1 DMF/H2O solution (200 µL, final conc. 25 mM) and $NaBH_3CN$ (50 equiv.) was added. The resulting solution was stirred at room temperature for 19 h. The reaction was analyzed by HPLC, which showed the formation of linear and cyclic dimers side products along with desired cyclic peptide.

Procedure for High Concentration Studies by CyClick Method. Linear peptide AVGPFE(CHO)Y **1.1a** was cyclized at high concentrations (100 mM) with our CyClick procedure.

CyClick method: Linear peptide AVGPFE(CHO)Y **1.1a** (3.5 mg, final conc. 100 mM) was dissolved in 1:1 DMF/H2O solution (44 µL) and DMAP (21 equiv.) was added. The resulting solution was stirred at room temperature for 8 h. The reaction was analyzed by HPLC, which showed the formation of only desired cyclic peptide **1.2a** with 89% conversion. The formation of any dimers or polymers was not observed under the reaction conditions.

HPLC Trace of High Concentration Reaction by CyClick Method (100 mM)

Cyclization of linear peptides (100 mM conc.)

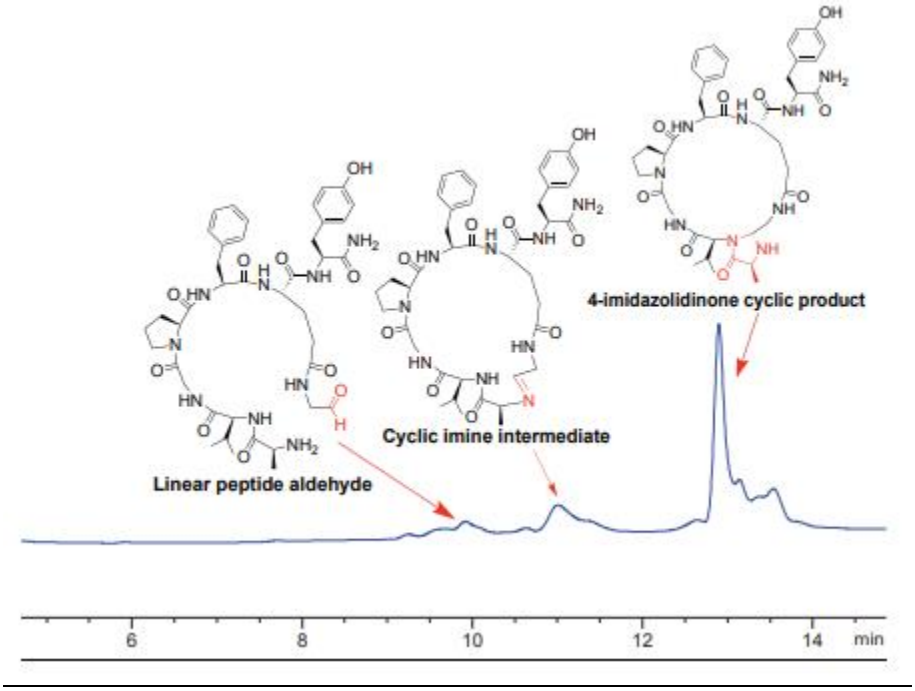

General Procedures for Rate Studies. Linear peptide AVGPFE(CHO)Y **1.1a** (1 mg, 0.001 mmol) was dissolved in 1:1 DMF/H_2O solution (1800 µL, final conc. 0.67 mM) and DMAP (7 equiv.) was added. The resulting solution was stirred at room temperature. Samples (100 µL) were taken after regular intervals of time and reaction was quenched by adding it into 400µL of pre-frozen water followed by freezing the sample at -80 °C. The frozen samples were then lyophilized and dissolved in 120 µL of 1:1 H_2O/ACN and injected immediately into the HPLC for determining the % conversion to a macrocyclic peptide **1.2a** at different time intervals. Rate study was done in triplicate. We use average of three trials to plot the rate curve. 0 min sample is sample taken after addition of all the reagents of the CyClick reaction.

Rate Studies for Macrocyclization of Peptide 1.1a to 1.2a by CyClick Chemistry

Time (min)	Macrocyclic peptide **1.2a** formation **Trial 1**	Macrocyclic peptide **1.2a** formation **Trial 2**	Macrocyclic peptide **1.2a** formation **Trial 3**	Macrocyclic peptide **1.2a** formation Average of three trials
0	9%	8%	9%	8.6%
1	11.4%	10.5%	11.6%	11.1%
2	12%	12%	12%	12%
3	12%	11%	11%	11.3%
5	14%	14.6%	17%	15.2%
7	17%	20%	17%	18%
9	18%	19.2%	18%	18.4%
12	20.6%	19.4%	20%	20%
17	24%	24%	27.3%	25.1%
22	36%	37%	36.5%	36.5%
27	38.2%	39%	38.5%	38.5%
37	44.2%	46%	51%	47%
60	54.3%	53%	53.7%	53.6%
90	63%	62.5%	63%	62.8%
120	65%	65.4%	67%	65.8%
250	83%	84%	83.5%	83.5%

Rate Studies for Macrocyclization of Peptide 1.1a to 1.2a by CyClick Chemistry

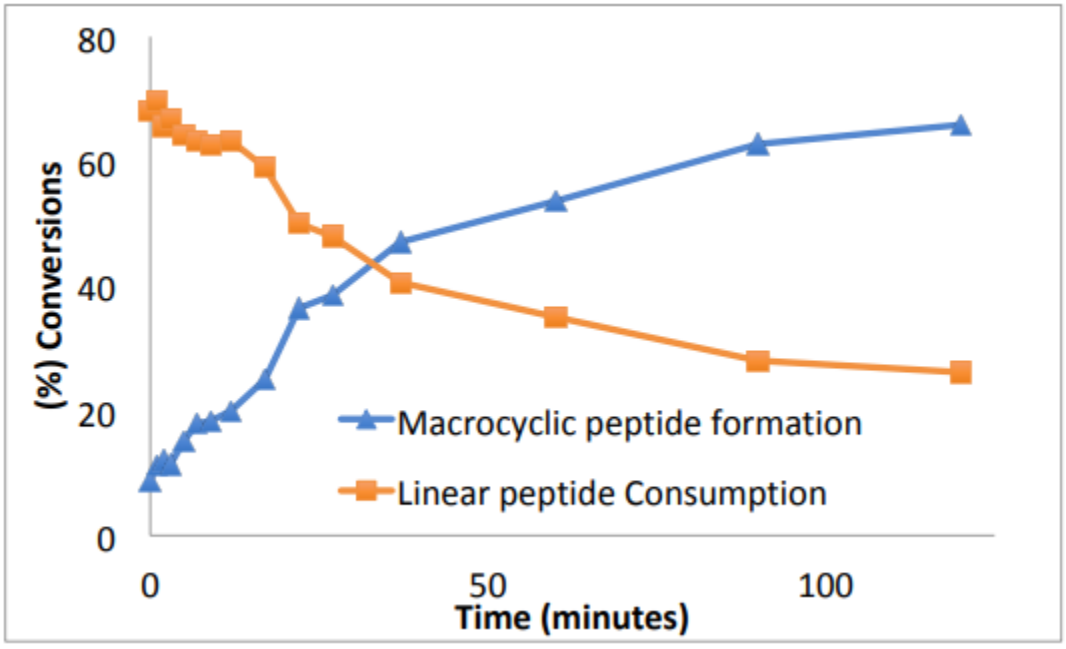

Peptide Characterization and HRMS Traces

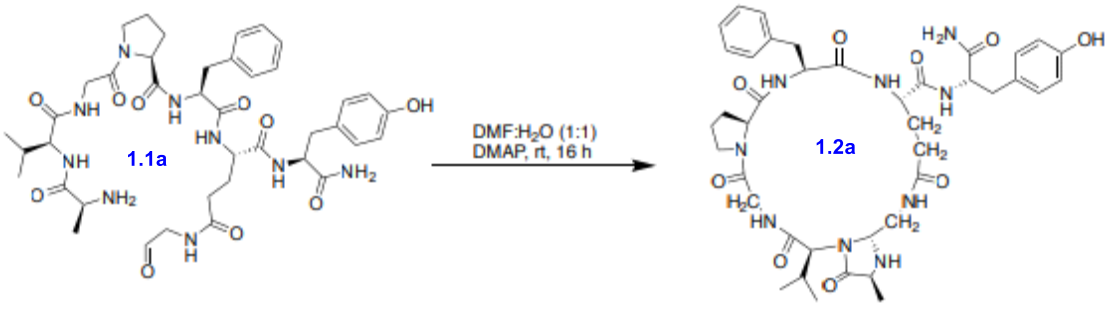

cyc(Ala-Val-Gly-Pro-Phe-Glu)Tyr (1.2a). LCMS: m/z 804.4 (calcd [M+H]+ = 804.3), m/z 826.4 (calcd [M+Na]+ = 826.3), Purity: >95% (HPLC analysis at 220 nm). Retention time: 12.8.

HRMS spectra of the macrocyclized product 1.2a

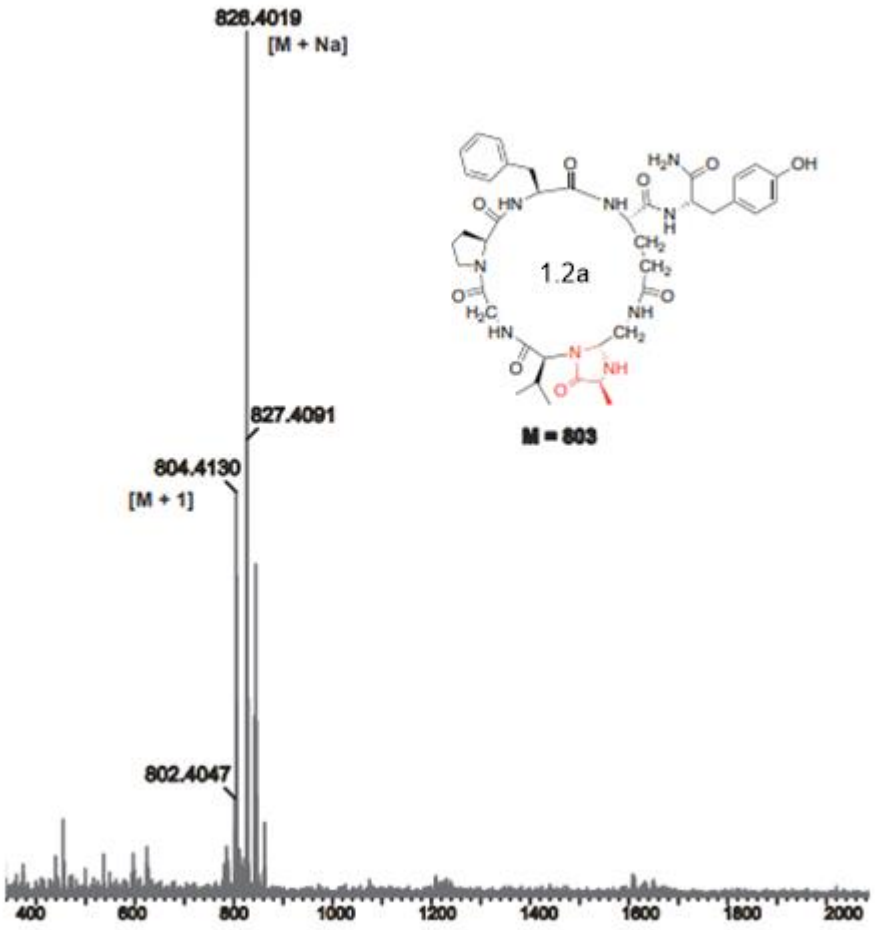

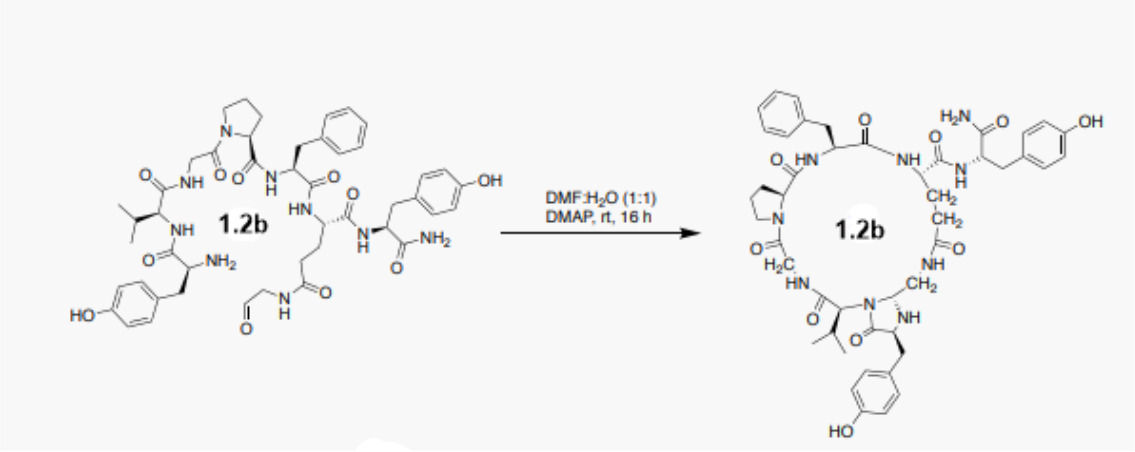

cyc(Tyr-Val-Gly-Pro-Phe-Glu)-Tyr LCMS: m/z 896.4 (calcd [M+H]+ = 896.3), m/z 918.4 (calcd [M+Na]+ = 918.4), m/z 934.3 (calcd [M+K]+ = 934.4), Purity: >95% (HPLC analysis at 220 nm). Retention time: 18.3

HRMS spectra of the macrocyclized product **1.2b**

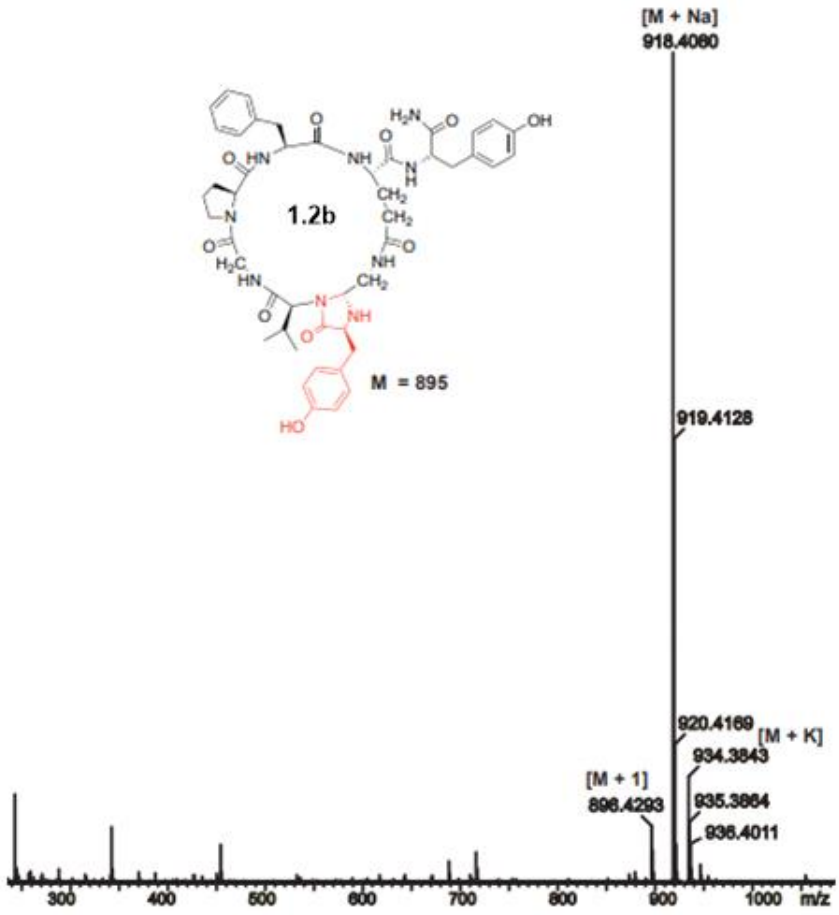

Conversion of Linear Peptide 1.1c to Cyclic Peptide 1.2c

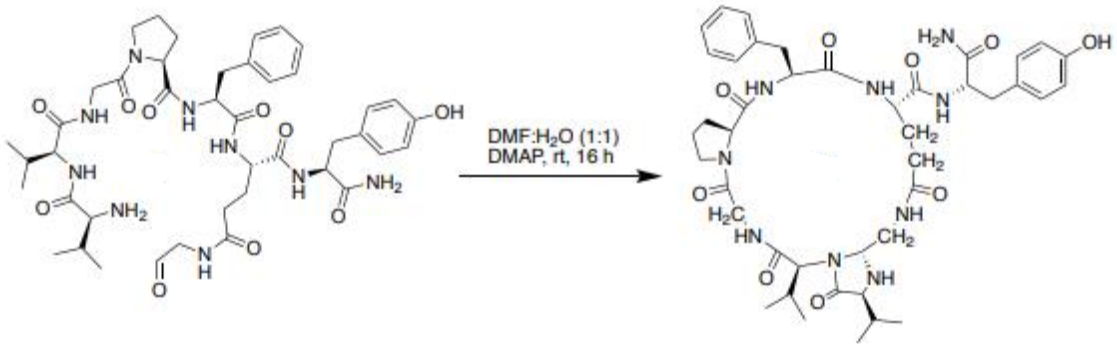

***cyc*(Val-Val-Gly-Pro-Phe-Glu)Tyr)** LCMS: *m/z* 832.4 (calcd $[M+H]^+$ = 832.4), *m/z* 854.4 (calcd $[M+Na]^+$ = 854.4, Purity: >95% (HPLC analysis at 220 nm). Retention time: 14.7

HRMS spectra of the macrocyclized product

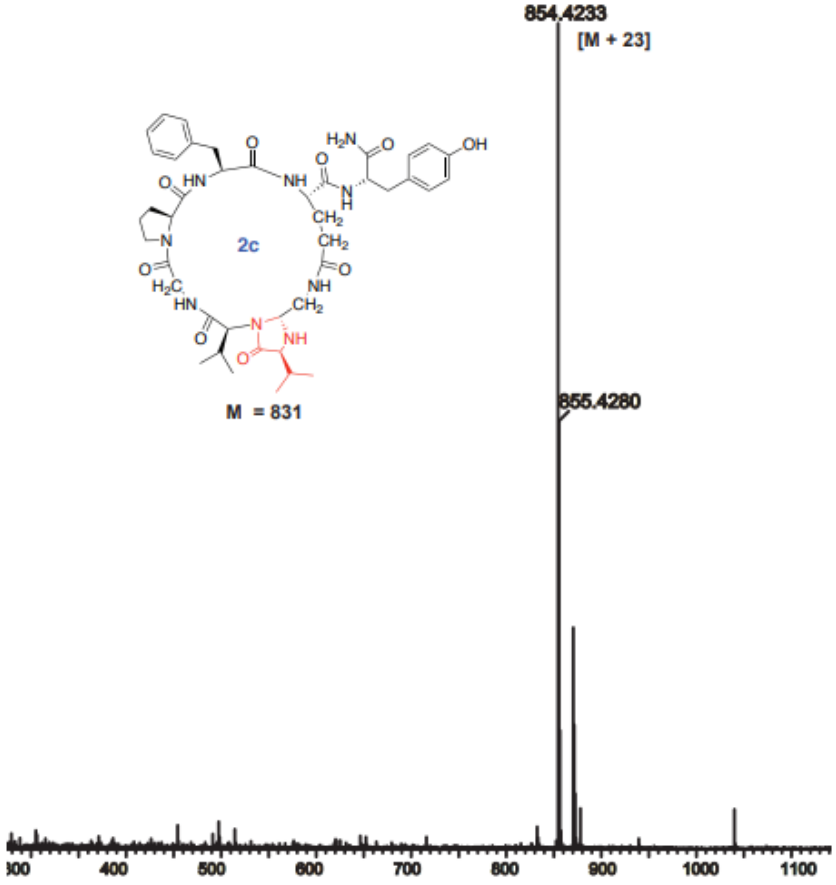

Conversion of Linear Peptide 1.1d to Cyclic Peptide 1.2d

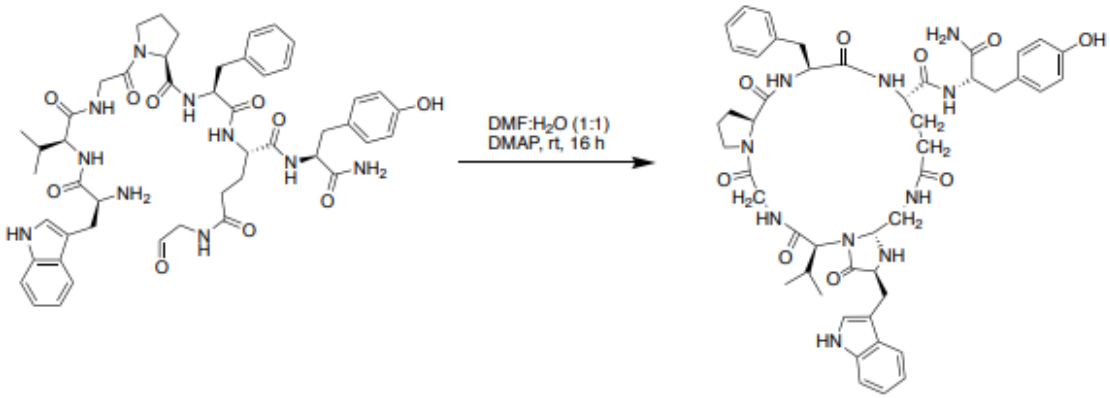

***cyc*(Trp-Val-Gly-Pro-Phe-Glu)-Tyr** LCMS: *m/z* 917.4 (calcd $[M+H]^+$ = 917.4), Purity: >95% (HPLC analysis at 220 nm). Retention time: 16.5

HRMS spectra of the macrocyclized product

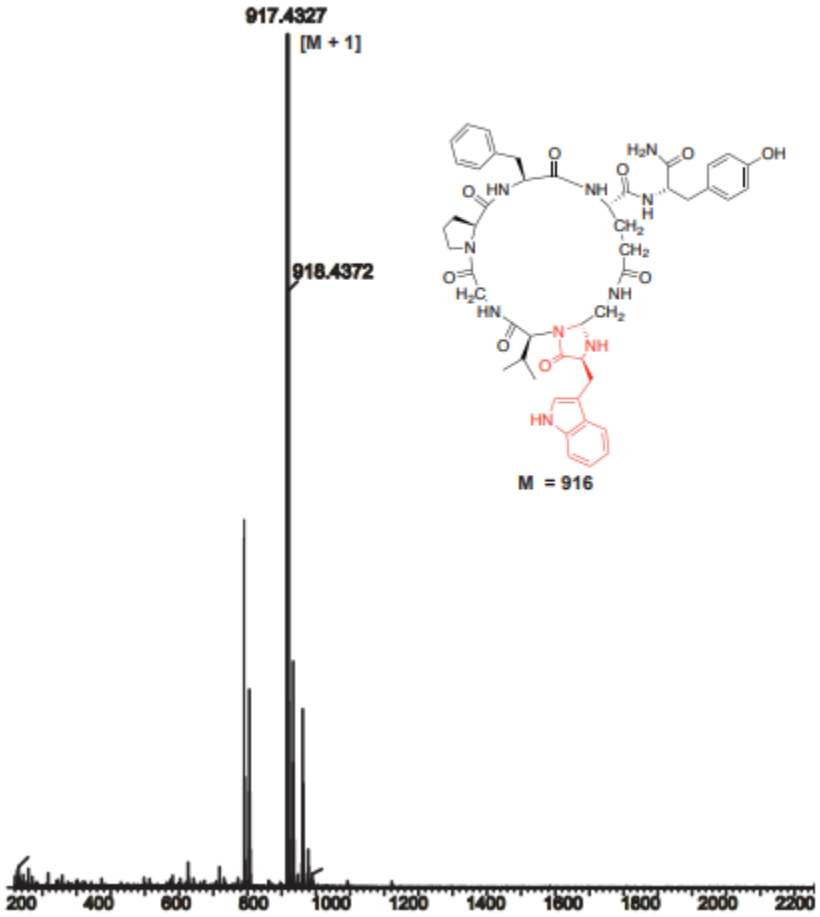

Conversion of Linear Peptide 1.1e to Cyclic Peptide 1.2e

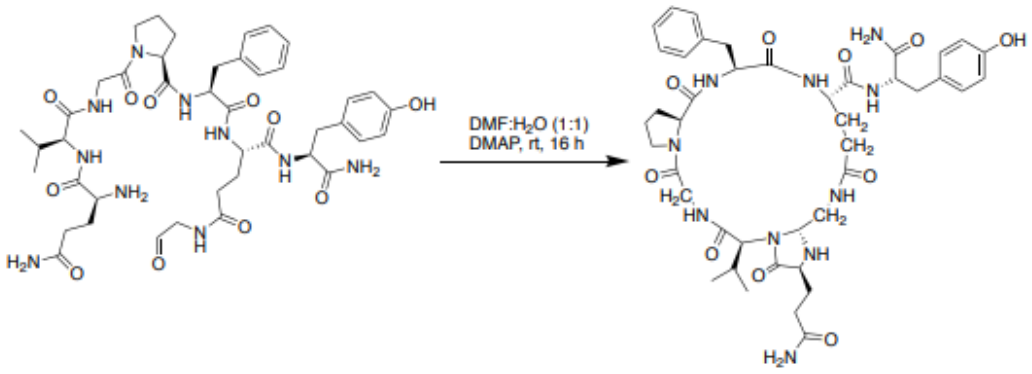

***cyc*(Gln-Val-Gly-Pro-Phe-Glu)-Tyr** LCMS: *m/z* 861.4 (calcd $[M+H]^+$ = 861.3), *m/z* 883.4 (calcd $[M+Na]^+$ = 883.3), Purity: >95% (HPLC analysis at 220 nm). Retention time: 13.6

HRMS spectra of the macrocyclized product

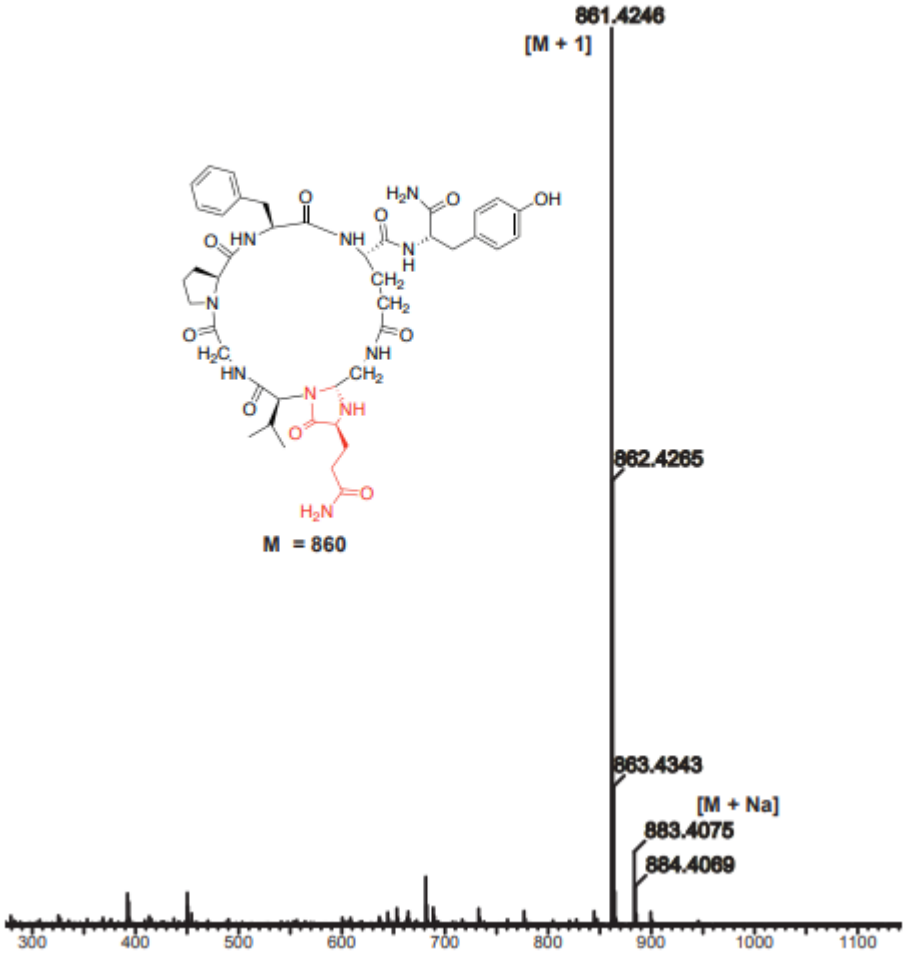

Conversion of Linear Peptide 1.1f to Cyclic Peptide 1.2f

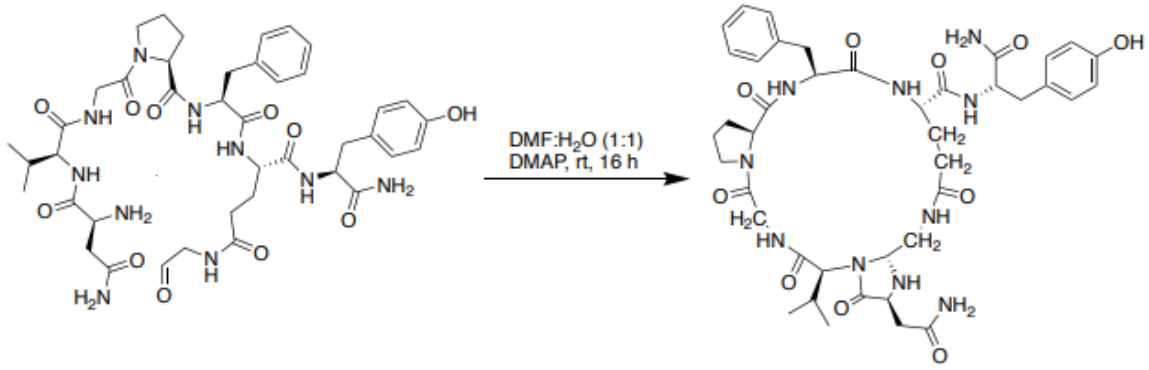

***cyc*(Asn-Val-Gly-Pro-Phe-Glu)-Tyr** LCMS: *m/z* 847.4 (calcd $[M+H]^+$ = 847.4), *m/z* 869.4 (calcd $[M+Na]^+$ = 869.4), Purity: >95% (HPLC analysis at 220 nm). Retention time: 14.4

HRMS spectra of the macrocyclized product .

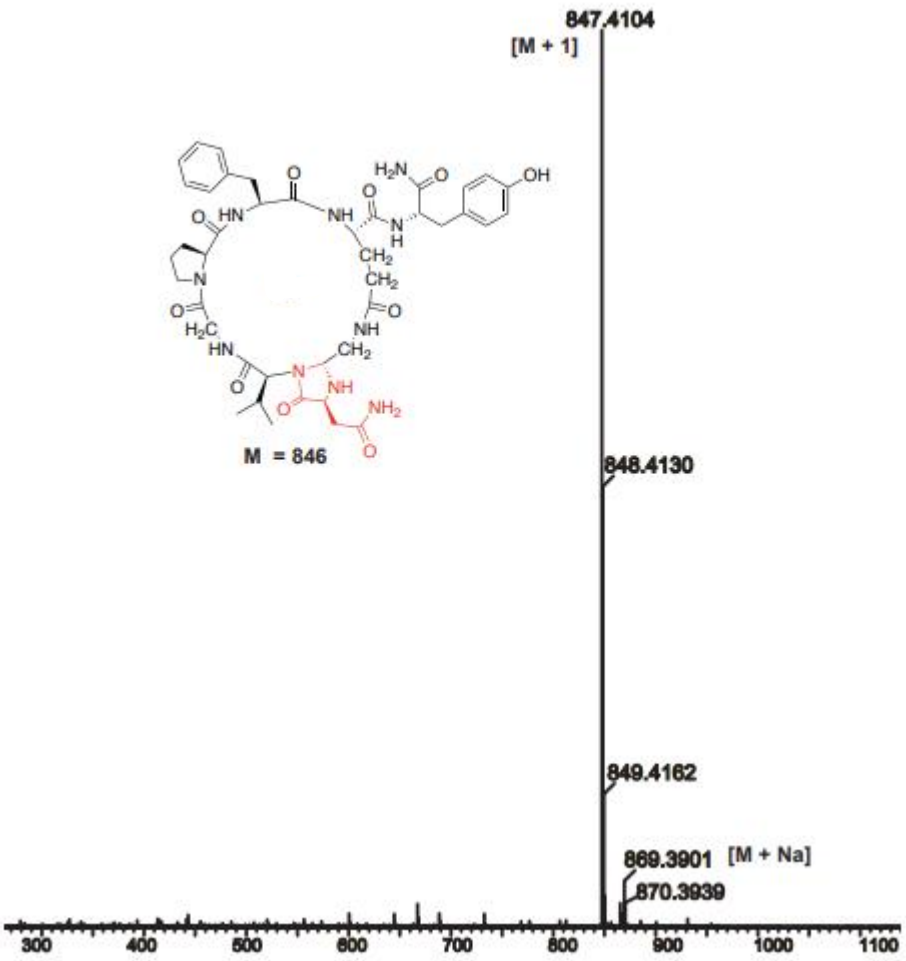

Conversion of Linear Peptide 1.1g to Cyclic Peptide 1.2g

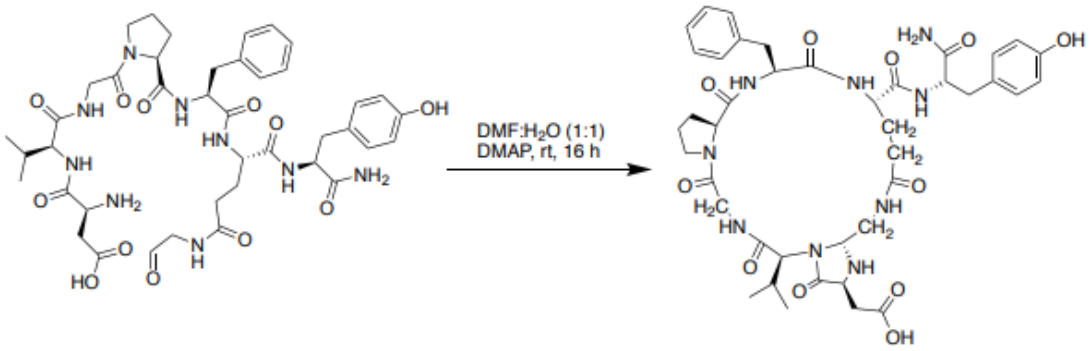

***cyc*(Asp-Val-Gly-Pro-Phe-Glu)-Tyr** LCMS: *m/z* 848.4 (calcd $[M+H]^+$ = 848.3), *m/z* 870.4 (calcd $[M+Na]^+$ = 870.3), *m/z* 886.4 (calcd $[M+K]^+$ = 886.3), Purity: >95% (HPLC analysis at 220 nm). Retention time: 14.9

HRMS spectra of the macrocyclized product

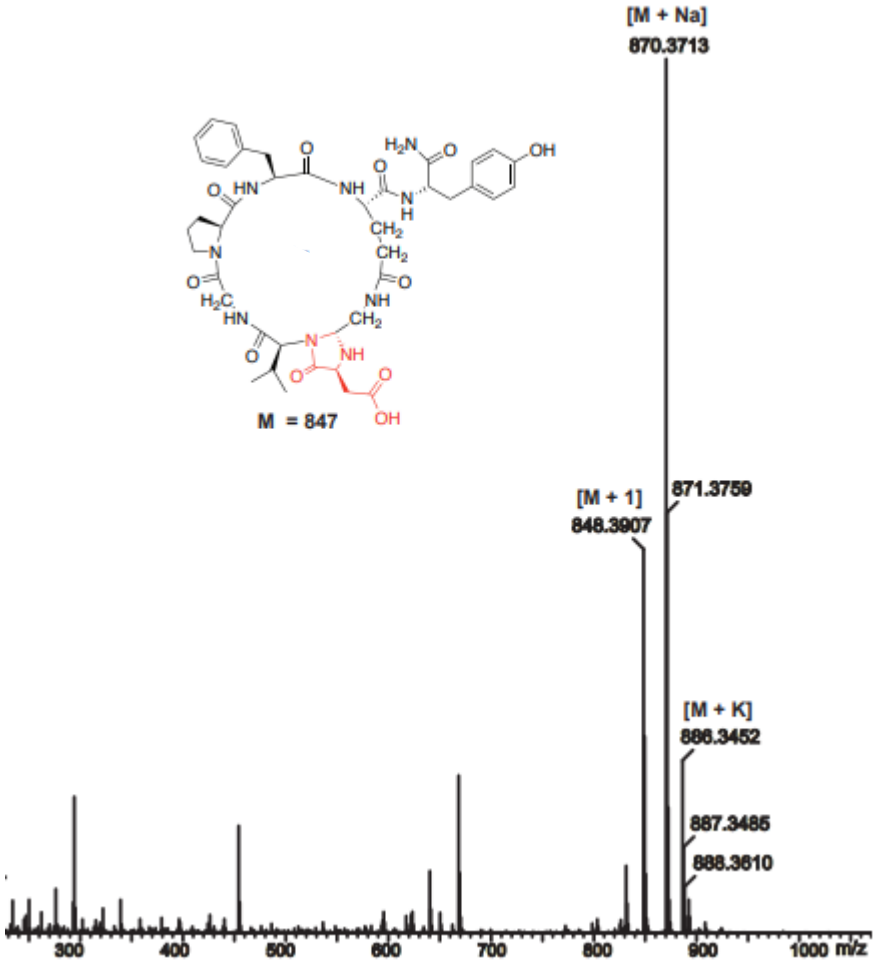

Conversion of Linear Peptide 1.1h to Cyclic Peptide 1.2h

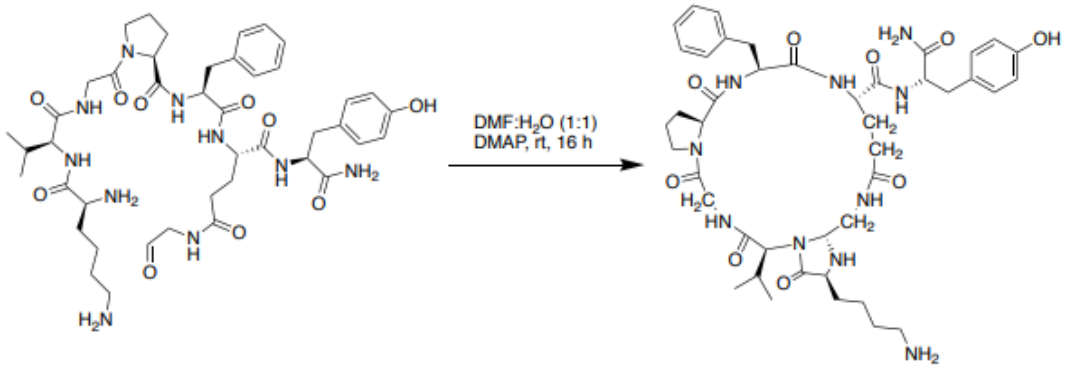

***cyc*(Lys-Val-Gly-Pro-Phe-Glu)-Tyr** LCMS: *m/z* 861.5 (calcd $[M+H]^+$ = 861.4), *m/z* 883.4 (calcd $[M+Na]^+$ = 883.4), Purity: >95% (HPLC analysis at 220 nm). Retention time: 11.3

HRMS spectra of the macrocyclized product

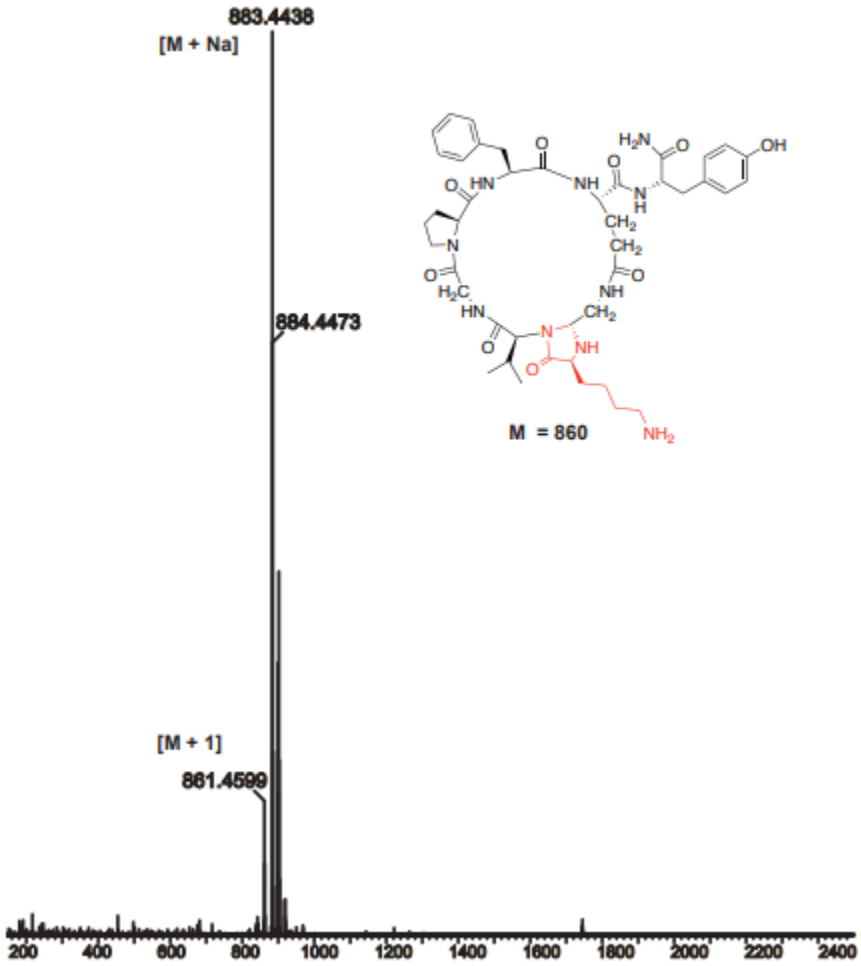

Cyclization of Linear Peptide 1.1i to Cyclic Peptide 1.2i and 1.2i'

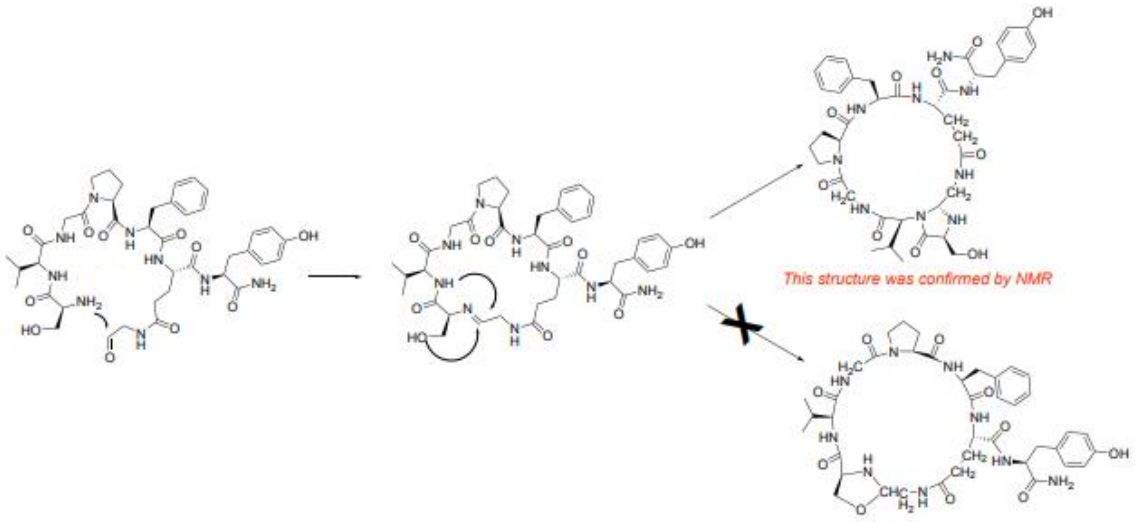

***cyc*(Ser-Val-Gly-Pro-Phe-Glu)-Tyr** LCMS: *m/z* 820.4 (calcd $[M+H]^+$ = 820.3), Purity: >95% (HPLC analysis at 220 nm). Retention time: 1.95

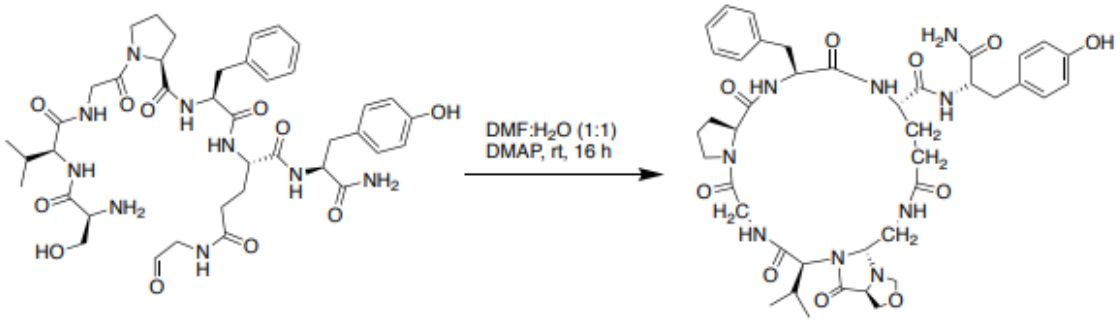

***cyc*(Ser(CO)-Val-Gly-Pro-Phe-Glu)-Tyr** LCMS: *m/z* 832.4 (calcd $[M+H]^+$ = 832.3), Purity: >95% (HPLC analysis at 220 nm). Retention time: 2.13

HRMS spectra of the macrocyclized product

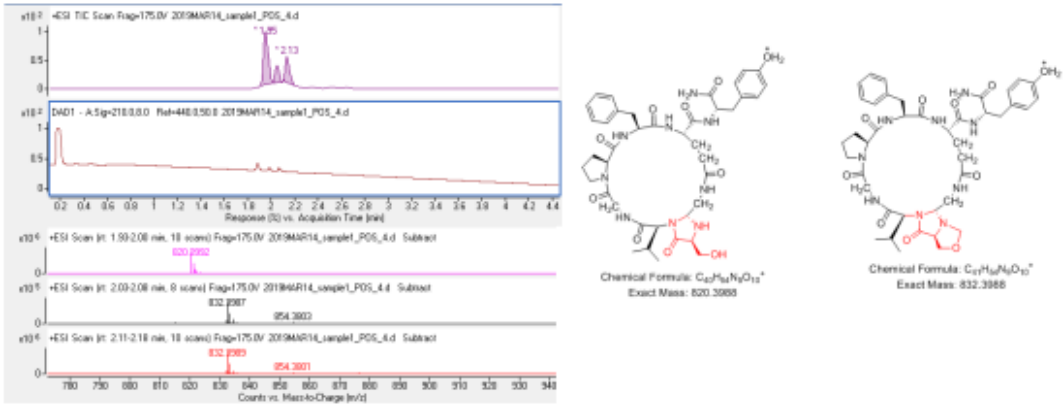

Cyclization of Linear Peptide 1.1i to Cyclic Peptide 1.2j

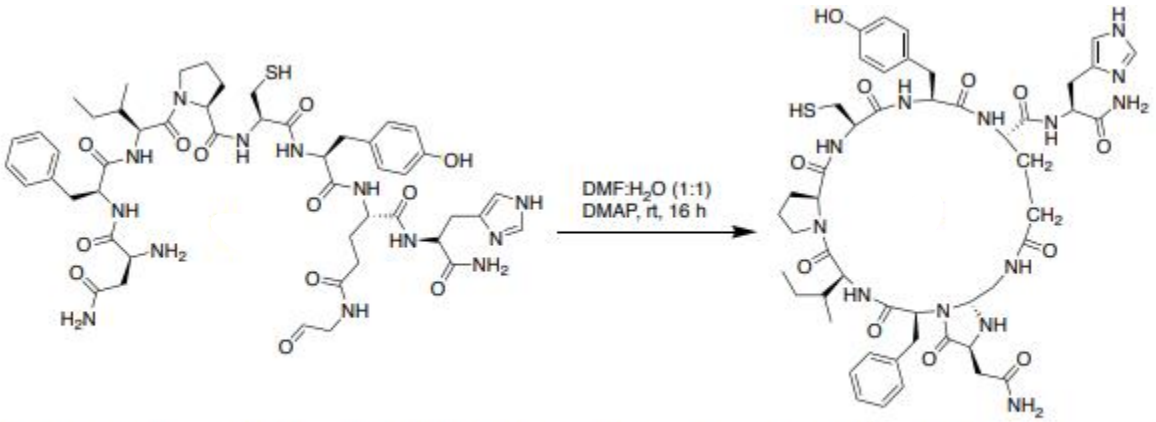

***cyc*(Asn-Phe-Ile-Pro-Cys-Tyr-Glu)-His** LCMS: *m/z* 1044.5 (calcd $[M+H]^+$ = 1044.4), Purity: >95% (HPLC analysis at 220 nm). Retention time: 16.8

HRMS spectra of the macrocyclized product

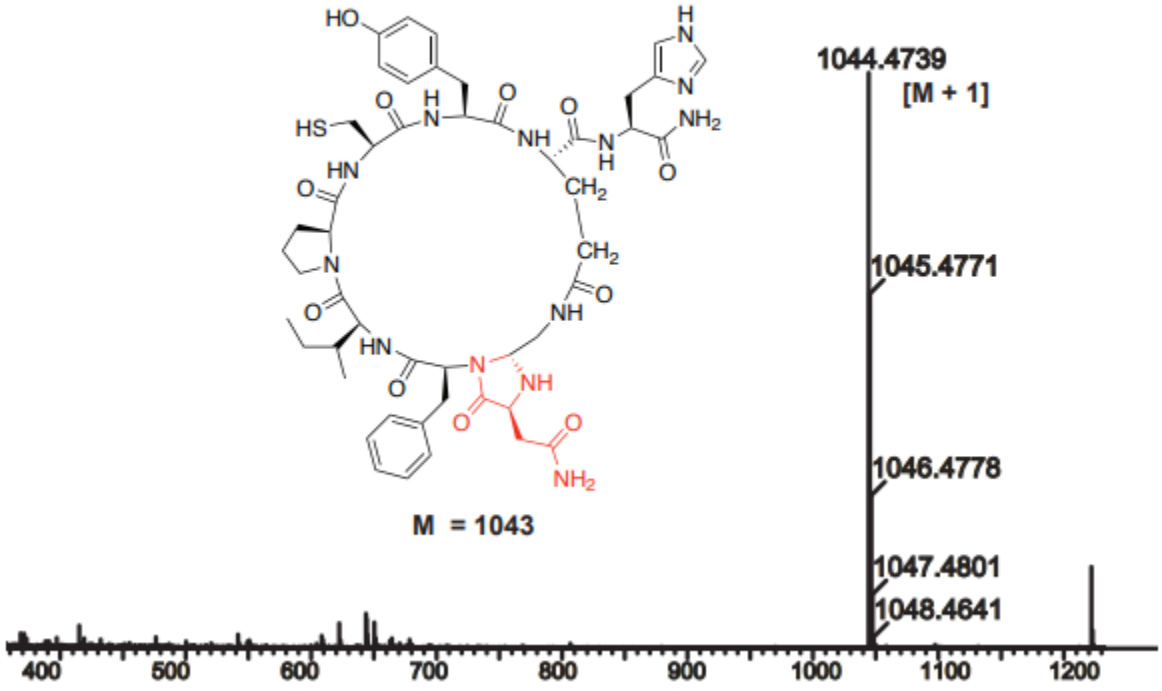

Cyclization of Linear Peptide 1.1k to Cyclic Peptide 1.2k

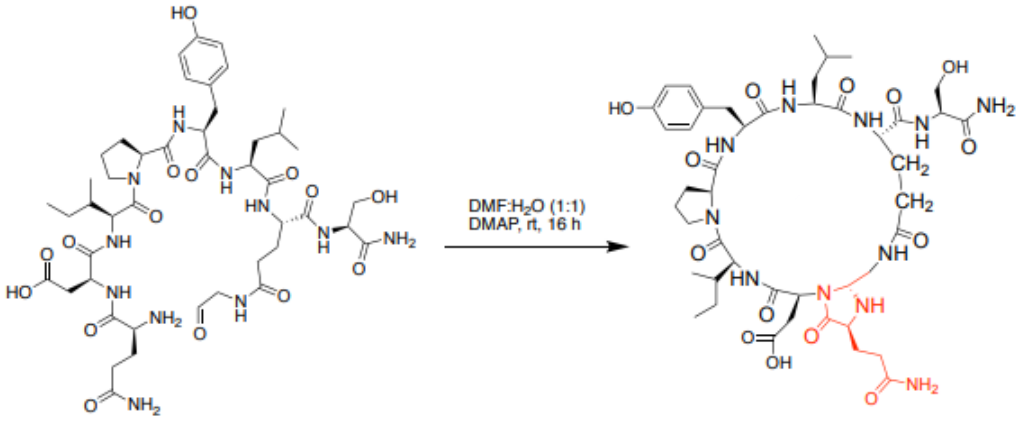

***cyc*(Gln-Asp-Ile-Pro-Tyr-Leu-Glu)-Ser** LCMS: *m/z* 986.5 (calcd $[M+H]^+$ = 986.4), *m/z* 1008.5 (calcd $[M+Na]^+$ = 1008.4), Purity: >95% (HPLC analysis at 220 nm). Retention time: 14.2

HRMS spectra of the macrocyclized product

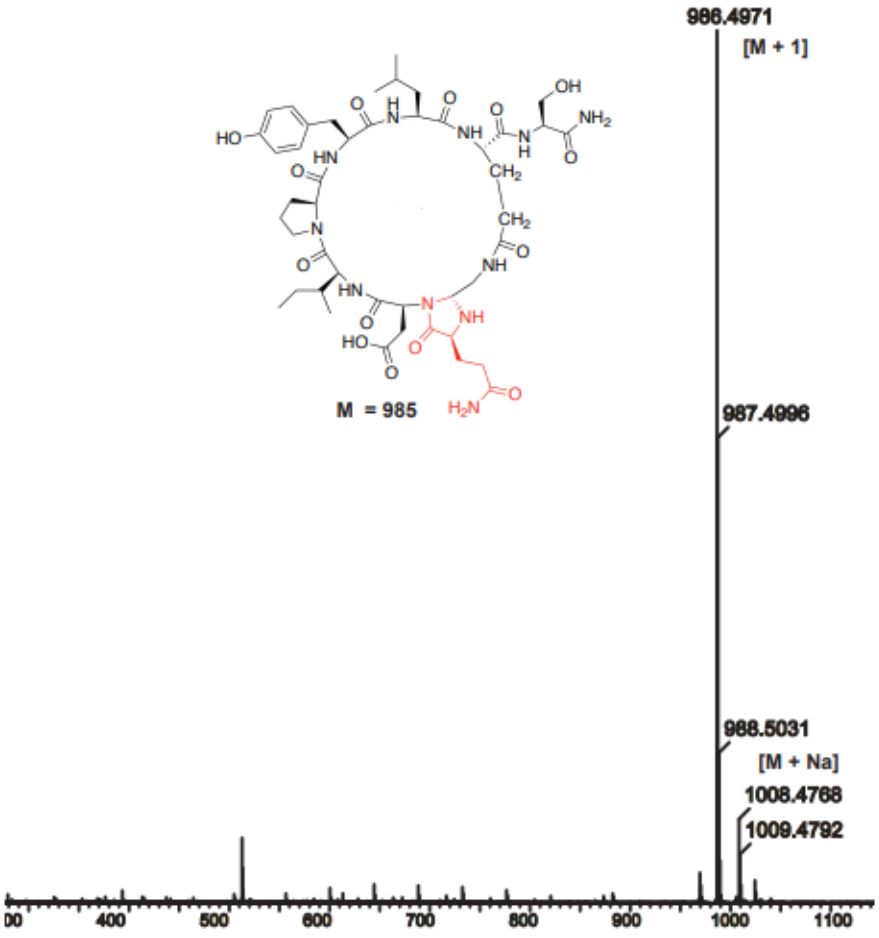

Cyclization of Linear Peptide 1.1l to Cyclic Peptide 1.2l

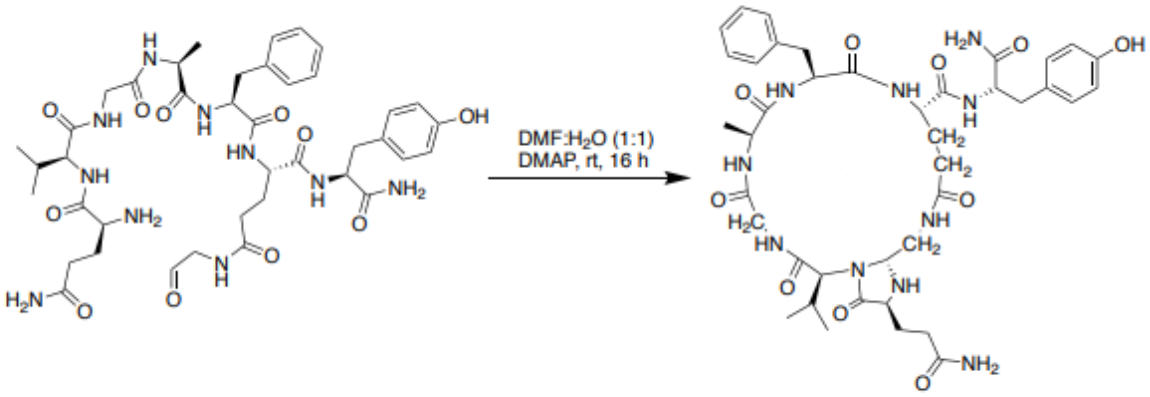

***cyc*(Gln-Val-Gly-Ala-Phe-Glu)-Tyr** . LCMS: *m/z* 835.4 (calcd $[M+H]^+$ = 835.4), *m/z* 857.4 (calcd $[M+Na]^+$ = 857.4), Purity: >95% (HPLC analysis at 220 nm). Retention time: 12.5

HRMS spectra of the macrocyclized product .

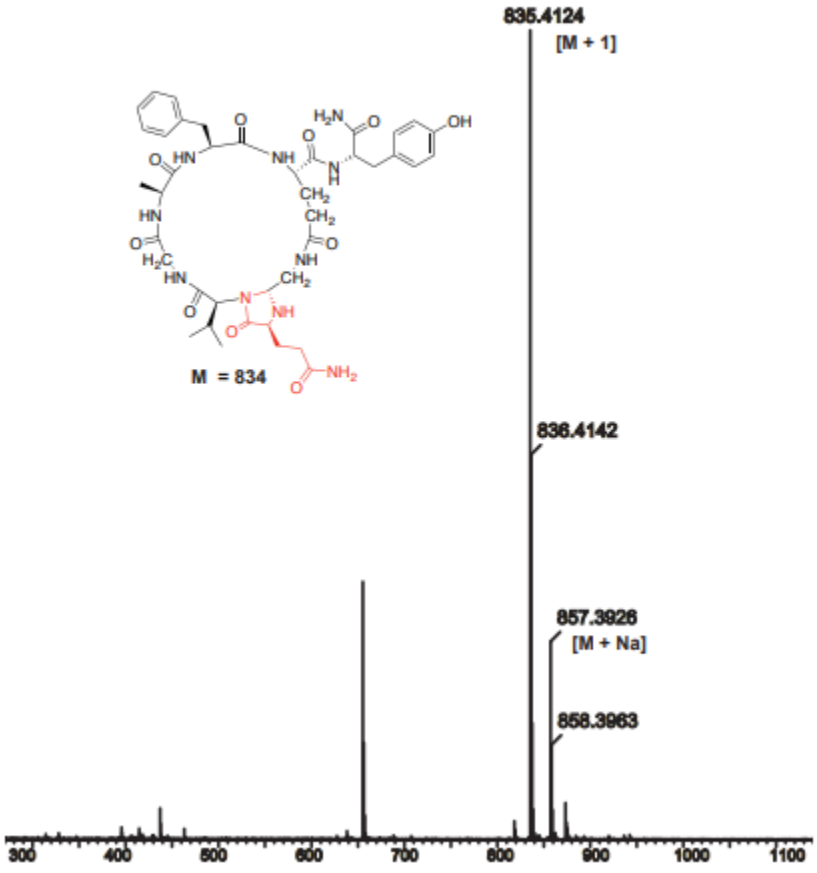

Cyclization of Linear Peptide 1.1m to Cyclic Peptide 1.2m

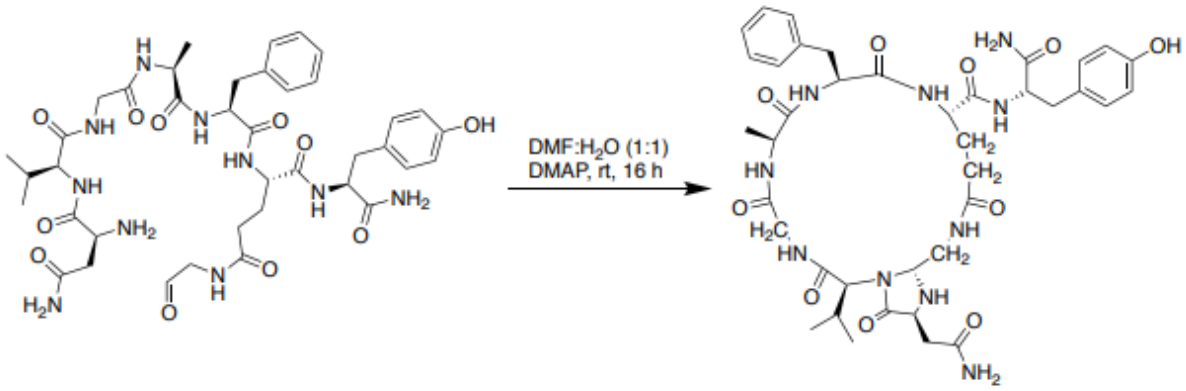

***cyc*(Asn-Val-Gly-Ala-Phe-Glu)-Tyr** LCMS: *m/z* 821.4 (calcd $[M+H]^+$ = 821.4), *m/z* 844.4 (calcd $[M+H]^+$ = 844.4), Purity: >95% (HPLC analysis at 220 nm). Retention time: 12.4

HRMS spectra of the macrocyclized product

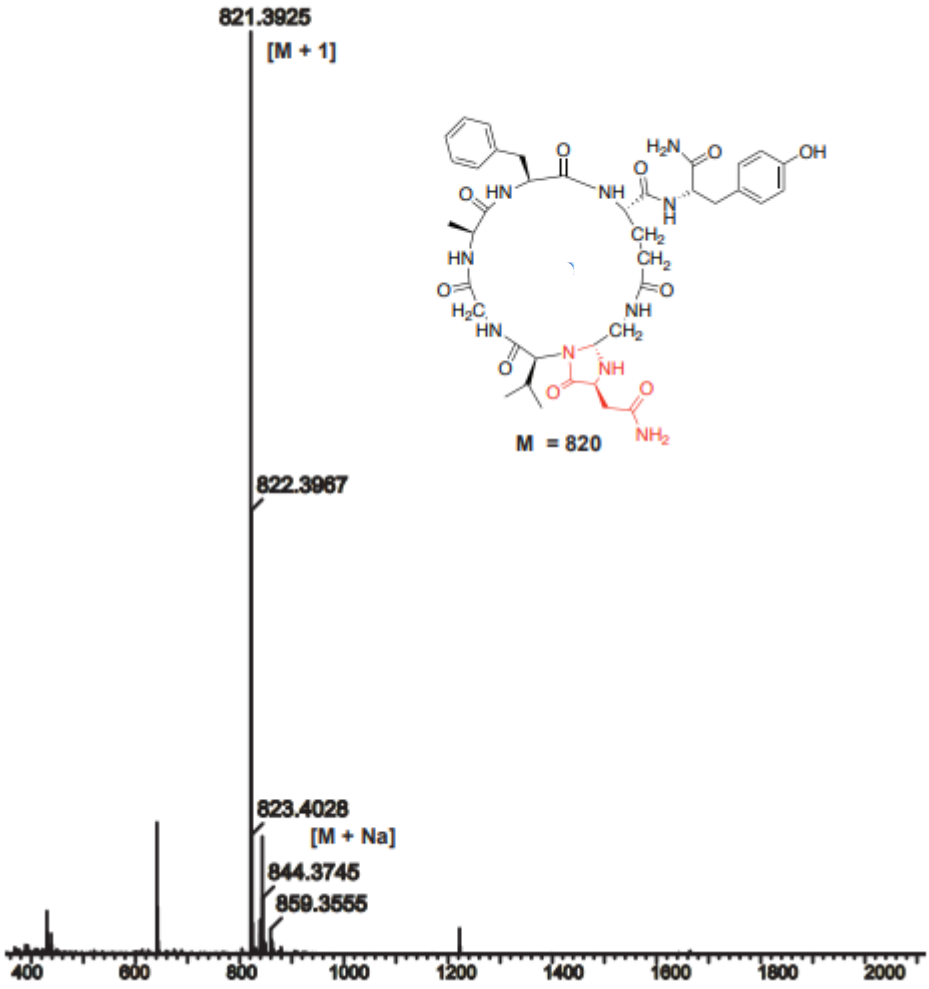

Cyclization of Linear Peptide 1.1n to Cyclic Peptide 1.2n

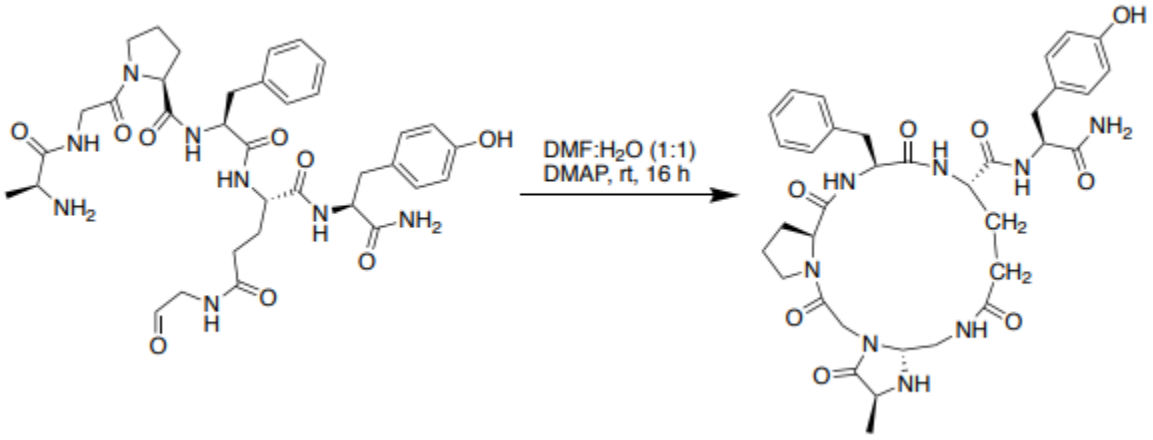

***cyc*(Ala-Gly-Pro-Phe-Glu)-Tyr** LCMS: *m/z* 705.3 (calcd $[M+H]^+$ = 705.4), *m/z* 727.3 (calcd $[M+Na]^+$ = 727.4), *m/z* 743.2 (calcd $[M+K]^+$ = 743.4), Purity: >95% (HPLC analysis at 220 nm). Retention time: 12.8

HRMS spectra of the macrocyclized product

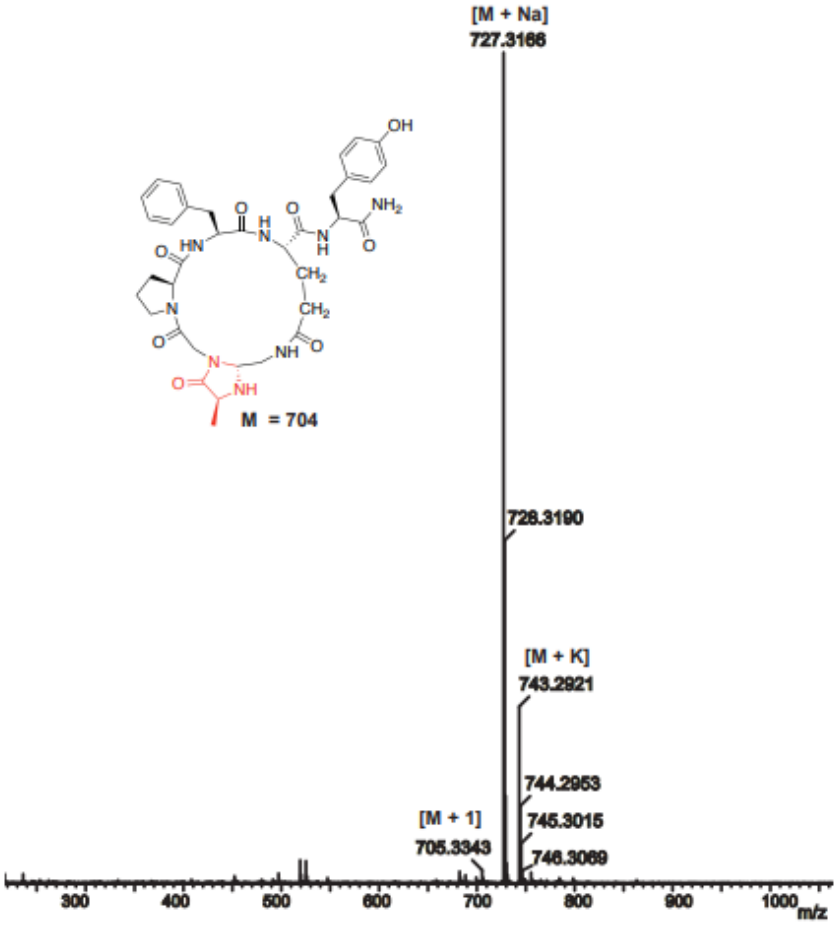

Cyclization of Linear Peptide 1.1o to Cyclic Peptide 1.2o

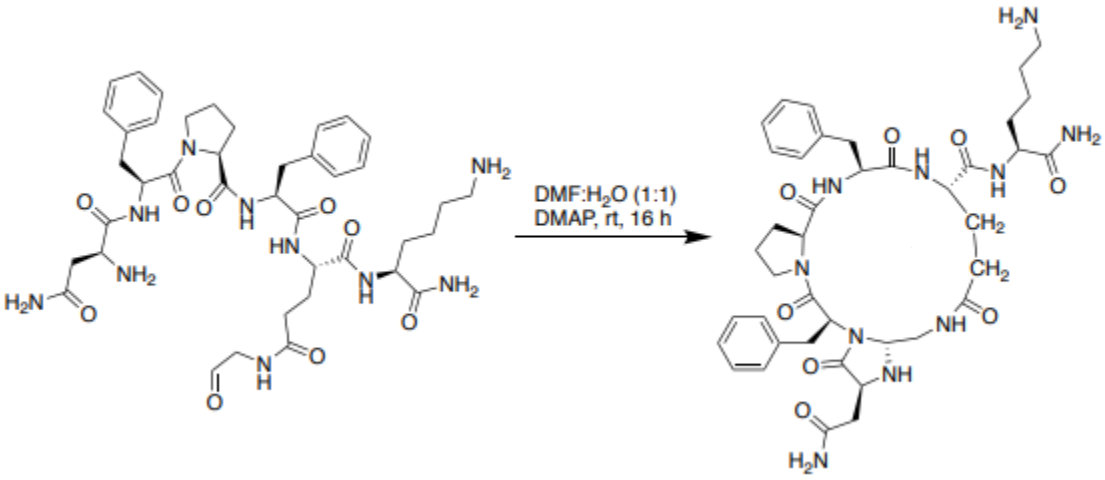

***cyc*(Asn-Phe-Pro-Phe-Glu)-Lys** LCMS: *m/z* 803.4 (calcd $[M+H]^+$ = 803.4), *m/z* 402.2 (calcd [(m+2)/2 = 402.2), Purity: >95% (HPLC analysis at 220 nm). Retention time: 10.7

HRMS spectra of the macrocyclized product

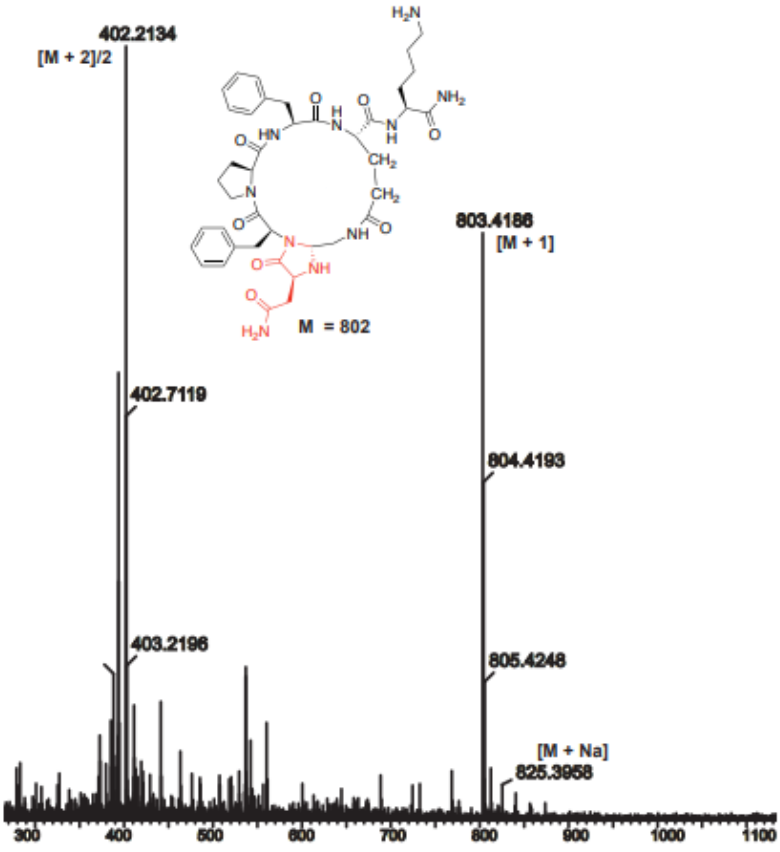

Cyclization of Linear Peptide 1.1p to Cyclic Peptide 1.2p

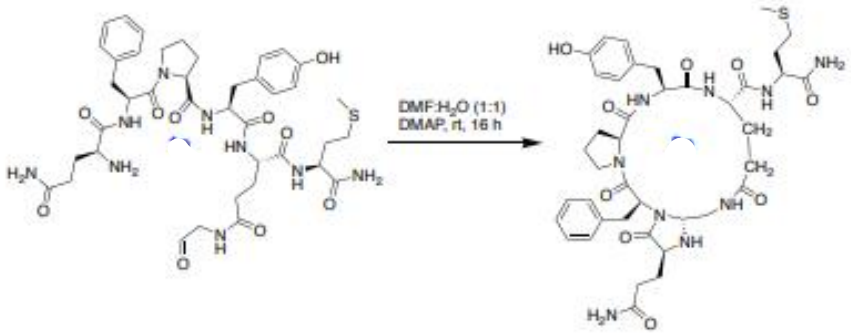

***cyc*(Gln-Phe-Pro-Tyr-Glu)-Met** LCMS: *m/z* 836.4 (calcd $[M+H]^+$ = 836.4), *m/z* 858.4 (calcd $[M+Na]^+$ = 858.4), Purity: >95% (HPLC analysis at 220 nm). Retention time: 14.0

HRMS spectra of the macrocyclized product

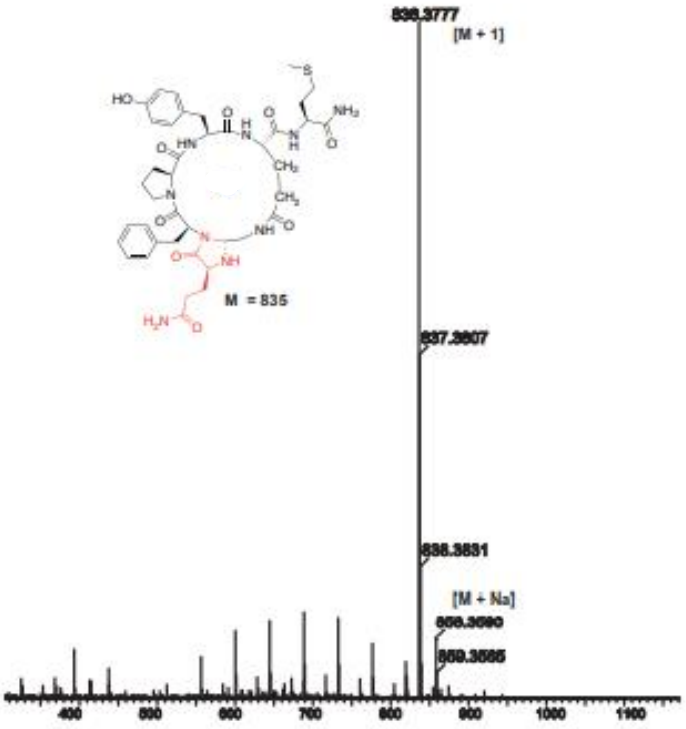

Cyclization of Linear Peptide 1.1q to Cyclic Peptide 1.2q

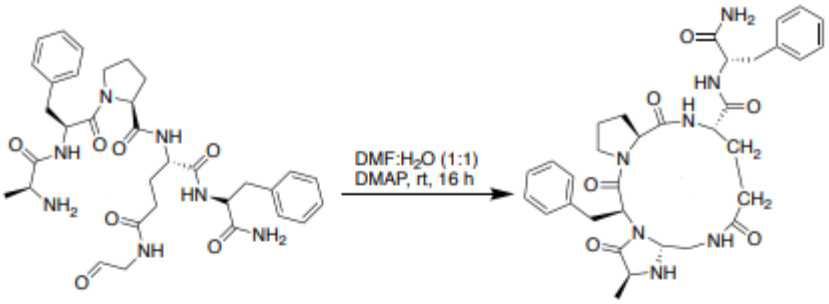

***cyc*(Ala-Phe-Pro-Glu)-Phe** . LCMS: *m/z* 654.3 (calcd $[M+Na]^+$ = 654.4), Purity: >95% (HPLC analysis at 220 nm). Retention time: 12.0

HRMS spectra of the macrocyclized product

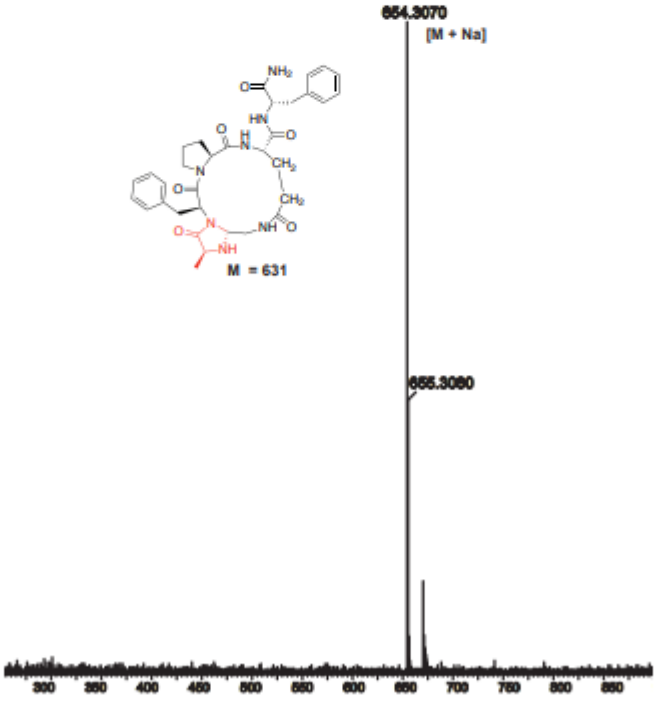

Cyclization of Linear Peptide 1.1r to Cyclic Peptide 1.2r

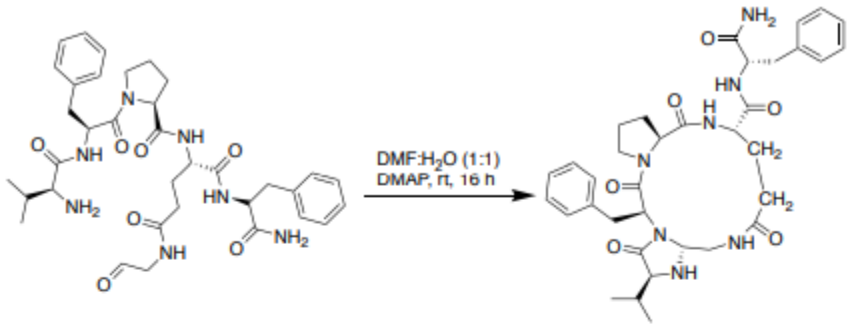

***cyc*(Val-Phe-Pro-Glu)-Phe** . LCMS: *m/z* 682.3 (calcd $[M+Na]^+$ = 682.4), *m/z* 698.3 (calcd $[M+K]^+$ = 698.4), Purity: >95% (HPLC analysis at 220 nm). Retention time: 14.5

HRMS spectra of the macrocyclized product .

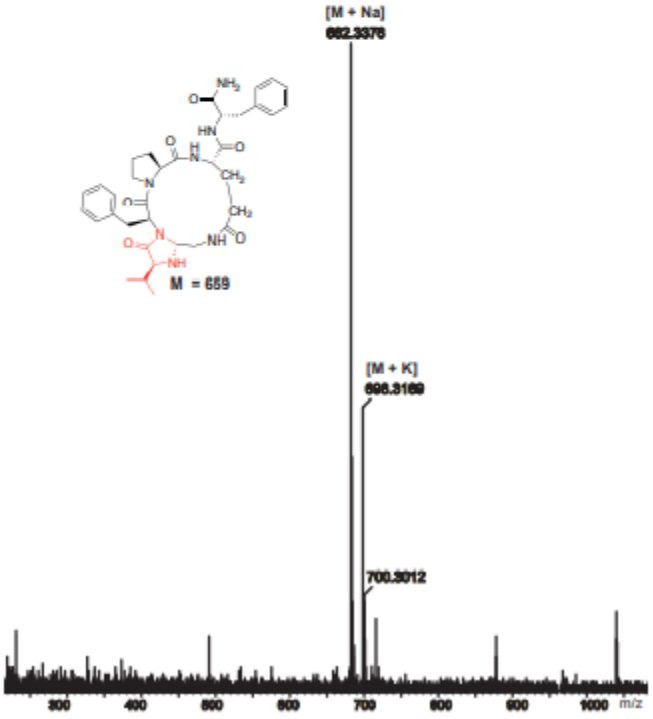

Cyclization of Linear Peptide 1.1t to Cyclic Peptide 1.2t

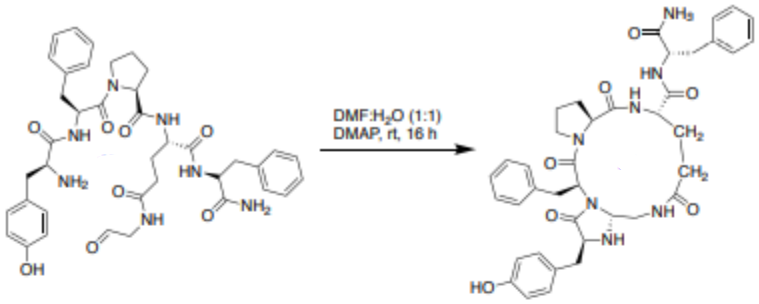

***cyc*(Tyr-Phe-Pro-Glu)-Phe** LCMS: *m/z* 746.3 (calcd $[M+Na]^+$ = 746.4), *m/z* 762.3 (calcd $[M+K]^+$ = 762.4), Purity: >95% (HPLC analysis at 220 nm). Retention time: 14.4

HRMS spectra of the macrocyclized product

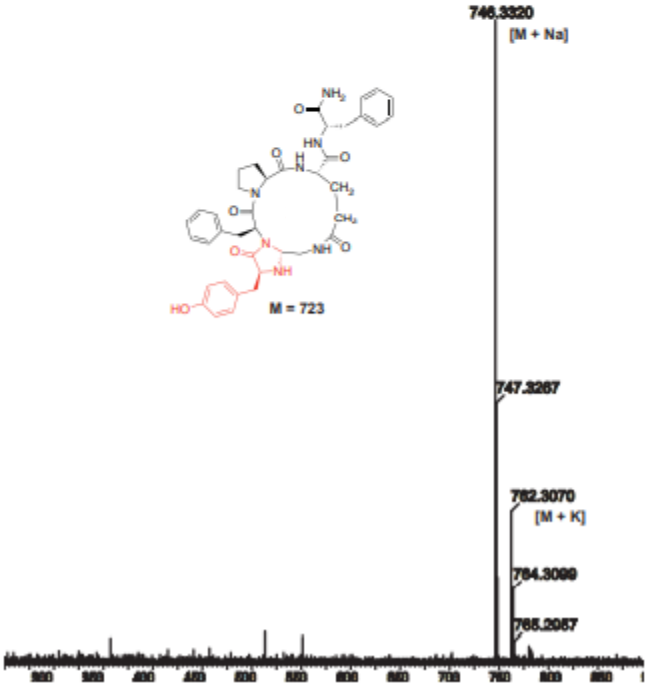

Cyclization of Linear Peptide 1.1u to Cyclic Peptide 1.2u

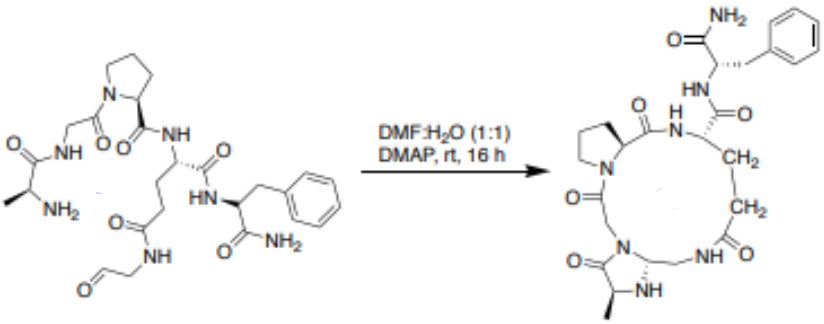

***cyc*(Ala-Gly-Pro-Glu)-Phe** LCMS: *m/z* 564.2 (calcd $[M+Na]^+$ = 564.4), *m/z* 580.2 (calcd $[M+K]^+$ = 580.4), Purity: >95% (HPLC analysis at 220 nm). Retention time: 9.26

HRMS spectra of the macrocyclized product

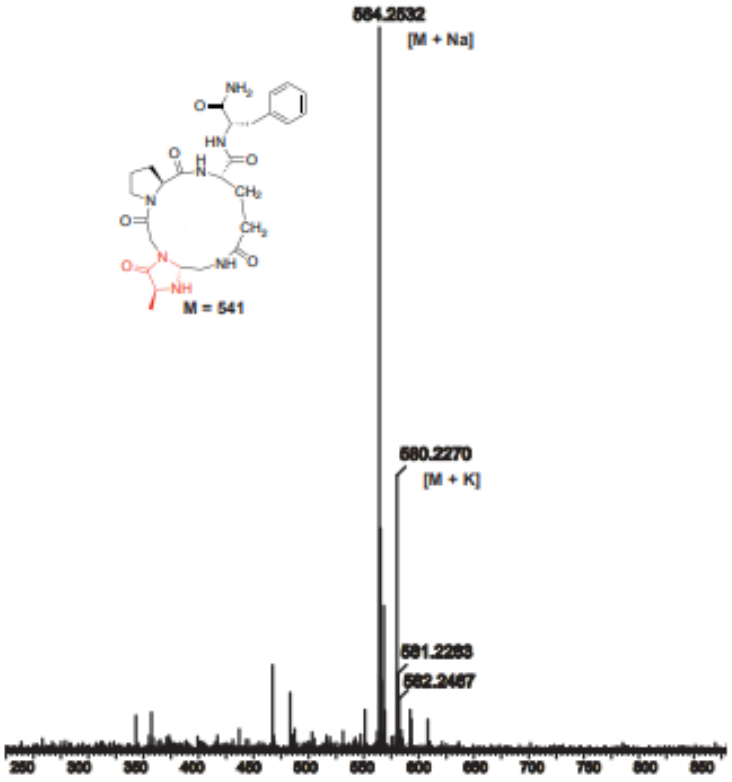

Cyclization of Linear Peptide 1.1v to Cyclic Peptide 1.2v

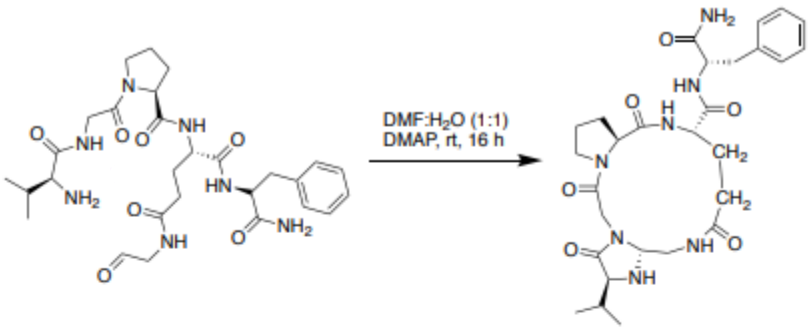

***cyc*(Val-Gly-Pro-Glu)-Phe** LCMS: *m/z* 592.3 (calcd $[M+Na]^+$ = 592.4), *m/z* 608.3 (calcd $[M+K]^+$ = 608.4), Purity: >95% (HPLC analysis at 220 nm). Retention time: 12.7

HRMS spectra of the macrocyclized product

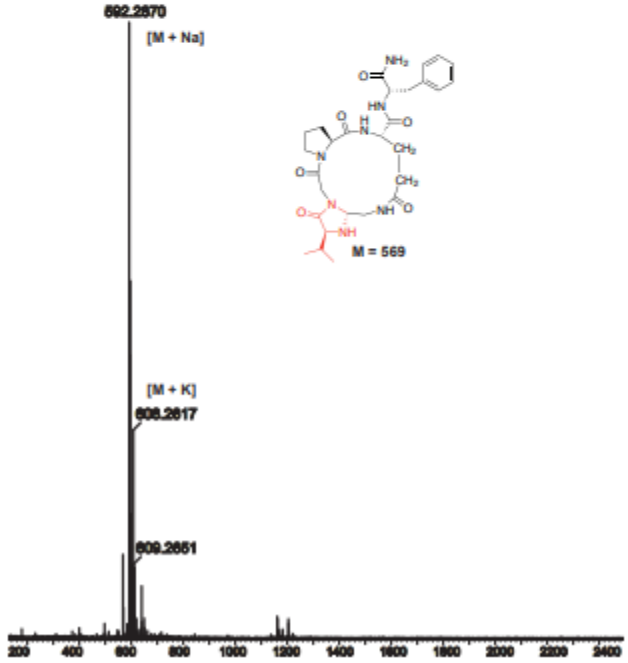

Cyclization of Linear Peptide 1.1w to Cyclic Peptide 1.2w

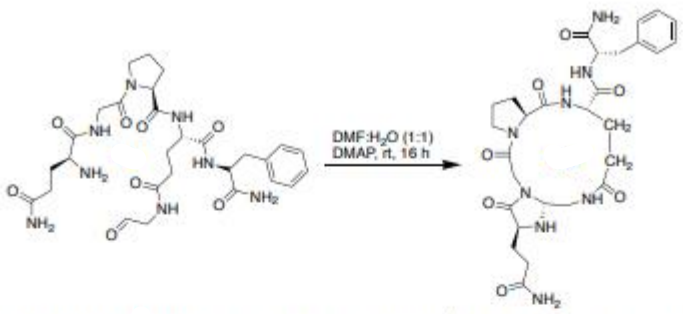

***cyc*(Gln-Gly-Pro-Glu)-Phe** LCMS: *m/z* 599.3 (calcd $[M+H]^+$ = 599.3), Purity: >95% (HPLC analysis at 220 nm). Retention time: 10.0

HRMS spectra of the macrocyclized product

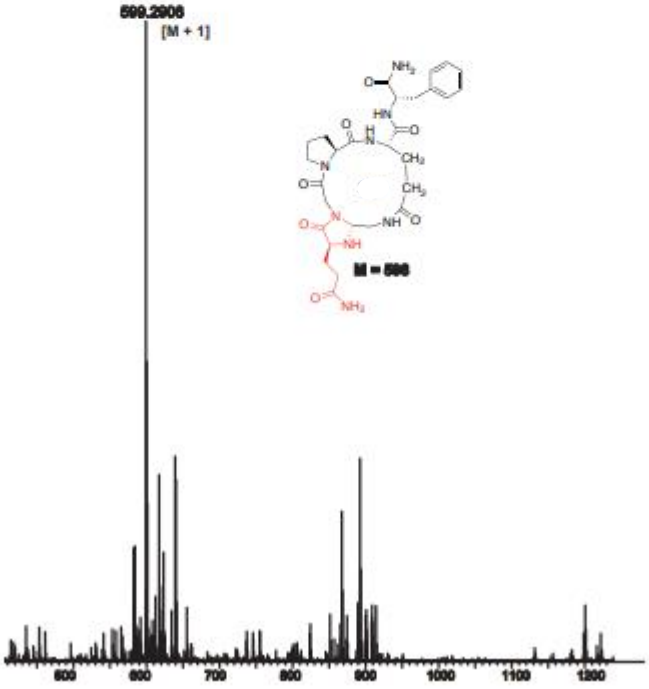

Cyclization of Linear Peptide 1.1x to Cyclic Peptide 1.2x

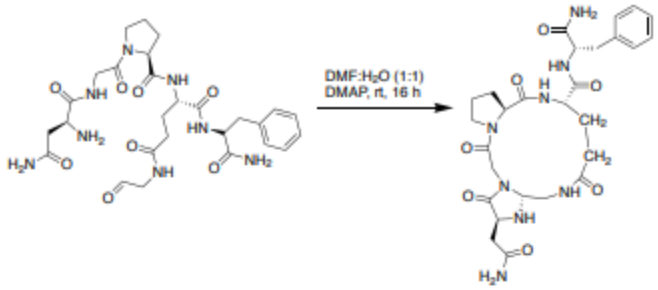

***cyc*(Asn-Gly-Pro-Glu-Phe)** LCMS: *m/z* 585.3 (calcd $[M+H]^+$ = 585.3), *m/z* 607.3 (calcd $[M+Na]^+$ = 607.3), Purity: >95% (HPLC analysis at 220 nm). Retention time: 10.1

HRMS spectra of the macrocyclized product

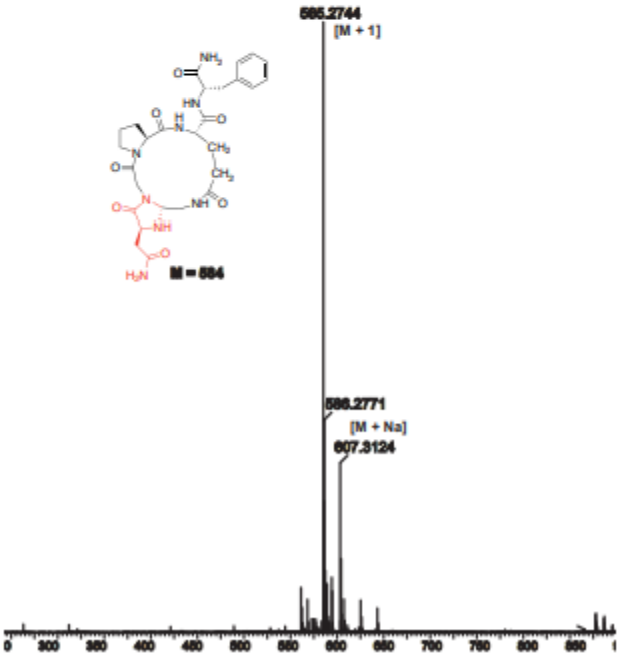

Macrocyclization to form Cyclic Peptide 1.3a

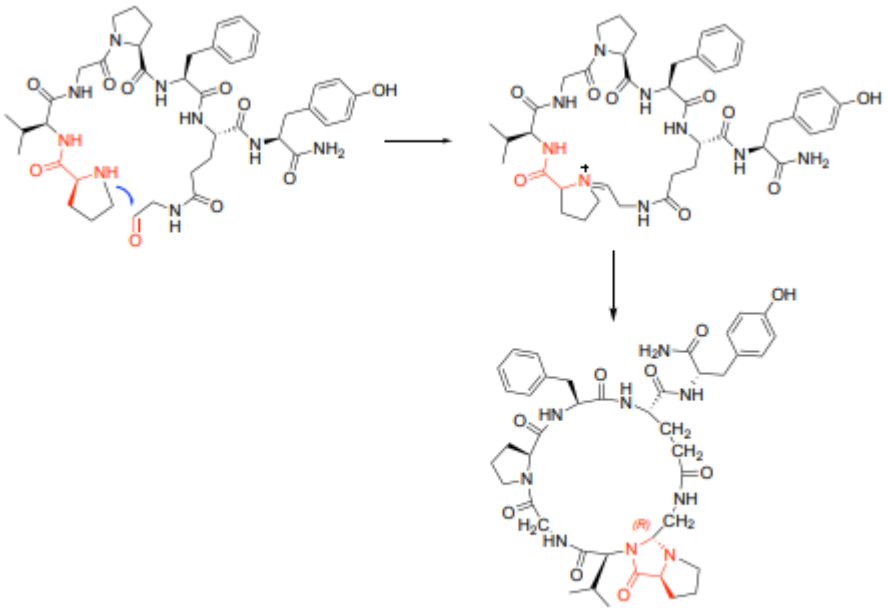

***cyc*(Pro-Val-Gly-Pro-Phe-Glu)-Tyr** Purity: >95% (HPLC analysis at 220 nm). Retention time: 12.8.

The NMR data for Cyclic peptide **1.3a** is shown below in the NMR section

Macrocyclization to form Cyclic Peptide 1.3b

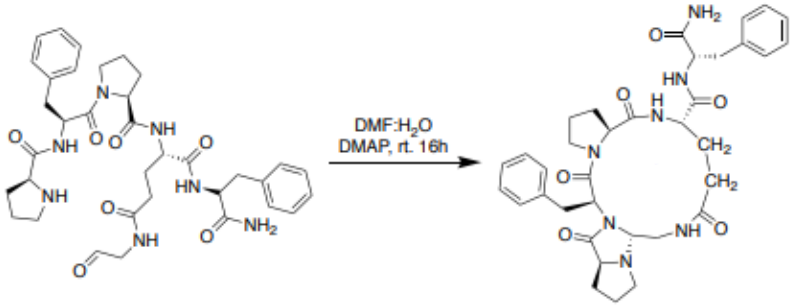

***cyc*(Pro-Phe-Pro-Glu)-Phe** LCMS: *m/z* 658.3 (calcd $[M+H]^+$ = 658.5), *m/z* 680.3 (calcd $[M+Na]^+$ = 680.5), *m/z* 698.3 (calcd $[M+K]^+$ = 698.5), Purity: >95% (HPLC analysis at 220 nm). Retention time: 13.0

HRMS spectra of the macrocyclized product

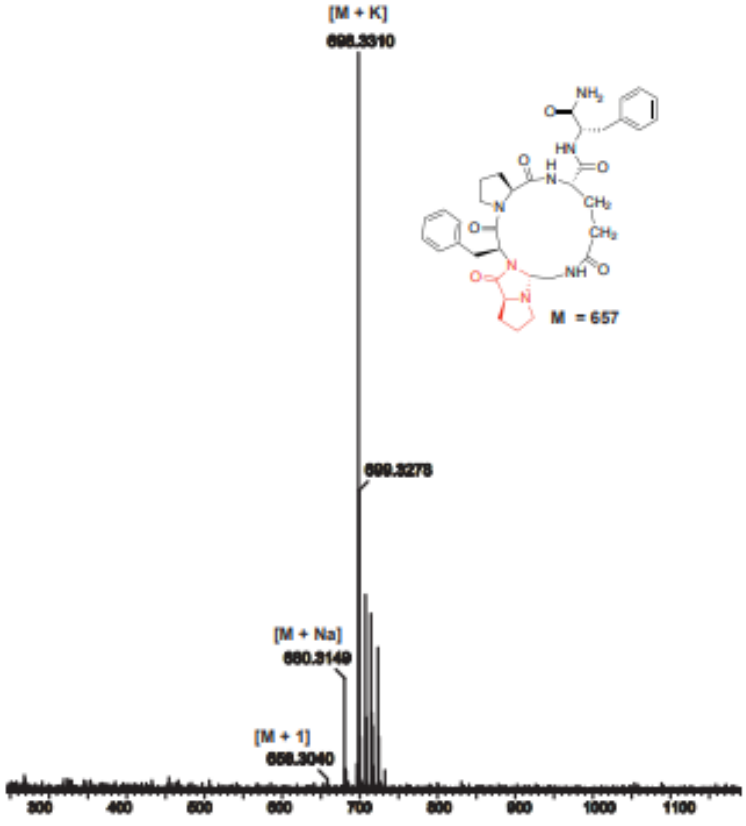

Macrocyclization to form Cyclic Peptide 1.7a

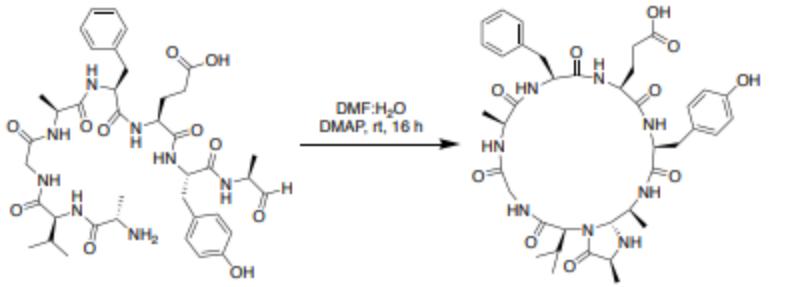

***cyc*(Ala-Val-Gly-Ala-Phe-Glu-Tyr)-Ala)** 、 LCMS: *m/z* 793.4 (calcd $[M+H]^+$ = 793.4), Purity: >95% (HPLC analysis at 220 nm). Retention time: 1.7

HRMS spectra of the macrocyclized product

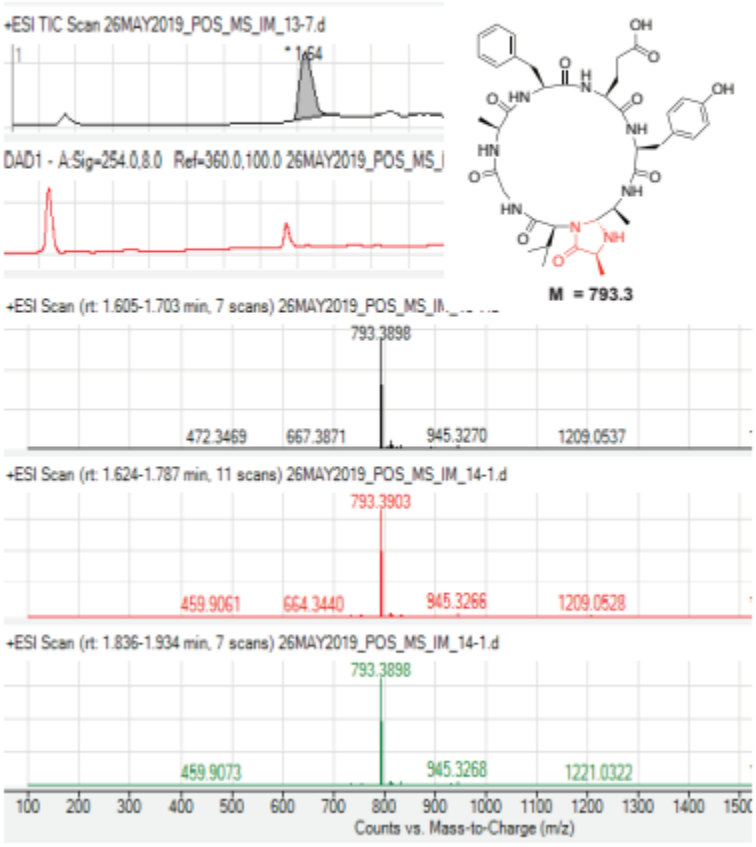

Macrocyclization to form Cyclic Peptide 1.7b

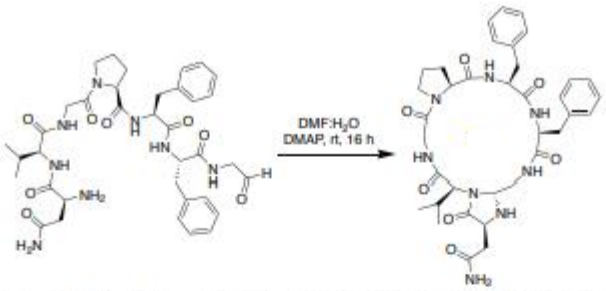

***cyc*(Gln-Val-Gly-Pro-Phe-Phe-Gly)** LCMS: *m/z* 703.3 (calcd $[M+H]^+$ = 703.3), Purity: >95% (HPLC analysis at 220 nm). Retention time: 16.8

MS spectrum of the macrocyclized product

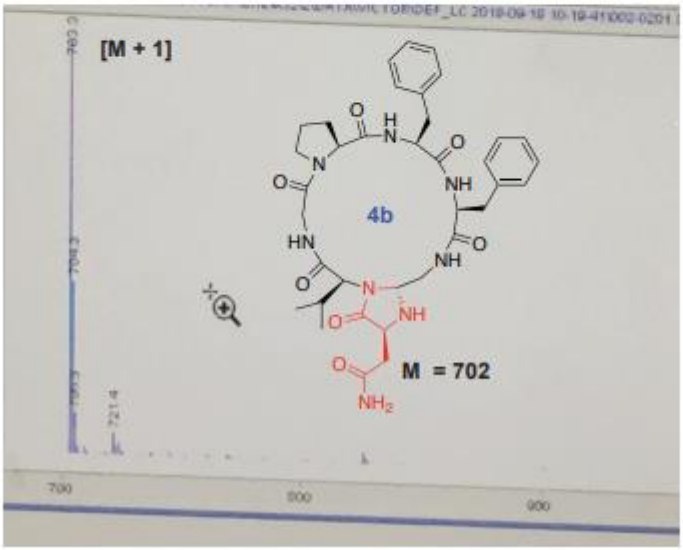

Macrocyclization to form Cyclic Peptide 1.7c

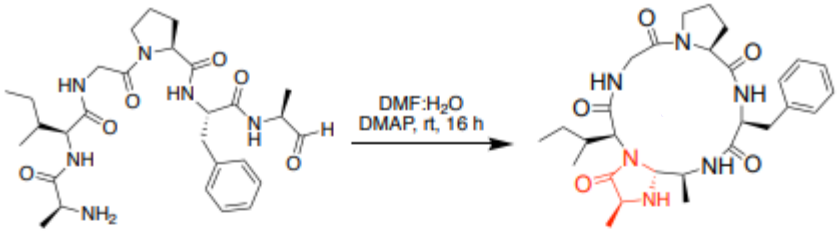

***cyc*(Ala-Ile-Gly-Pro-Phe-Ala)** LCMS: *m/z* 562.4 (calcd $[M+Na]^+$ = 563.5), Purity: >95% (HPLC analysis at 220 nm). Retention time: 11.3-12.3

MS spectrum of the macrocyclized product

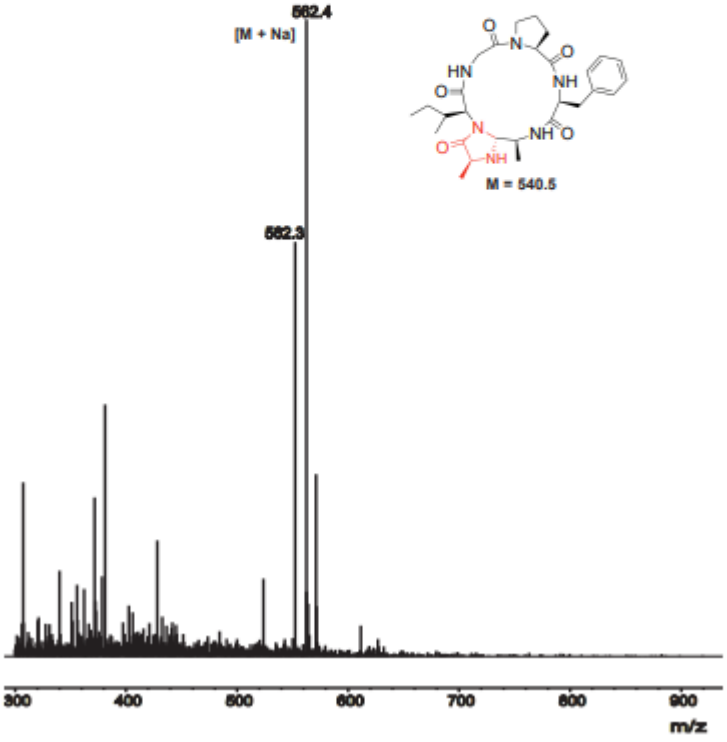

Macrocyclization to form Cyclic Peptide 1.7d

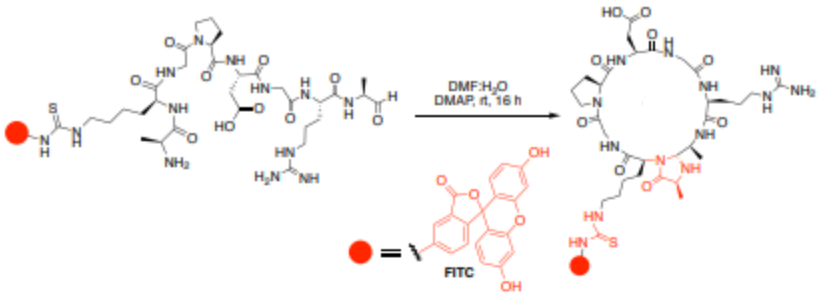

***cyc*(Ala-Lys-Gly-Pro-Asp-Gly-Arg-Ala)-FITC** LCMS: *m/z* 1126.4 (calcd $[M+H]^+$ = 1126.5), *m/z* 563.7 (calcd [(*M*+2)/2] = 563.7), Purity: >95% (HPLC analysis at 220 nm). Retention time: 13.5

HRMS spectra of the macrocyclized product

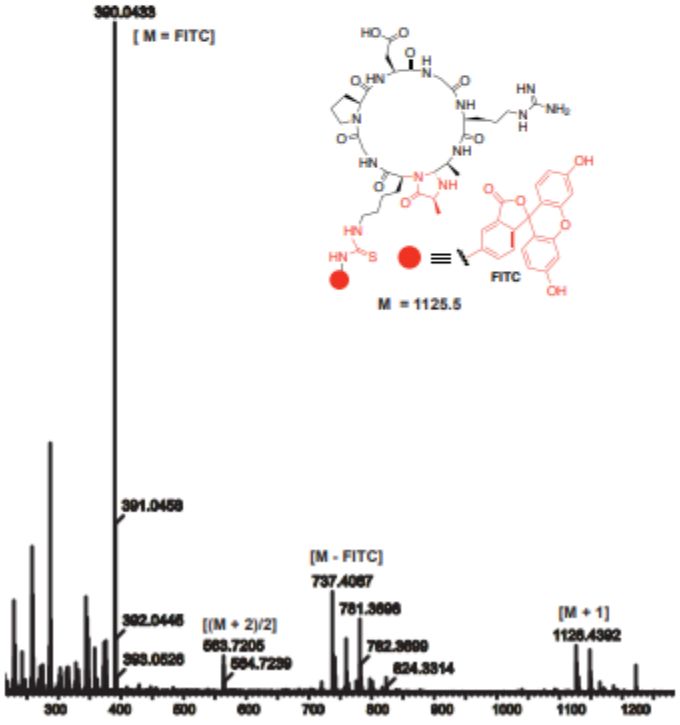

Macrocyclization to form Cyclic Peptide 1.7e

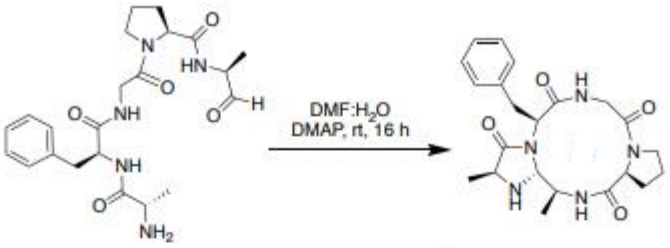

***cyc*(Ala-Phe-Gly-Pro-Ala)** . LCMS: *m/z* 428.2 (calcd $[M+H]^+$ = 428.2), Purity: >95% (HPLC analysis at 220 nm). Retention time: 8.2-9.7

HRMS spectra of the macrocyclized product

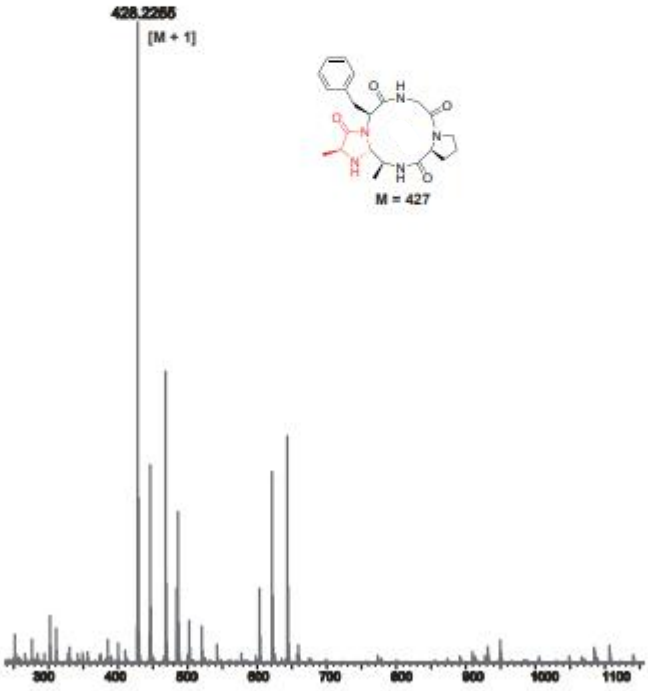

Macrocyclization to form Cyclic Peptide 1.7f

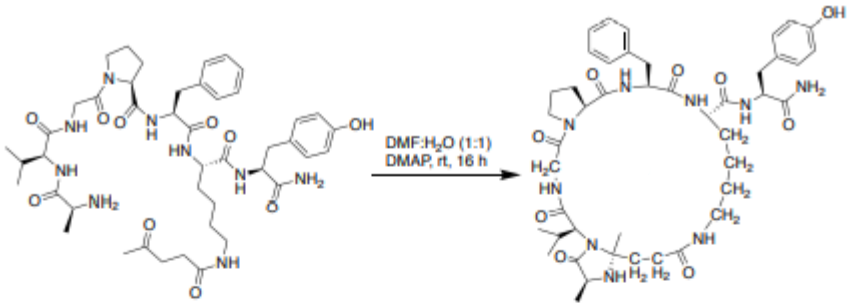

***cyc*(Ala-Val-Gly-Pro-Phe-Lys(CO)-Tyr** . LCMS: *m/z* 884.4 (calcd $[M+Na]^+$ = 884.5), *m/z* 900.4 (calcd $[M+K]^+$ = 900.5), Purity: >95% (HPLC analysis at 220 nm). Retention time: 10.7

HRMS spectra of the macrocyclized product

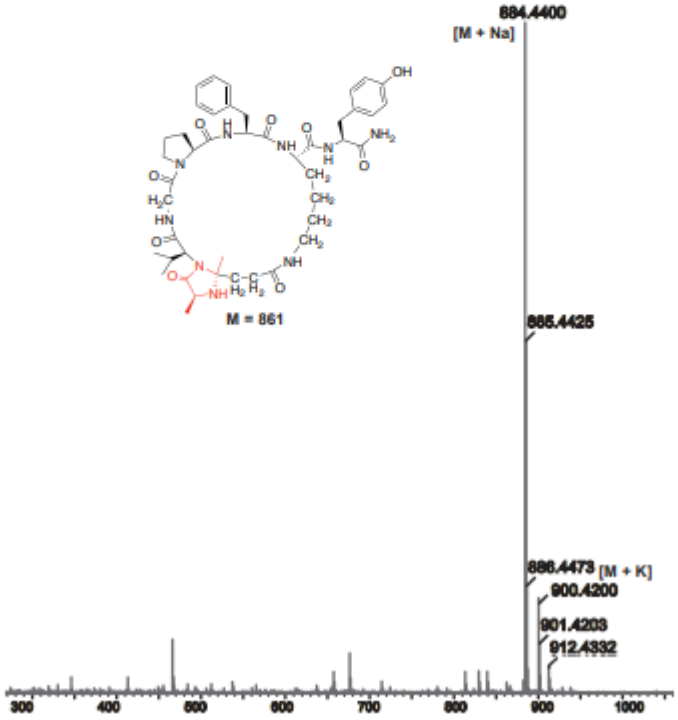

Macrocyclization of 1.4g to form Cyclic Peptide 1.7g

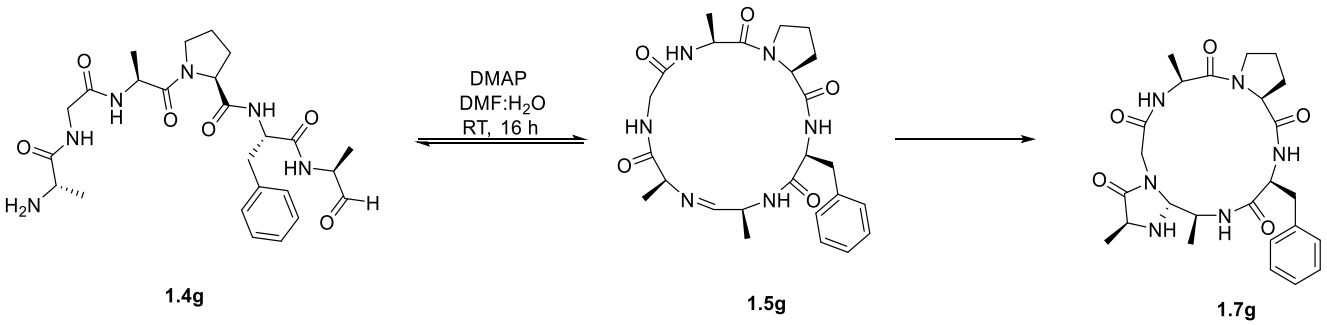

1.4g **1.5g** **1.7g**

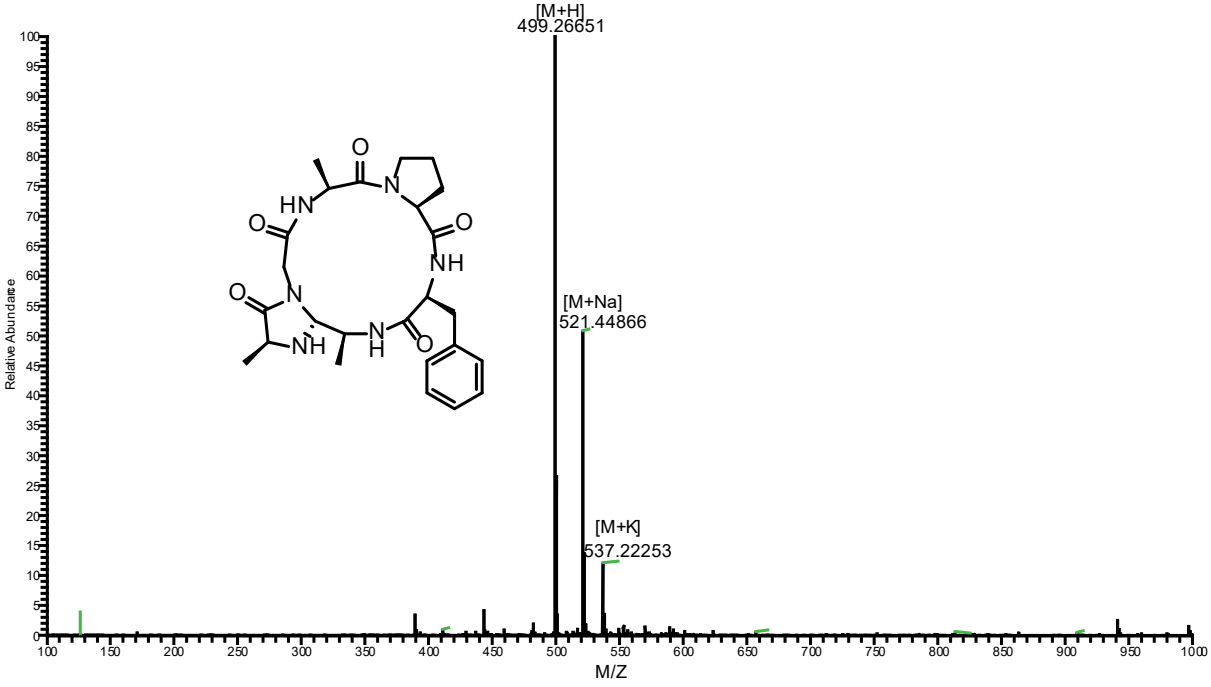

Control Reaction of Tetrapeptide

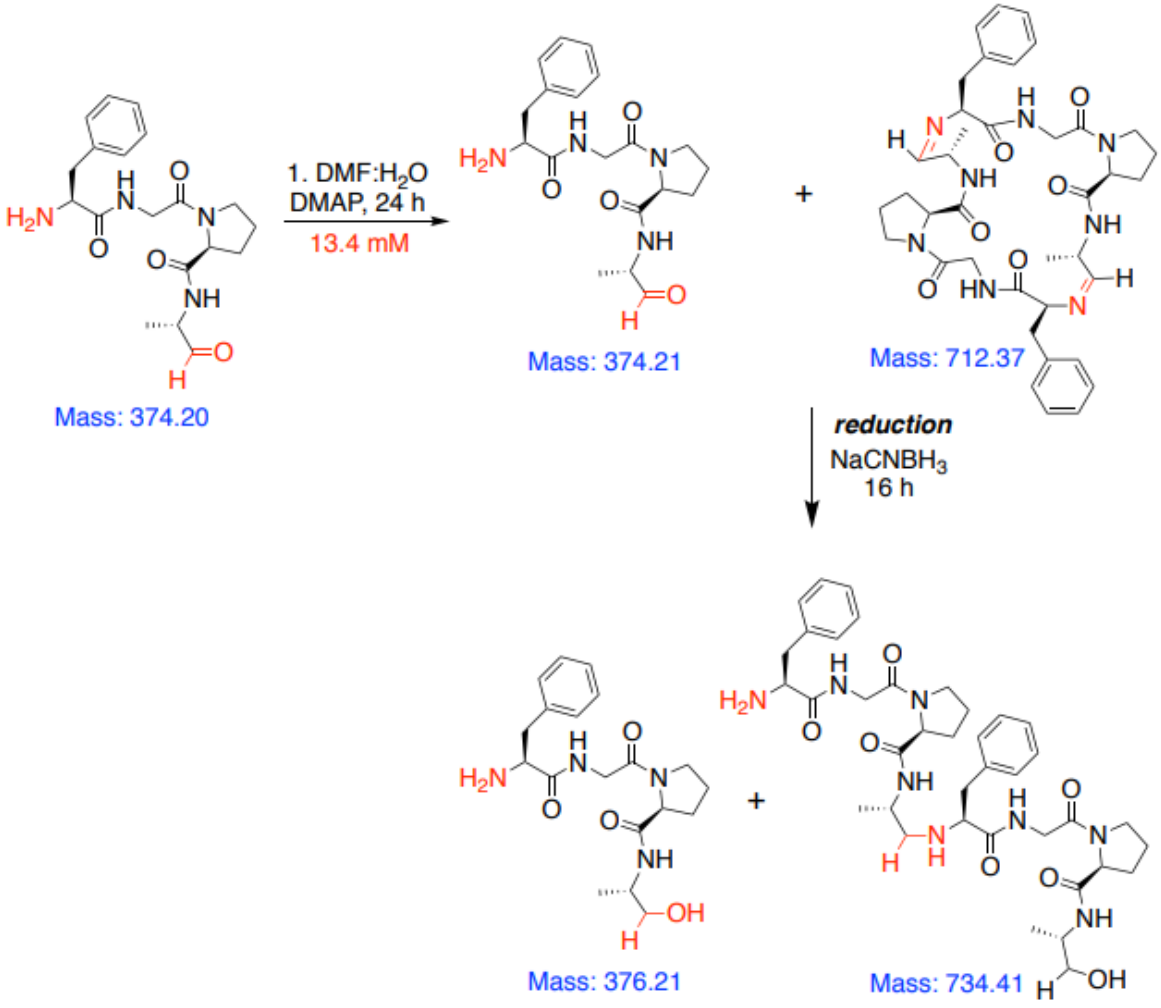

Reaction with tetrapeptide FGPA(CHO): Lypholized peptide FGPA(CHO) (1.5 mg, 12.8 mM) was mixed with excess of DMAP (30 equiv., 384 mM) in a 1:1 DMF:H2O solution (300 µL). The reaction was shaken at room temperature for 24 h.

Identification of the products of tetrapeptide aldehyde reaction. The cyclic imine intermediate exhibits mass equivalent to the desired 4-imidazolidinone products. We knew that a tetrapeptide aldehyde would give a 9-membered ring, which is impossible of course, but to confirm the

formation of any linear and cyclodimer by CyClick chemistry, we carried out reduction with sodium cyanoborohydride. In an effort to determine the nature of the product of tetrapeptide reaction, sodium cyanoborohydride (50 equiv.) was added and reaction was stirred for additional 16 h. The resulting products were analyzed with LC-MS. The result showed the formation of reduced linear tetrapeptide and reduced dimerized peptide. We did not observe the formation of any CyClick product.

HRMS spectra of the tetrapeptide reaction before reduction

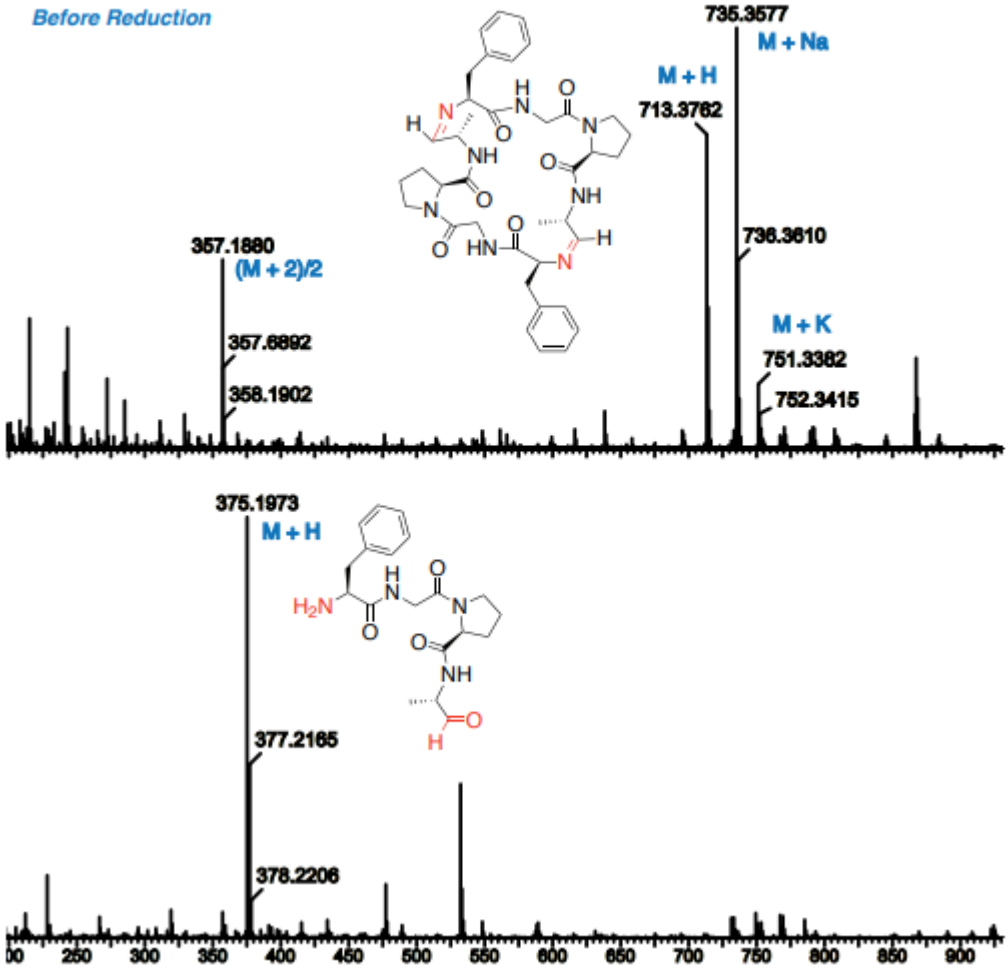

HRMS spectra of the tetrapeptide reaction after reduction

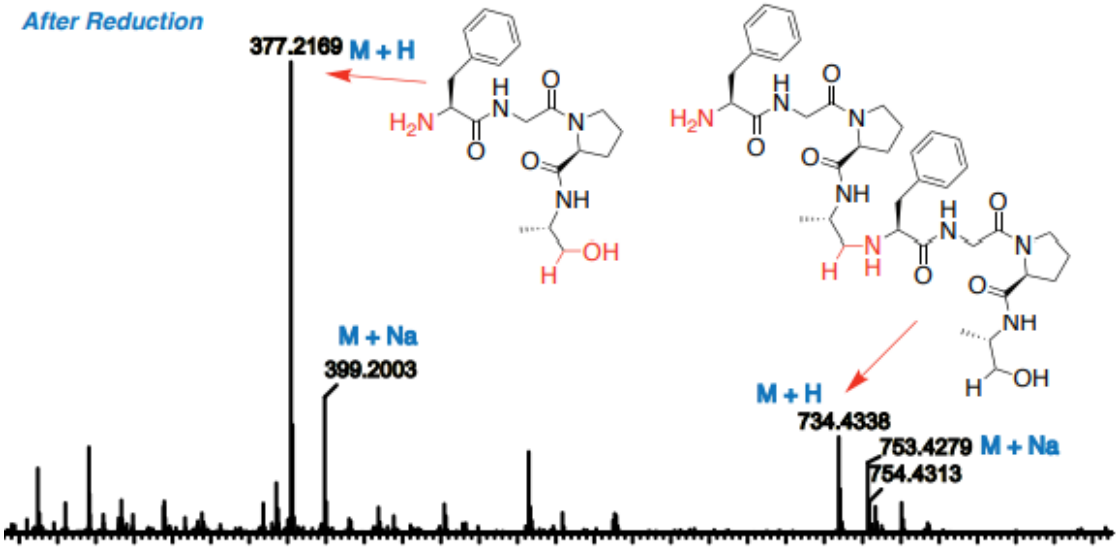

HSQC NMR data of fused bicyclic five membered 5-imino-oxazolidine cyc peptide 1.2i'

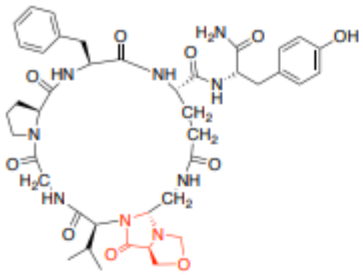

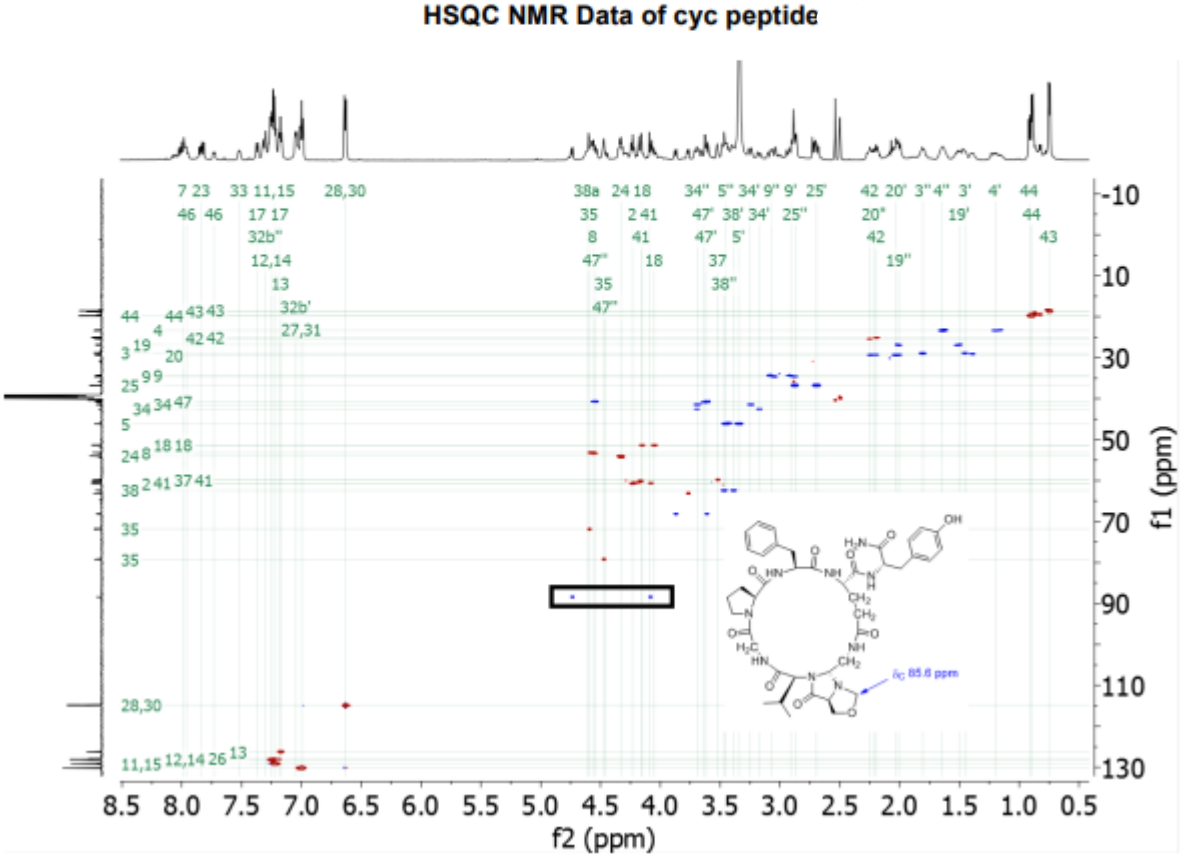

NMR Data of fused bicyclic five membered pyrrolo[1,2-c]imidazolone cyclic peptide 1.3a

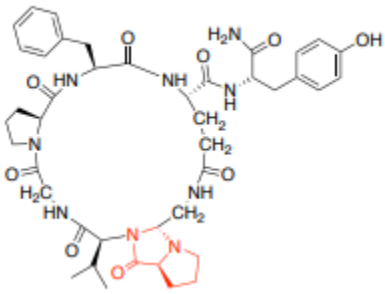

NMR data for "Sample 1.3a"

Residue	Atom Name	Numbering	d_H (ppm), multiplicity	d_C (ppm)
Pro	N	1	--	--
	C_aH	2	4.22, d (*J* = 9.1 Hz)	60.59
	C_bH_2	3	1.40, m; 1.81, m	29.14
	C_gH_2	4	1.14, m; 1.62, m	23.21
	C_dH_2	5	3.34, m; 3.45, t (*J* = 8.9 Hz)	46.11
	CO	6	--	172.15
Phe	NH	7	8.01, d (*J* = 8.7 Hz)	--
	C_aH	8	4.56, ddd (*J* = 10.6, 9.1, 6.8 Hz)	53.23
	C_bH_2	9	2.94, dd (*J* = 14.3, 11.4 Hz); 3.07, m	34.25
	C_1	10	--	138.22
	C_2H, C_6H	11, 15	7.22, m	129.01
	C_3H, C_5H	12, 14	7.25, m	128.09
	C_4	13	7.18, t (*J* = 6.9 Hz)	126.18
	CO	16	--	170.71
Glu	NH	17	7.19, m	--
	C_aH	18	4.11, m	51.50
	C_bH_2	19	1.48, m; 2.00, m	26.89
	C_gH_2	20	1.95, m; 2.15, dd (*J* = 15.2, 8.2 Hz)	29.47
	C_dO	21	--	171.54
	CO	22	--	170.54
Tyr	NH	23	7.84, d (*J* = 8.7 Hz)	--
	C_aH	24	4.33, td (*J* = 8.6, 5.0 Hz)	54.06
	C_bH_2	25	2.70, dd (*J* = 13.9, 9.0 Hz); 2.88, m	36.72
	C_1	26	--	127.88
	C_2H, C_6H	27, 31	7.00, d (*J* = 8.0 Hz)	130.10
	C_3H, C_5H	28, 30	6.64, d (*J* = 8.0 Hz)	114.82
	C_4OH	29	9.16, s	155.74
	$CONH_2$	32	7.04, s; 7.31, s	172.82
Linker	NH	33	7.30, m	--
	C_aH_2	34	3.14, br d (*J* = 12.9 Hz); 3.74, m	42.43
	C_bH	35	4.41, br s	78.43
Pro	N	36	--	--
	C_aH	37	3.60, dd (*J* = 8.9, 4.5 Hz)	63.72
	C_bH_2	38	1.73, m; 1.96, m	27.88
	C_gH_2	39	1.53, m; 1.59, m	24.37
	C_dH_2	40	2.65, m; 3.08, m	55.75
	CO	41	--	175.71
Val	N	42	--	--
	C_aH	43	4.06, d (*J* = 11.1 Hz)	60.27
	C_bH	44	2.22, m	25.11
	$C_{g1}H_3$, $C_{g2}H_3$	45, 46	0.81, d (*J* = 6.5 Hz); 0.93, d (*J* = 6.4 Hz)	19.08, 19.85
	CO	47		169.37
Gly	NH	48	7.60, dd (*J* = 8.2, 2.4 Hz)	--
	C_aH_2	49	3.63, dd (*J* = 16.6, 2.6 Hz); 4.48, dd (*J* = 16.9, 8.7 Hz)	40.76
	CO	50	--	169.39

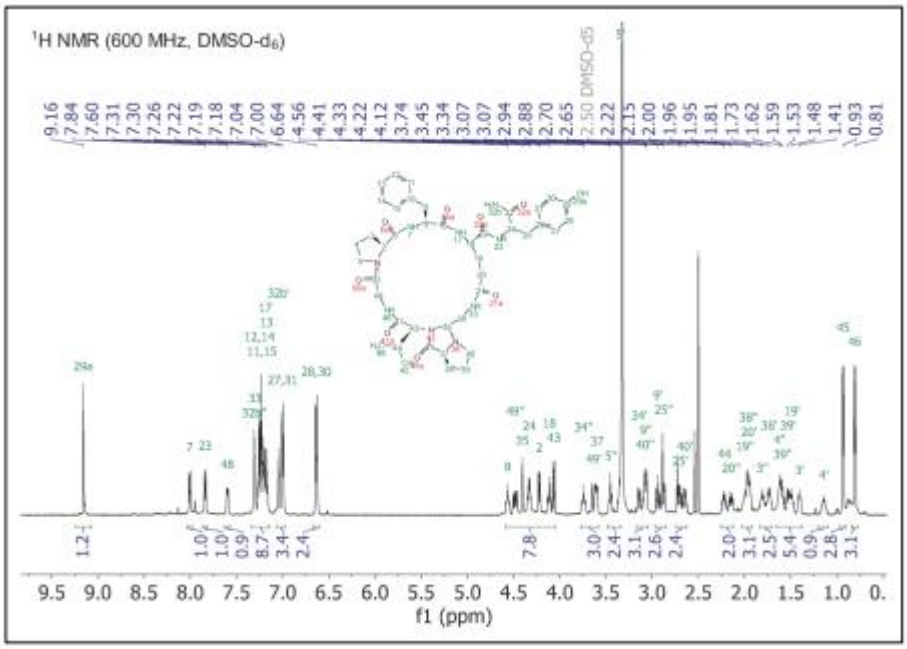
^{1}H NMR (600 MHz, DMSO-d$_6$)
f1 (ppm)

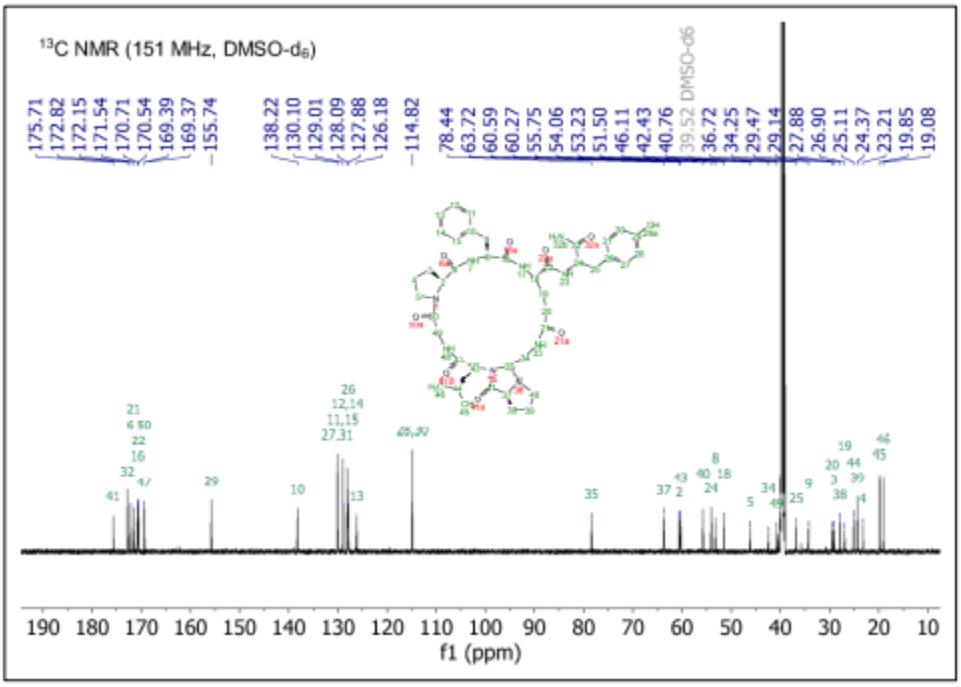
^{13}C NMR (151 MHz, DMSO-d$_6$)
f1 (ppm)

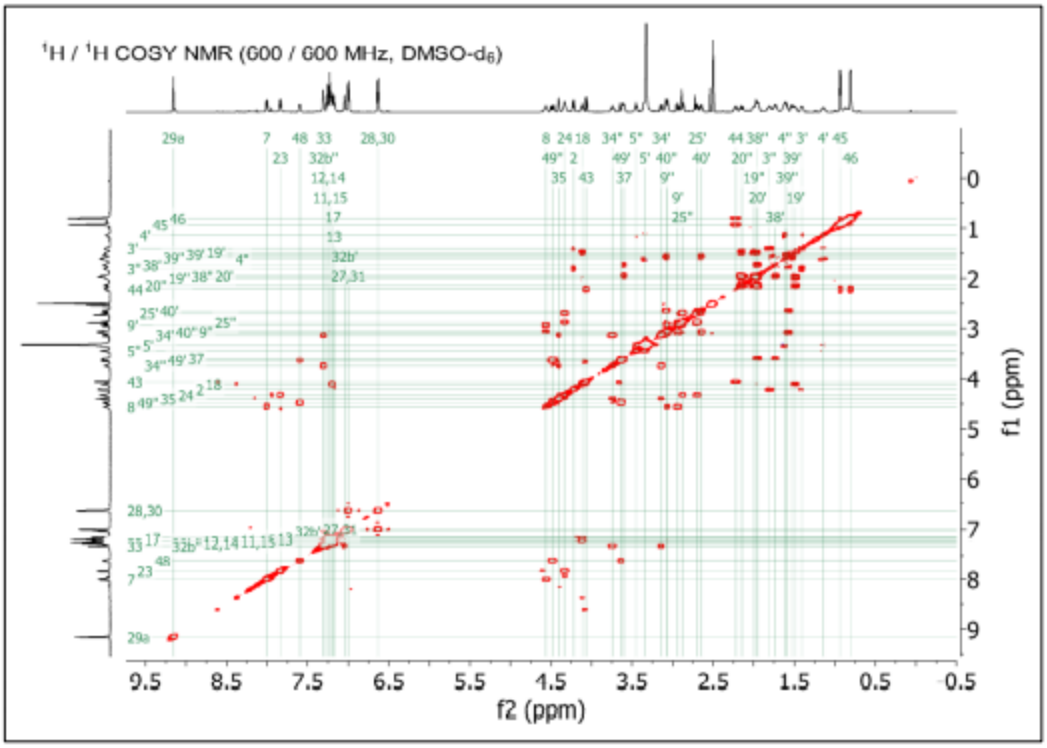
¹H / ¹H COSY NMR (600 / 600 MHz, DMSO-d6)
f2 (ppm)
f1 (ppm)

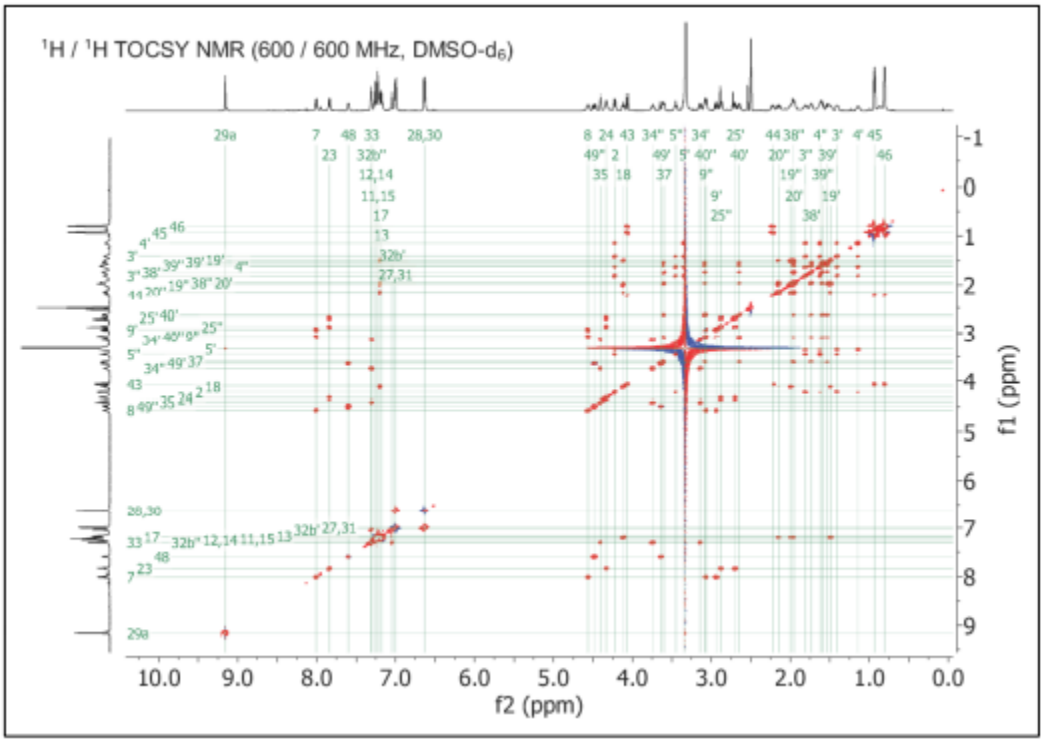
¹H / ¹H TOCSY NMR (600 / 600 MHz, DMSO-d6)
f2 (ppm)
f1 (ppm)

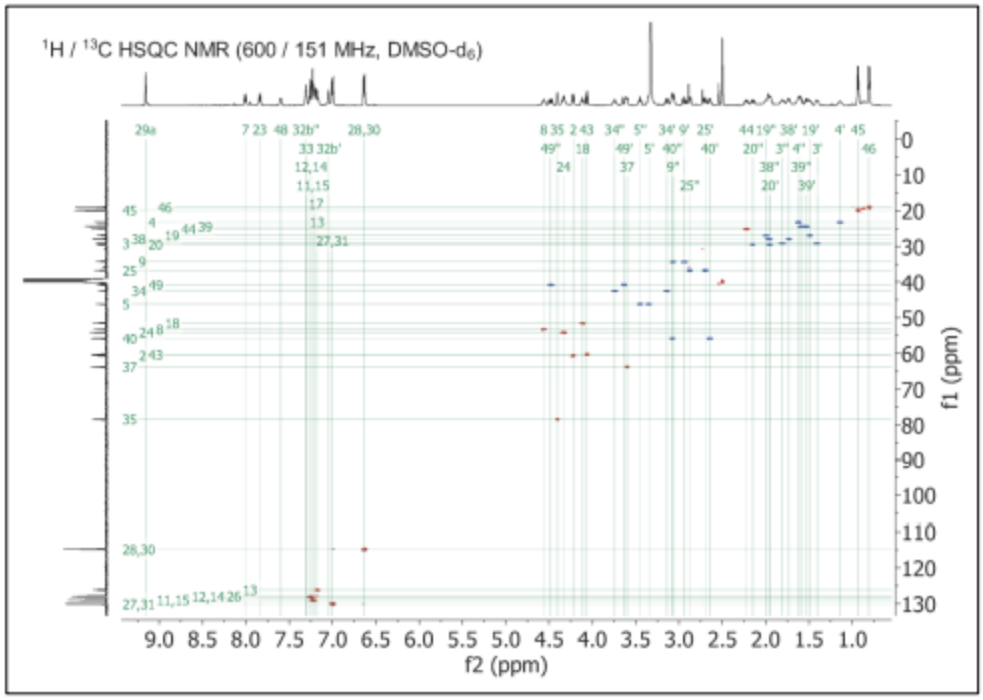
^{1}H / ^{13}C HSQC NMR (600 / 151 MHz, DMSO-d$_6$)
f2 (ppm)
f1 (ppm)

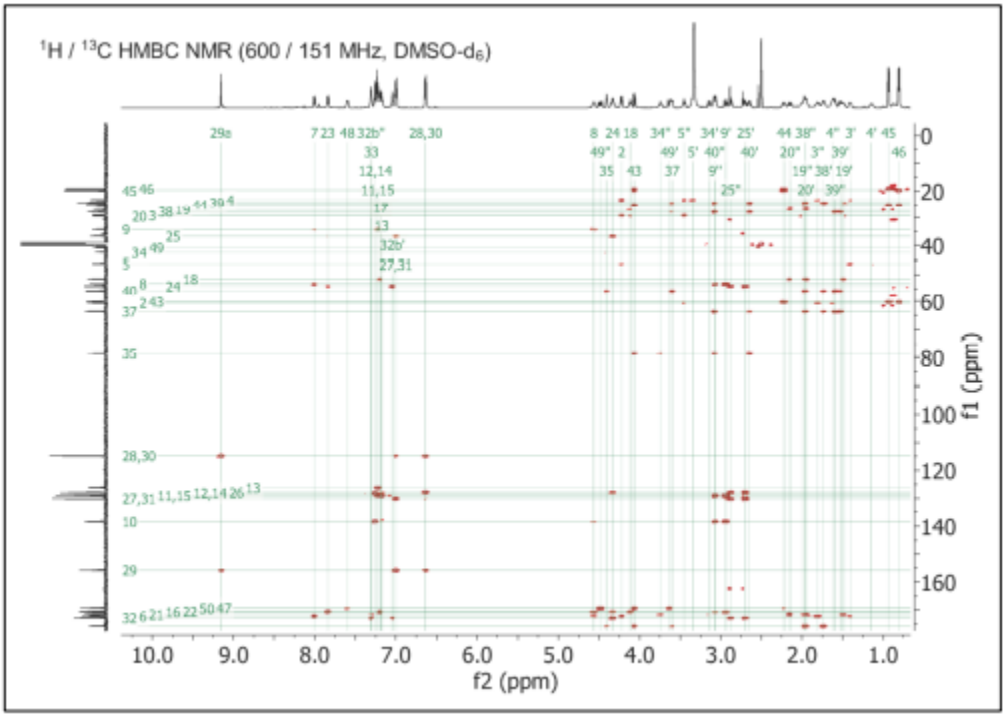
^{1}H / ^{13}C HMBC NMR (600 / 151 MHz, DMSO-d$_6$)
f2 (ppm)
f1 (ppm)

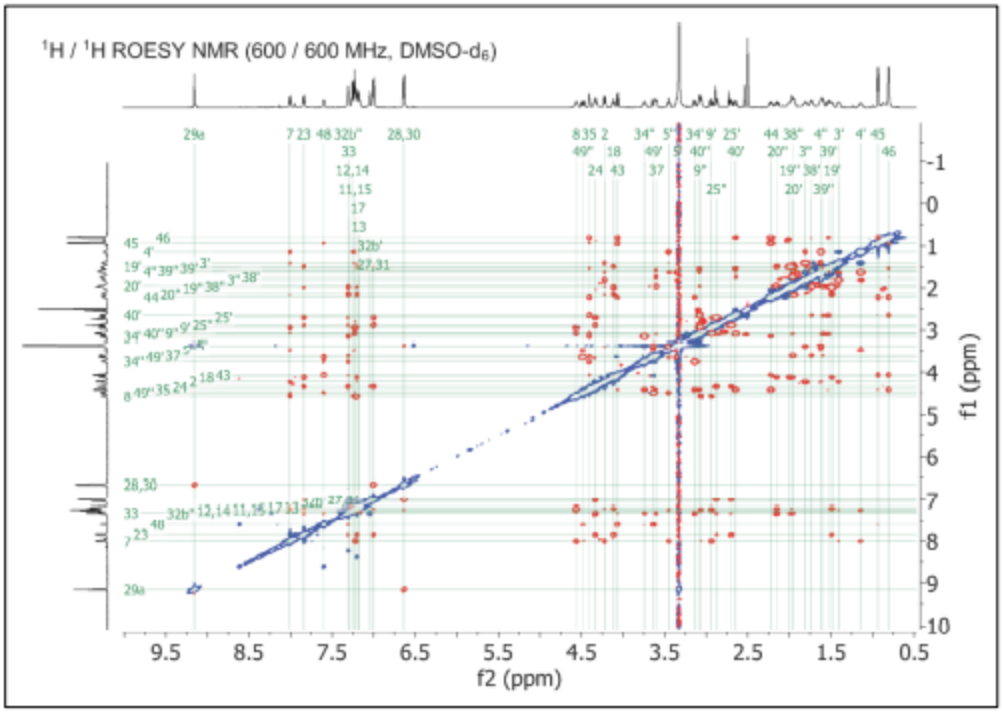

Structural impact of head-to-tail 4-imidazolidinone cyclic peptide 1.7a by NMR

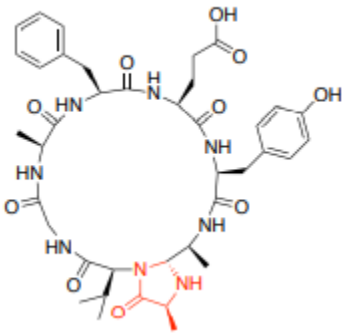

^{1}H NMR (600 MHz, CD_3CN / H_2O, 7:3, v/v, 298 K)

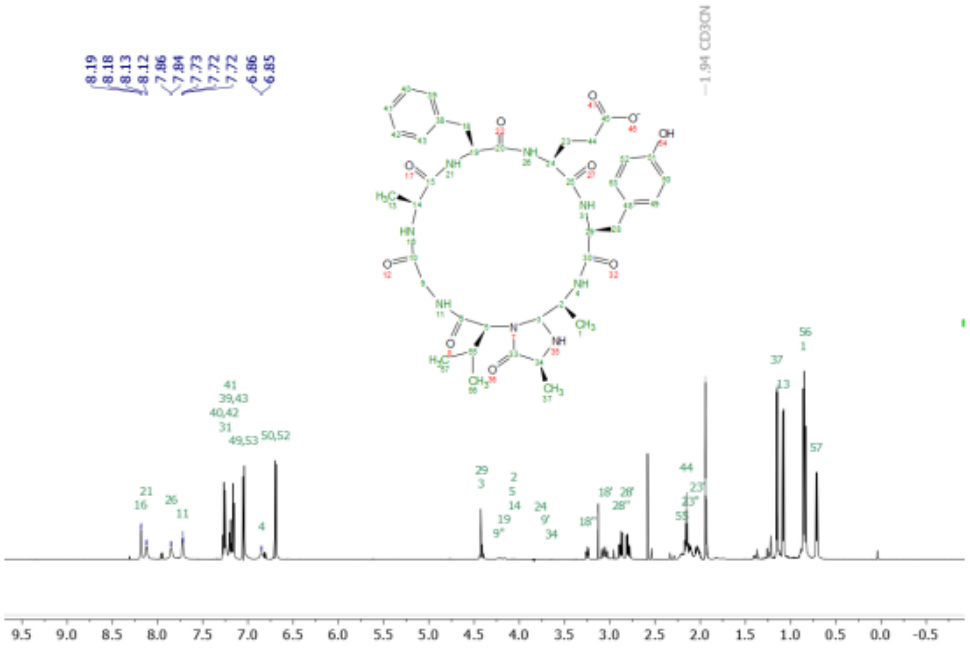

^{13}C NMR (151 MHz, CD_3CN / H_2O, 7:3, v/v, 298 K)

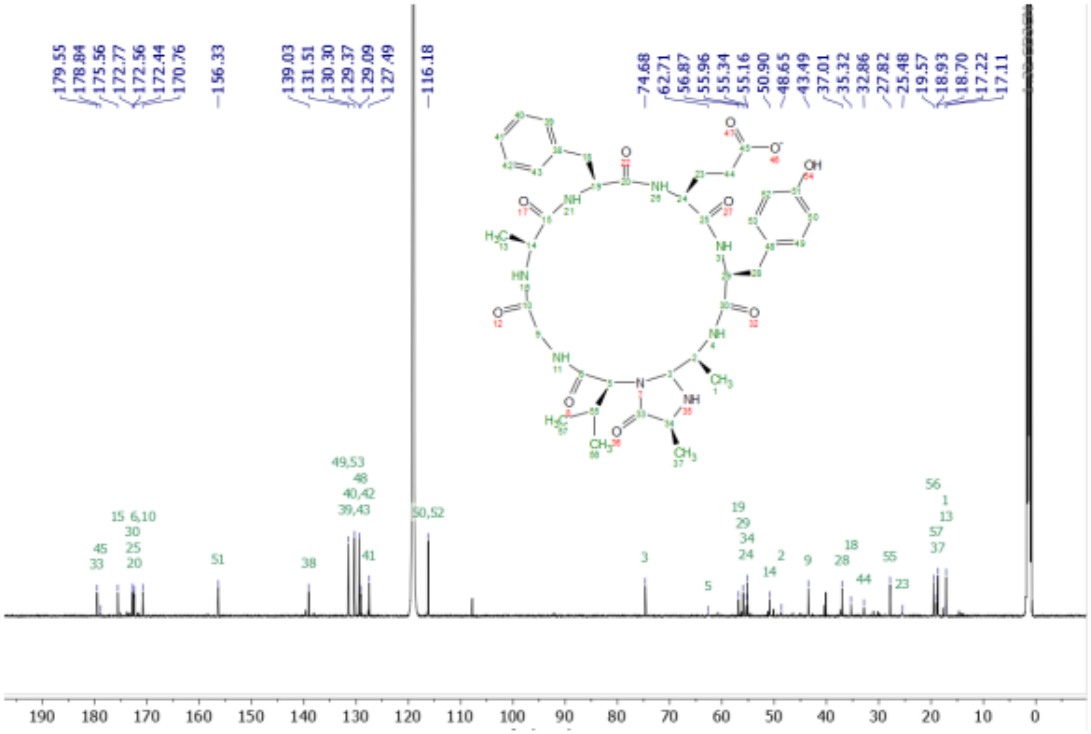

^{1}H / ^{1}H DQF-COSY NMR (600 / 600 MHz, CD3CN / H2O, 7:3, v/v, 298 K)

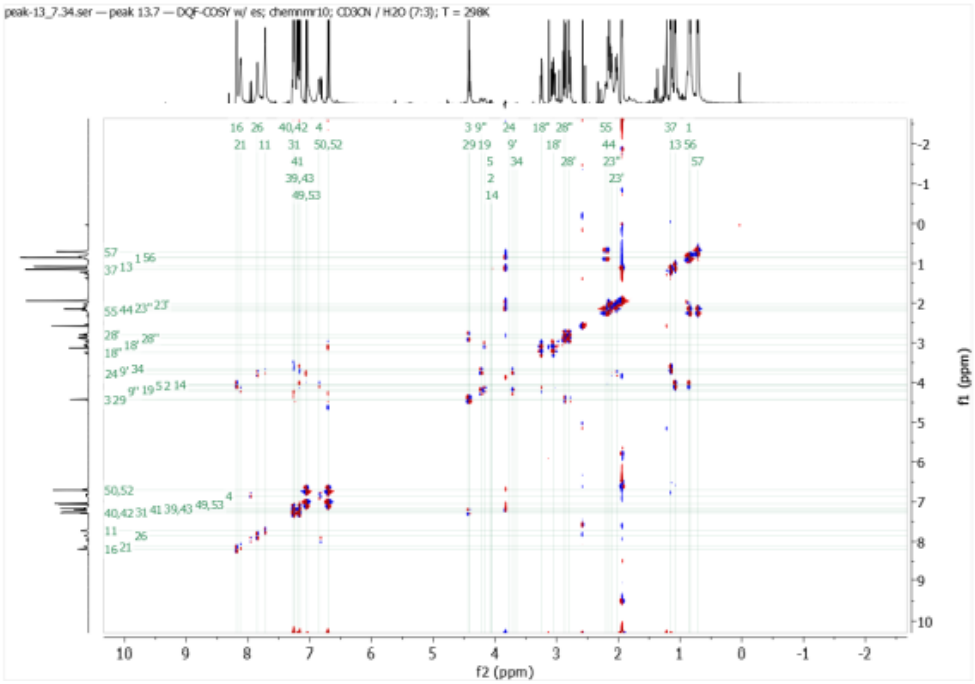

^{1}H / ^{1}H TOCSY NMR (600 / 600 MHz, CD_3CN / H_2O, 7:3, v/v, 298 K)

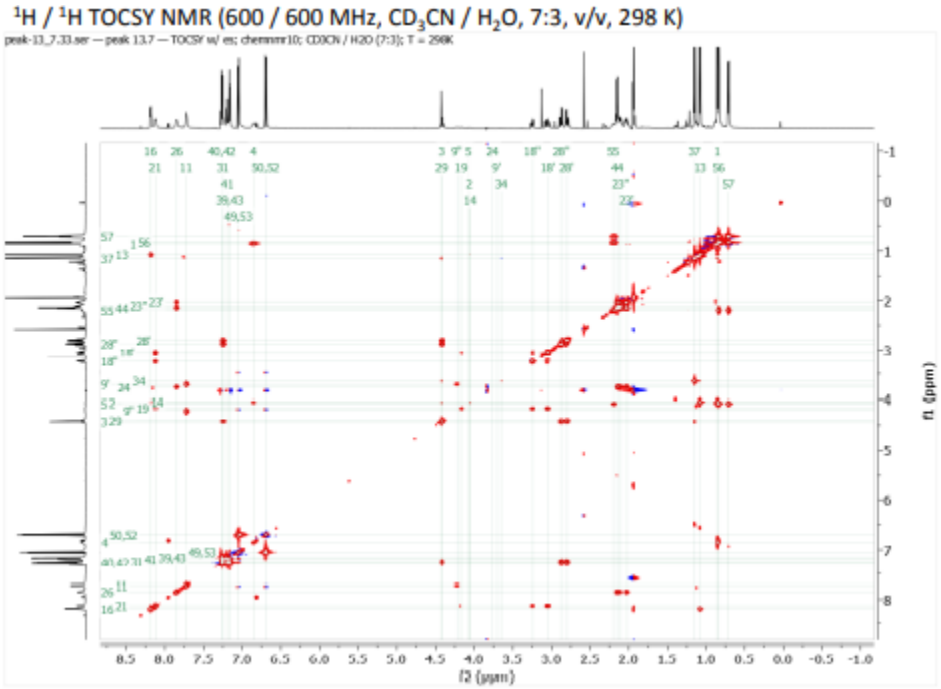

^{1}H / ^{13}C HSQC NMR (600 / 151 MHz, CD_3CN / H_2O, 7:3, v/v, 298 K)

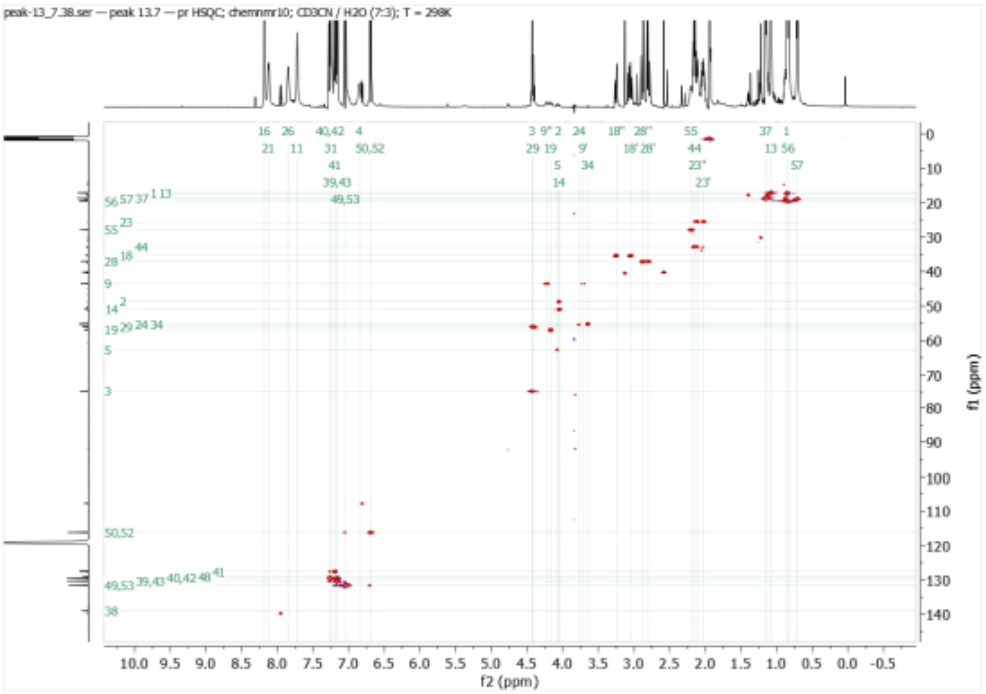

^{1}H / ^{13}C HMBC NMR (600 / 151 MHz, CD_3CN / H_2O, 7:3, v/v, 298 K)

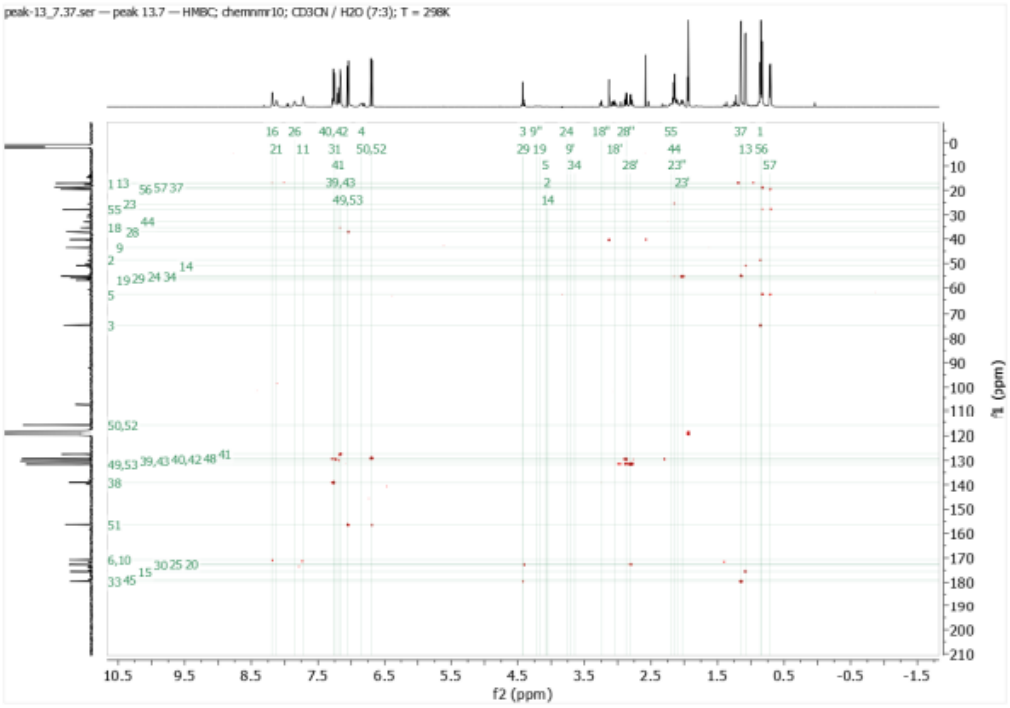

^{1}H / ^{13}C band selective HMBC NMR (600 / 151 MHz, CD3CN / H2O, 7:3, v/v, 298 K)

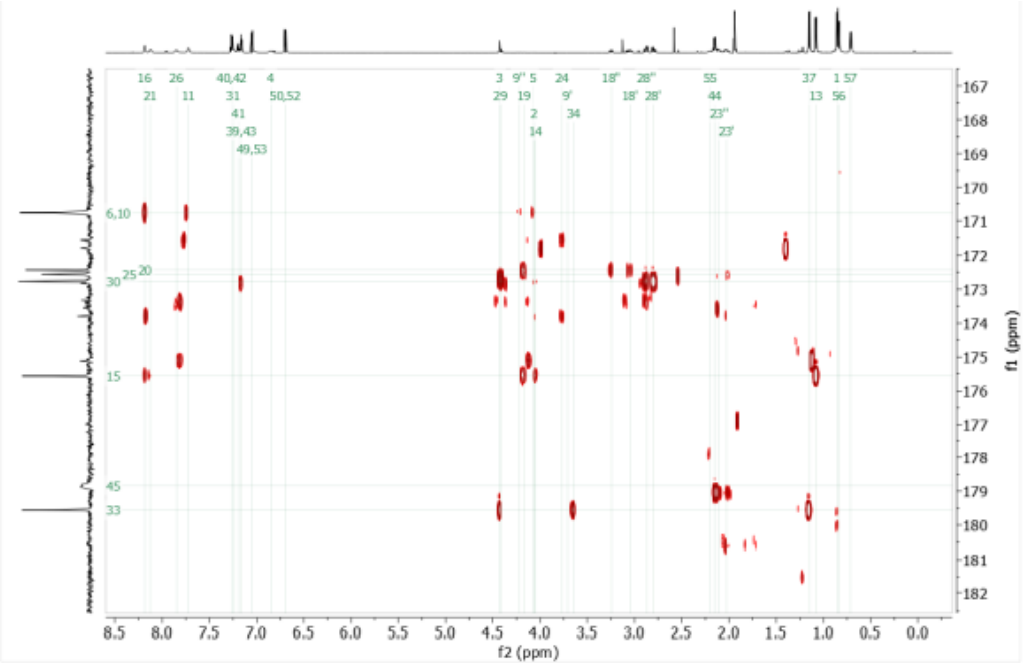

^{1}H / ^{1}H ROESY NMR (600 / 600 MHz, CD3CN / H2O, 7:3, v/v, 298 K)

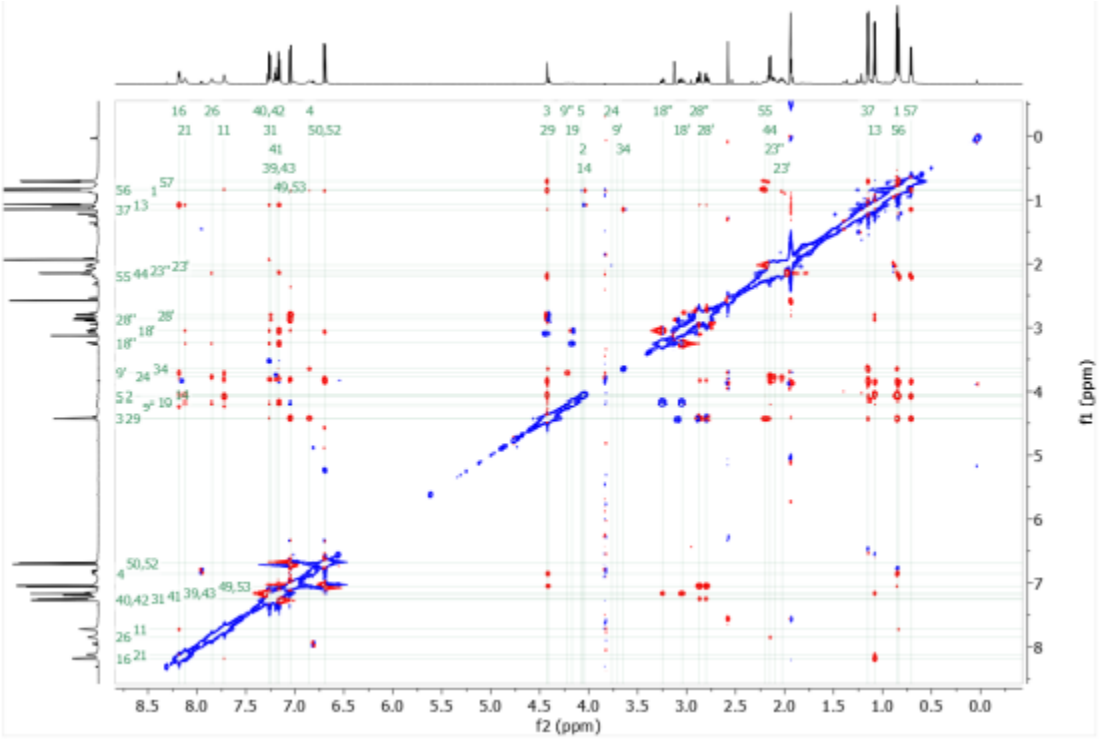

Variable temperature VT-NMR of head-to-tail cyclic peptide **1.7a**

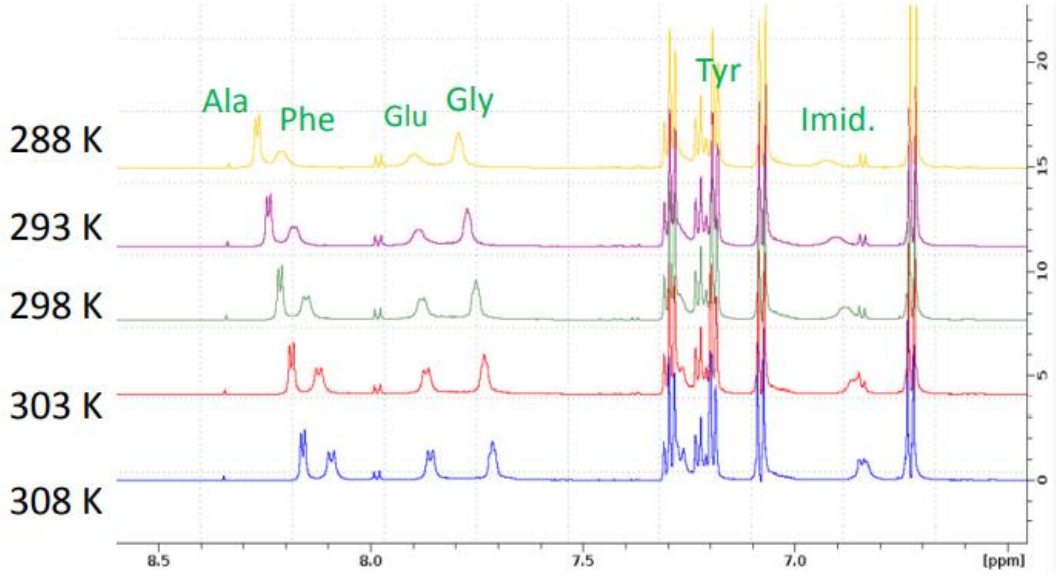

Temperature coefficients were used to determine H-bonding.

	T (K):	288	293	298	303	308	$\Delta\delta_{NH}/\Delta T$
residue	$^3J_{H\alpha,NH}$ (Hz)	chemical shift (ppm)					ppb/K
Ala	5.4	8.238	8.211	8.185	8.156	8.131	-5.4
Phe	7.4	8.181	8.151	8.124	8.094	8.065	-5.8
Glu	7.2	7.867	7.858	7.850	7.840	7.830	-1.8
Gly	4.7	7.764	7.743	7.724	7.704	7.685	-3.9
Tyr	6.3	7.254	7.251	7.248	7.247	7.242	-0.6
Imid.	8.0	6.896	6.875	6.853	6.829	6.810	-4.4

referencing versus CD2HCN peak at 1.94 ppm

H-bonding for $\Delta\delta_{NH}/\Delta T > -4.6$

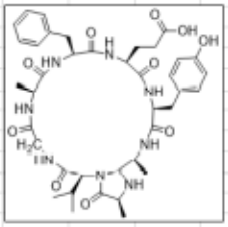

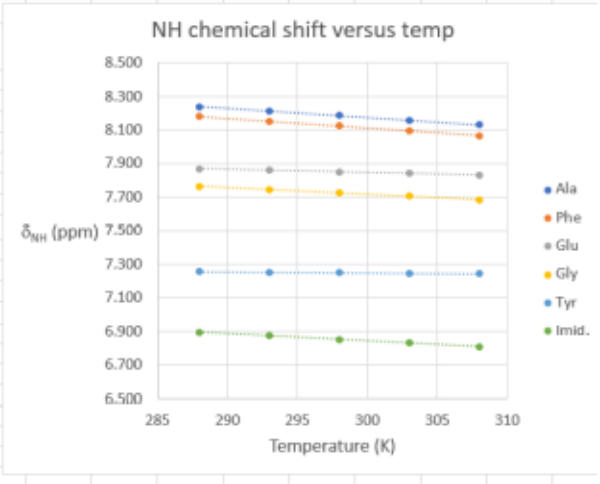

Temperature coefficients > -4.6 ppb/DT may show H-bonding. Tyr and Glu appear to be H-bound, while Gly and the Imidazoline residues are borderline.

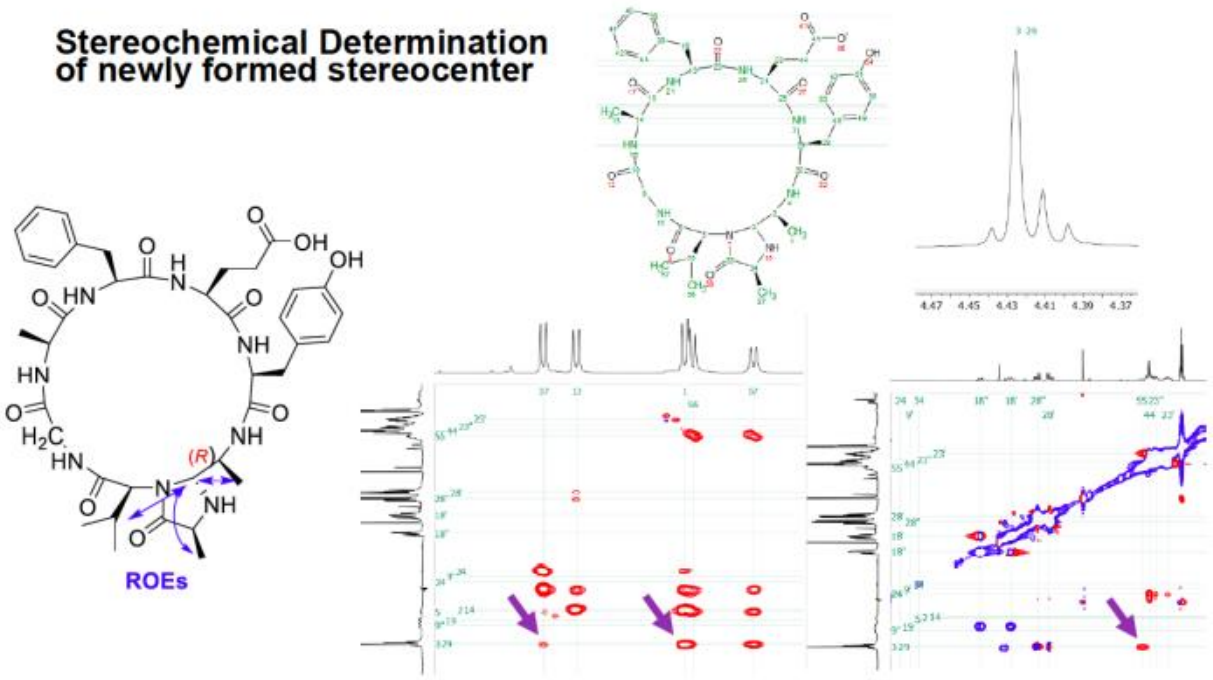

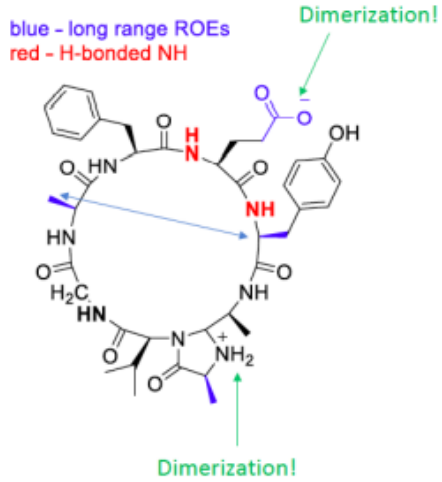

Weak ROEs were observed between Imid methyl and Glu methylene protons. This appears to indicate dimerization. However, to minimize dimerization, the sample would need to be diluted which would have hurt NMR sensitivity. Thus, these ROEs were simply ignored. On the otherhand, two long ROEs were observed between Ala methyl and both Tyr methylenes. This appears to be consistent, along with hydrogen bonding for Tyr, with Phe or Glu involved in a turn.

ROE distance restraints

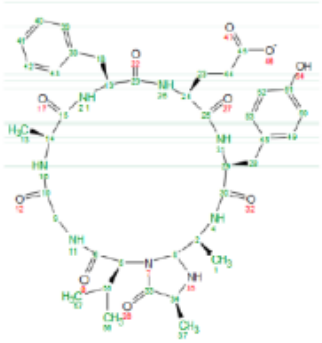

class	restraint
strong	1.8-2.7 Å
medium	1.8-3.3 Å
weak	1.8-5.0 Å

Volume integrals from ROESY spectrum were converted into distance restraints by bracketing them into strong, medium, and weak ROEs.

Summary of ROEs used as distance constraints:

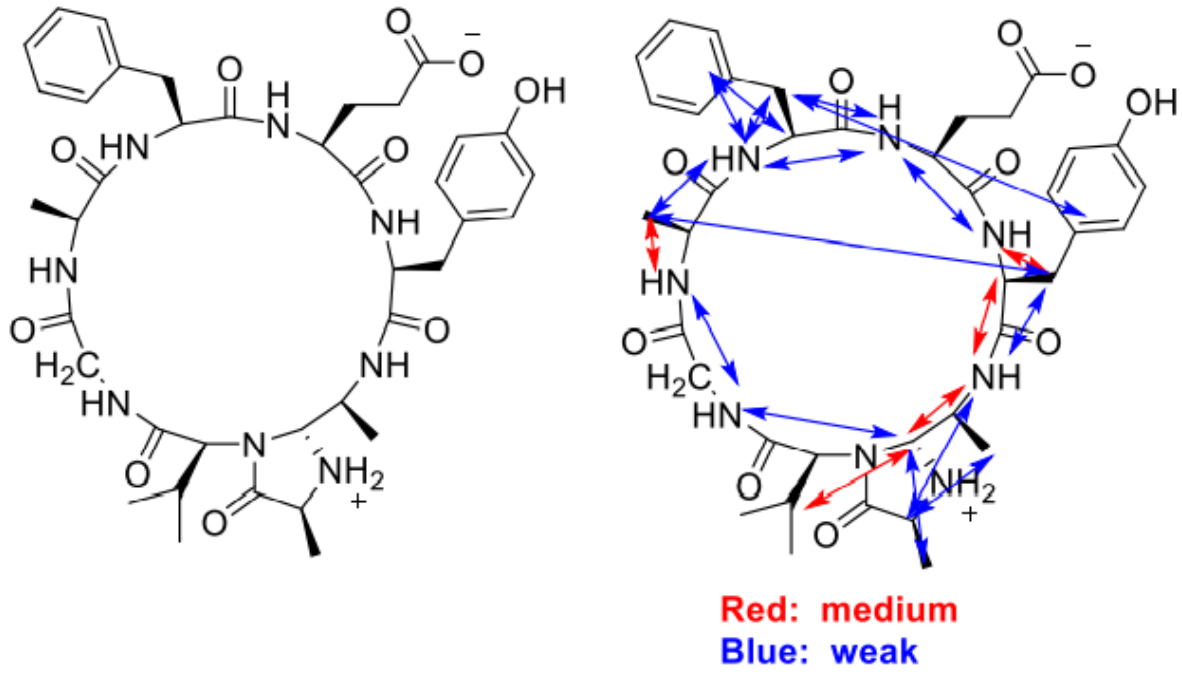

Note: The internuclear distance between Tyr aromatic protons was used as a calibrant for a strong ROE upon which to bracket the other observed ROEs.

Secondary structure determination of **1.7a** by NMR coupling constants and ForceGen.

Running forcegen with NMR restraints

The program was run using the command:
sf-tools.exe –molconstraint nmr-cons -pquant testprep macro-ex.mol2 macgeom

where:
- nmr-cons is a text file containing the NMR distance and dihedral restraints
- macro-ex.mol2 is the unoptimized initial structure in mol2 format
- macgeom is the file of output structures

Distance Restraints

```
# Type Pen   Dist Wiggle  a1   a2
nmr    1.0   4.24 0.5     39   134
nmr    1.0   3.87 0.5     39   96
...
# Type Pen   Dist Wgl  a1N a2N  a1list a2list
qnmr   1.0   2.86 0.5  1   3    96     15 16 17
qnmr   1.0   2.78 0.5  1   3    98     15 16 17
...
```

-Note that # is a comment line; tabs can be used between parameters
-Pen is a penalty value (kcal/mol/Å^2)
-Dist is in Å
-Wiggle (or Wgl) allows for free movement (in this case, ±0.5 Å) up to which a quadratic penalty is applied
-qNMR type restraint is to centroid of symmetry-related group of protons
-a1N and a2N are the number of atoms in the list (e.g., 1 to 6)

Dihedral Restraints

```
# Type   Pen   L_Bound  U_Bound  a1 a2 a3 a4
torsion 0.3   -150     -90      36 38 40 56
torsion 0.3   -160     -80      93 95 97 112
...
```

-L_Bound and U_Bound are the lower and upper bounds for dihedral angles, which are generated from Karplus-type curves using coupling constants

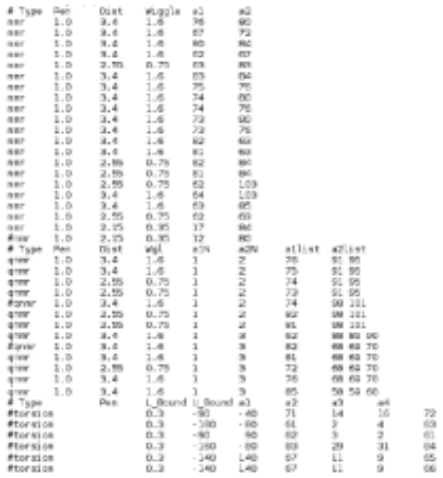

This is an example of the restraint file used for our peptide. The # are comments. Forcegen was run with and without using dihedral angle restraints (torsions). Here, we decided to use distance restraints (ROEs), and then calculate J-couplings using DFT as a way to eliminate incorrect structures.

Cnum	NViol	MeanViol		Constraint							
0	0	0.0000	nmr	1.0	3.4	1.6	76	80			
1	0	0.0000	nmr	1.0	3.4	1.6	67	72			
2	0	0.0000	nmr	1.0	3.4	1.6	80	84			
3	7	0.0692	nmr	1.0	3.4	1.6	62	67			
4	34	0.0302	nmr	1.0	2.55	0.75	63	83			
5	0	0.0000	nmr	1.0	3.4	1.6	83	84			
6	0	0.0000	nmr	1.0	3.4	1.6	75	76			
7	0	0.0000	nmr	1.0	3.4	1.6	74	80			
8	0	0.0000	nmr	1.0	3.4	1.6	74	76			
9	0	0.0000	nmr	1.0	3.4	1.6	73	80			
10	0	0.0000	nmr	1.0	3.4	1.6	73	76			
11	0	0.0000	nmr	1.0	3.4	1.6	82	83			
12	0	0.0000	nmr	1.0	3.4	1.6	81	83			
13	448	0.1707	nmr	1.0	2.55	0.75	82	84			
14	28	0.3238	nmr	1.0	2.55	0.75	81	84			
15	467	0.8157	nmr	1.0	2.55	0.75	82	103			
16	0	0.0000	nmr	1.0	3.4	1.6	84	103			
17	10	0.0990	nmr	1.0	3.4	1.6	83	85			
18	38	0.1460	nmr	1.0	2.55	0.75	62	83			
19	162	0.1375	nmr	1.0	2.15	0.35	17	84			
20	0	0.0000	qnmr	1.0	3.4	1.6	1	2	76	91	95
21	0	0.0000	qnmr	1.0	3.4	1.6	1	2	75	91	95
22	0	0.0000	qnmr	1.0	2.55	0.75	1	2	74	91	95
23	0	0.0000	qnmr	1.0	2.55	0.75	1	2	73	91	95
24	0	0.0000	qnmr	1.0	2.55	0.75	1	2	82	98	101
25	0	0.0000	qnmr	1.0	2.55	0.75	1	2	81	98	101
26	0	0.0000	qnmr	1.0	3.4	1.6	1	3	62	88	89 90
27	102	0.5388	qnmr	1.0	3.4	1.6	1	3	81	68	69 70
28	24	0.1128	qnmr	1.0	2.55	0.75	1	3	72	68	69 70
29	0	0.0000	qnmr	1.0	3.4	1.6	1	3	76	68	69 70
30	1	0.5586	qnmr	1.0	3.4	1.6	1	3	85	58	59 60

After running forcegen, violations of distance restraints was used as a way to ensure that these were correctly assigned ROEs and should be used in the model. If there were too many violations, then these were removed.

Filter by J-couplings

Best conformer: conf#284

MAE: 0.77

			conf#100	conf#101	conf#102	conf#103	conf#104	conf#105	conf#106	conf#107	conf#108	conf#109	conf#10
Coupling	expt J (Hz)	MAE:	15.425	16.68	15.32	16.14	15.83	7.5	-1	20.75	16.17	19.55	20.41
(62,61)	1.0	error:	2.123	1.844	2.286	2.269	1.836	1.25	null	2.883	2.269	3.121	2.628
(63,61)	8.6	error:	7.365	6.867	6.125	6.091	6.972	8.121	null	6.849	6.084	5.354	5.731
(67,65)	4.5	error:	4.725	5.622	4.61	5.415	0.887	3.179	null	5.036	5.41	6.013	3.804
(67,66)	4.5	error:	9.839	8.438	10.015	9.056	7.925	3.569	null	9.273	9.051	7.879	10.669
(72,71)	5.4	error:	8.396	10.626	7.371	10.22	9.874	6.907	null	10.594	10.214	10.428	9.504
(76,75)	7.4	error:	8.096	8.202	9.594	6.952	6.455	7.003	null	8.488	6.945	5.673	9.137
(80,79)	7.2	error:	9.998	7.954	8.63	8.279	8.54	9.614	null	10.689	8.288	8.95	10.266
(84,83)	8.4	error:	9.41	8.134	9.602	8.944	7.028	8.389	null	6.387	8.975	7.611	8.544

1000 conformers!

This approach was then applied to our peptide. A python script was written to filter conformers with J-couplings that fit the observed. The set with total absolute error < 10 Hz was then used to generate an accurate ensemble.

Post J-coupling filtering

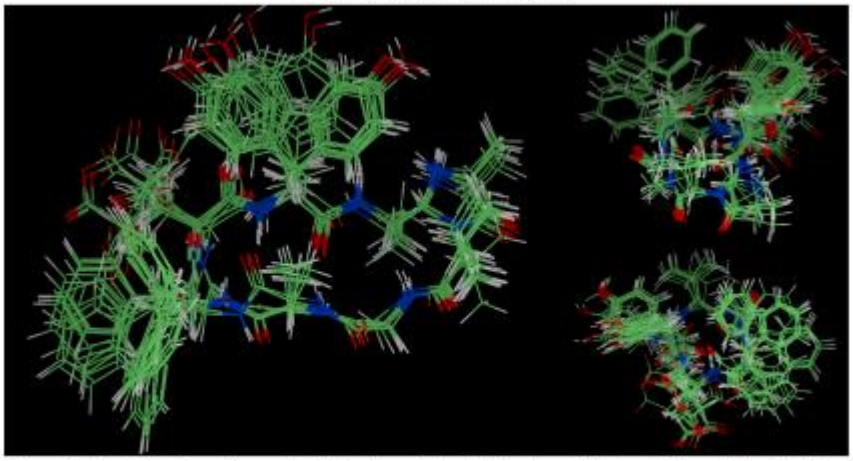

This is the results from the J-coupling constant filtering, which exhibits a type II β-turn at Glu and Phe. The H-bond is also observed for Tyr. The imidazoline group is conformationally constrained with limited flexibility.

Forcegen was then re-run with the Tyr NH to Ala C=O hydrogen bond as a constraint. This then generated a more accurate structure, which shows that the Ala NH hydrogen bond is not present.

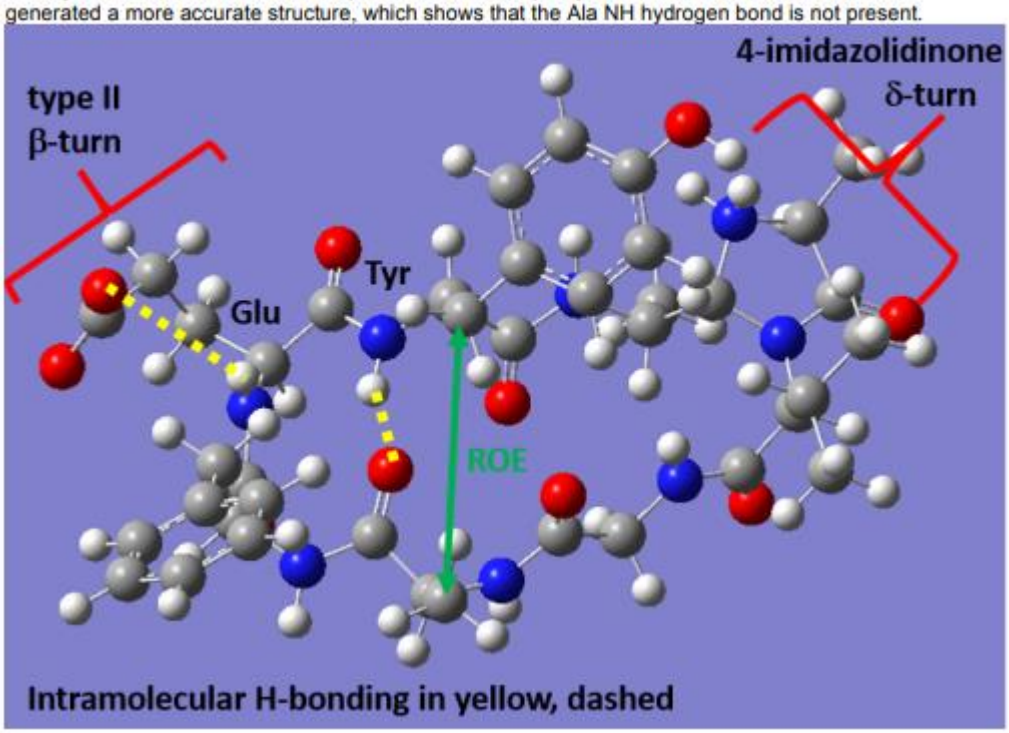

pH Stability Studies. Cyclic peptide cyc(NVGPFEY) **1.2f** (2.5 mg) was dissolved in H_2O to form a stock solution (500 µL, conc. 7 mM). 100 µL of the stock was added to 400 µL of sodium phosphate buffer (10 mM) at the following pH values: 3.5, 5.5, 7.5, 8.5, 10.5 (total conc. 1.4 mM). The reactions were shaken at room temperature. Samples were analyzed by injecting them in HPLC after regular intervals of time. No degradation of cyc(NVGPFEY) **1.2f** was observed even after 24 h at different pH values.

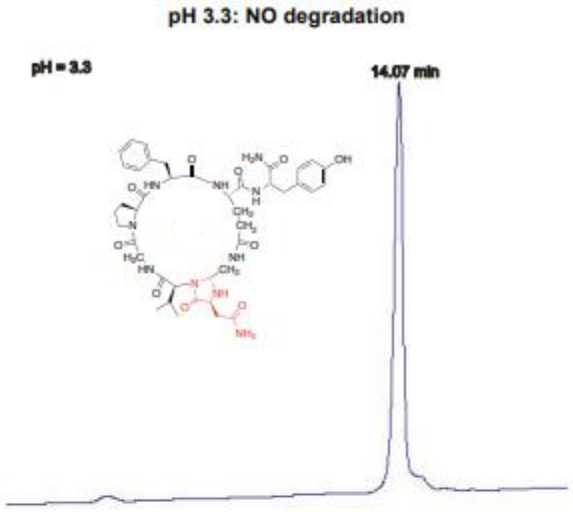

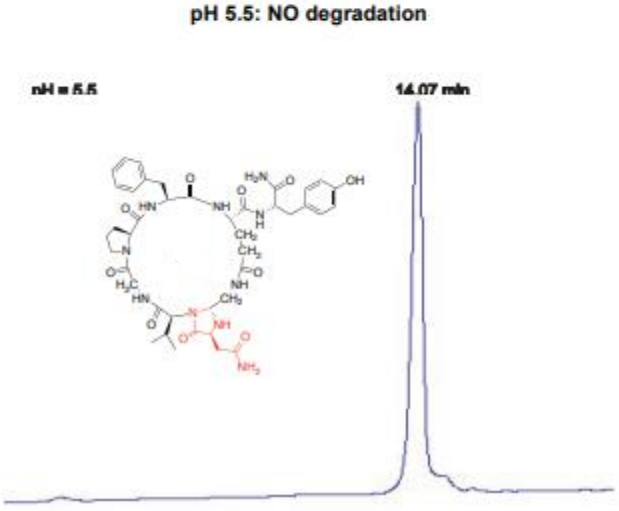

pH 7.5: NO degradation

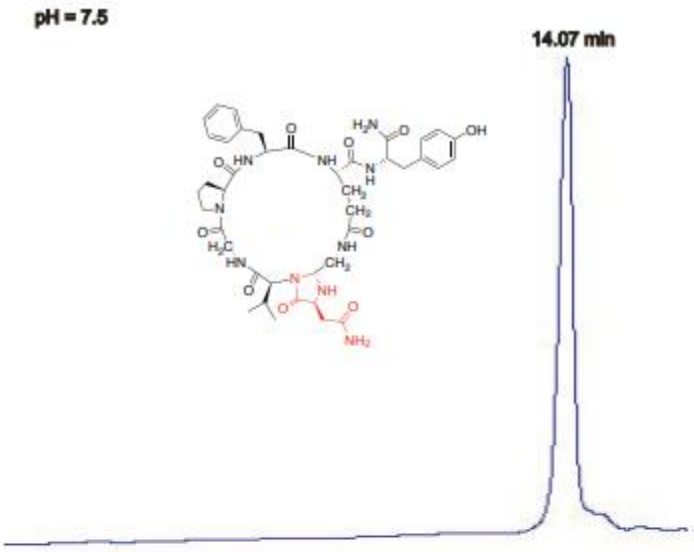

pH 8.5: NO degradation

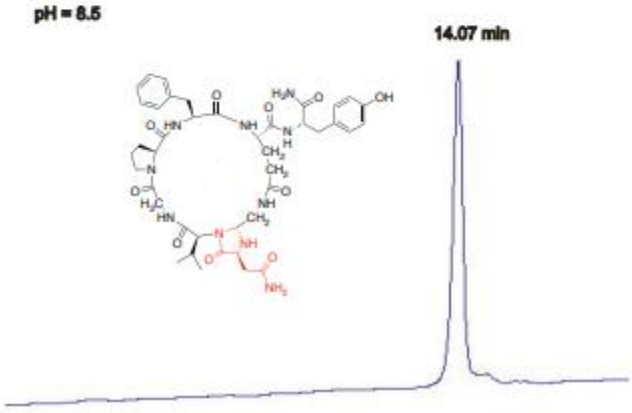

Enzymatic Degradation Studies. Linear peptide AVGPFEY and cyclic peptide cyc(AVGPFEY) **1.2a** were individually dissolved in 10 mM Tris buffer pH 7.5 (final conc. 1.5 mM). A chymotrypsin stock solution was created by the addition of 1 mg chymotrypsin in 100µL $CaCl_2$ (0.01 M), 100 µL tris buffer (0.1 M pH 7.5), 100 µL HCl (1 mM). 10 µL of the chymotrypsin stock solution was added to both linear peptide AVGPFEY and cyclic peptide cyc(AVGPFEY) **1.2a** solutions. Samples (100 µL) were taken after regular intervals of time from both linear and cyclic peptide solutions. 100 µL of each sample was quenched with 400 µL of frozen water and solutions were frozen at –80 °C at the following time intervals: 0 min, 5 min, 15 min, 30 min, 45 min, 60 min, 90 min, 120 min and 480 min. Each sample was lyophilized and analyzed using HPLC and LCMS.

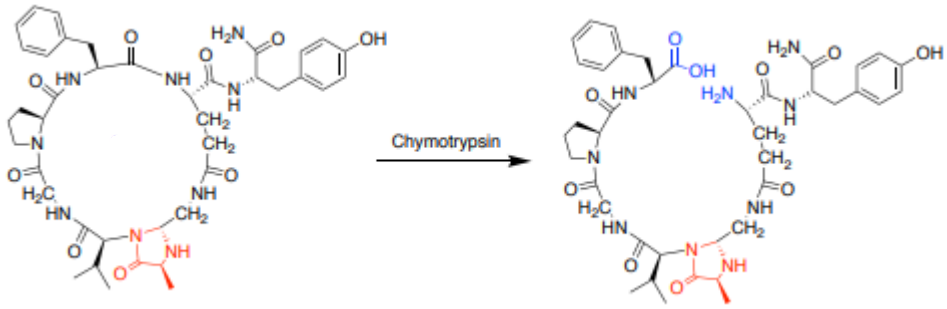

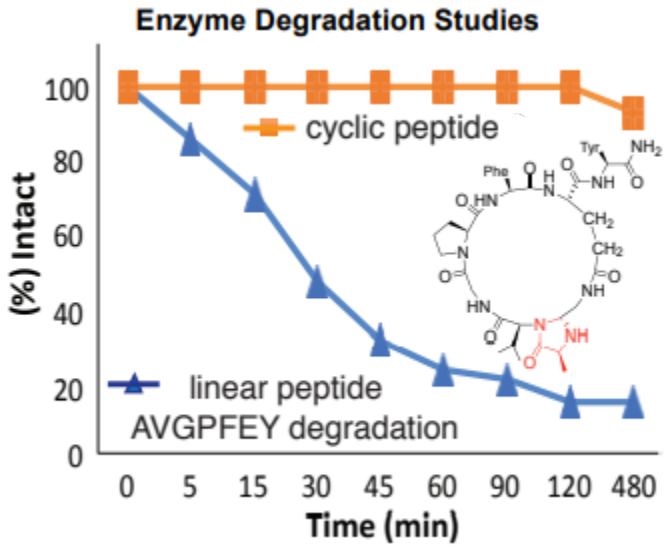

Enzyme Degradation of Linear Peptide

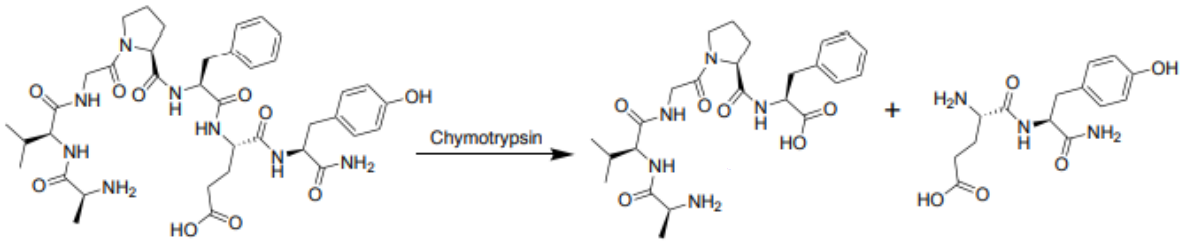

1.1a **1.1a'**

HPLCs for Enzymatic Degradation of Linear Peptide **1.1a**

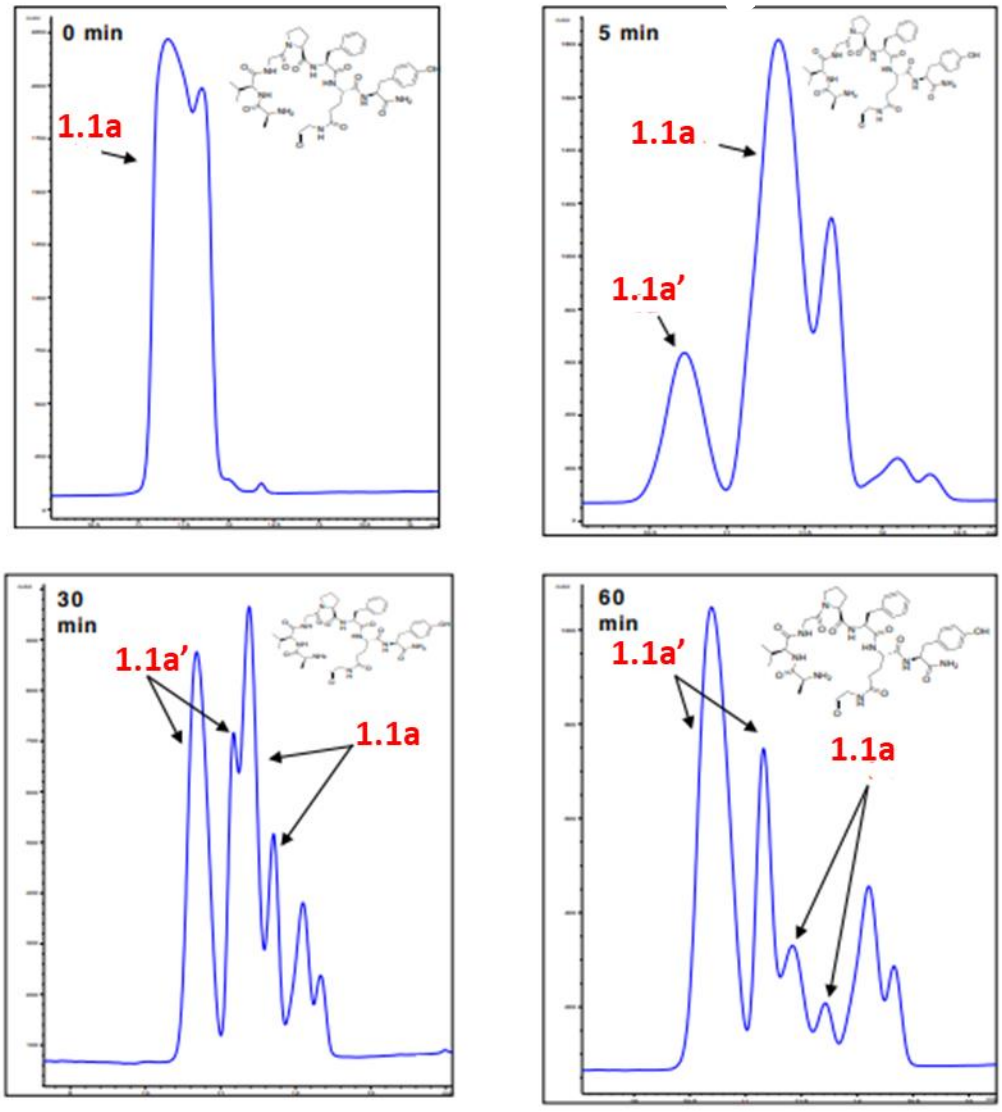

Data for Reversibility of CyClick Chemistry

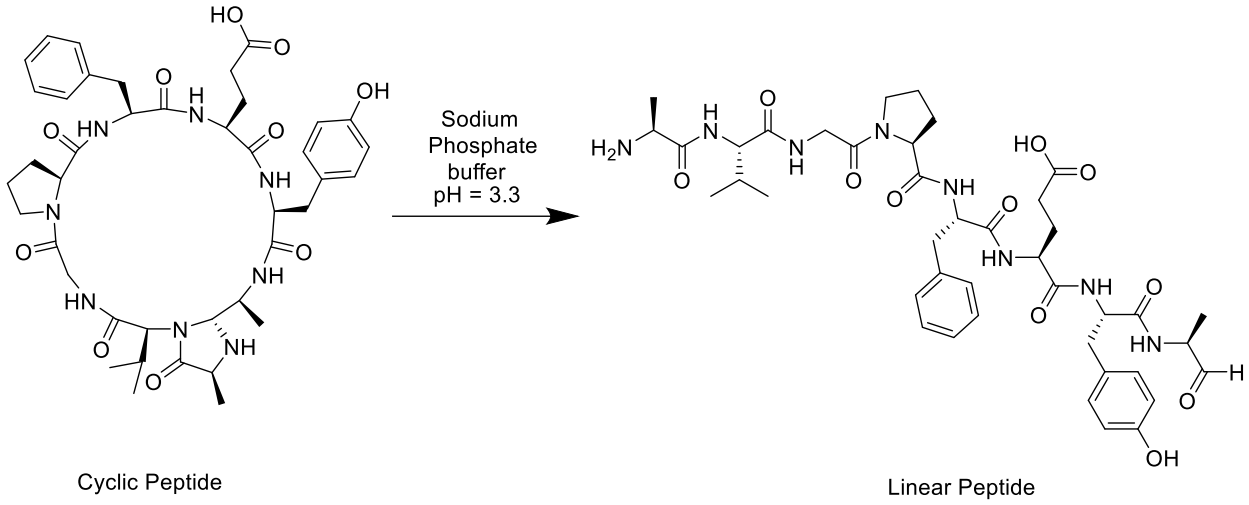

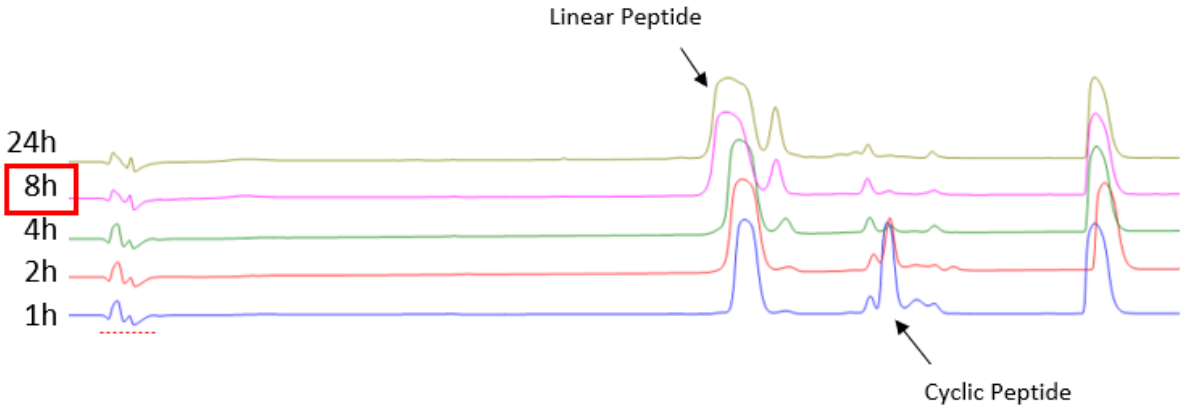

Benchmark of computational methods

To validate the computational method used in the manuscript, we benchmarked the single point energies of key transition states and intermediated along the reaction coordinate of CyClick of **1.4e** (Figure 13 in the manuscript) (**Table S1**). We tested various single point energies using different basis sets (entries 2 and 3), density functionals (entries 4, 5, 6, 7), and solvation models (entries 8, 9). All tested computational methods produced consistent results, suggesting that **TS2-R** is the rate-limiting transition state. Moreover, all methods predicts **TS2-R** has a lower free energy of activation than **TS2-S**, which is consistent with the experimental observation.

Benchmark of computational method (ΔG in kcal/mol)

	Single point computational method tested	**5**	**TS1**	**6**	**TS2-R**	**TS2-S**	**7-R**	**7-S**
1	M062X[i]/def2tzvpp[ii]/ SMD[iii] (solvent=water) *[method used in manuscript]*	0.0	17.7	16.0	20.0	36.1	-3.9	-6.9
2	M062X/6-31+g(d)/ SMD (solvent=water)	0.0	18.6	15.5	19.3	35.6	-5.1	-8.1
3	M062X/6-311+g(d,p)/ SMD (solvent=water)	0.0	17.7	16.1	19.6	35.6	-4.6	-7.4
4	b3lyp[iv]-D3[v]/ def2tzvpp/ SMD (solvent=water)	0.0	16.1	15.3	18.6	33.4	-0.7	-4.4
5	M06[vi]/ def2tzvpp/ SMD(solvent=water)	0.0	18.8	17.1	19.6	36.1	-2.5	-5.9
6	M062X-D3/ def2tzvpp/ SMD(solvent=water)	0.0	17.7	16.0	19.9	35.8	-4.0	-7.1
7	ωb97xd[vii]/ def2tzvpp/ SMD(solvent=water)	0.0	16.7	16.4	19.9	34.6	-5.0	-8.7
8	M062X/def2tzvpp/ PCM[viii] (solvent=water)	0.0	17.8	16.6	17.9	37.7	-6.7	-9.5
9	M062X/def2tzvpp/ CPCM[ix] (solvent=water)	0.0	17.9	16.7	18.0	37.7	-6.6	-9.5

Effect of additive on the CyClick chemistry

We observed that addition of 4-Dimethylaminopyridine (DMAP) improves the conversion percentage to form the imidazolidinone cyclic peptide product. Our computed reaction coordinate profile (**Figure S2**) suggested that in presence of the organic base DMAP, the CyClick mechanism still favors the intramolecular hydrogen bonding (IMHB) enabled zwitterionic mechanism (solid black pathway). The rate-limiting transition state remained to be the collapse of the zwitterion (**STS2**) with 23.0 kcal/mol free energies of activation. The formation of the imidazolidinone cyclic peptide product is thermodynamically more favorable (-6.4 kcal/mol) compared to that without DMAP (-3.9 kcal/mol). The DMAP assisted zwitterionic pathway (dashed black pathway) requires 29.3 kcal/mol free energies of activation (**STS3**), making it the less favorable pathway. We will show some more details regarding the two zwitterionic pathways in **Figure S3**. The competing anionic pathway (red pathway), along which DMAP is responsible

for the deportation of the cyclic imine intermediate, has significantly higher free energy barrier of 38.9 kcal/mol (**STS4**), and unlikely to take place at room temperature.

Computed reaction coordinate profile of intramolecular CyClick reaction of 4 with DMAP

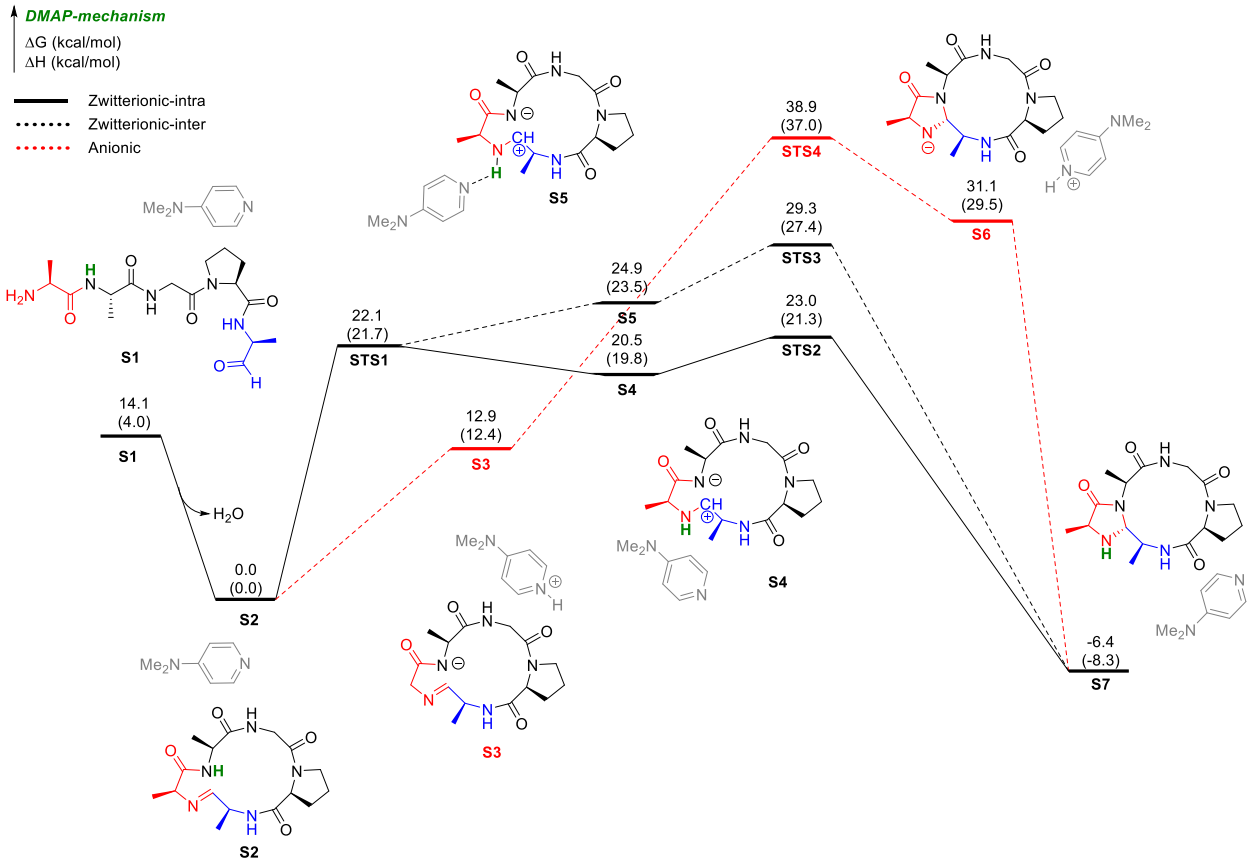

The optimized geometries of the zwitterionic intermediates and transition states. On the top of the figure, S4 and STS2, which are stabilized by intramolecular hydrogen bonding (IMHBs), have lower free energy barriers compared to S5 and STS3, which are stabilized intermolecularly by DMAP.

IMHB

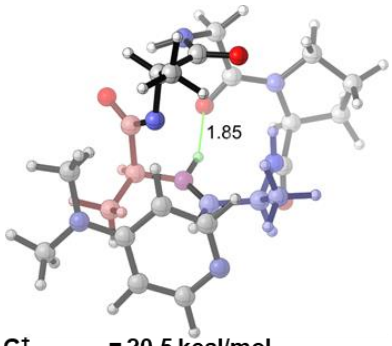

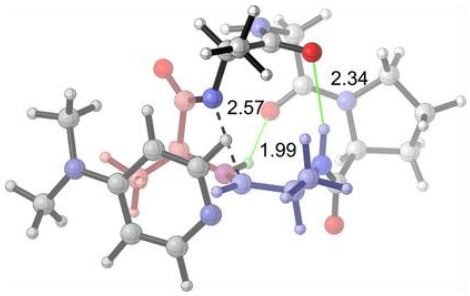

$\Delta G^{\ddagger}_{S4\ (IMHB)}$ = 20.5 kcal/mol

$\Delta G^{\ddagger}_{STS2\ (IMHB)}$ = 23.0 kcal/mol

DMAP does not directly interact with the zwitterionic IM4 nor TS4

DMAP

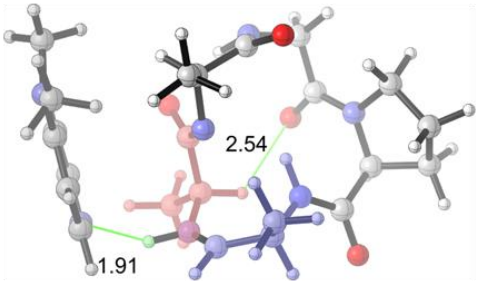

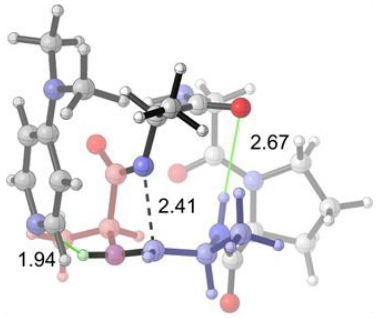

$\Delta G^{\ddagger}_{S5\ (DMAP)}$ = 24.9 kcal/mol

$\Delta G^{\ddagger}_{STS3\ (DMAP)}$ = 29.4 kcal/mol

Cyclization of Linear Peptides to form Cyclic Tetrapeptide

Cyclization of Linear Peptide 1.8a to form Cyclic Tetrapeptide 1.9a

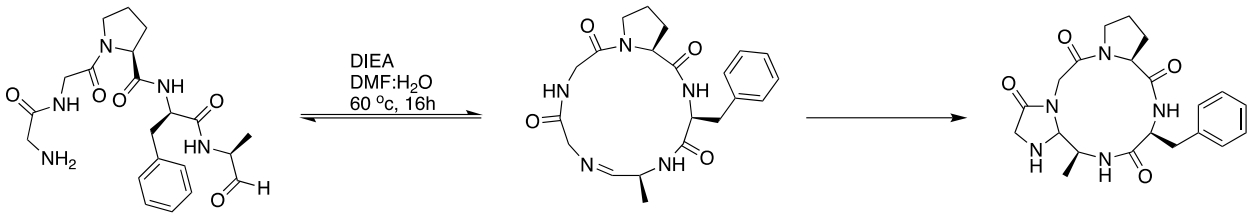

***cyc*-4-Imz-Gly(-Gly-Pro-Phe-Ala) (1.9a).** LCMS: *m/z* 414.1883 (calcd $[M+H]^+$ = 414.21), Purity: >95% (HPLC analysis at 220 nm). Retention time: 9.81 min

HRMS spectra of the macrocyclized product **1.9a**

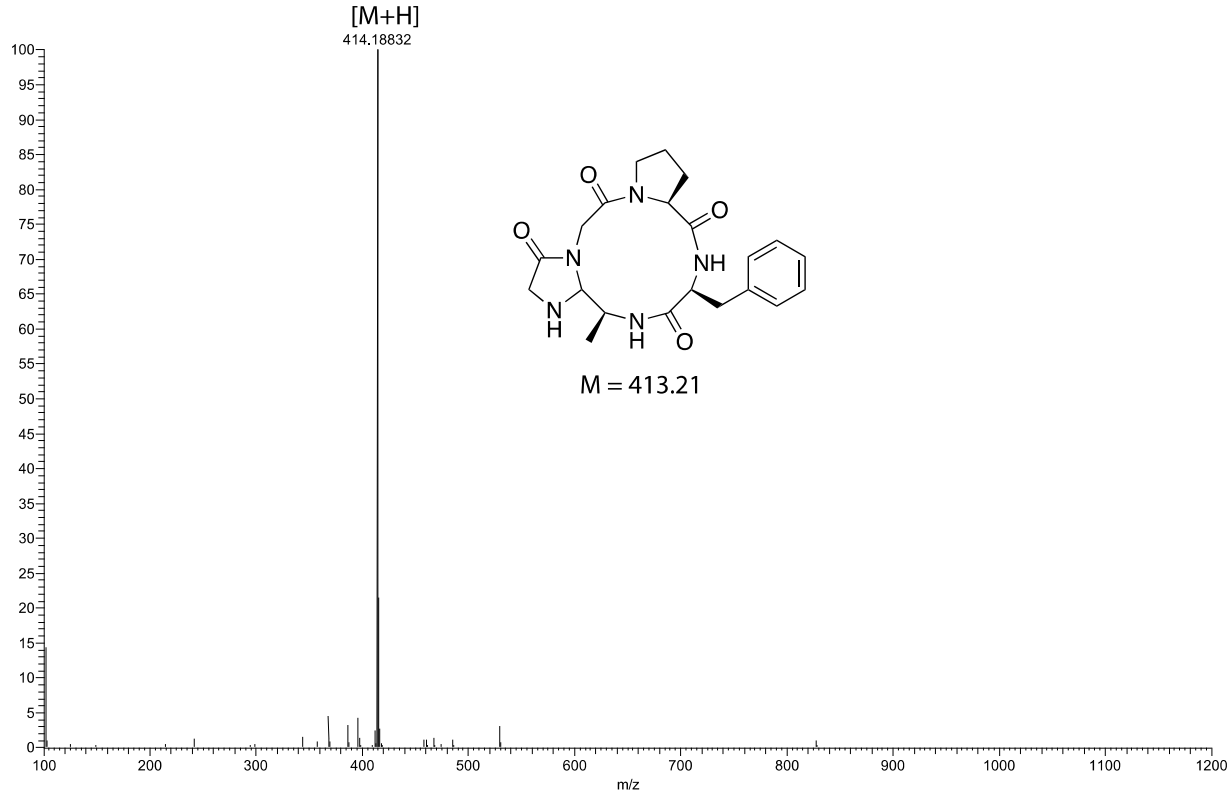

Cyclization of Linear Peptide 1.8b to form Cyclic Tetrapeptide 1.9b

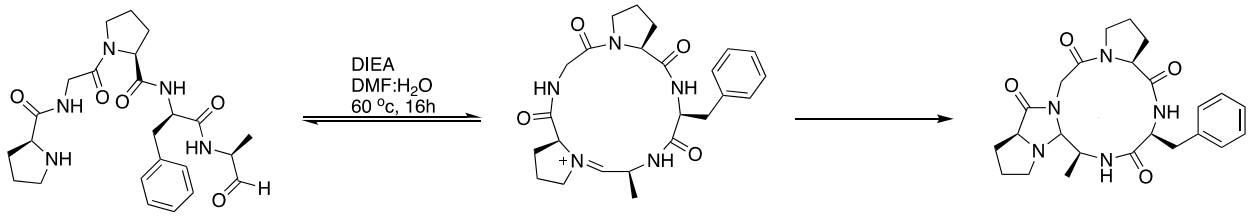

***cyc*-4-Imz-Pro(-Gly-Pro-Phe-Ala) (1.9b).** LCMS: *m/z* 454.2162 (calcd $[M+H]^+$ = 454.25), Purity: >95% (HPLC analysis at 220 nm). Retention time: 13.59 min

HRMS spectra of the macrocyclized product **1.9b**

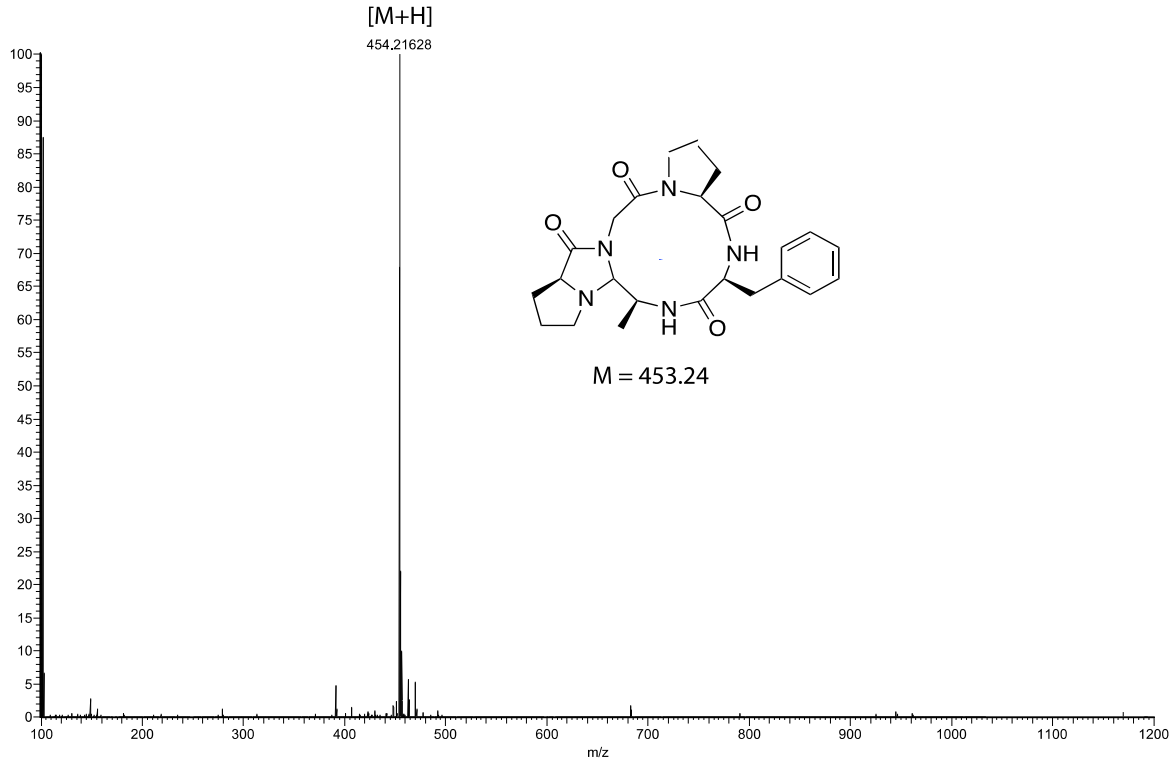

Cyclization of Linear Peptide 1.8c to form Cyclic Tetrapeptide 1.9c

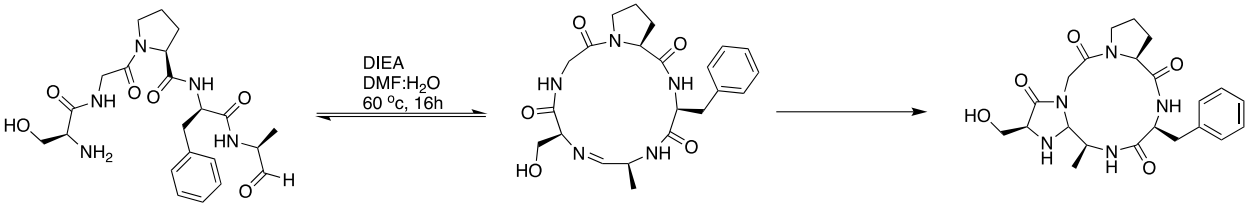

***Cyc*-4-Imz-Ser(-Gly-Pro-Phe-Ala) (1.9c).** LCMS: *m/z* 444.1983 (calcd $[M+H]^+$ = 444.22), Purity: >95% (HPLC analysis at 220 nm). Retention time: 11.26 min

HRMS spectra of the macrocyclized product **1.9c**

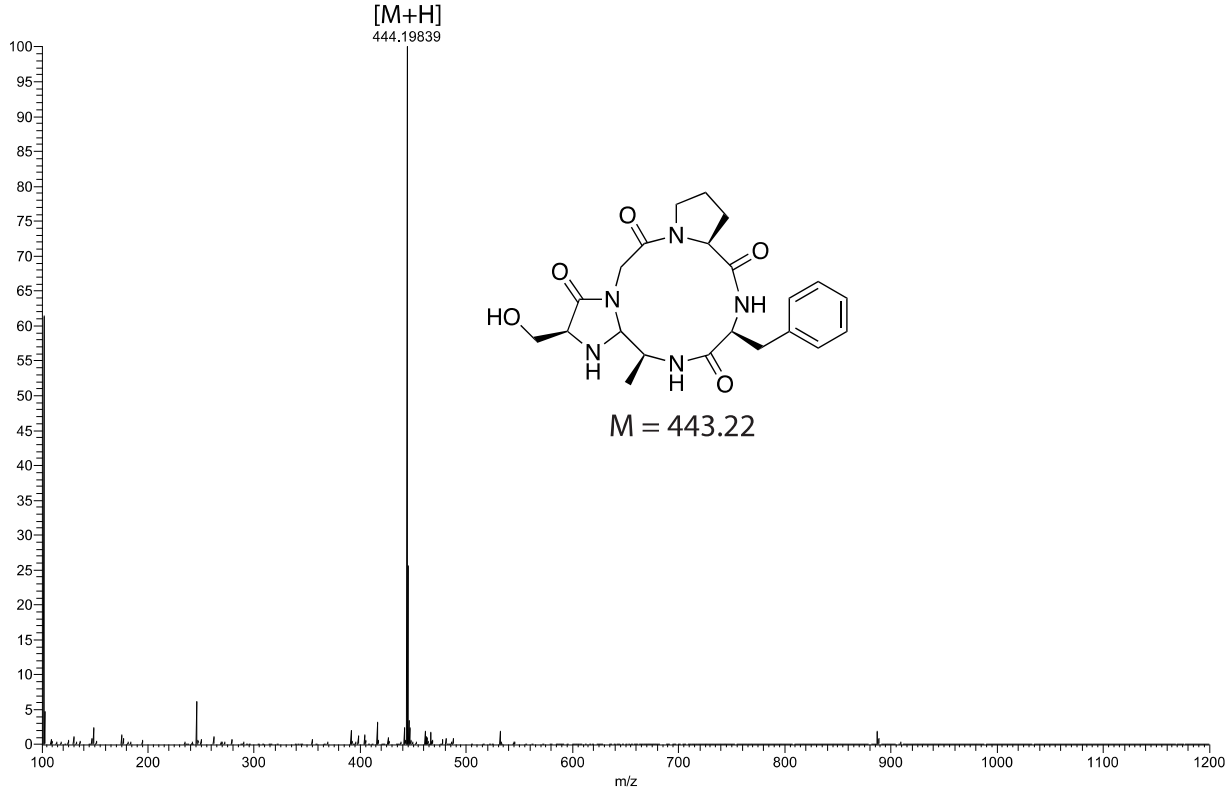

Cyclization of Linear Peptide 1.8d to form Cyclic Tetrapeptide 1.9d

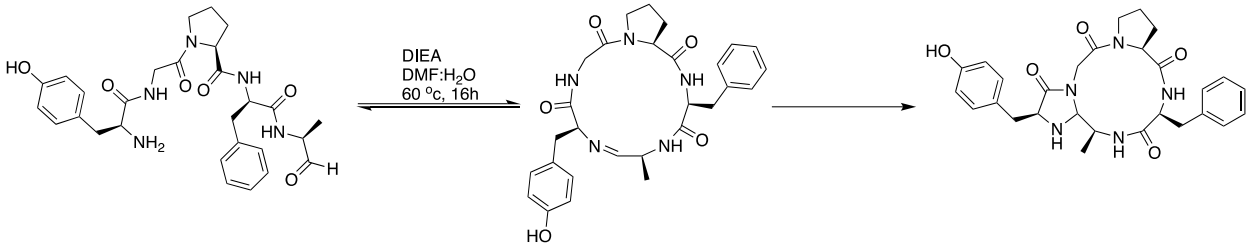

***cyc*-4-Imz-Tyr(-Gly-Pro-Phe-Ala) (1.9d).** LCMS: *m/z* 520.2243 (calcd $[M+H]^+$ = 520.26), Purity: >95% (HPLC analysis at 220 nm). Retention time: 13.98 min

HRMS spectra of the macrocyclized product **1.9d**

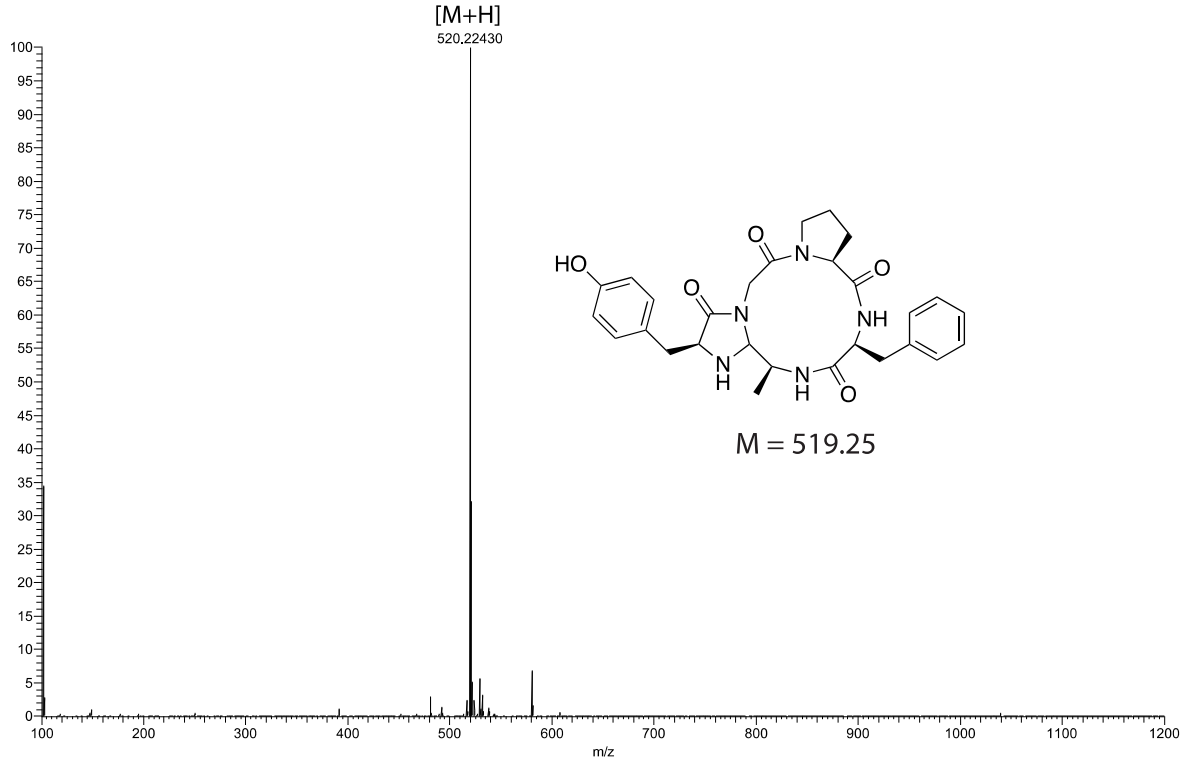

Cyclization of Linear Peptide 1.8e to form Cyclic Tetrapeptide 1.9e

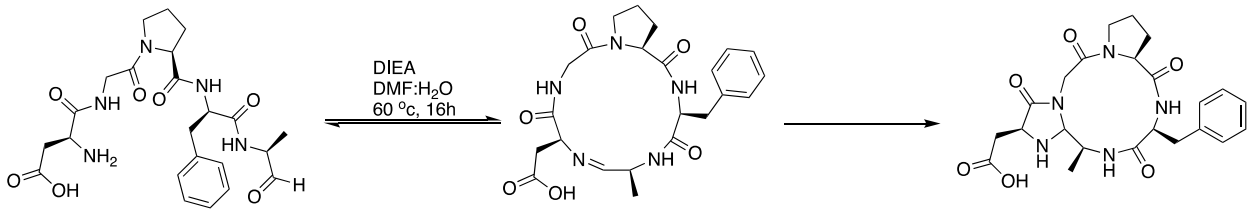

***Cyc*-4-Imz-Asp(-Gly-Pro-Phe-Ala (1.9e).** LCMS: *m/z* 472.2198 (calcd $[M+H]^+$ = 472.22), *m/z* 494.2027 (calcd $[M+Na]^+$ = 494.22), Purity: >95% (HPLC analysis at 220 nm). Retention time: 12.19 min

HRMS spectra of the macrocyclized product **1.9e**

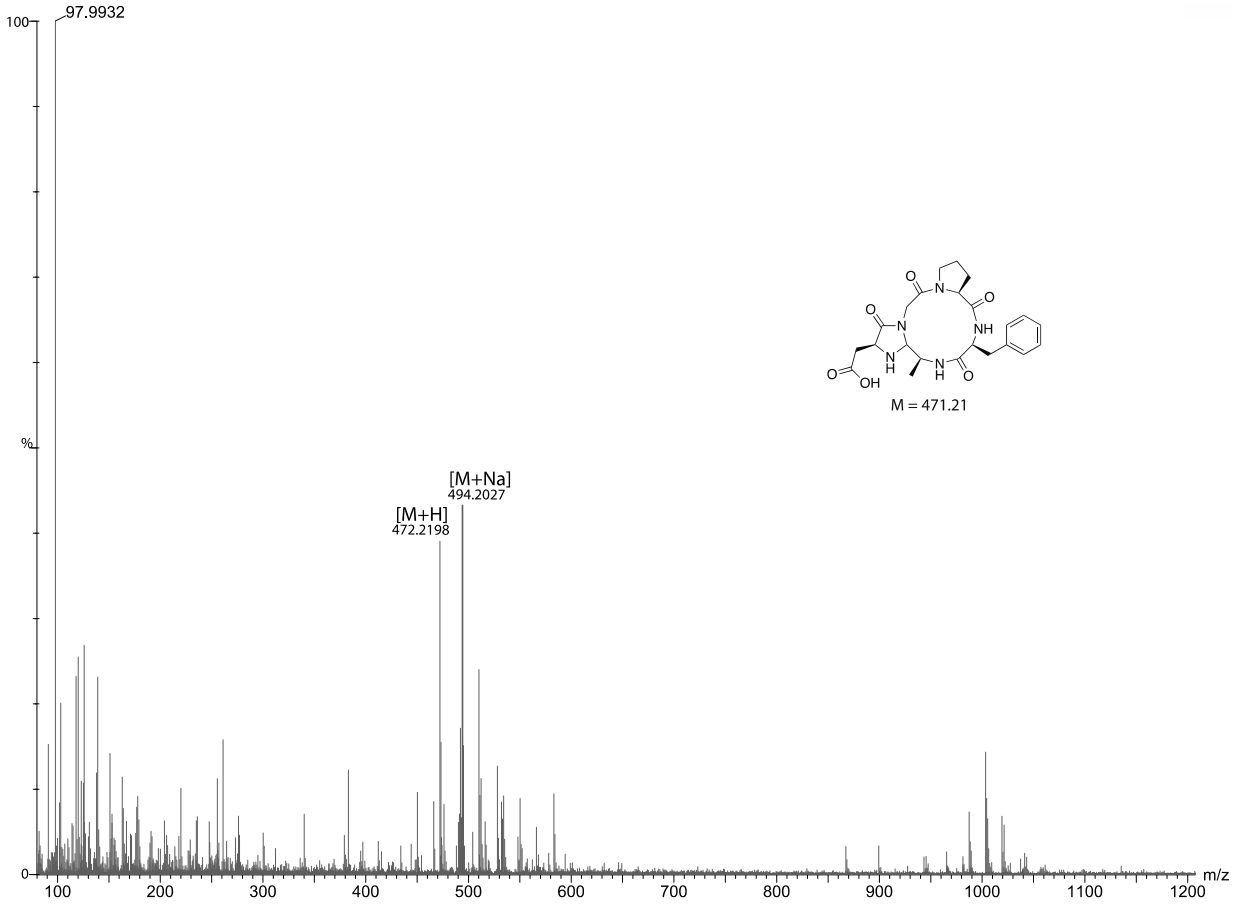

Cyclization of Linear Peptide 1.8f to form Cyclic Tetrapeptide 1.9f

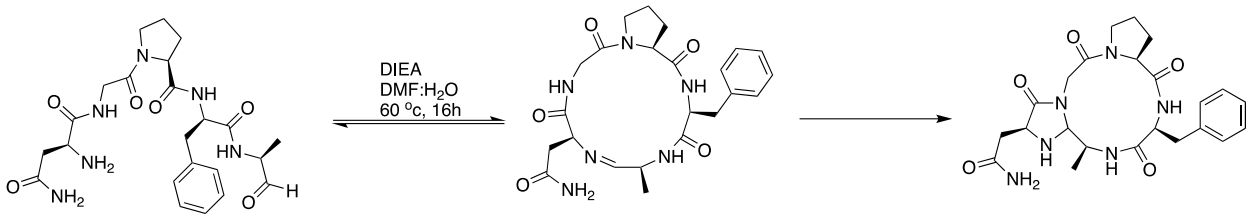

***Cyc*-4-Imz-Asn(-Gly-Pro-Phe-Ala) (1.8f).** LCMS: *m/z* 471.2367 (calcd $[M+H]^+$ = 471.24), *m/z* 493.2187 (calcd $[M+Na]^+$ = 493.24), Purity: >95% (HPLC analysis at 220 nm). Retention time: 10.18 min

HRMS spectra of the macrocyclized product **1.8f**

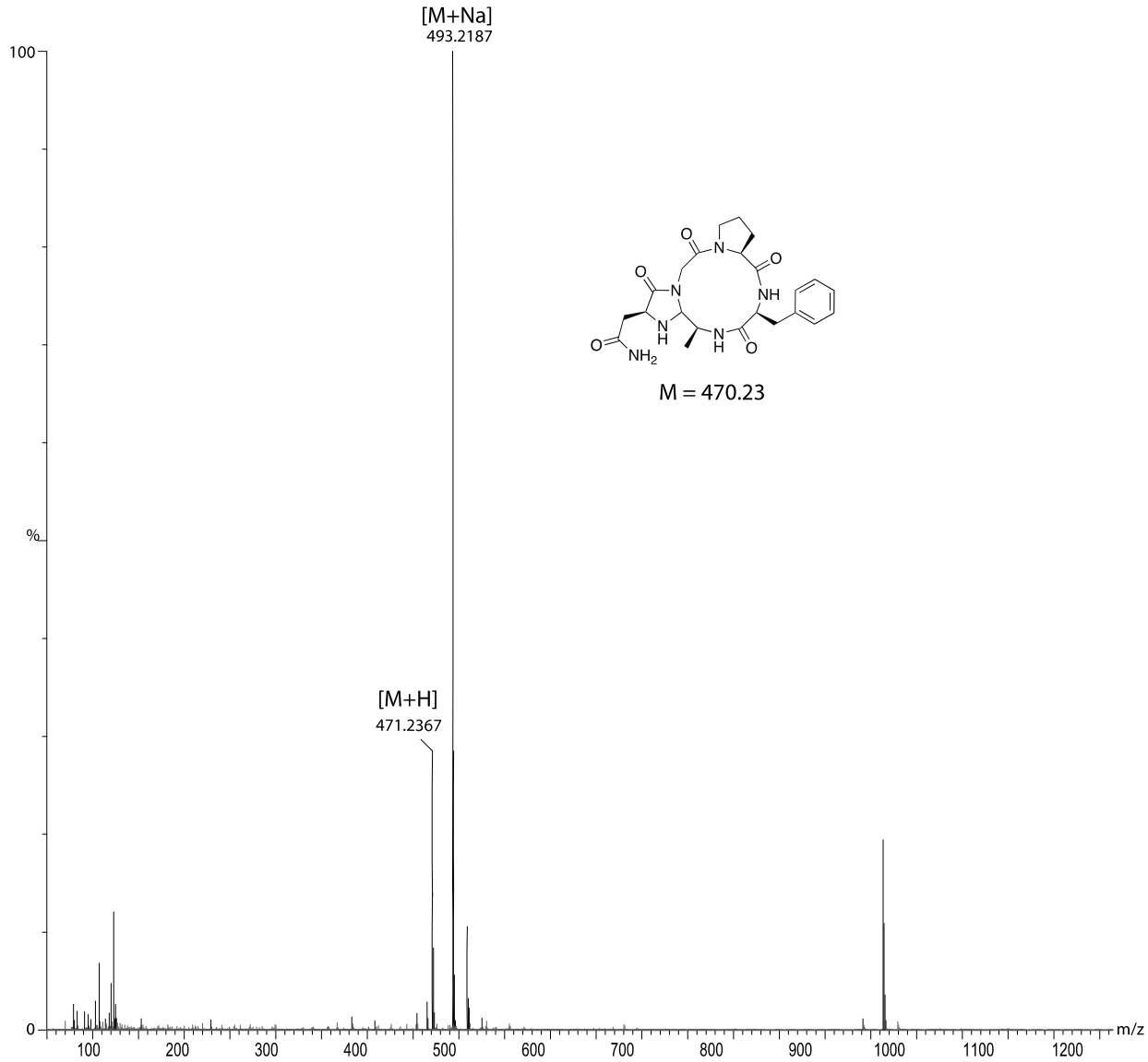

Data for Application of CyClick for the Formation of Peptide-Peptoid Hybrids

HRMS of compound 1.11a

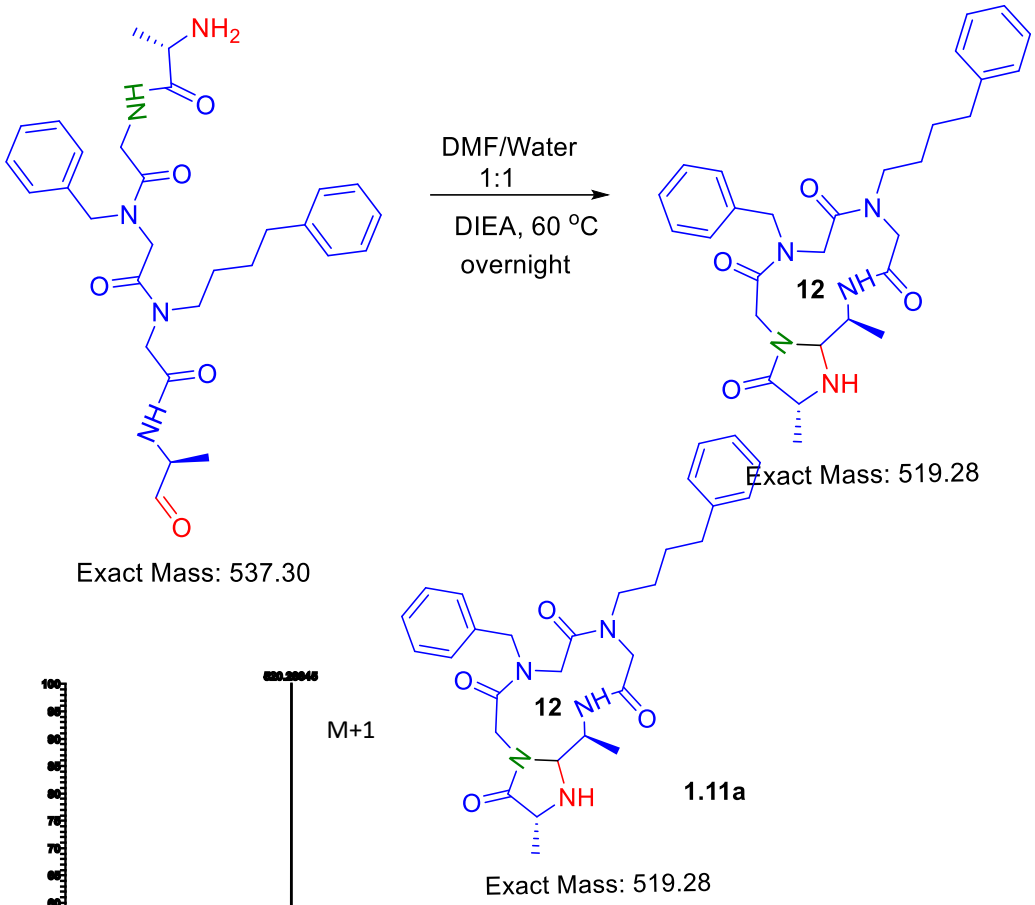

HRMS of compound 1.11b

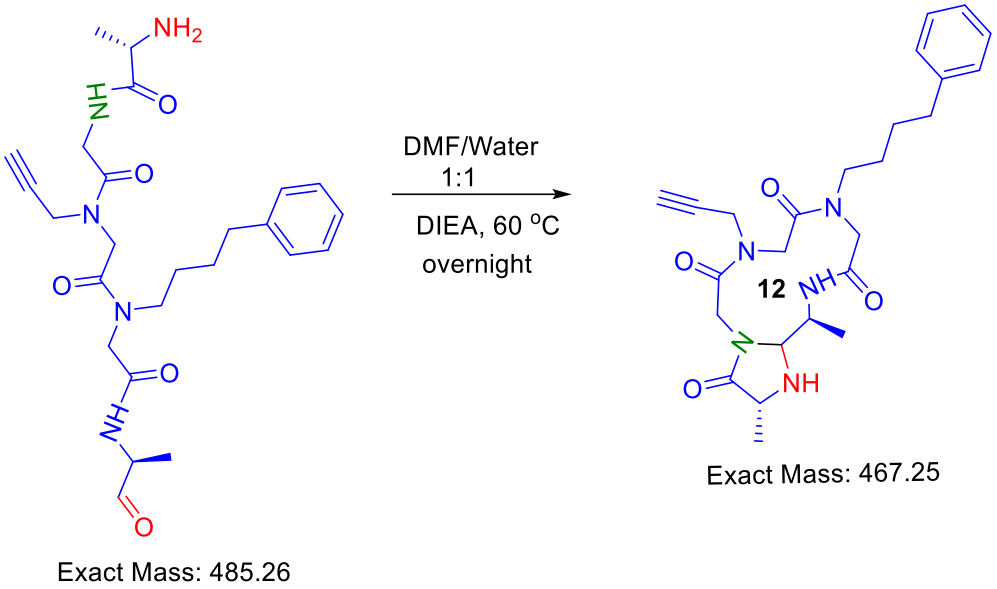

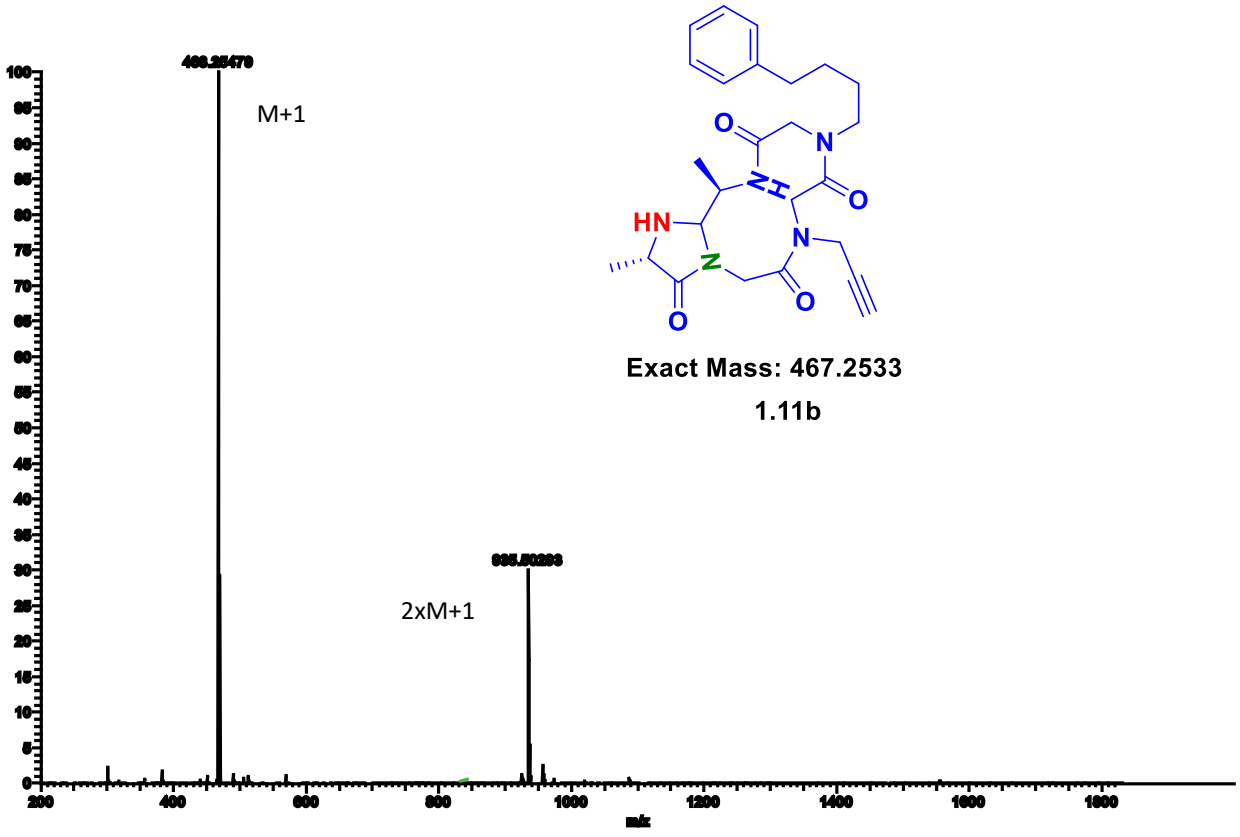

Exact Mass: 467.2533

1.11b

HRMS of compound 1.11c

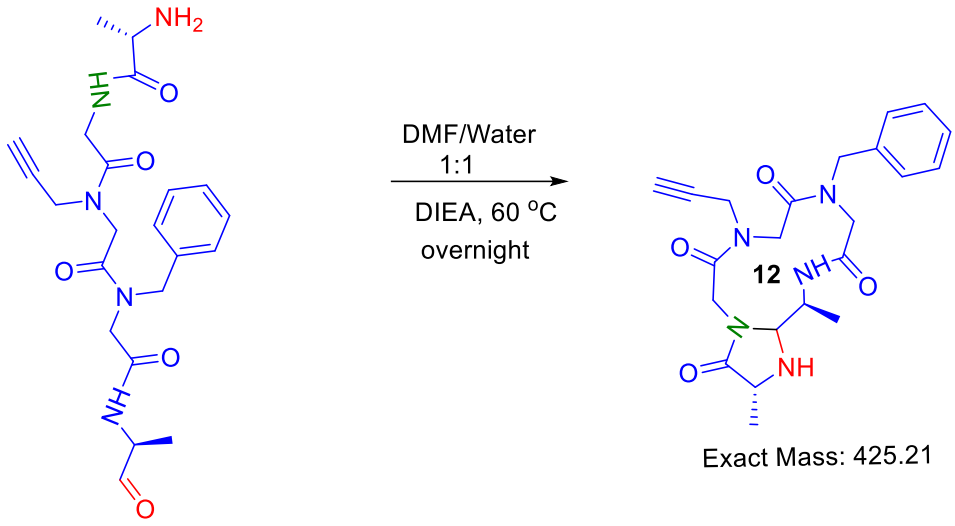

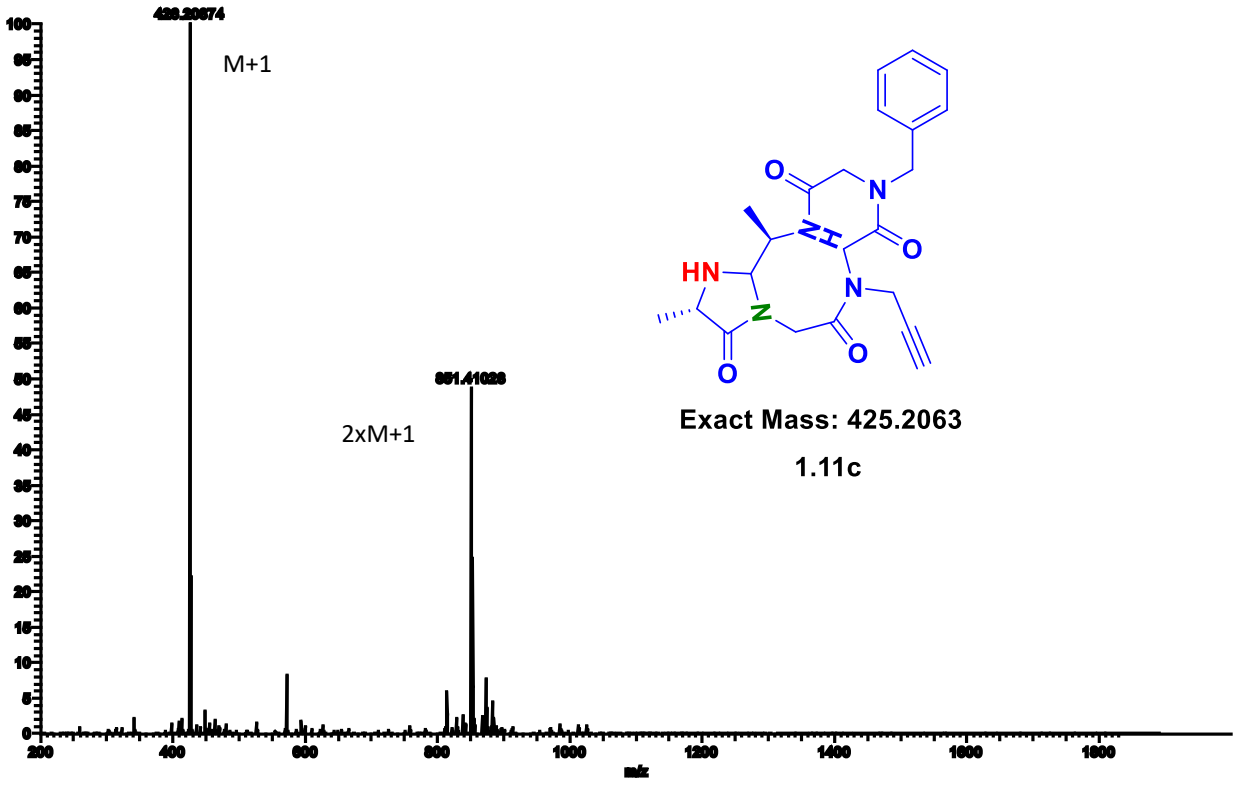

HRMS of compound 1.11d

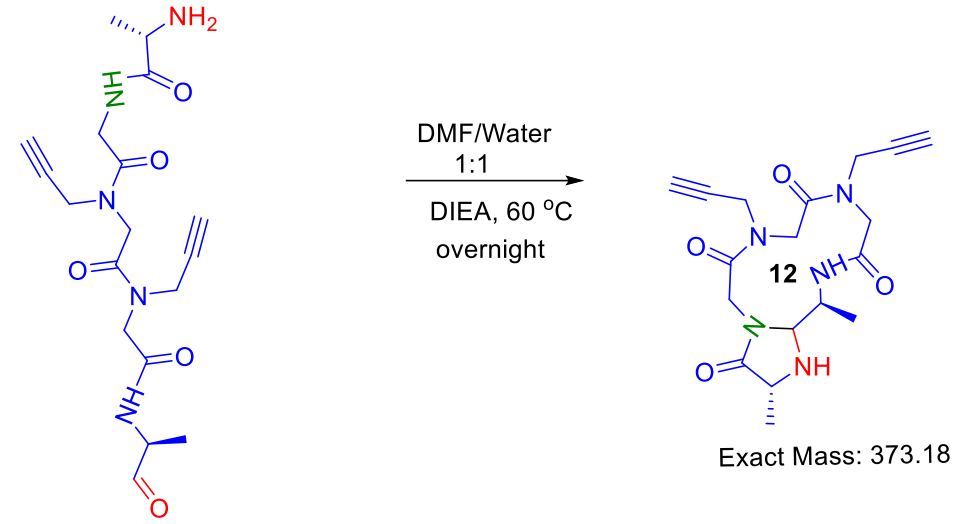

Exact Mass: 391.19

Exact Mass: 373.18

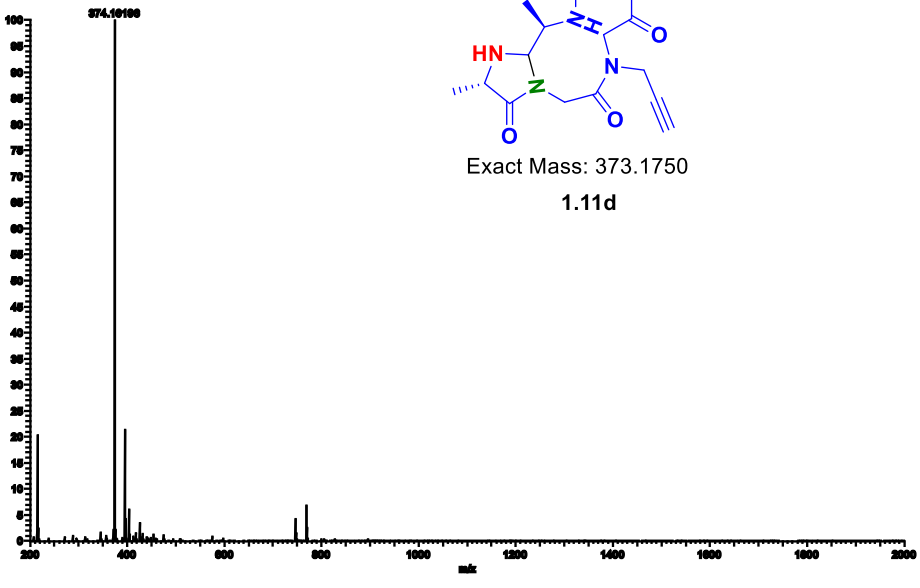

Exact Mass: 373.1750

1.11d

HMRS for CyClick Peptide-Peptiod 1.11e

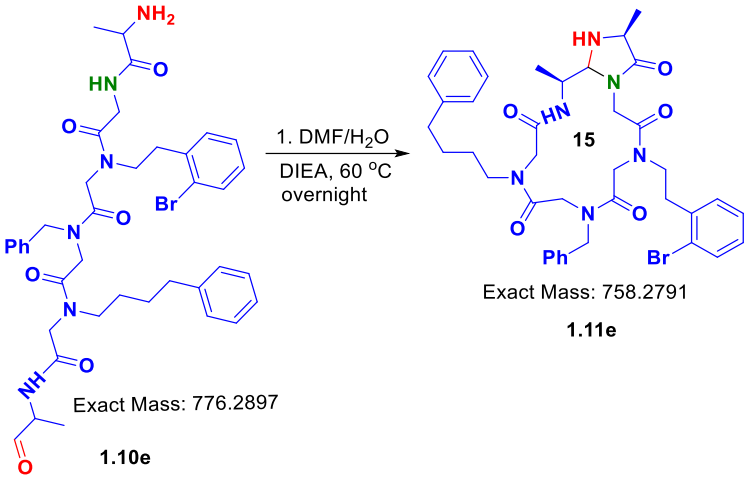

cyclic peptide-peptoid 1.11e. LCMS: *m/z* ($_{79}$Br) 759.2809 (calcd [*M*+H]+ = 759.2870), *m/z* 761.2793 (calcd [*M*+H]$^+$ = 761.2870), Purity: >95% (HPLC analysis at 220 nm). Retention time in HPLC: 23.376min.

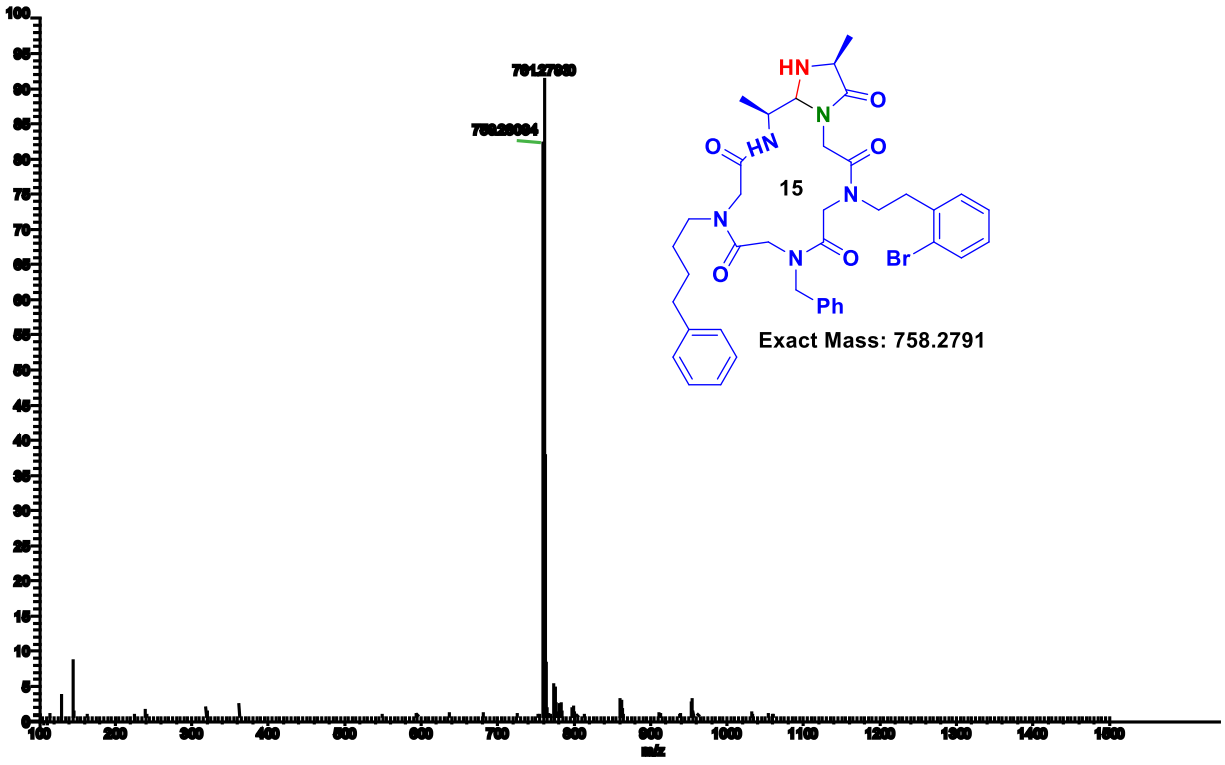

HRMS of Cyclic Peptide-Peptoid Hybrid 1.11f

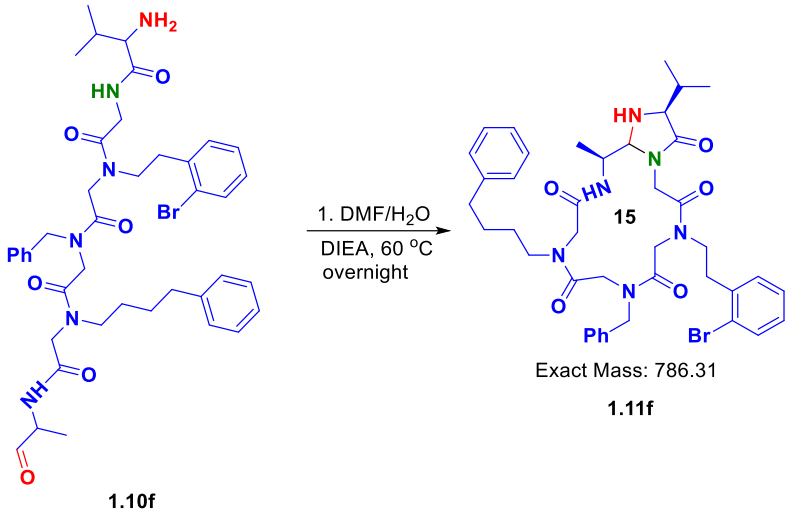

cyclic peptoid 1.11f. LCMS: *m/z* ($_{79}$Br) 787.2793 (calcd [*M*+H]+ = 787.3183), *m/z* ($_{81}$Br) 789.2775 (calcd ($_{81}$Br) [*M*+H]$^+$ = 789.3183), Purity: >95% (HPLC analysis at 220 nm). Retention time in HPLC: 26.892min.

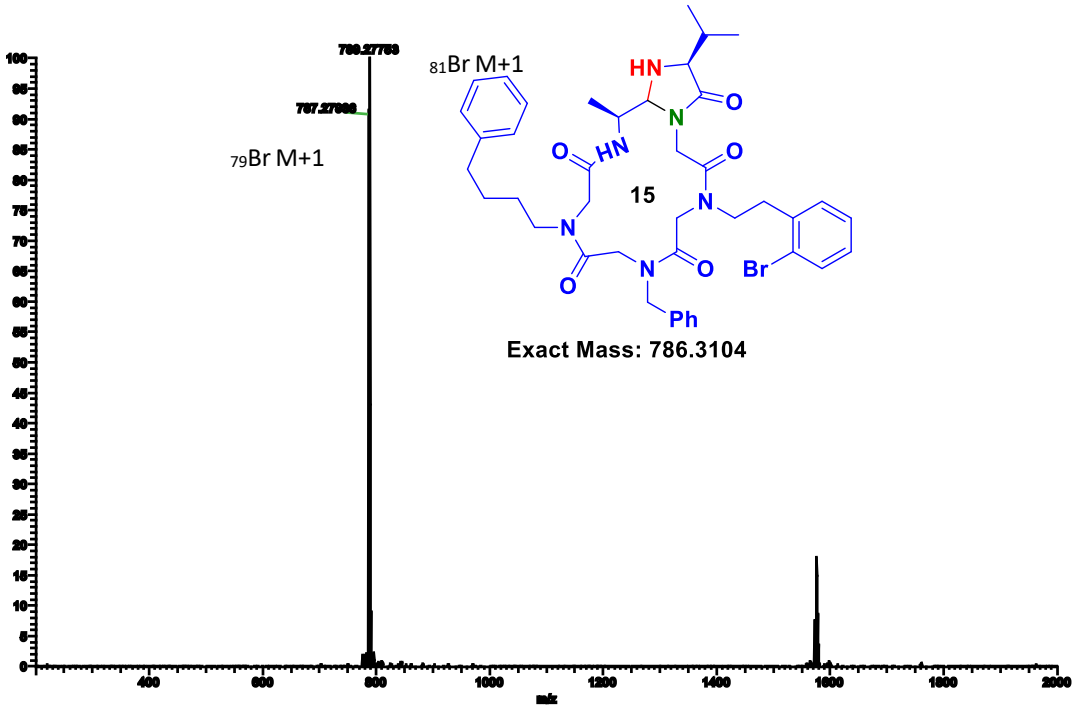

HRMS of Cyclic Peptide-Peptoid Hybrid 1.11g

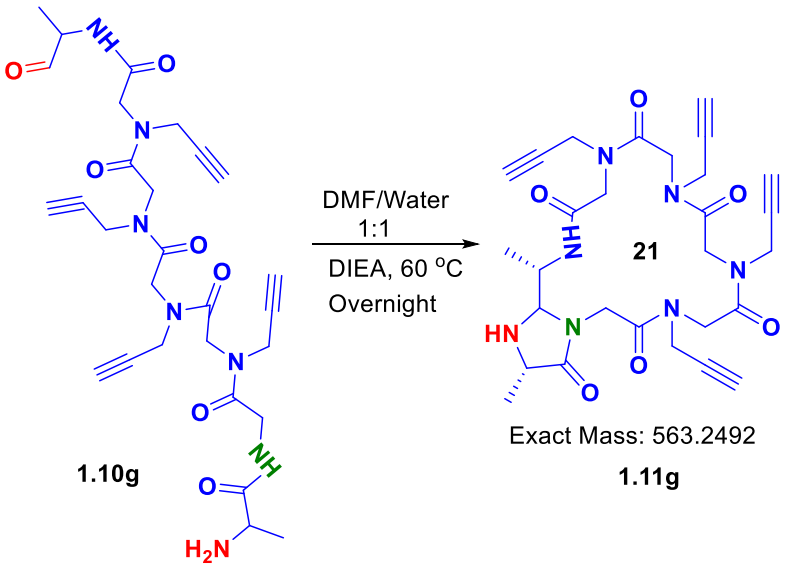

cyclic peptoid 1.11g. LCMS: *m/z* 564.2541 (calcd [*M*+H]$^+$ =564.2571), *m/z* 586.2358 (calcd [*M*+Na]+ = 586.2390), Purity: >95% (HPLC analysis at 220 nm). Retention time in HPLC: 9.219min.

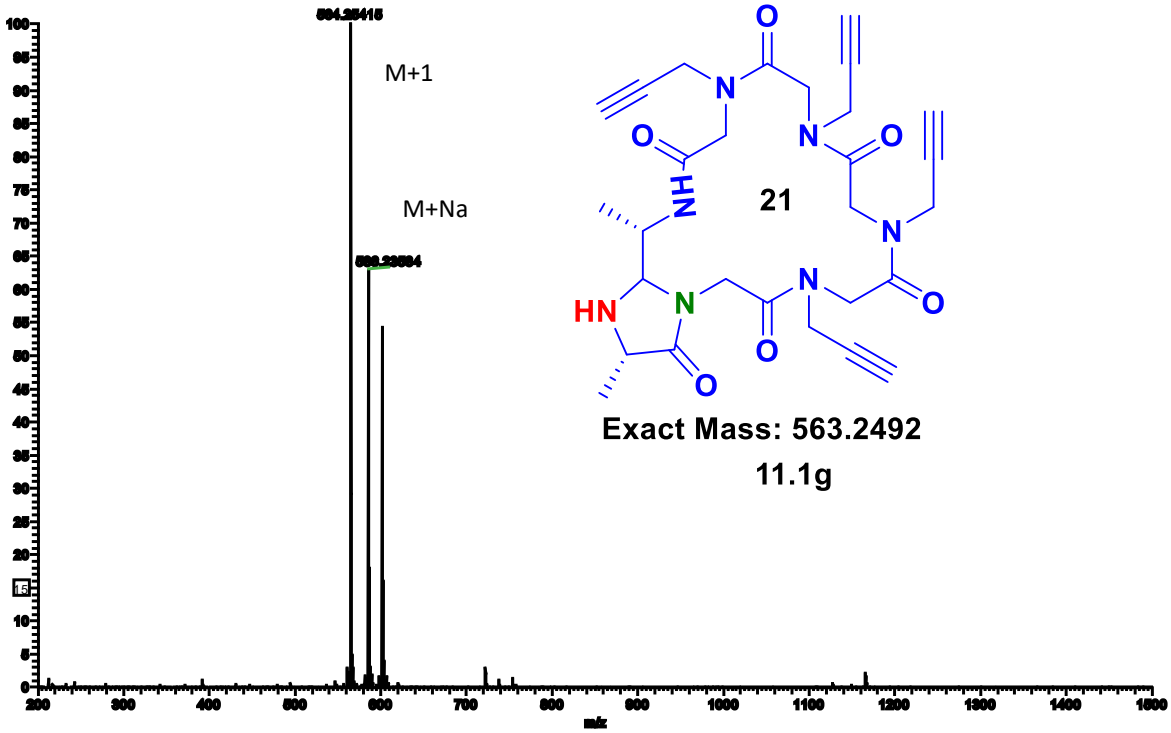

HRMS of Cyclic Peptide-Peptoid Hybrid 1.11h

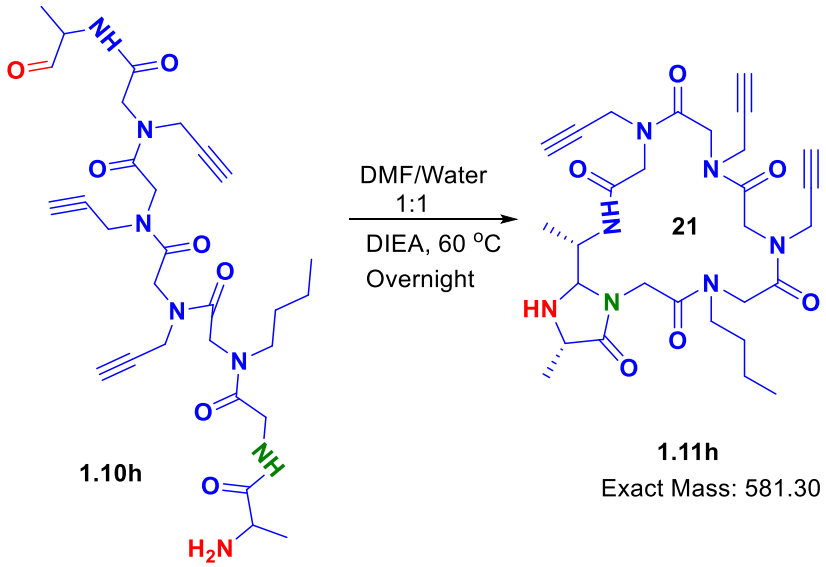

cyclic peptoid 1.11h. LCMS: *m/z* 582.2992 (calcd [*M*+H]$^+$ =582.3040), *m/z* 604.2805 (calcd [*M*+Na]+ = 604.2860), Purity: >95% (HPLC analysis at 220 nm). Retention time in HPLC: 14.949min.

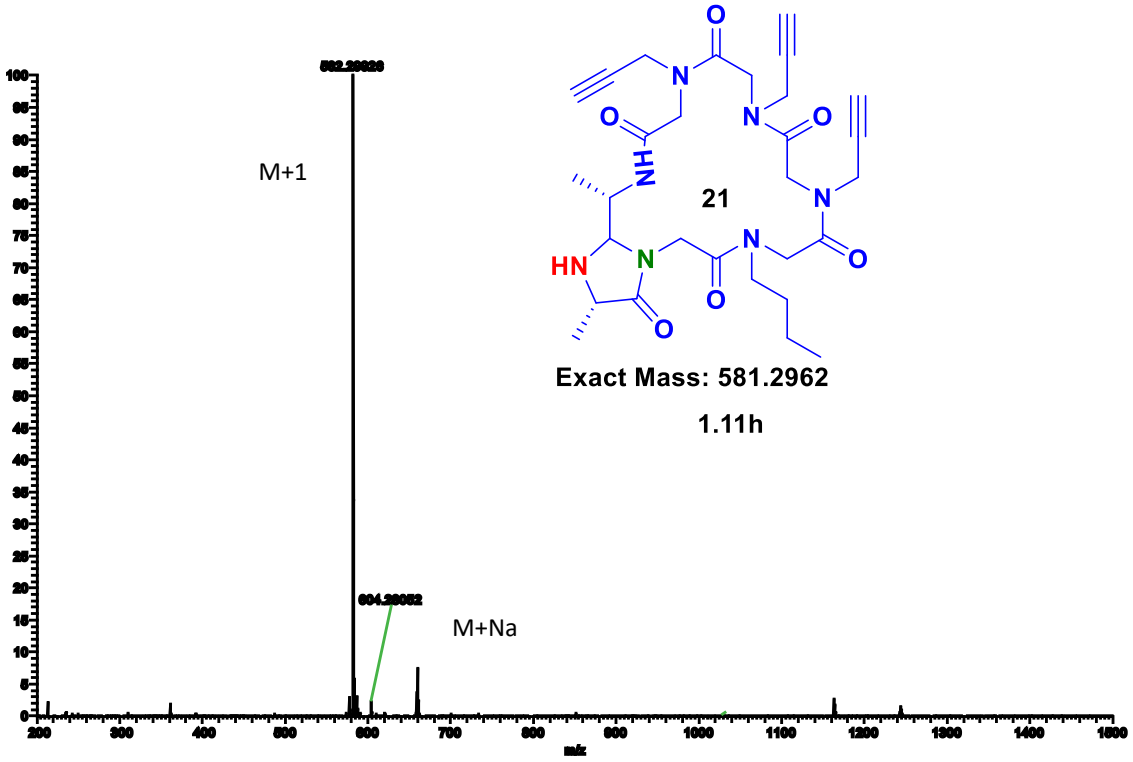

HRMS of Cyclic Peptide-Peptoid Hybrid 1.11i

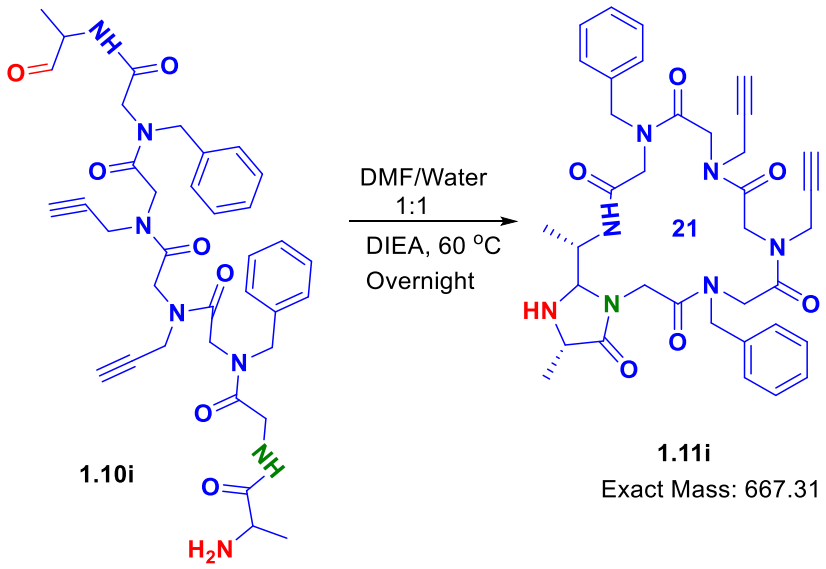

cyclic peptoid 2e. LCMS: *m/z* 668.2827 (calcd [*M*+H]$^+$ =668.3197), *m/z* 1335.5589 (calcd [2x*M*+H]+ = 1335.6315), Purity: >95% (HPLC analysis at 220 nm). Retention time in HPLC: 15.987.

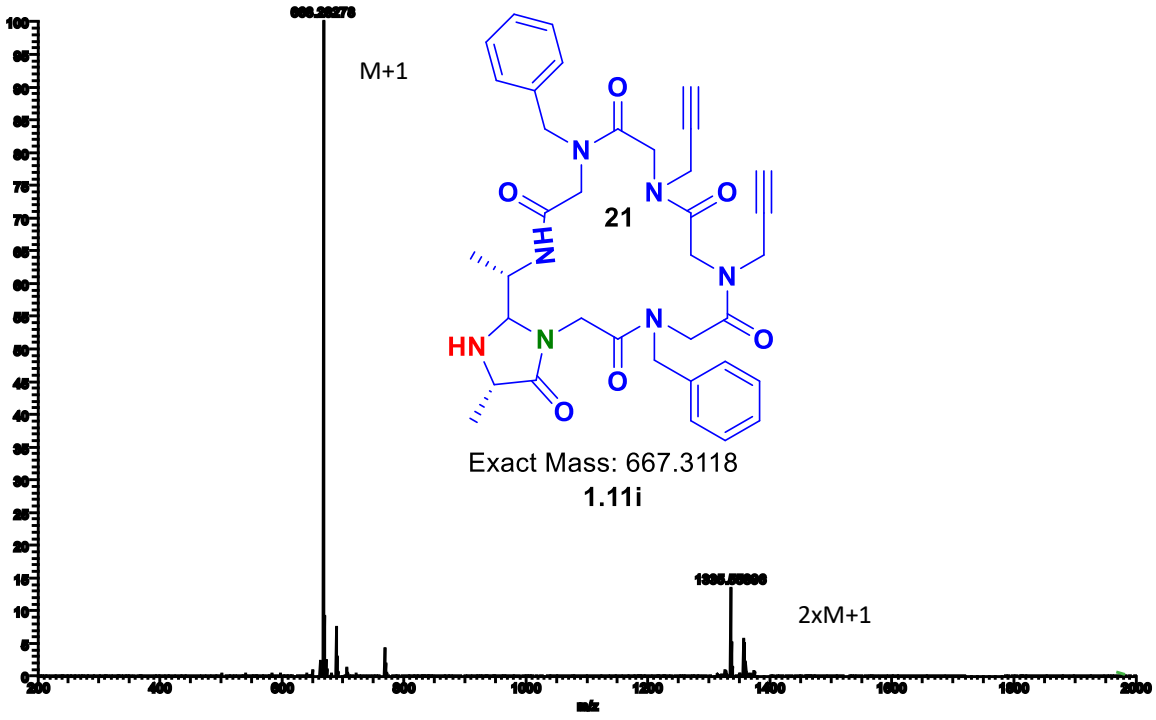

HRMS of Cyclic Peptide-Peptoid Hybrid 1.11j

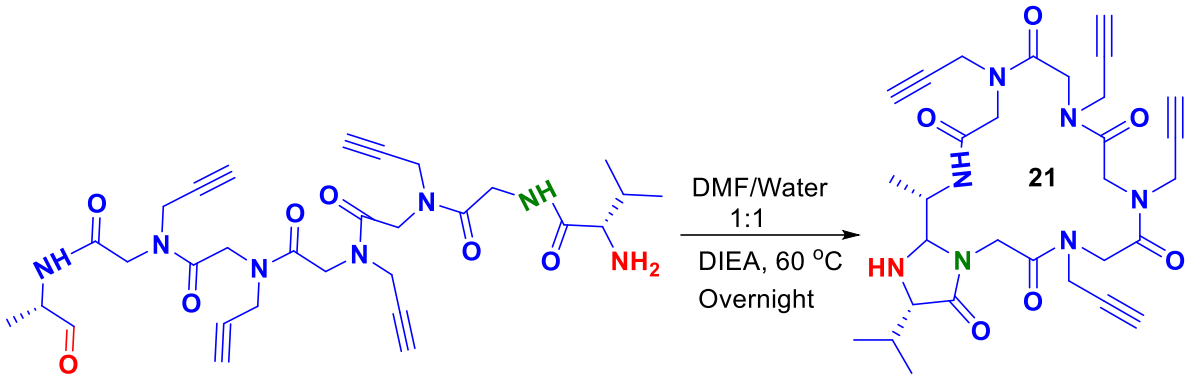

Exact Mass: 609.2911

1.10j

Exact Mass: 591.2805

1.11j

cyclic peptide-peptoid 1.11j. LCMS: *m/z* 592.2503 (calcd [*M*+H]$^+$ = 592.2884), *m/z* 1183.4940 (calcd [2x*M*+H]+ = 1183.5689), Purity: >95% (HPLC analysis at 220 nm). Retention time in HPLC: 12.356min

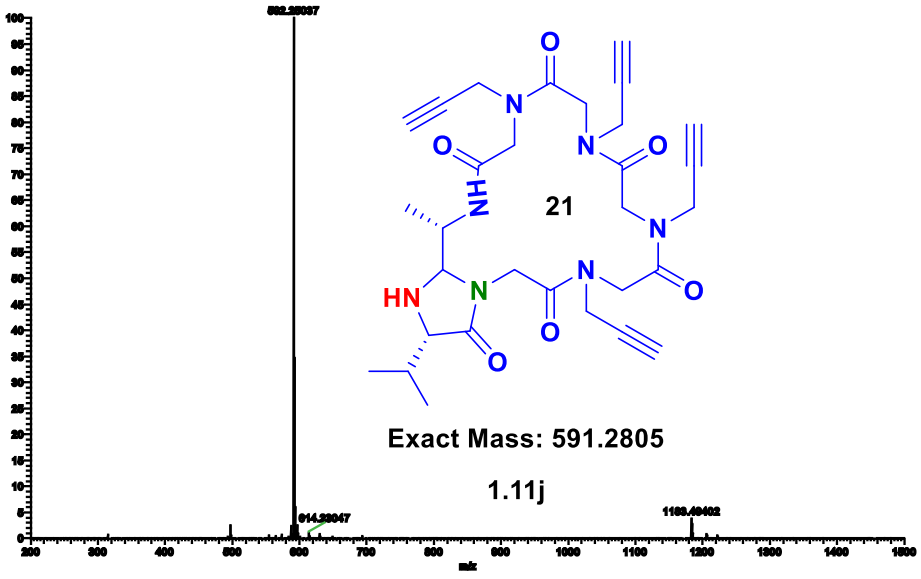

HRMS of Cyclic Peptide-Peptoid Hybrid 1.11k

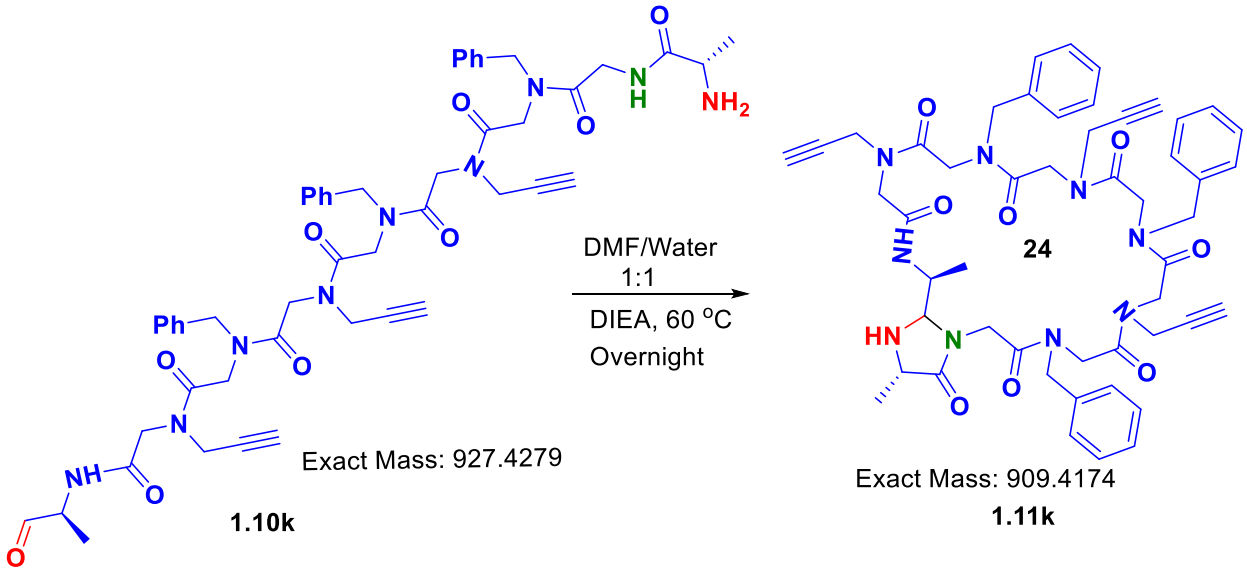

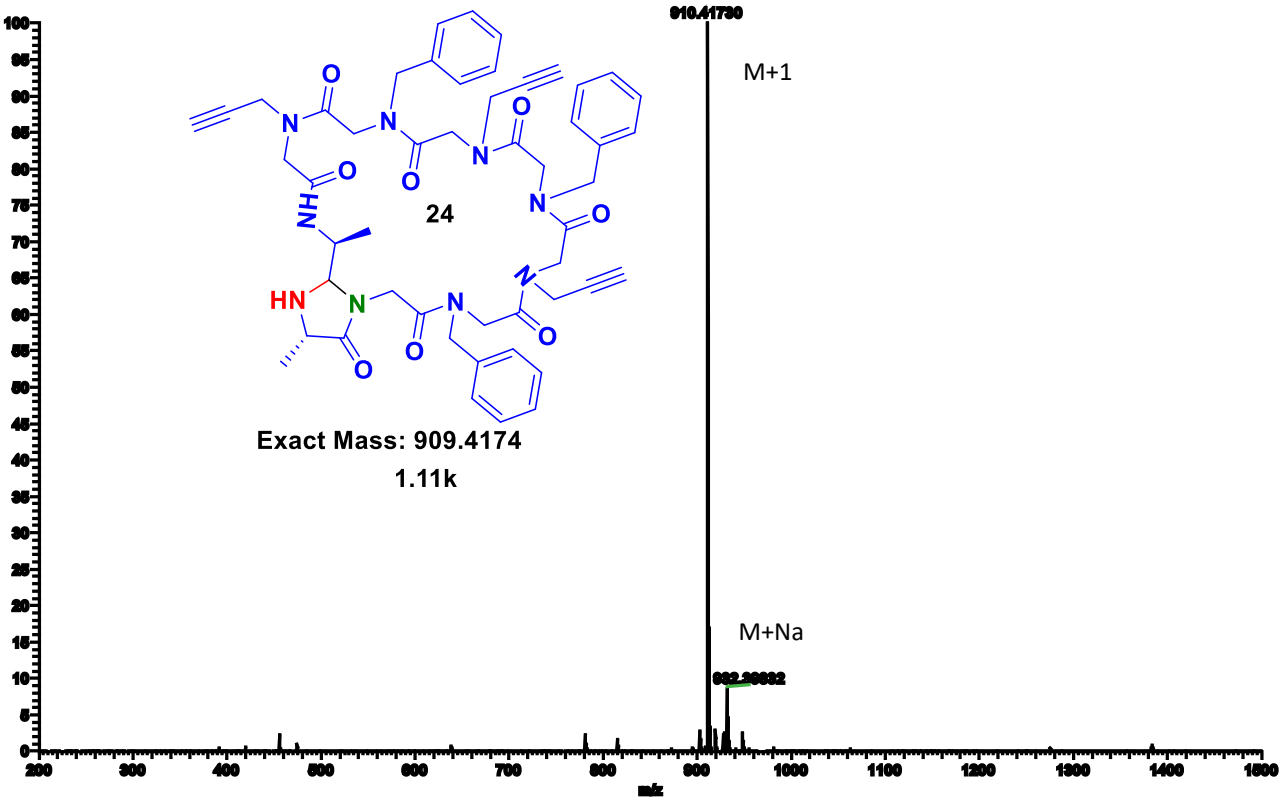

HRMS of Cyclic Peptide-Peptoid Hybrid 1.11l

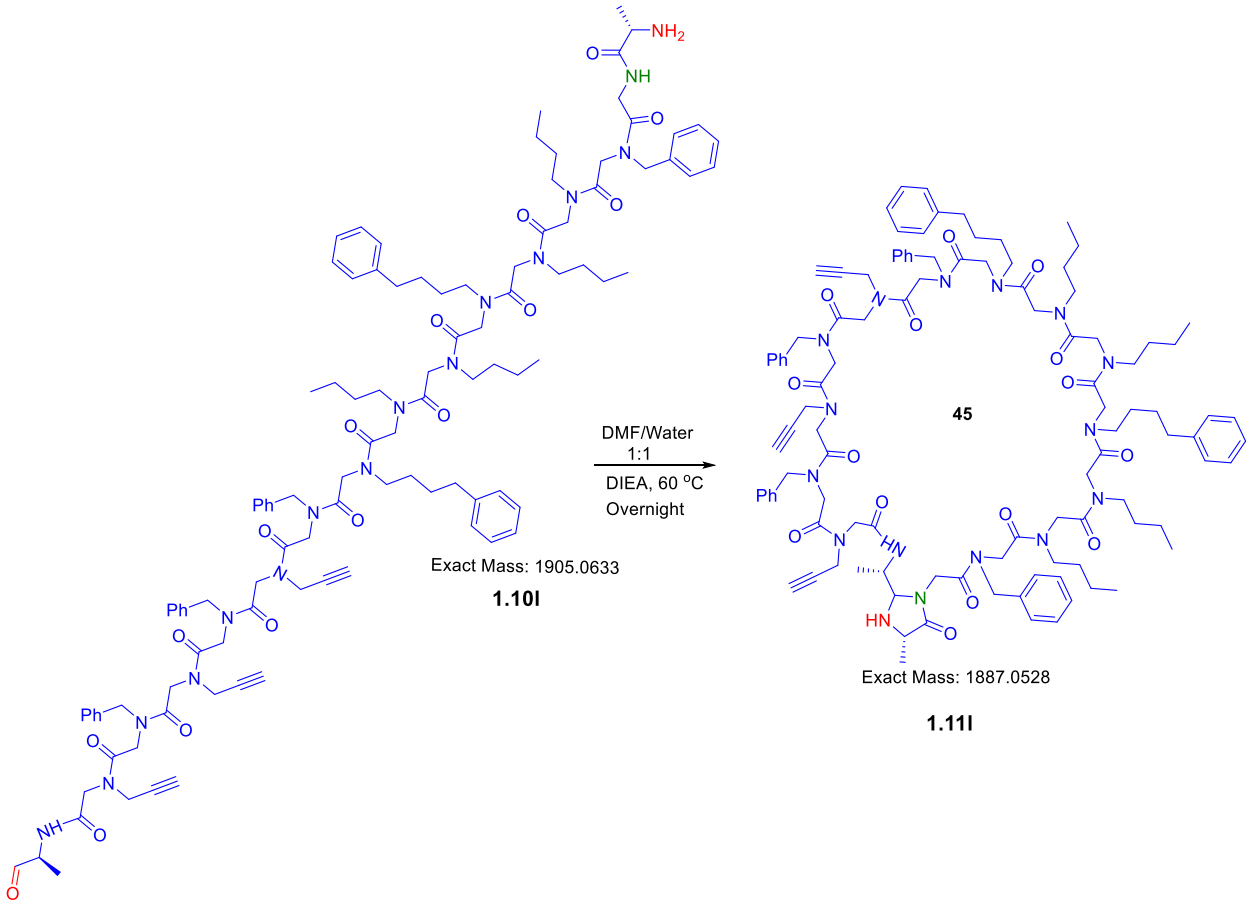

Exact Mass: 1905.0633

1.10l

Exact Mass: 1887.0528

1.11l

HRMS of Cyclic Peptide-Peptoid Hybrid 1.11l

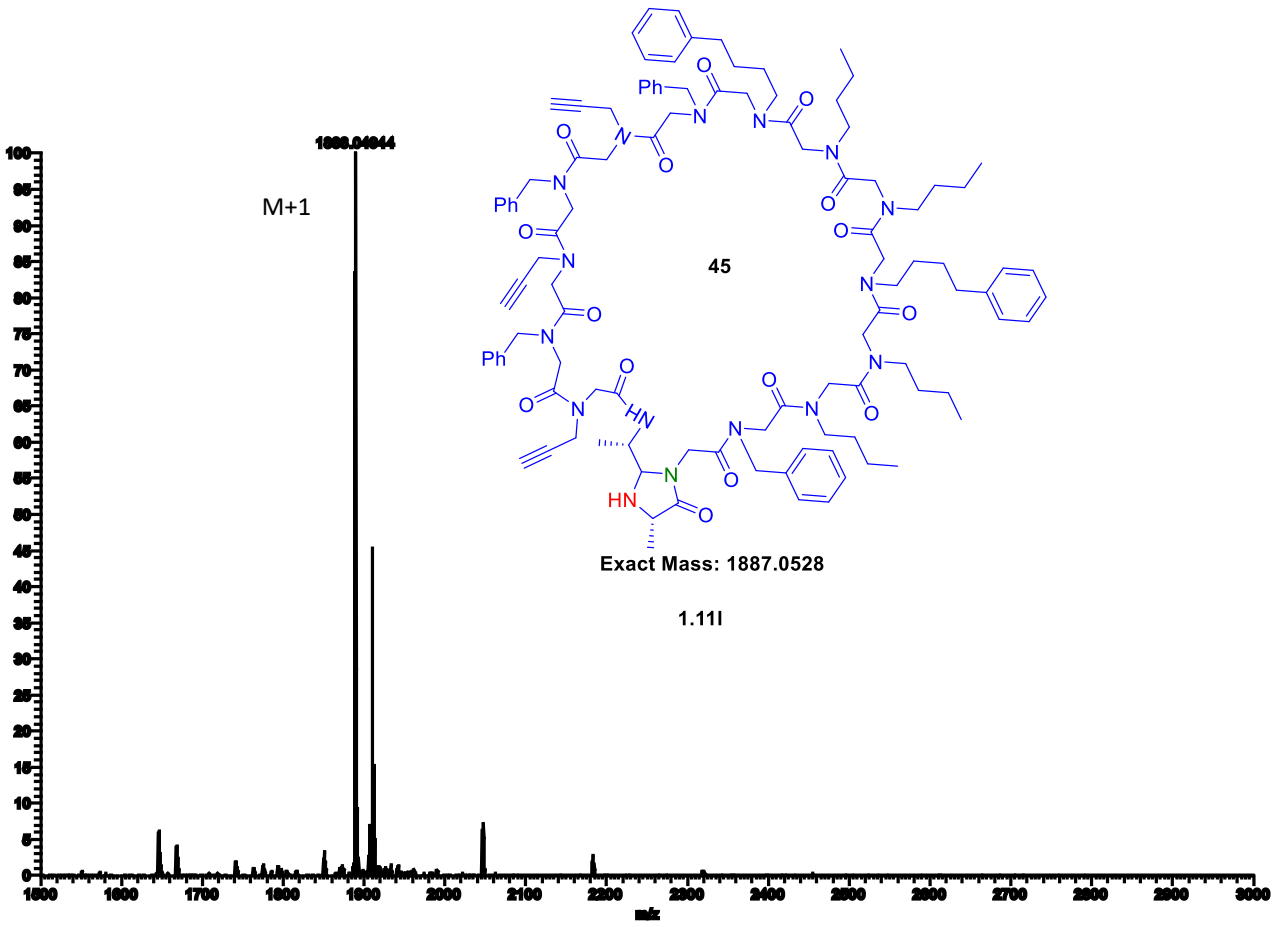

HRMS of Cyclic Peptide-Peptoid Hybrid 1.11m

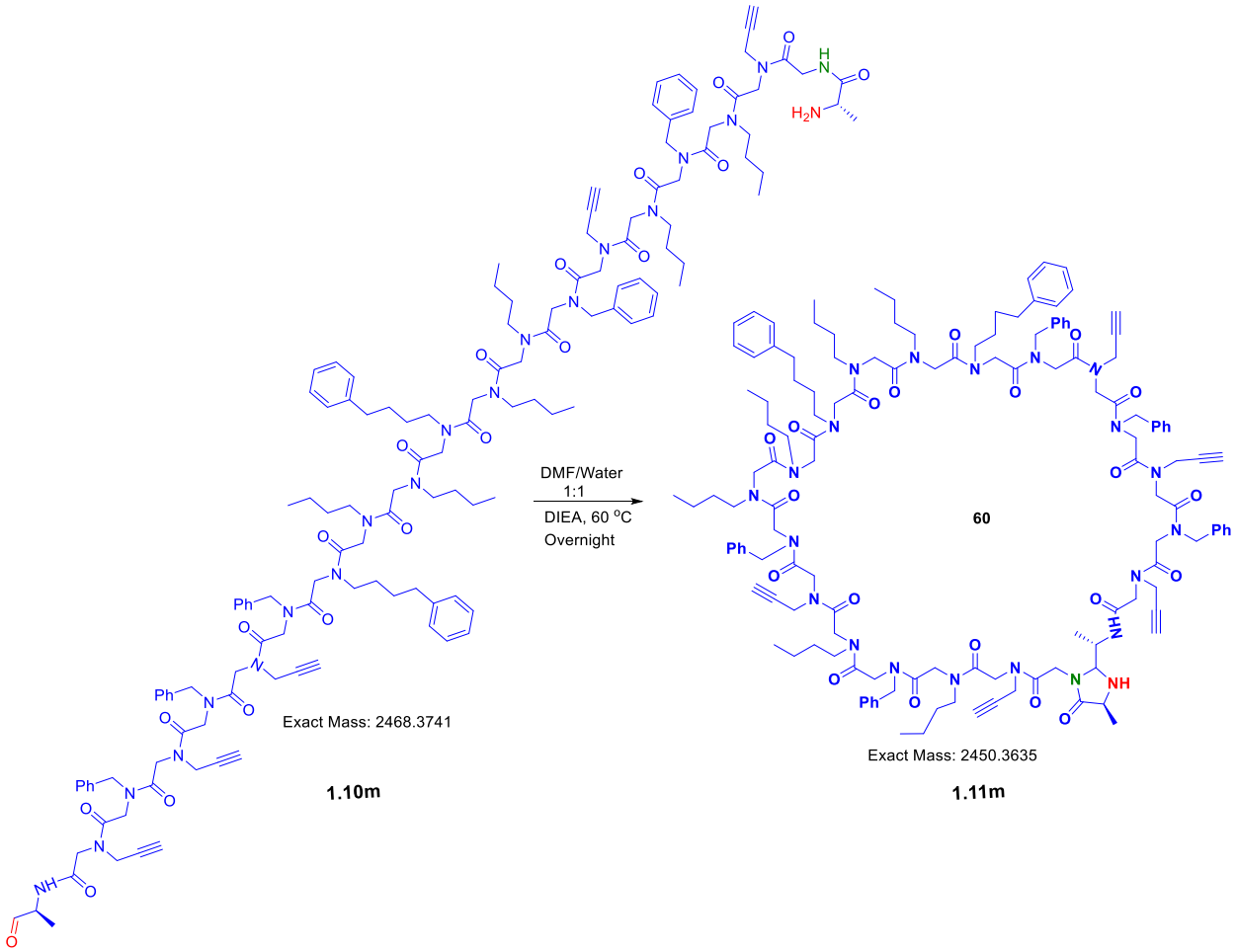

cyclic peptoid 2i. LCMS: *m/z* 2451.2158 (calcd $[M+H]^+$ = 2451.3714), Purity: >95% (HPLC analysis at 220 nm). Retention time in HPLC: 26.892min

HRMS of Cyclic Peptide-Peptoid Hybrid 1.11m

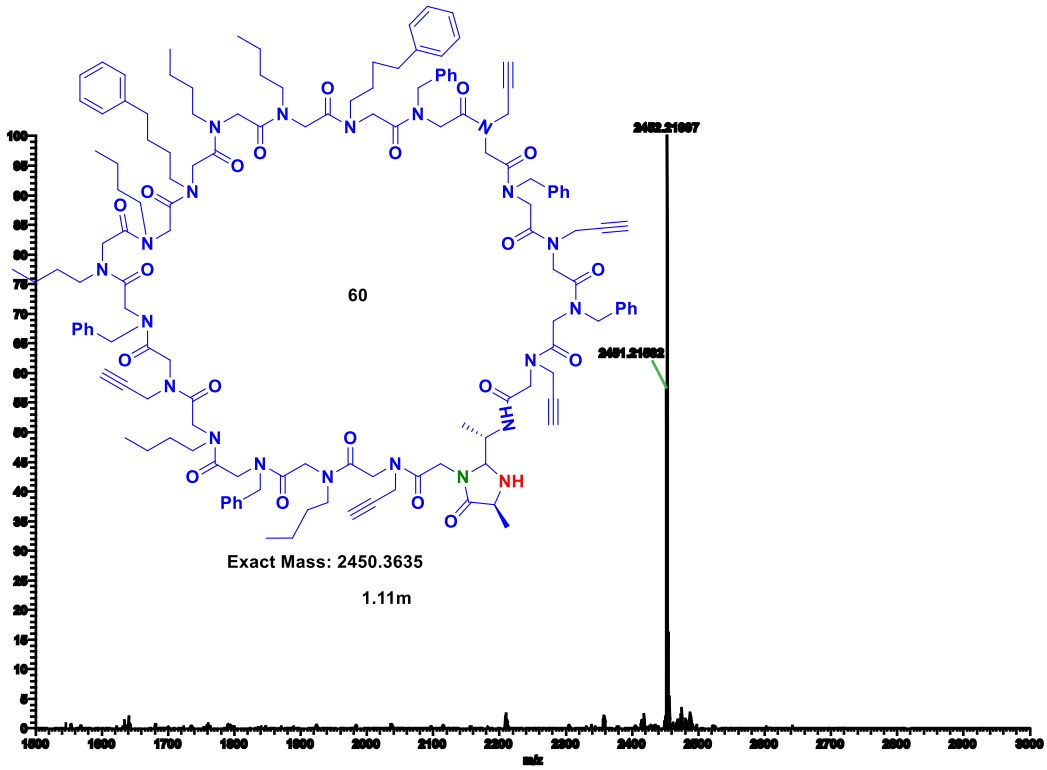

HRMS of Cyclic Peptide-Peptoid Hybrid 1.11o

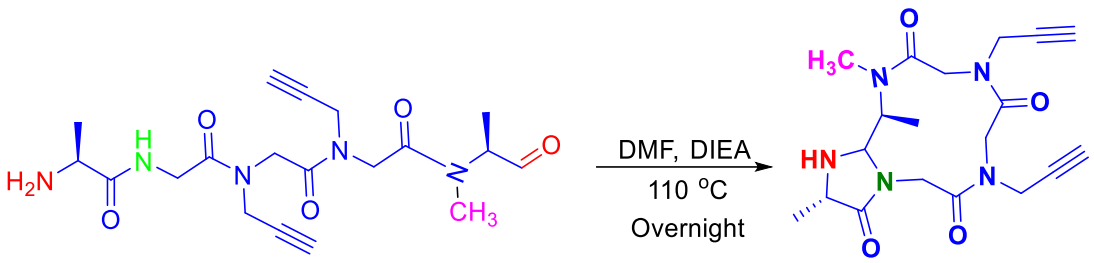

Exact Mass: 405.20

1.10o

Exact Mass: 387.19

1.11o

cyclic peptoid 1.11o. LCMS: *m/z* 388.1774 (calcd $[M+H]^+$ = 388.1985), Purity: >95% (HPLC analysis at 220 nm). Retention time in HPLC: 9.499min

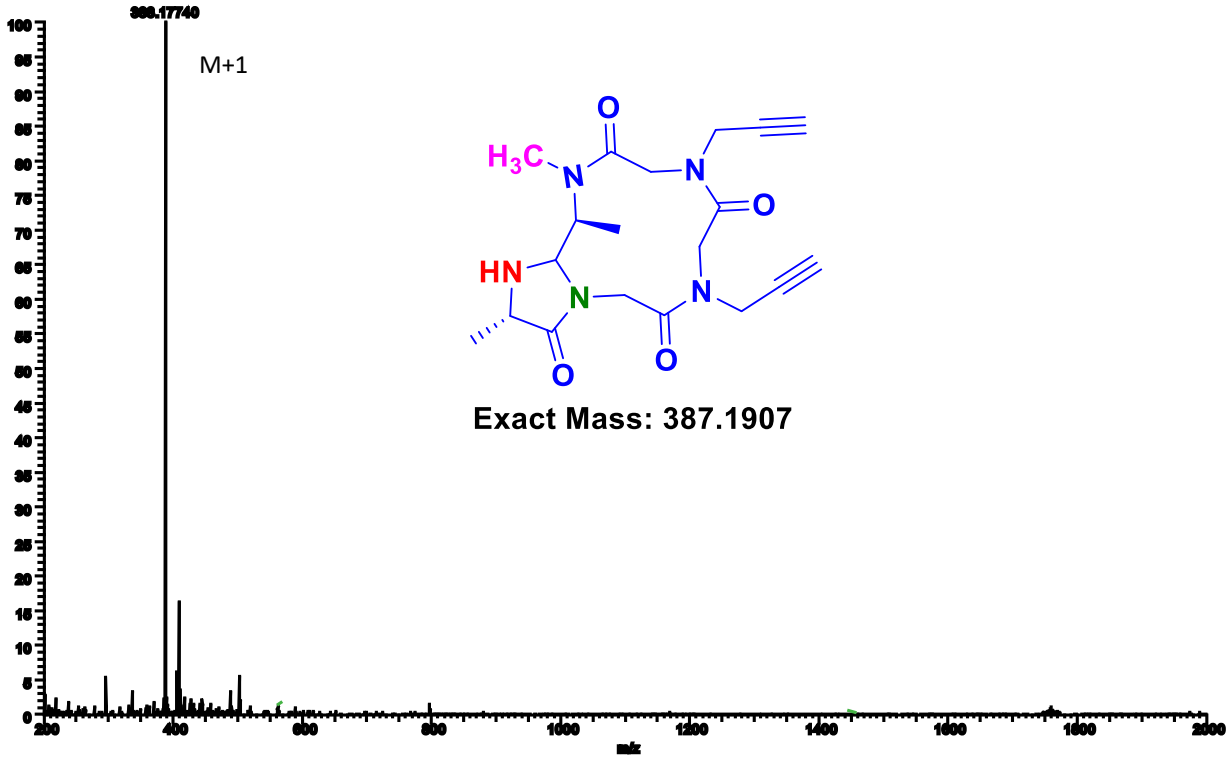

Exact Mass: 387.1907

HRMS of Cyclic Peptide-Peptoid Hybrid 1.12p

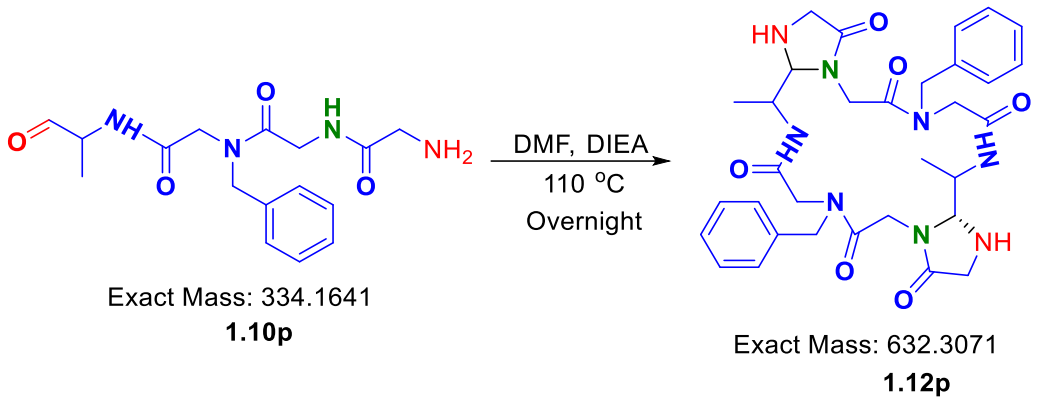

Exact Mass: 334.1641
1.10p

Exact Mass: 632.3071
1.12p

cyclic peptide-peptoid 1.12p hybrid. LCMS: *m/z* 633.3128 (calcd [*M*+H]$^+$ = 633.3149), *m/z* 655.2946 (calcd) [2x*M*+H]$^+$ =655.2969) Purity: >95% (HPLC analysis at 220 nm). Retention time in HPLC: 28min

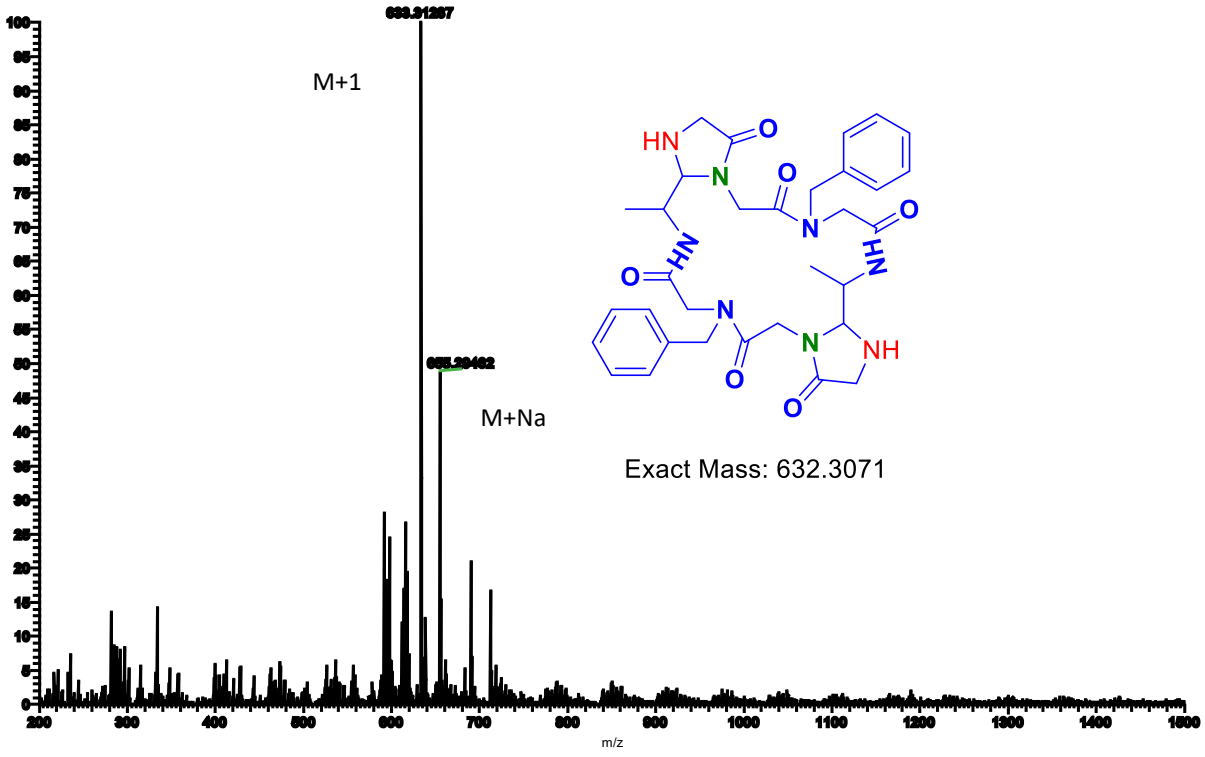

Exact Mass: 632.3071

Experimental Data for Chapter 2

Computational Methods: All calculations were performed using Gaussian 09 of programs. All geometry optimizations were performed using methodology, B3LYP/6-311++G(d,p) level of theory. This methodology has been shown to be accurate in predicting the properties and optimized geometries of various twisted amide derivatives.[2] The absence of imaginary frequencies was essential in the characterization of the structures as minima on the potential energies surface. All the optimized geometries were verified as minima with no imaginary frequencies. The structural representations were generated using Avogadro software (Avogadro-1.2.0n-win32).

DFT Calculations for Ground State Distortion of Amides

Substrate	Twist Angles (τ)	Nitrogen Pyramidization (X_N)	C=O Bond length	N-C(O) Bond length	Rotational Energy Barrier (Kcal)
2E	3.60	0.5	1.227	1.362	17.1
2.1a	21.30	9.1	1.207	1.419	9.8
2.1b	24.00	16.2	1.205	1.425	6.9
2.1c	28.65	21.8	1.215	1.427	11.4
2.1d	27.3	19.9	1.206	1.430	7.3

Cartesian Coordinates for 2E (in Å):

S	-3.0355010	-0.4580340	-0.7598180
S	-2.1138870	-2.4391330	1.2869700
O	-0.9875350	2.9050430	-0.4286750
O	0.6460810	-2.6879190	-0.1970360
O	-0.7462280	1.6590430	1.4338310
N	-0.5226190	-0.7034240	-0.0890800
C	4.4750080	0.4877050	0.0836270
C	3.4473950	0.8983370	0.9309980
C	4.2549280	-0.5425390	-0.8317710
C	2.1912440	0.2996590	0.8524310
C	3.0113270	-1.1615110	-0.8968450
C	1.9679000	-0.7300140	-0.0683720
C	-0.6107970	0.5970780	-0.7654420
C	-1.7984410	0.4865330	-1.7314410
C	0.6748830	-1.4851780	-0.1182120
C	-1.1496740	4.0886820	0.3841030

C	-0.7950650	1.7529110	0.2371170
C	-1.7750710	-1.2648240	0.2078270
H	3.6242290	1.6798930	1.6611340
H	5.4486770	0.9609740	0.1430090
H	5.0558310	-0.8705670	-1.4844050
H	2.8377040	-1.9851470	-1.5790770
H	1.3980730	0.6068810	1.5224880
H	0.3117320	0.7906840	-1.3145150
H	-1.5244380	-0.0738680	-2.6260750
H	-1.2962890	4.9040290	-0.3199400
H	-2.0155640	3.9797580	1.0372740
H	-2.1944650	1.4602660	-2.0077710
H	-0.2573130	4.2553560	0.9879310

Energy of Optimized Geometry: -782.634 Hartree

There was no Imaginary Frequency for this molecule

Basis Set: b3lyp/6-311G

Cartesian Coordinates for 2.1a (in Å):

C1	0.0798450	0.0122650	-0.1092920
C2	-0.0394150	-0.6603410	-1.4970100
O3	-0.3979580	0.4411280	-2.4079550
C4	-0.8250520	1.5547230	-1.6877850
N5	-0.5763090	1.3075780	-0.3247650
C6	-1.0119020	2.0407080	0.8069680
O7	-1.0924680	1.4257630	1.8884260
C8	-1.3172640	3.4829680	0.6984390
C9	-0.5443500	4.3578120	-0.0798710
C10	-0.8116670	5.7263680	-0.0592460
C11	-1.8573270	6.2274370	0.7221990
C12	-2.6271460	5.3588320	1.5036280
C13	-2.3500190	3.9932240	1.5029610
C14	1.5222880	0.2054970	0.3380440
O15	2.0825800	-1.0102690	0.6158500

O16	2.1132380	1.2772450	0.4324260
C17	3.4845670	-1.0216770	1.0776150
O18	-1.3323930	2.5277030	-2.2175950
H19	-0.4390110	-0.5516240	0.6617060
H20	0.8873070	-1.097510	-1.8499060
H21	-0.8396570	-1.3955820	-1.5251720
H22	0.2668760	3.9772160	-0.6811350
H23	-0.2083600	6.3984970	-0.6539310
H24	-2.0678740	7.2887630	0.7261710
H25	-3.4332590	5.7448470	2.1127080
H26	-2.9189830	3.3137590	2.1216790
H27	3.7098870	-2.0683500	1.2437120
H28	4.1294200	-0.5951310	0.3126380
H29	3.5706960	-0.4484540	1.9975500

Energy of Optimized Geometry: -894.757 Hartree

There was no Imaginary Frequency for this molecule

Cartesian Coordinates for 2.1b (in Å):

C1	0.0798450	0.0122650	-0.1092920
C2	-0.0394150	-0.6603410	-1.4970100
O3	-0.3979580	0.4411280	-2.4079550
C4	-0.8250520	1.5547230	-1.6877850
N5	-0.5763090	1.3075780	-0.3247650
C6	-1.0119020	2.0407080	0.8069680
O7	-1.0924680	1.4257630	1.8884260
C8	-1.3172640	3.4829680	0.6984390
C9	-0.5443500	4.3578120	-0.0798710
C10	-0.8116670	5.7263680	-0.0592460
C11	-1.8573270	6.2274370	0.7221990
C12	-2.6271460	5.3588320	1.5036280
C13	-2.3500190	3.9932240	1.5029610
C14	1.5222880	0.2054970	0.3380440
O15	2.0825800	-1.0102690	0.6158500
O16	2.1132380	1.2772450	0.4324260

C17	3.4845670	-1.0216770	1.0776150
O18	-1.3323930	2.5277030	-2.2175950
H19	-0.4390110	-0.5516240	0.6617060
H20	0.8873070	-1.0975100	-1.8499060
H21	-0.8396570	-1.3955820	-1.5251720
H22	0.2668760	3.9772160	-0.6811350
H23	-0.2083600	6.3984970	-0.6539310
H24	-2.0678740	7.2887630	0.7261710
H25	-3.4332590	5.7448470	2.1127080
H26	-2.9189830	3.3137590	2.1216790
H27	3.7098870	-2.0683500	1.2437120
H28	4.1294200	-0.5951310	0.3126380
H29	3.5706960	-0.4484540	1.9975500

Energy of Optimized Geometry: -1217.710 Hartree

There was no Imaginary Frequency for this molecule

Cartesian Coordinates for 2.1c (in Å):

C1	0.0470190	-0.0370890	-0.2599050
C2	-0.2100150	-0.6348250	-1.6553790
S3	-2.0136620	-0.2276190	-2.0451860
C4	-1.9353760	1.2425930	-0.8982910
N5	-0.7370560	1.2151330	-0.1678100
C6	-0.4613890	2.0776990	0.9352630
C7	-0.8588420	3.4978100	0.8701090
O8	0.1676440	1.5998330	1.8970500
C9	-0.8499710	4.2199380	-0.3331390
C10	-1.1464170	5.5817320	-0.3305160
C11	-1.4674960	6.2276140	0.8678060
C12	-1.4737760	5.5124580	2.0700500
C13	-1.1588100	4.1548010	2.0742870
O14	-2.8409620	2.0592680	-0.8016140
C15	1.5407980	0.1608940	-0.0651620
O16	1.984220	1.3601110	-0.5368470
O17	2.2725240	-0.7205500	0.3832890

C18	3.4206280	1.6538300	-0.3773210
H19	-0.2734510	-0.7301510	0.5180040
H20	0.4128440	-0.1699270	-2.4131380
H21	-0.0777350	-1.7105690	-1.6534590
H22	-0.5994380	3.7241200	-1.2596310
H23	-1.1318690	6.1363280	-1.2588460
H24	-1.7084590	7.2823880	0.8651470
H25	-1.7203620	6.0111540	2.9974380
H26	-1.1432160	3.5924480	2.9971150
H27	3.5460540	2.6438660	-0.7993310
H28	3.6776010	1.6405920	0.6792070
H29	4.0120500	0.9157650	-0.9143240

Energy of Optimized Geometry: -1217.737 Hartree

There was no Imaginary Frequency for this molecule

Cartesian Coordinates for 2.1d (in Å):

C1	0.0798450	0.0122650	-0.1092920
C2	-0.0394150	-0.6603410	-1.497010
O3	-0.3979580	0.4411280	-2.4079550
C4	-0.8250520	1.5547230	-1.6877850
N5	-0.5763090	1.3075780	-0.3247650
C6	-1.0119020	2.0407080	0.8069680
O7	-1.0924680	1.4257630	1.8884260
C8	-1.3172640	3.4829680	0.6984390
C9	-0.5443500	4.3578120	-0.0798710
C10	-0.8116670	5.7263680	-0.0592460
C11	-1.8573270	6.2274370	0.7221990
C12	-2.6271460	5.3588320	1.5036280
C13	-2.3500190	3.9932240	1.5029610
C14	1.5222880	0.2054970	0.3380440
O15	2.0825800	-1.0102690	0.615850
O16	2.1132380	1.2772450	0.4324260
C17	3.4845670	-1.0216770	1.0776150
O18	-1.3323930	2.5277030	-2.2175950

H19	-0.4390110	-0.5516240	0.6617060
H20	0.8873070	-1.0975100	-1.8499060
H21	-0.8396570	-1.3955820	-1.5251720
H22	0.2668760	3.9772160	-0.6811350
H23	-0.2083600	6.3984970	-0.6539310
H24	-2.0678740	7.2887630	0.7261710
H25	-3.4332590	5.7448470	2.1127080
H26	-2.9189830	3.3137590	2.1216790
H27	3.7098870	-2.0683500	1.2437120
H28	4.1294200	-0.5951310	0.3126380
H29	3.5706960	-0.4484540	1.9975500

Energy of Optimized Geometry: -1540.687 Hartree

There was no Imaginary Frequency for this molecule

Rotational Energy Profile for compound 2E

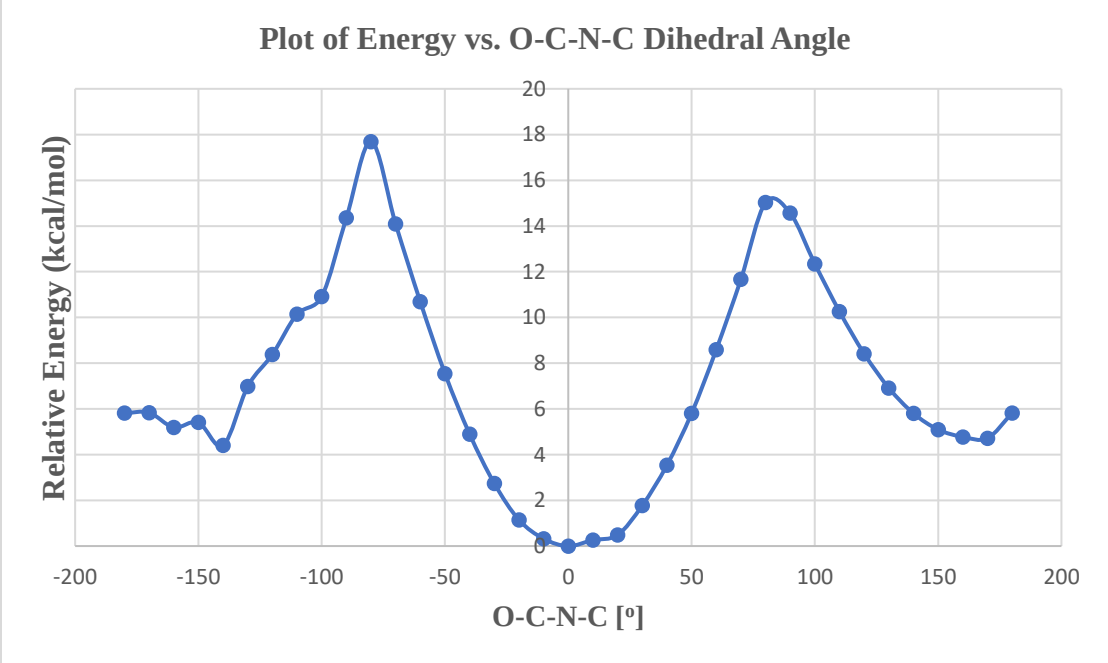

Rotational Energy Profile for compound 2.1a

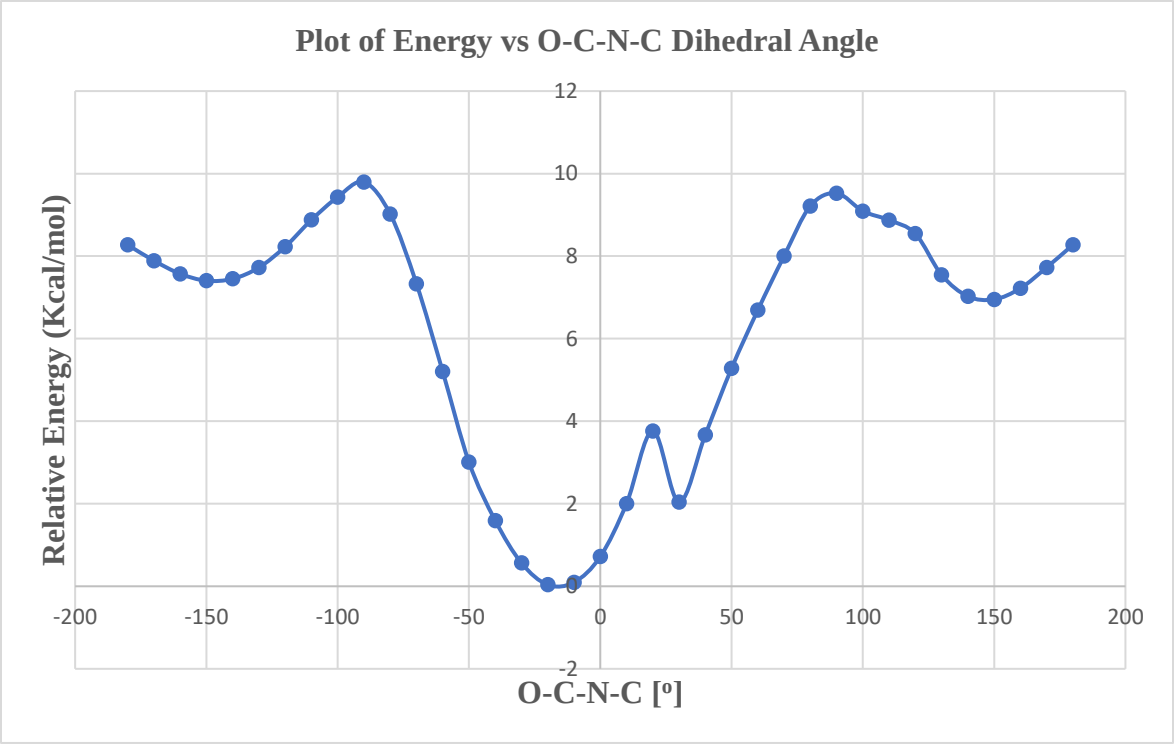

Rotational Energy Profile for compound 2.1b

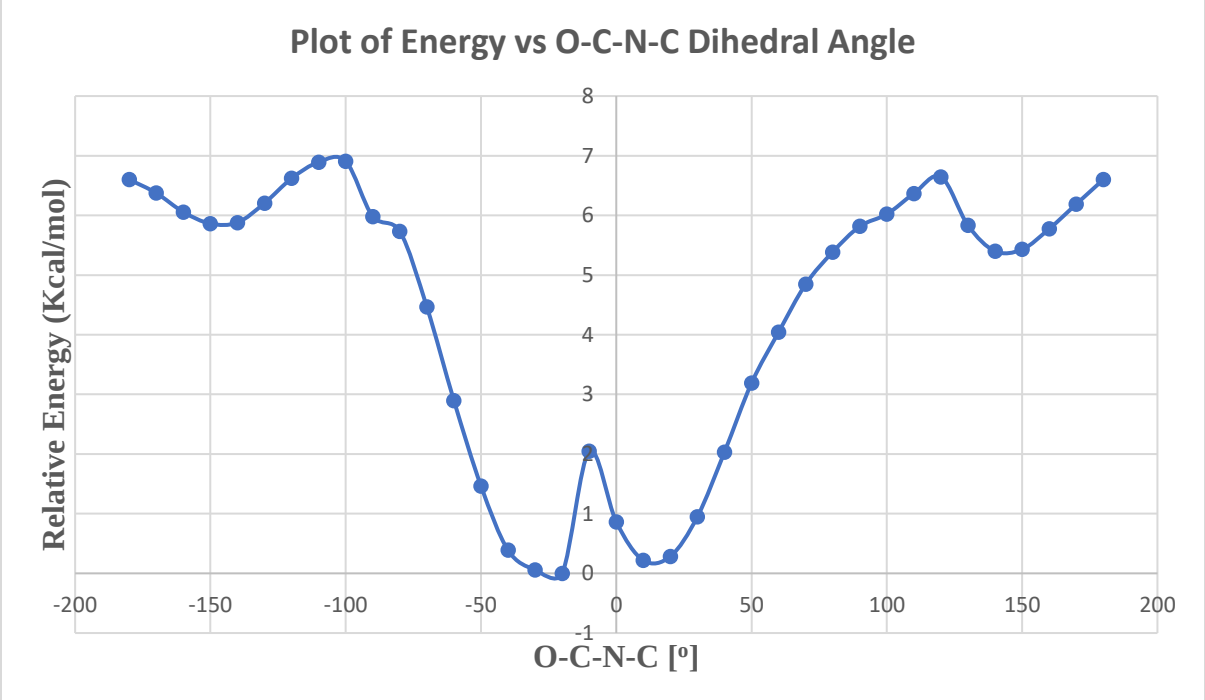

Rotational Energy Profile for compound 2.1c

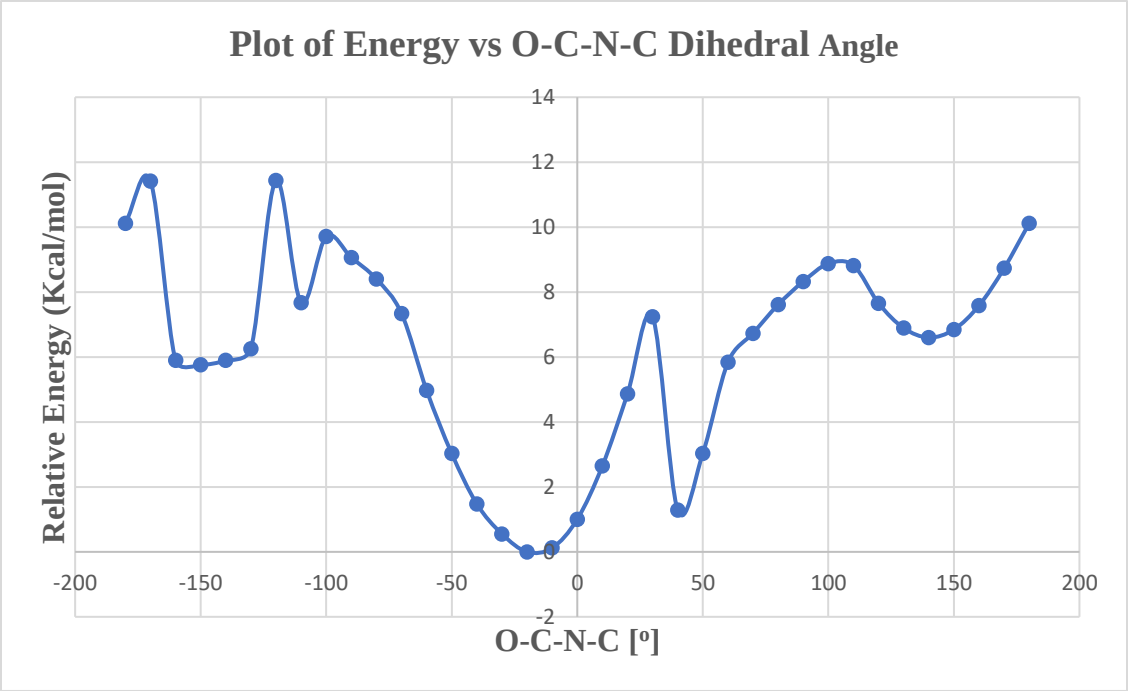

Rotational Energy Profile for compound 2.1d

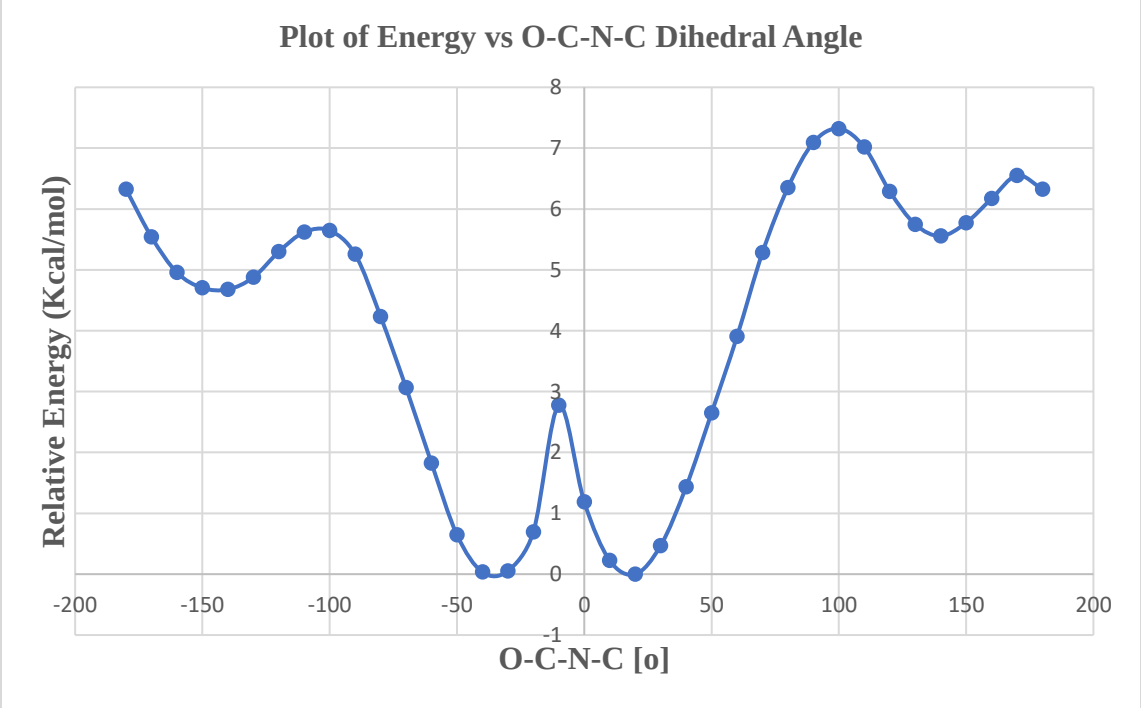

Synthesis of Small Molecule Twisted amides.

Synthesis of Compound 2A

To a solution of serine methyl ester hydrochloride salt (6.45 mmol) in dry dichloromethane (80 mL) was added 1.1 equiv. of triethylamine (Et_3N) and 1.3 equiv. of N, N'-Disuccinimidyl carbonate (DSC) and left to stir at room temperature for 16 h. The volatiles were removed under reduced pressure. Crude residue was purified by column chromatography using mixture of ethyl acetate and hexanes as an eluent to get the product 2**A** with 42% yield.

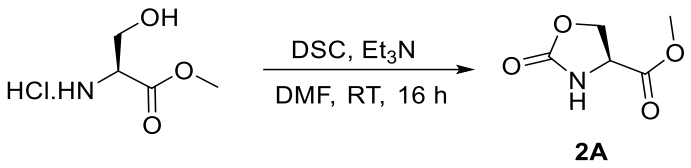

2A

Synthesis of Compound 2B

To a solution of serine methyl ester hydrochloride salt (6.45 mmol) in dry dichloromethane (80 mL) was added 1.1 equiv. of Et_3N and 1.2 equiv. of 1,1'-Thiocarbonyldiimidazole (thio-CDI) and left to stir at room temperature for 16 h. The solvent was removed under reduced pressure. Crude residue was purified by column chromatography using mixture of ethyl acetate and hexanes as an eluent to get the product 2**B** with 62% yield.

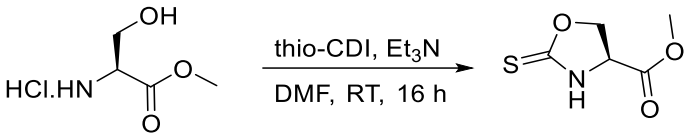

2B

Synthesis of Compound 2C

To a solution of cysteine methyl ester hydrochloride salt (6.45 mmol) in dry dichloromethane (80 mL) was added 1.1 equiv. of Et_3N and 1.3 equiv. of DSC and left to stir at room temperature for 16 h. The volatiles were removed under reduced pressure. Crude residue was purified by column chromatography using mixture of ethyl acetate and hexanes as an eluent to get the product 2**C** with 40% yield.

2C

Synthesis of Compound 2D[3]

To a solution of cysteine methyl ester hydrochloride salt (6.45 mmol) in dry dichloromethane (80 mL) was added 1.1 equiv. of Et_3N and 1.3 equiv. carbon disulfide and left to stir at room temperature for 16 h. The volatiles were removed under reduced pressure resulting in a white solid residue. This was then suspended in ethyl acetate and filtered through a short plug of silica gel column. The eluent was concentrated using a rotavap and a second column chromatography was done using eluents ethyl acetate and hexane to generate pure Compound 2D with yield of 60%.

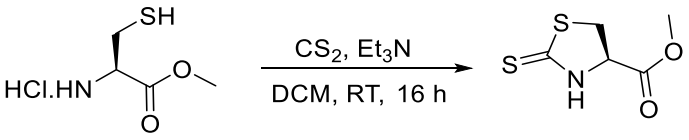

2D

Synthesis of Compounds 2.1a-2.1d

The solution of compounds 2**A-2D** (1 equiv., 10 mM) in dry THF was flushed with nitrogen. It was then placed in an ice bath for 15 minutes to lower the temperature to 0 ^oC followed by the addition of NaH (1.5 equiv.) and left for stirring for 30 minutes. Next, benzoyl chloride (2 equiv.) was added to the reaction mixture and left to stir for 5 h. The reaction was quenched by the addition of 1M HCl solution. The remaining THF left in the reaction was removed using the rotavap. Ethyl acetate was added to the reaction mixture, followed by washing with a saturated brine solution. Ethyl acetate was removed using the rotavap. The crude residue was purified by column chromatography using mixture of ethyl acetate and hexane as an eluent to get the products **2.1a-2.1d**.

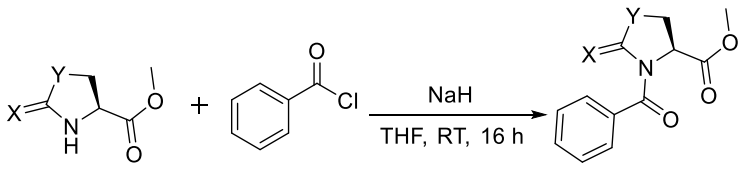

2A-2D

2A: X=O, Y=O
2B: X=S, Y=O
2C: X=O, Y=S
2D: X=S, Y=S

2.1a-2.1d

2.1a: X=O, Y=O
2.1b: X=S, Y=O
2.1c: X=O, Y=S
2.1d: X=S, Y=S

NMR of Small Molecule Twisted Amides 2.1a-2.1d

NMR Data for Compound 2.1b

Methyl (S)-3-benzoyl-2-thioxooxazolidine-4-carboxylate: ^{1}H NMR (400 MHz, $CDCl_3$) δ 7.78-7.76 (m, 2H), 7.61-7.56 (m, 1H), 7.45 (t, *J* = 7.8 Hz, 2H), 5.33-5.29 (m, 1H), 4.84 (td, *J* = 9.4, 0.64 Hz, 1H), 4.61 (ddd *J* = 9.4, 6.12, 0.6 Hz, 1H), 3.84 (s, 3H). ^{13}C NMR (100 MHz, $CDCl_3$) δ 185.48, 170.70, 168.21, 132.98, 132.75, 129.63, 128.19, 69.27, 50.25, 53.49.

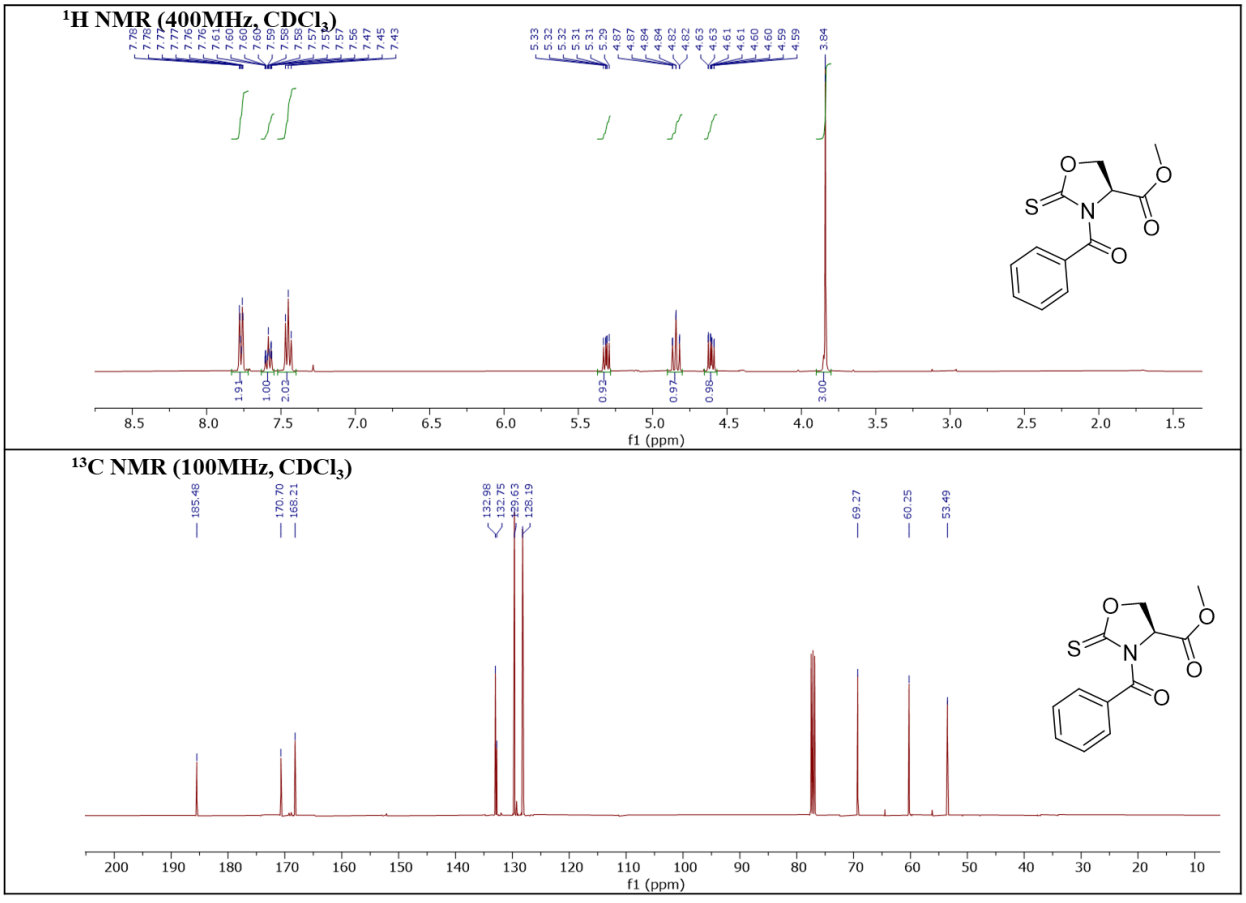

NMR Data for Compound 2.1c

Methyl (R)-3-benzoyl-2-oxothiazolidine-4-carboxylate: ^{1}H NMR (400 MHz, $CDCl_3$) δ 7.70-7.67 (m, 2H), 7.57-7.53 (m, 1H), 7.46-7.42 (m, 2H), 5.18 (dd, *J* = 8.08, 3.44 Hz, 1H), 3.85 (s, 3H), 3.71 (dd, *J* = 11.64, 8.2 Hz, 1H), 3.40 (dd, *J* = 11.6, 3.4 Hz, 1H), ^{13}C NMR (100 MHz, $CDCl_3$) δ 170.80, 169.37, 169.36, 133.19, 132.57, 129.09, 128.05, 59.90, 53.31, 28.42.

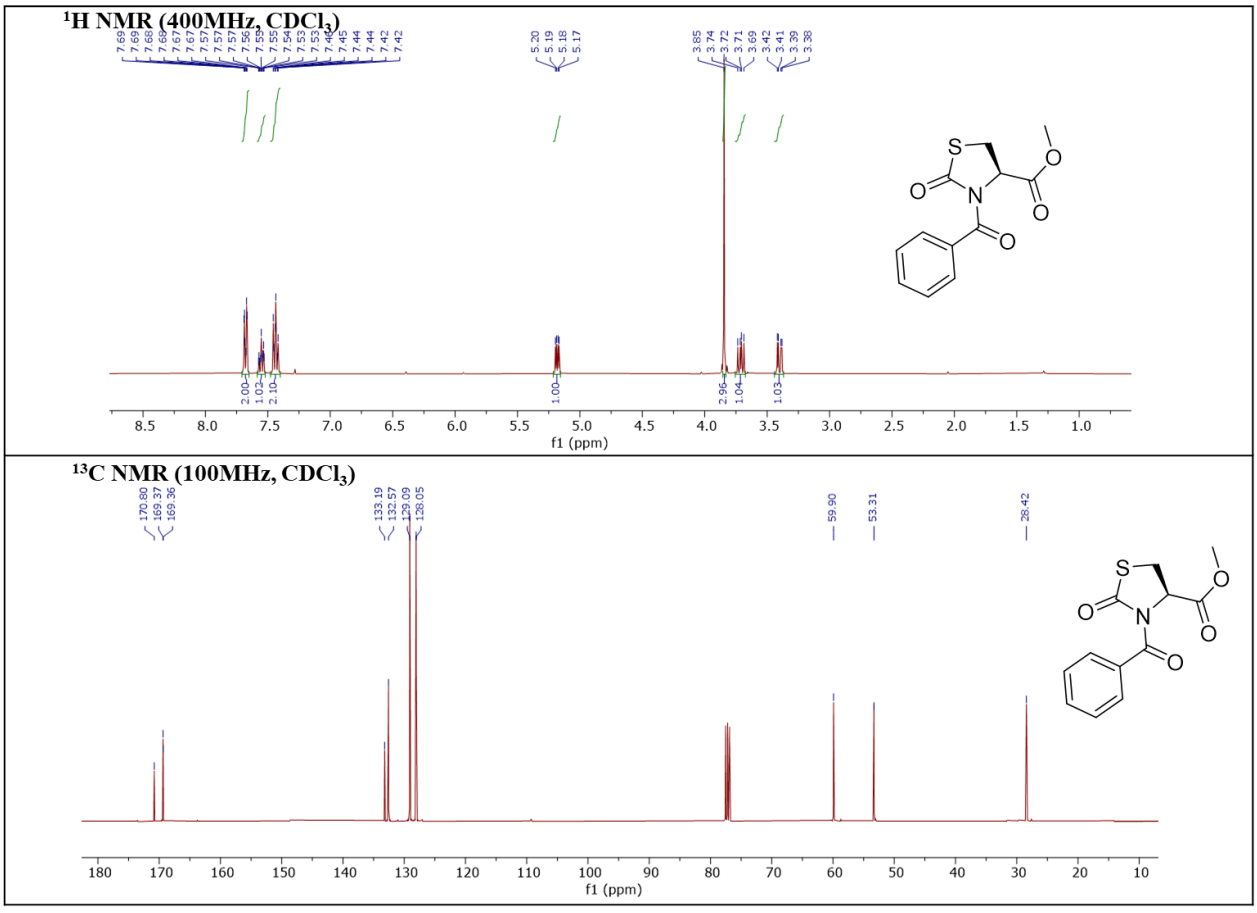

NMR Data for Compound 2.1d

Methyl (R)-3-benzoyl-2-thioxothiazolidine-4-carboxylate: ^{1}H NMR (400 MHz, $CDCl_3$) δ 7.79-7.42 (m, 2H), 7.59-7.54 (m, 1H), 7.46-7.42 (m, 2H), 5.53 (dd, *J* = 8.04, 5.6 Hz, 1H), 3.87 (s, 3H), 3.82 (dd, *J* = 11.48, 7.96 Hz, 1H), 3.58 (dd, *J* = 11.48, 5.48 Hz, 1H). ^{13}C NMR (100 MHz, $CDCl_3$) δ 200.22, 171.13, 168.74, 133.40, 132.90, 129.64, 128.34, 68.02, 53.42, 32.23.

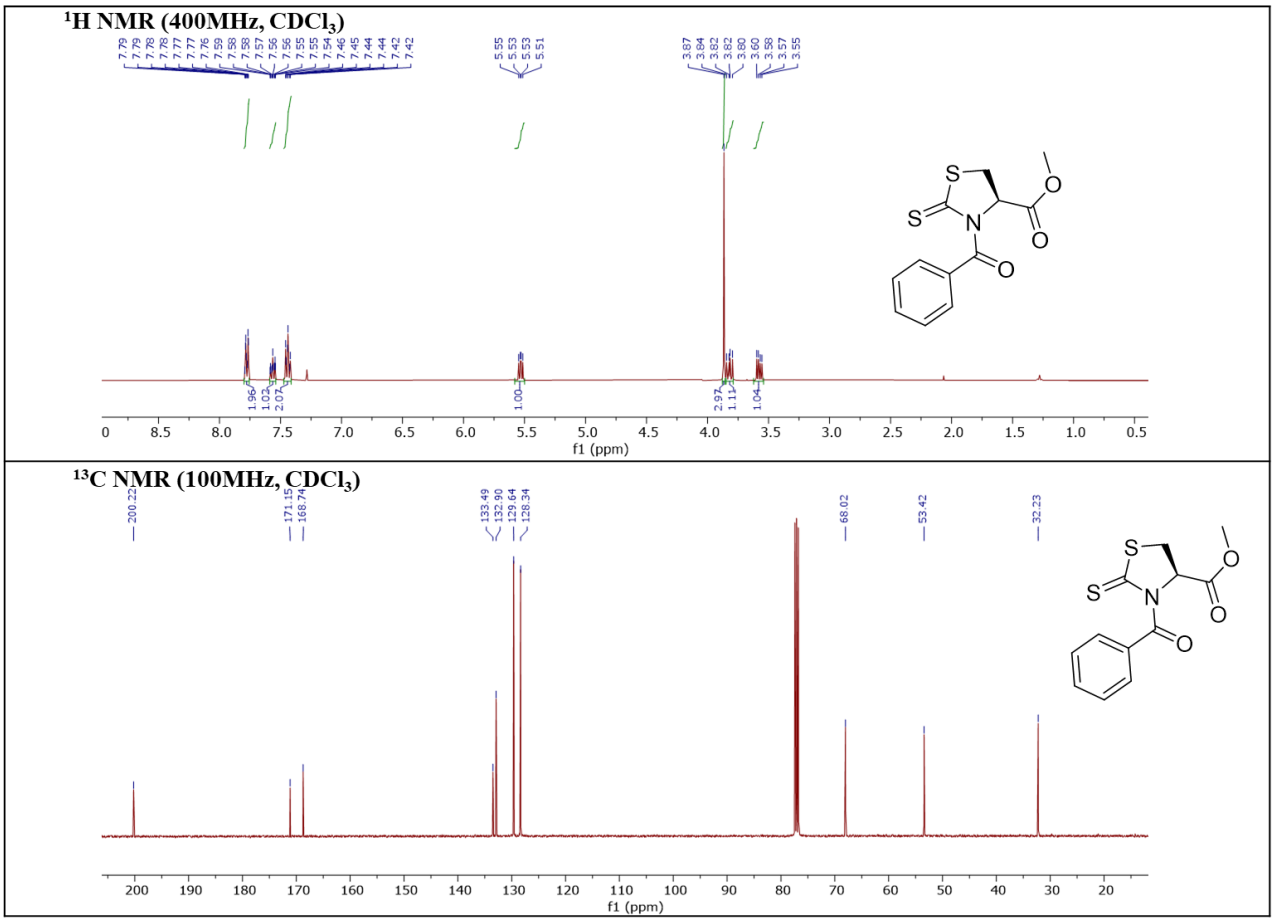

Experimental Data for Transamidations of Twisted Amides
Optimization of Reaction Conditions for Transamidation

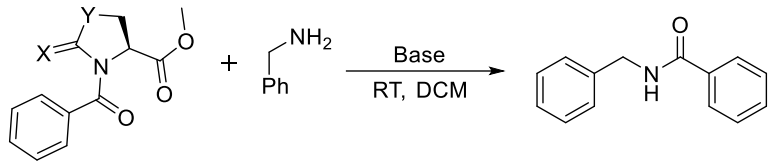

2.1a-2.1d

2.1a: X=O, Y=O
2.1b: X=S, Y=O
2.1c: X=O, Y=S
2.1d: X=S, Y=S

2.2a

Entry	Twisted amide	Y	X	Base	Yield (%)	Time (h)
1	2.1d	S	S	LiHMDS	<10	16
2	2.1d	S	S	LDA	<10	16
3	2.1d	S	S	NaH	<10	16
4	2.1d	S	S	KOtBu	<10	16
5	2.1d	S	S	DBU	20	16
6	2.1d	S	S	DIPEA	70	16
7	**2.1d**	**S**	**S**	**Triethylamine**	**96**	**2**
8	2.1c	S	O	Triethylamine	69	12
9	2.1a	O	O	Triethylamine	71	16
10	**2.1b**	**O**	**S**	**Triethylamine**	**94**	**2**

Reaction Conditions: Twisted amides **2.1a-2.1d** (0.07 mmol), amine (1.5 equiv.), base (1.5 equiv.) in DCM (5 mL) at room temperature.

Procedure for transamidation reactions

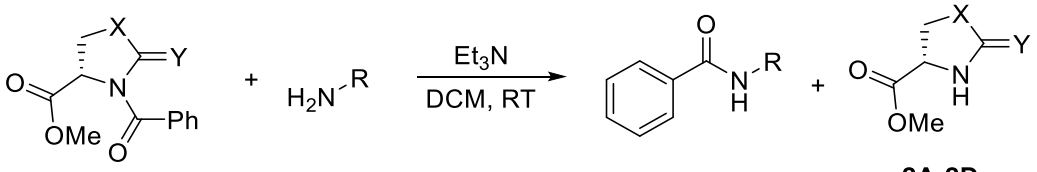

2.1a-2.1d

X = O or S
Y = O or S

2A-2D

X = O or S
Y = O or S

To a solution of twisted amide **2.1a-2.1d** (0.07 mmol) in DCM (5 mL) was added benzylamine (1.5 equiv.), and base (1.5 equiv.) sequentially, and the reaction mixture was stirred at room temperature until the starting material consumed as monitored by TLC. Volatiles removed under reduced pressure and crude residue was purified by column chromatography using mixture of ethyl acetate and hexane as an eluent. The resulting products were characterized by ^{1}H NMR and ^{13}C-NMR.

Synthesis of 2.2a from 2.1d on a gram scale: To a solution of twisted amide **2.1d** (1g, 3.5 mmol) in DCM (100 mL) was added benzylamine (1.5 equiv.), and triethylamine (1.5 equiv.) sequentially, and the reaction mixture was stirred at room temperature until the starting material consumed as monitored by TLC. Volatiles removed under reduced pressure and crude residue was purified by column chromatography using mixture of ethyl acetate and hexane (1:5) as an eluent. The resulting product **2.2a** (0.680 g, 90% yield) was characterized by ^{1}H NMR and ^{13}C-NMR

Control Reaction

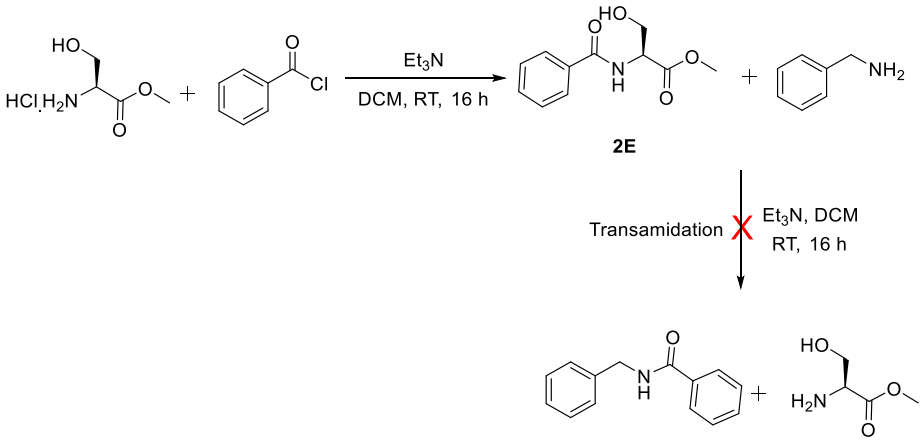

Synthesis of compound 2E

Serine methyl ester (6.45 mmol) was added in one portion to a solution of benzoyl chloride (6.45 mmol) in DCM (100 mL) at 0 ^{O}C. Triethylamine (1.8 mL, 12.9 mmol) was dissolved in DCM (10 mL). Triethylamine solution was added slowly and the resulting reaction mixture was left to stir from 0 ^{o}C to room temperature for 3 h. The reaction progress was monitored by TLC. After completion, the reaction was diluted with more DCM followed by washing with saturated brine and sodium bicarbonate solution. The organic layer was concentrated using the rotavap followed by column chromatography using a mixture of ethyl acetate and hexane to generate compound E.

Transamidation reaction of compound 2E.

Compound 2E (0.07 mmol) was dissolved in DCM (5 mL) followed by the addition of triethylamine (1.5 equiv.) and benzylamine (1.5 equiv.). The reaction was left for stirring overnight at room temperature for 16 h and analyzed by TLC. No modification of the compound E was observed under the reaction conditions.

General procedure for transamidation of 2.1b and 2.1d.

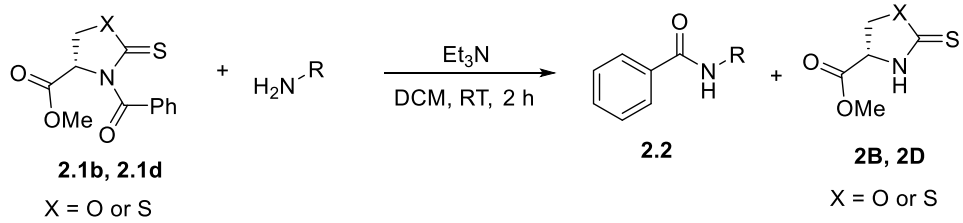

To a solution of twisted amide **2.1b** or **2.1d** (0.07 mmol) in DCM (5 mL) was added respective amine (1.5 equiv.), and triethylamine (1.5 equiv.) sequentially, and the reaction mixture was stirred at room temperature for 2 h. Volatiles removed under reduced pressure and crude residue was purified by column chromatography using mixture of ethyl acetate and hexane as an eluent. The resulting products were characterized by ^{1}H NMR and ^{13}C-NMR.

NMR DATA FOR TRANSAMIDATION REACTIONS

NMR Data for Compound 2.2a

N-benzylbenzamide: ^{1}H NMR (600 MHz, $CDCl_3$) δ 7.79 (d, *J* = 7.5 Hz, 2H), 7.50 (t, *J* = 7.3 Hz, 1H), 7.42 (t, *J* = 7.5 Hz, 2H), 7.36-7.35 (m, 4H), 7.31-7.29 (m, 1H), 6.55(s, 1H), 4.64 (d, *J* = 5.6 Hz, 2H). ^{13}C NMR (151 MHz, $CDCl_3$) δ 167.5, 138.2, 134.3, 131.7, 128.9, 128.7, 128.0, 127.7, 127.1, 44.2.

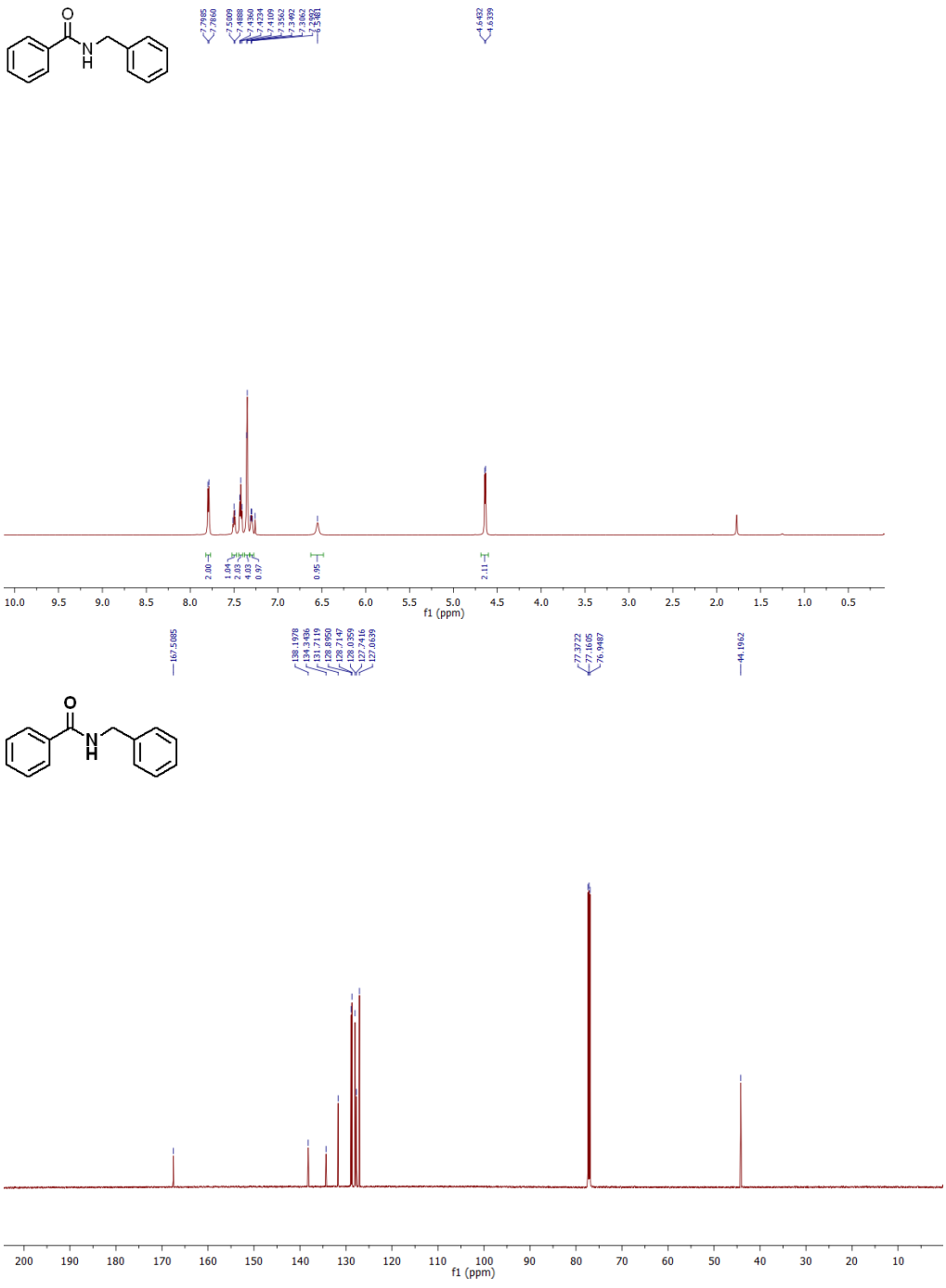

NMR Data for Compound 2.2b

N-(Prop-2-yn-1-yl)benzamide:[1]H NMR (600 MHz, $CDCl_3$) δ 7.78 (d, *J* = 7.8 Hz, 2H), 7.52 (t, *J* = 7.3 Hz, 1H), 7.44 (t, *J* = 7.4 Hz, 2H), 6.32 (s, 1H), 4.26 – 4.25 (m, 2H), 2.28 (s, 1H). ^{13}C NMR (151 MHz, $CDCl_3$) δ 167.2, 133.9, 132.0, 128.8, 127.1, 79.6, 72.1, 29.9.

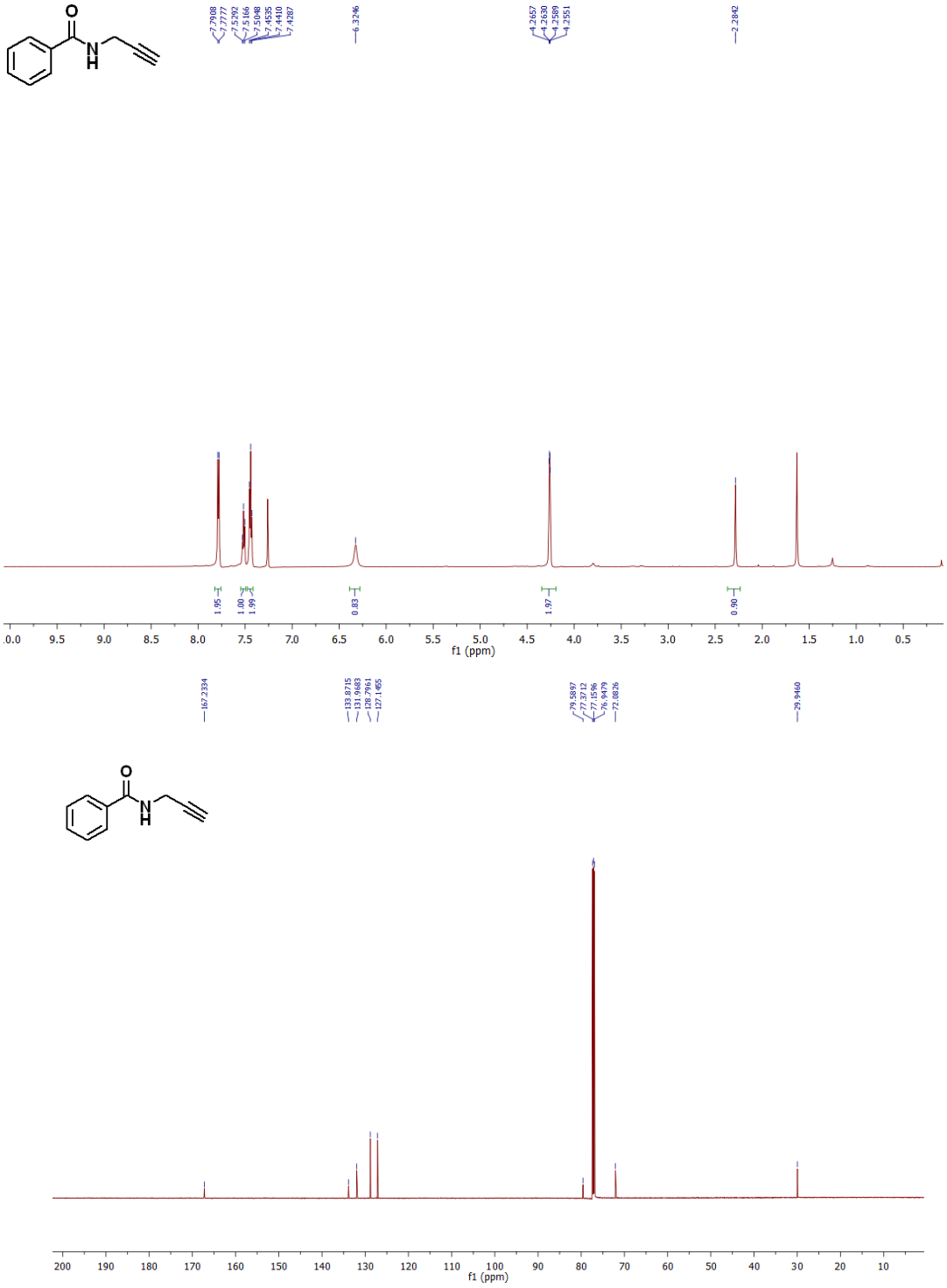

NMR Data for Compound 2.2c

N-(2,2-dimethoxyethyl)benzamide:^{1}H NMR (400 MHz, $CDCl_3$) δ 7.77 (d, *J* = 7.4 Hz, 2H), 7.50 (t, *J* = 7.2 Hz, 1H), 7.43 (t, *J* = 7.4 Hz, 2H), 6.36 (s, 1H), 4.49 (t, *J* = 5.2 Hz, 1H), 3.62 – 3.59 (m, 2H), 3.43 (s, 6H). ^{13}C NMR (101 MHz, $CDCl_3$) δ 167.7, 134.5, 131.7, 128.7, 127.1, 102.9, 54.7, 41.6.

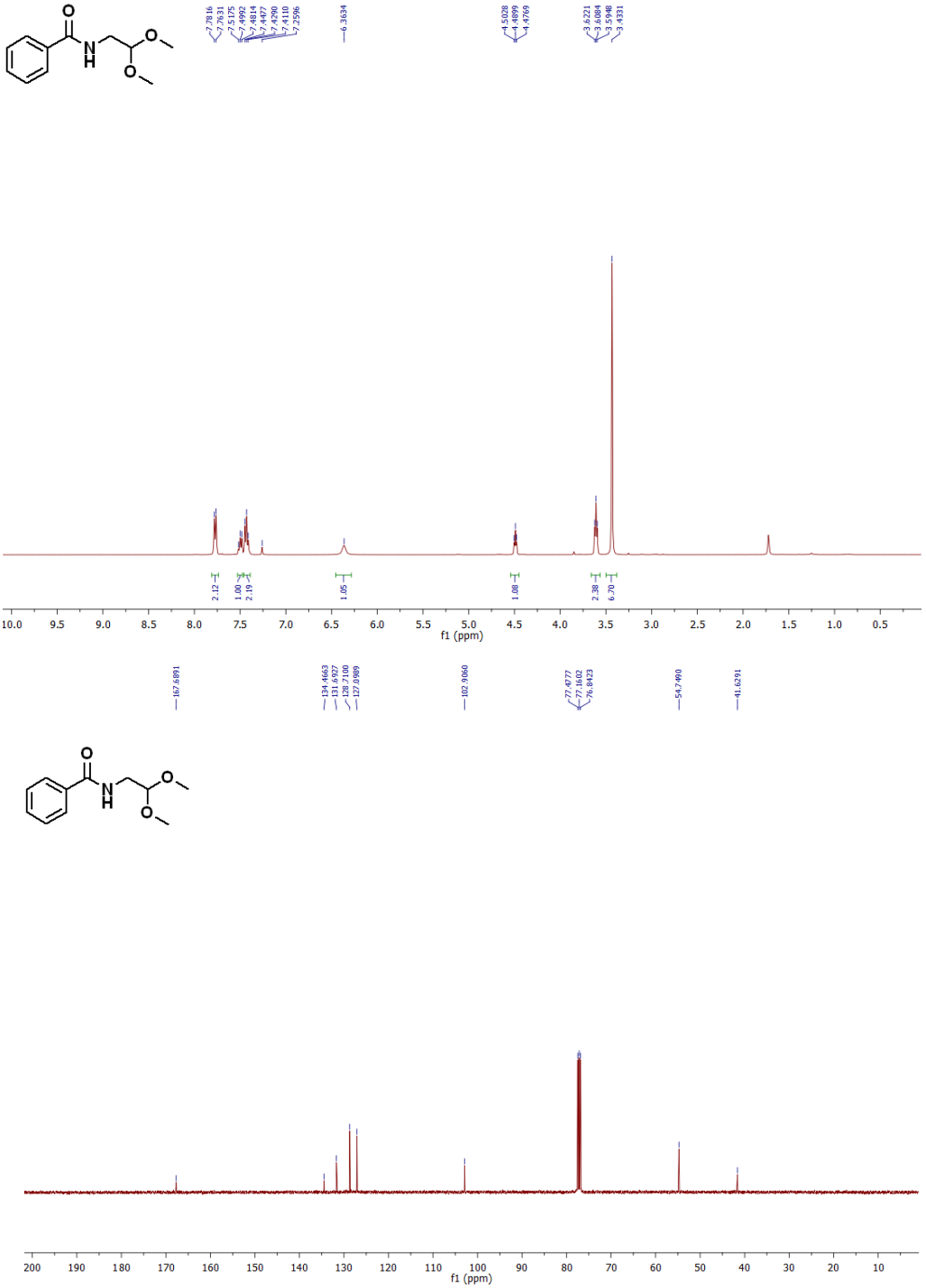

NMR Data for Compound 2.2d

<u>N-isopropylbenzamide:</u> ^{1}H NMR (600 MHz, $CDCl_3$) δ 7.75 (d, *J* = 7.2 Hz, 2H), 7.48 (t, *J* = 7.3 Hz, 1H), 7.42 (t, *J* = 7.5 Hz, 2H), 5.94 (s, 1H), 4.29 (heptet, *J* = 6.6 Hz, 1H), 1.26 (d, *J* = 6.6 Hz, 6H). ^{13}C NMR (101 MHz, $CDCl_3$) δ 166.8, 135.1, 131.4, 128.6, 126.9, 42.0, 23.0.

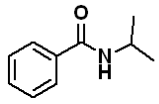

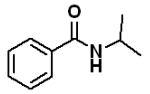

NMR Data for Compound 2.2e

N-Octylbenzamide: ^{1}H NMR (600 MHz, $CDCl_3$) δ 7.76 – 7.75 (m, 2H), 7.5 – 7.47 (m, 1H), 7.43 – 7.41 (m, 2H), 6.14 (s, 1H), 3.46 – 3.43 (m, 2H), 1.64 – 1.58 (m, 2H), 1.40 – 1.23 (m, 10H), 0.88 (t, *J* = 6.0 Hz, 3H). ^{13}C NMR (151 MHz, $CDCl_3$) δ 167.6, 135.0, 131.4, 128.7, 126.9, 40.3, 31.9, 29.8, 29.4, 29.3, 27.1, 22.8, 14.2.

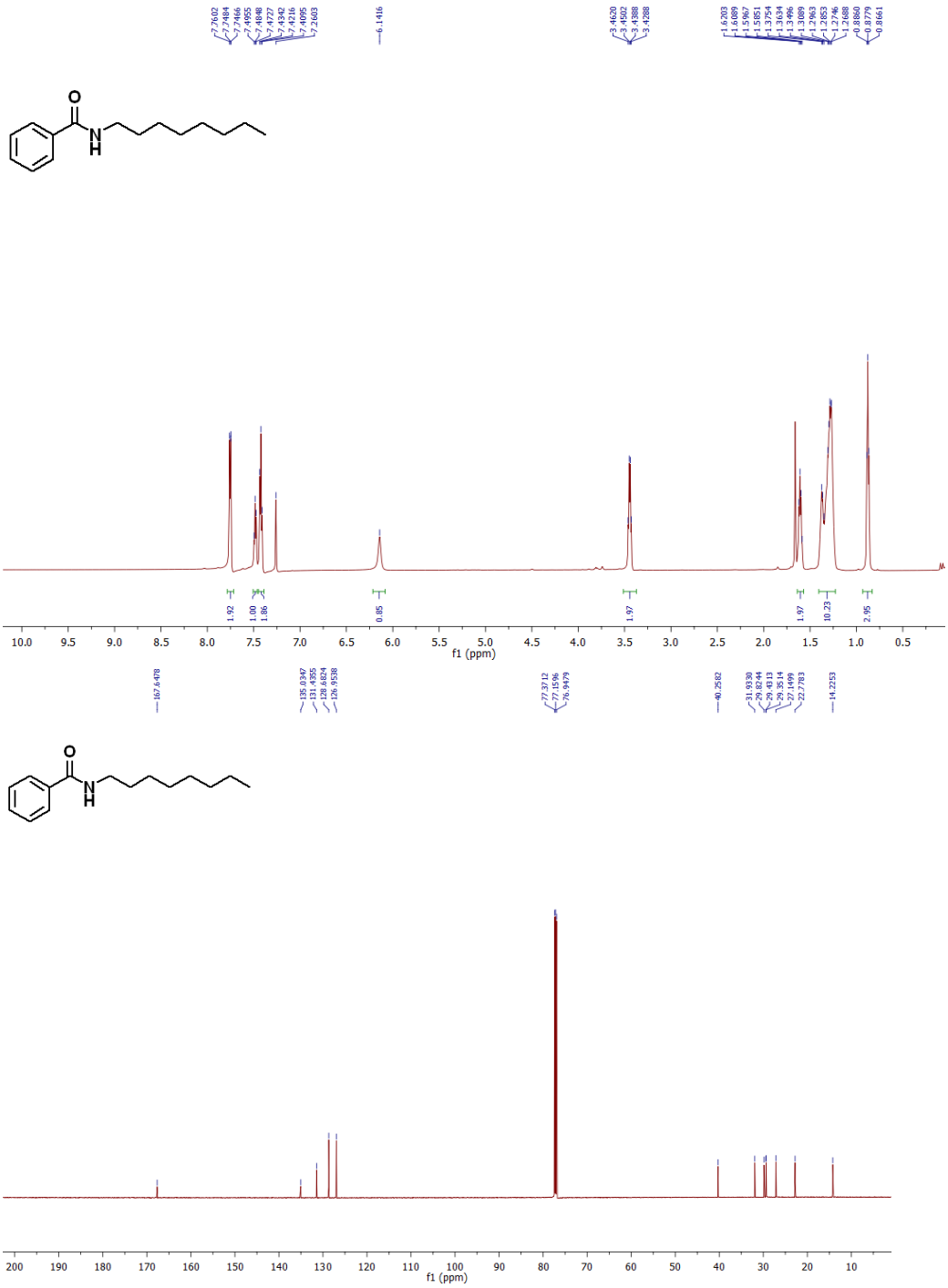

NMR Data for Compound 2.2f

<u>tert-butyl 4-benzoylpiperazine-1-carboxylate</u>: ^{1}H NMR (500 MHz, $CDCl_3$) δ 7.44 – 7.40 (m, 5H), 3.73 – 3.39 (m, 8H), 1.46 (s, 9H). ^{13}C NMR (126 MHz, $CDCl_3$) δ 170.7, 154.7, 135.6, 130.0, 128.7, 127.2, 80.5, 47.6, 42.2, 28.5.

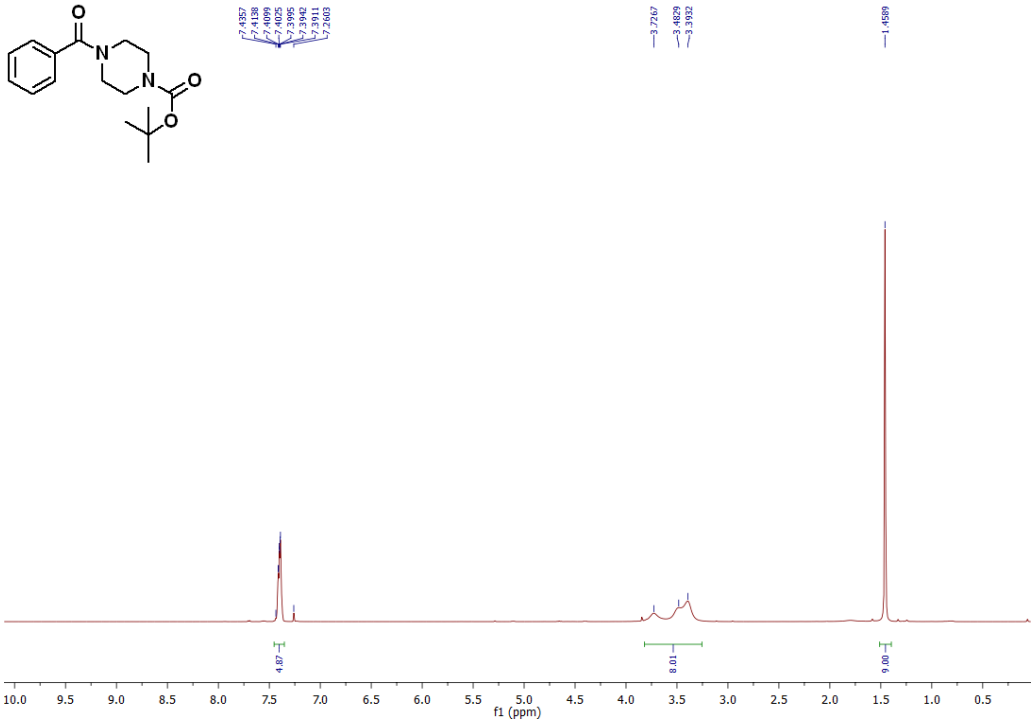

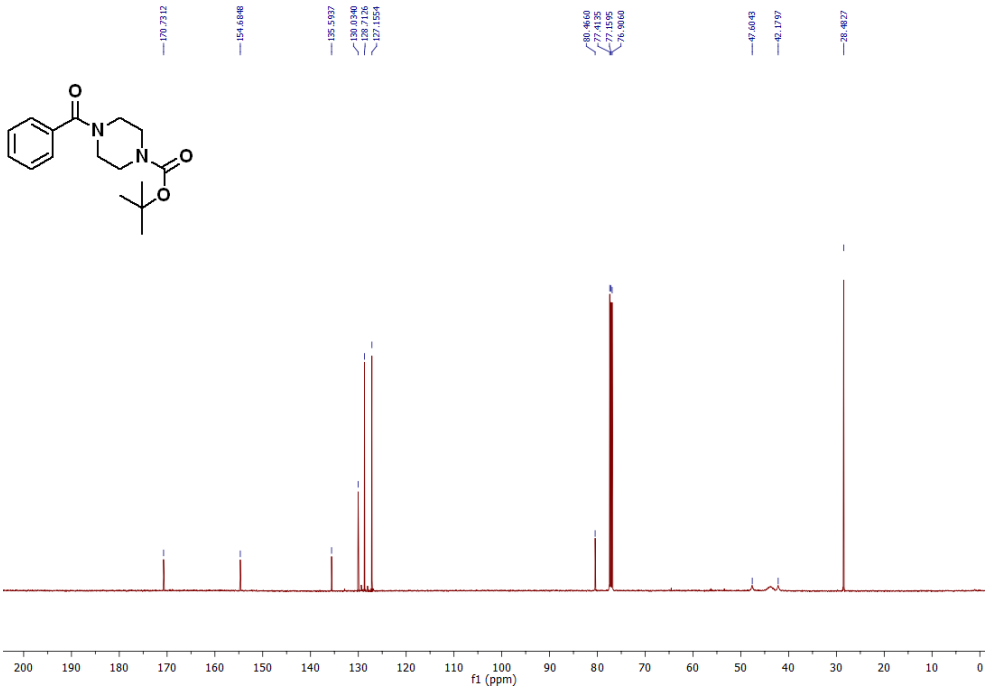

NMR Data for Compound 2.2g

Morpholino(phenyl)methanone: ^{1}H NMR (400 MHz, $CDCl_3$) δ 7.41 (bs, 5H), 3.86 – 3.35 (m, 8H). ^{13}C NMR (101 MHz, $CDCl_3$) δ 170.6, 135.5, 130.0, 128.7, 127.2, 67.1, 48.6.

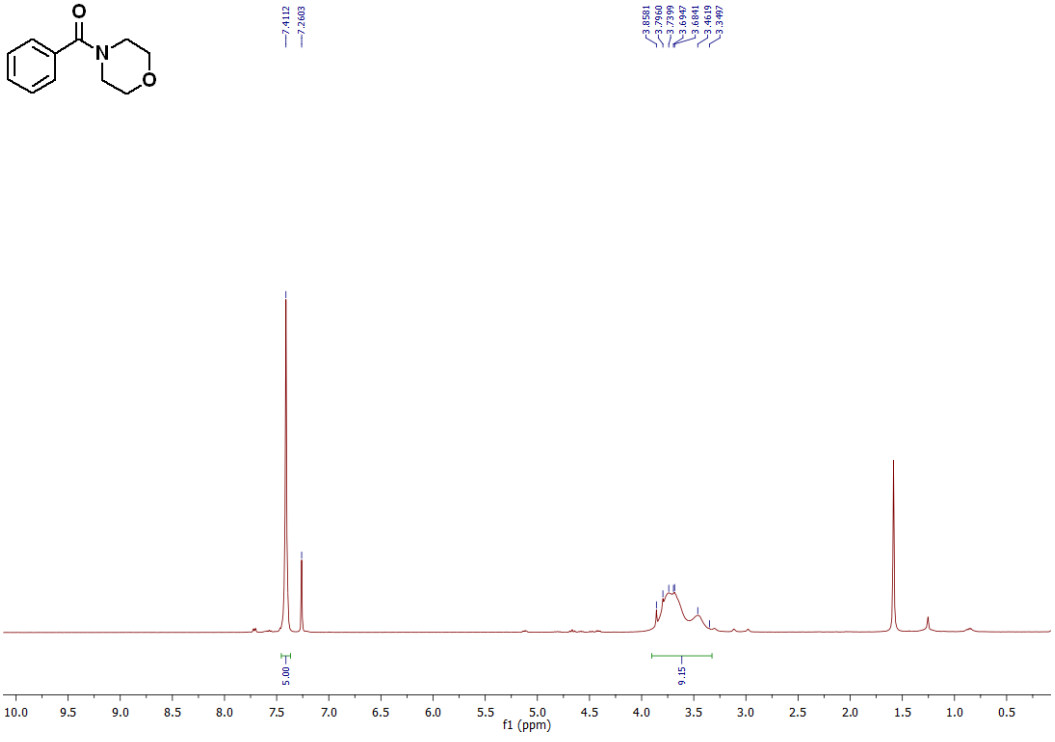

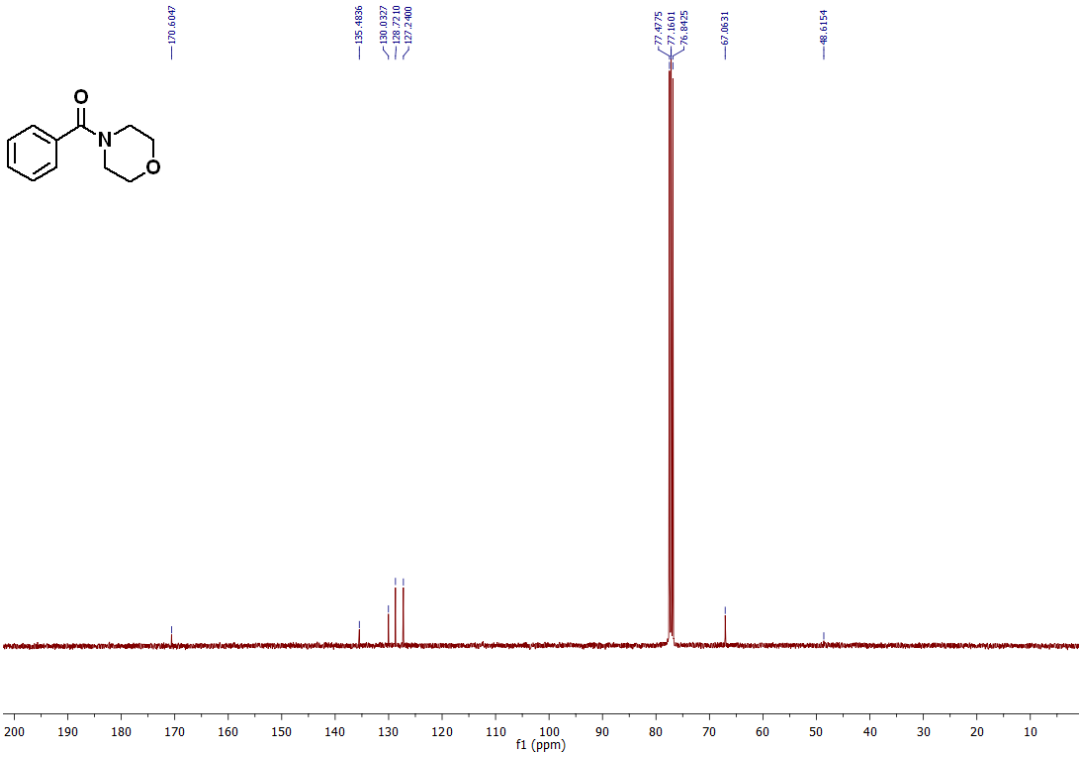
170.6947
135.4836
130.0327
128.7210
127.2400
77.4775
77.1601
76.8425
67.0631
48.6154
O
N
O
200
190
180
170
160
150
140
130
120
110
100
90
80
70
60
50
40
30
20
10
f1 (ppm)

NMR Data for Compound 2.2h

Phenyl(piperidin-1-yl)methanone: ^{1}H NMR (600 MHz, $CDCl_3$) δ 7.38 (bs, 5H), 3.71 (bs, 2H), 3.33 (bs, 2H), 1.74 – 1.63 (m, 4H), 1.51 (bs, 2H). ^{13}C NMR (101 MHz, $CDCl_3$) δ 170.4, 136.7, 129.5, 128.5, 126.9, 48.9, 43.3, 26.6, 25.7, 24.7.

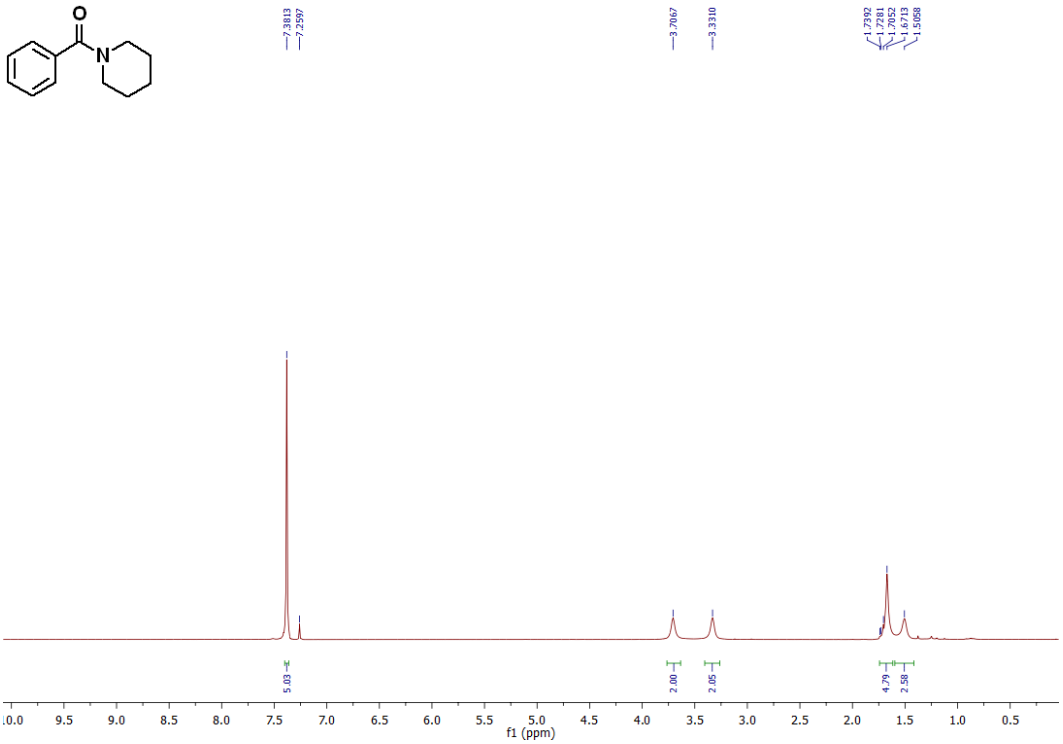

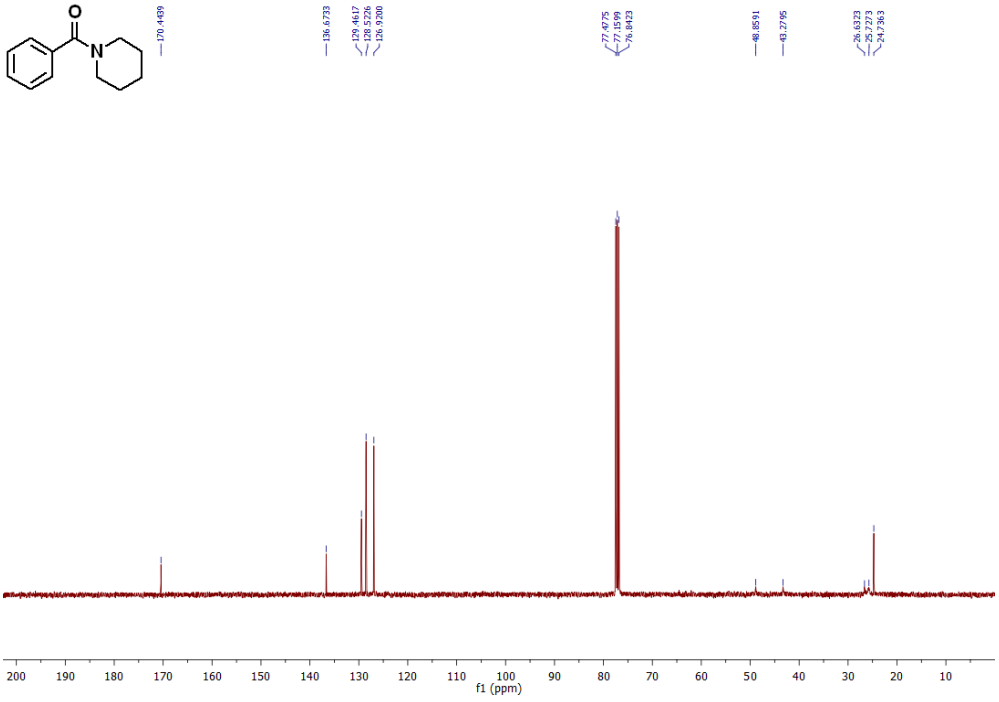

NMR Data for Compound 2.2i

phenyl(pyrrolidin-1-yl)methanone: ^{1}H NMR (400 MHz, $CDCl_3$) δ 7.51 – 7.49 (m, 2H), 7.40 – 7.36 (s, 3H), 3.64 (t, *J* = 6.8 Hz, 2H), 3.41 (t, *J* = 6.5 Hz, 2H), 1.98 – 1.92 (m, 2H), 1.89 – 1.84 (m, 2H). ^{13}C NMR (151 MHz, $CDCl_3$) δ 169.9, 137.4, 129.9, 128.4, 127.2, 49.7, 46.3, 26.5, 24.6.

NMR Data for Compound 2.2j

N-(2-bromoethyl)benzamide: ^{1}H NMR (400 MHz, $CDCl_3$) δ 7.95 (d, *J* = 7.4 Hz, 2H), 7.49 – 7.46 (m, 1H), 7.41 (t, *J* = 7.4 Hz, 2H), 4.44 (t, *J* = 9.5 Hz, 2H), 4.10 (*J* = 9.5 Hz, 2H). ^{13}C NMR (101 MHz, $CDCl_3$) δ 164.8, 131.4, 128.5, 128.3, 127.9, 67.7, 55.1.

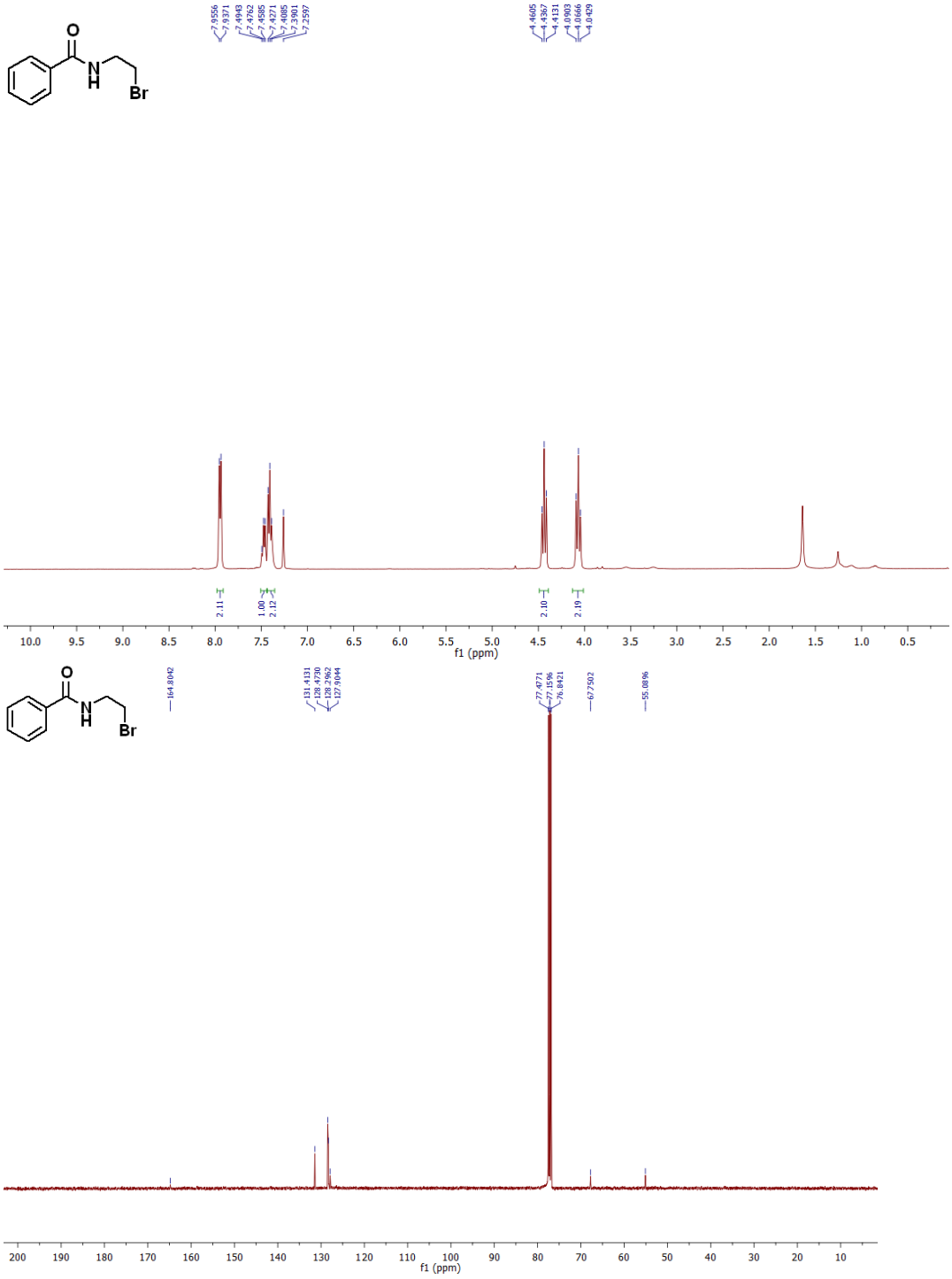

NMR Data for Compound 2.2k

<u>methyl benzoylprolinate</u>: ^{1}H NMR (500 MHz, $CDCl_3$) δ 7.57 – 7.55 (m, 2H), 7.43 – 7.35 (m, 3H), 4.68 – 4.65 (m, 1H), 3.77 (s, 3H), 3.66 – 3.62 (m, 1H), 3.55 – 3.50 (m, 1H), 2.33 – 2.31 (m, 1H), 2.04 – 2.00 (m, 2H), 1.91 – 1.86 (m, 1H). ^{13}C NMR (126 MHz, $CDCl_3$) δ 172.9, 169.8, 136.3, 130.3, 128.3, 127.4, 59.2, 52.4, 50.0, 29.5, 25.5.

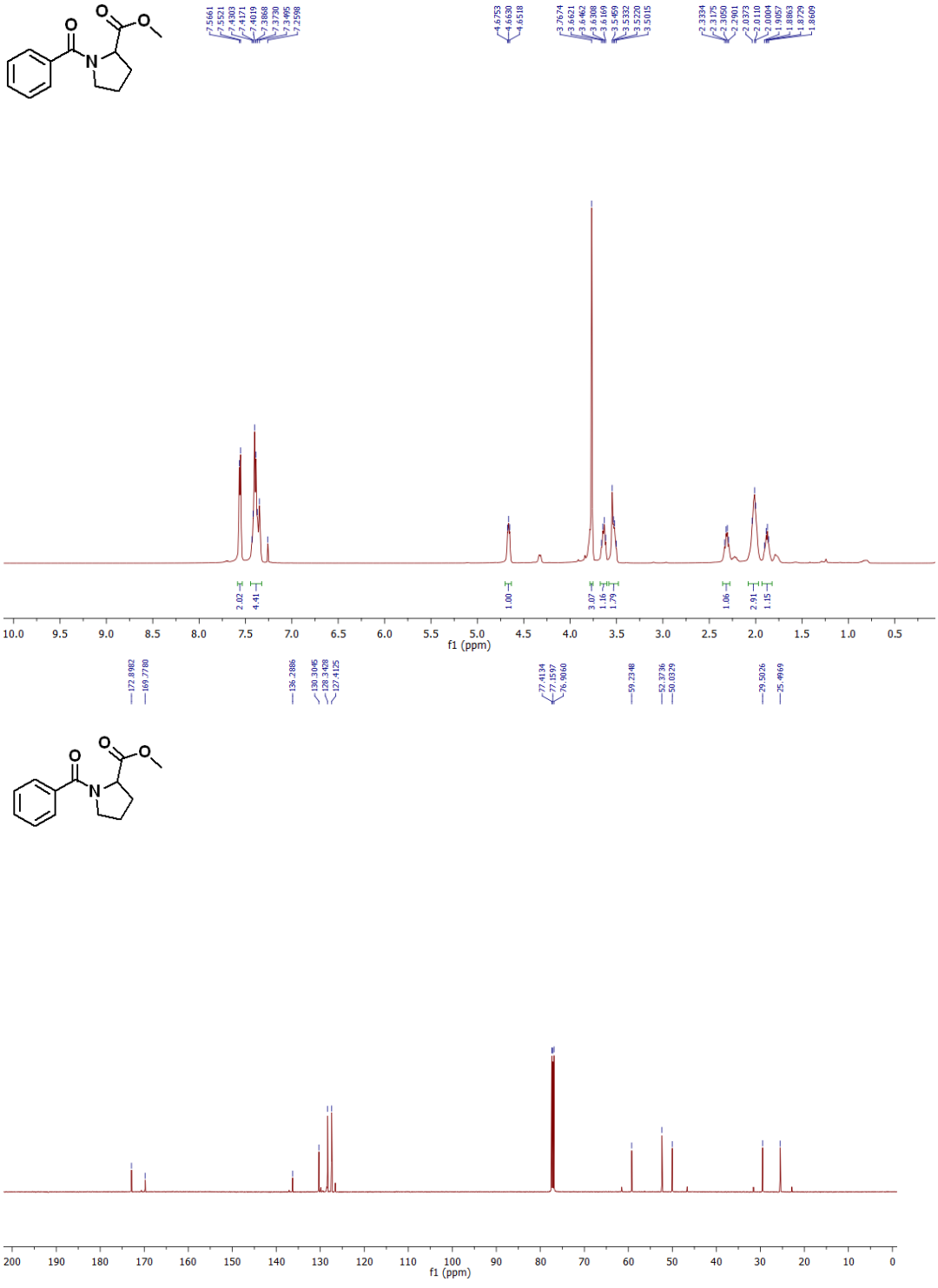

NMR Data for Compound 2.2l

<u>Methyl benzoylphenylalaninate</u>: ^{1}H NMR (600 MHz, $CDCl_3$) δ 7.72 (d, *J* = 7.2 Hz, 2H), 7.51 (t, *J* = 7.4 Hz, 1H), 7.42 (t, *J* = 7.6 Hz, 2H), 7.31 – 7.24 (m, 3H), 7.13 (d, *J* = 7.0 Hz, 2H), 6.59 (d, *J* = 6.7 Hz, 1H), 5.11 – 5.08 (m, 1H), 3.77 (s, 3H), 3.26 (ddd, *J* = 39.4, 13.9, 5.6 Hz, 2H). ^{13}C NMR (151 MHz, $CDCl_3$) δ 172.2, 167.0, 136.0, 134.0, 131.9, 129.5, 128.8, 127.3, 127.1, 53.6, 52.6, 38.0.

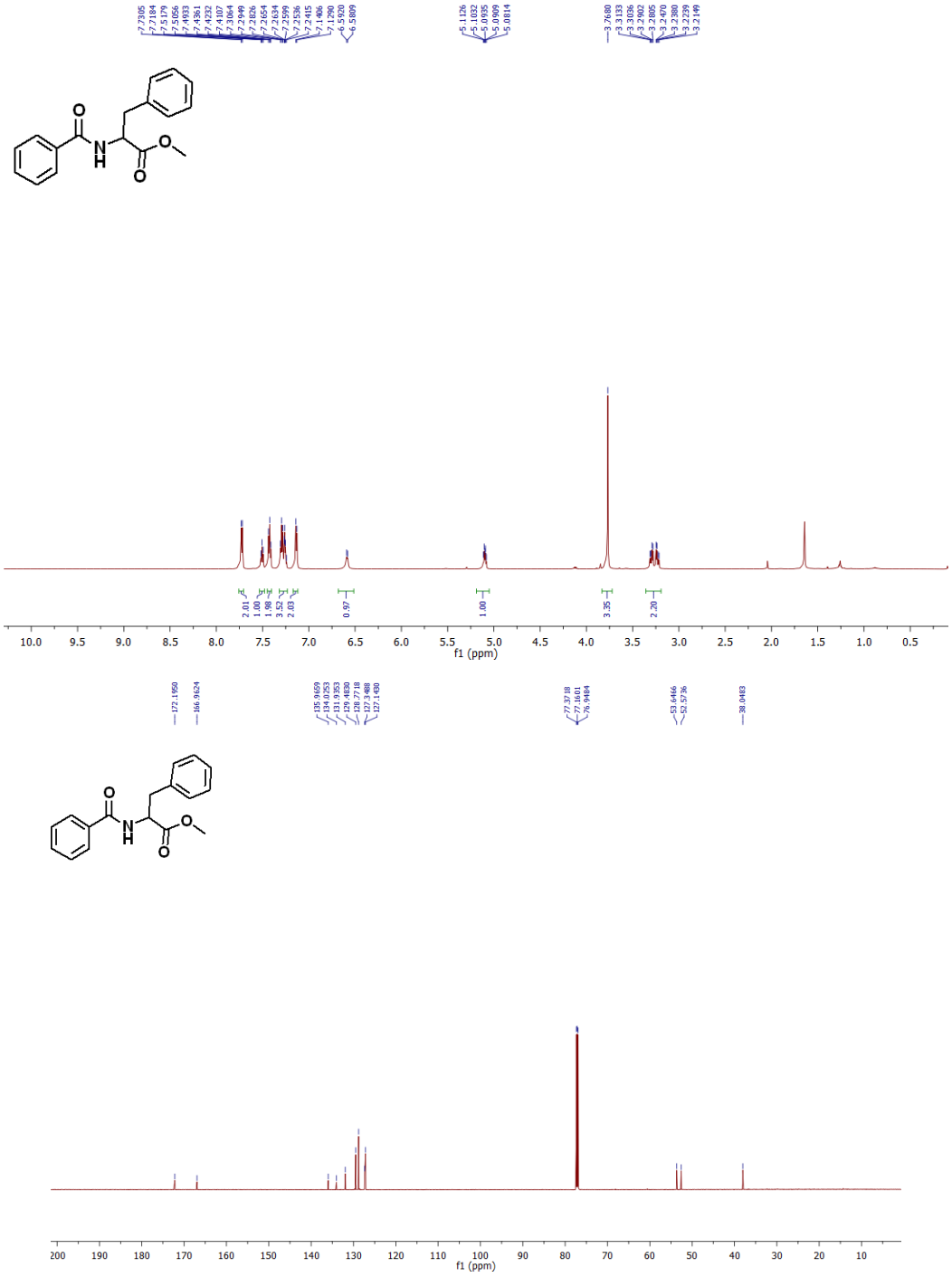

Experimental Details for Esterification Reactions
Optimization of reaction conditions for esterification.

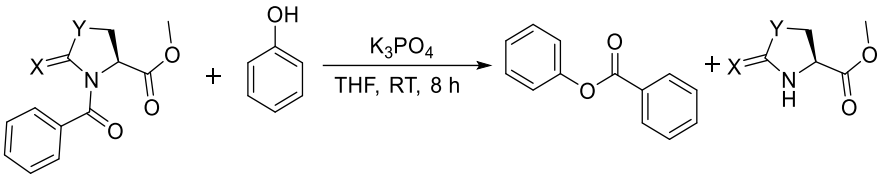

2.1a-2.1d
X = O or S
Y = O or S

2.3a

2A-2D
X = O or S
Y = O or S

Entry	Twisted amide	Y	X	Yield (%)
1	**2.1d**	**S**	**S**	**62**
2	2.1c	S	O	60
3	2.1a	O	O	62
4	2.1b	O	S	53

Reaction Conditions: Twisted amides **2.1a-2.1d** (0.142 mmol), alcohol (1.5 equiv.), K_3PO_4 (5 equiv.) in THF (7 mL) at room temperature for 8 h.

Procedure for esterification reactions

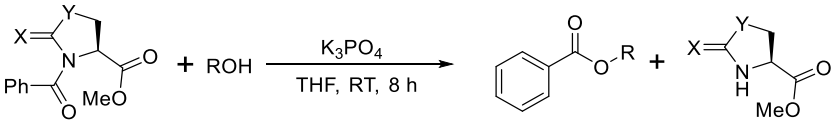

2.1a-2.1d
2.1a: X=O, Y=O
2.1b: X=S, Y=O
2.1c: X=O, Y=S
2.1d: X=S, Y=S

2.3

2A-2D
2A: X=O, Y=O
2B: X=S, Y=O
2C: X=O, Y=S
2D: X=S, Y=S

To a solution of twisted amide **2.1a-2.1d** (0.142 mmol) in THF (7 mL) was added alcohol (1.5 eq.), and K_3PO_4 (5 eq.) sequentially, and the reaction mixture was stirred at room temperature for 8 h. Volatiles removed under reduced pressure and crude residue was purified by column chromatography using mixture of ethyl acetate and hexane as an eluent to get the desired ester **2.3**. The resulting products were characterized by ^{1}H NMR and ^{13}C-NMR.

General procedure for esterification of 1b and 1d.

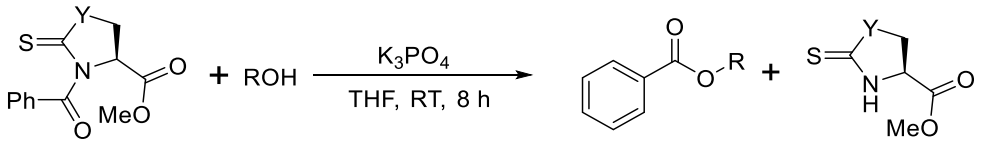

2.1b, 2.1d **2.3** **2B, 2D**

2.1b: Y=O
2.1d: Y=S

2B: Y=O
2D: Y=S

To a solution of twisted amide **2.1b** or **2.1d** (0.142 mmol) in THF (7 mL) was added respective alcohol (1.5 eq.), and K_3PO_4 (5 eq.) sequentially, and the reaction mixture was stirred at room temperature for 8 h. Volatiles removed under reduced pressure and crude residue was purified by column chromatography using mixture of ethyl acetate and hexane as an eluent. The resulting products were characterized by ^{1}H NMR and ^{13}C-NMR.

I. NMR Data for Esterification Reactions

NMR DATA FOR 2.3a

Phenyl benzoate: ^{1}H NMR (400 MHz, $CDCl_3$) δ 8.26-8.24 (m, 3H), 7.67 (t, *J* = 7.4 Hz, 1H), 7.55 (t, *J* = 7.76 Hz, 2H), 7.47 (t, *J* = 7.94, 2H), 7.33-7.25 (m, 2H). ^{13}C NMR (100 MHz, $CDCl_3$) δ 165.2, 150.9, 133.6, 130.2, 129.6, 129.5, 128.6, 125.9, 121.7.

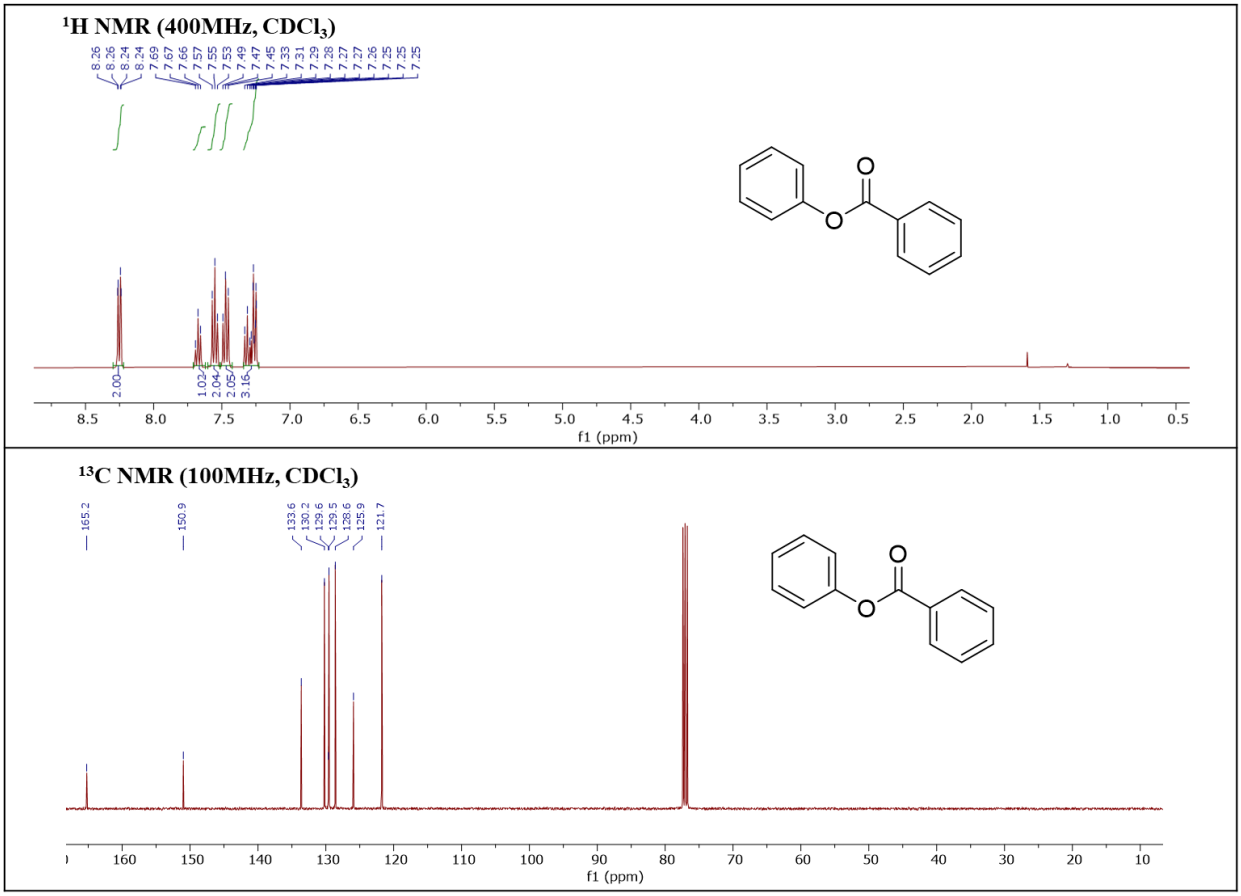

NMR DATA FOR 2.3b

4-Bromophenyl benzoate: ^{1}H NMR (400 MHz, $CDCl_3$) δ 8.19 (d, *J* = 7.68 Hz, 2H), 7.63 (t, *J* = 7.74 Hz, 1H), 7.56-7.50 (m, 4H), 7.12 (d, *J* = 8.48 Hz, 2H). ^{13}C NMR (100 MHz, $CDCl_3$) δ 164.96, 150.08, 133.90, 132.63, 130.30, 129.28, 128.74, 123.64, 119.08.

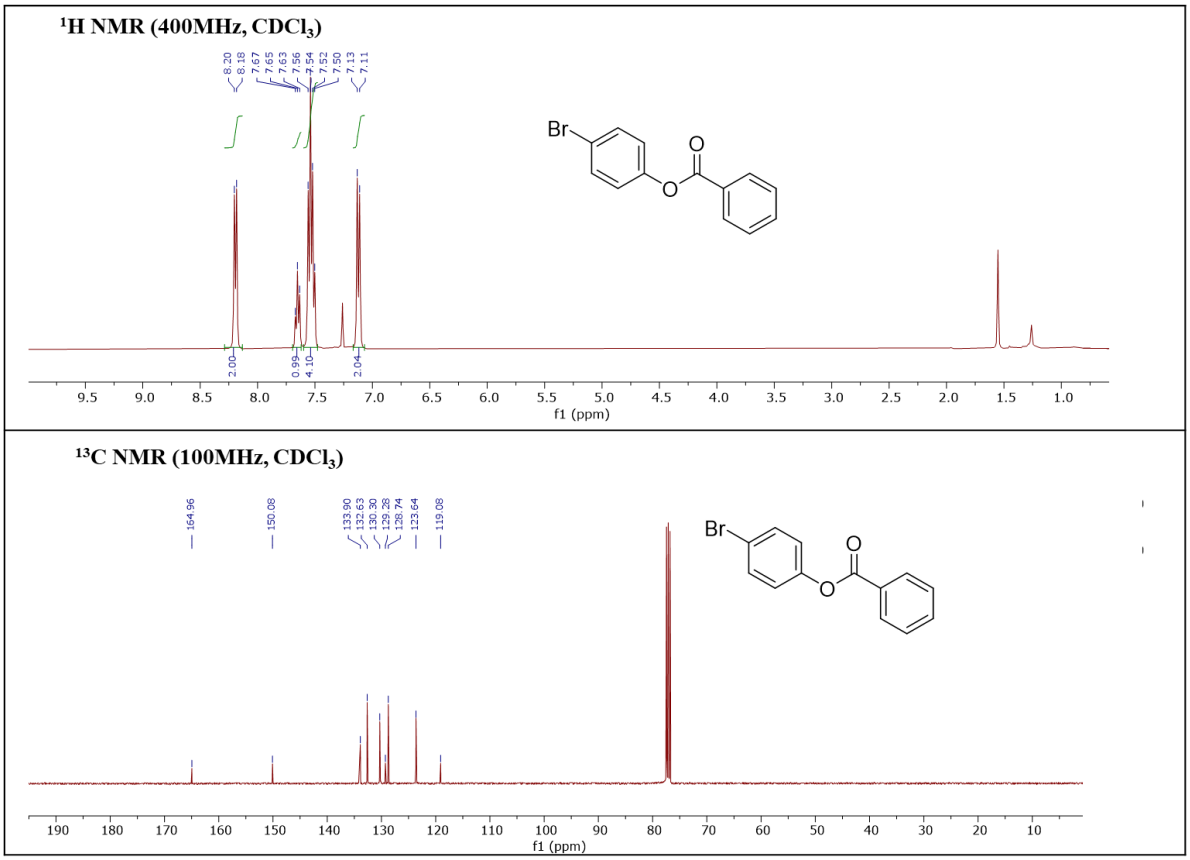

NMR DATA FOR 2.3c

4-Methoxyphenyl benzoate: ^{1}H NMR (600 MHz, $CDCl_3$) δ 8.20 (d, *J* = 7.08 Hz, 2H), 7.62 (t, *J* = 7.50 Hz, 1H), 7.5 (t, *J* = 7.77Hz 2H), 7.15-7.12 (m, 2H), 7.95-7.92 (m, 2H), 3.82 (s, 3H). ^{13}C NMR (151 MHz, $CDCl_3$) δ 165.56, 157.32, 144.43, 133.51, 130.14, 129.65, 128.55, 122.46, 114.53, 55.62.

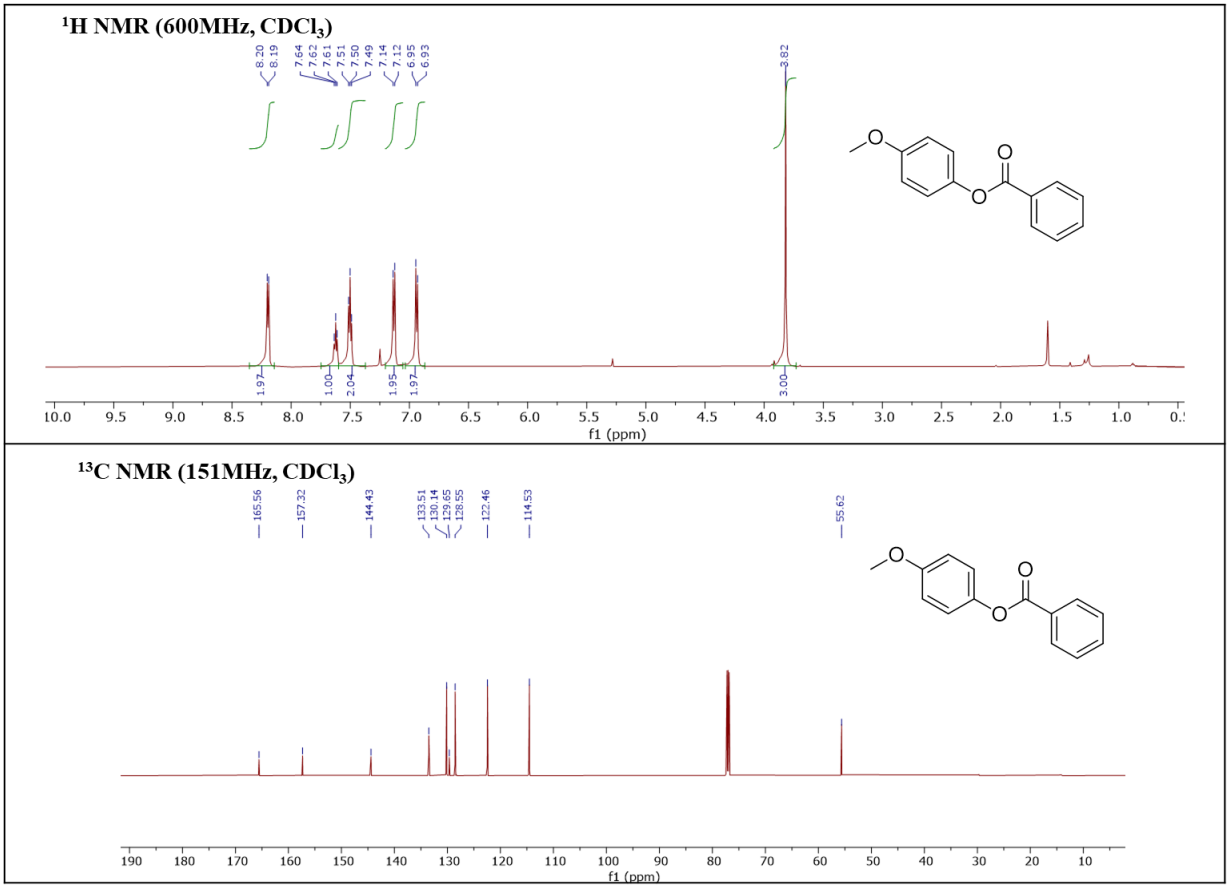

NMR DATA FOR 2.3d

3-Formylphenyl benzoate: ^{1}H NMR (400 MHz, $CDCl_3$) δ 10.06 (s, 1H), 8.25-8.23 (m, 2H), 7.85-7.82 (m, 1H), 7.79 (t, *J* = 2 Hz, 1H), 7.71-7.62 (m, 2H), 7.58-7.52 (m, 3H). ^{13}C NMR (100 MHz, $CDCl_3$) δ 191.19, 164.91, 151.57, 137.86, 133.97, 130.27, 130.24, 129.01, 128.72, 127.95, 127.35, 122.55.

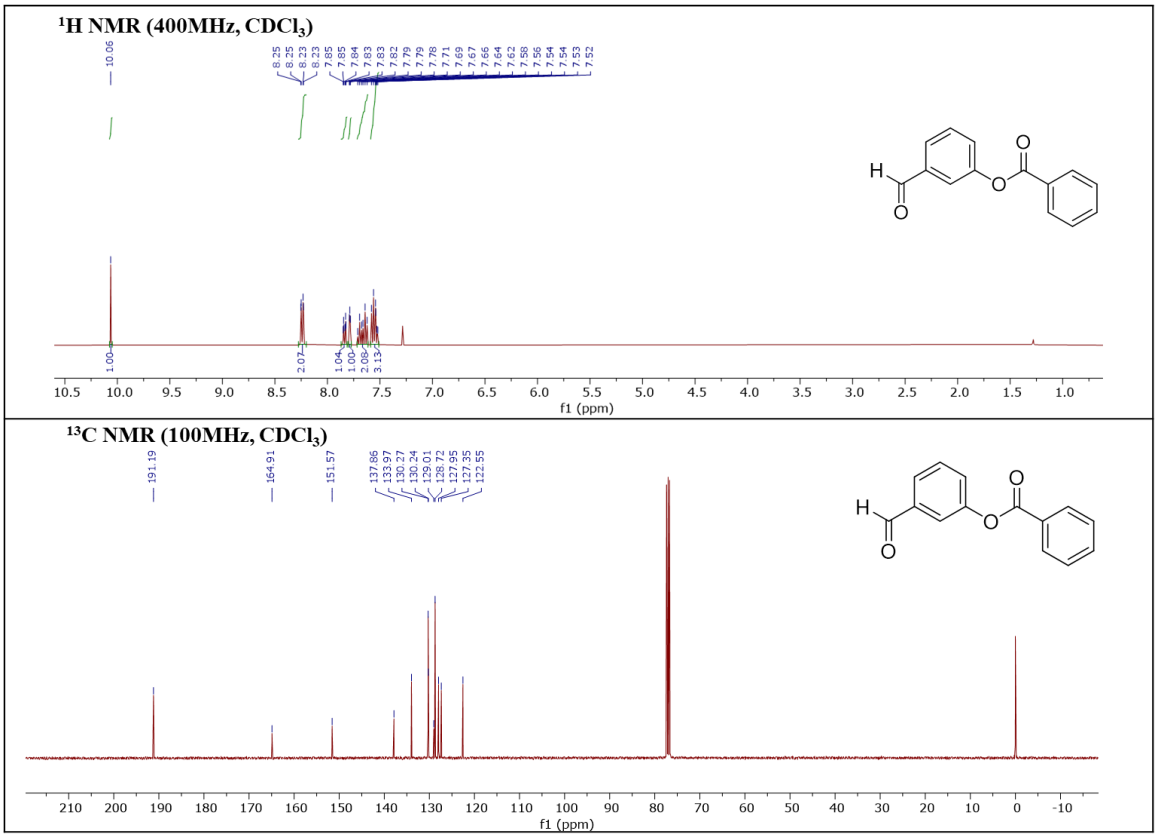

NMR DATA FOR 2.3e

<u>4-Acetylphenyl benzoate</u>: ^{1}H NMR (600MHz, $CDCl_3$) δ 8.21 (d, *J* = 7.08 Hz, 2H), 8.04 (d, *J* = 8.07 Hz, 2H), 7.66 (t, *J* = 7.5 Hz, 1H), 7.53 (t, *J* = 7.8 Hz, 2H), 7.33 (d, *J* = 8.7 Hz, 2H), 2.62 (s, 3H). ^{13}C NMR (100 MHz, $CDCl_3$) δ 196.92, 166.51, 155.43, 134.82, 133.96, 130.28, 130.04, 129.96, 128.71, 121.97, 37.66.

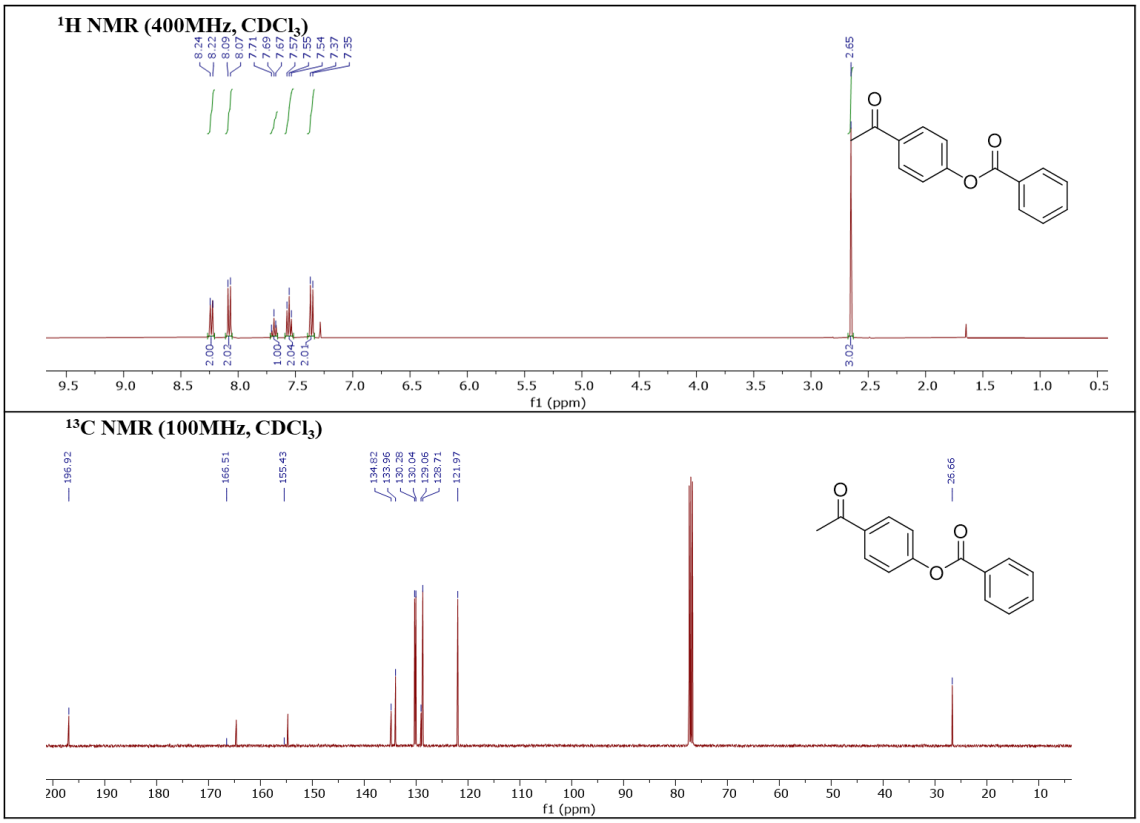

NMR DATA FOR 2.3f

4-(Trifluoromethyl)phenyl benzoate: ^{1}H NMR (400MHz, $CDCl_3$) δ 8.25-8.23 (m, 2H), 7.75-7.68 (m, 3H), 7.56 (t, *J* = 7.84 Hz, 2H), 7.39 (d, *J* = 8.8 Hz, 2H). ^{13}C NMR (100 MHz, $CDCl_3$) δ 164.69, 153.50, 153.48, 153.47, 134.00, 130.29, 128.97, 128.72, 128.36, 128.04, 126.94, 126.90, 126.87, 126.83, 125.28, 122.57, 122.29.

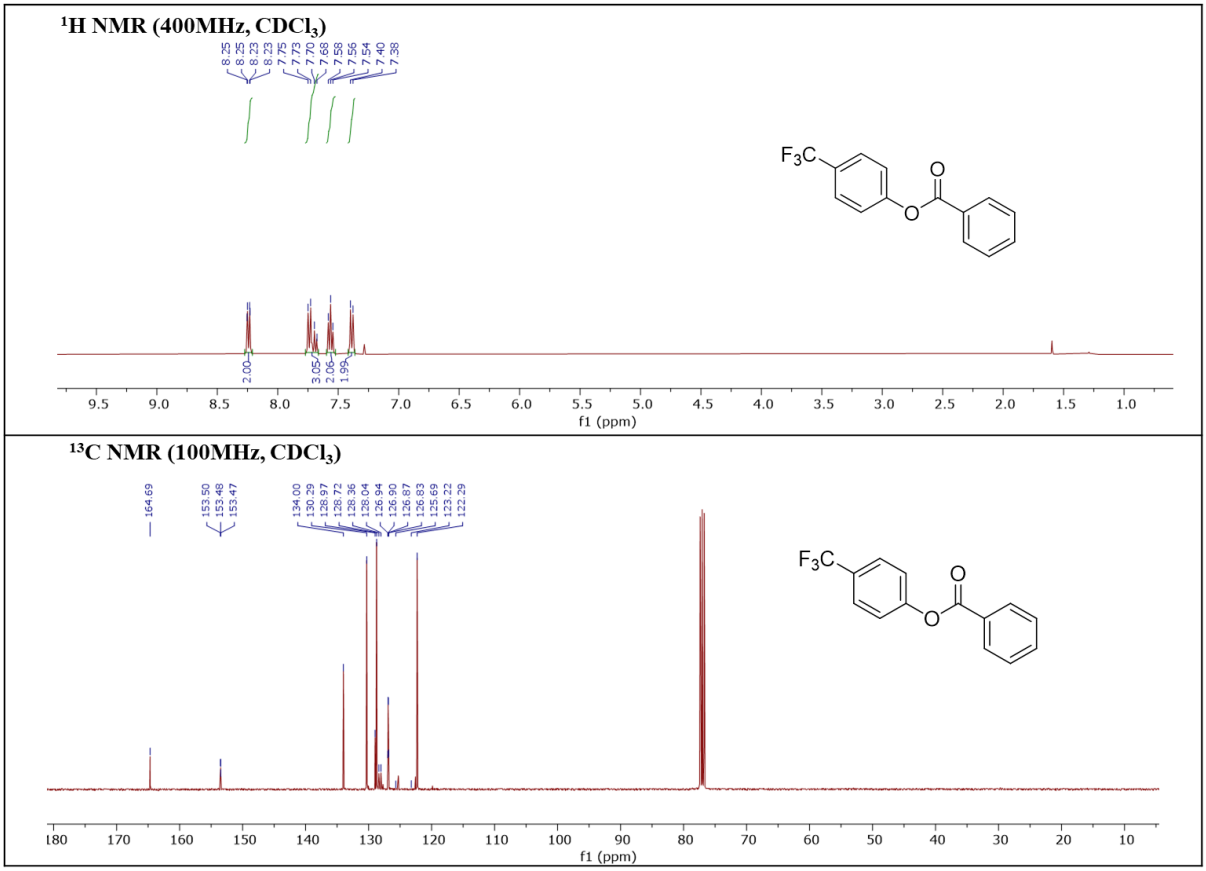

NMR DATA FOR 2.3g

<u>Naphthalen-1-yl benzoate</u>: ^{1}H NMR (600 MHz, $CDCl_3$) δ 8.26 (d, *J* = 7.44 Hz, 2H), 7.91-7.82 (m, 3H), 7.70 (s, 1H), 7.65 (t, *J* = 7.56 Hz, 1H), 7.54-7.47 (m, 4H), 7.37-7.35 (m, 1H). ^{13}C NMR (151 MHz, $CDCl_3$) δ 165.37, 148.60, 133.83, 133.65, 131.52, 130.23, 129.57, 129.47, 128.61, 127.81, 127.69, 126.59, 125.73, 121.25, 118.70.

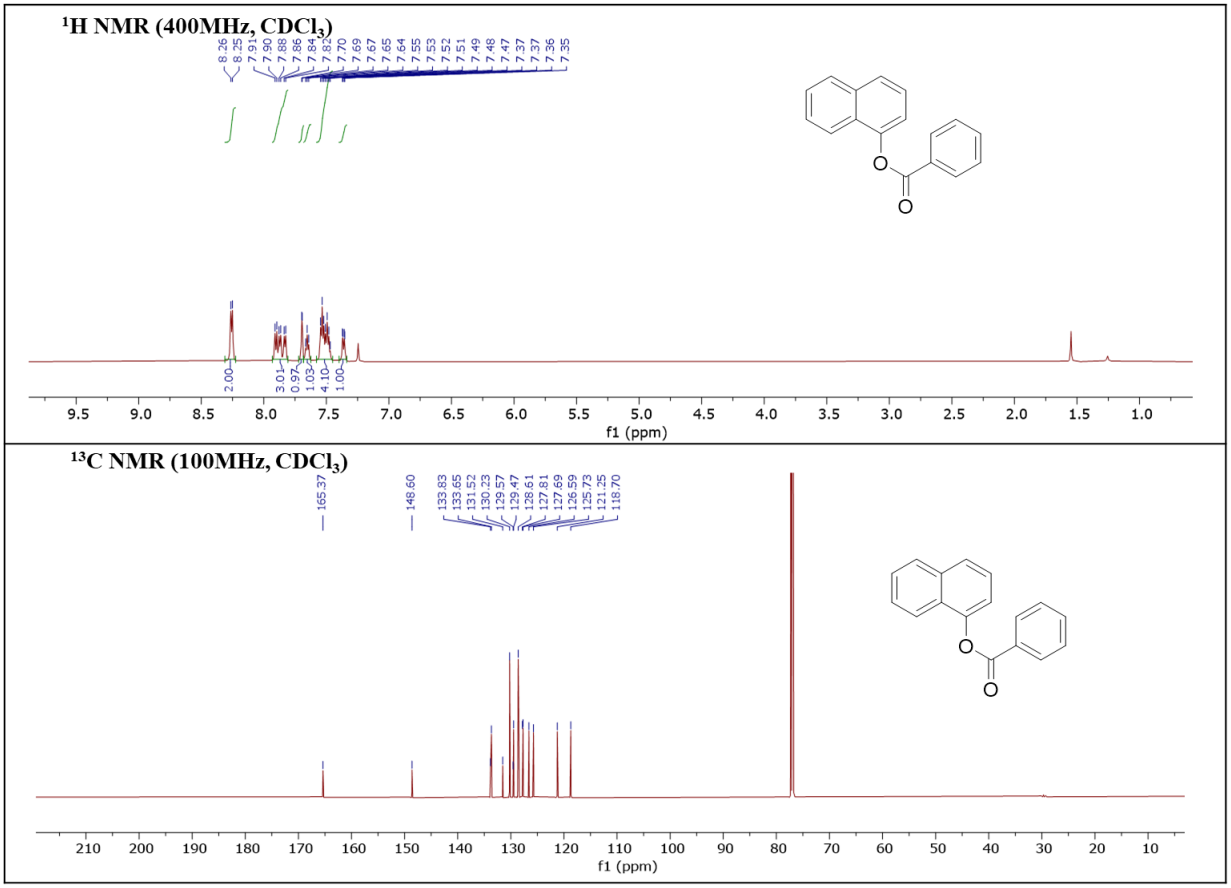

NMR DATA FOR 2.3h

2,6-dimethylphenyl benzoate: ^{1}H NMR (600 MHz, $CDCl_3$) δ 8.18 (d, *J* = 7.68 Hz, 2H), 7.58 (t, *J* = 7.44 Hz, 1H), 7.46 (t, *J* = 7.77 Hz, 2H), 7.05-7.00 (m, 3H), 2.12 (s, 6H). ^{13}C NMR (100 MHz, $CDCl_3$) δ 164.38, 148.35, 133.59, 130.38, 130.20, 129.33, 128.65, 128.63, 125.93, 16.40.

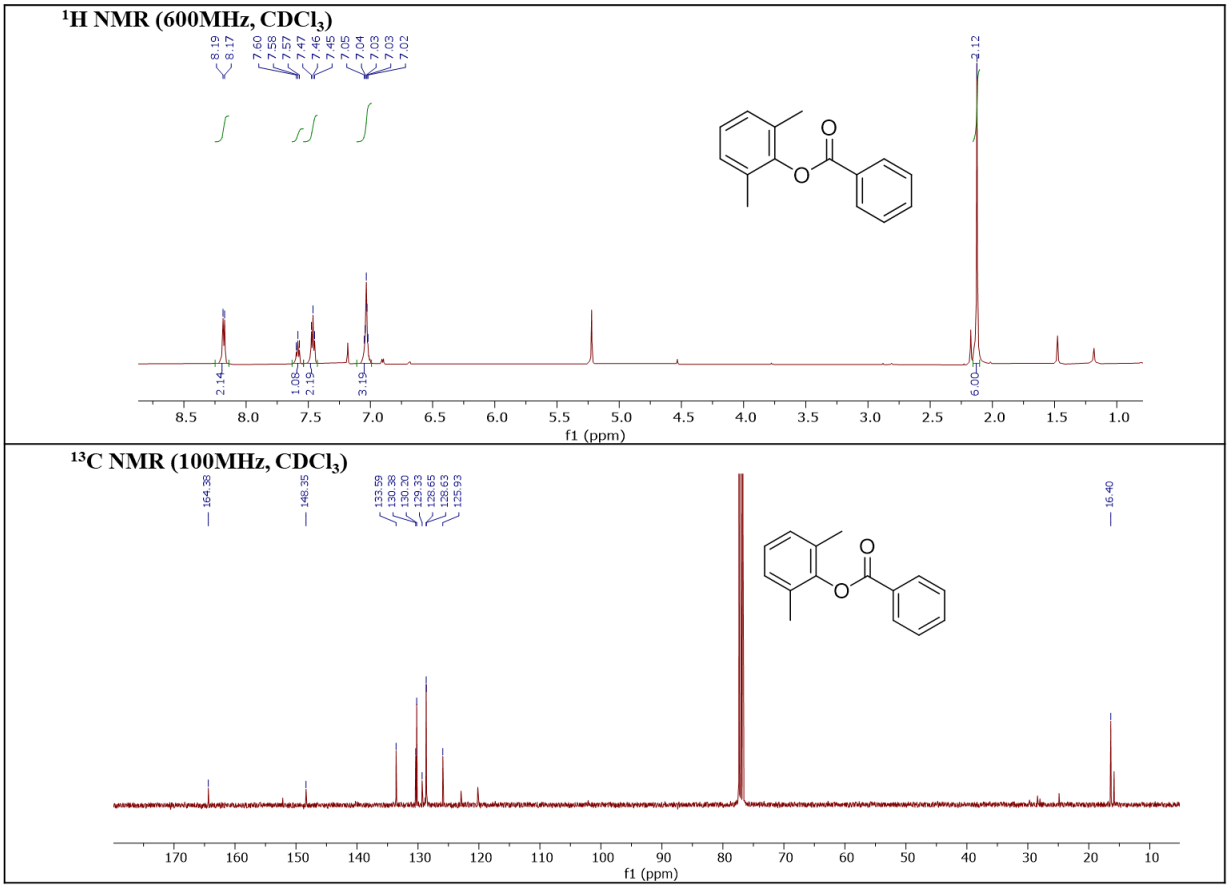

NMR DATA FOR 2.3i

<u>2-Nitrobenzyl Benzoate</u>: ^{1}H NMR (600 MHz, $CDCl_3$) δ 8.14 (d, *J* = 8.28 Hz, 1H), 8.11 (d, *J* = 8.22 Hz, 1H), 7.69-7.65 (m, 2H), 7.60 (d, *J* = 7.44 Hz, 1H), 7.52-7.47 (m, 3H), 5.79 (s, 1H). ^{13}C NMR (151 MHz, $CDCl_3$) δ 165.94, 147.62, 133.81, 133.41, 132.39, 129.78, 129.57, 128.92, 128.80, 128.57, 125.13, 63.35.

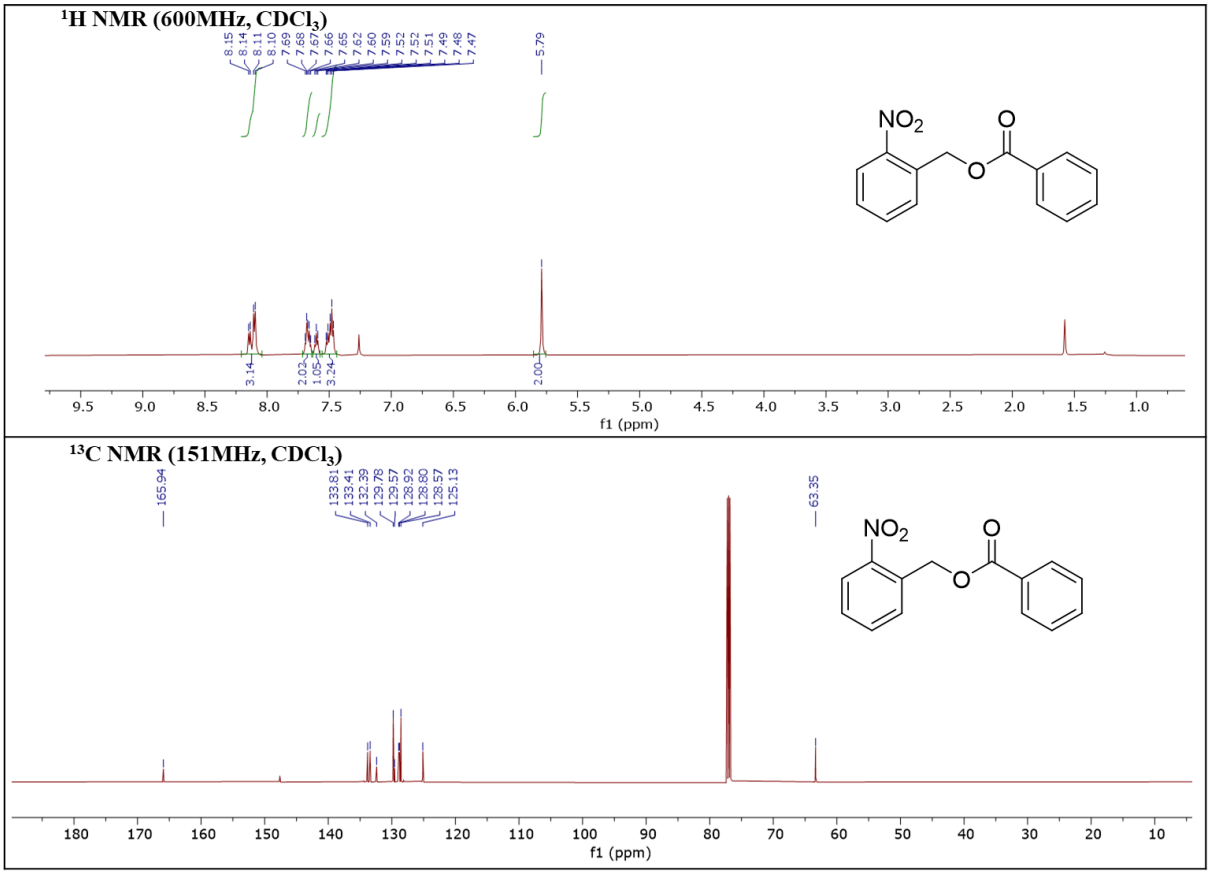

NMR DATA FOR 2.3j

<u>Benzyl Benzoate</u>:^{1}H NMR (400 MHz, $CDCl_3$) δ 8.08 (d, *J* = 7.68 Hz, 2H), 7.56 (t, *J* = 7.38 Hz, 1H), 7.46-7.33 (m, 7H), 5.38 (s, 2H). ^{13}C NMR (100 MHz, $CDCl_3$) δ 166.61, 136.24, 133.19, 130.32, 129.88, 128.77, 128.54, 128.41, 128.33, 66.86.

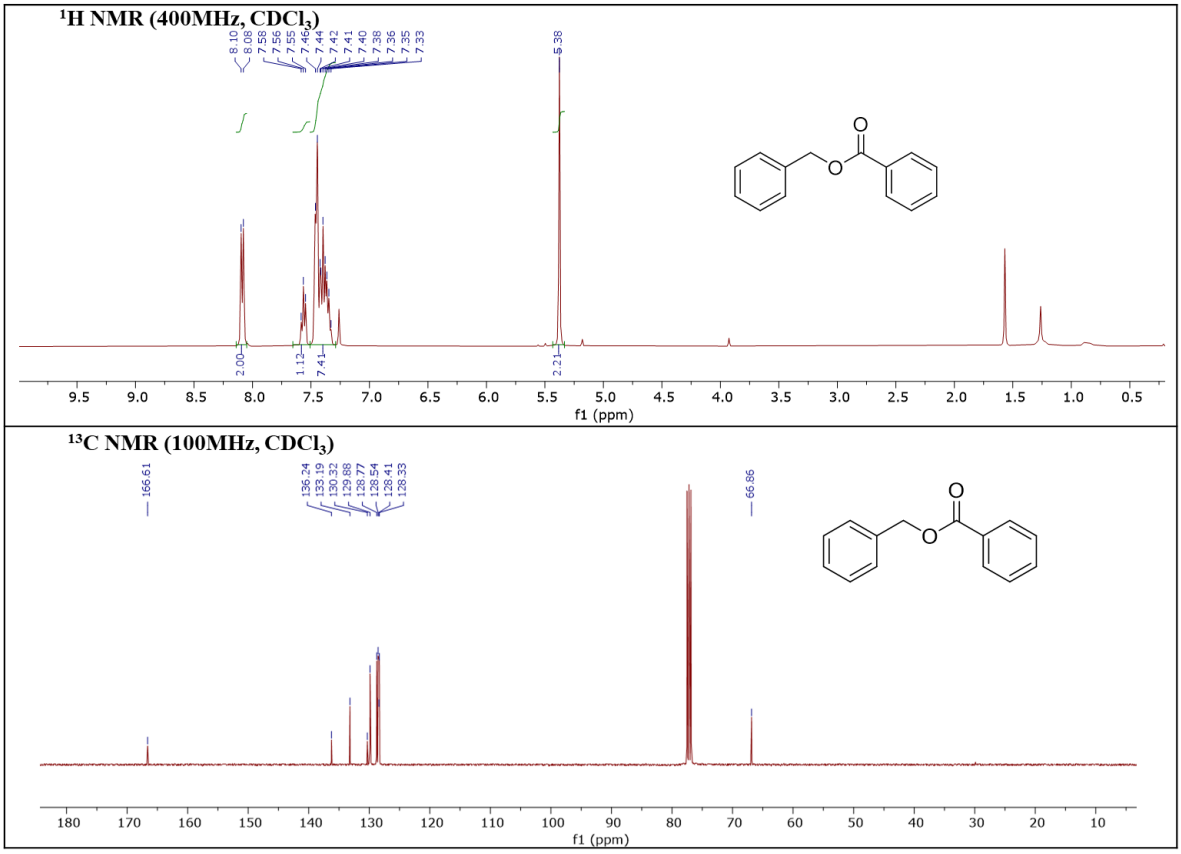

Experimental Details for Nucleophilic Addition of Twisted Peptides

Synthesis of Twisted Peptides by Thiocarbonyl Insertion

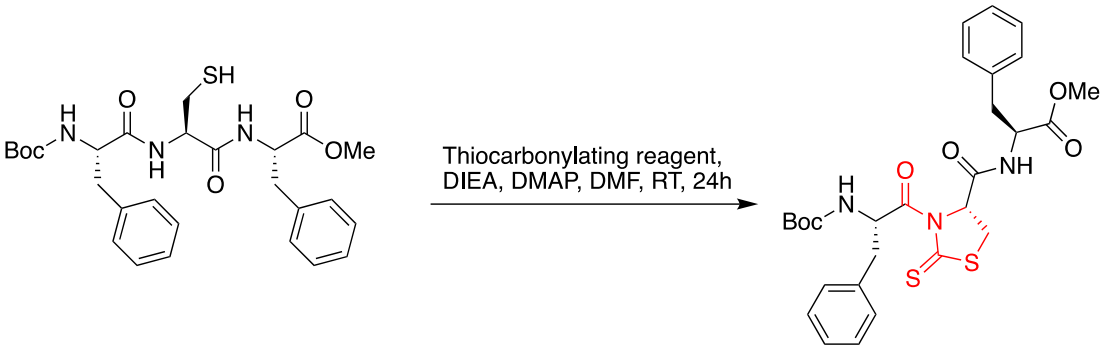

Thiocarbonylating reagent (equiv.)	DIEA (equiv.)	DMAP (equiv.)	Product (%)
1,1'-Thiocarbonyldiimidazole (10 equiv.)	1.5	5	No product
Di (2-pyridyl) thionocarbonate (1 equiv.)	1.5	5	No product
Pentafluorophenyl chlorothionoformate (1 equiv.)	1.5	5	No product
1,1′-Thiocarbonyldi-2(1H)-pyridon (1 equiv.)	1.5	5	No product

Structures of thiocarbonylating reagents used in this study:

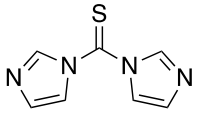
1,1'-Thiocarbonyldiimidazole

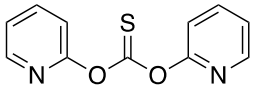
Di(2-pyridyl) thionocarbonate

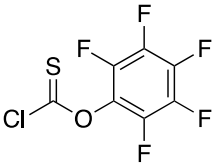
Pentafluorophenyl chlorothionoformate

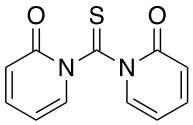
1,1′-Thiocarbonyldi-2(1H)-pyridon

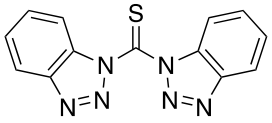
Bis(1-benzotriazolyl)methanethione

Procedure of thiocarbonyl addition in peptide using side chain of cysteine in solution phase.

To a solution of a peptide Boc-FCF-OMe (0.0064 mmol) in DMF (1 mL) was added respective thiocarbonylating reagent (1-10 equiv.), DMAP (5 equiv.) and triethylamine (1.5 equiv.) sequentially, and the reaction mixture was stirred at room temperature for 24 h. DMF removed under reduced pressure and crude residue was analyzed using HPLC and MS to get the desired thiocarbonyl-activated amide product. The HPLC was done using a linear gradient of 0-80% of acetonitrile (0.1% FA) in water (0.1% FA) for 30 mins at room temperature and with a flow rate of 1.0

mL min^{-1} (l = 220 nm). The resulting products were characterized by LCMS. The modification to desired thiocarbonyl-activated amide product was not observed under varying above conditions.

Synthesis of Twisted Peptides by Thiocarbonyl Insertion on solid support

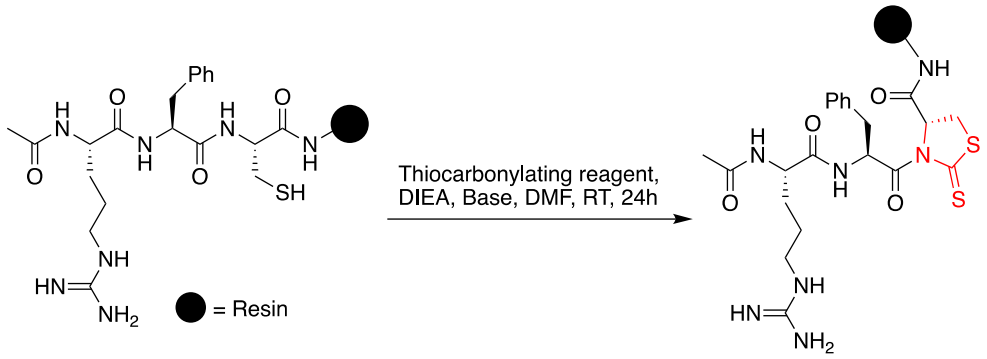

Thiocarbonylating reagent (equiv.)	DIEA (equiv.)	Base (equiv.)	Product (%)
1,1'-Thiocarbonyldiimidazole (10 equiv.)	10	DBU (10)	No product
1,1'-Thiocarbonyldiimidazole (5 equiv.)	5	DMAP (5)	< 5%
1,1'-Thiocarbonyldiimidazole (10 equiv.)	10	NaH (10)	No product
Di (2-pyridyl) thionocarbonate (10 equiv.)	10	NaH (10)	No product
Di (2-pyridyl) thionocarbonate (5 equiv.)	5	DMAP (5)	No product
Pentafluorophenyl chlorothionoformate (5 equiv.)	5	DMAP (5)	No product
Bis(1-benzotriazolyl)methanethione (1 equiv.)	1.5	DMAP (5)	No product
Bis(1-benzotriazolyl)methanethione (5 equiv.)	5	DMAP (5)	No product
1,1′-Thiocarbonyldi-2(1H)-pyridon (10 equiv.)	10	DBU (10)	No product
1,1′-Thiocarbonyldi-2(1H)-pyridon (5 equiv.)	10	DBU (5)	< 5%

Procedure of thiocarbonyl addition in peptide using side chain of cysteine on solid support.

Peptide AcO-RFC-solid support was synthesized on a 0.5 mmol scale by Fmoc solid phase peptide synthesis on a rink amide resin. To 50 mg of the peptide on solid support, a mixture of thiocarbonylating reagent (1-10 equiv.), DIEA (1.5-10 equiv.) and base (DMAP/DBU/NaH) (5-10 equiv.) dissolved in DMF (3 mL) was added. The resin with solution was left to shake on a hand wrist shaker in the solid phase tube for 24 h. The resulting modified peptide was cleaved from the resin using a cocktail of 95:2.5:2.5, trifluoroacetic acid: triethylsilane: water for 2 h. The resin was removed by filtration and the resulting solution was concentrated. The residue was diluted with ACN/water mixture. The crude residue was analyzed using HPLC and MS. The HPLC was done using a linear gradient of 0-80% of

acetonitrile (0.1% FA) in water (0.1% FA) for 30 mins at room temperature and with a flow rate of 1.0 mL min^{-1} (l = 220 nm). The resulting products were characterized by LCMS. The modification to desired thiocarbonyl-modified peptide was not observed under varying above conditions.

Synthesis of Twisted Peptide 2.4.

2.4

Peptide OAc-FSF was synthesized on a 0.5 mmol scale by Fmoc solid phase peptide synthesis on a rink amide resin. A mixture of DSC (20 equiv.), DIEA (20 equiv.) and DMAP (7 equiv.) dissolved in dry DMF (10 mL) was added to the resin loaded with the peptide. The resin with solution was left to shake on a hand wrist shaker in the solid phase tube for 16 h. The resulting modified peptide was cleaved from the resin using a cocktail of 95:2.5:2.5, trifluoroacetic acid: triethylsilane: water for 2 h. The resin was removed by filtration and the resulting solution was concentrated. The residue was diluted with ACN/water mixture. Efficient synthesis of the twisted peptide AcFOxaF **2.4** was confirmed via HPLC purification and mass spectrometry.

Procedure for transamidation of twisted peptide 2.4.

Transamidation of Twisted Peptide 2.4: To a solution of twisted peptide OAc-FOxaF **2.4** (0.0064 mmol) in DMF (1 mL) was added respective amine (5 equiv.), and triethylamine (5 equiv.) sequentially, and the reaction mixture was stirred at room temperature for 16 h. DMF removed under reduced pressure and crude residue was purified using HPLC to get the desired amide product. The HPLC was done using a linear gradient of 0-80% of Acetonitrile in water for 30 mins

at room temperature and with a flow rate of 1.0 mL min^{-1}. The resulting products were characterized by LCMS.

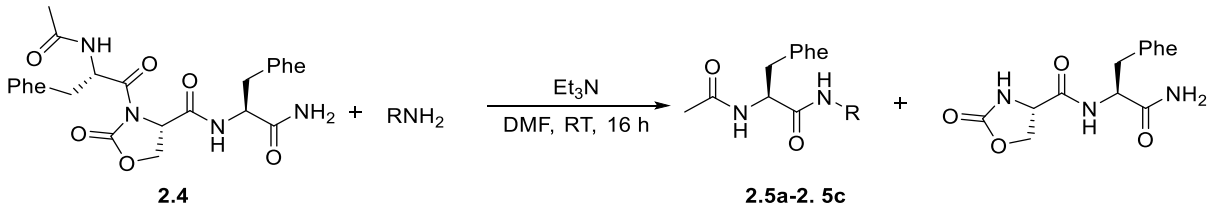

2.4 **2.5a-2. 5c**

Data for transamidation of twisted peptide 2.4.

Synthesis of 2.5a

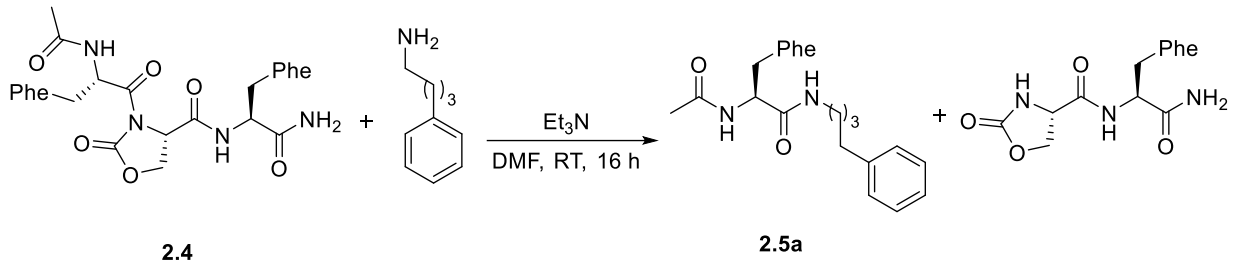

2.4 **2.5a**

5a. LCMS: *m/z* 339.20 (calcd $[M+H]^+$ = 339.20), *m/z* 361.18 (calcd $[M+Na]^+$ = 361.20), *m/z* 377.16 (calcd $[M+K]^+$ = 377.16), *m/z* 677.40 (calcd $[2M+H]^+$ = 677.40), *m/z* 699.38 (calcd $[2M+Na]^+$ = 699.40), *m/z* 715.36 (calcd $[2M+K]^+$ = 715.36), Purity: >95% (HPLC analysis at 220 nm). Retention time: 21.2 min.

HRMS spectra of 2.5a

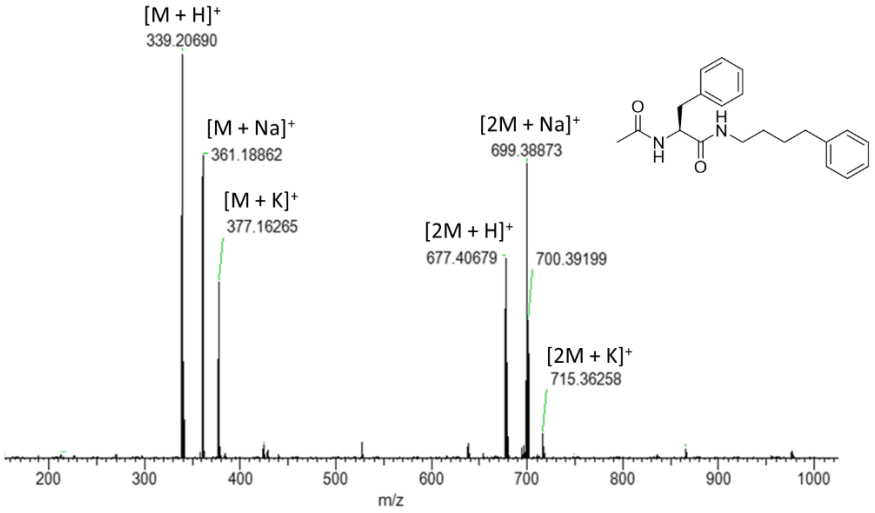

Synthesis of 2.5b

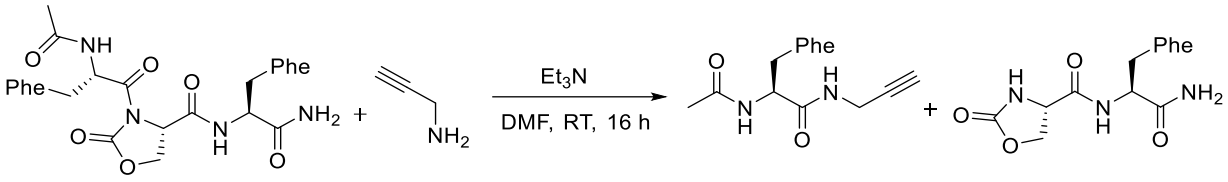

2.2 2.5b

2.5b. LCMS: *m/z* 267.11 (calcd [*M*+Na]$^+$ = 267.12), *m/z* 283.08 (calcd [*M*+K]$^+$ = 283.08), Purity: >95% (HPLC analysis at 220 nm). Retention time: 10.3 min.

HRMS spectra of 2.5b

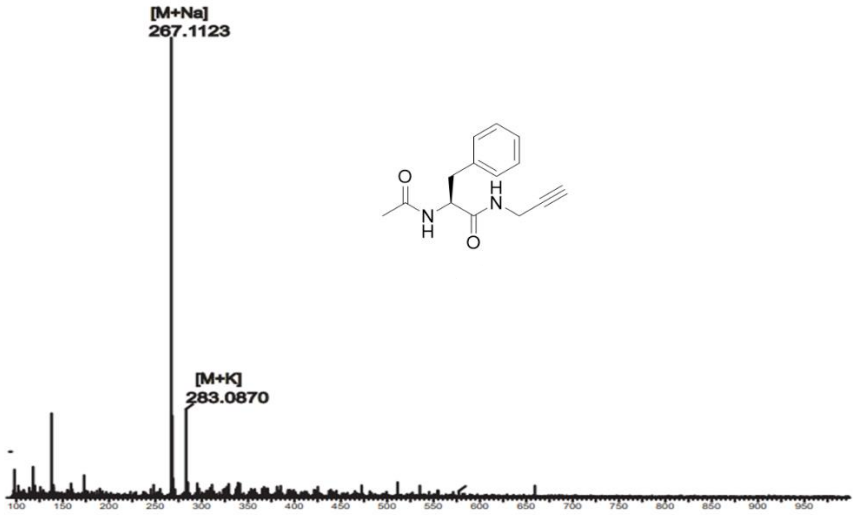

Synthesis of 2.5c

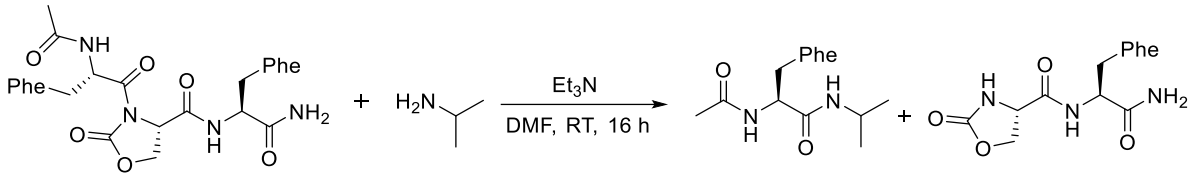

2.4 2.5c

2.5c. LCMS: *m/z* 271.14 (calcd $[M+Na]^+$ = 271.15), *m/z* 287.11 (calcd $[M+K]^+$ = 287.11), Purity: >95% (HPLC analysis at 220 nm). Retention time: 11.5 min.

HRMS spectra of 2.5c

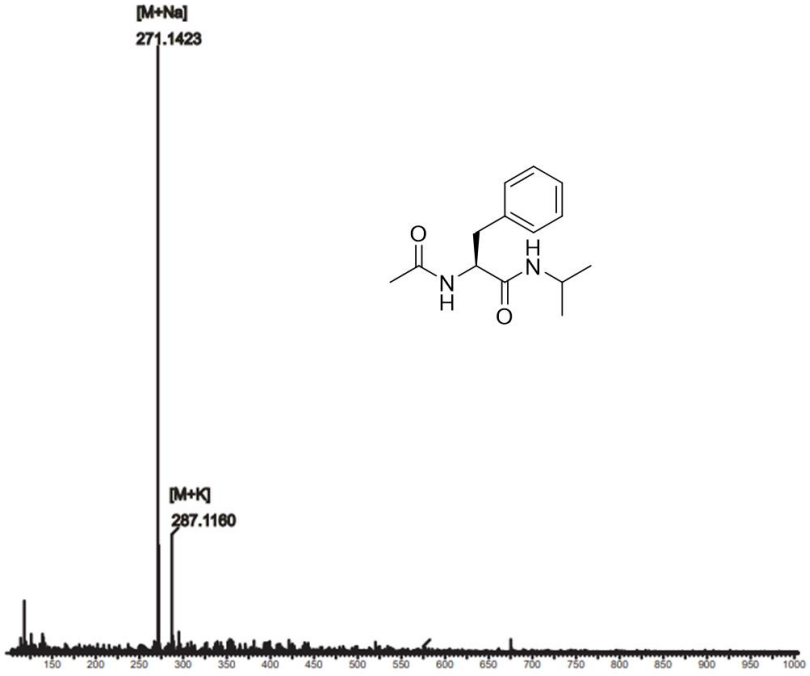

Procedure for esterification of twisted peptide 2.4.

Esterification of Twisted Peptide AcFOxaF 2.4: To a solution of twisted peptide OAc-FOxaF **2.4** (0.0064 mmol) in DMF (1 mL) was added respective alcohol (5 equiv.), and DMAP (5 equiv.) sequentially, and the reaction mixture was stirred at 50 ^{o}C for 16 h. DMF was removed under reduced pressure and crude residue was purified using HPLC. The HPLC was done using a linear gradient of 0-80% of acetonitrile in water for 30 mins at room temperature with a flow rate of 1.0 mL min^{-1} and detector wavelength of 220 nm. The resulting products were characterized by Mass Spectrometry and HPLC.

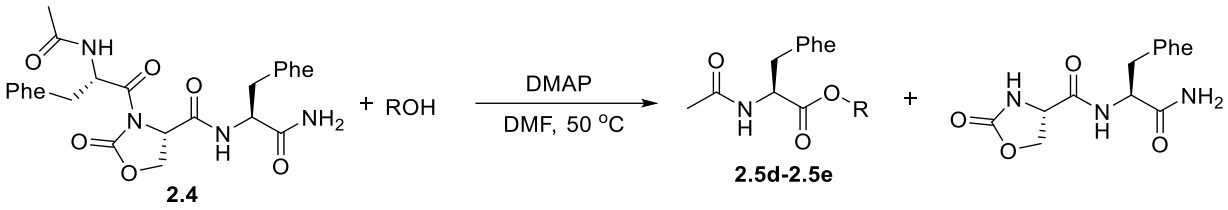

Data for Esterification of Twisted Peptides

HRMS spectra of 2.5d

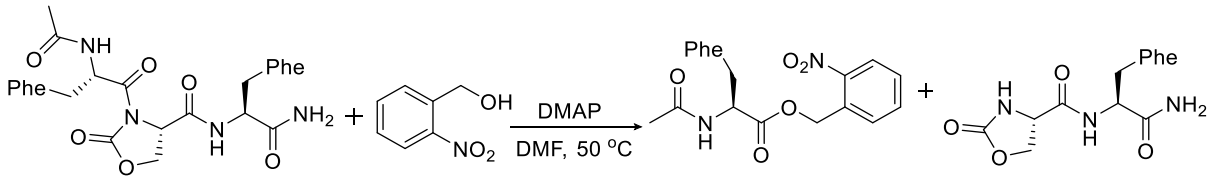

2.4 **2.5d**

2.5d. LCMS: *m/z* 342.12 (calcd $[M+H]^+$ = 343.12), *m/z* 365.11 (calcd $[M+Na]^+$ = 365.12), *m/z* 381.08 (calcd $[M+K]^+$ = 381.08) Purity: >95% (HPLC analysis at 220 nm). Retention time: 21.6 min

HRMS spectra of 2.5d

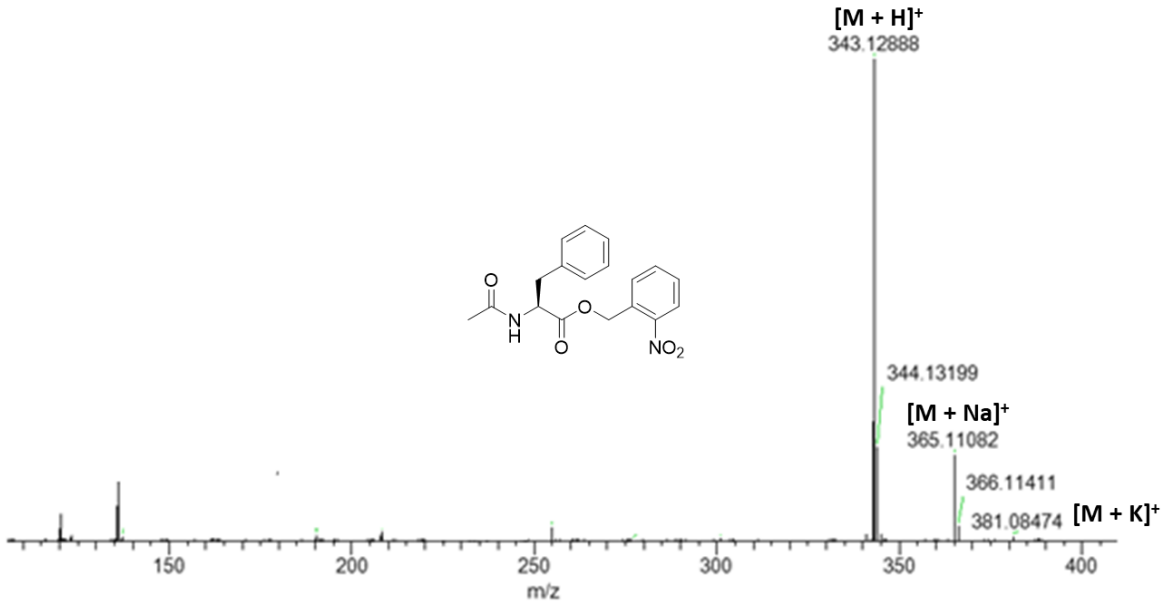

Synthesis of 2.5e

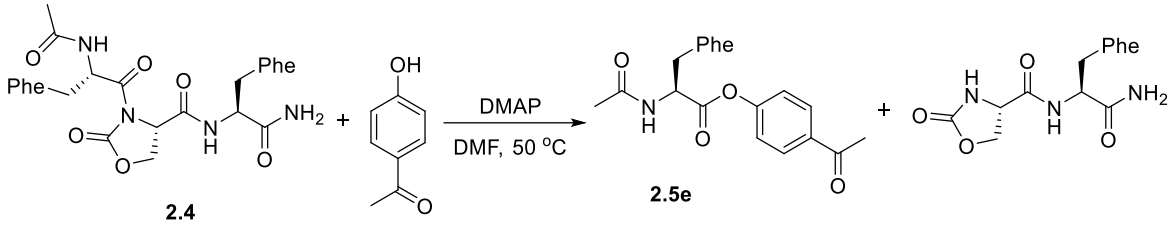

2.5e. LCMS: *m/z* 348.13 (calcd $[M+Na]^+$ = 348.12) Purity: >95% (HPLC analysis at 220 nm). Retention time: 19.3 min.

HRMS spectra of 2.5e

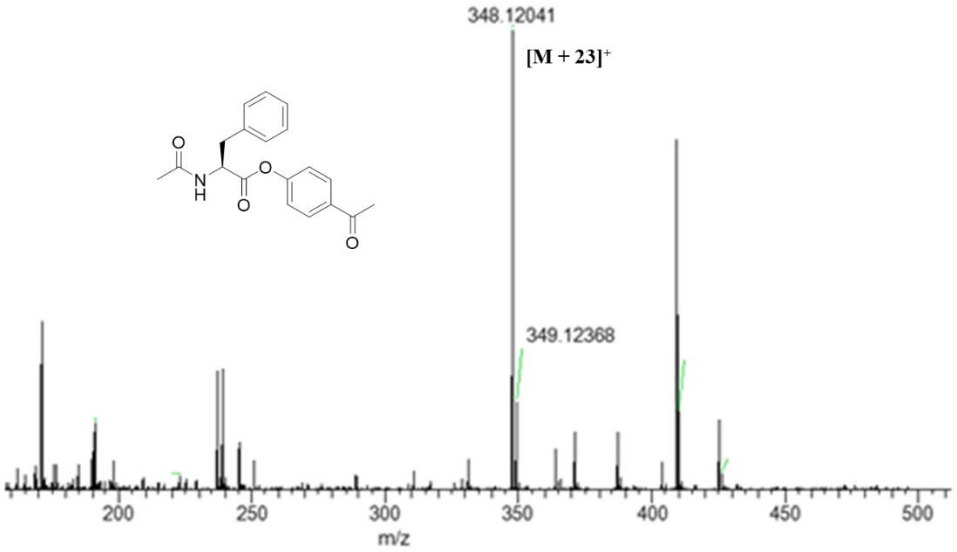

Racemization studies of amidation of twisted tetrapeptides.

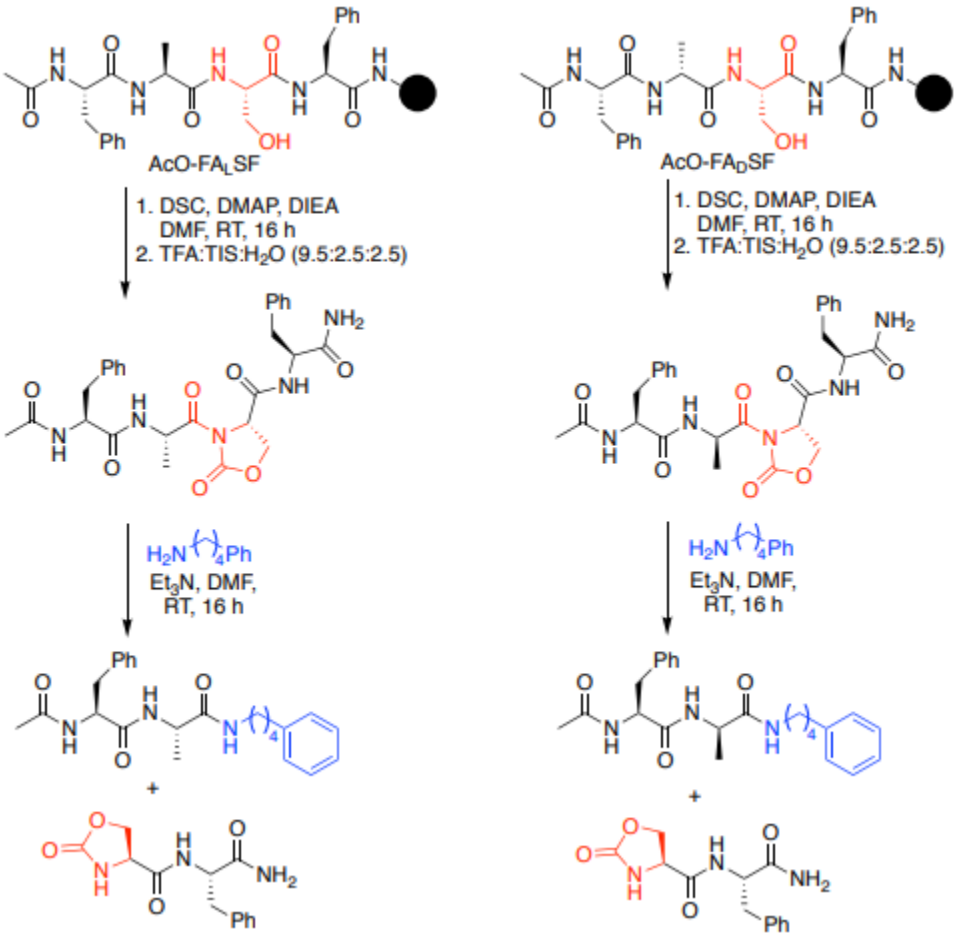

Tetrapeptides AcO-FA$_L$SF and AcO-FA$_D$SF were synthesized on a 0.5mmol scale by Fmoc solid phase peptide synthesis on a rink amide resin. A mixture of DSC (10 equiv.), DIEA (10 equiv.) and DMAP (7 equiv.) dissolved in DMF (10 mL) was added to the resin loaded with these peptides. The resins with solution were left to shake on a hand wrist shaker in the solid phase tube for 16 h. The resulting modified peptides were cleaved from the resin using a cocktail of 95:2.5:2.5, trifluoroacetic acid: triethylsilane: water for 2 h. The resins were removed by filtration and the resulting solutions were concentrated. The residues were diluted with ACN/water mixture. The twisted peptides AcO-FA$_L$OxaF and AcO-FA$_D$OxaF were purified by HPLC using a linear gradient of 0-80% of acetonitrile (0.1% FA) in water (0.1% FA) for 30 mins at room temperature and with a flow rate of 1.0 mL min^{-1}. The resulting twisted peptides AcOFA$_L$OxaF and AcO-FA$_D$OxaF were characterized by HPLC and LCMS.

AcO-FA$_L$OxaF:

LCMS of AcO-FA$_L$OxaF: m/z 538.32 (calcd $[M+H]^+$ = 538.23), m/z 1075.60 (calcd $[2M+1]^+$ = 1075.46).

HPLC AcO-FALOxaF: (C_{18}, ACN (0.1% FA)/H_2O (0.1% FA) = 0/80, flow rate = 1.0 mL/min, l = 220 nm) tR = 15.4 min. Purity: 80%, Volume ratios of elute (1.05: 1) (ACN: H_2O) 15.4 mL.

HPLC spectra of AcO-FA$_L$OxaF

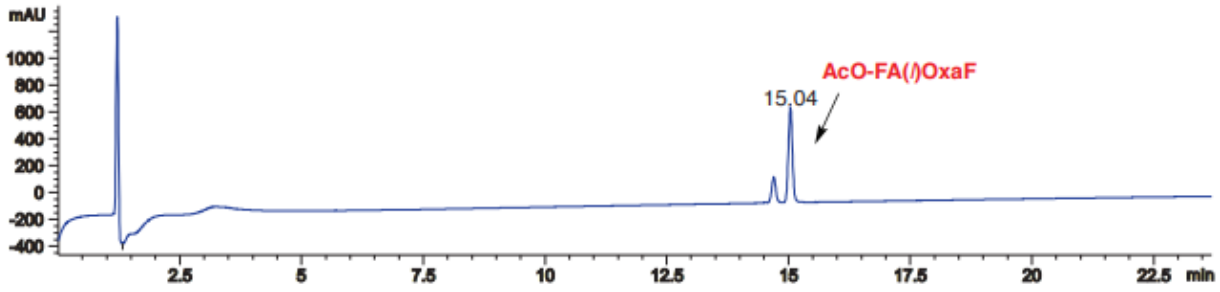

HPLC spectra of AcO-FA$_D$OxaF

HPLC AcO-FA$_D$OxaF: (C_{18}, ACN (0.1% FA)/H_2O (0.1% FA) = 0/80, flow rate = 1.0 mL/min, l = 220 nm) tR = 16.34 min. Purity: >95%, Volume ratios of elute (1.19: 1) (ACN: H_2O) 16.34mL.

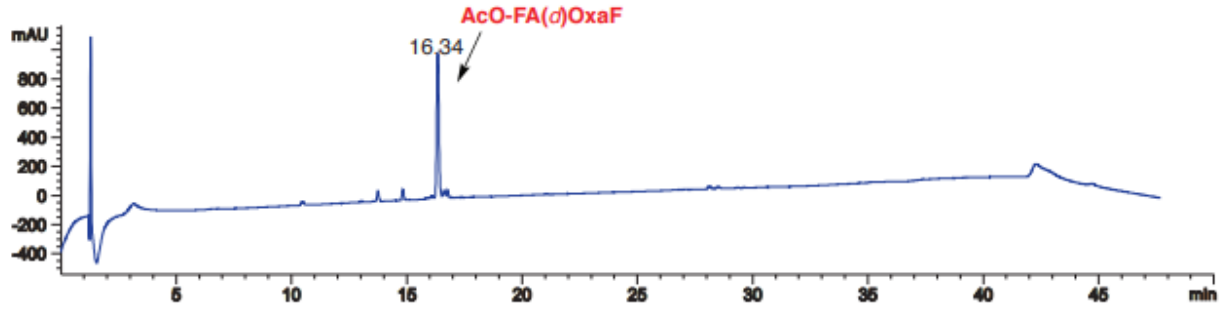

HRMS of AcO-FA$_L$OxaF

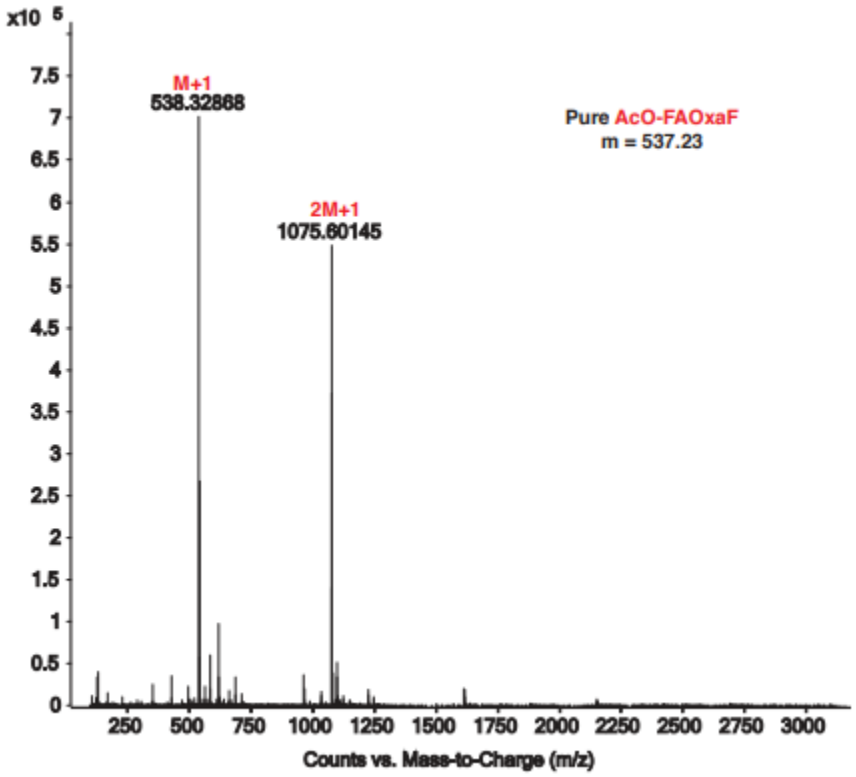

Procedure for transamidation of twisted peptides.

Transamidation of twisted peptides: To solution of twisted peptides AcO-FA$_L$**Oxa**F and AcOFA$_D$**Oxa**F (0.0064 mmol) in DMF (1 mL) was added 4-phenyl butylamine (5 equiv.), and triethylamine (5 equiv.) sequentially, and the reaction mixture was stirred at room temperature for 16 h. DMF removed under reduced pressure and crude residue was analyzed and purified using HPLC to get the desired amide products AcO-FA$_L$-4-phenyl butylamine and AcO-FA$_D$-4-phenyl butylamine. The resulting amide products AcO-FA$_L$-4-phenyl butylamine and AcO-

FA_D4-phenyl butylamine were characterized by LCMS. The amidation products were obtained with 90% conversion. No racemization was observed during the synthesis of twisted amides and formation of amidation products.

AcO-FA_L-4-phenyl butylamine:

LCMS of AcO-FA-4-phenyl butylamine: m/z 410.261 (calcd [M+H]+ = 410.116), m/z 432.244 (calcd [M+Na]+ = 432.116), m/z 819.516 (calcd [2M+1]+ = 819.232), m/z 841.498 (calcd [2M+Na]+ = 841.232).

HPLC of mixture of AcO-FA_L-4-phenyl butylamine + AcO-FA_D-4-phenyl butylamine: (C_{18}, 3 µm, 100X 4.6mm; ACN (0.1% FA)/H_2O (0.1% FA) = 43% ACN to 48% ACN in water in 30 min, flow rate = 0.5 mL/min, l = 220 nm) AcO-FA_L-4-phenyl butylamine tR = 13.4 min, AcOFA_D-4-phenyl butylamine tR = 13.6 min. Purity: >95%.

HPLC of AcO-FA_D-4-phenyl butylamine: C_{18}, 3 µm, 100X 4.6mm; ACN (0.1% FA)/H_2O (0.1% FA) = 43% ACN to 48% ACN in water in 30 min, flow rate = 0.5 mL/min, l = 220 nm) tR = 13.8 min. Purity: >95%.

HPLC spectra of mixture of isomers AcO-FA_L-4-phenyl butylamine and AcO-FA_D-4-phenyl butylamine

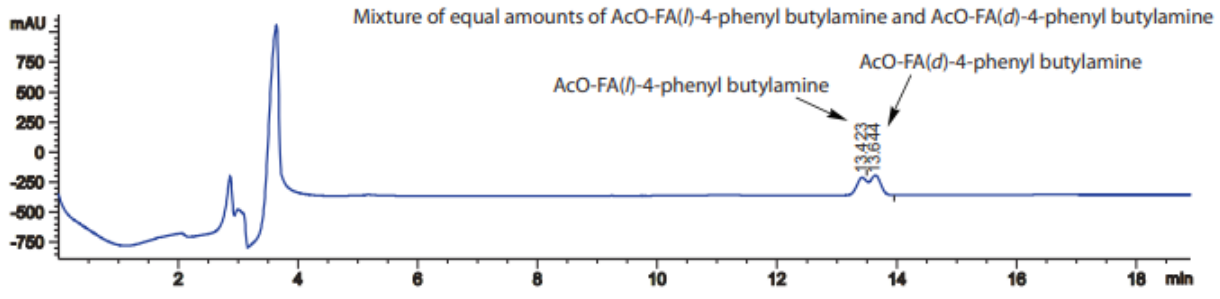

HPLC spectra of pure AcO-FA$_D$-4-phenyl butylamine

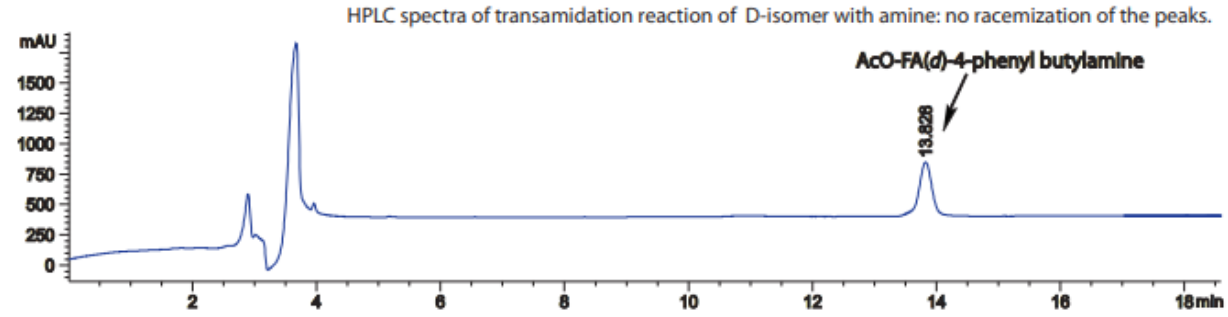

HRMS spectra of pure AcO-FA-4-phenyl butylamine.

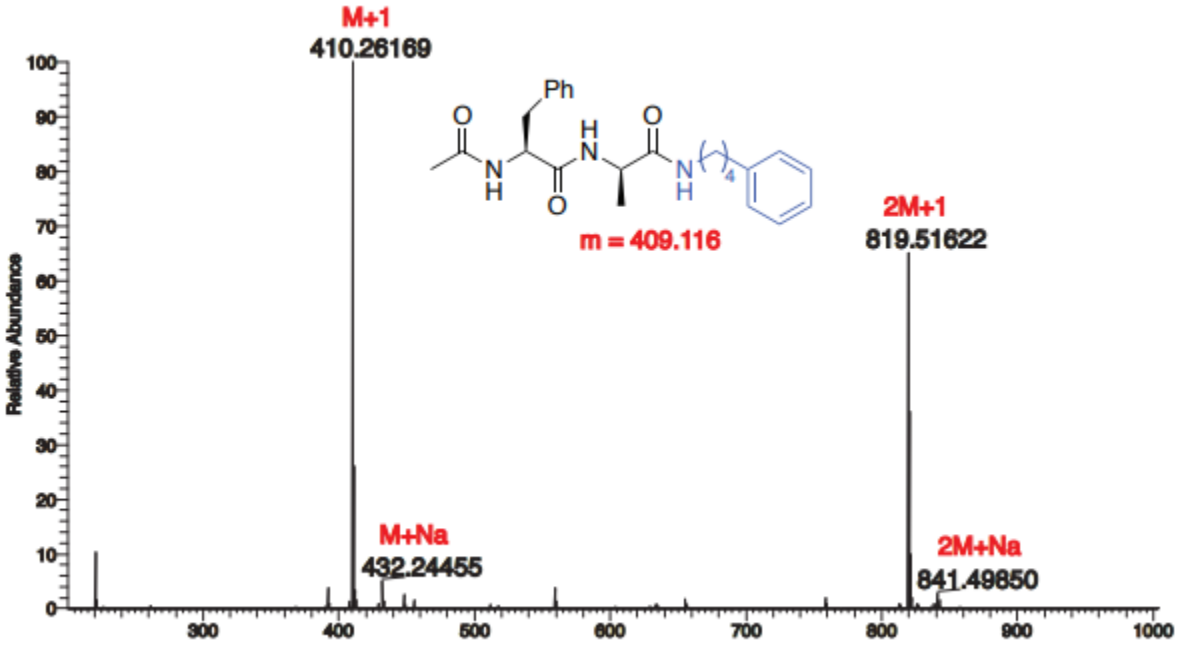

Synthesis of double twisted amide on a nonapeptide with multiple serines 2.6 followed by transamidation to generate double amidation products.

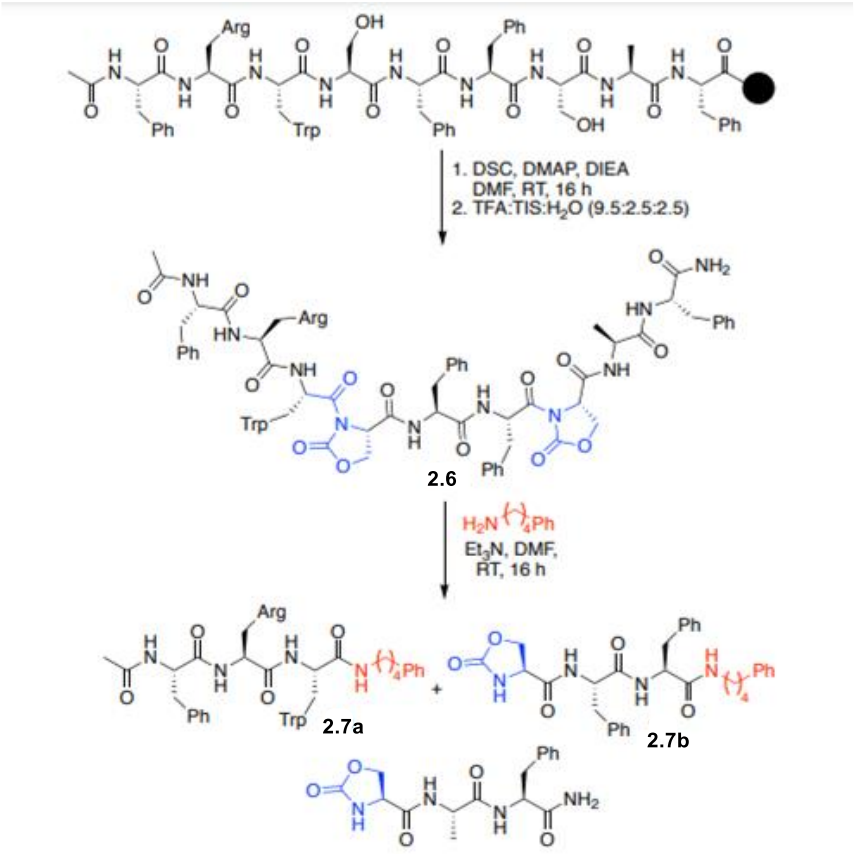

Nonapeptide AcO-FRWSFFSAF was synthesized on a 0.5 mmol scale by Fmoc solid phase peptide synthesis on a rink amide resin. A mixture of DSC (20 equiv.), DIEA (20 equiv.) and DMAP (14 equiv.) dissolved in DMF (10 mL) was added to the resin loaded with the peptide. The resin with solution was left to shake on a hand wrist shaker in the solid phase tube for 16 h. The resulting modified peptide was cleaved from the resin using a cocktail of 95:2.5:2.5, trifluoroacetic acid: triethylsilane: water for 2 h. The resin was removed by filtration and the resulting solution was concentrated. The residue was diluted with ACN/water mixture. The double twisted peptide

AcO-FRWOxaFFOxaAF **2.6** was purified by HPLC using a linear gradient of 0-80% of acetonitrile (0.1% FA) in water ((0.1% FA) for 30 mins at room temperature and with a flow rate of 1.0 mL min^{-1} . The resulting AcO-FRWOxaFFOxaAF **2.6** was characterized by LCMS. The twisted peptide AcO-FRWOxaFFOxaAF **2.6** was obtained with 80% conversion at retention time of 14.4 min.

AcO-FRWOxaFFOxaAF 2.6:

LCMS of 2.6: m/z 1287.720 (calcd $[M+H]^+$ = 1287.581), m/z 644.389 (calcd $[M+2/2]^+$ = 644.291).

HPLC of 2.6: (C_{18}, ACN (0.1% FA)/H_2O (0.1% FA) = 0/80, flow rate = 1.0 mL/min, l = 220 nm) tR = 14.4 min, Purity: >95%, Volume ratios of elute (1:1.08) (ACN: H_2O) 14.4 mL.

Procedure for transamidation of twisted peptide 2.6.

Transamidation of Twisted Peptide 2.6: To a solution of twisted peptide **AcO**FRW**Oxa**FF**Oxa**AF **2.6** (0.0064 mmol) in DMF (1 mL) was added 4-phenyl butylamine (5 equiv.), and triethylamine (5 equiv.) sequentially, and the reaction mixture was stirred at room temperature for 16 h. DMF removed under reduced pressure and crude residue was purified using HPLC to get the desired amide products **2.7a** and **2.7b.** The HPLC was done using a linear gradient of 0-80% of acetonitrile (0.1% FA) in water (0.1% FA) for 30 mins at room temperature and with a flow rate of 1.0 mL min^{-1} . The resulting amide products **2.7a** and **2.7b** were characterized by LCMS. The amidation products were obtained with >99% conversion.

AcO-FRW-4-phenyl butylamine 2.7a

LCMS of 2.7a: m/z 681.418 (calcd $[M+H]^+$ = 681.259), m/z 704.404 (calcd $[M+Na]^+$ = 703.259).

HPLC of 2.7a: (C_{18}, ACN (0.1% FA)/H_2O (0.1% FA) = 0/80, flow rate = 1.0 mL/min, l = 220 nm) tR = 13.4 min. >99% conversion, Volume ratios of elute (1: 1.2) (ACN: H_2O) 13.4 mL.

OxaFF-4-phenyl butylamine 2.7b

LCMS of 2.7b: m/z 557.302 (calcd $[M+H]^+$ = 557.168), m/z 595.259 (calcd $[M+K]^+$ = 595.168), m/z 1113.596 (calcd $[2M+1]^+$ = 1113.336), m/z 1151.553 (calcd $[2M+K]^+$ = 1151.336).

HPLC of 2.7b: (C_{18}, ACN (0.1% FA)/H_2O (0.1% FA) = 0/80, flow rate = 1.0 mL/min, l = 220 nm) tR = 18.3 min. >99% conversion, Volume ratios of elute (1.56: 1) (ACN: H_2O) 18.3 mL.

HPLC traces of pure 6 and after transamidation reaction with 4-phenyl butylamine.

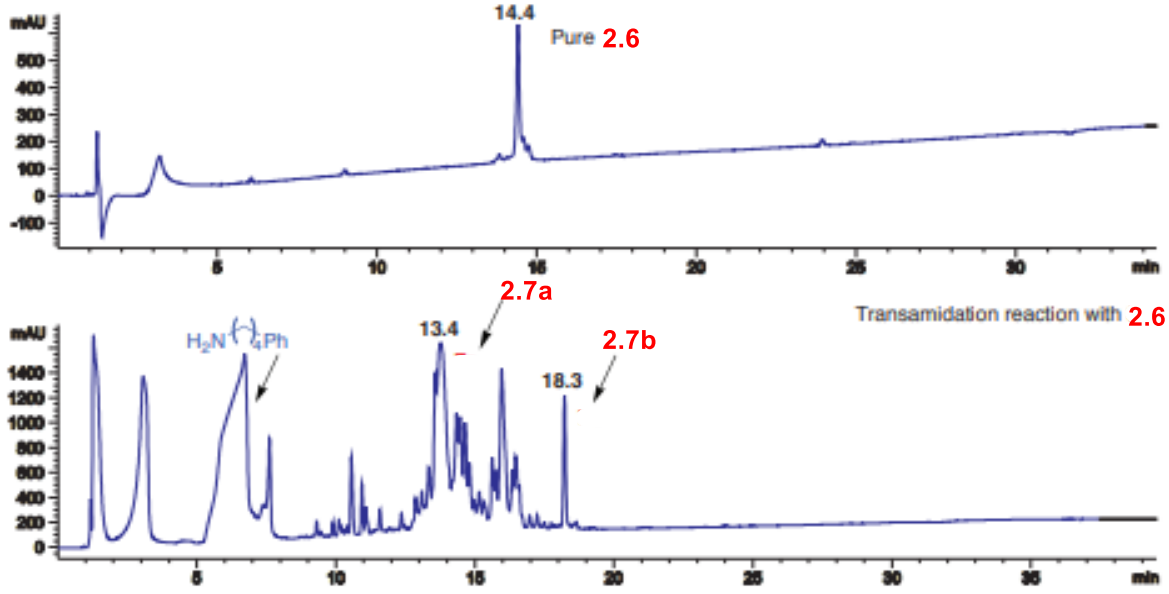

HRMS of pure 2.6

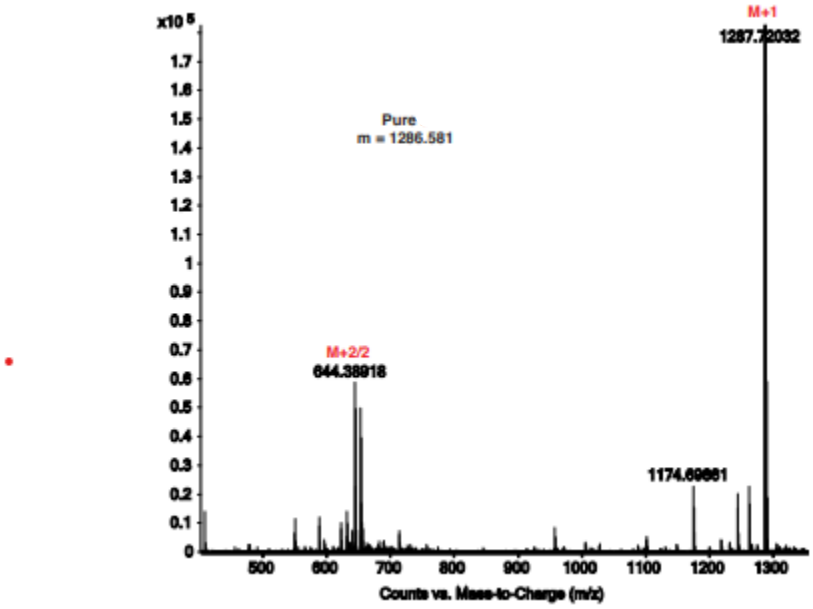

HRMS of transamidation product 2.7a

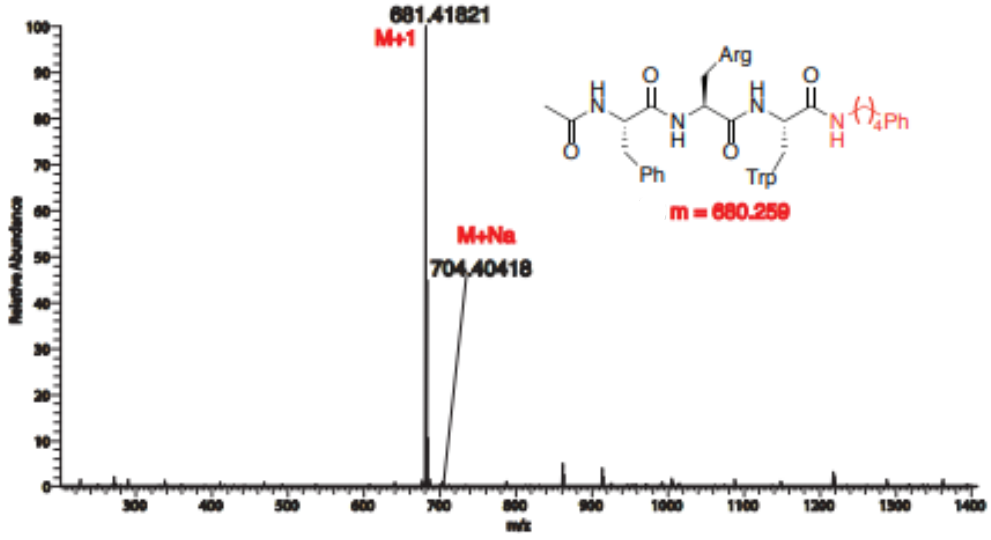

HRMS of transamidation product 2.7b

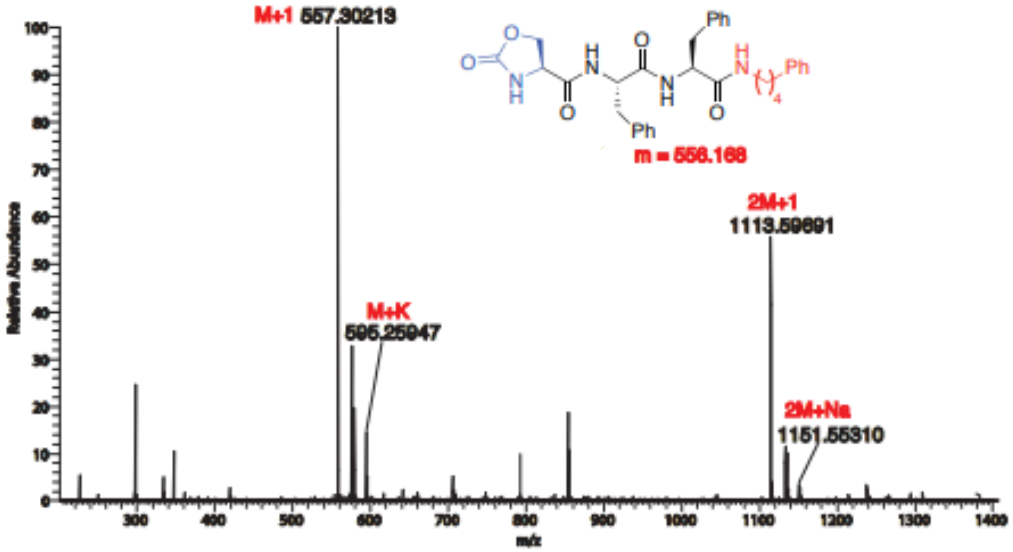

Experimental Detail for Suzuki Reaction

Optimization of Reaction Conditions for Suzuki Reaction

General Procedure for Suzuki reactions.

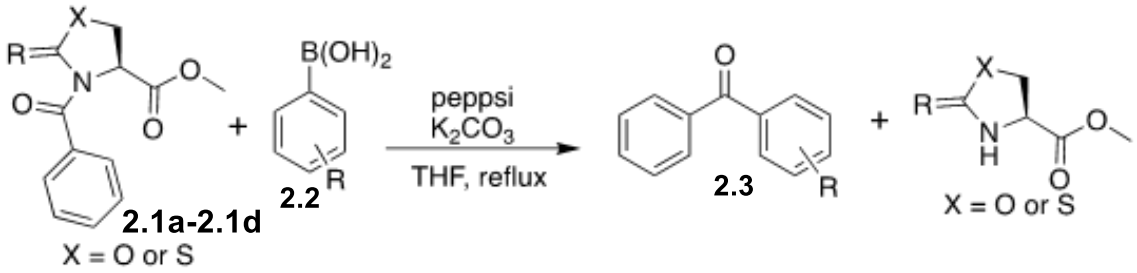

To a solution of twisted amide **2.1a-2.1d** (17.43-19.67 mg, 0.07 mmol) in dry THF (5 mL) was added respective arene boronic acid (2 eq.), potassium carbonate (3 eq.), and Pd-peppsi catalyst (0.4 eq.) in one portion under inert atmosphere and the reaction mixture was sealed and stirred at reflux conditions for overnight. Volatiles removed under reduced pressure and crude residue was purified by column chromatography using mixture of ethyl acetate and hexane (1:4) as an eluent to get the desired ketone product **2.10**. The resulting products were characterized by ^{1}H NMR and ^{13}C-NMR.

Control Reaction with unmodified analog 2E

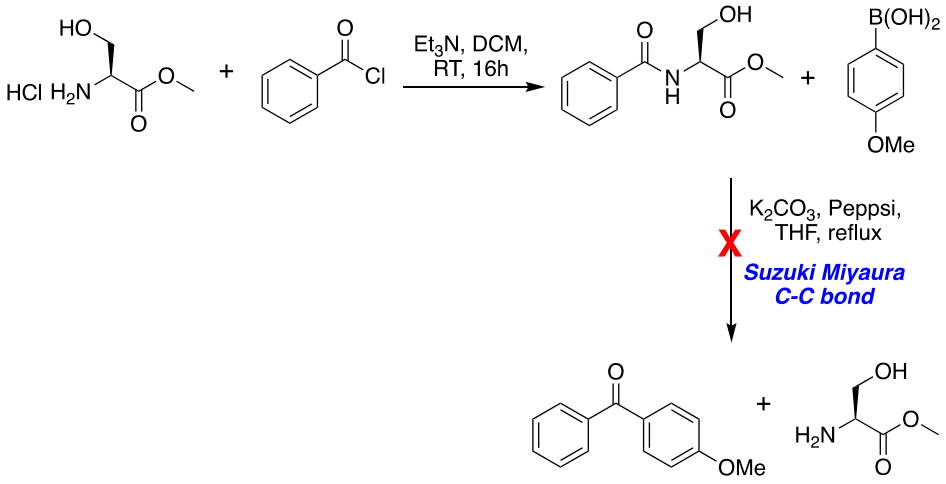

NMR DATA FOR SUZUKI REACTIONS

NMR Data for Compound 2.10a[6]

(4-methoxyphenyl)(phenyl)methanone 2.10a: ^{1}H NMR (500 MHz, $CDCl_3$) δ 7.83 (d, *J* = 8.6 Hz, 2H), 7.76 (d, *J* = 7.9 Hz, 2H), 7.57 (t, *J* = 7.3 Hz, 1H), 7.47 (t, *J* = 7.5 Hz, 2H), 6.97 (d, *J* = 8.6 Hz, 2H), 3.89 (s, 3H). ^{13}C NMR (126 MHz, $CDCl_3$) δ 195.5, 163.2, 138.3, 132.5, 132.0, 131.9, 129.7, 128.2, 113.5, 55.6. white solid; **2.10a** product from **2.1b** (10.38 mg) 70% yield; **2.10a** from **2.1d** (9.79 mg) 66% yield.

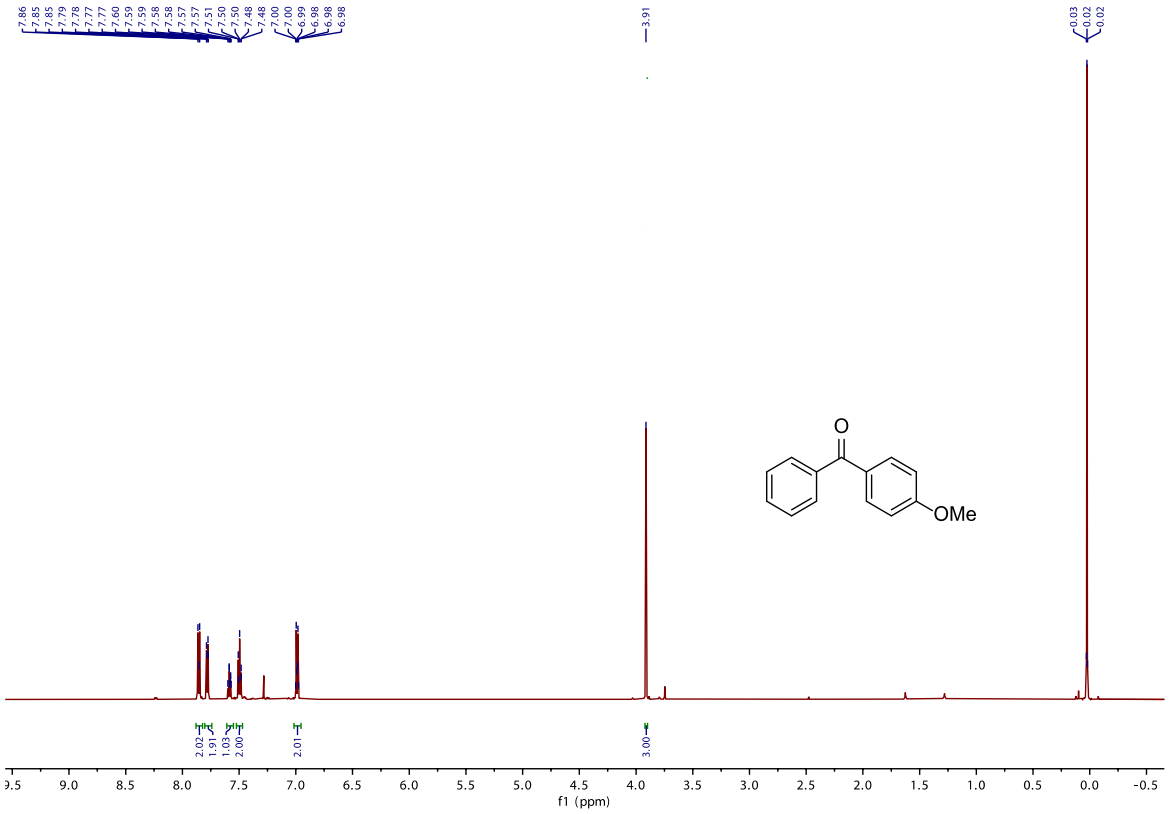

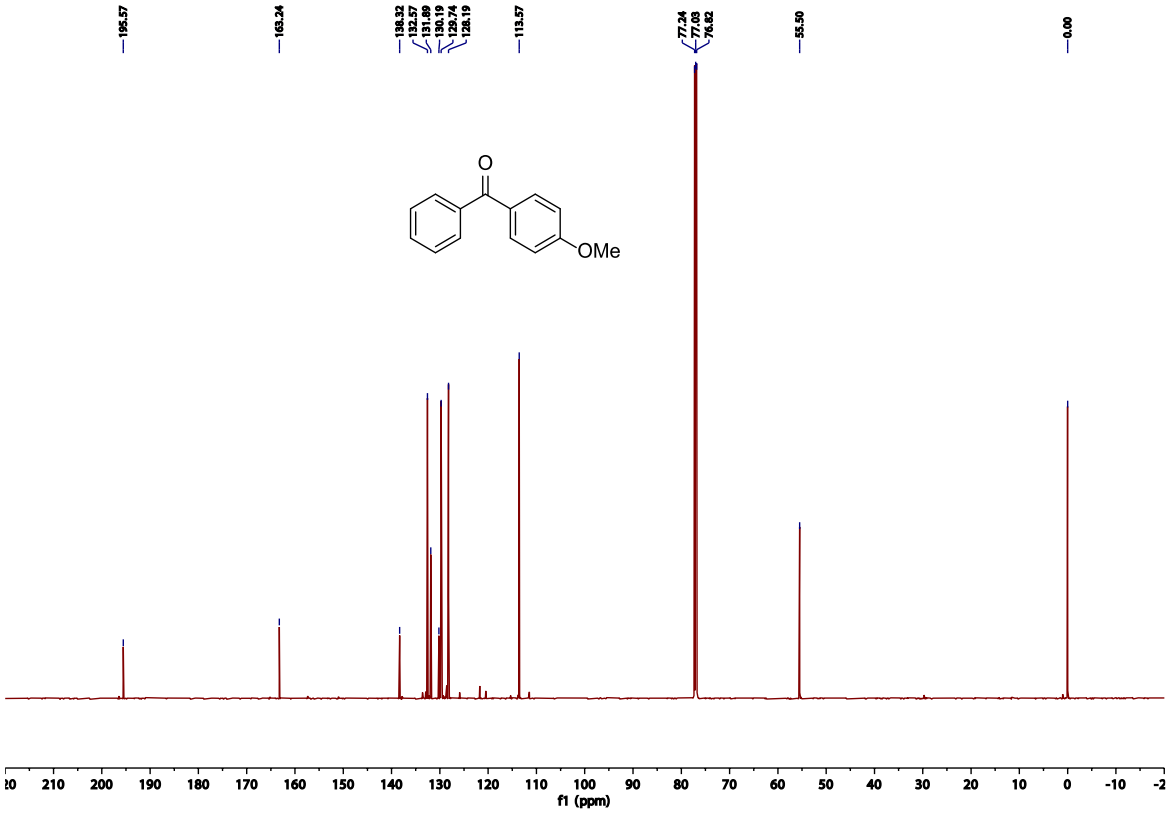

NMR Data for Compound 2.10b[6]

Benzophenone 2.10b: ^{1}H NMR (600 MHz, $CDCl_3$) δ 7.82 (d, *J* = 7.1 Hz, 2H), 7.60 (t, *J* = 7.4 Hz, 1H), 7.52 (t, *J* = 7.7 Hz, 2H). ^{13}C NMR (151 MHz, $CDCl_3$) δ 196.7, 137.6, 132.4, 130.0, 128.2. white solid; **2.10b** product from **2.1b** (8.92 mg) 70% yield; **2.10b** from **2.1d** (8.79 mg) 69% yield.

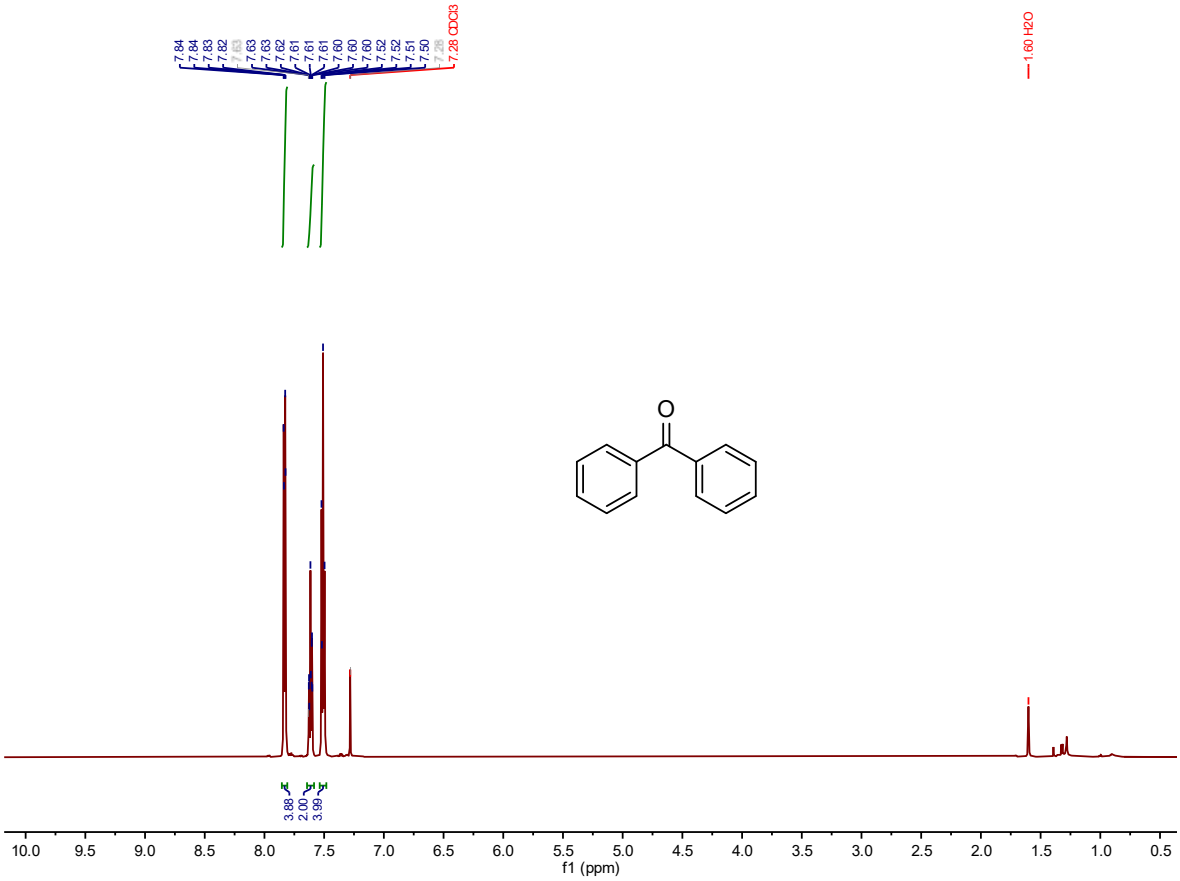
7.84
7.84
7.83
7.82
7.63
7.63
7.62
7.61
7.61
7.61
7.60
7.60
7.60
7.52
7.52
7.51
7.50
7.26 CDCl3
1.60 H2O
O
3.88
2.00
3.99
10.0
9.5
9.0
8.5
8.0
7.5
7.0
6.5
6.0
5.5
5.0
4.5
4.0
3.5
3.0
2.5
2.0
1.5
1.0
0.5
f1 (ppm)

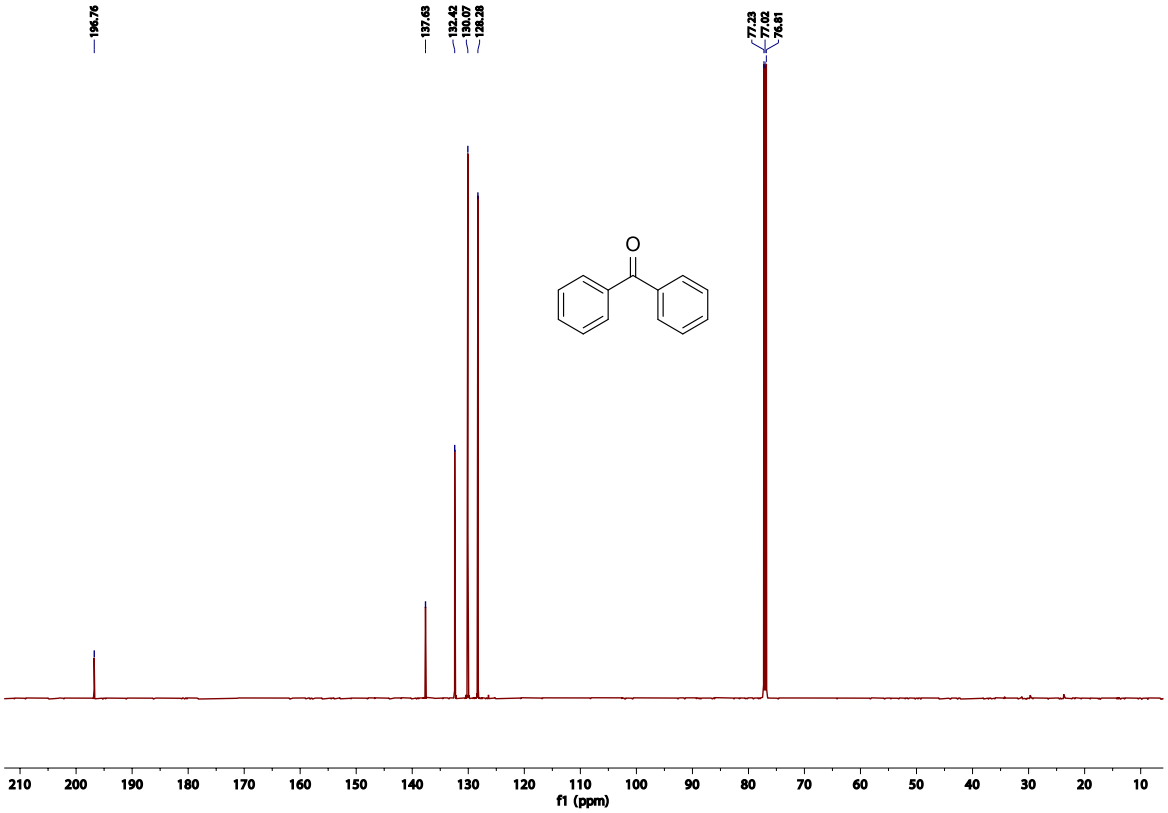
196.76
137.63
132.42
130.07
128.28
77.23
77.02
76.81
O
210
200
190
180
170
160
150
140
130
120
110
100
90
80
70
60
50
40
30
20
10
f1 (ppm)

NMR Data for Compound 2.10c[7]

1-(4-benzoylphenyl)ethan-1-one 2.10c: ^{1}H NMR (400 MHz, $CDCl_3$) δ 1H NMR (400 MHz, Chloroform-d) δ 8.08 – 8.04 (m, 2H), 7.90 – 7.86 (m, 2H), 7.84 – 7.80 (m, 2H), 7.68 – 7.61 (m, 1H), 7.54 – 7.48 (m, 2H), 2.68 (s, 3H). ^{13}C NMR (101 MHz, $CDCl_3$) δ 197.7, 196.1, 141.5, 139.7, 137.1, 133.1, 130.3, 130.2, 128.6, 128.3, 27.0. white solid; **2.10c** product from **2.1b** (5.64 mg) 36% yield; **2.10c** from **2.1d** (7.84 mg) 50% yield.

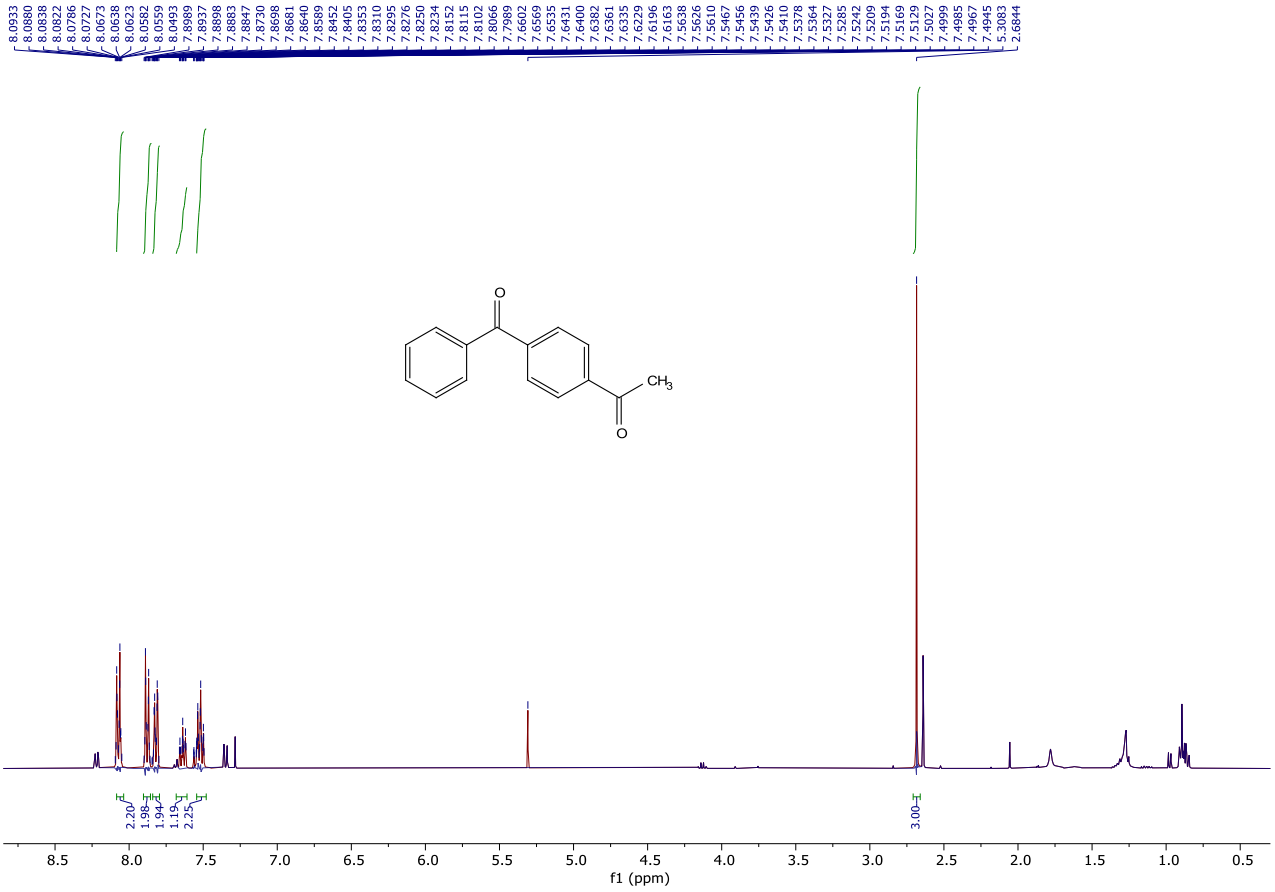

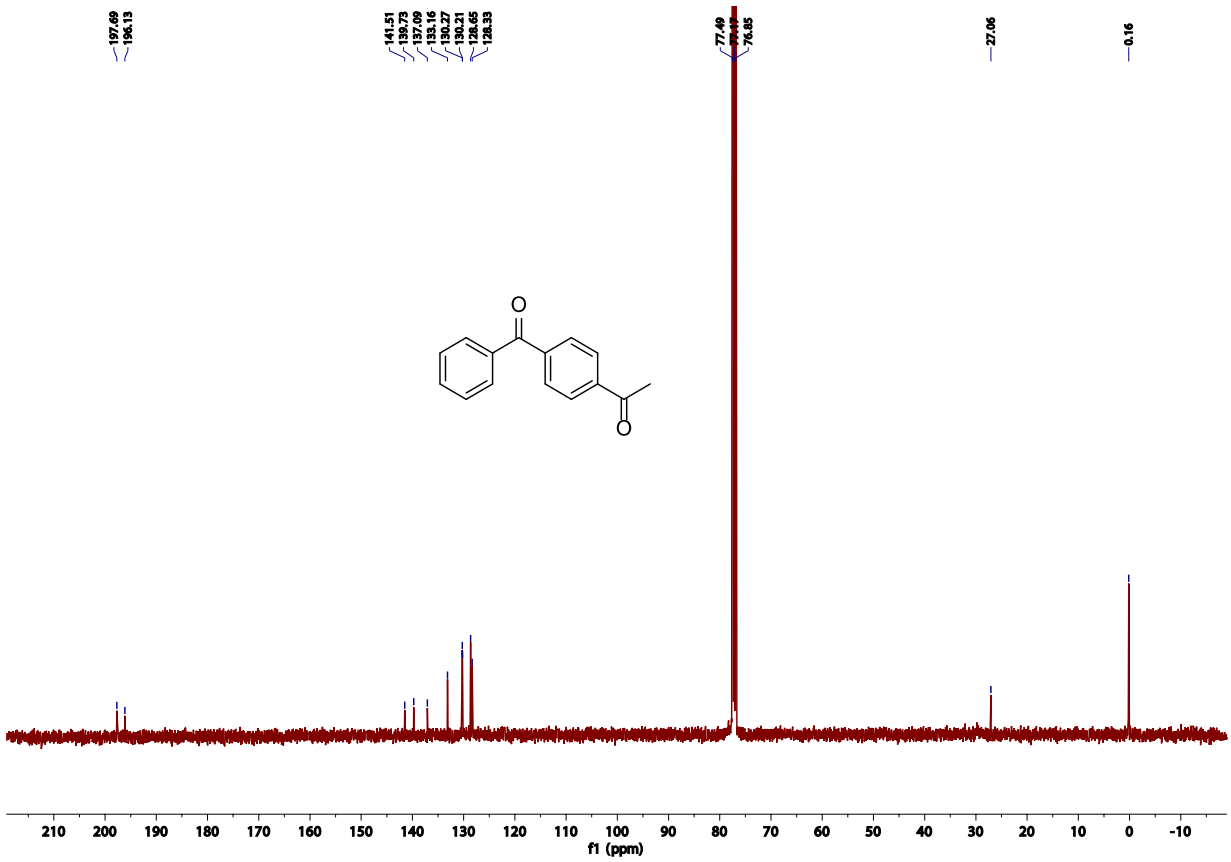
197.69
196.13
141.51
139.73
137.09
133.16
130.27
130.21
128.65
128.33
77.49
77.16
76.85
27.06
0.16
O
O
210 200 190 180 170 160 150 140 130 120 110 100 90 80 70 60 50 40 30 20 10 0 -10
f1 (ppm)

NMR Data for Compound 2.10d[8]

4-benzoylbenzonitrile 2.10d: ^{1}H NMR (400 MHz, Chloroform-d) δ 8.26 – 8.14 (m, 2H), 7.93 – 7.88 (m, 1H), 7.85 – 7.79 (m, 2H), 7.71 – 7.64 (m, 1H), 7.60 – 7.51 (m, 3H).^{13}C NMR (101 MHz, $CDCl_3$) δ 195.2, 141.4, 136.5, 133.5, 132.3, 130.4, 130.2, 128.8, 118.2, 115.8. white solid; **2.10d** product from **2.1b** (6.52 mg) 45% yield; **2.10d** from **2.1d** (5.94 mg) 41% yield.

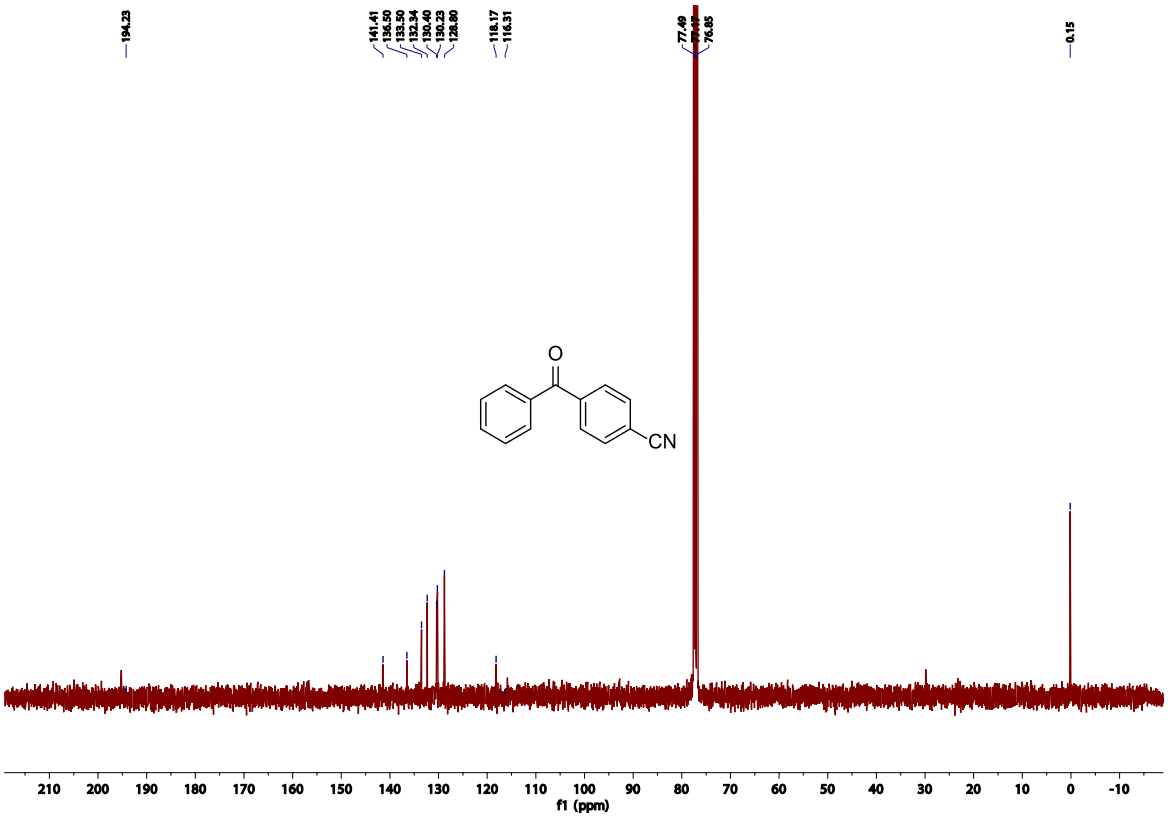

NMR data of compound 2.10e[7]

(4-nitrophenyl)(phenyl)methanone 2.10e: ^{1}H NMR (400 MHz, $CDCl_3$) δ 8.35 (d, *J* = 8.4 Hz, 2H), 7.94 (d, *J* = 8.4 Hz, 2H), 7.81 (d, *J* = 7.6 Hz, 2H), 7.66 (t, *J* = 7.3 Hz, 1H), 7.53 (t, *J* = 7.5 Hz, 2H). ^{13}C NMR (101 MHz, $CDCl_3$) δ 195.0, 150.0, 143.0, 136.4, 133.6, 130.8, 130.2, 128.8, 123.7. white solid; **2.10e** product from **2.1b** (7.46 mg) 47% yield; **2.10e** from **2.1d** (6.99 mg) 44% yield.

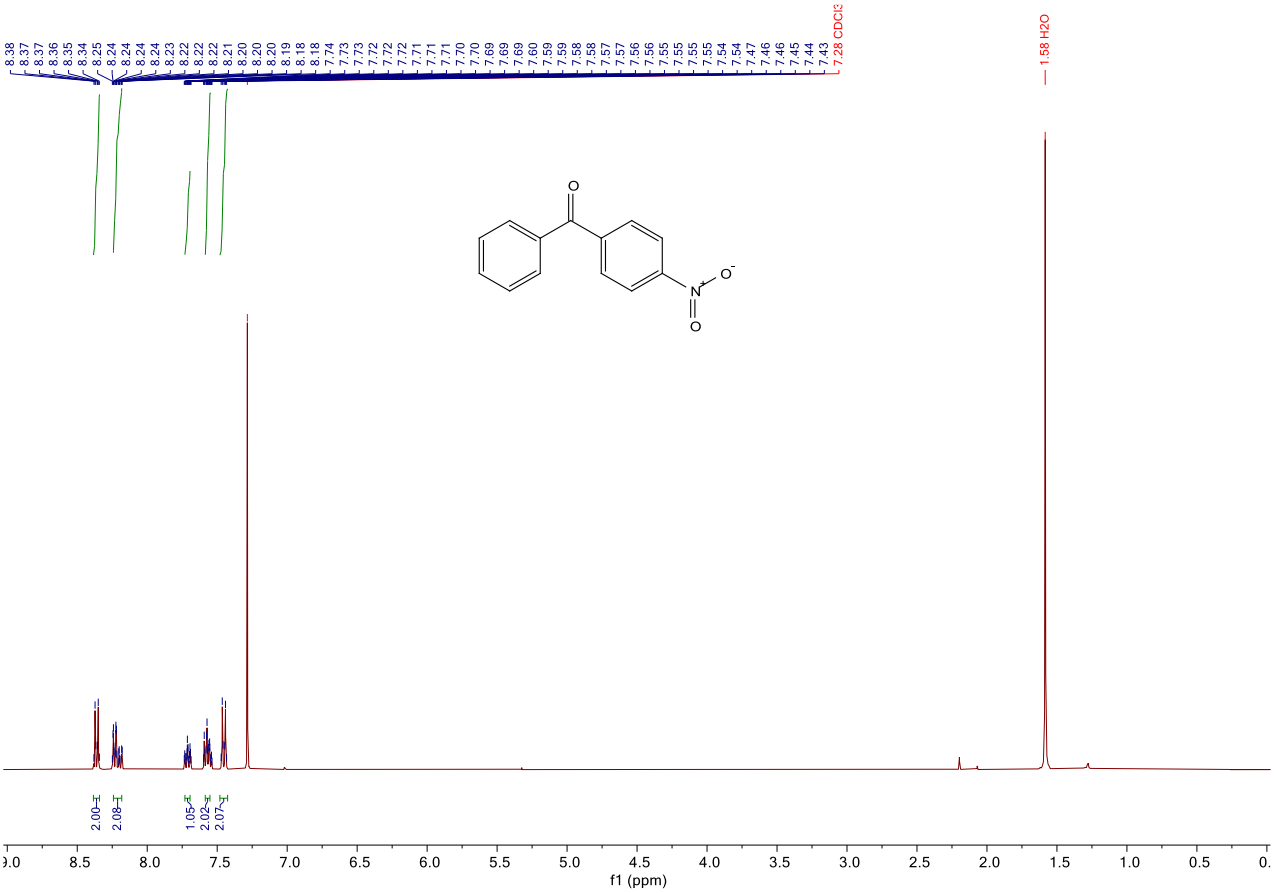

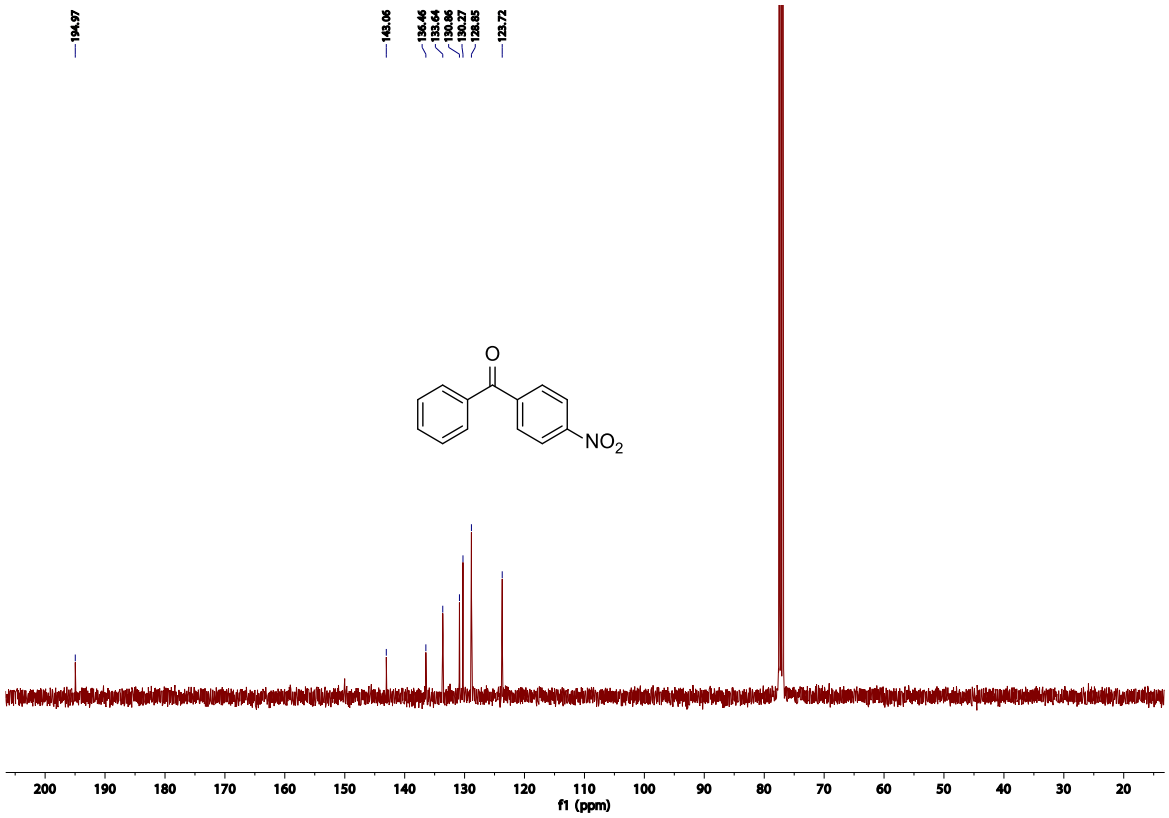
194.97
143.06
136.46
133.64
130.86
130.27
128.85
123.72
O
NO2
200
190
180
170
160
150
140
130
120
110
100
90
80
70
60
50
40
30
20
f1 (ppm)

NMR Data for Compound 2.10f[7]

(4-fluorophenyl)(phenyl)methanone 2.10f: ^{1}H NMR (500 MHz, $CDCl_3$) δ 7.85 (dd, *J* = 8.6, 5.5 Hz, 2H), 7.77 (d, *J* = 7.4 Hz, 2H), 7.60 (t, *J* = 7.4 Hz, 1H), 7.49 (t, *J* = 7.7 Hz, 2H), 7.16 (t, *J* = 8.6 Hz, 2H). ^{13}C NMR (126 MHz, $CDCl_3$) δ 195.4, 165.5 (d, *J* = 254.1 Hz), 137.6, 132.9, 132.8, 132.6, 130.0, 128.5, 115.6 (d, *J* = 22.0 Hz). ^{19}F NMR (471 MHz, $CDCl_3$) δ -106.0. white solid; **2.10f** product from **2.1b** (9.24 mg) 66% yield; **2.10f** from **2.1d** (8.4 mg) 60% yield.

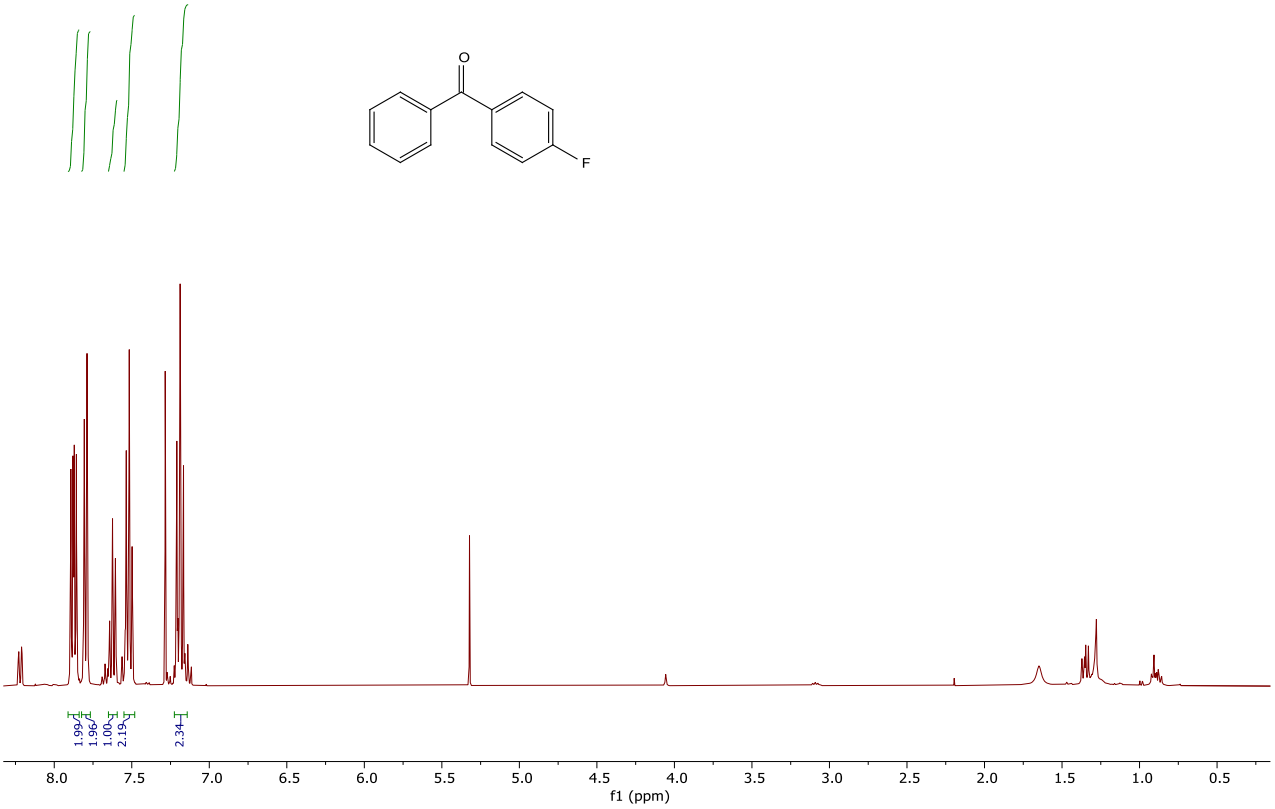

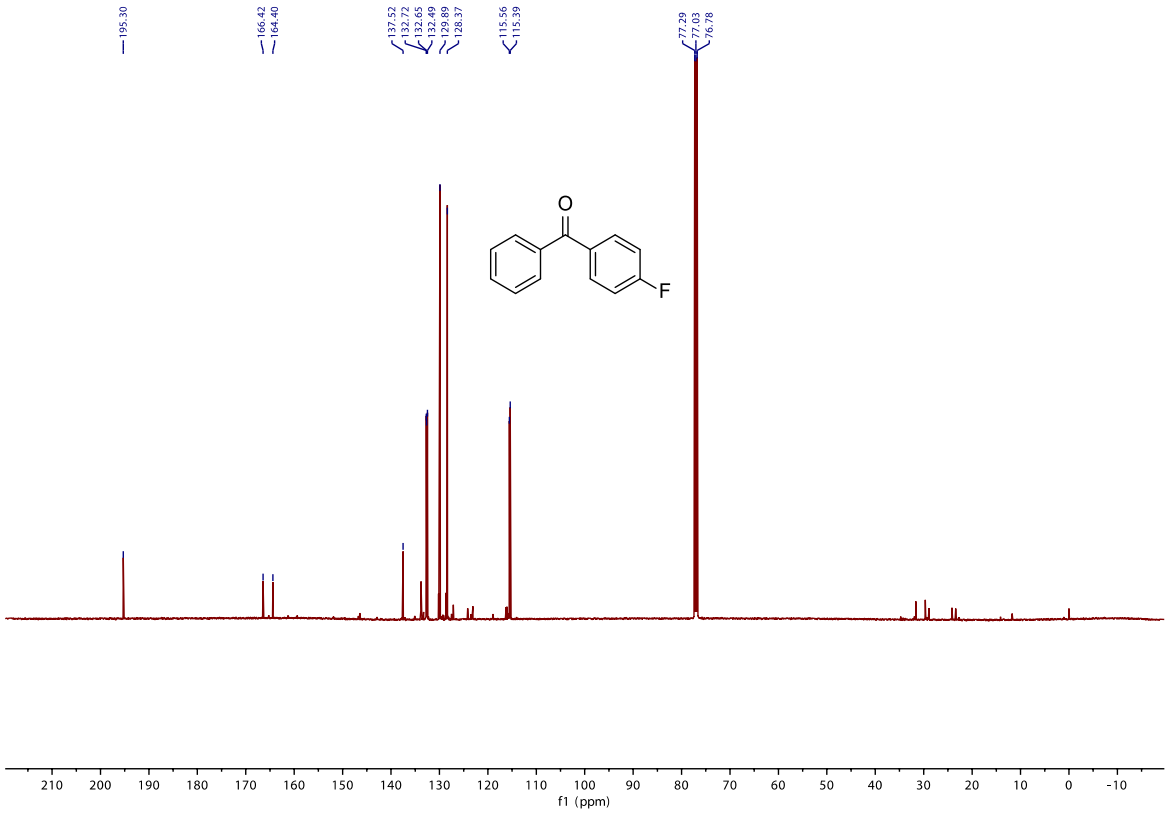
195.30
166.42
164.40
137.52
132.72
132.65
132.49
129.89
128.37
115.56
115.39
77.29
77.03
76.78
O
F
210 200 190 180 170 160 150 140 130 120 110 100 90 80 70 60 50 40 30 20 10 0 -10
f1 (ppm)

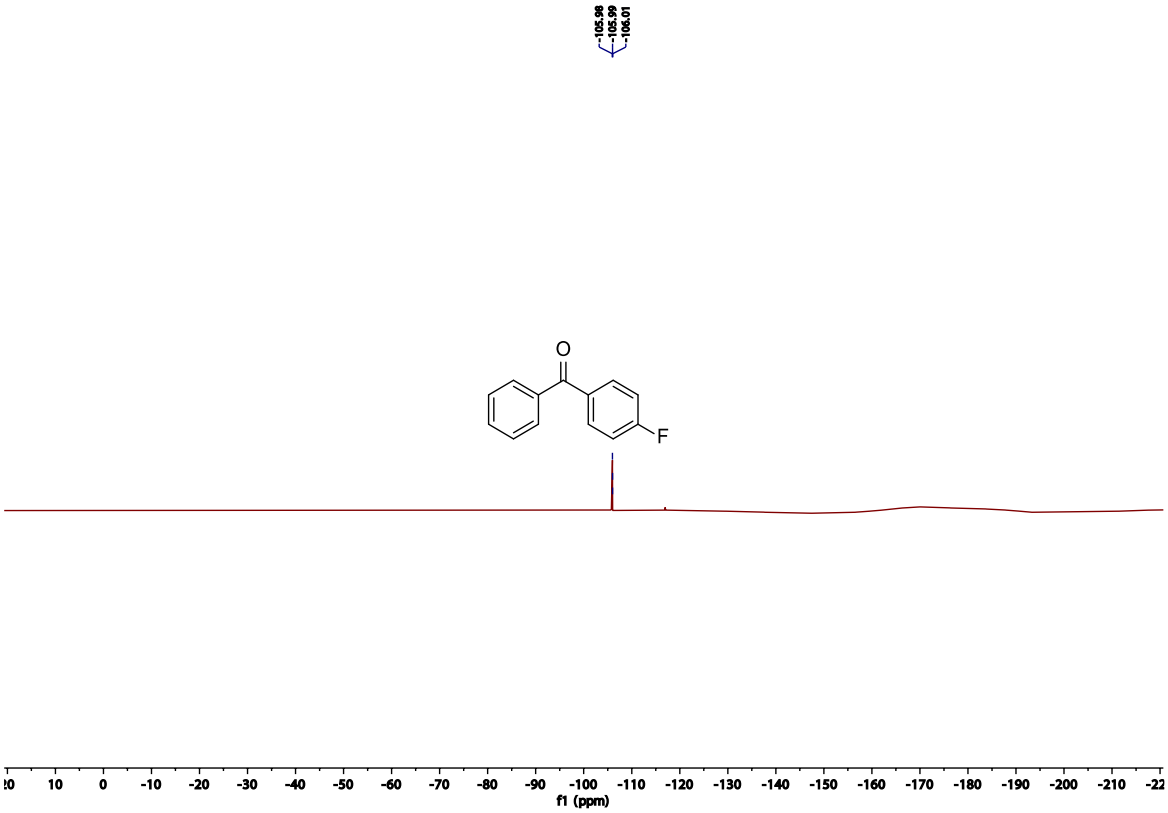
-105.98
-105.99
-106.01
O
F
10
0
-10
-20
-30
-40
-50
-60
-70
-80
-90
-100
-110
-120
-130
-140
-150
-160
-170
-180
-190
-200
-210
f1 (ppm)

NMR Data for Compound 2.10g[9]

2-benzoylbenzaldehyde 2.10g: ^{1}H NMR (400 MHz, $CDCl_3$) δ 10.03 (s, 1H), 8.04 (m, 1H), 7.80 (d, *J* = 7.6 Hz, 2H), 7.74-7.64 (s, 2H), 7.61 (t, *J* = 7.2 Hz, 1H), 7.53 – 7.44 (m, 3H). ^{13}C NMR (101 MHz, $CDCl_3$) δ 196.7, 190.8, 141.6, 137.2, 135.6, 133.8, 133.5, 130.8, 130.2, 130.1, 129.0, 128.8. white solid; **2.10g** product from **2.1b** (8.37 mg) 57% yield; **2.10g** from **2.1d** (7.79 mg) 53% yield.

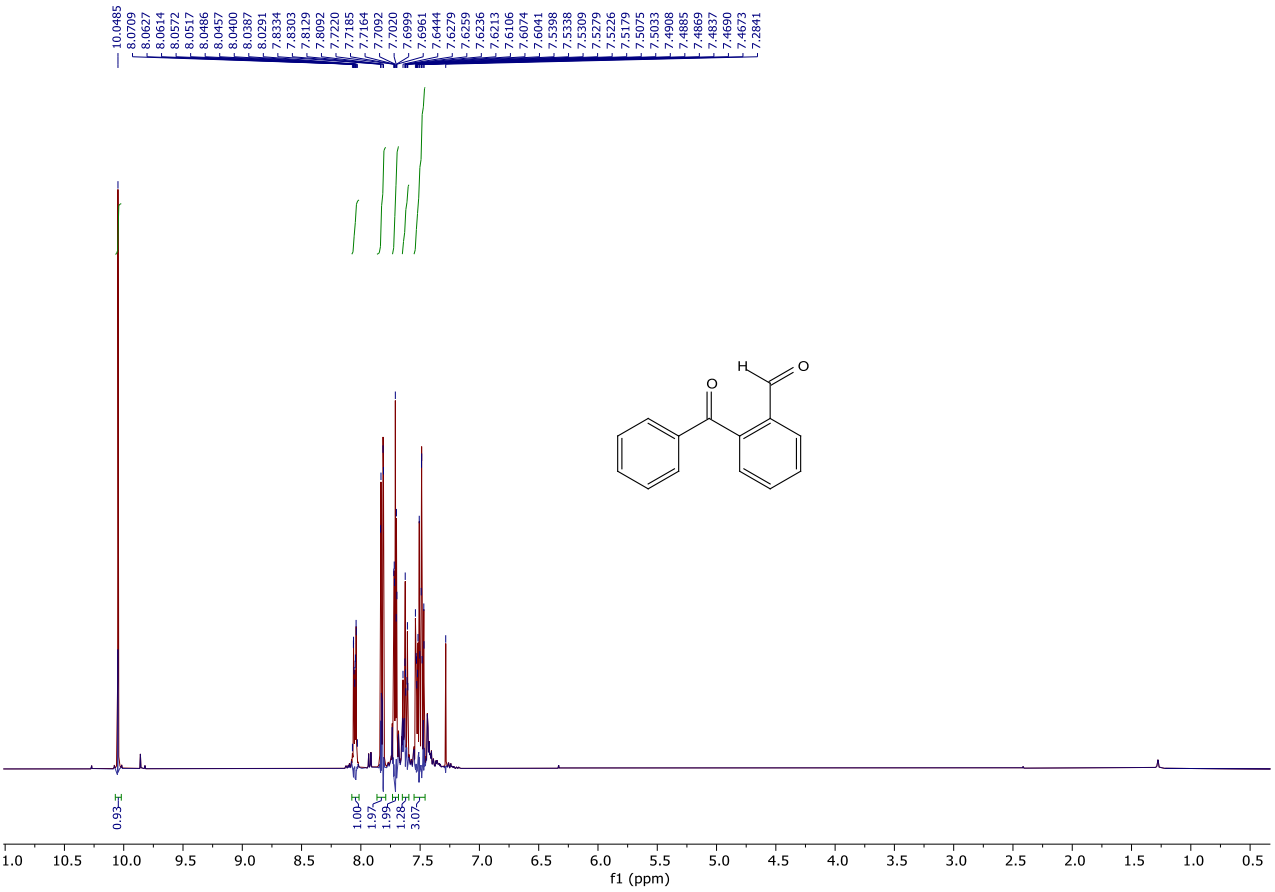

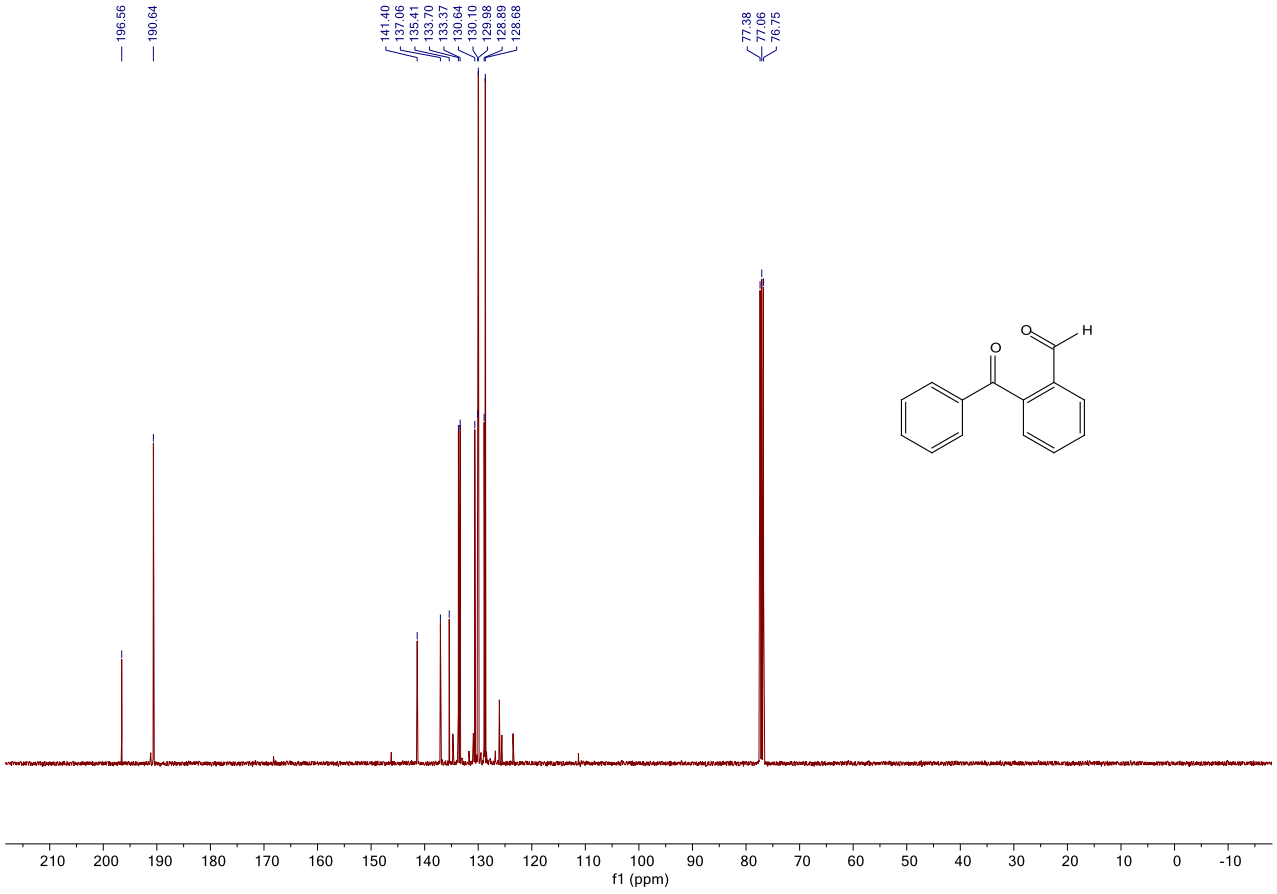

NMR Data for Compound 2.10h[6]

Methyl 4-benzoylbenzoate 2.10h: ^{1}H NMR (400 MHz, $CDCl_3$) δ 8.15 (d, *J* = 8.1 Hz, 2H), 7.82 (dd, *J* = 15.1, 8.1 Hz, 4H), 7.62 (t, *J* = 7.4 Hz, 1H), 7.50 (t, *J* = 7.5 Hz, 2H), 3.97 (s, 3H). ^{13}C NMR (101 MHz, $CDCl_3$) δ 196.2, 166.5, 141.5, 137.1, 133.4, 133.1, 130.3, 129.9, 129.7, 128.6, 52.6. white solid; **2.10h** product from **2.1b** (4.7 mg) 28% yield; **210h** from **2.1d** (4.87 mg) 29% yield.

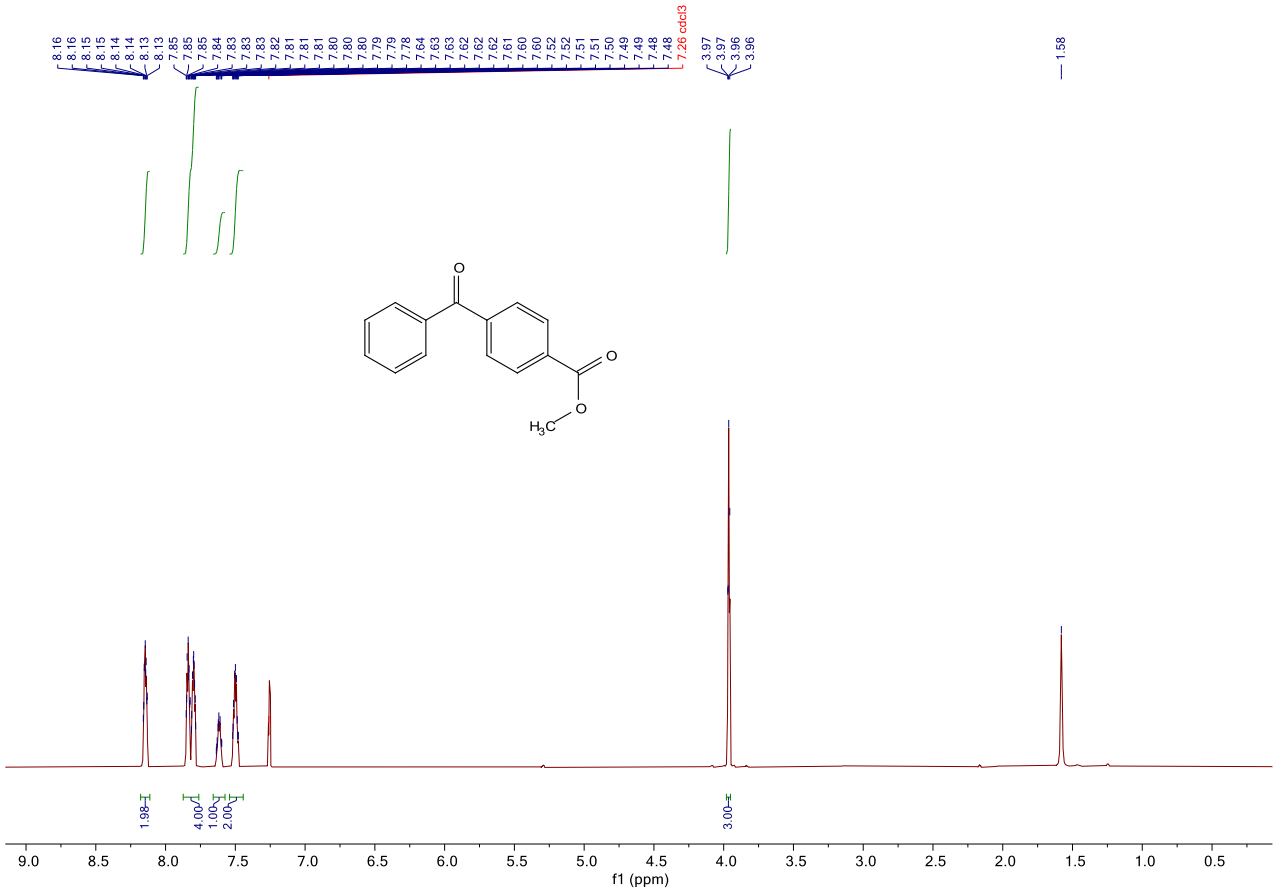
8.16
8.16
8.15
8.15
8.14
8.14
8.13
8.13
7.85
7.85
7.85
7.84
7.83
7.83
7.83
7.82
7.81
7.81
7.81
7.80
7.80
7.80
7.79
7.79
7.78
7.64
7.63
7.63
7.62
7.62
7.62
7.61
7.60
7.60
7.52
7.52
7.51
7.51
7.50
7.49
7.49
7.48
7.48
7.26 cdcl3
3.97
3.97
3.96
3.96
1.58
O
O
O
H3C
1.98
4.00
1.00
2.00
3.00
9.0
8.5
8.0
7.5
7.0
6.5
6.0
5.5
5.0
4.5
4.0
3.5
3.0
2.5
2.0
1.5
1.0
0.5
f1 (ppm)

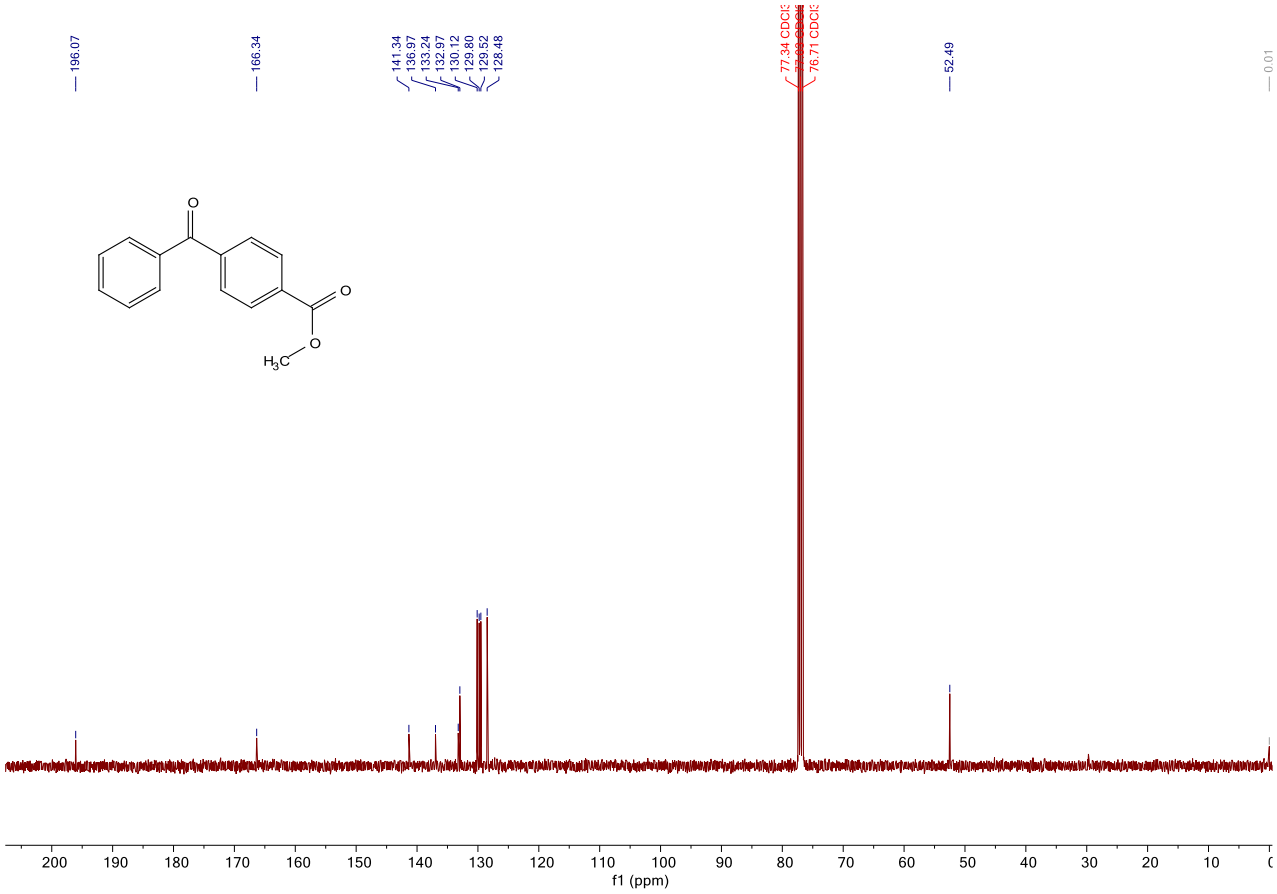
196.07
166.34
141.34
136.97
133.24
132.97
130.12
129.80
129.52
128.48
77.34 CDCl3
76.71 CDCl3
52.49
0.01
O
O
O
H3C
200
190
180
170
160
150
140
130
120
110
100
90
80
70
60
50
40
30
20
10
f1 (ppm)

NMR Data for Compound 2.10i[10]

Phenyl(4-vinylphenyl)methanone 2.10i: ^{1}H NMR (400 MHz, $CDCl_3$) δ 7.79 (d, *J* = 7.6 Hz, 4H**)**, 7.61-7.57 (m, 1H), 7.52-7.47 (m, 4H), 6.79 (dd, *J* = 17.6, 11.0 Hz, 1H), 5.90 (d, *J* = 17.6 Hz, 1H), 5.41 (d, *J* = 10.8 Hz, 1H). ^{13}C NMR (101 MHz, $CDCl_3$) δ 196.4, 141.7, 137.9, 136.8, 136.1, 132.5, 130.7, 130.1, 128.4, 126.2, 116.7. white solid; **2.10i** product from **2.1b** (12.66 mg) 87% yield; **2.10i** from **2.1d** (13.68 mg) 84% (pure) yield.

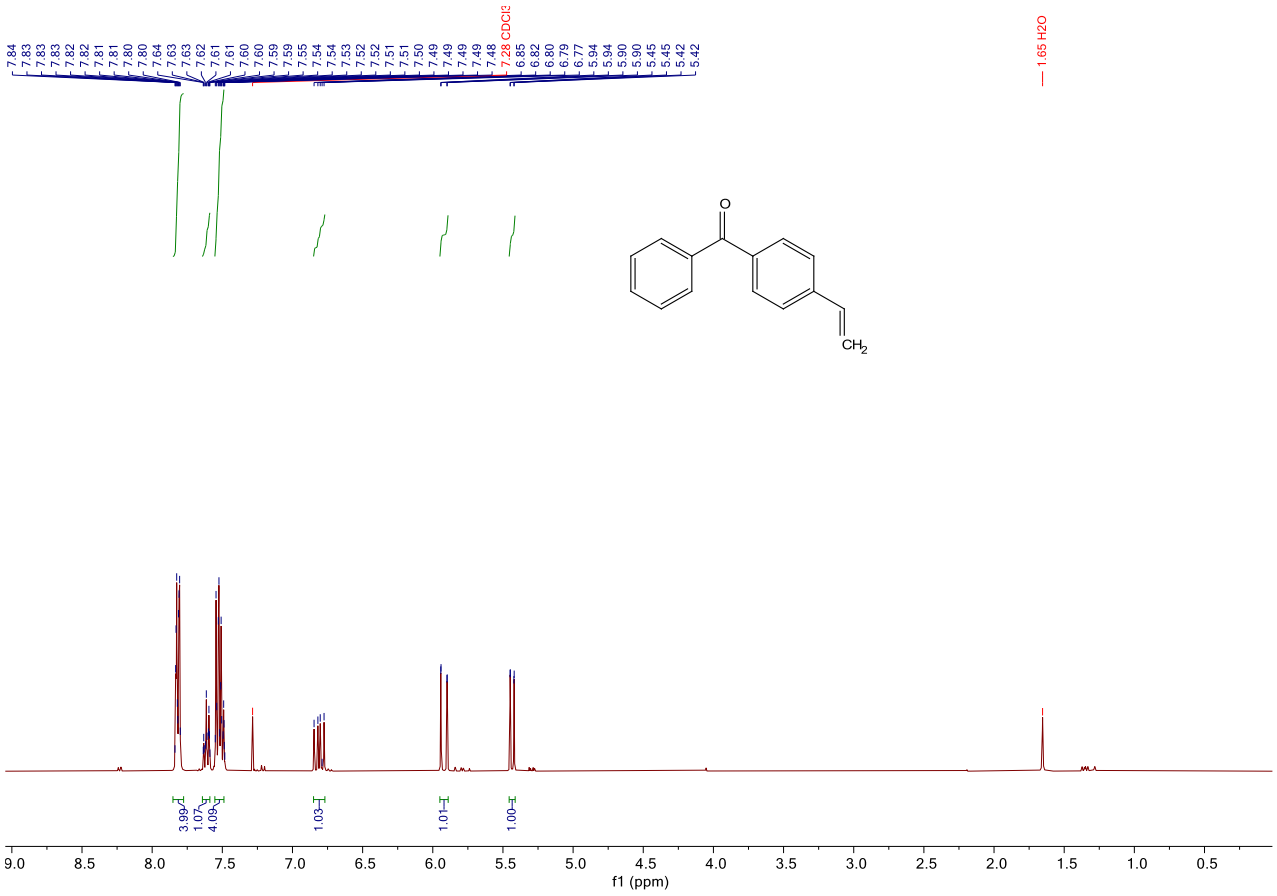

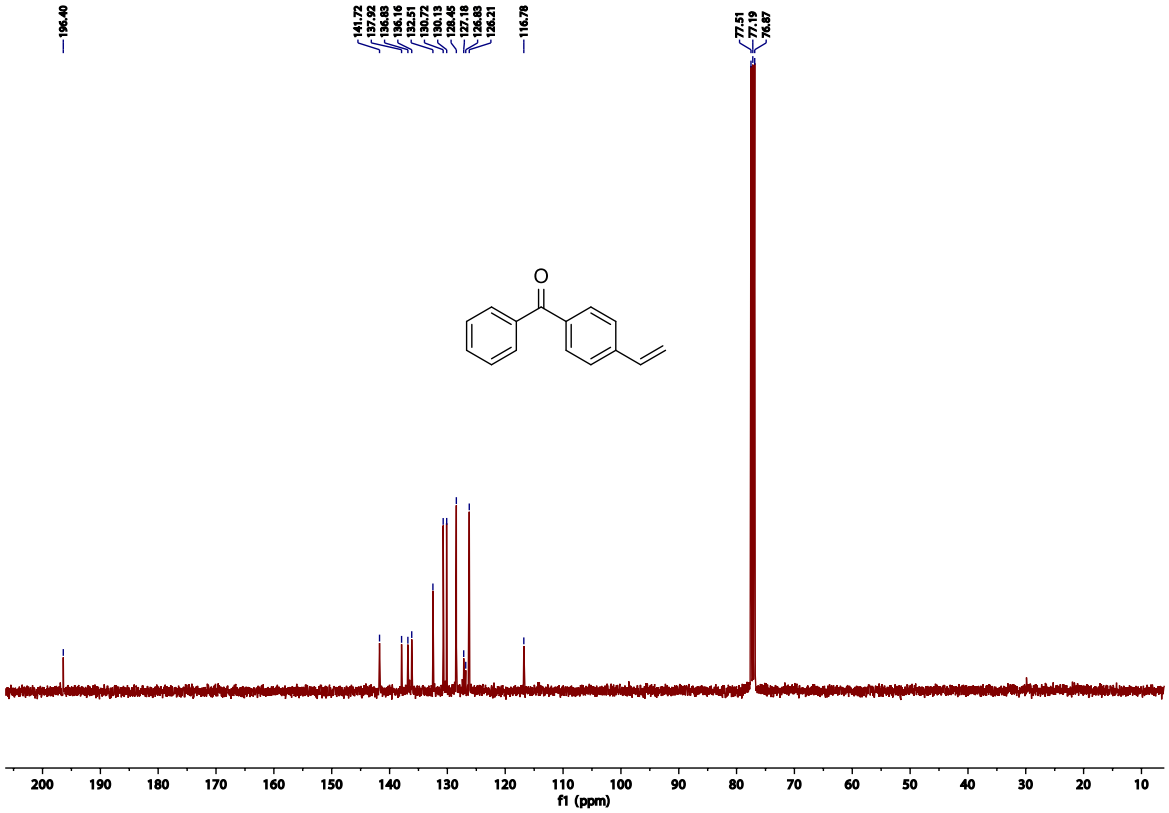
196.40
141.72
137.82
134.68
134.16
132.51
130.72
130.13
128.45
127.18
126.83
126.21
116.78
77.51
77.19
76.87
O
200
190
180
170
160
150
140
130
120
110
100
90
80
70
60
50
40
30
20
10
f1 (ppm)

NMR Data for Compound 2.10j[11]

(2,3-dihydrobenzo[b][1,4]dioxin-6-yl)(phenyl)methanone 2.10j: ^{1}H NMR (400 MHz, $CDCl_3$) δ 7.76 (d, *J* = 7.5 Hz, 2H), 7.56 (t, *J* = 7.2 Hz, 1H), 7.46 (t, *J* = 7.4 Hz, 2H), 7.41 – 7.36 (m, 2H), 6.93 (d, *J* = 8.3 Hz, 1H), 4.37 – 4.25 (m, 4H). ^{13}C NMR (101 MHz, $CDCl_3$) δ 195.5, 147.8, 143.3, 138.2, 132.1, 131.1, 129.9, 128.3, 124.6, 119.9, 117.2, 64.8, 64.3. white solid; **2.10j** product from **2.1b** (12.76 mg) 76% yield; **2.10j** from **2.1d** (10.92 mg) 65% yield.

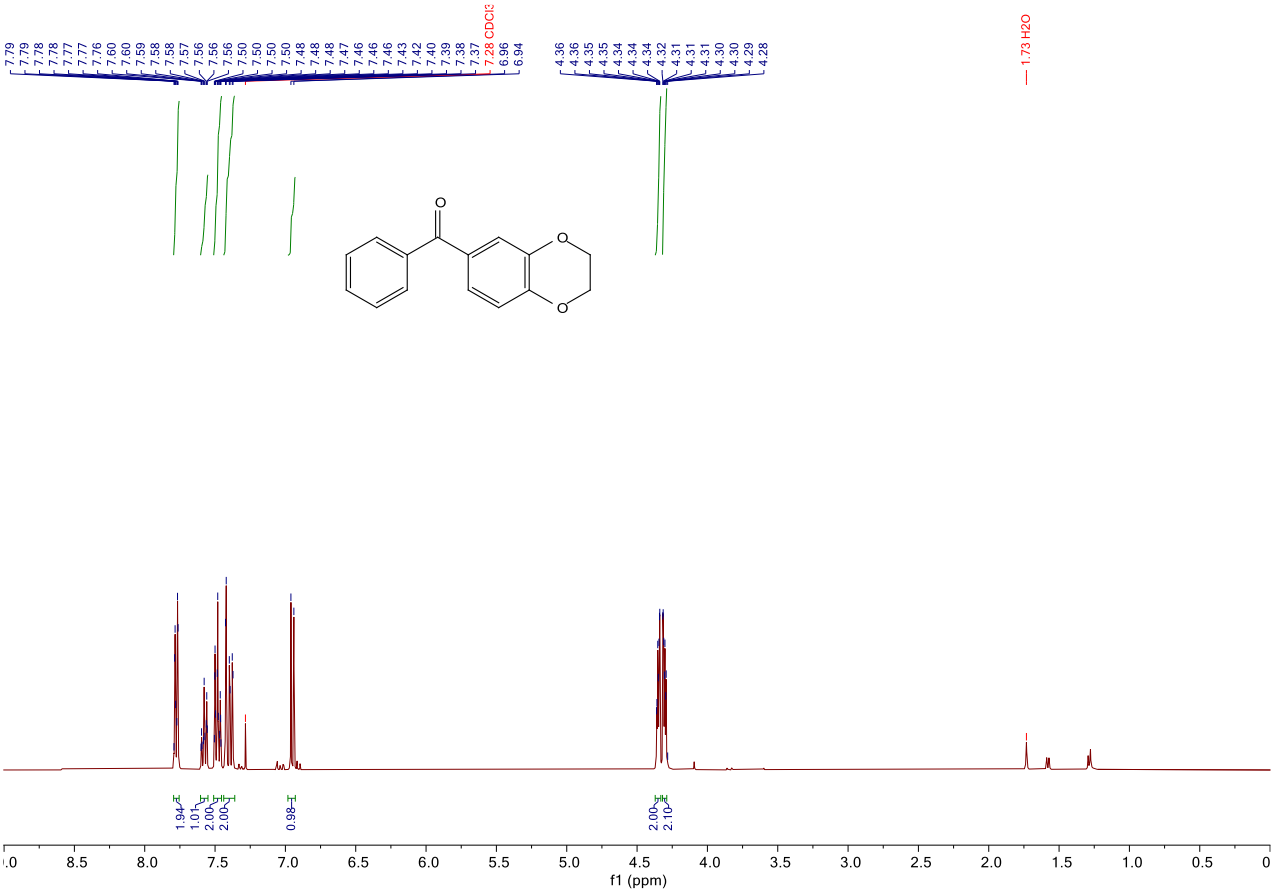

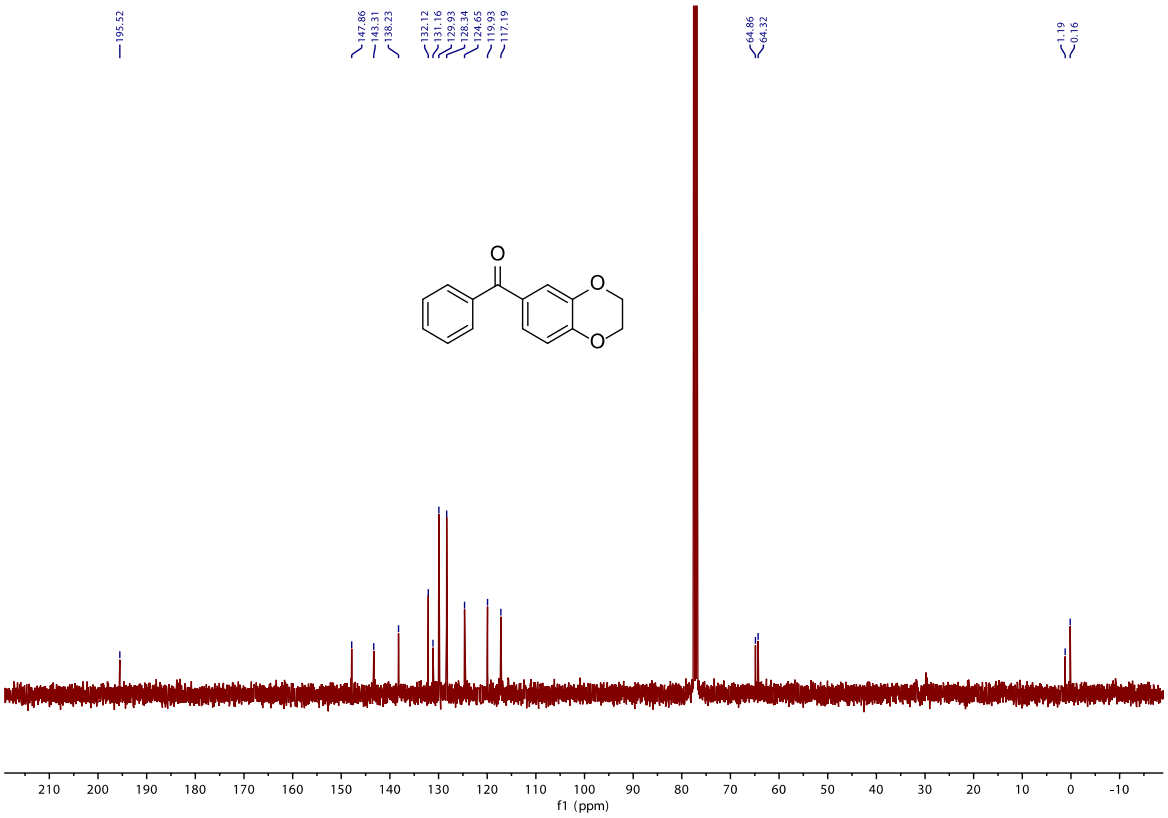
195.52
147.86
143.31
138.23
132.12
131.16
129.93
128.34
124.45
119.93
117.19
64.86
64.32
1.19
0.16
O
O
O
210 200 190 180 170 160 150 140 130 120 110 100 90 80 70 60 50 40 30 20 10 0 -10
f1 (ppm)

NMR Data for Compound 2.10k[6]

Phenyl(thiophen-3-yl)methanone 2.10k: ^{1}H NMR (400 MHz, $CDCl_3$) δ 7.93 (d, *J* = 2.7 Hz, 1H), 7.85 (d, *J* = 7.4 Hz, 2H), 7.61 – 7.57(m, 2H), 7.49 (t, *J* = 7.7 Hz, 2H), 7.39 (dd, *J* = 4.9, 3.0 Hz, 1H). ^{13}C NMR (101 MHz, $CDCl_3$) δ 190.2, 141.4, 138.8, 134.1, 132.4, 129.5, 128.8, 128.5, 126.3. white solid; **2,10k** product from **2.1b** (9.21 mg) 70% yield; **2.10k** from **2.1d** (8.55 mg) 65% yield.

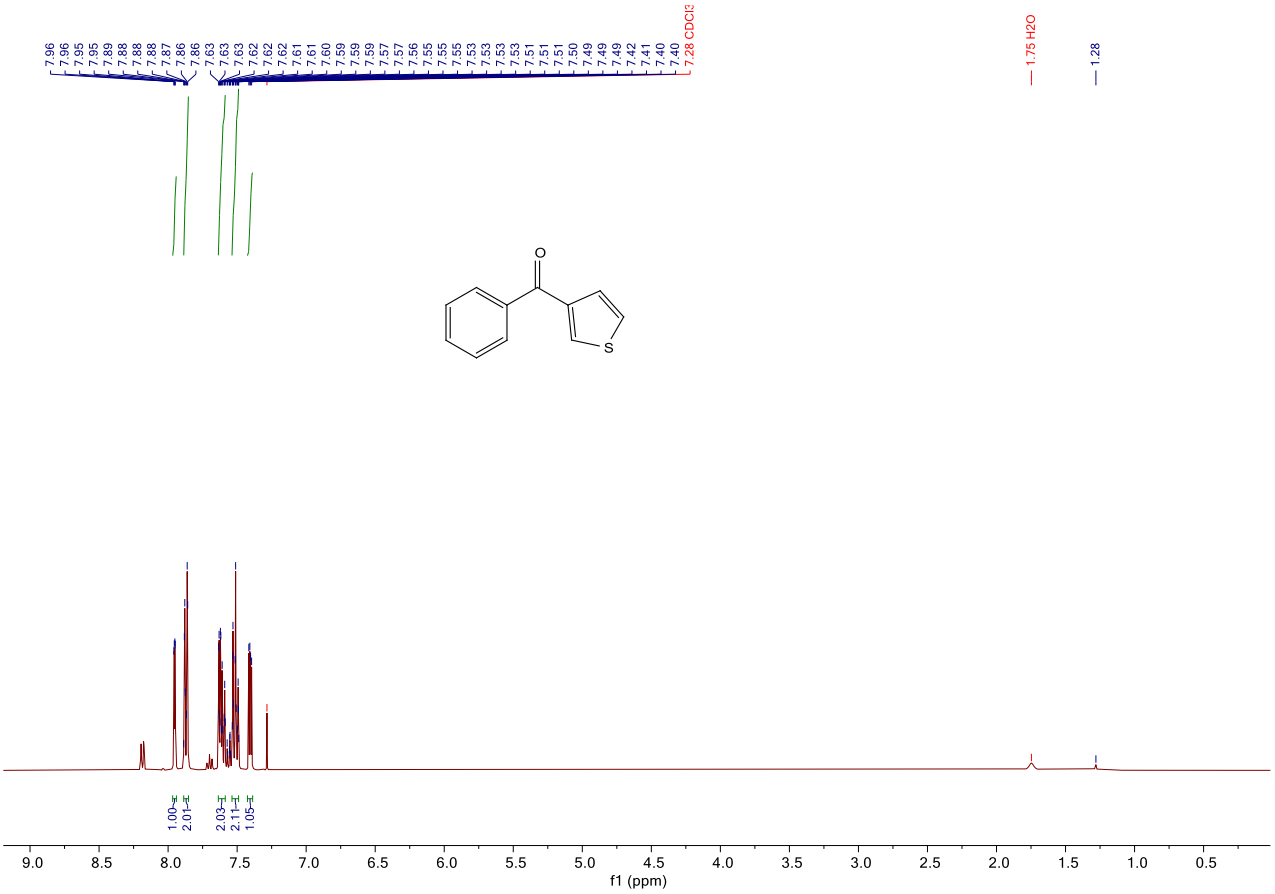

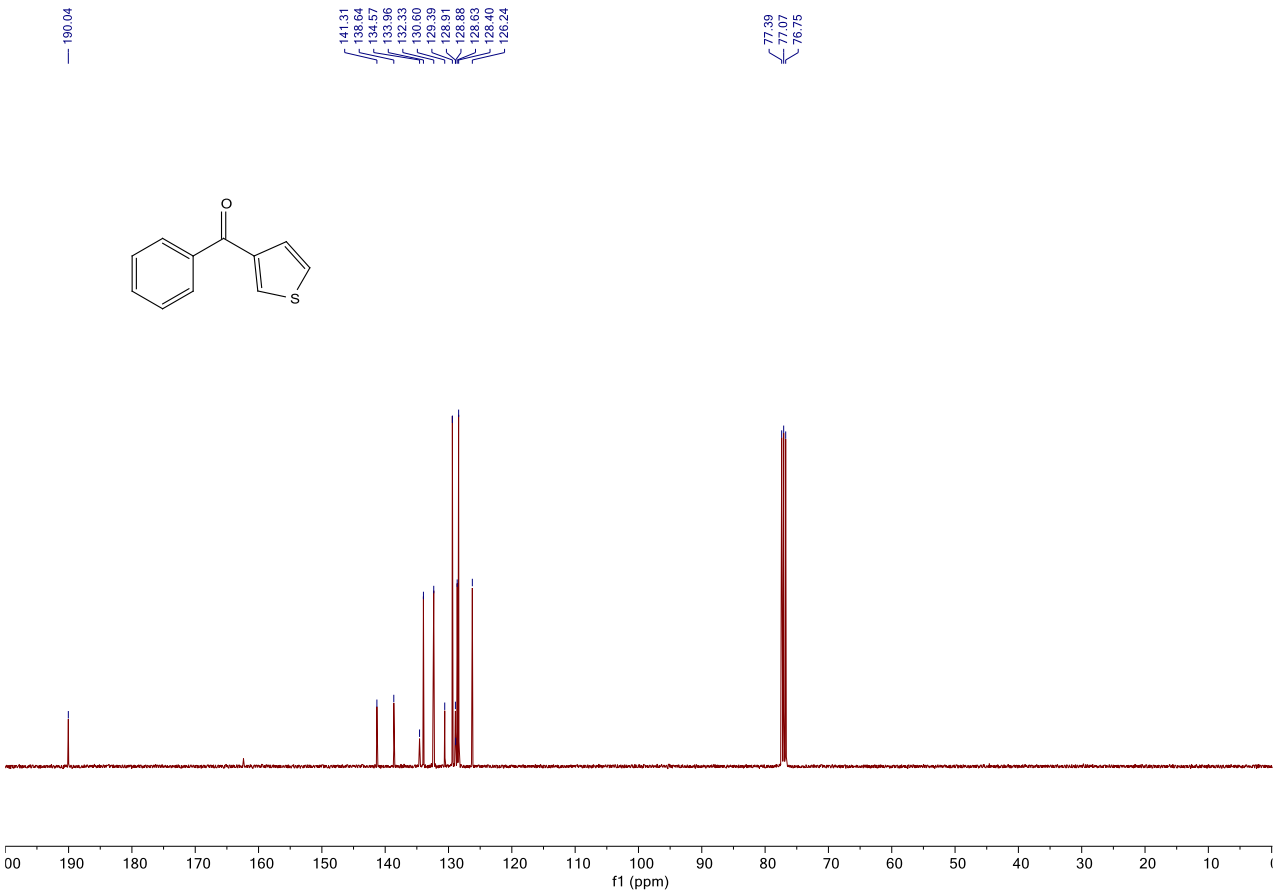
190.04
141.31
138.64
134.57
133.96
132.33
130.60
129.39
128.91
128.88
128.63
128.40
126.24
77.39
77.07
76.75
O
S
190
180
170
160
150
140
130
120
110
100
90
80
70
60
50
40
30
20
10
f1 (ppm)

NMR Data for Compound 2.10l[12]

Naphthalen-2-yl(phenyl)methanone 2.10l: ^{1}H NMR (600 MHz, $CDCl_3$) δ 8.27 (s, 1H), 7.95 (s, 2H), 7.92 (dd, *J* = 8.1, 3.7 Hz, 2H), 7.87 (d, *J* = 7.3 Hz, 2H), 7.62 (m, 2H), 7.59 – 7.50 (m, 3H). ^{13}C NMR (151 MHz, $CDCl_3$) δ 196.9, 138.0, 135.4, 135.0, 132.5, 132.4, 132.0, 130.2, 129.6, 128.48, 128.47, 128.45, 128.0, 126.9, 125.9. white solid; **2.10l** product from **2.1b** (11.2 mg) 69% yield; **2.10l** from **2.1d** (13.8 mg) 85% yield.

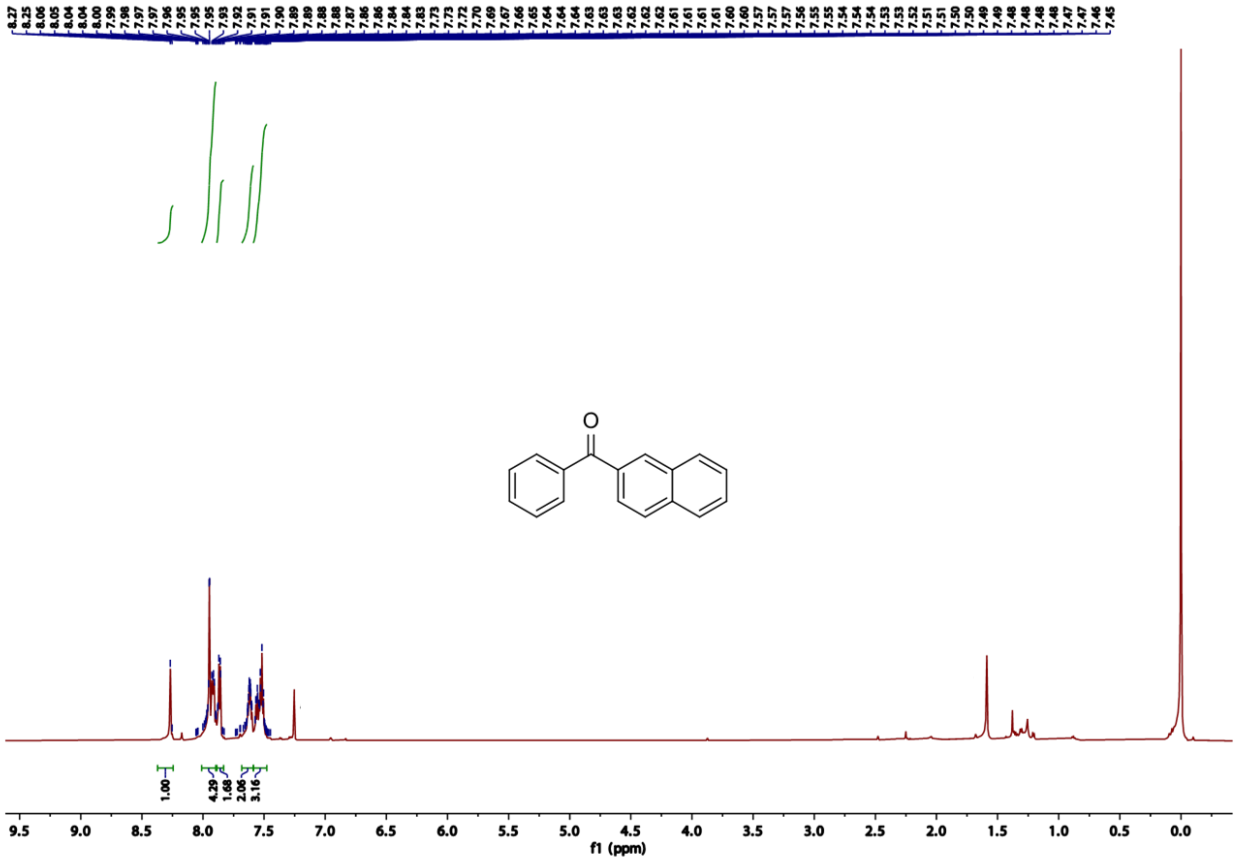

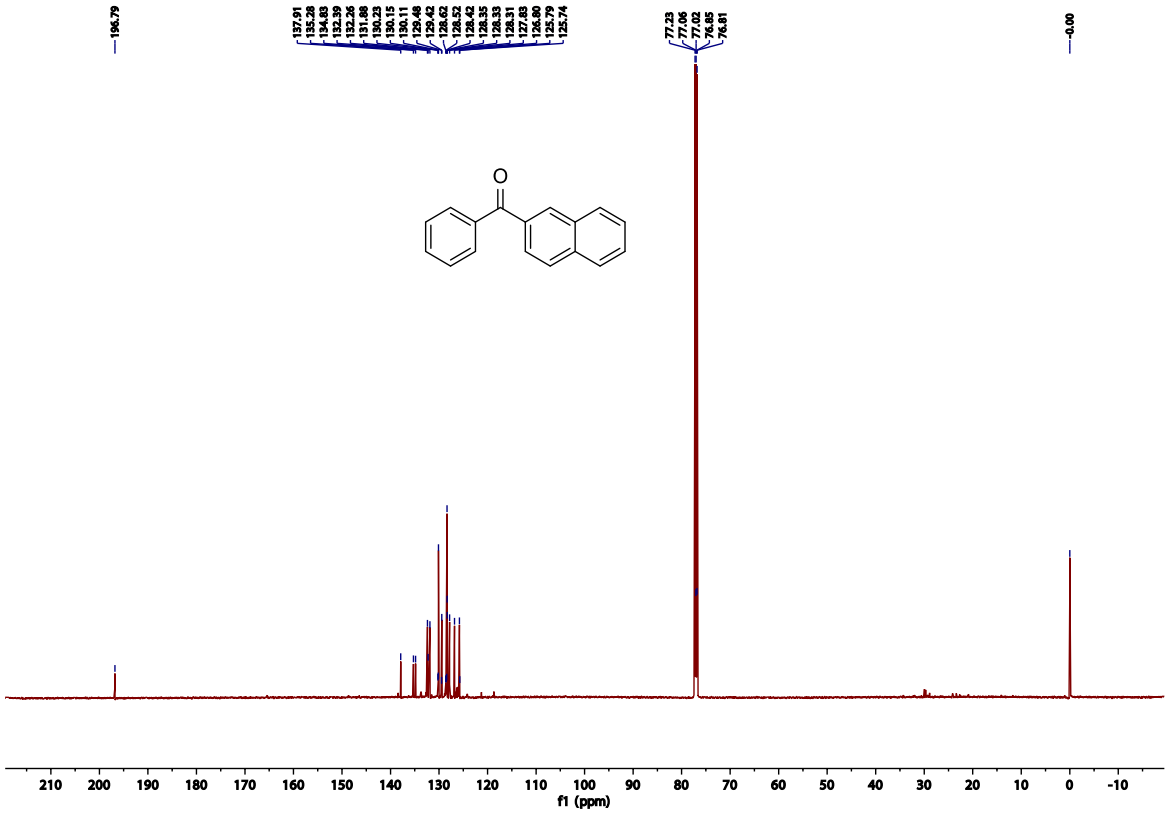
196.79
137.91
135.28
134.83
132.39
132.26
131.88
130.23
130.15
130.11
129.48
129.42
128.62
128.52
128.42
128.35
128.33
128.31
127.61
126.80
125.79
125.74
77.23
77.06
77.02
76.85
76.81
0.00
O
210 200 190 180 170 160 150 140 130 120 110 100 90 80 70 60 50 40 30 20 10 0 -10
f1 (ppm)

NMR Data for Compound 2.10m[12]

Phenyl(pyren-1-yl)methanone 2.10m: ^{1}H NMR (400 MHz, $CDCl_3$) δ 8.36 (d, *J* = 9.2 Hz, 1H), 8.27 – 8.18 (m, 4H), 8.13 – 8.05 (m, 4H), 7.90 (d, *J* = 7.5 Hz, 2H), 7.62 (t, *J* = 7.4 Hz, 1H), 7.48 (t, *J* = 7.7 Hz, 2H). ^{13}C NMR (101 MHz, $CDCl_3$) δ 198.6, 138.9, 133.3, 133.27, 133.2, 131.3, 130.8, 130.76, 129.9, 129.3, 129.0, 128.6, 127.4, 127.1, 126.6, 126.2, 126.1, 125.0, 124.9, 124.6, 123.9. white solid; **2.10m** product from **2.1b** (15.95 mg) 74% yield; **2.10m** from **2.1d** (19.62 mg) 91% yield.

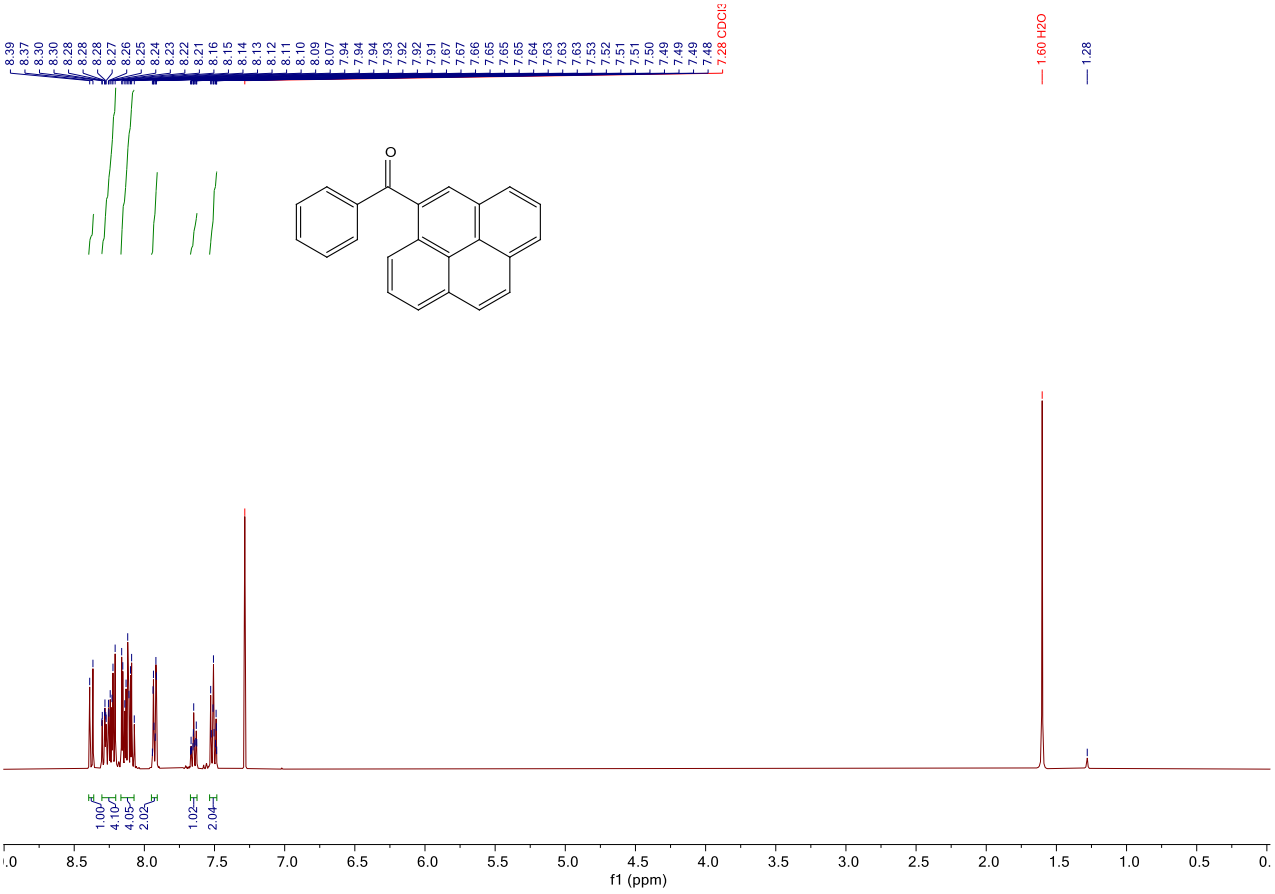

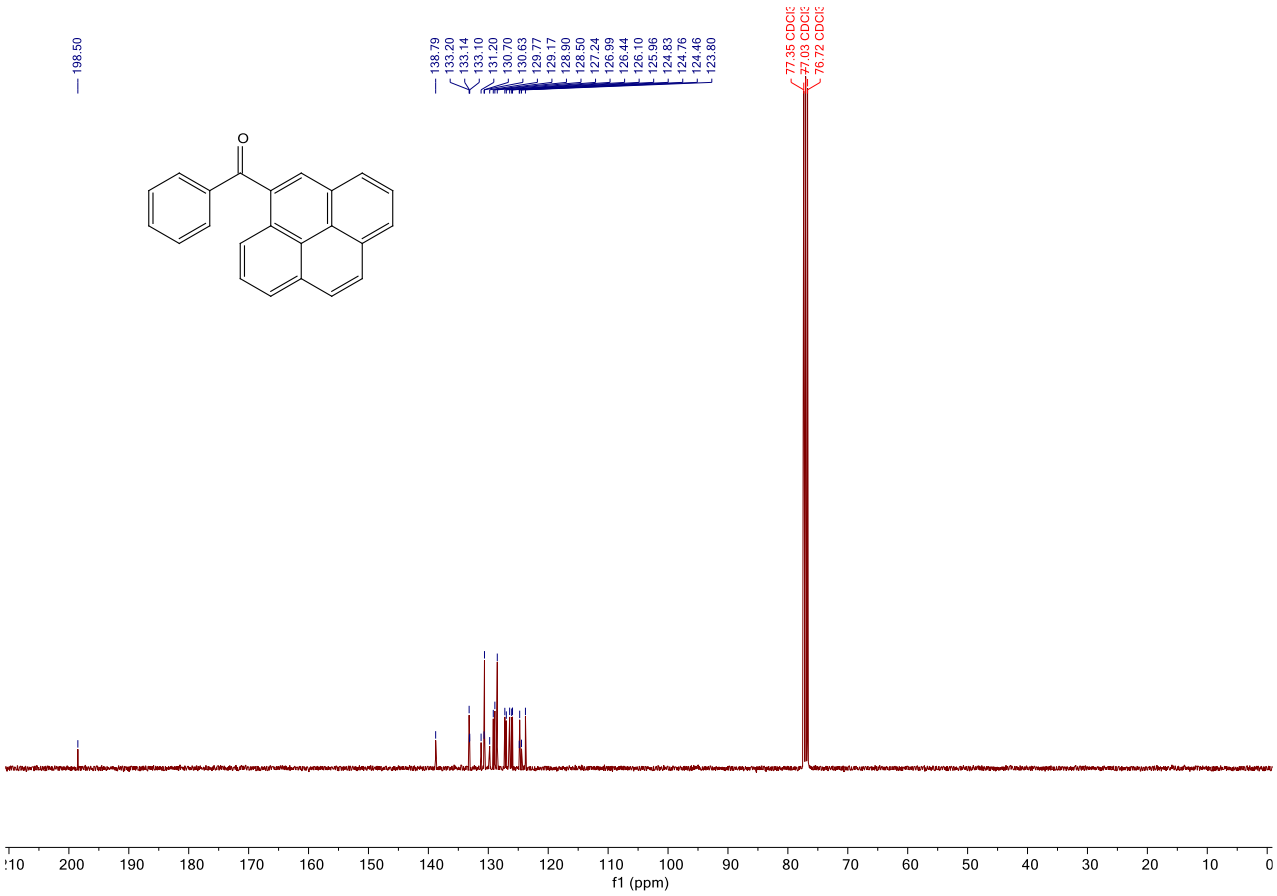
198.50
138.79
133.20
133.14
133.10
131.20
130.70
130.63
129.77
129.17
128.90
128.50
127.24
126.99
126.44
126.10
125.96
124.83
124.76
124.46
123.80
77.35 CDCl3
77.03 CDCl3
76.72 CDCl3
O
f1 (ppm)

NMR Data for Compound 2.10n[13]

(9H-Fluoren-2-yl)(phenyl)methanone 2.10n: ^{1}H NMR (400 MHz, $CDCl_3$) δ 8.03 (s, 1H), 7.88-7.83 (m, 5H), 7.60 (d, *J* = 6.9 Hz, 2H), 7.51 (t, *J* = 7.4 Hz, 2H), 7.46 – 7.37 (m, 2H), 3.98 (s, 2H). ^{13}C NMR (101 MHz, $CDCl_3$) δ 196.9, 146.1, 144.6, 143.2, 140.7, 138.3, 136.0, 132.3, 130.1, 129.8, 128.4, 128.1, 127.2, 127.0, 125.4, 121.0, 119.6, 37.1. white solid; **2.10n** product from **2.1b** (16.63 mg) 88% yield; **2.10n** from **2.1d** (12.85 mg) 68% yield.

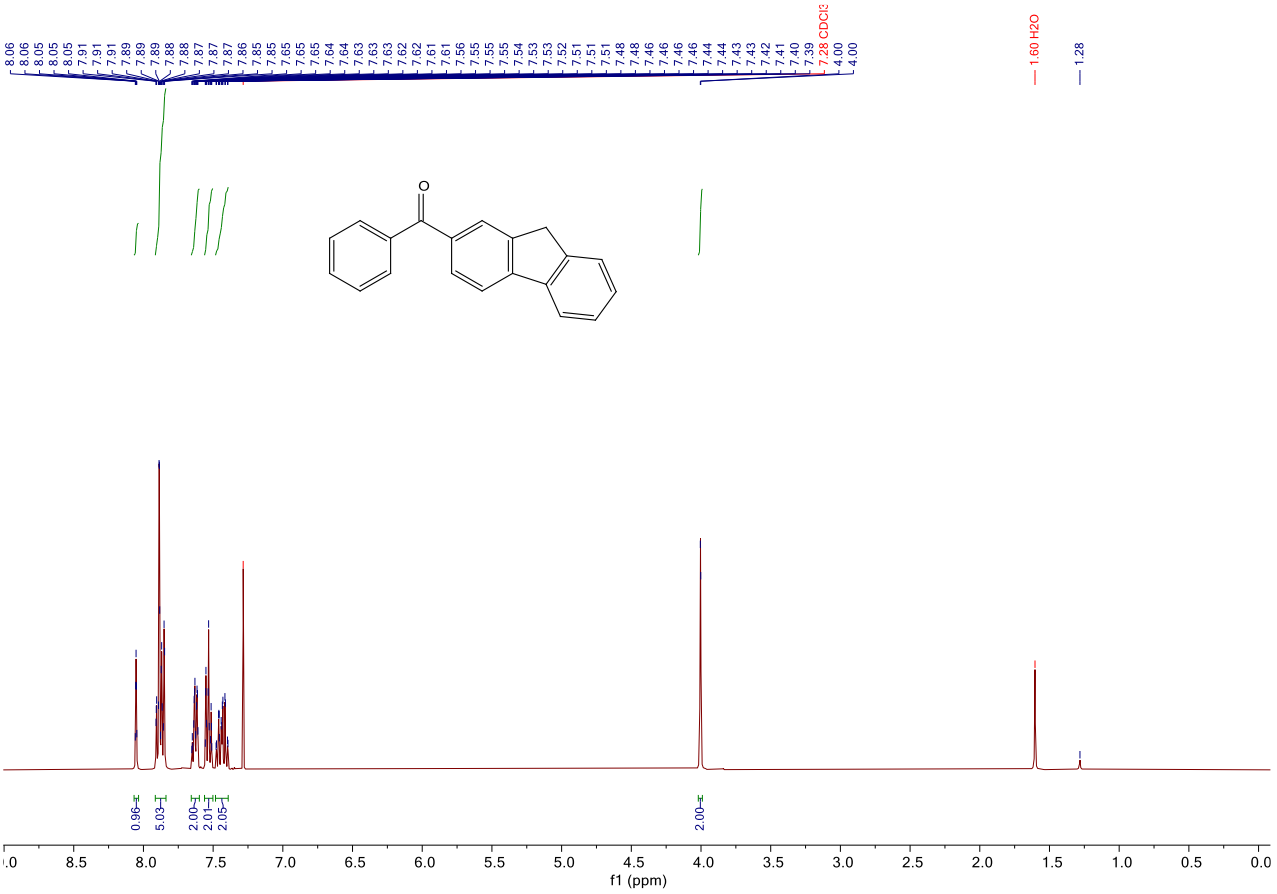

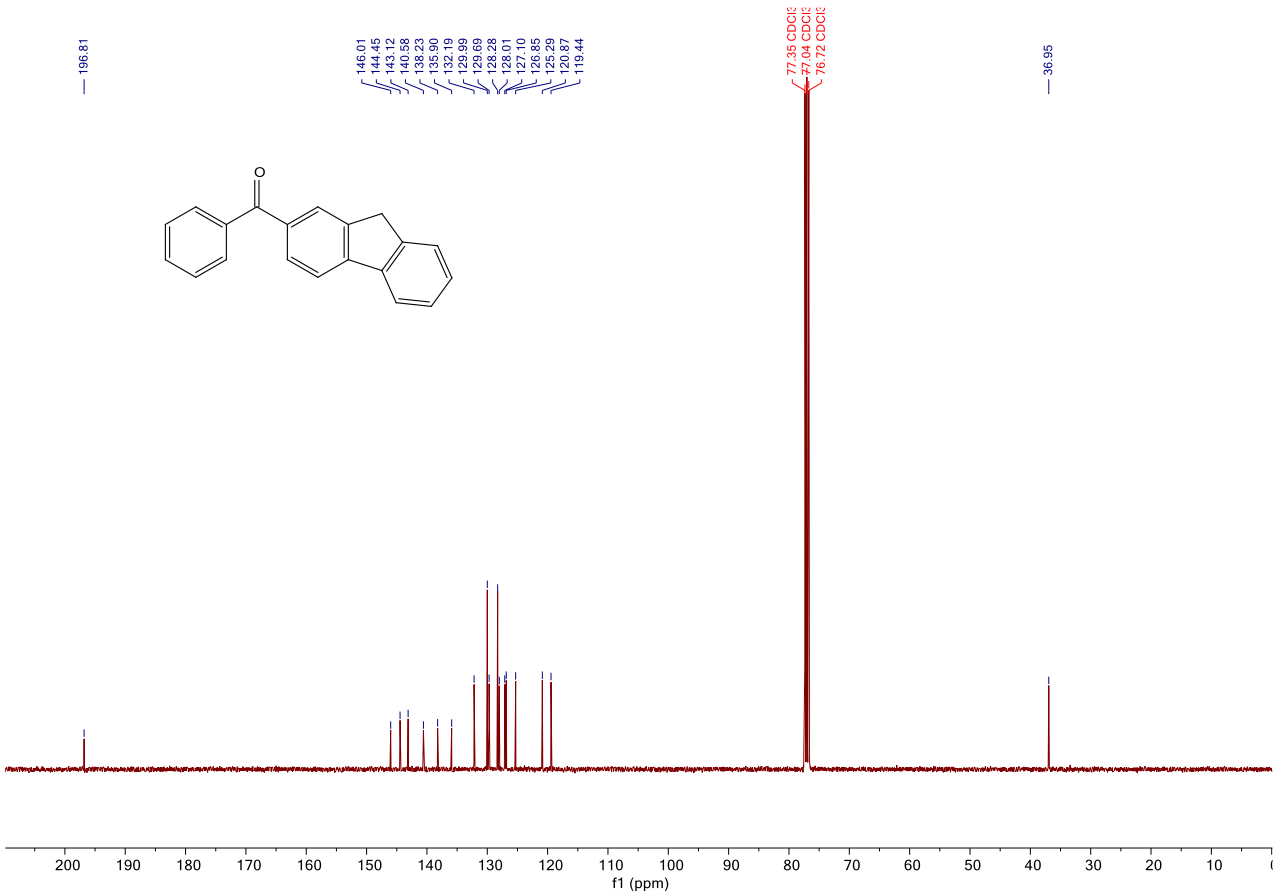
196.81
146.01
144.45
143.12
140.58
138.23
135.90
132.19
129.99
129.69
128.28
128.01
127.10
126.85
125.29
120.87
119.44
77.35 CDCl3
77.04 CDCl3
76.72 CDCl3
36.95
O
200
190
180
170
160
150
140
130
120
110
100
90
80
70
60
50
40
30
20
10
f1 (ppm)

Optimization of reaction NMR Data for Compound 3o[14]

(E)-1-phenylhex-2-en-1-one 2.10o: ^{1}H NMR (400 MHz, $CDCl_3$) δ 7.93 (d, *J* = 7.5 Hz, 2H), 7.55 (t, *J* = 7.3 Hz, 1H), 7.47 (t, *J* = 7.5 Hz, 2H), 7.06 (dt, *J* = 15.2, 7.1 Hz, 1H), 6.88 (d, *J* = 15.5, 1H), 2.33-2.29 (m, 2H), 1.61 – 1.51 (m, 2H), 0.98 (t, *J* = 7.3 Hz, 3H). ^{13}C NMR (101 MHz, $CDCl_3$) δ 191.1, 150.0, 138.2, 132.7, 128.7, 128.6, 126.2, 35.0, 21.6, 13.9. white solid; **2.10o** product from **2.1b** (8.4 mg) 69% yield; **2.10o** from **2.1d** (9.74 mg) 80% yield.

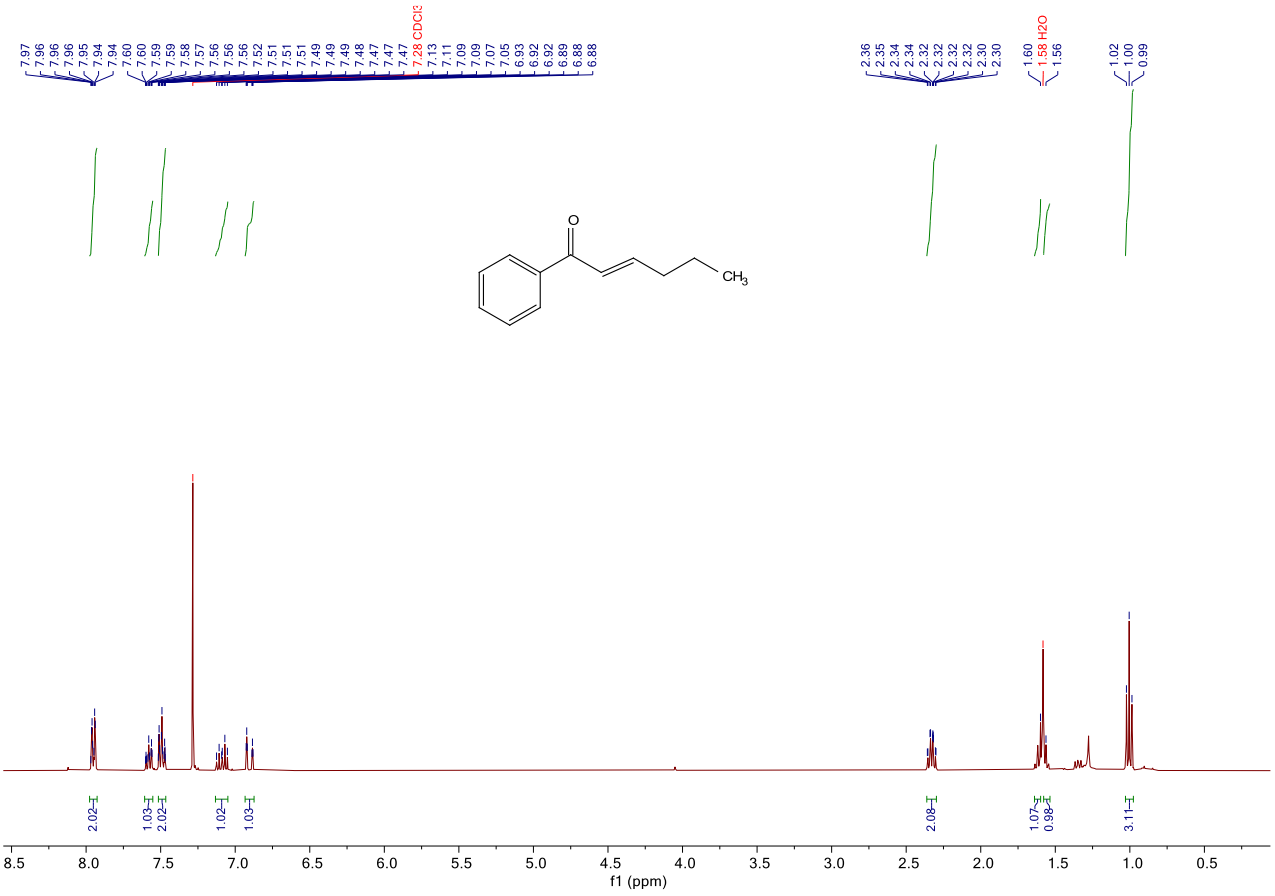

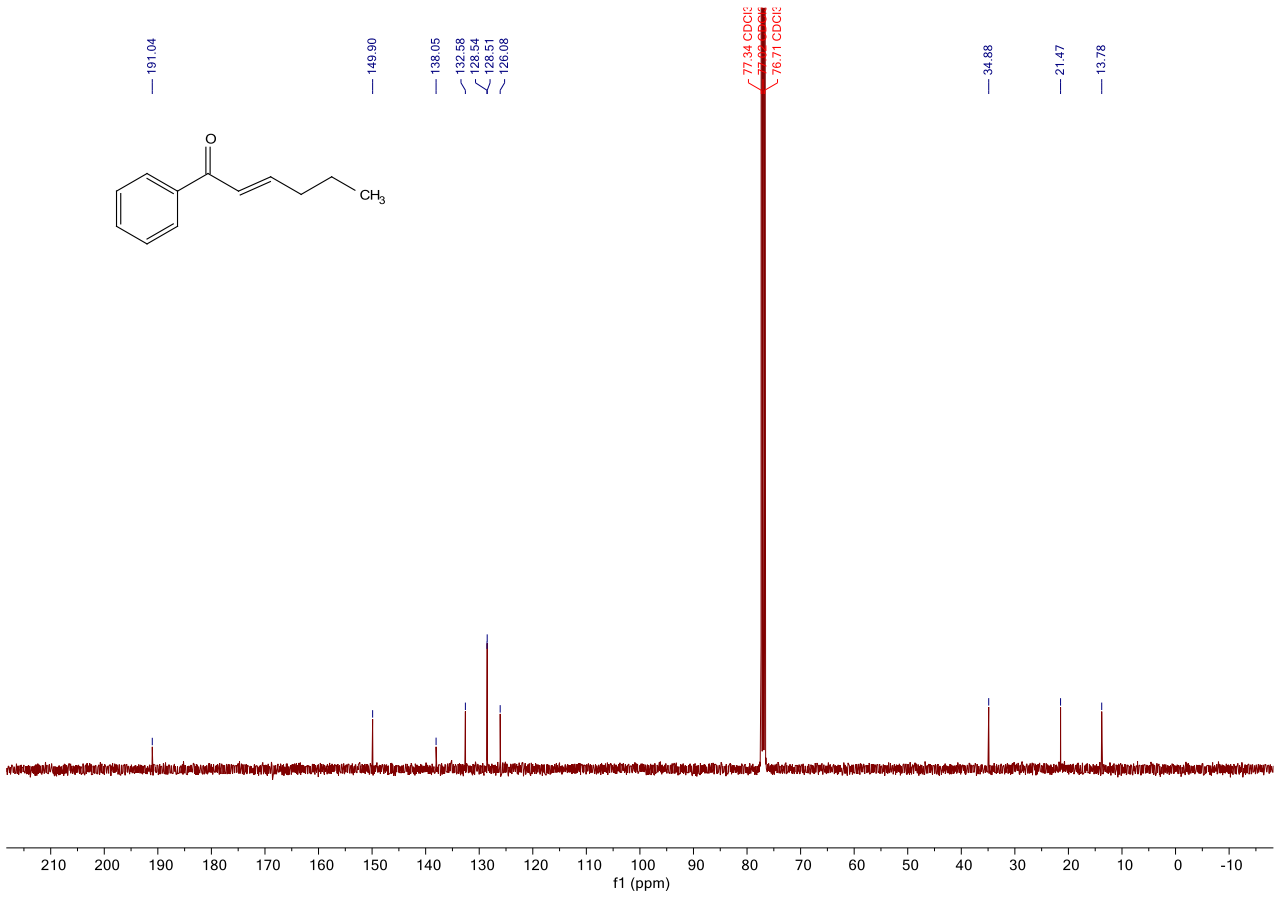
191.04
149.90
138.05
132.58
128.54
128.51
126.08
77.34 CDCl3
76.71 CDCl3
34.88
21.47
13.78
O
CH3
210 200 190 180 170 160 150 140 130 120 110 100 90 80 70 60 50 40 30 20 10 0 -10
f1 (ppm)

NMR Data for Compound 2.10p[15]

(E)-1-phenylnon-2-en-1-one 2.10p: ^{1}H NMR (500 MHz, $CDCl_3$) δ 7.92 (d, *J* = 7.4 Hz, 2H), 7.55 (t, *J* = 7.4 Hz, 1H), 7.46 (t, *J* = 7.7 Hz, 2H), 7.07 (dt, *J* = 15.2, 6.6 Hz, 1H), 6.87 (d, *J* = 15.2, 1H), 2.32 (q, *J* = 7.1 Hz, 2H), 1.52 (pentet, *J* = 7.5, 2H), 1.39 – 1.25 (m, 6H), 0.89 (t, *J* = 6.6 Hz, 3H).^{13}C NMR (126 MHz, $CDCl_3$) δ 191.2, 150.4, 138.2, 132.7, 128.7, 128.6, 126.0, 33.0, 31.8, 29.1, 28.3, 22.7, 14.2. white solid; **2.10p** product from **2.1b** (10.58 mg) 70% yield; **2.10p** from **2.1d** (11.79 mg) 78% yield.

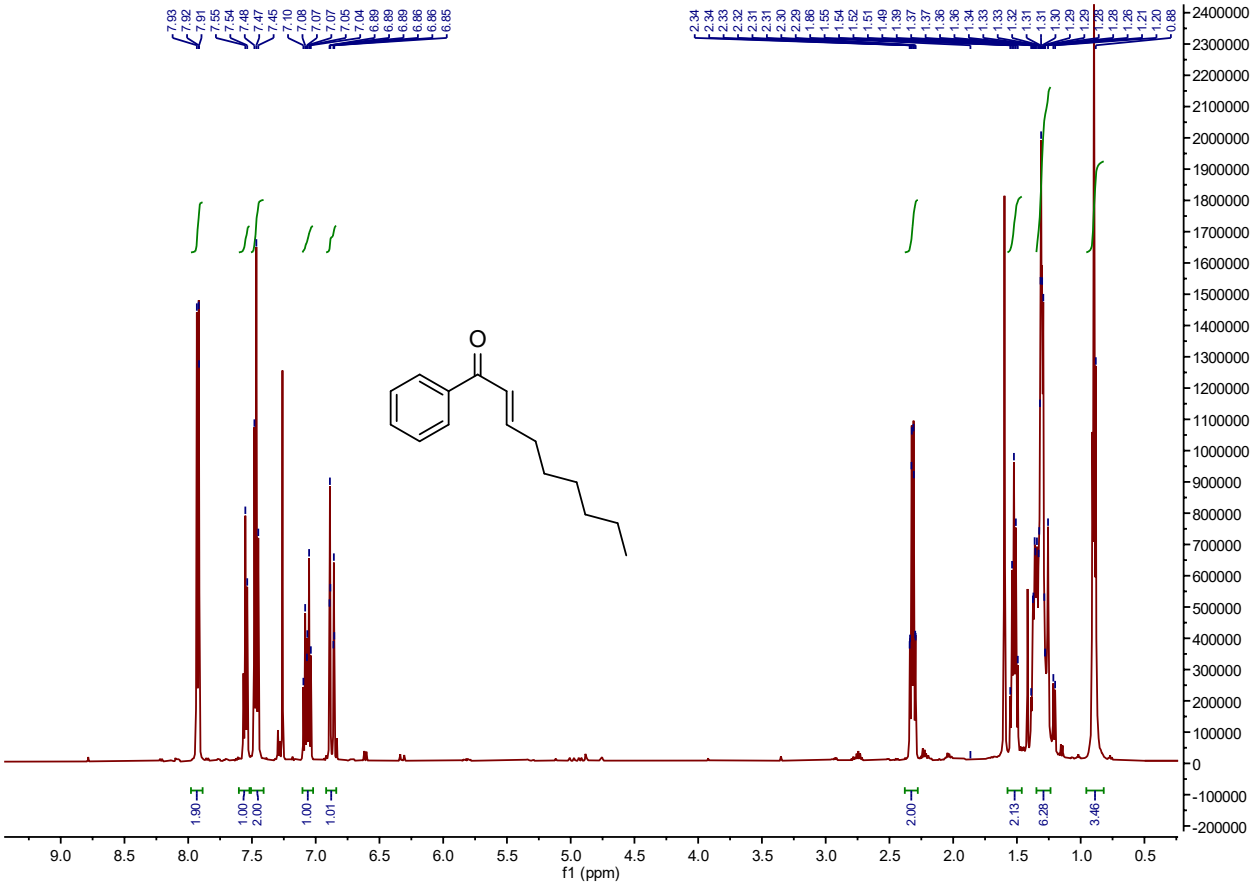

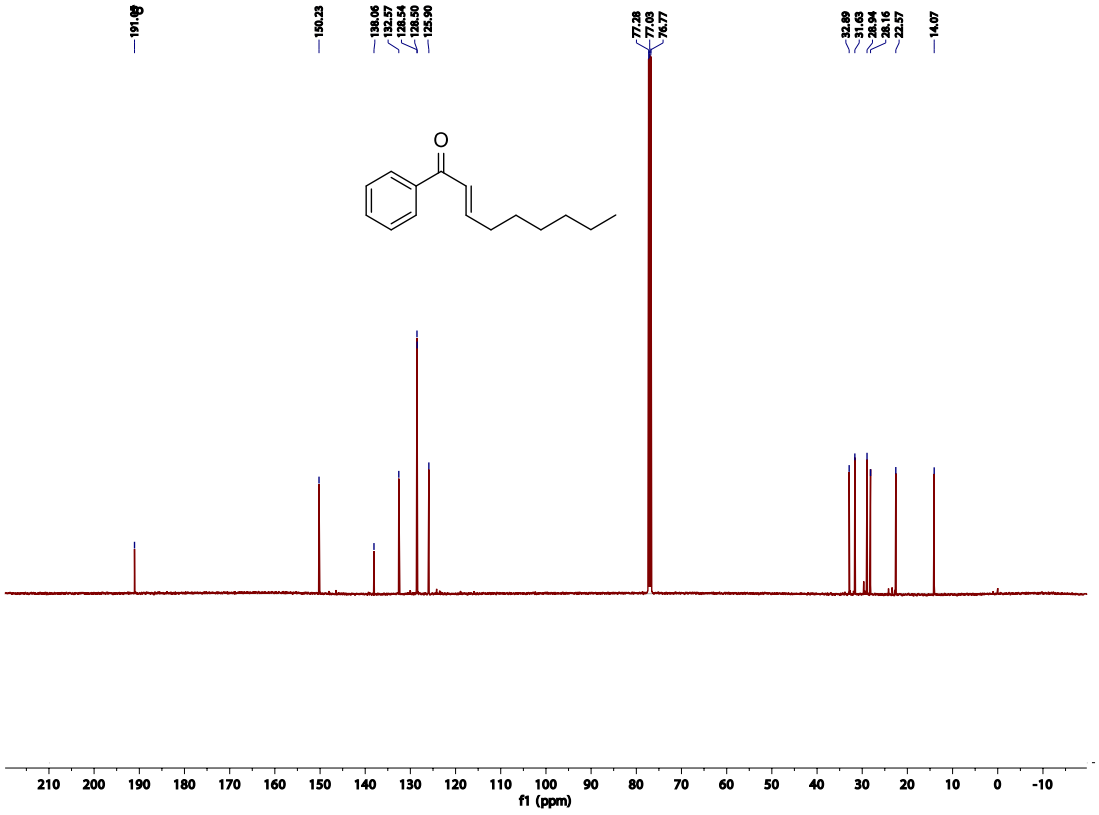
191.49
150.23
138.06
132.57
128.54
128.50
125.90
77.28
77.03
76.77
32.89
31.63
28.94
28.16
22.57
14.07
O
210 200 190 180 170 160 150 140 130 120 110 100 90 80 70 60 50 40 30 20 10 0 -10
f1 (ppm)

NMR Data for Compound 2.10q[14]

(E)-chalcone 2.10q: ^{1}H NMR (400 MHz, $CDCl_3$) δ 8.03 (d, *J* = 7.3 Hz, 2H), 7.82 (d, *J* = 15.7 Hz, 1H), 7.68 – 7.64 (m, 2H), 7.60 (t, *J* = 7.3 Hz, 1H), 7.56-7.50 (m, 3H), 7.46 – 7.40 (m, 3H). ^{13}C NMR (101 MHz, $CDCl_3$) δ 190.8, 145.0, 138.4, 135.0, 132.9, 130.7, 129.1, 128.8, 128.7, 128.6, 122.3. white solid; **2.10q** product from **2.1b** (8.82 mg) 60% yield; **2.10q** from **2.1d** (9.85 mg) 67% yield.

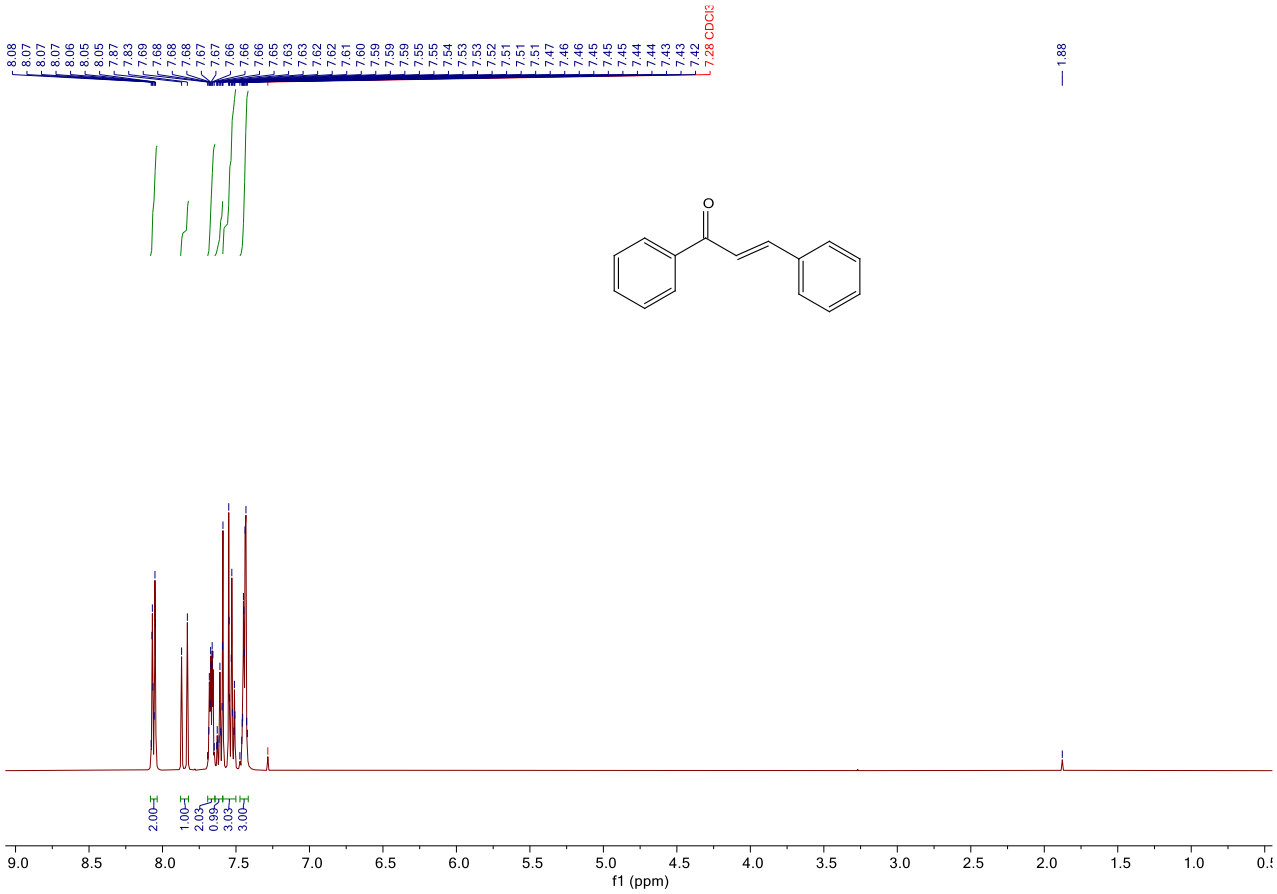

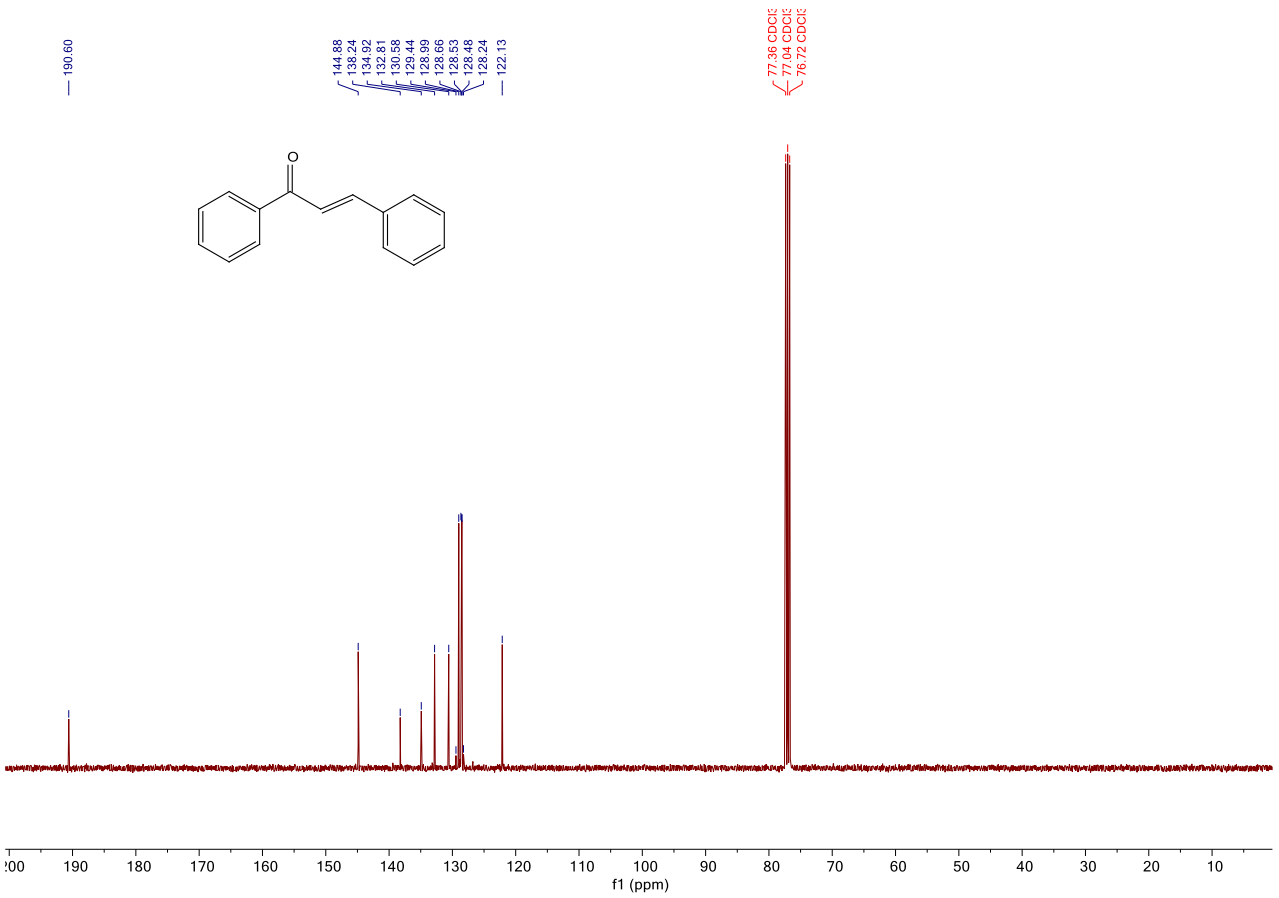
190.60
144.88
138.24
134.92
132.81
130.58
129.44
128.99
128.66
128.53
128.48
128.24
122.13
77.36 CDCl3
77.04 CDCl3
76.72 CDCl3
O
200
190
180
170
160
150
140
130
120
110
100
90
80
70
60
50
40
30
20
10
f1 (ppm)

Experimental Detail for Friedel Craft Acylation of Twisted Amides

Conditions for Friedel-Crafts acylation.

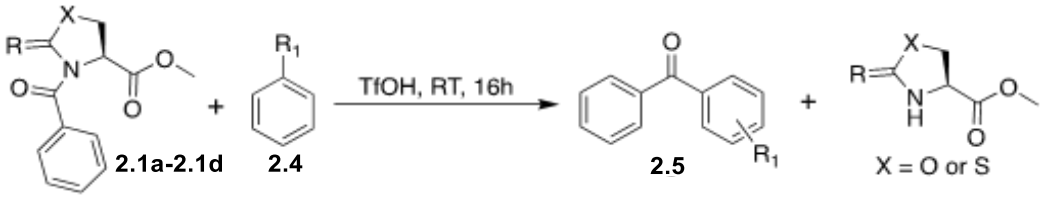

Entries	X	R	2.1a-2.1d	R_1	Solvent	Acid Catalyst (3 eq.)	Yield (%)
1	S	S	**2.1d**	OMe	-	Cu(OTf)3	0%
2	S	S	**2.1d**	OMe	-	TMS(OTf)3	0%
3	S	S	**2.1d**	OMe	DCM	TfOH	0%
4	S	S	**2.1d**	OMe	-	TfOH	90%
5	O	O	**2.1a**	Me	-	TfOH	62%
6	O	S	**2.1b**	Me	-	TfOH	50%
7	S	O	**2.1c**	Me	-	TfOH	73%
8	S	S	**2.1d**	Me	-	TfOH	87%

Reaction Conditions: Twisted amides **2.1a-2.1d** (50 mg each, 2.1a; 0.2 mmol, 2.1b=2.1c; 0.189 mmol, 2.1d; 0.178 mmol), TfOH (5 equiv.) in dry arene solvent (5 mL) under inert conditions at room temperature for 16 h.

General Procedure for Friedel-Crafts Reaction

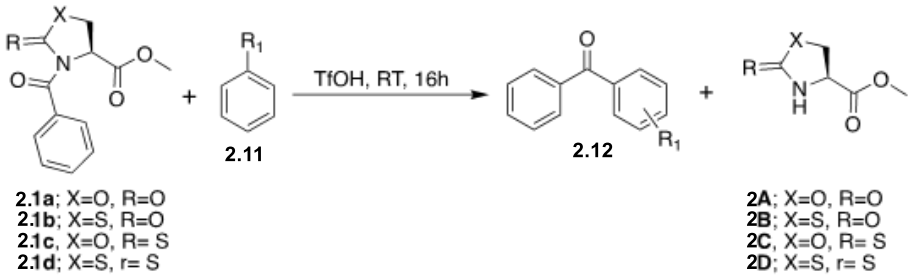

To a solution of twisted amide **2.1a-2.1d** (50 mg each, **2.1a**; 0.2 mmol, **2.1b**=**2.1c**; 0.189 mmol, **2.1d**; 0.178 mmol) in dry arene solvent (5 mL) under inert conditions, TfOH (5 eq.) was added sequentially, and the reaction mixture was stirred at room temperature for 16 h. Volatiles removed under reduced pressure and crude residue was purified by column chromatography using mixture of ethyl acetate and hexane (1:4) as an eluent to get the desired ketone **2.12**. The resulting products were characterized by ^{1}H NMR and ^{13}C-NMR.

Control Reaction

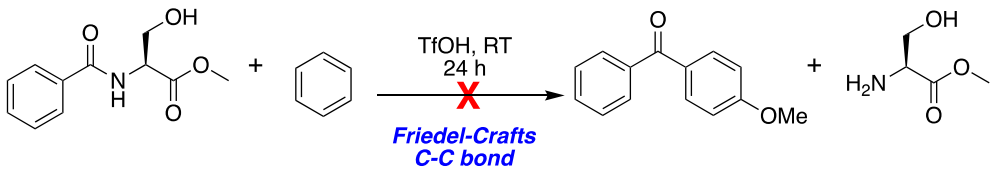

Friedel-Crafts reaction of compound 2E.

Compound **2E** (50mg, 0.224 mmol) was dissolved in dry benzene (5 mL) followed by the addition of TfOH (5 equiv.) in one portion under inert atmosphere and the reaction mixture was sealed and stirred at room temperature for 16h and analyzed by TLC. No modification of the compound **2E** was observed under the reaction conditions.

XIII. Supplementary Figure S7. General procedure for Friedel-Crafts reactions of 1b and 1d.

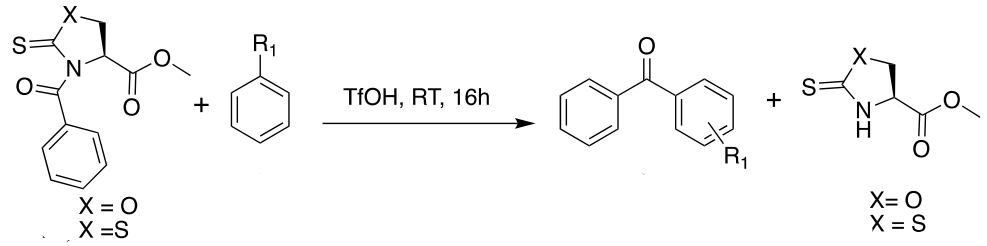

To a solution of twisted amide **2.1b** or **2.1d** (**2.1b**-50mg (0.189 mmol); **2.1d**-50mg (0.178 mmol) in arene dry solvent (5 mL), TfOH (5 eq.) was added sequentially under inert atmosphere, and the reaction mixture was stirred at room temperature for 16 h. Volatiles removed under reduced pressure and crude residue was purified by column chromatography using mixture of ethyl acetate and hexane (1:4) as an eluent to get the desired ketone **2.12**. The resulting products were characterized by ^{1}H NMR and ^{13}C-NMR.

NMR DATA FOR Friedel-Crafts Reaction

NMR DATA FOR 2.12a[16]

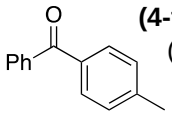

(4-fluorophenyl)(phenyl)methanone 2.12a: ^{1}H NMR (400 MHz, Chloroform-*d*) δ 7.84 – 7.78 (m, 2H), 7.78 – 7.71 (m, 2H), 7.66 – 7.58 (m, 1H), 7.56 – 7.46 (m, 2H), 7.37 – 7.26 (m, 2H), 2.47 (s, 3H). ^{13}C NMR (101 MHz, $CDCl_3$) δ 196.6, 143.3, 137.9, 134.8, 132.2, 130.3, 129.9, 129.0, 128.2, 21.7. white solid; **2.12a** product from **2.1b** (18.52 mg) 50% yield; **2.12a** from **2.1d** (30.7 mg) 88% yield.

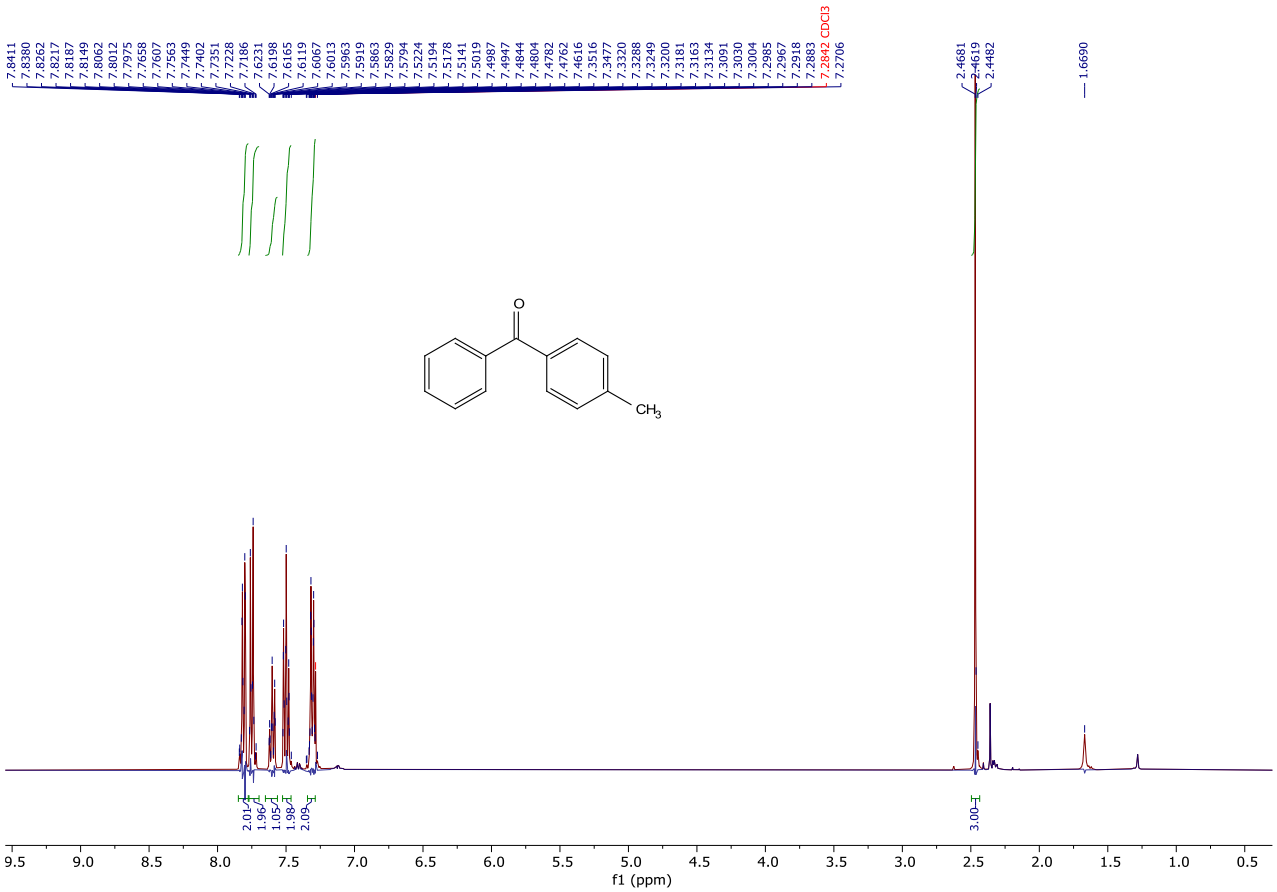
7.8411
7.8380
7.8262
7.8217
7.8187
7.8149
7.8062
7.8012
7.7975
7.7658
7.7607
7.7563
7.7449
7.7402
7.7351
7.7228
7.7186
7.6231
7.6198
7.6165
7.6119
7.6067
7.6013
7.5963
7.5919
7.5863
7.5829
7.5794
7.5224
7.5194
7.5178
7.5141
7.5019
7.4987
7.4947
7.4844
7.4804
7.4782
7.4762
7.4616
7.3516
7.3477
7.3320
7.3288
7.3249
7.3200
7.3181
7.3163
7.3134
7.3091
7.3030
7.3004
7.2985
7.2967
7.2918
7.2883
7.2842 CDCl3
7.2706
2.4681
2.4619
2.4482
1.6690
O
CH3
2.01
1.96
1.05
1.98
2.09
3.00
9.5
9.0
8.5
8.0
7.5
7.0
6.5
6.0
5.5
5.0
4.5
4.0
3.5
3.0
2.5
2.0
1.5
1.0
0.5
f1 (ppm)

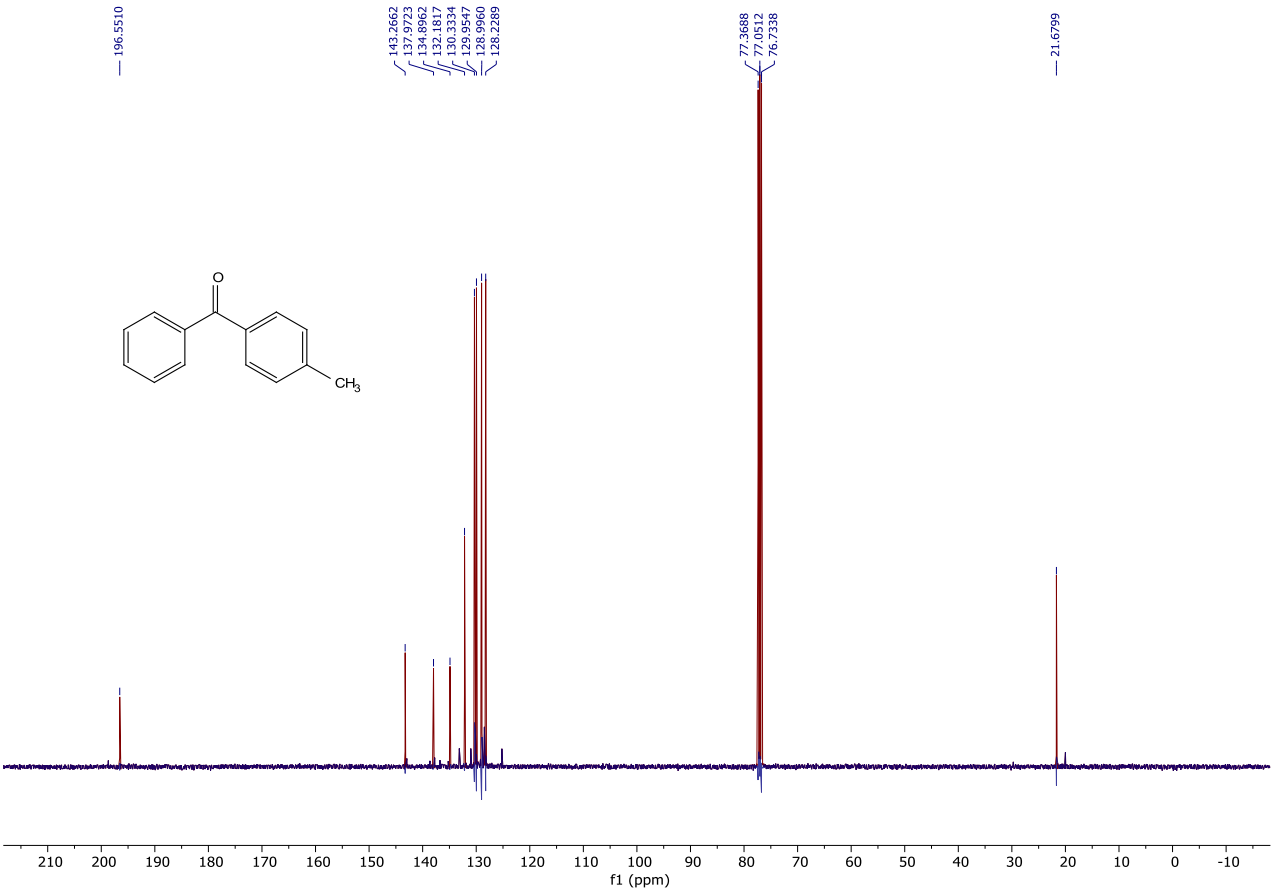
196.5510
143.2662
137.9723
134.8962
132.1817
130.3334
129.9547
128.9960
128.2289
77.3688
77.0512
76.7338
21.6799
O
CH3
210 200 190 180 170 160 150 140 130 120 110 100 90 80 70 60 50 40 30 20 10 0 -10
f1 (ppm)

NMR DATA FOR 2.12b[17]

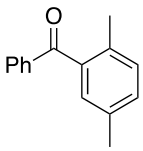

(**4-fluorophenyl)(phenyl)methanone 2.12b**: ^{1}H NMR (400 MHz, Dichloromethane-d_2) δ 1H NMR (400 MHz,) δ 7.83 – 7.67 (m, 2H), 7.65 – 7.53 (m, 1H), 7.50 – 7.37 (m, 2H), 7.27 – 7.14 (m, 2H), 7.12 – 7.00 (m, 1H), 2.33 (s, 3H), 2.24 (s, 3H).^{13}C NMR (101 MHz, $CDCl_3$) δ ^{13}C NMR (101 MHz, CH_2Cl_2) δ 200.26, 140.39, 139.62, 136.65, 135.17, 134.75, 132.62, 132.54, 131.71, 130.58, 130.17, 22.33, 20.93. White solid **2.12b** product from **2.1b** (32.5 mg) 82% yield; **2.12b** from **2.1d** (20.2 mg) 54% yield.

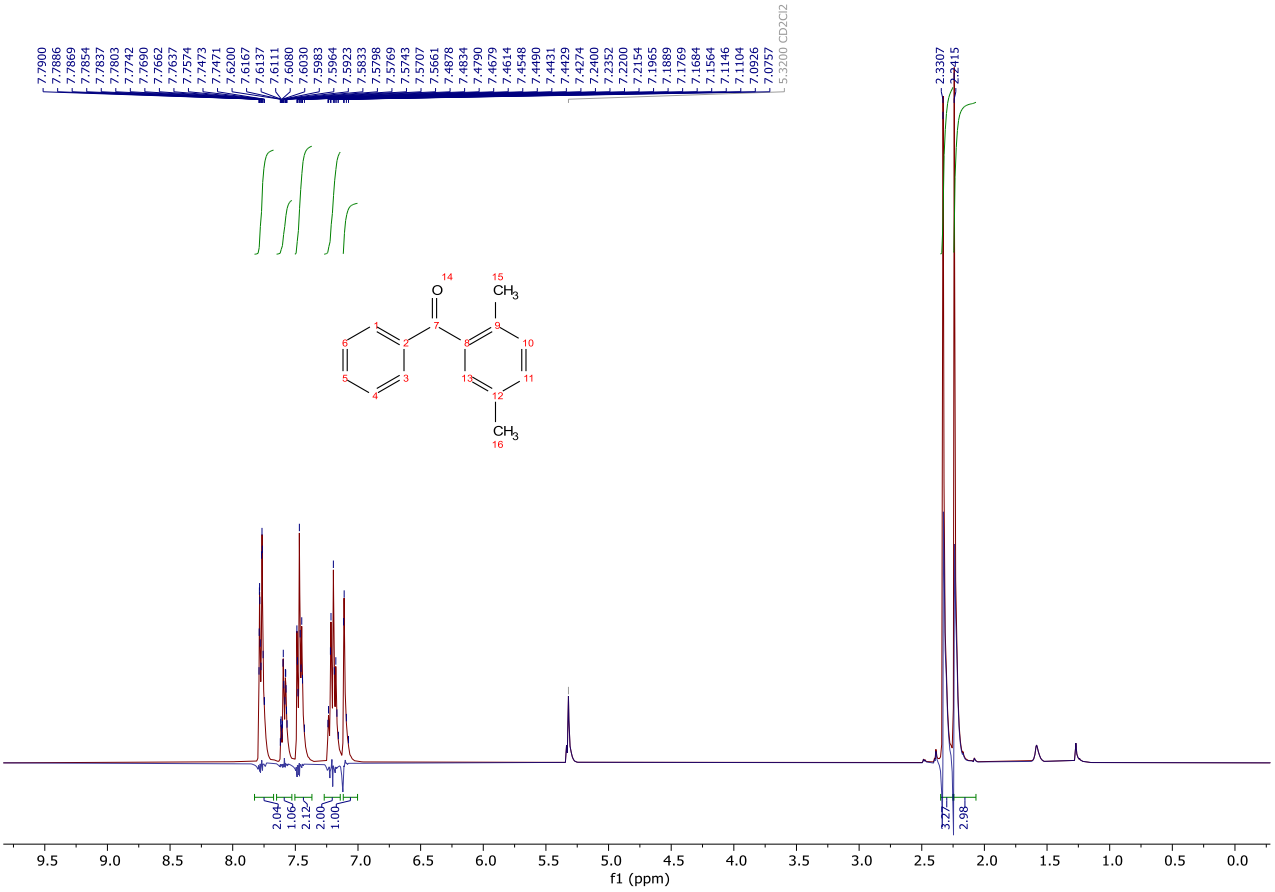

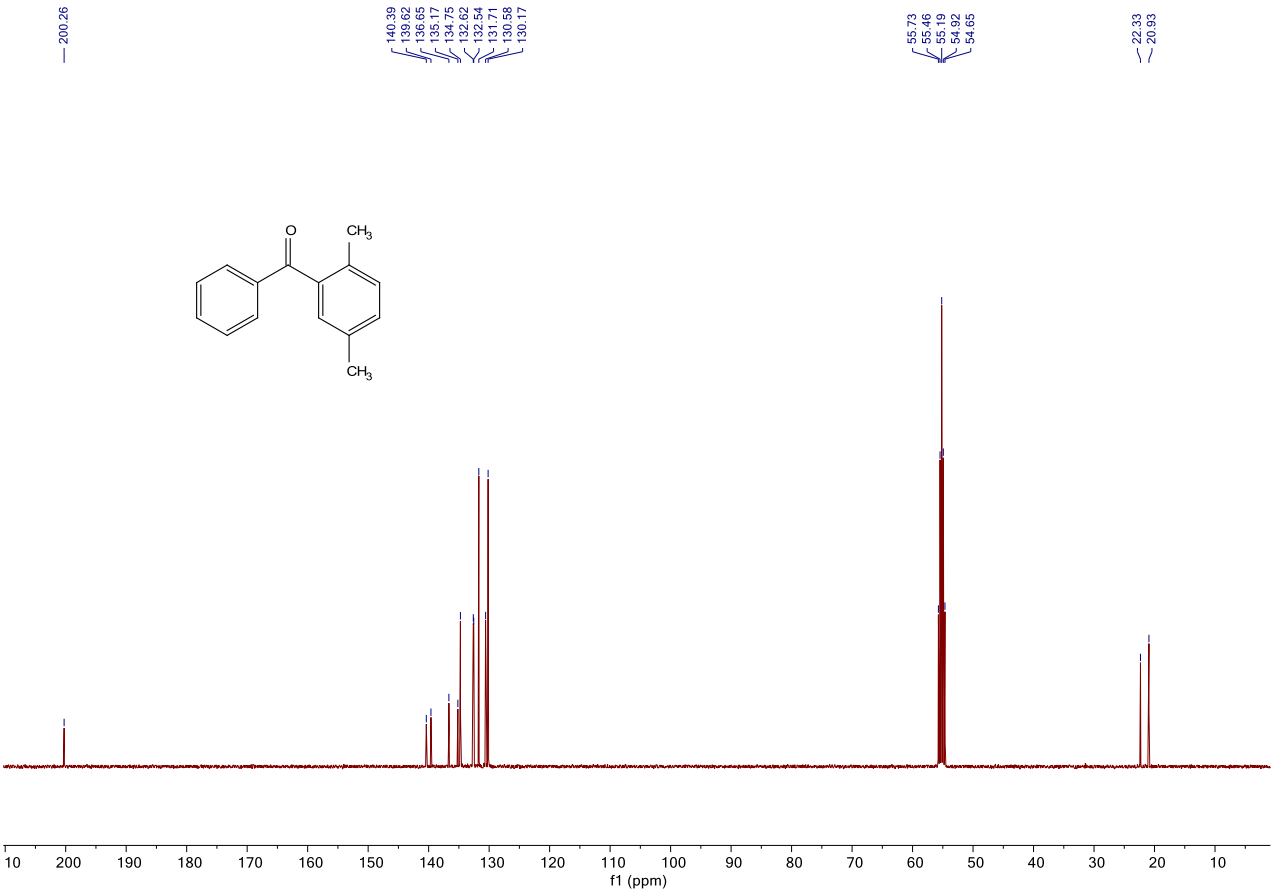
200.26
140.39
139.62
136.65
135.17
134.75
132.62
132.54
131.71
130.58
130.17
55.73
55.46
55.19
54.92
54.65
22.33
20.93
O
CH3
CH3
10
200
190
180
170
160
150
140
130
120
110
100
90
80
70
60
50
40
30
20
10
f1 (ppm)

NMR DATA FOR 2.12c[16]

(4-fluorophenyl)(phenyl)methanone 2.12c: ^{1}H NMR (400 MHz, Dichloromethanne-d_2) δ 7.80 – 7.68 (m, 2H), 7.62 – 7.51 (m, 1H), 7.49 – 7.37 (m, 2H), 7.21 (dd, J = 8.9, 3.1 Hz, 1H), 7.12 (s, 1H), 7.06 (d, J = 7.9 Hz, 1H), 2.39 (s, 3H), 2.30 (s, 3H). δ 13C NMR (101 MHz, CD_2Cl_2) δ 199.93, 142.49, 140.00, 138.91, 137.39, 134.52, 133.54, 131.67, 130.84, 130.08, 127.47, 22.83, 21.53. White solid. **2.12c** product from **2.1b** (27.8 mg) 70% yield; **2.12c** from **2.1d** (26.5 mg) 71% yield.

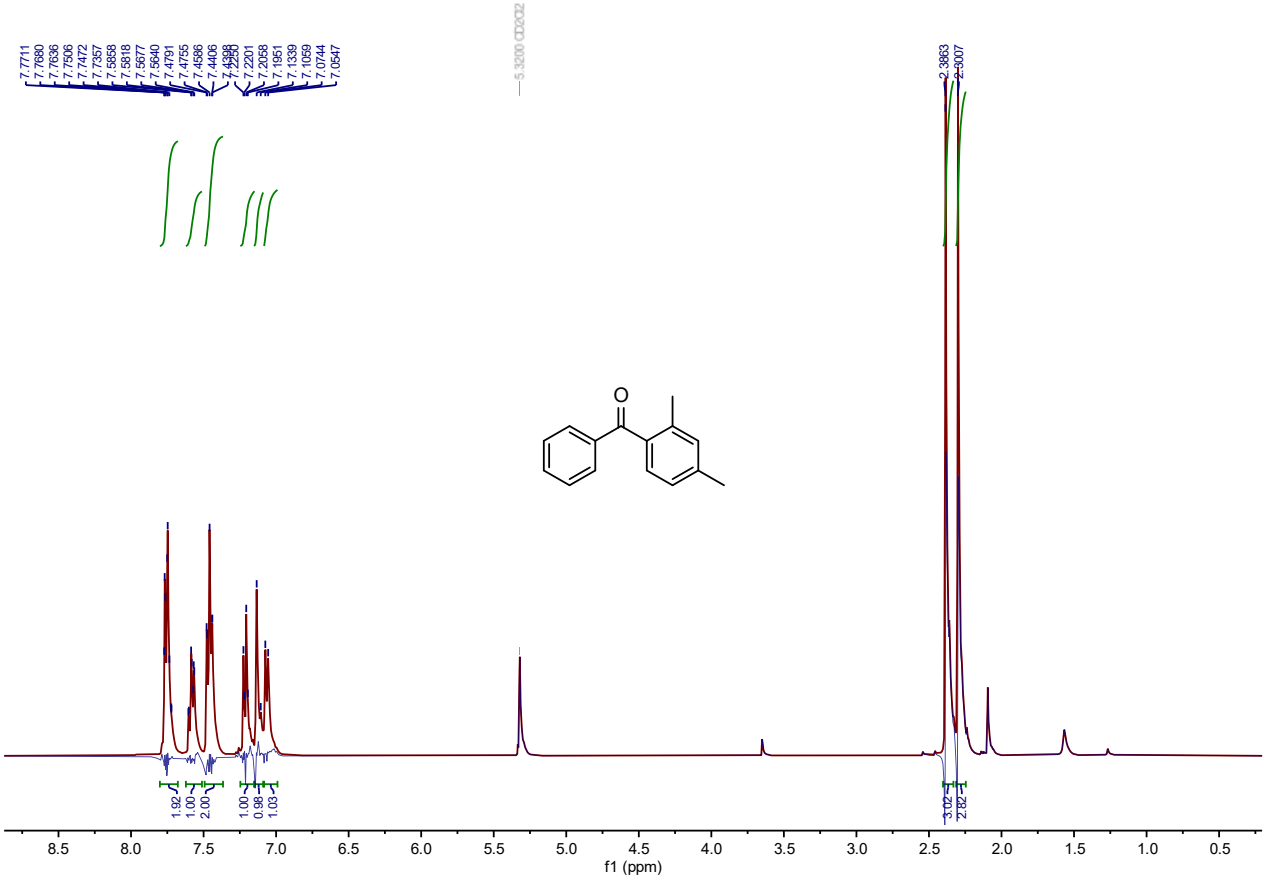

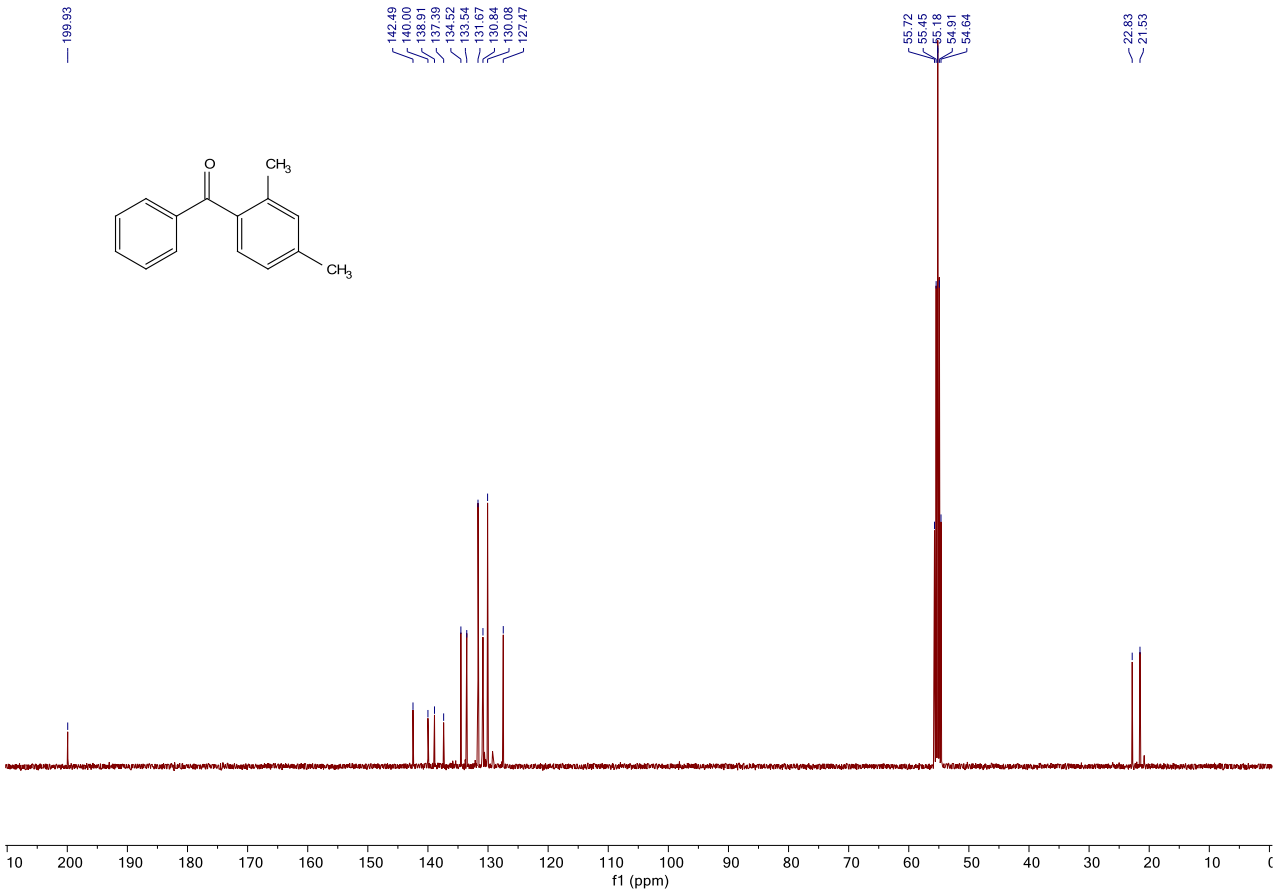
199.93
142.49
140.00
138.91
137.39
134.52
133.54
131.67
130.84
130.08
127.47
55.72
55.45
55.18
54.91
54.64
22.83
21.53
O
CH3
CH3
f1 (ppm)

NMR DATA FOR 2.12d[16]

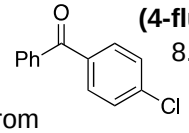

(4-fluorophenyl)(phenyl)methanone 2.12d: ^{1}H NMR (600 MHz, Chloroform-*d*) δ 7.77 (t, *J* = 8.7 Hz, 4H), 7.60 (t, *J* = 7.4 Hz, 1H), 7.53 – 7.39 (m, 4H). ^{13}C NMR (151 MHz, $CDCl_3$) δ 195.5, 138.9, 137.3, 135.9, 132.6, 131.5, 129.9, 128.6, 128.4. White solid. **2.12d** product from **2.1b** (26.5 mg) 65% yield; **2.12d** from **2.1d** (33.8 mg) 88% yield.

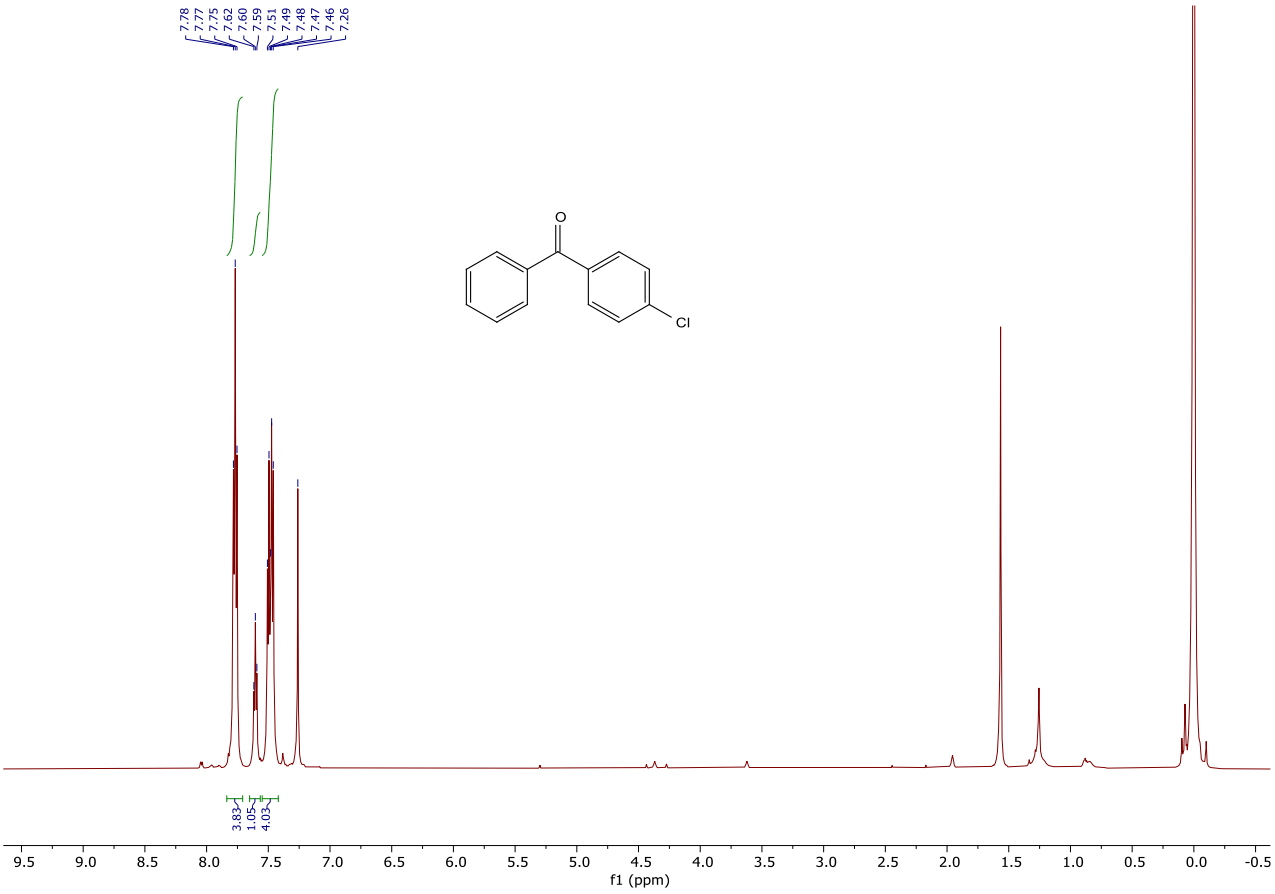

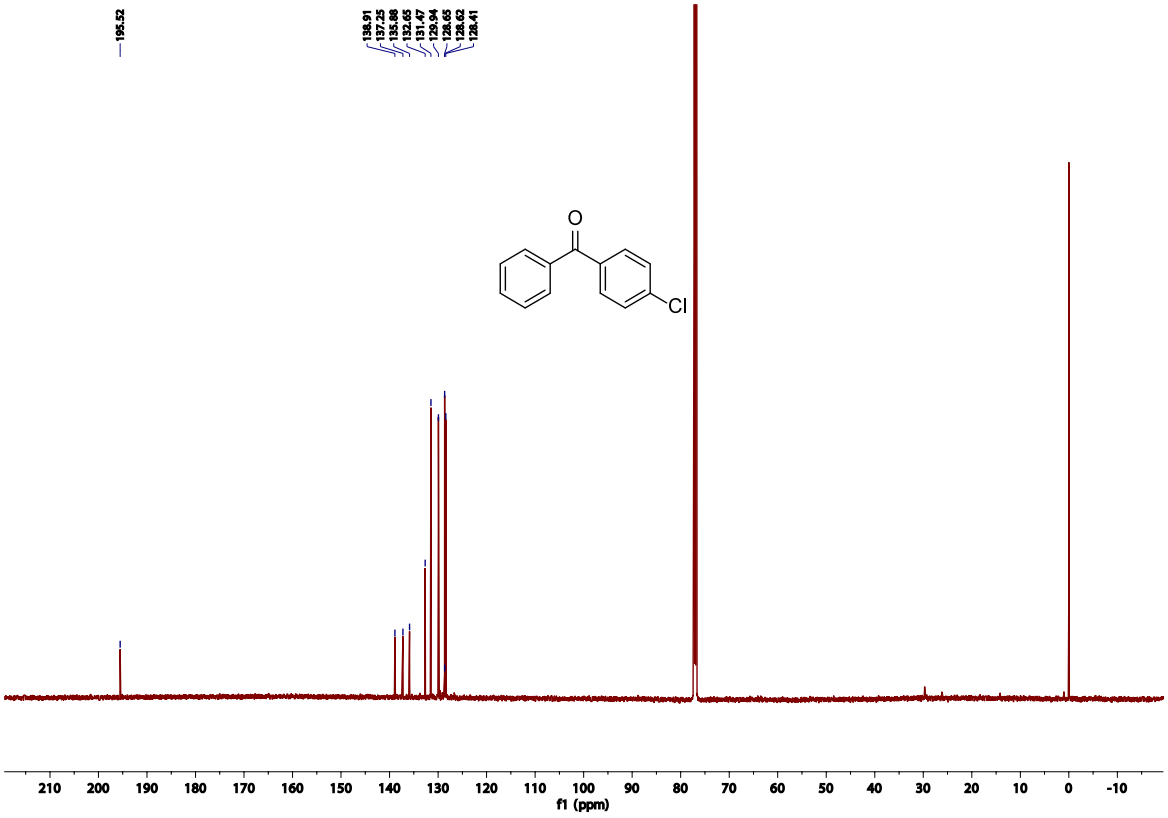
195.52
138.91
137.25
135.68
132.66
131.47
129.94
128.65
128.62
128.41
O
Cl
210
200
190
180
170
160
150
140
130
120
110
100
90
80
70
60
50
40
30
20
10
0
-10
f1 (ppm)

NMR DATA FOR 2.12e

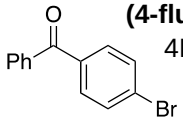

(4-fluorophenyl)(phenyl)methanone 2.12e: ^{1}H NMR (600 MHz, Chloroform-*d*) δ 7.81-7.74 (m, 4H), 7.60 (t, *J* = 7.4 Hz, 1H), 7.54 – 7.44 (m, 4H). ^{13}C NMR (151 MHz, $CDCl_3$) δ 195.6, 137.2, 136.3, 132.7, 131.6, 131.6, 130.1, 129.9, 128.4, 127.5. White solid. **2.12e** product from **2.1b** (27.5 mg) 56% yield; **2.12e** from **2.1d** (32.4 mg) 70% yield.

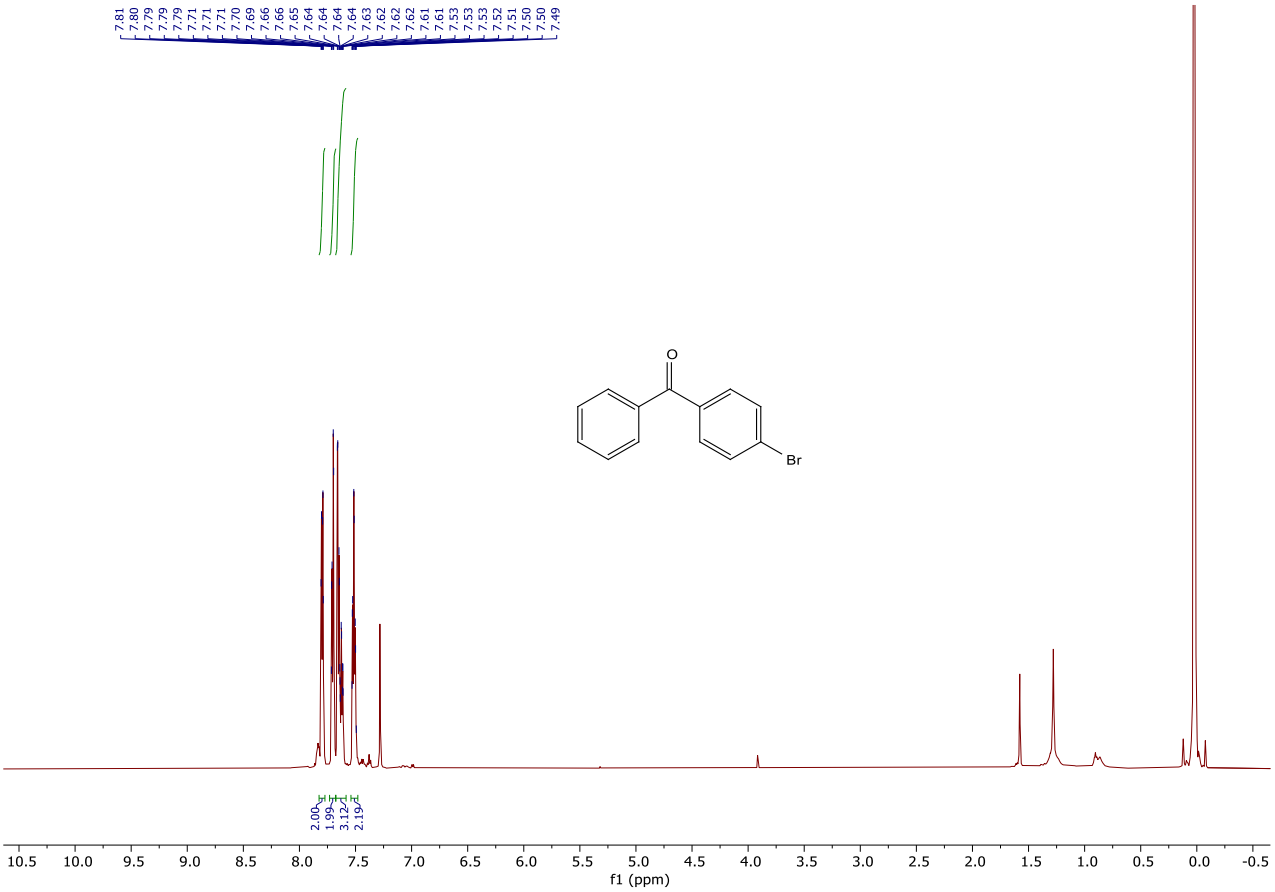

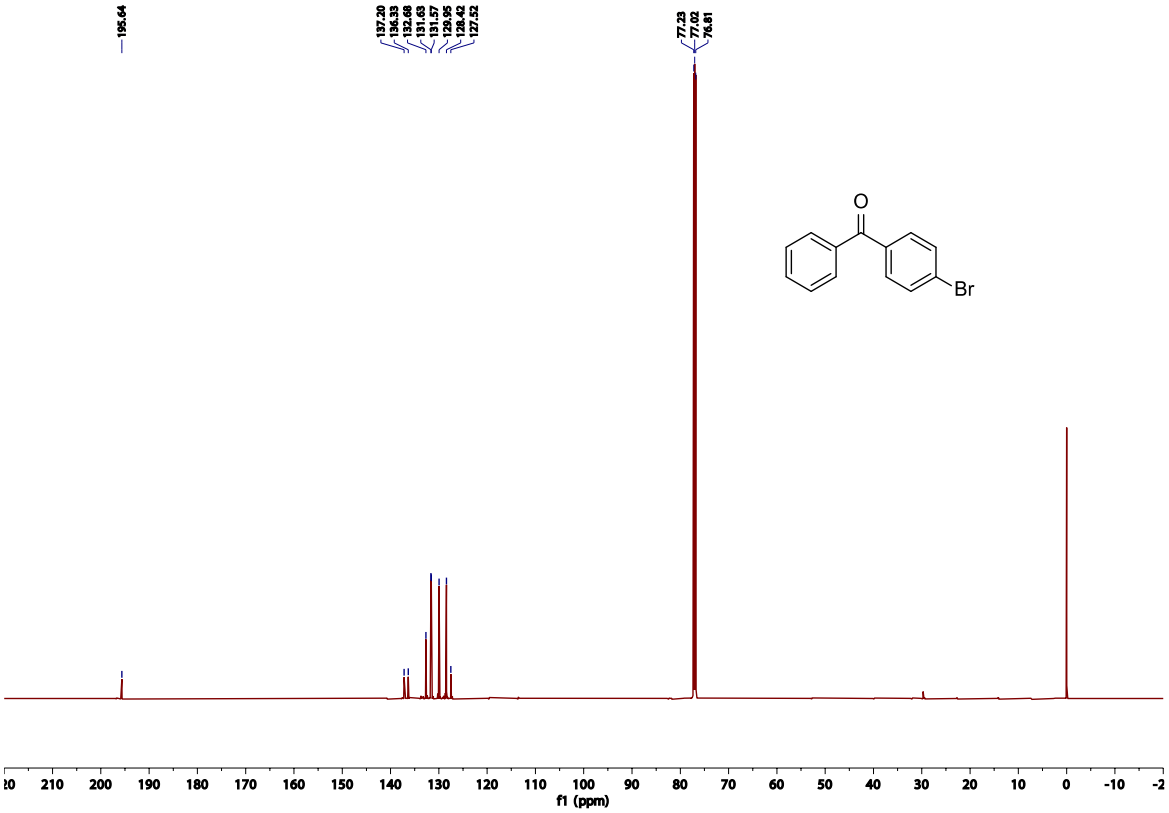

NMR DATA FOR 2.12f

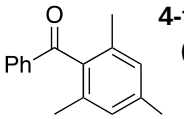

4-fluorophenyl)(phenyl)methanone 2.12f: ^{1}H NMR (600 MHz, Chloroform-*d*) δ 7.88 – 7.80 (m, 2H), 7.64 – 7.57 (m, 1H), 7.47 (t, *J* = 7.6 Hz, 2H), 6.93 (s, 2H), 2.36 (s, 3H), 2.11 (s, 6H). ^{13}C NMR (151 MHz, $CDCl_3$) δ 200.8, 138.5, 137.3, 136.9, 134.2, 133.5, 129.4, 128.8, 128.3, 21.2, 19.4. White solid. **2.12f** product from **2.1b** (29.2 mg) 69% yield; **2.12f** from **2.1d** (28.7 mg) 72% yield.

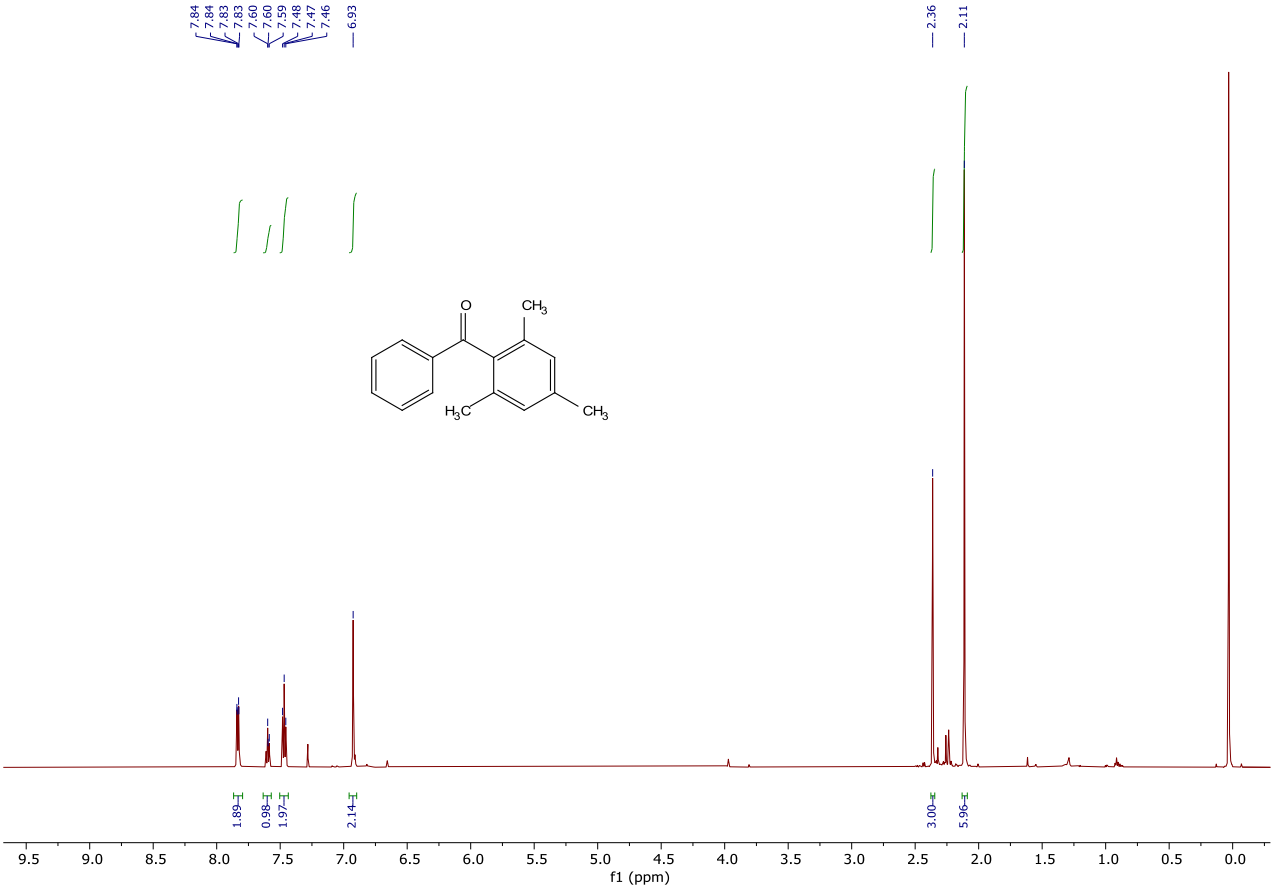

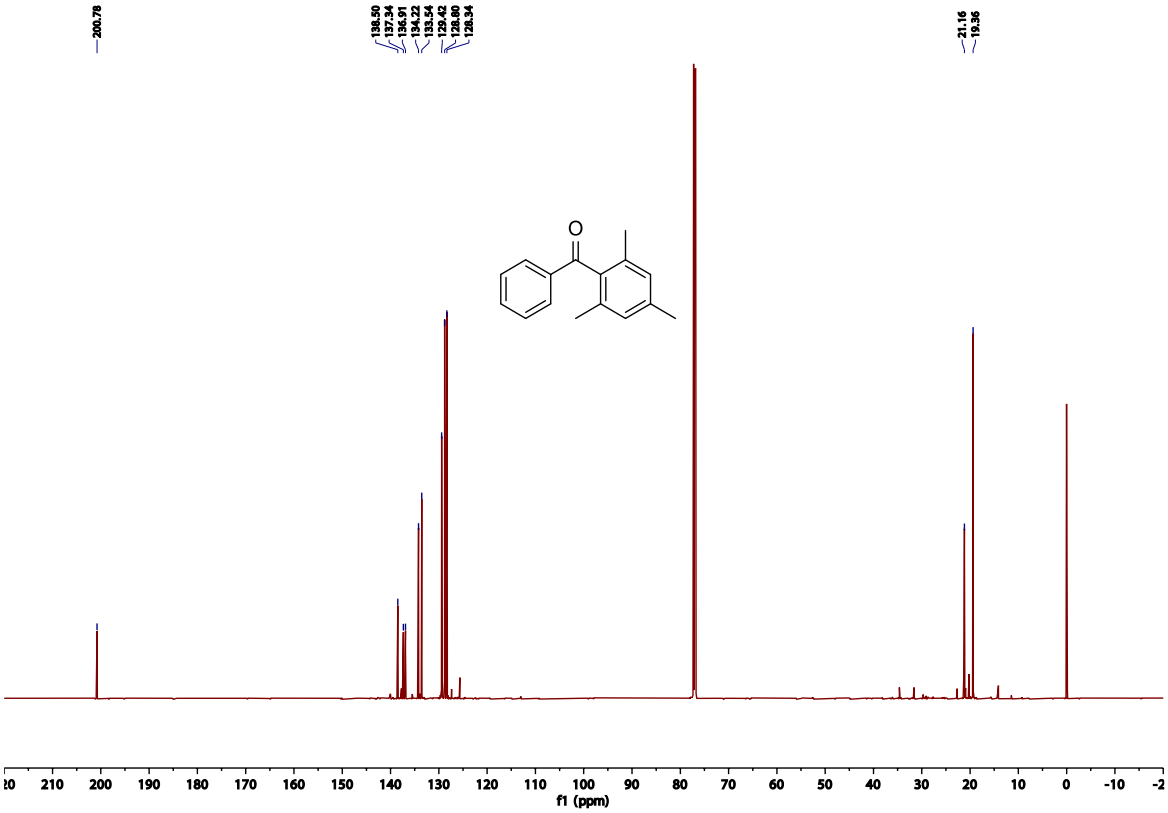
200.78
138.50
137.34
135.91
134.22
133.54
129.42
128.60
128.34
21.16
19.36
O
f1 (ppm)

Synthesis of Twisted Polyamides 2.13.

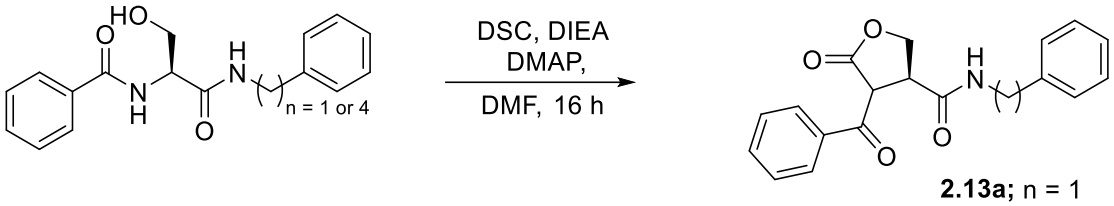

2.13a; n = 1
2.13b; n =4

2.13c

General procedure for selective synthesis of twisted amides: A polyamide containing serine residue (0.82 mmol) was dissolved in 30 mL of anhydrous DMF. To the reaction mixture, DSC (5 equiv.), DMAP (5 equiv.) and DIEA (5 equiv.) were added and left to stir overnight. The reaction was monitored by TLC followed by concentration using a rotary evaporator and purification by column chromatography in 40% ethyl acetate in hexane with **2.13a** (white solid, 70% yield), **2.13b** (white solid, 66 % yield) and **2.13c** (white solid, 63 % yield). The resulting activated amides **2.13a** and **2.13b** were characterized by ^{1}H NMR and ^{13}C-NMR.

NMR DATA of the Twisted Polyamides 2.13a and 2.13b

NMR DATA FOR 2.13a.

(R)-3-benzoyl-2-oxo-N-(4-phenylbutyl)oxazolidine-4-carboxamide: ^{1}H NMR (600 MHz, Acetone) δ 8.06 (s, 1H), 7.68 (ddq, J = 7.0, 2.7, 1.2 Hz, 2H), 7.56 (dddt, J = 9.4, 6.8, 2.7, 1.3 Hz, 1H), 7.49 – 7.41 (m, 2H), 7.37 – 7.28 (m, 4H), 7.29 – 7.18 (m, 1H), 5.18 (dddd, J = 9.0, 4.7, 3.2, 1.5 Hz, 1H), 4.79 – 4.71 (m, 1H), 4.52 (dd, J = 15.1, 6.1 Hz, 1H), 4.46 (dd, J = 15.1, 5.7 Hz, 1H), 4.44 – 4.40 (m, 1H). **^{13}C NMR (151 MHz, CDCl3)** δ 174.32, 173.53, 158.00, 144.05, 138.93, 136.92, 134.04, 133.60, 132.81, 132.63, 132.23, 71.05, 62.55, 48.08.

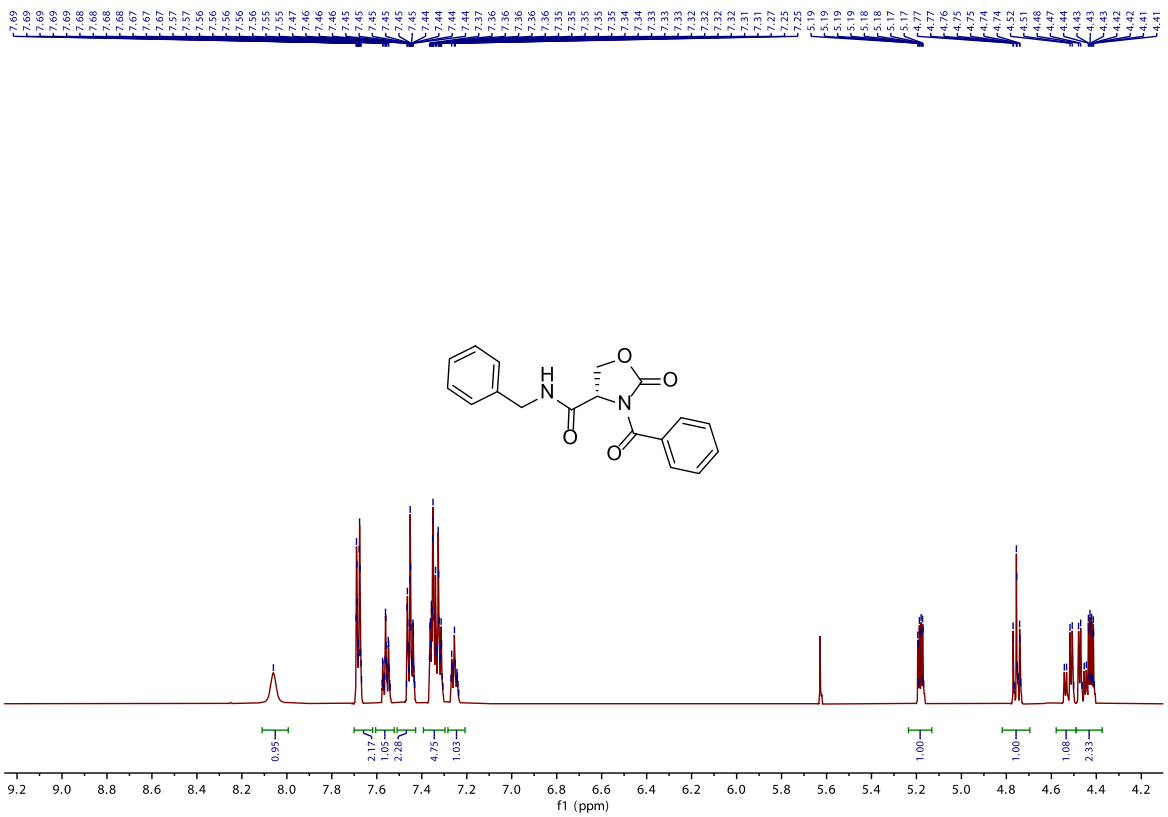
7.69 7.69 7.69 7.69 7.68 7.68 7.68 7.67 7.67 7.67 7.57 7.57 7.56 7.56 7.56 7.56 7.55 7.55 7.47 7.46 7.46 7.45 7.45 7.45 7.45 7.44 7.44 7.44 7.44 7.37 7.36 7.36 7.36 7.35 7.35 7.35 7.35 7.34 7.34 7.33 7.33 7.32 7.32 7.32 7.32 7.31 7.31 7.27 7.25 7.25
5.19 5.19 5.19 5.18 5.18 5.17 5.17 4.77 4.77 4.76 4.75 4.74 4.74 4.52 4.51 4.48 4.47 4.44 4.43 4.43 4.43 4.42 4.42 4.41 4.41
H
N
O
O
N
O
O
0.95
2.17
1.05
2.28
4.75
1.03
1.00
1.00
1.08
2.33
9.2 9.0 8.8 8.6 8.4 8.2 8.0 7.8 7.6 7.4 7.2 7.0 6.8 6.6 6.4 6.2 6.0 5.8 5.6 5.4 5.2 5.0 4.8 4.6 4.4 4.2
f1 (ppm)

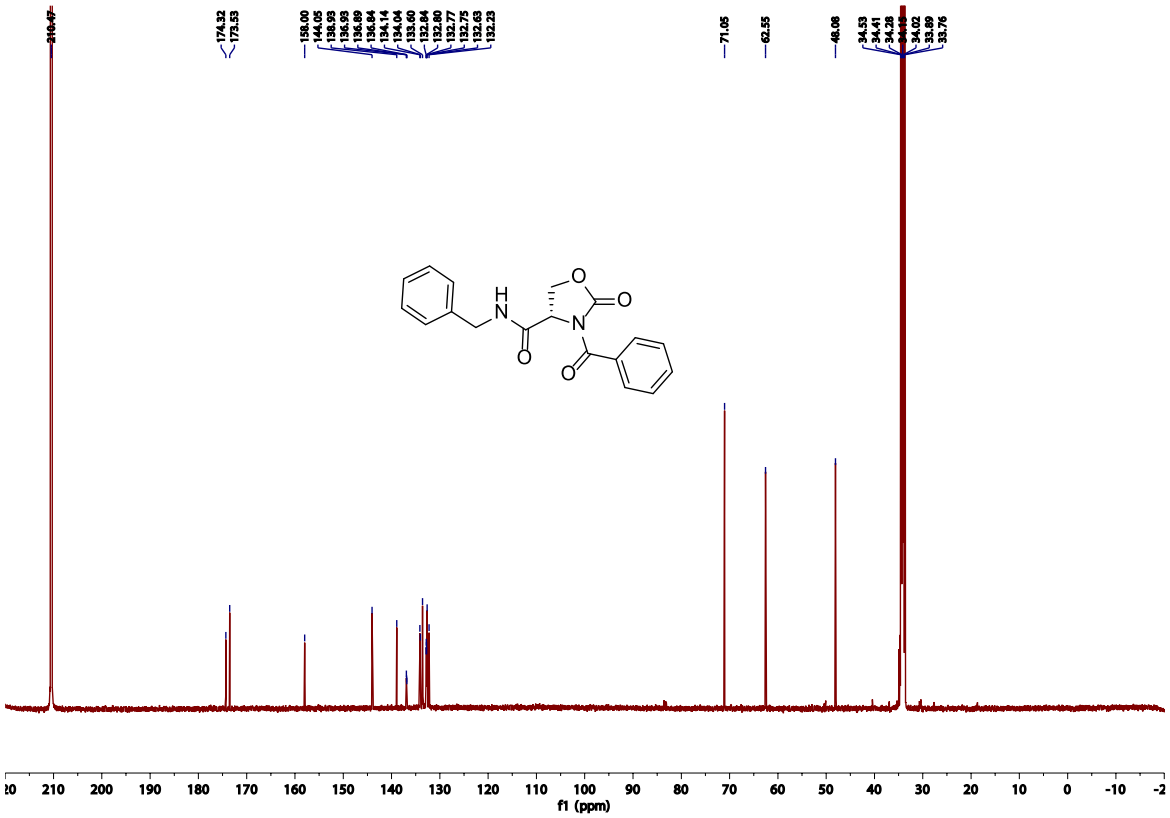

NMR DATA FOR 2.13b.

R)-3-benzoyl-2-oxo-N-(4-phenylbutyl)oxazolidine-4-carboxamide: ^{1}H NMR (400 MHz, Acetone) δ 7.67 (td, J = 8.2, 4.8 Hz, 3H), 7.60 – 7.53 (m, 1H), 7.46 (dd, J = 8.4, 7.1 Hz, 2H), 7.31 – 7.06 (m, 4H), 5.09 (dd, J = 9.0, 4.3 Hz, 1H), 4.72 (t, J = 8.8 Hz, 1H), 4.37 (dd, J = 9.0, 4.3 Hz, 1H), 3.43 – 3.22 (m, 2H), 2.65 (td, J = 7.4, 2.1 Hz, 2H), 1.69 (qd, J = 8.9, 5.6 Hz, 2H), 1.58 (ddd, J = 12.4, 9.4, 6.1 Hz, 2H). **^{13}C NMR (101 MHz, Acetone)** δ 169.06, 168.14, 152.83, 142.41, 133.76, 131.67, 128.88, 128.36, 128.19, 127.60, 125.59, 65.91, 57.35, 38.90, 35.14, 28.71, 28.51.

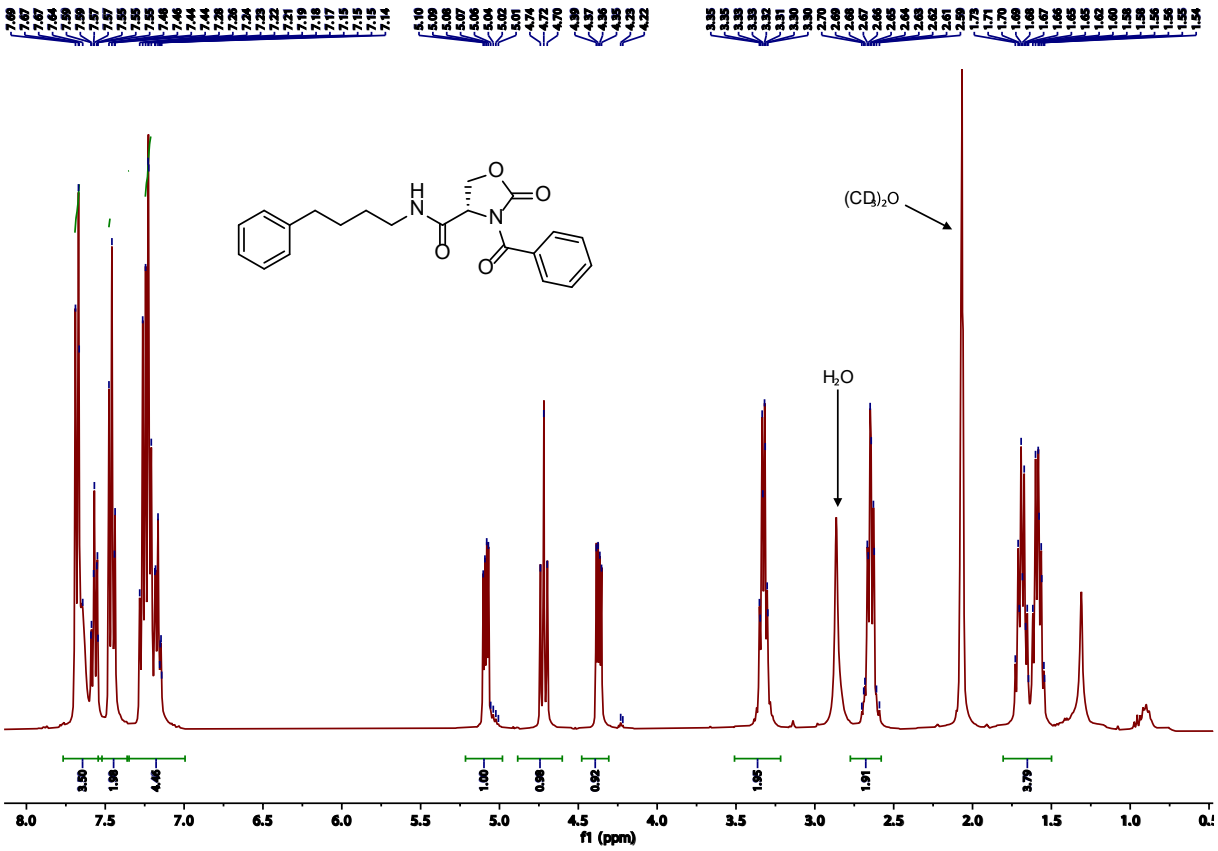
(CD3)2O
H2O
3.50
1.88
4.46
1.00
0.98
0.92
1.95
1.91
3.79
8.0
7.5
7.0
6.5
6.0
5.5
5.0
4.5
4.0
3.5
3.0
2.5
2.0
1.5
1.0
f1 (ppm)

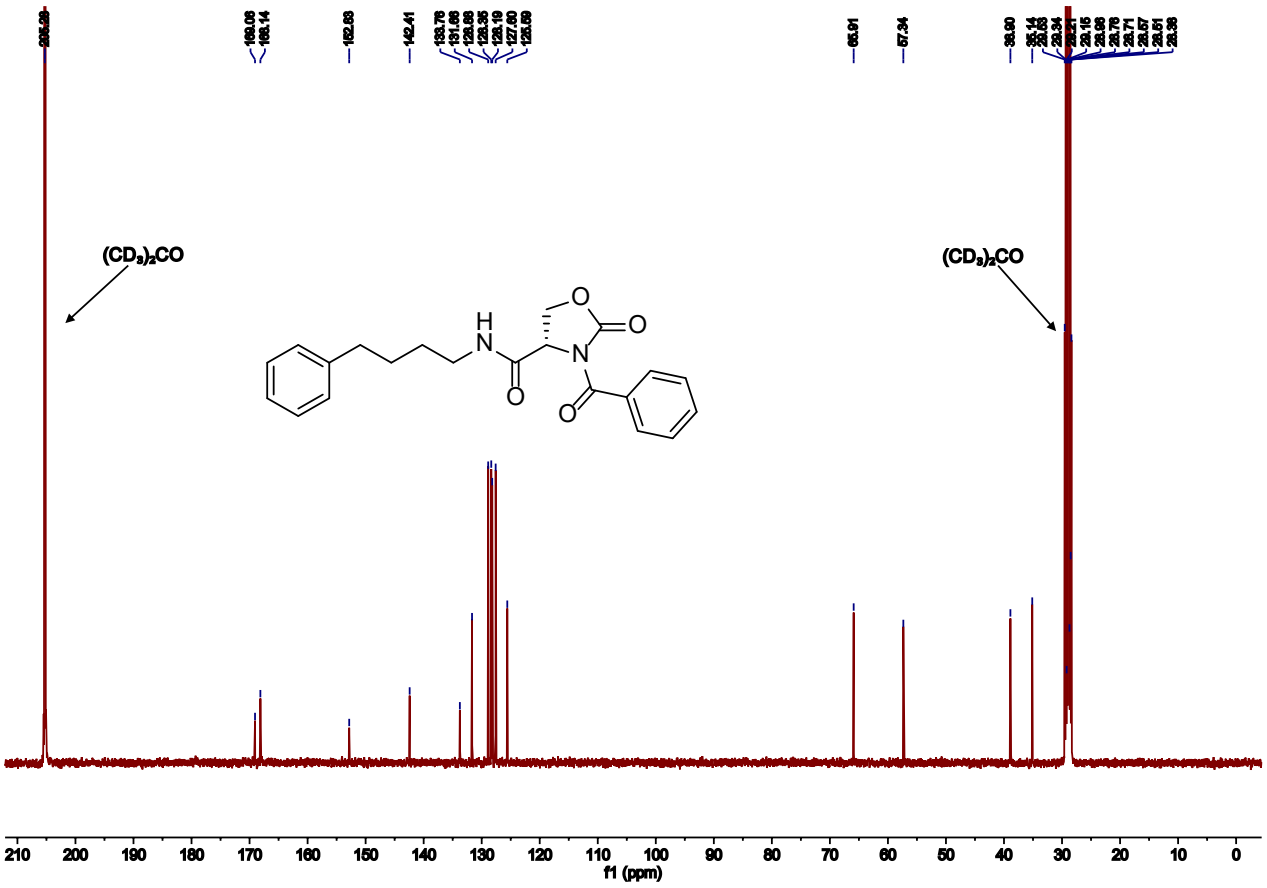

Procedure for Friedel-Crafts reaction of twisted peptide 2.13.

Optimization reaction for Friedel-Crafts acylation with polyamide 2.13a: To a solution of twisted amide **2.13a** (0.273 mm) in dry anisole solvent or dry anisole and HFIP co-solvents (1:3) (5 mL, indicated below in the table) under inert conditions, TfOH (10 equiv.) was added to the reaction mixture and allowed to stir at 50 ^{o}C for the time indicated in the table below. The reaction was analyzed by TLC, volatiles removed under reduced pressure and reaction mixture was purified by column chromatography using mixture of ethyl acetate and hexane (1:4) as an eluent to get the desired ketone **2.10a** as white solid. The resulting ketone product **2.10a** was characterized by ^{1}H NMR and ^{13}C-NMR.

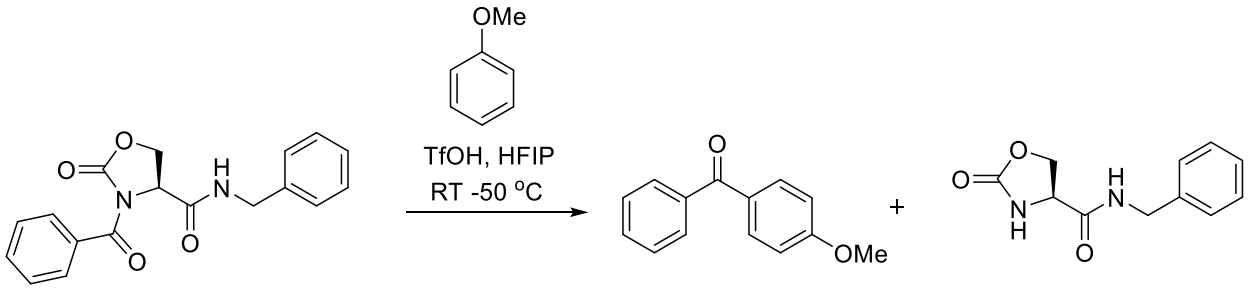

2.13a **2.10b**

Entry	Solvent	Temperature (^{o}C)	Yield (%)	Time (h)
1	Anisole	RT	0	16

2	75:25 HFIP/Anisole	RT	25	10
3	75:25 HFIP/Anisole	45	73	10

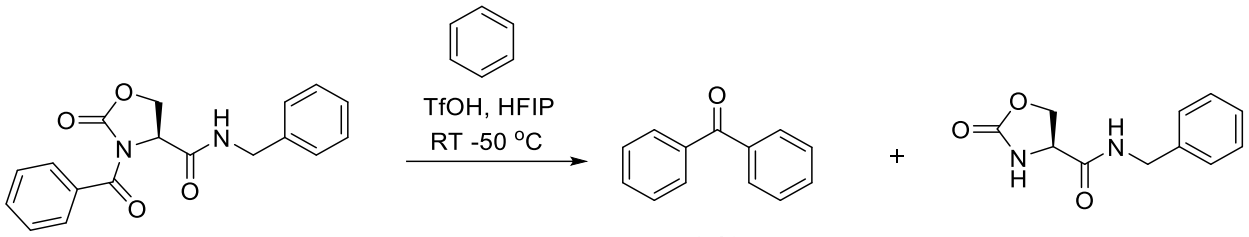

2.13a **2.10a**

General procedure of Friedel-Crafts acylation with polyamide 2.13a: To a solution of twisted amide **2.13a** (0.273 mmol) in dry arene and HFIP co-solvents (1:3) (5 mL; benzene) under inert conditions, TfOH (10 equiv.) was added to the reaction mixture and allowed to stir at 50 °C for 10 h. The reaction was analyzed by TLC, volatiles removed under reduced pressure and reaction mixture was purified by column chromatography using mixture of ethyl acetate and hexane (1:4) as an eluent to get the desired ketone **2.10b** as white solid in 67% yield. The resulting ketone product **2.10b** was characterized by ^{1}H NMR and ^{13}C-NMR.

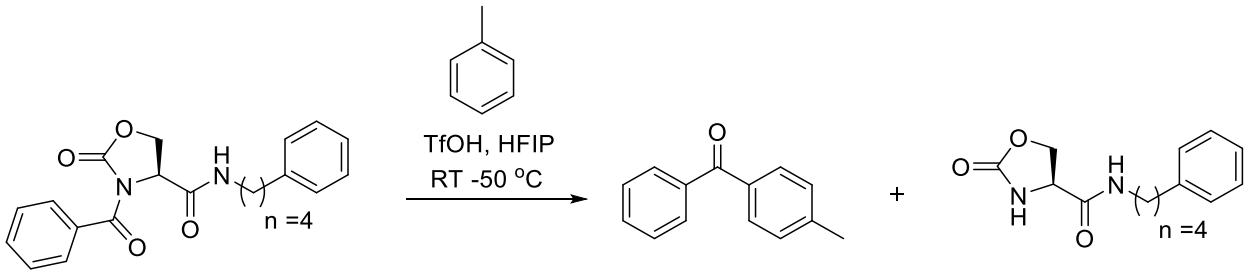

2.13b **2.12a**

General procedure of Friedel-Crafts acylation with polyamide 2.13b: To a solution of twisted amide **2.13b** (0.273 mmol) in dry arene and HFIP co-solvents (1:3) (5 mL; toluene) under inert conditions, TfOH (10 equiv.) was added to the reaction mixture and allowed to stir at 50 °C for 10 h. The reaction was analyzed by TLC, volatiles removed under reduced pressure and reaction mixture was purified by column chromatography using mixture of ethyl acetate and hexane (1:4) as an eluent to get the desired ketone **2.12a** as white solid in 53% yield. The resulting ketone product **2.12a** was characterized by ^{1}H NMR and ^{13}C-NMR

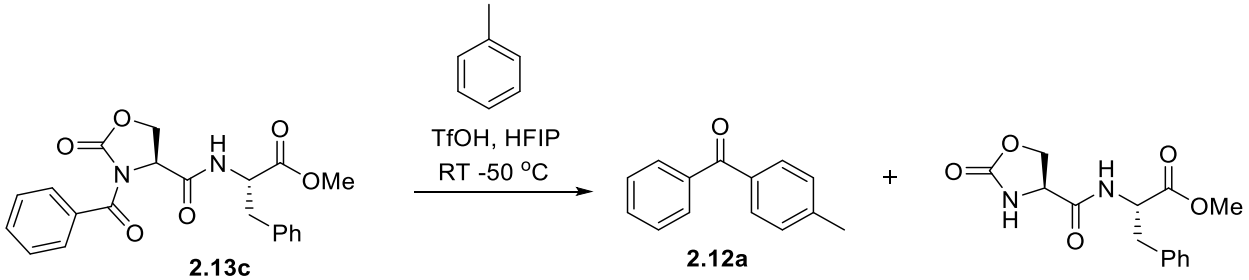

2.13c **2.12a**

General procedure of Friedel-Crafts acylation with peptide 2.13c: To a solution of twisted peptide **2.13c** (0.0126 mmol) in dry toluene and HFIP co-solvents (1:3) (600 µL) under inert conditions, TfOH (10 equiv., 0.126 mmol) was added to the reaction mixture and allowed to stir at 50 ^{o}C for 10 h. The reaction was analyzed by HPLC, volatiles removed under reduced pressure and reaction mixture was purified HPLC. The HPLC was done using a linear gradient of 0-80% of acetonitrile in water for 30 mins at room temperature with a flow rate of 1.0 mL min^{-1} and detector wavelength (l = 220 nm) to get the desired ketone **2.12a** in 68% yield. The resulting ketone product **2.12a** was characterized by ^{1}H NMR and ^{13}C-NMR and LCMS.

HPLC spectra of twisted polyamide 2.13c and products of Friedel-Crafts reaction with 2.13c.

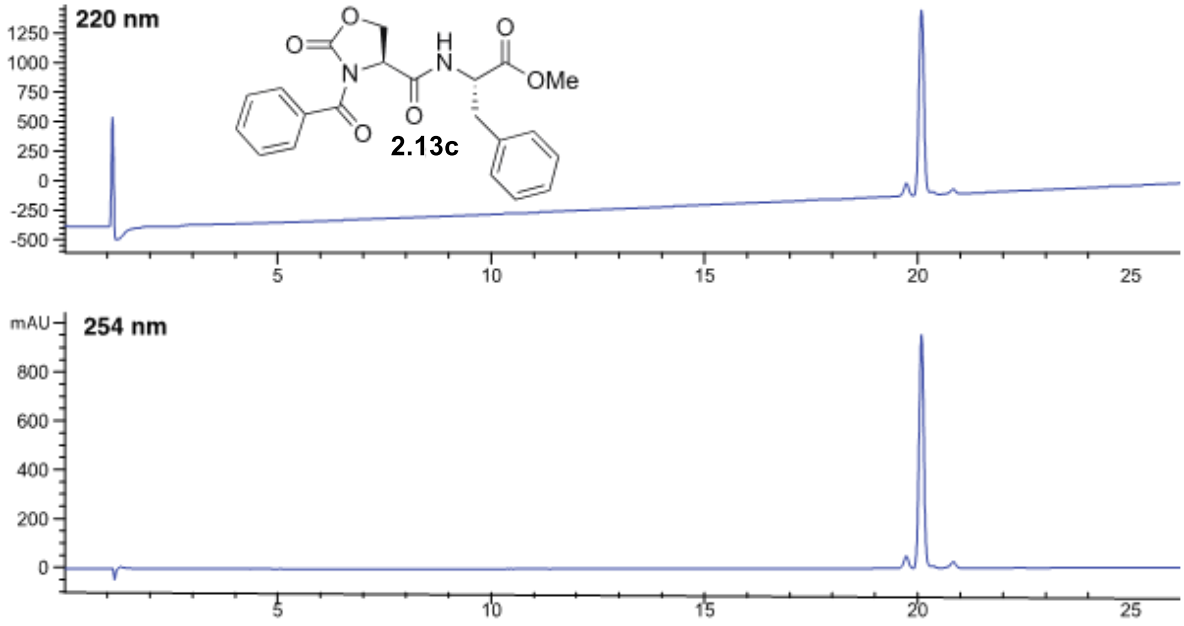

HPLC spectra of reaction of twisted polyamide 2.13c

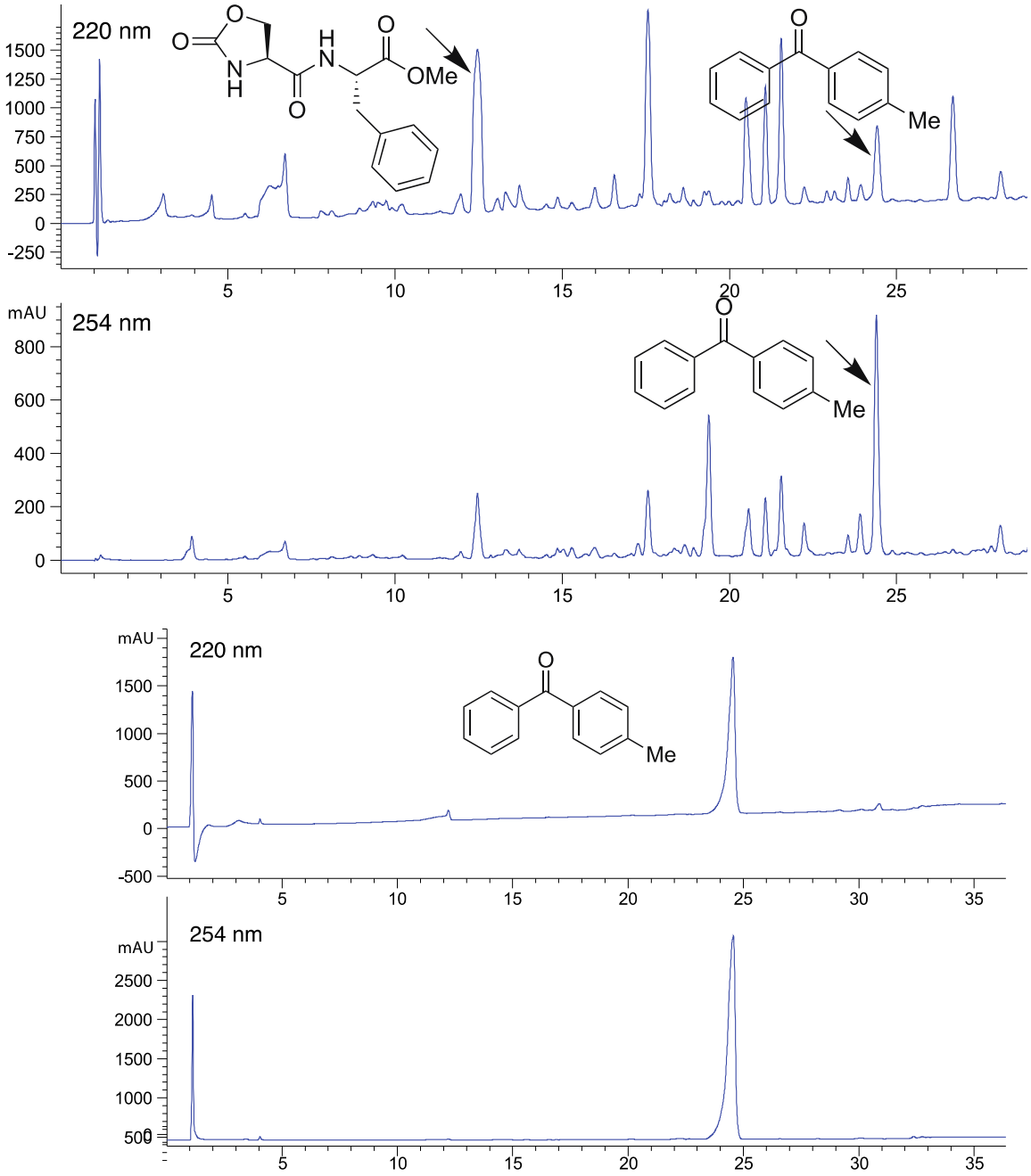

HRMS spectra of twisted polyamide 2.13c and products of Friedel-Crafts reaction with 2.13c.

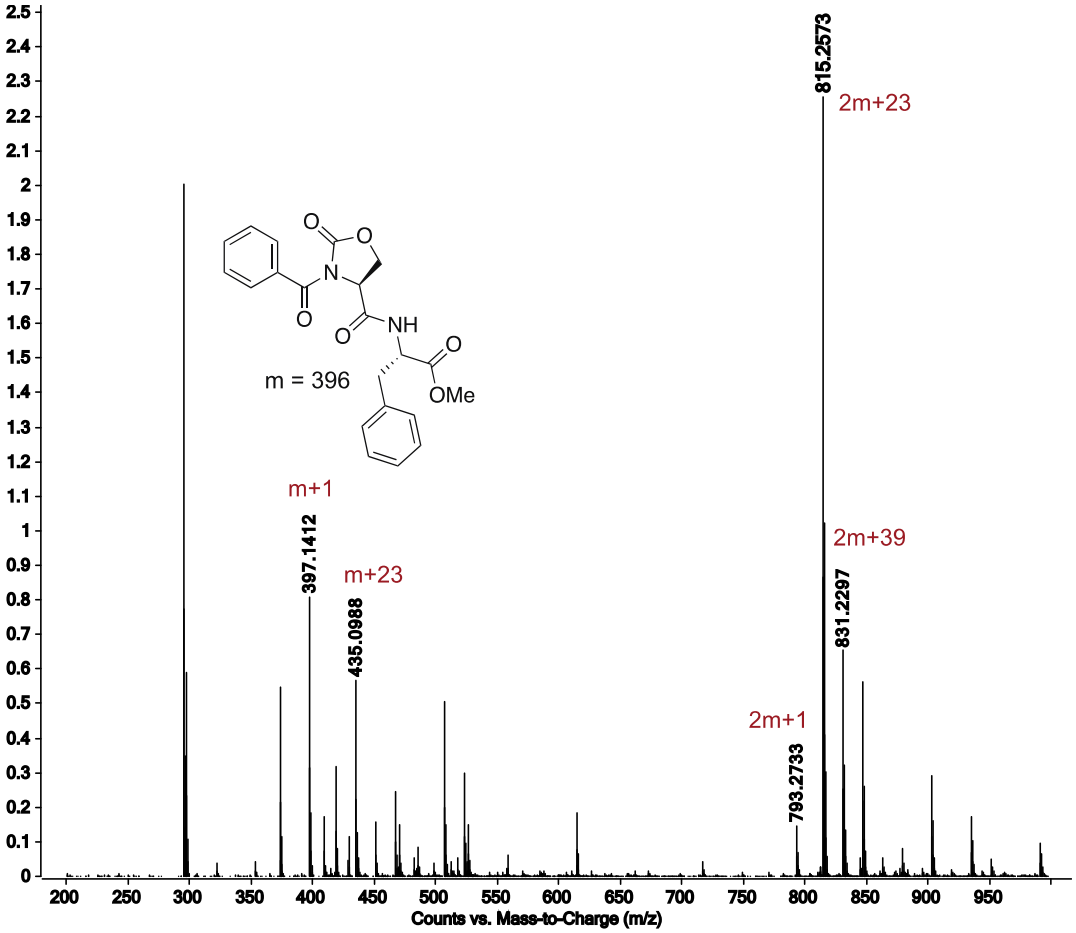
815.2573
2m+23
m = 396
m+1
397.1412
m+23
435.0988
2m+39
831.2297
2m+1
793.2733
Counts vs. Mass-to-Charge (m/z)

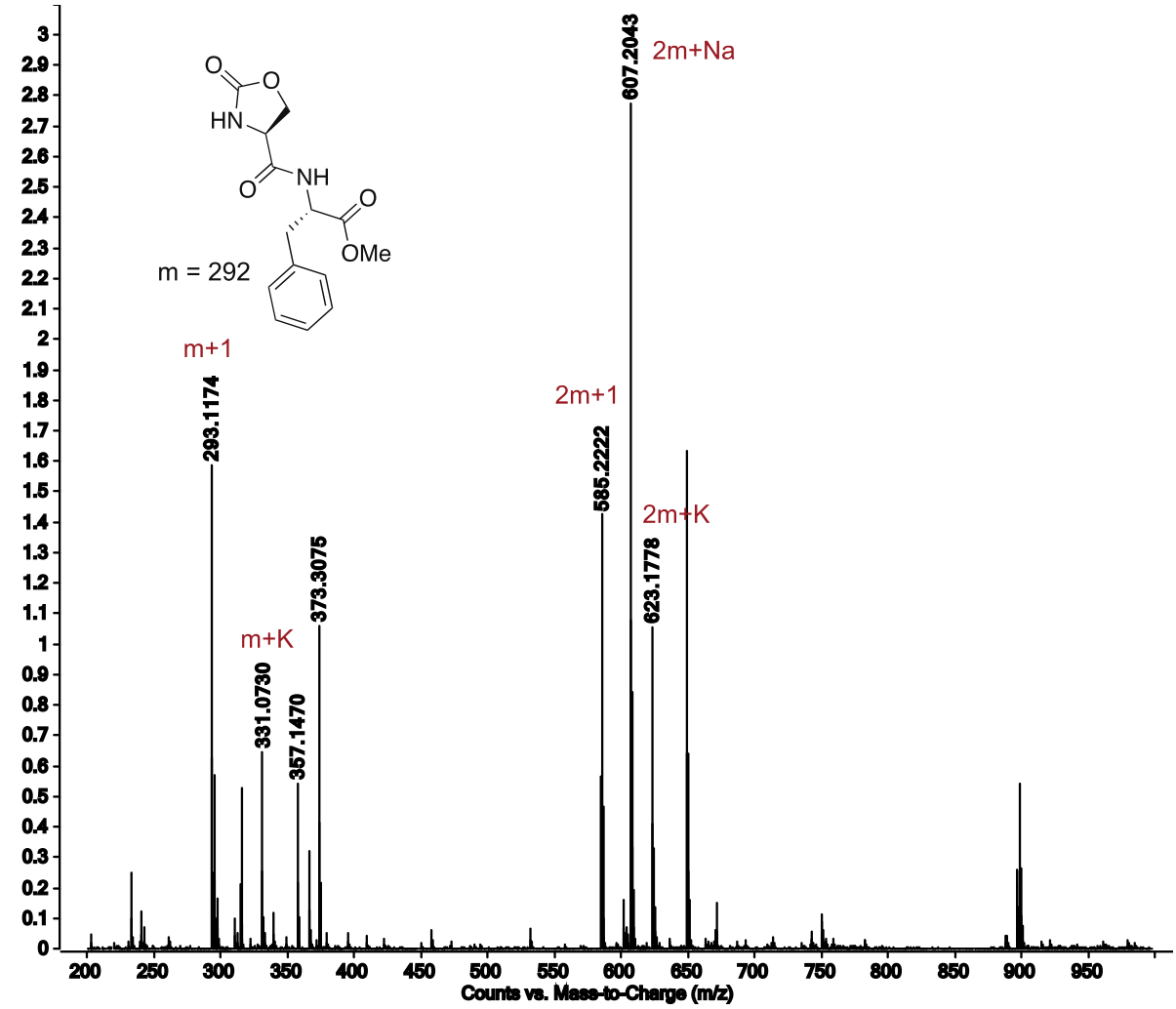

Synthesis of polyamide starting materials

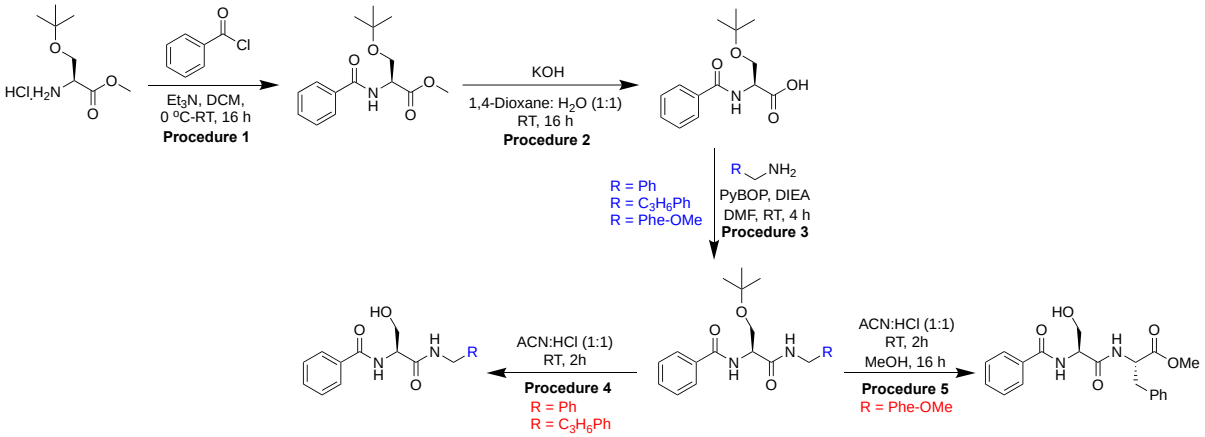

Procedure 1. H-Ser(tBu)-OMe HCl (19.04 mmol) was added to a solution containing benzoyl chloride (20.95 mmol, 1.1 equiv.) in DCM (100 mL) at 0°C. Triethylamine (5.3 mL, 38.09 mmol, 2 equiv.) was added dropwise to the reaction within a period of 30 minutes and mixture was left to stir from 0°C to room temperature overnight. The reaction progress was monitored by TLC. The reaction was then diluted with more DCM and washed with saturated brine and sodium bicarbonate solution. The organic layer was

extracted and concentrated using rotary evaporator. The product, methyl N-benzoyl-O-(tert-butyl) serinate, was purified by column chromatography using a mixture of ethyl acetate and hexane (2:3) (with 85.7 % yield. The resulting product was white solid characterized by ^{1}H, ^{13}C NMR and HRMS.

Procedure 2. Methyl N-benzoyl-O-(tert-butyl) serinate (4558 mg, 16.31 mmol) was added to a solution containing 50 mL of 1,4 Dioxane and 50 mL of water. KOH (913 mg, 16.31 mmol) was added to the reaction mixture and left at room temperature to stir overnight. The reaction progress was monitored by TLC. 1N HCl solution was added to the reaction mixture gradually until a pH of 3.5 was attained. The mixture was diluted using ethyl acetate and washed with water. The organic layer was extracted and concentrated using rotary evaporator. The product, N-benzoyl-O-(tert-butyl) serine, was purified through column chromatography using a mixture of ethyl acetate, hexane and formic acid (4:1) with 85.5% yield. The resulting product was white solid and characterized by ^{1}H, ^{13}C NMR and HRMS.

Procedure 3. N-benzoyl-O-(tert-butyl) serine (925 mg, 3.49 mmol) was dissolved in DMF (20 mL) and PyBOP (1814 mg, 3.49 mmol) was added to the solution. Benzylamine (0.381 mL, 3.49 mmol) was dissolved in DMF (5 mL) followed by the addition of N,N-Diisopropylethyamine (DIEA) (0.604 mL, 3.49 mmol) to the solution. The reaction mixture was left to stir for 4 hours. The reaction progress was monitored by TLC and concentrated using rotary evaporator. The product, N-(1-(benzylamino)-3-(tert-butoxy)-1-oxopropan-2-yl) benzamide, was purified by column chromatography using a mixture of ethyl acetate and hexane (2:3). (R = Ph; white solid, yield = 88.9%); (R = C_3H_6Ph; white solid, yield = 64.8%); (R = Phe-OMe; white solid, yield = 74.6%). The resulting products were characterized by ^{1}H, ^{13}C NMR and HRMS.

Procedure 4. N-(1-(benzylamino)-3-(tert-butoxy)-1-oxopropan-2-yl) amide (1100 mg, 3.10 mmol) was dissolved in a reaction mixture containing acetonitrile (60 mL) and 12 N HCl (60 mL). The reaction mixture was left to stir at room temperature for 2 hours. The reaction progress was monitored by TLC. The reaction was quenched by adding sodium bicarbonate. A work-up was done by adding DCM to the mixture and the organic layer was extracted and concentrated using rotary evaporator. The product, N-(1-(benzylamino)-3-hydroxy-1-oxopropan-2-yl) benzamide, was purified by column chromatography using a mixture ethyl acetate and hexane (4:1). (R = Ph; white solid, yield = 39.1%); (R = C_3H_6Ph; white solid, yield = 40.3%). The resulting products were characterized by ^{1}H, ^{13}C NMR and HRMS.

Procedure 5. Methyl N-benzoyl-O-(tert-butyl) serylphenylalaninate (1110 mg, 2.60 mmol) was dissolved in a mixture of acetonitrile (60 mL) and hydrochloric acid (60 mL). The reaction mixture was left to stir at room temperature for 2 h. The reaction mixture was concentrated using rotary evaporator. The reaction product was diluted in methanol and left to stir overnight. The product, methyl benzoyl-seryl-phenylalaninate, was purified using column chromatography using a mixture of ethyl acetate and hexane (4:1) with 39.5% yield as white solid. The resulting product was characterized by ^{1}H, ^{13}C NMR and HRMS.

NMR Data of the Starting Materials

^{1}HNMR DATA after procedure 1: methyl N-benzoyl-O-(tert-butyl)-L-serinate

methyl N-benzoyl-O-(tert-butyl)-L-serinate: ^{1}H NMR (600 MHz, $CDCl_3$) δ 7.32 (ddt, *J* = 6.9, 3.4, 1.4 Hz, 2H), 7.01 (dddd, *J* = 10.7, 5.0, 2.5, 1.3 Hz, 1H), 6.97 – 6.91 (m, 2H), 6.48 (d, *J* = 8.1 Hz, 1H), 4.42 (ddh, *J* = 8.1, 3.1, 1.6 Hz, 1H), 3.43 – 3.36 (m, 1H), 3.28 – 3.22 (m, 3H), 3.19 (dqd, *J* = 8.1, 2.6, 1.1 Hz, 1H), 0.66 – 0.62 (m, 9H).

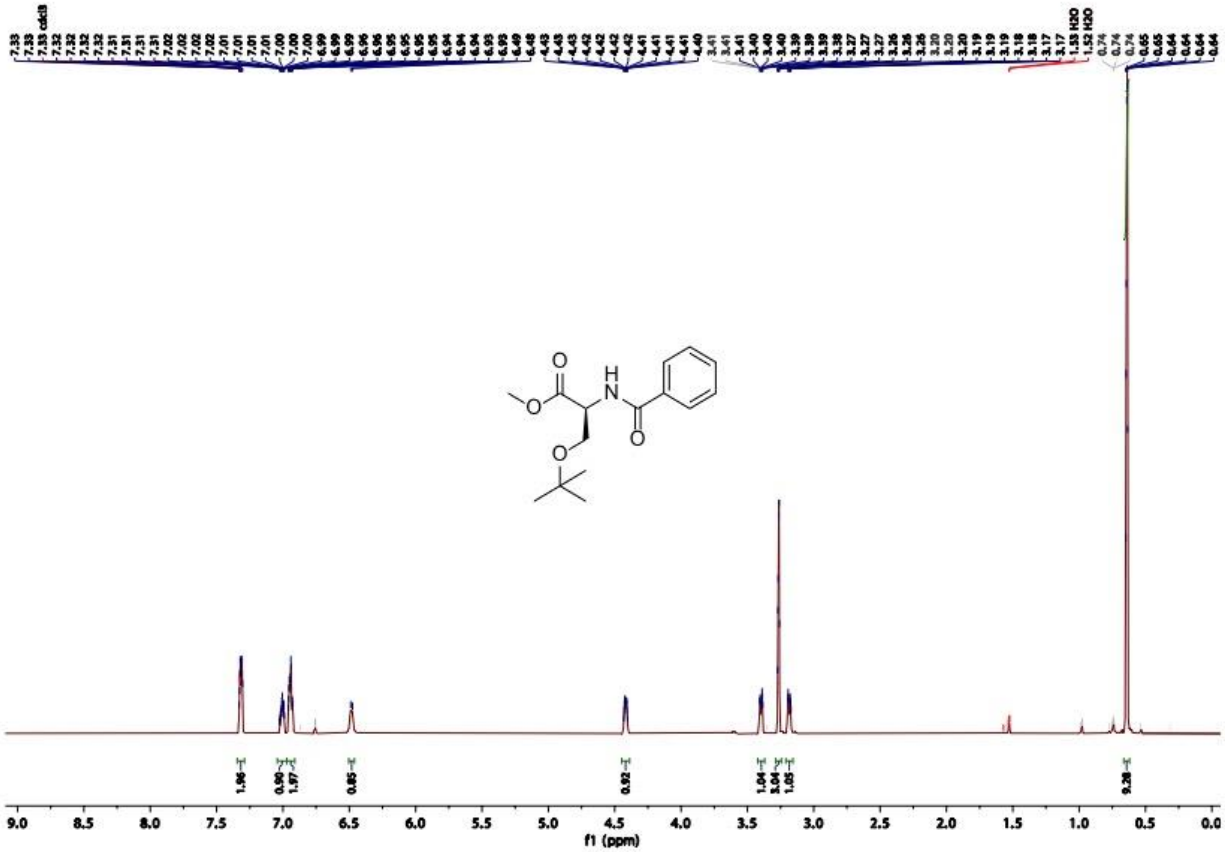

HRMS DATA after procedure 1: methyl N-benzoyl-O-(tert-butyl)-L-serinate

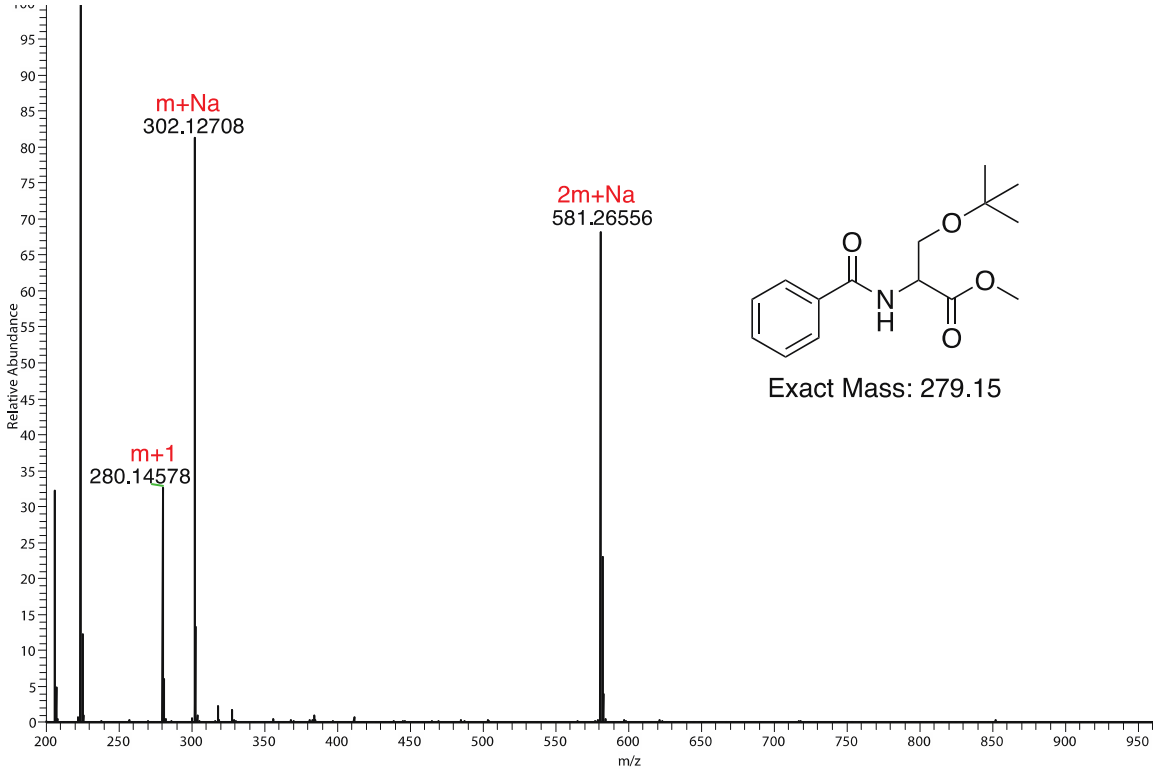

^{1}H and ^{13}C NMR DATA after procedure 2: N-benzoyl-O-(tert-butyl)-L-serine

N-benzoyl-O-(tert-butyl)-L-serine :^{1}H NMR (400 MHz, $CDCl_3$) δ 7.84 (dt, *J* = 7.0, 1.4 Hz, 2H), 7.58 – 7.49 (m, 1H), 7.45 (dd, *J* = 8.2, 6.6 Hz, 2H), 7.17 (d, *J* = 7.9 Hz, 1H), 4.95 (dt, *J* = 8.0, 3.4 Hz, 1H), 3.99 (dd, *J* = 9.2, 3.0 Hz, 1H), 3.75 (dd, *J* = 9.3, 3.8 Hz, 1H), 1.19 (s, 9H). **^{13}C NMR (101 MHz, CDCl3)** δ 174.13, 167.83, 133.63, 131.97, 128.66, 127.25, 74.13, 61.72, 53.26, 27.33.

^{1}HNMR DATA of N-benzoyl-O-(tert-butyl)-L-serine

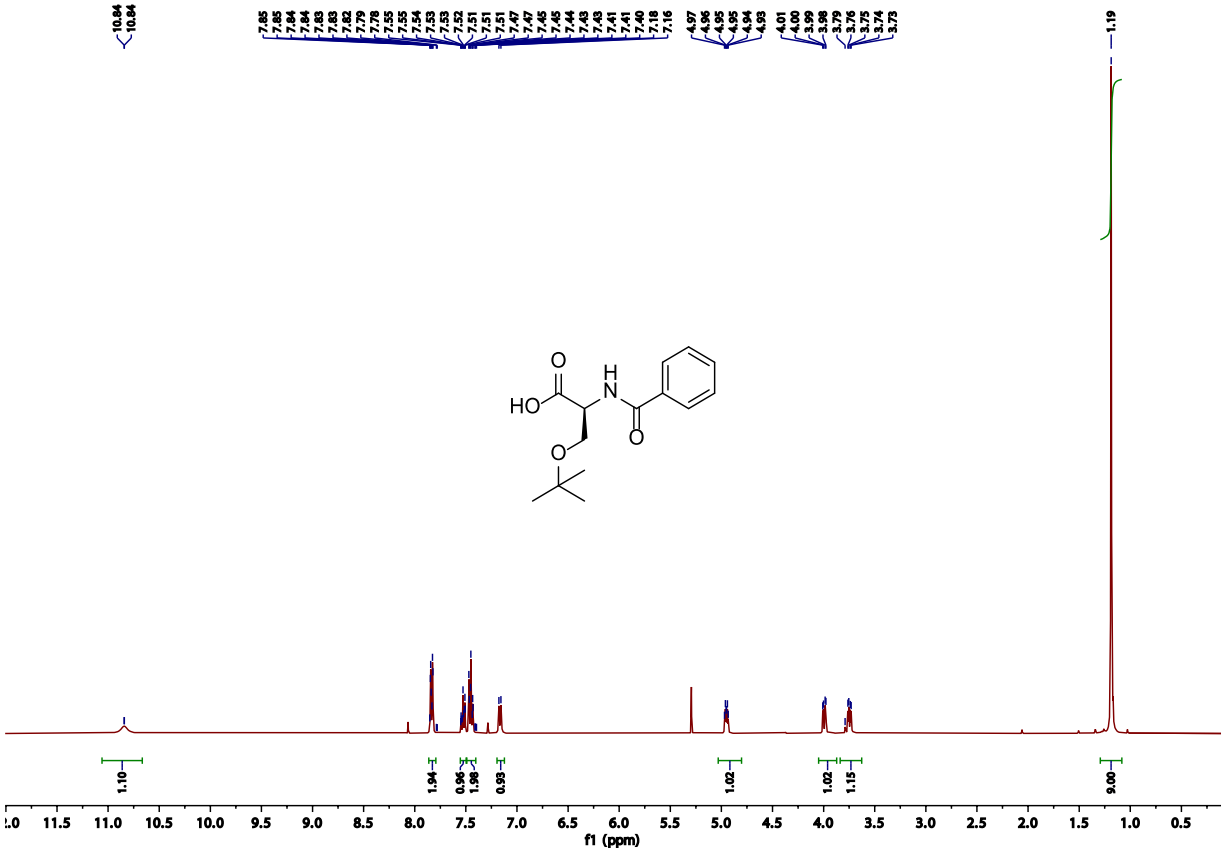

^{13}C NMR DATA of N-benzoyl-O-(tert-butyl)-L-serine

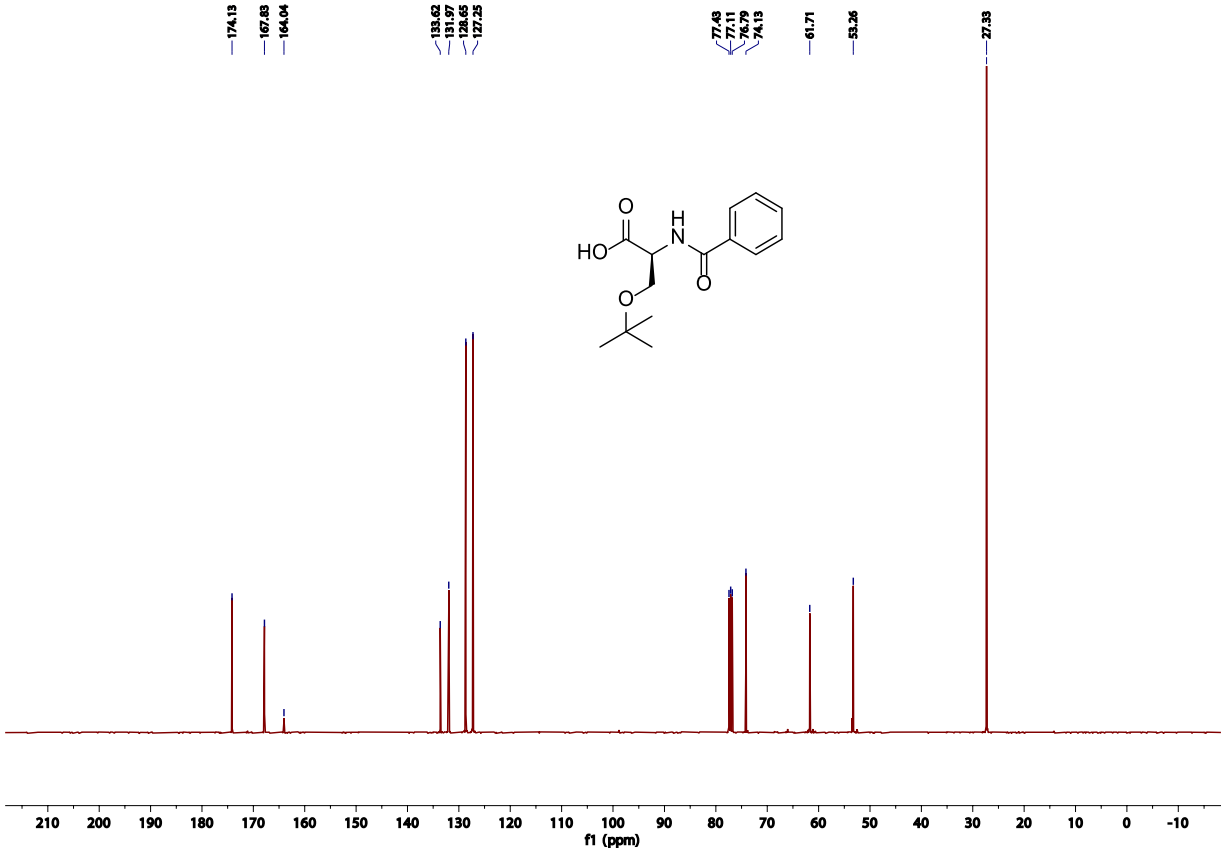

HRMS DATA of N-benzoyl-O-(tert-butyl)-L-serine

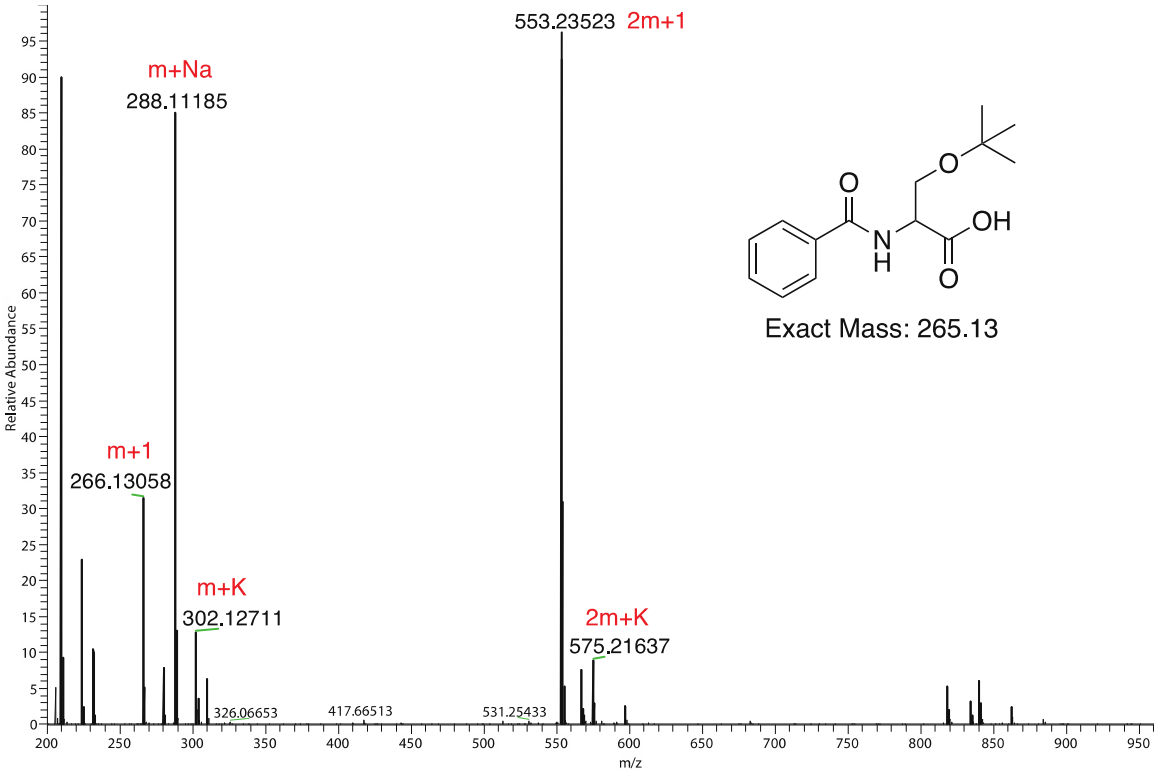

^{1}H NMR DATA after procedure 3 for R = Ph

NMR DATA FOR (S)-*N*-(1-(benzylamino)-3-(*tert*-butoxy)-1-oxopropan-2-yl)benzamide ^{1}H NMR (400 MHz, Chloroform-*d*) δ 7.87 – 7.84 (m, 2H), 7.57 – 7.52 (m, 1H), 7.49 – 7.44 (m, 2H), 7.38 – 7.30 (m, 5H), 7.11 (d, *J* = 7.3 Hz, 1H), 4.66 (ddd, *J* = 8.7, 6.0, 4.0 Hz, 1H), 4.58 (dd, *J* = 14.9, 6.1 Hz, 1H), 4.48 (dd, *J* = 14.9, 5.5 Hz, 1H), 4.01 (dd, *J* = 8.6, 4.1 Hz, 1H), 3.44 (t, *J* = 8.6 Hz, 1H), 1.20 (s, 9H). **^{13}C NMR (101 MHz, Chloroform-*d*)** δ 170.42, 167.17, 137.90, 133.78, 131.85, 128.72, 128.63, 127.58, 127.55, 127.12, 74.43, 61.47, 53.28, 43.66, 27.44.

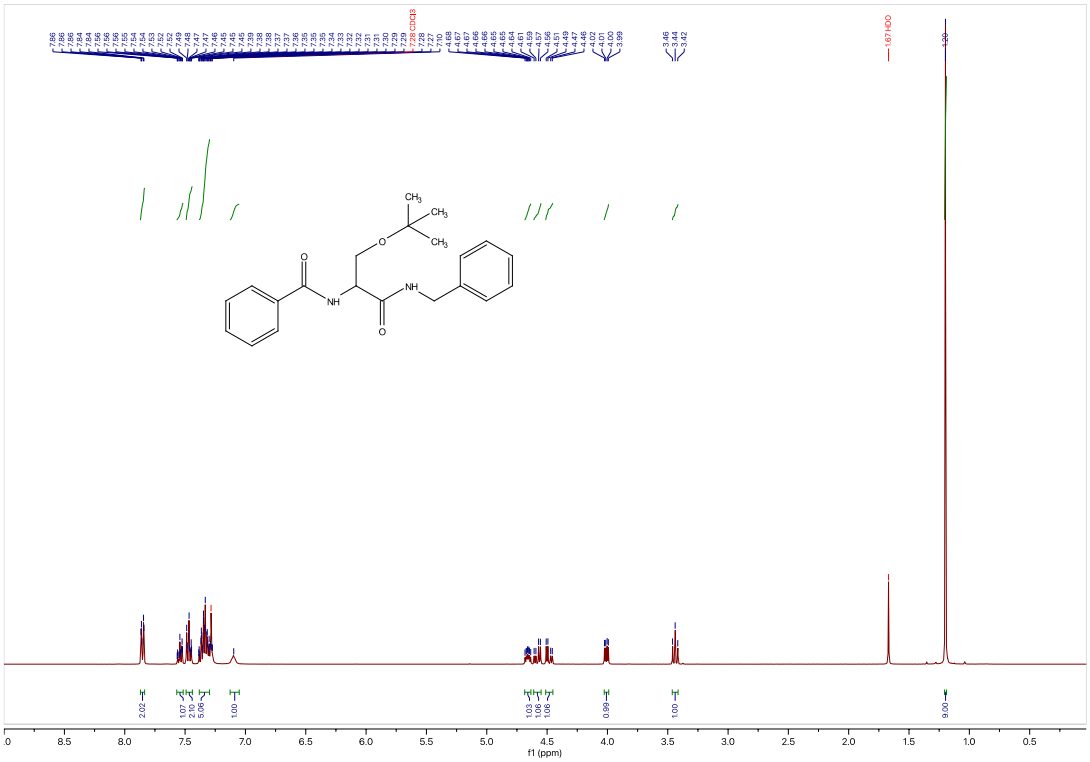

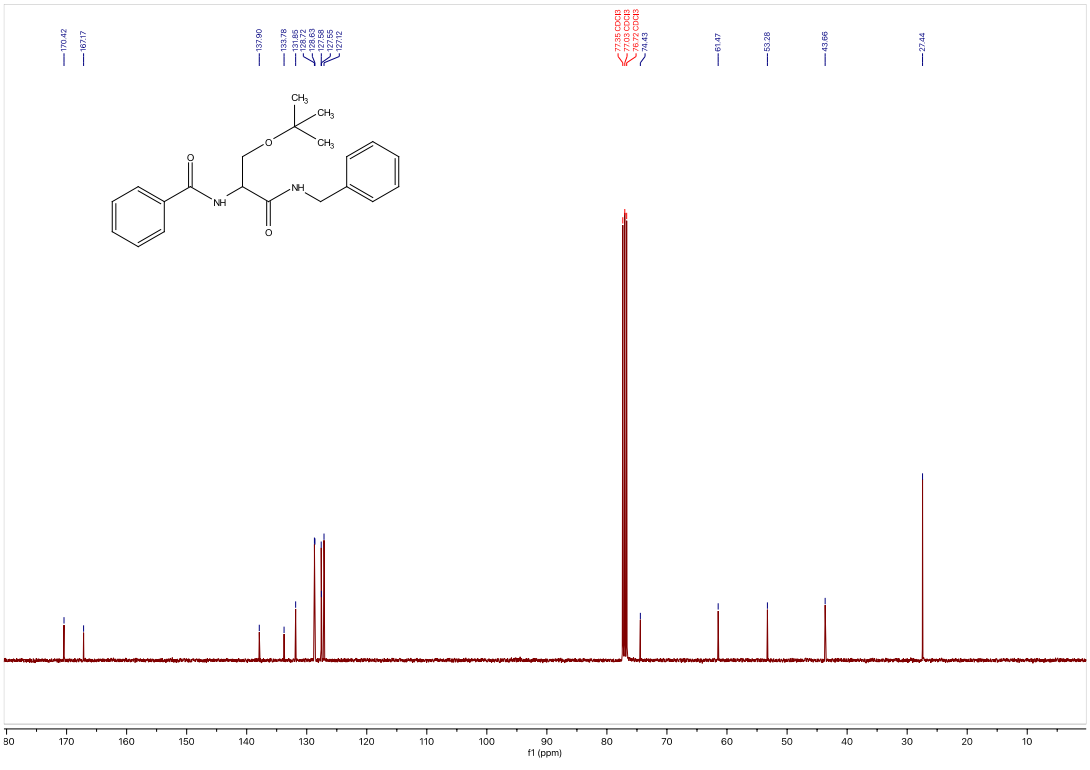

^{1}H NMR DATA after procedure 3 for R = C_3H_6Ph

NMR DATA for (S)-N-(3-(tert-butoxy)-1-oxo-1-((4-phenylbutyl)amino)propan-2-yl)benzamide: ^{1}H NMR (400 MHz, $CDCl_3$): δ 7.86 – 7.83 (m, 2H), 7.56 – 7.52 (m, 1H), 7.49 – 7.45 (m, 2H), 7.32 – 7.28 (m, 2H), 7.22 – 7.17 (m, 3H), 6.77 (s, 1H), 4.56 (ddd, *J* = 8.8, 5.9, 4.1 Hz, 1H), 3.98 (dd, *J* = 8.6, 4.1 Hz, 1H), 3.40 (d, *J* = 8.9 Hz, 1H), 3.34 (ddd, *J* = 14.1, 6.7, 5.3 Hz, 2H), 2.67 (t, *J* = 7.5 Hz, 2H), 1.70 (tt, *J* = 7.4, 2.4 Hz, 2H), 1.63 – 1.56 (m, 2H), 1.25 (s, 9H). **^{13}C NMR (101 MHz, Chloroform-*d*)** δ 170.39, 167.16, 141.99, 133.84, 131.81, 128.61, 128.41, 128.36, 127.10, 125.85, 74.43, 61.45, 53.21, 39.42, 35.48, 29.14, 28.67, 27.54.

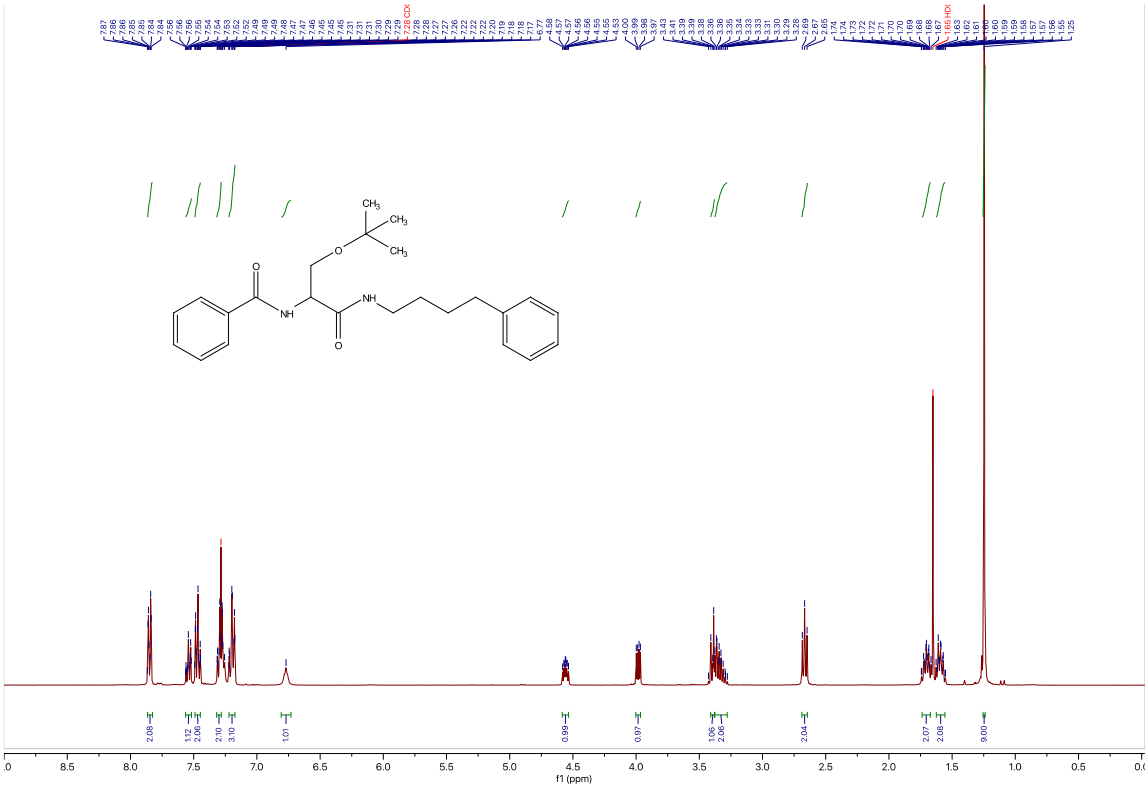

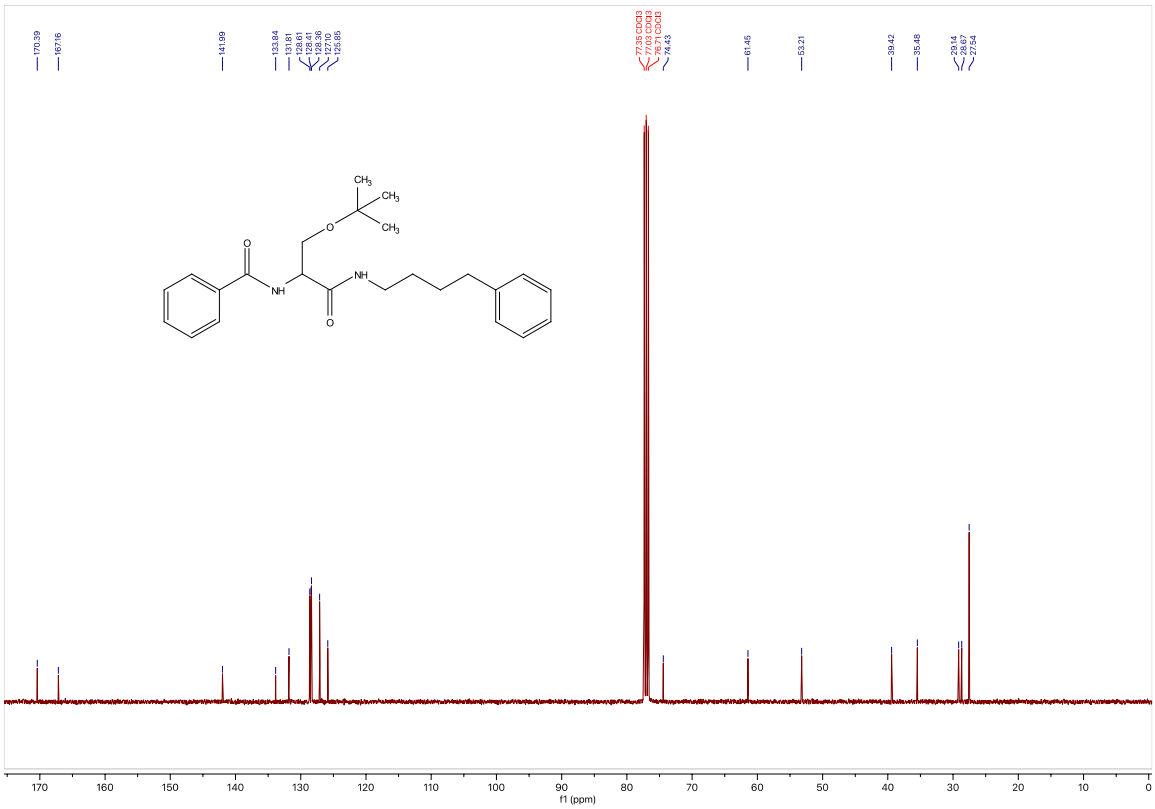

HRMS DATA after procedure 3 for R = C_3H_6Ph

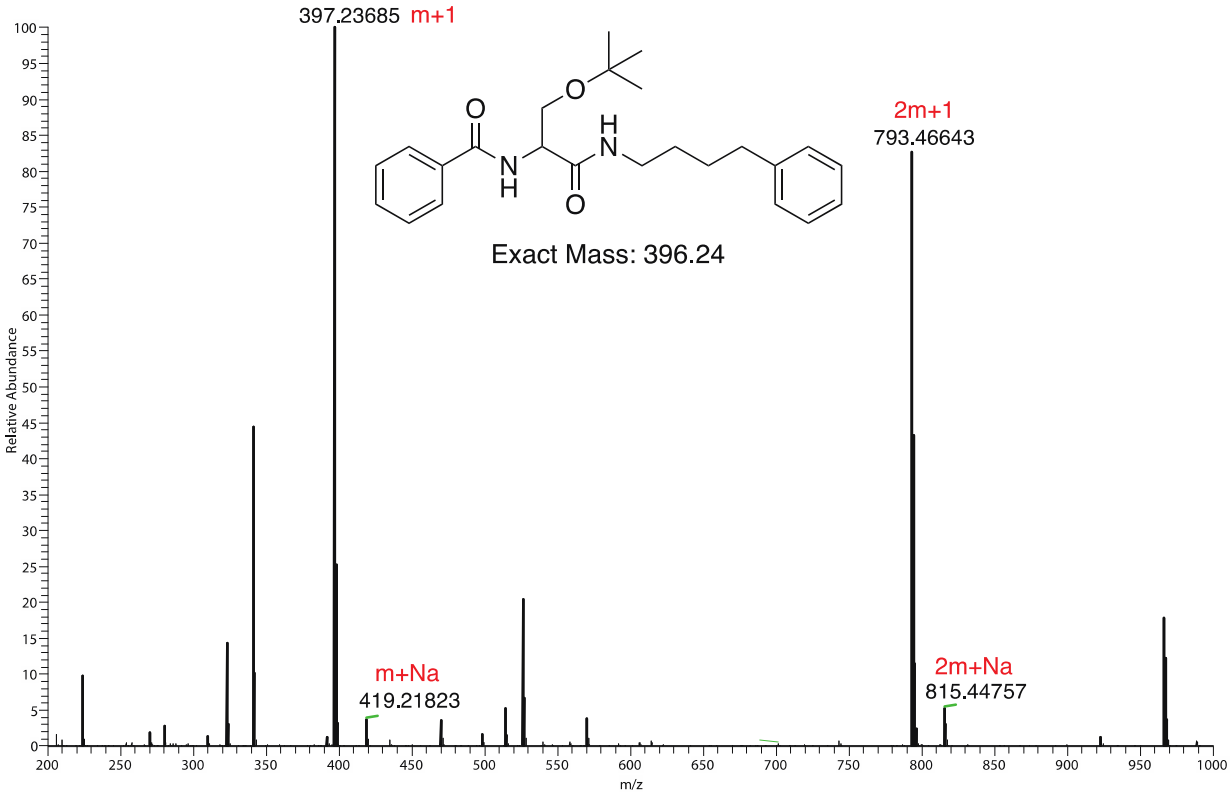

NMR DATA after procedure 3 for R = Phe-OMe

NMR DATA for Methyl *N*-benzoyl-*O*-(*tert*-butyl)serylphenylalaninate ^{1}H NMR (400 MHz, Chloroform-*d*) δ 7.83 (td, *J* = 8.5, 1.4 Hz, 2H), 7.56 – 7.42 (m, 4H), 7.31 – 7.26 (m, 2H), 7.17 – 7.12 (m, 2H), 4.95 – 4.89 (m, 1H), 4.62 (ddd, *J* = 9.5, 5.7, 3.9 Hz, 1H), 4.00 – 3.95 (m, 1H), 3.75 (d, *J* = 2.3 Hz, 3H), 3.40 (dt, *J* = 10.2, 8.6 Hz, 1H), 3.24 – 3.11 (m, 2H), 1.20 (d, *J* = 9.5 Hz, 9H). **^{13}C NMR (101 MHz, Chloroform-*d*)** δ 170.35, 170.14, 167.25, 135.75, 135.73, 131.87, 131.84, 129.27, 129.25, 128.64, 128.62, 128.58, 127.18, 127.15, 127.12, 127.11, 74.53, 61.17, 53.52, 53.48, 52.99, 52.36, 52.32, 38.04, 37.99, 27.35.

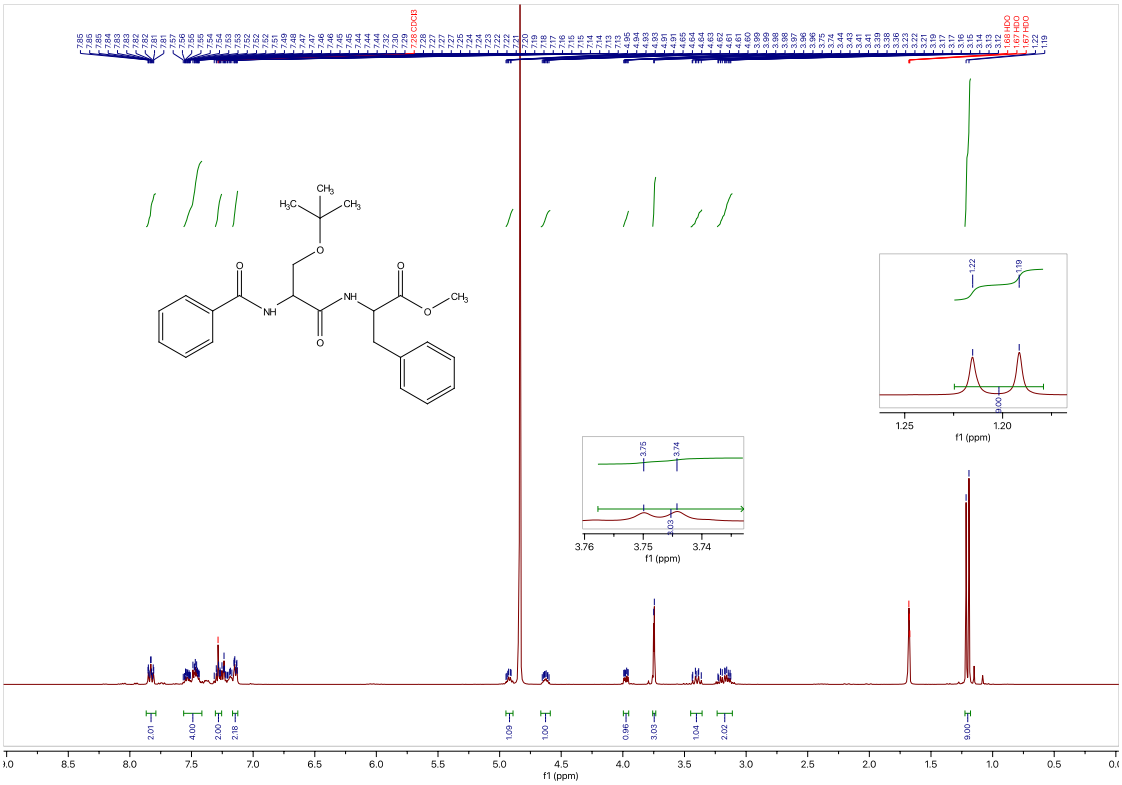

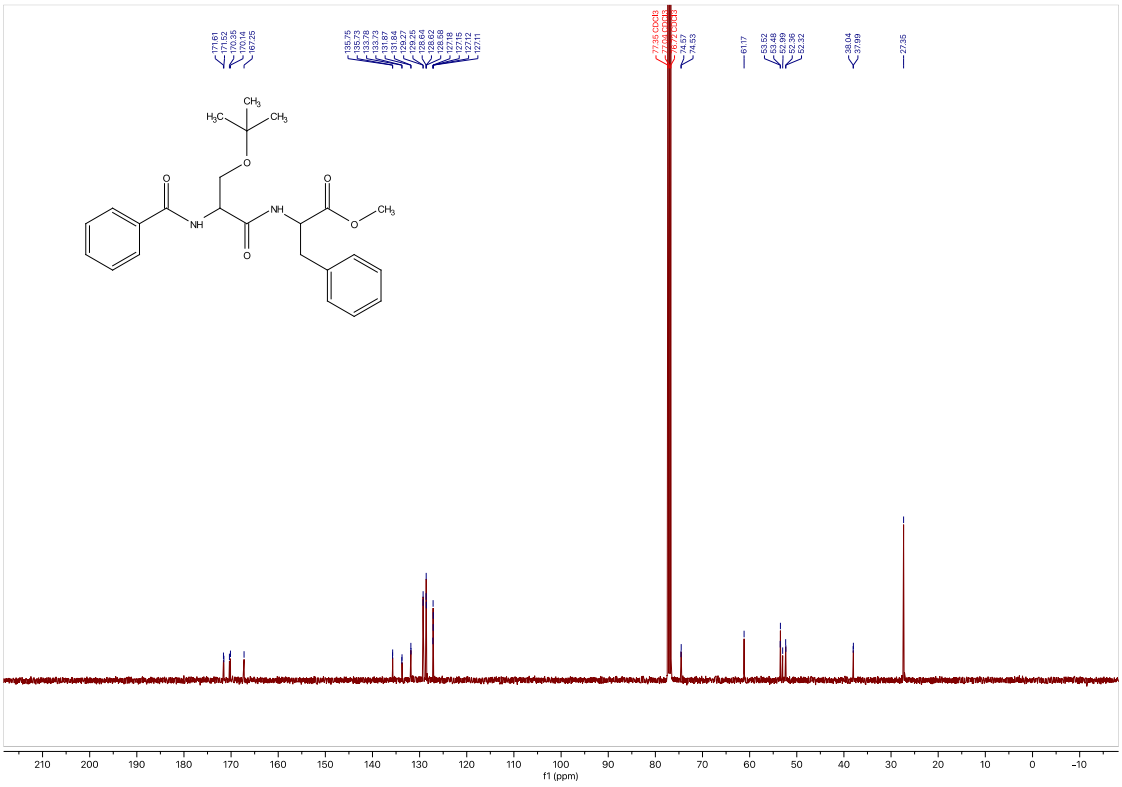

HRMS DATA after procedure 3 for R = Phe-OMe

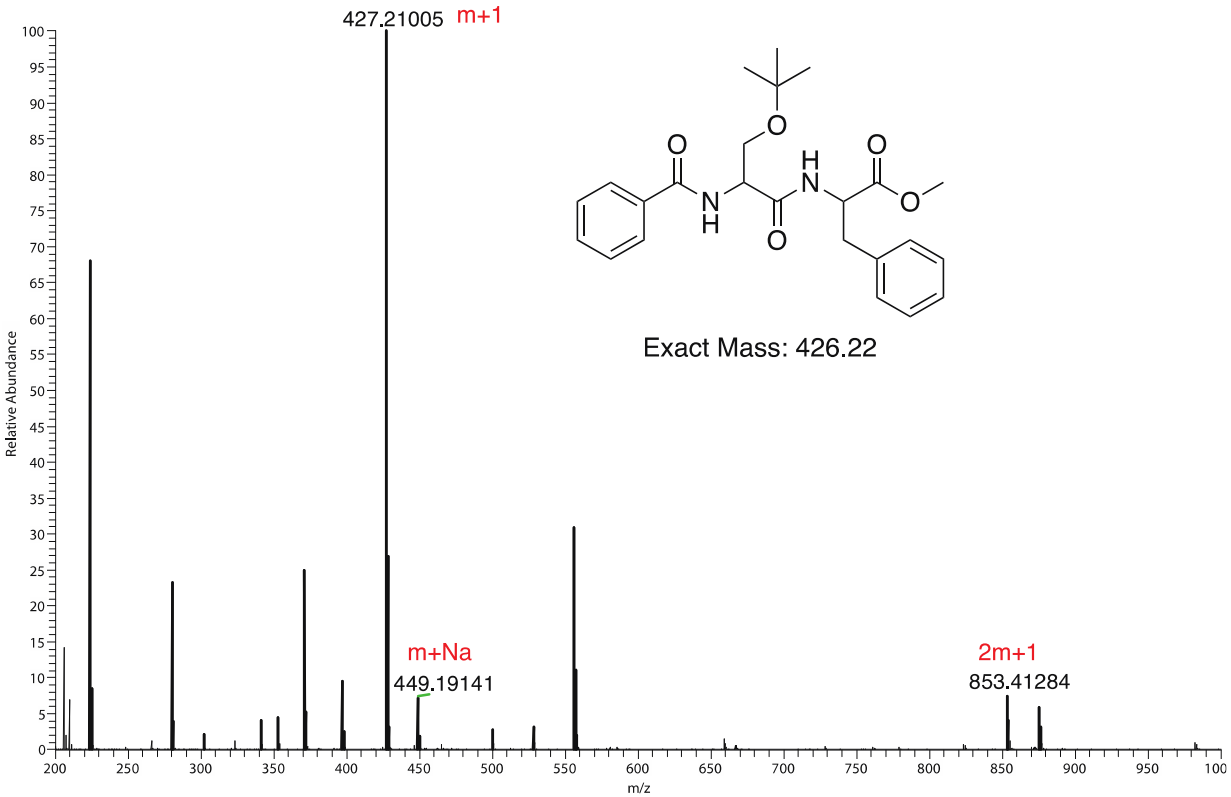

^{1}H NMR DATA after procedure 4 for R = Ph

***N*-(1-(benzylamino)-3-hydroxy-1-oxopropan-2-yl)benzamide ^{1}H NMR (400 MHz, Chloroform-*d*)** δ 7.83 – 7.79 (m, 2H), 7.58 – 7.54 (m, 1H), 7.49 – 7.39 (m, 4H), 7.35 – 7.29 (m, 3H), 4.70 (ddd, *J* = 7.4, 4.9, 3.0 Hz, 1H), 4.54 – 4.44 (m, 2H), 4.29 (dd, *J* = 11.3, 3.1 Hz, 1H), 3.77 (d, *J* = 11.4 Hz, 1H), 3.66 (s, 1H). **^{13}C NMR (101 MHz, Chloroform-*d*)** δ 171.05, 168.28, 137.66, 133.15, 132.21, 128.75, 127.55, 127.45, 127.18, 62.79, 54.04, 43.49.

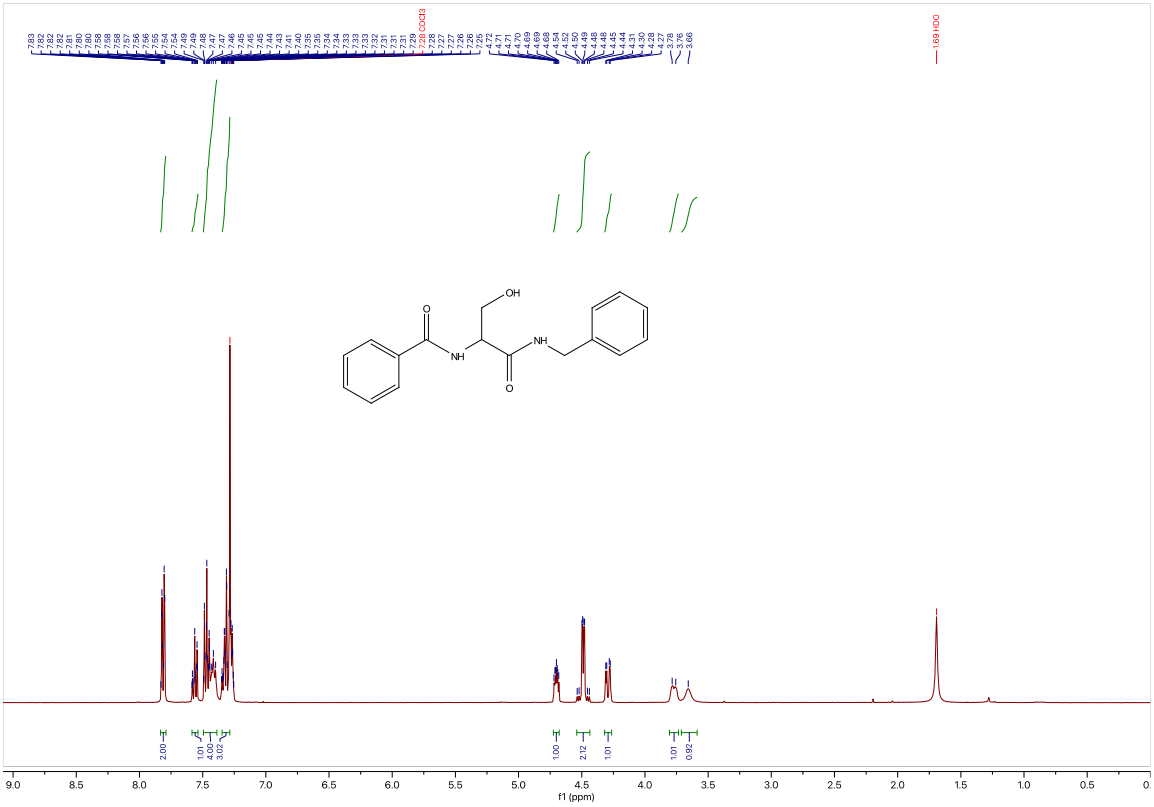

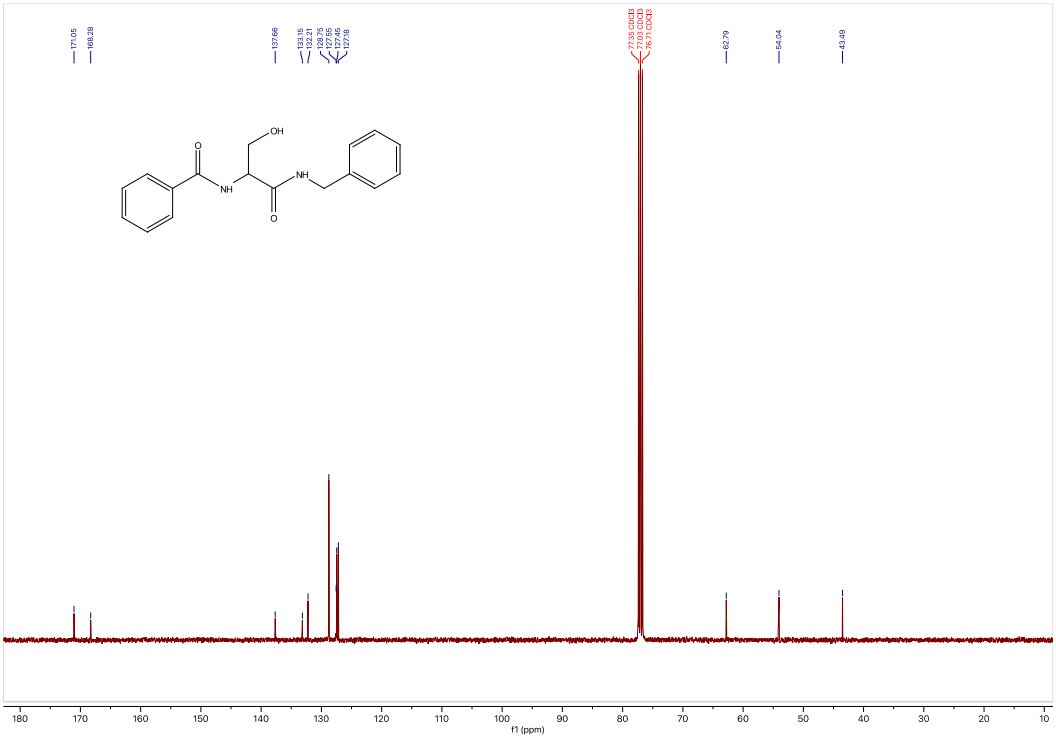

HRMS DATA after procedure 4 for R = Ph

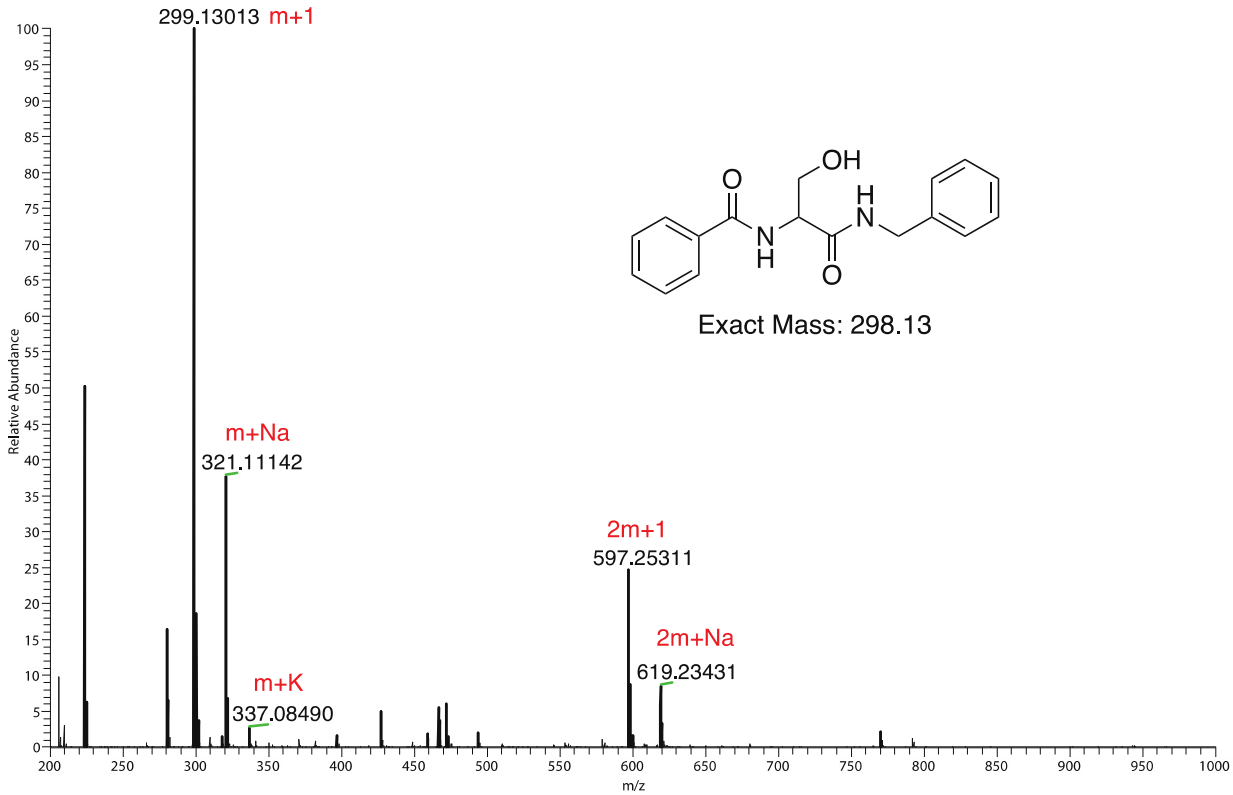

^{1}H NMR DATA after procedure 4 for R = C_3H_6Ph

***N*-(3-hydroxy-1-oxo-1-((4-phenylbutyl)amino)propan-2-yl)benzamide ^{1}H NMR (400 MHz, Chloroform-*d*)** δ 7.86 – 7.79 (m, 2H), 7.58 – 7.52 (m, 1H), 7.50 – 7.40 (m, 3H), 7.26 (d, *J* = 1.5 Hz, 1H), 7.18 – 7.11 (m, 3H), 4.66 (ddd, *J* = 7.0, 5.2, 3.4 Hz, 1H), 4.22 (dd, *J* = 11.4, 3.4 Hz, 1H), 3.75 (dd, *J* = 11.4, 5.2 Hz, 1H), 3.31 (q, *J* = 6.6 Hz, 2H), 2.62 (t, *J* = 7.4 Hz, 2H), 1.70 – 1.54 (m, 4H). **^{13}C NMR (101 MHz, Chloroform-*d*)** δ 170.94, 168.23, 141.99, 133.23, 132.17, 128.72, 128.36, 128.34, 127.19, 125.82, 62.91, 54.23, 39.42, 35.43, 28.95, 28.57

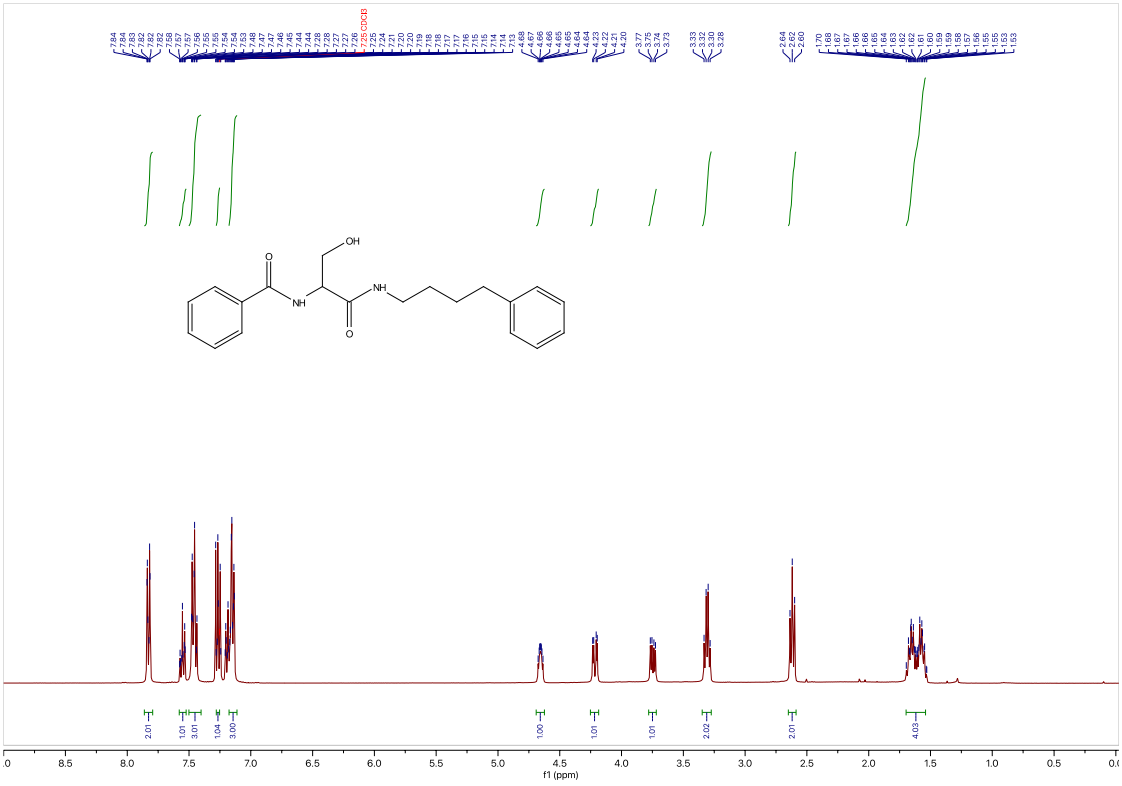

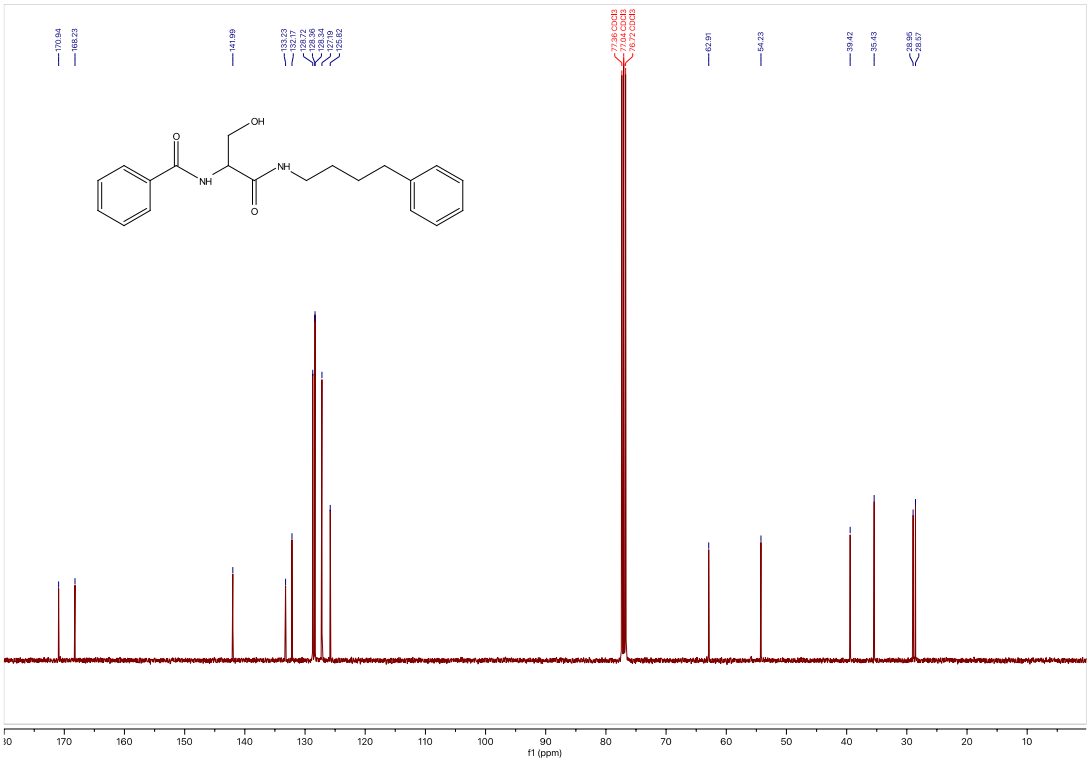

HRMS DATA after procedure 4 for R = C_3H_6Ph

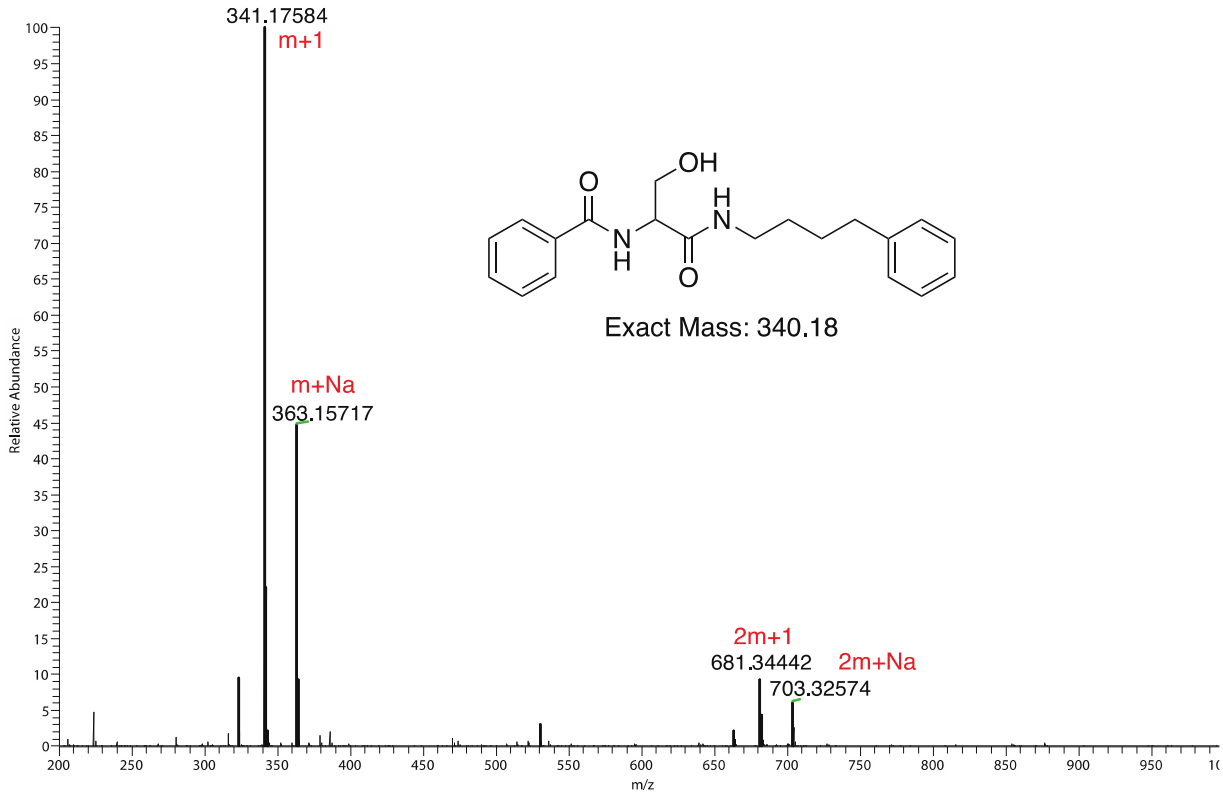

^{1}H NMR DATA after procedure 5

NMR DATA for methyl benzoyl-L-seryl-L-phenylalaninate: ^{1}H NMR (600 MHz, CD_3COCD_3) δ 7.96 – 7.89 (m, 2H), 7.78 (q, *J* = 10.0 Hz, 2H), 7.57 – 7.52 (m, 1H), 7.51 – 7.44 (m, 2H), 7.25 – 7.13 (m, 5H), 4.79 – 4.71 (m, 2H), 4.30 (br s, 1H), 3.95 – 3.89 (m, 1H), 3.85 (dh, *J* = 16.6, 5.6 Hz, 1H), 3.67 – 3.63 (m, 3H), 3.14 (ddd, *J* = 13.7, 9.1, 5.6 Hz, 1H), 3.05 (ddd, *J* = 13.8, 7.4, 2.8 Hz, 1H).

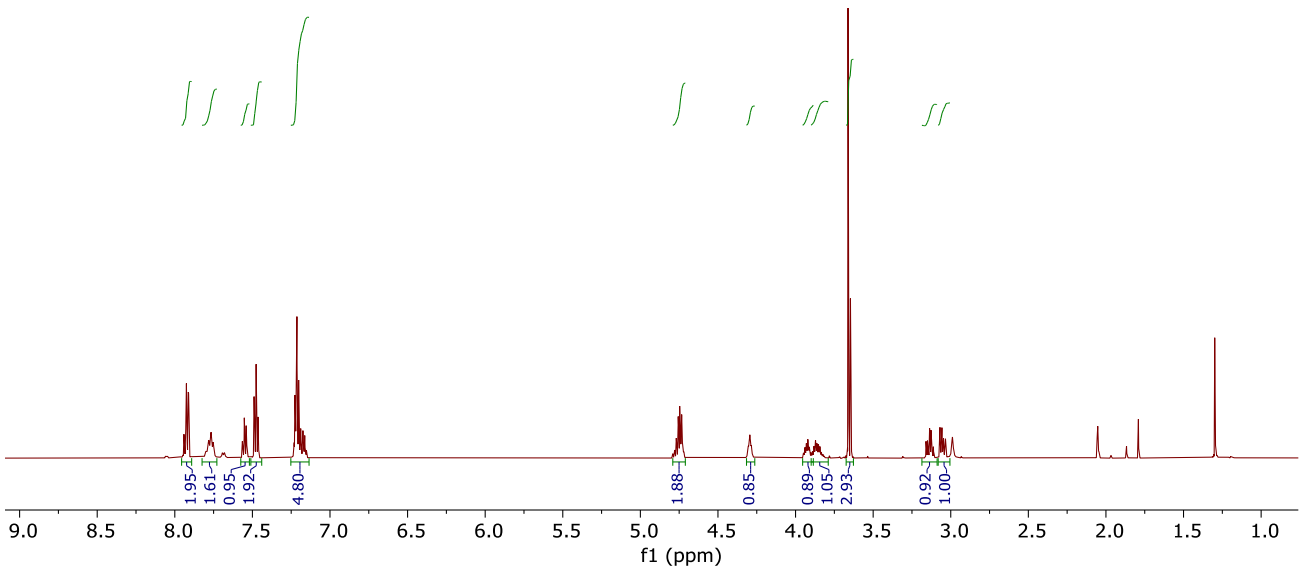

HRMS DATA after procedure 5

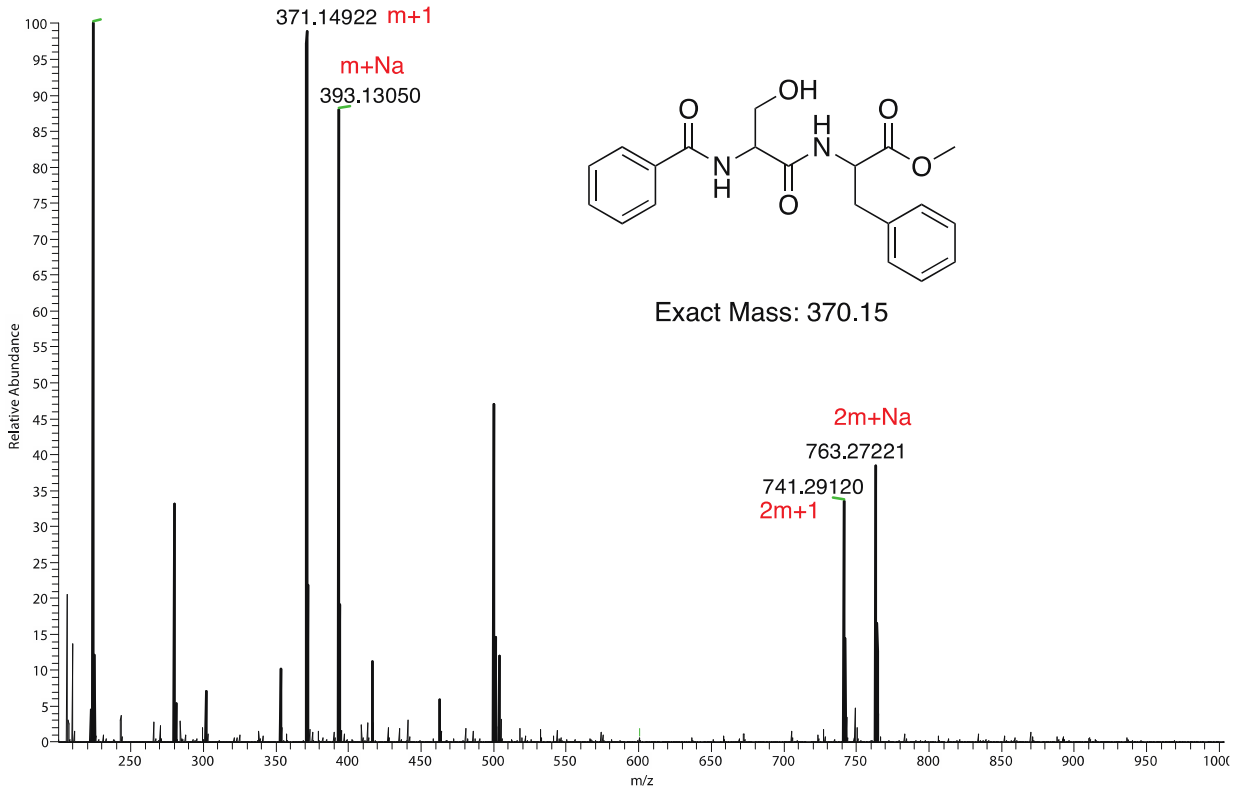

Supplementary Information for Chapter 3

General procedure for synthesis of protein aldehyde 3.5.

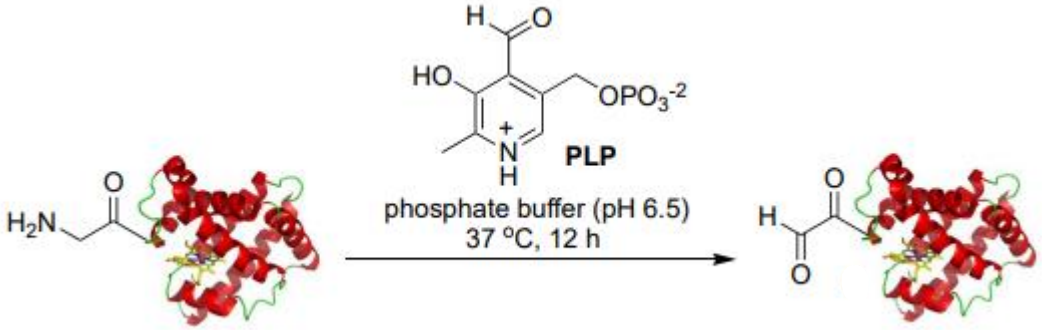

To a protein with glycine at the N-terminus (5 mg) was added PLP solution in 25 mM sodium phosphate buffer (pH 6.5). The pyridoxal 5-phosphate (PLP) stock solution should be prepared immediately before use, as this compound has been reported to degrade in aqueous solution (Ball, 2006). The PLP solution was made in the same buffer (25 mM sodium phosphate buffer (pH 6.5) in which the transamination reaction was carried out. After the addition of PLP to the buffer it is important to check and adjust the pH, as the phosphate group of PLP may significantly alter the pH of the buffer solution. For a transamination reaction with 10 mM PLP, the following guidelines may be followed to make 1 mL of a 2Å~ (20 mM) PLP stock solution: Add 5.3 mg of pyridoxal 5-phosphate monohydrate from Sigma to 1 mL of 25 mM phosphate buffer, pH 6.5, followed by the addition of 24 µL of 1 M NaOH and brief vortexing. Check the pH with a microelectrode and adjust to 6.5 if necessary. Carefully check the pH of this solution. If the pH of the PLP stock was not adjusted this solution may be overly acidic, leading to protein precipitation or suboptimal levels of conversion. The 800 µl of PLP stock solution was added to the protein. Combine the protein and the PLP stock solution to give a final concentration of 10 mM PLP and 10 - 500 µM protein at pH 6.5. Incubate at 37 °C for 4–20 h. These conditions represent the standard conditions for most proteins and can be used as a starting point for optimization with each new protein target. Factors that may be varied include the concentration of PLP, the reaction temperature, the

incubation time, and the pH. The reaction may be completed in as little as an hour, typically when a higher concentration of PLP (up to 100 mM) is used. The pure protein and protein aldehyde were analyzed by ultra-performance LC system (ACQUITY, Waters Corp., USA) coupled with a quadrupole time-of-flight mass spectrometer (Q-Tof Premier, Waters).

General procedure for synthesis of protein ketones.

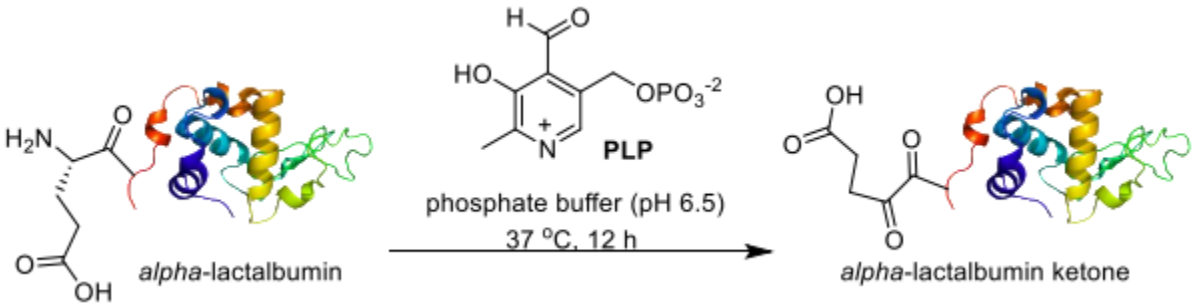

A protein alpha lactalbumin (5 mg) was dissolved in 25 mM sodium phosphate buffer (pH 6.5). The pyridoxal 5-phosphate (PLP) stock solution should be prepared immediately before use, as this compound has been reported to degrade in aqueous solution (Ball, 2006). The PLP solution should be made in the same buffer in which the transamination reaction will be run, typically 10 to 50 mM phosphate buffer at pH 6.5. After the addition of PLP to the buffer it is important to check and adjust the pH, as the phosphate group of PLP may significantly alter the pH of the buffer solution. It is often convenient to make the PLP stock solution at two times the desired concentration for the reaction, assuming that it will be added to the protein solution in a 1:1 volume ratio. For a transamination reaction with 10 mM PLP, the following guidelines may be followed to make 1 mL of a 2Å~ (20 mM) PLP stock solution: Add 5.3 mg of pyridoxal 5-phosphate monohydrate from Sigma to 1 mL of 25 mM phosphate buffer, pH 6.5, followed by the addition of 24 uL of 1 M NaOH and brief vortexing. Check the pH with a microelectrode and adjust to 6.5 if necessary. Carefully check the pH of this solution. If the pH of the PLP stock was not adjusted

this solution may be overly acidic, leading to protein precipitation or suboptimal levels of conversion. The PLP stock solution was added to the protein solution in a 1:1 volume ratio. Combine the protein solution and the PLP stock solution to give a final concentration of 10 mM PLP and 10 - 500 µM protein at pH 6.5. Incubate at 37 °C for 4–20 h. These conditions represent the standard conditions for most proteins, and can be used as a starting point for optimization with each new protein target. Factors that may be varied include the concentration of PLP, the reaction temperature, the incubation time, and the pH. The reaction may be completed in as little as an hour, typically when a higher concentration of PLP (up to 100 mM) is used. The pure protein and protein aldehyde were analyzed by ultra-performance LC system (ACQUITY, Waters Corp., USA) coupled with a quadrupole time-of-flight mass spectrometer (Q-Tof Premier, Waters).

General procedure and the rate studies for synthesis of nitro-peptide conjugate 3.3a.

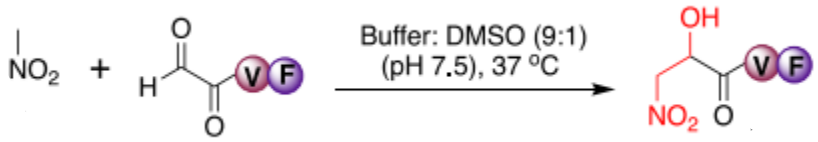

To a solution of peptide aldehyde CHO-VF (**3.2a**, 1.5 mM) in phosphate buffer (pH 7.5, 50 mM): DMSO (9:1) (2 mL) was added nitromethane (**3.1a**, 5 equiv. 7.5 mM). The reaction mixture was stirred at 37 °C and monitored by injecting the sample in HPLC after regular intervals of time and analyzed by LCMS. % conversion to nitro-peptide adduct **3.3a** was determined by integrating the area of HPLC peaks. The adduct **3.3a** was purified by HPLC and characterized by MS and NMR. Product **3.3a** was isolated as a mixture of diastereomers with 7:3 diastereomeric ratio (d.r.).

Rate studies for the synthesis of nitro-peptide conjugate **3.3a**

a.

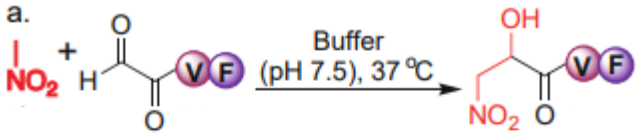

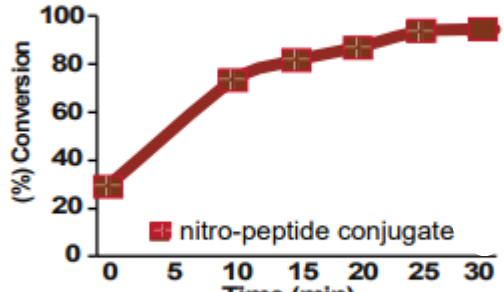

b.

Reaction	Rate ($M^{-1}S^{-1}$)	Relative rate
Henry	14.94	245
Oxime	0.061 (100 mM catalyst)	1

Kinetic Studies of Henry Bioconjugation:

To a solution of peptide aldehyde CHO-VF (**3.2a**) in 50 mM phosphate buffer pH 7.5 was added a solution of nitromethane (**3.1a**) in 50 mM phosphate buffer pH 7.5 while maintaining the total concentration of reactants 0.625 mM in 1:1 ratio. For analysis, a sample (50 µL) was taken from the mixture and injected to analytical HPLC (X Terra C18 column {5 µm} with a gradient of 0 to 80% MeCN with 0.1% formic acid in 30 min). Second-order rate constant was found as an average of 14.94 M-1S -1 over two runs.

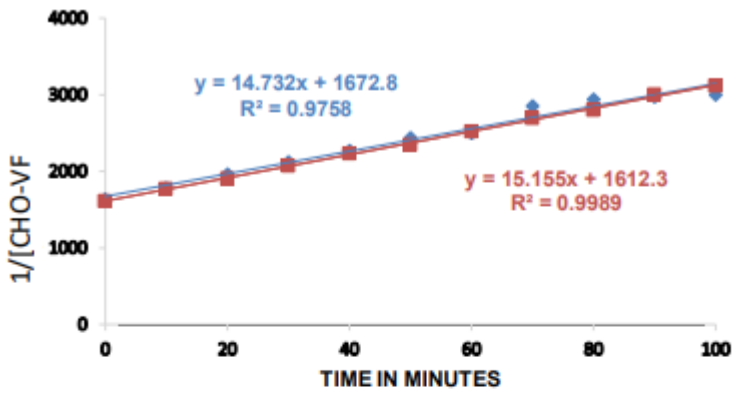

Comparison of Rate studies of Henry Bioconjugation with other Aldehyde bioconjugation reactions.

Reaction	Conditions	Rate ($M^{-1}S^{-1}$)
Henry Bioconjugation	0.625 mM aldehyde 0.625 mM nitromethane pH = 7.5, PB	**14.94**
Oxime Bioconjugation	1 mM aldehyde 1 mM aminooxy pH = 7.5, PB	**0.015 (uncatalysed)** **0.061 (100 mM p-methoxyaniline)**
Oxime Bioconjugation	1 mM aldehyde 1 mM aminooxy pH = 4.5, PB	0.057 (uncatalysed) 0.68 (10 mM aniline)
Hydrazone Bioconjugation	1 mM aldehyde 1 mM hydrazine pH 5.7	0.0031 (uncatalysed) 0.21 (10 mM aniline)
iso-Pictet Spengler	0.5 mM aldehyde 0.5 mM indole	10.6 (pH 4.5) 0.26 (pH 7.0)
Thiazolidinedione aldol	10 mM aldehyde 10 mM Thiazolidinedione	0.0078 (pH 7.0)

Characterization of nitro-peptide conjugate 3a by NMR and HRMS.

HRMS of 3.3a

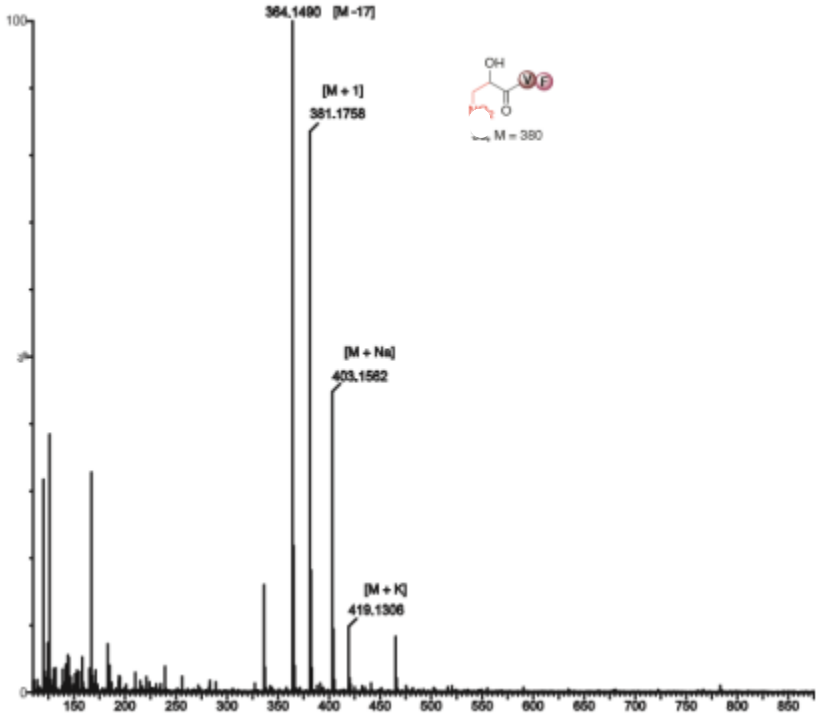

Characterization of nitro-peptide conjugate 3.3a by NMR and HRMS.

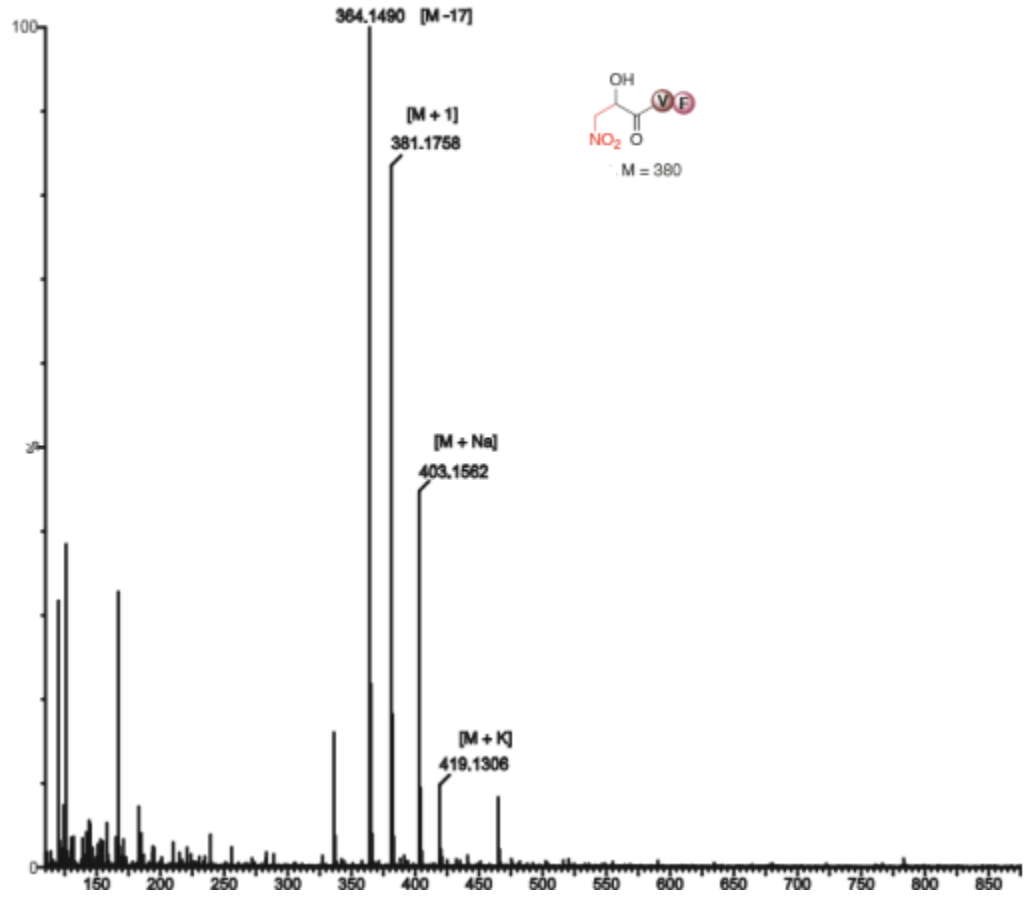

NMR data and spectra of **3.3a** ^{1}H NMR (600 MHz, DMF-d7) :δ 8.34 (d, J = 8.0 Hz, 1H-minor), 8.26 (d, J = 7.9 Hz, 1H-major), 7.85 (d, J = 8.5 Hz, 1H-major), 7.78 (d, J = 8.7 Hz, 1H-minor), 7.61 (s, 1H-minor), 7.58 (s, 1H-major), 7.30 – 7.26 (m, 4H-major & 4H-minor), 7.22 – 7.19 (m, 2H-major & 2H-minor), 7.09 (s, 1H-minor), 6.99 (s, 1H-major), 5.00 – 4.98 (m, 1H-major & 1H-minor), 4.84 – 4.82 (m, 1H-major & 1H-minor), 4.71 – 4.68 (m, 2H-major & 2H-minor), 4.38 – 4.35 (m, 1H-minor), 4.33 – 4.30 (m, 1H- major), 3.18 – 3.15 (m, 1Hmajor & 1H-minor), 3.00 – 2.89 (m, 1H-major & 1H-minor), 2.15 – 2.09 (m, 1H-major & 1H-minor), 0.87 – 0.82 (m, 6H-

major & 6H-minor). d.r.: 7:3 was determined by integration of proton NMR signal; δmajor : 4.32, δminor : 4.36. The ratio of two isomers was concluded from the integration of ^{1}H NMR of nitro-peptide conjugate **3.3a** as shown below. There are multiple diastereomeric peaks in the ^{1}H NMR. For example integration of the peak for the proton 6 at δ major : 4.32 and δ minor : 4.36 clearly showed the ratio of two diastereoisomers (major diastereoisomer showed integration of 0.9781 and minor diastereoisomer showed integration of 0.3800). From these two values, we calculated the diastereomeric ratio (d.r.) (0.9781/1.3581) to be 72 % of the major diastereoisomer. Similar diastereomeric peaks were observed for other protons in the ^{1}H NMR spectra of nitro-peptide conjugate **3.3a** such as protons 10 and 5. These calculations clearly showed the 7:3 diastereomeric ratio.

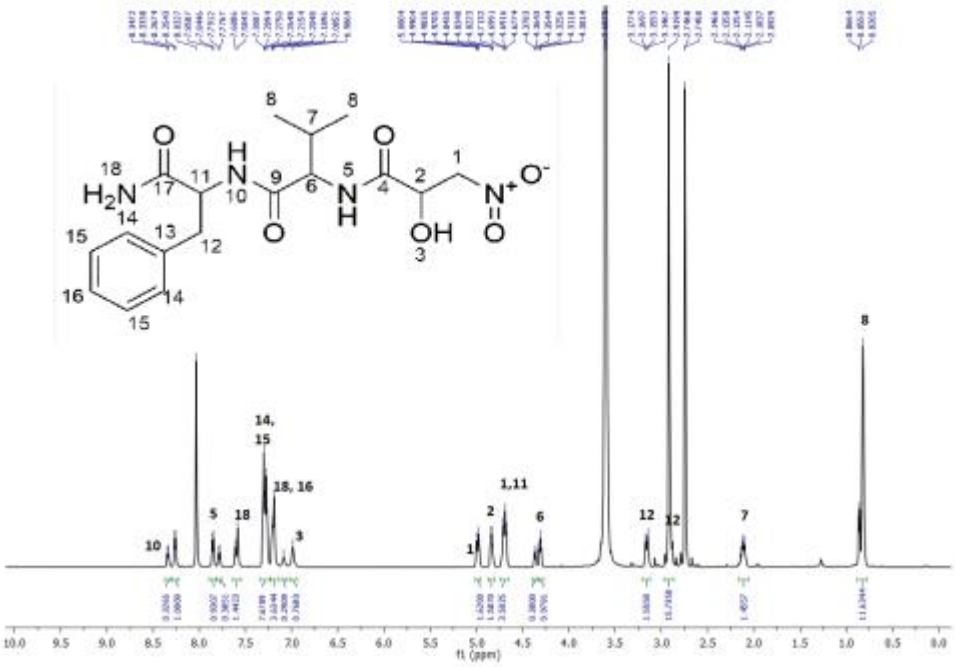

^{13}C NMR (151 MHz, DMF-d$_7$) δ 173.42(minor), 173.40(major), 170.9(minor), 170.8(major), 170.1(major), 170.0(minor), 138.54(minor), 138.51(major), 129.6, 128.4, 126.65(minor),

126.62(major), 79.2, 69.8(major), 69.7(minor), 58.2(major), 57.8(minor), 54.6(minor), 54.5(major), 38.3, 31.9(minor), 31.7(major), 19.3(minor), 19.2(major), 17.7(major), 17.4(minor).

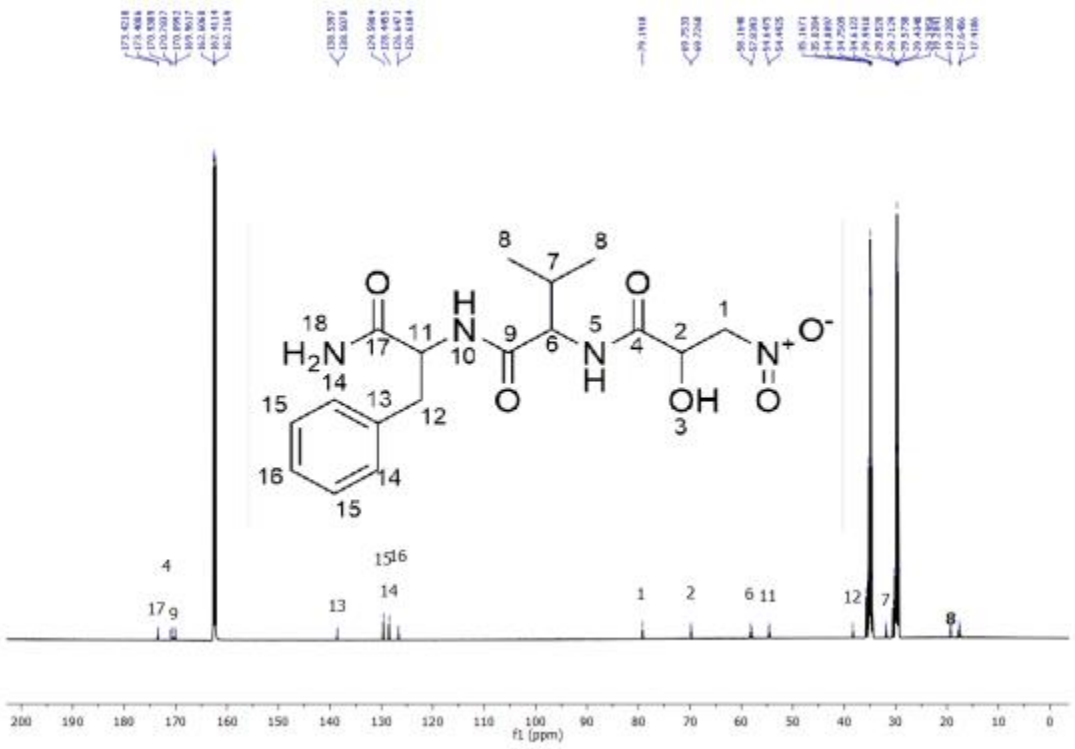

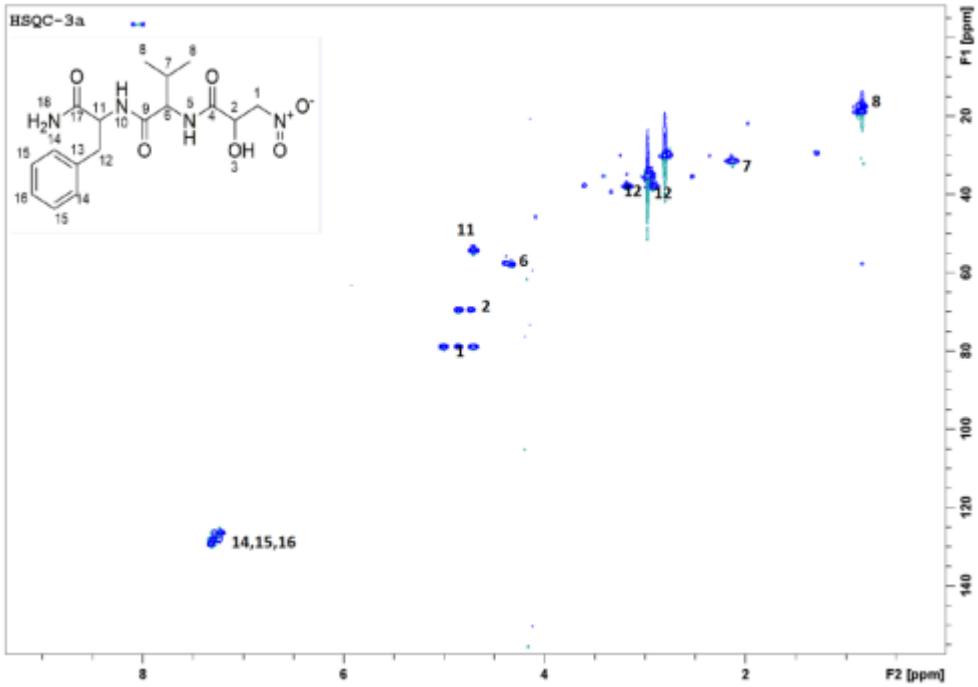

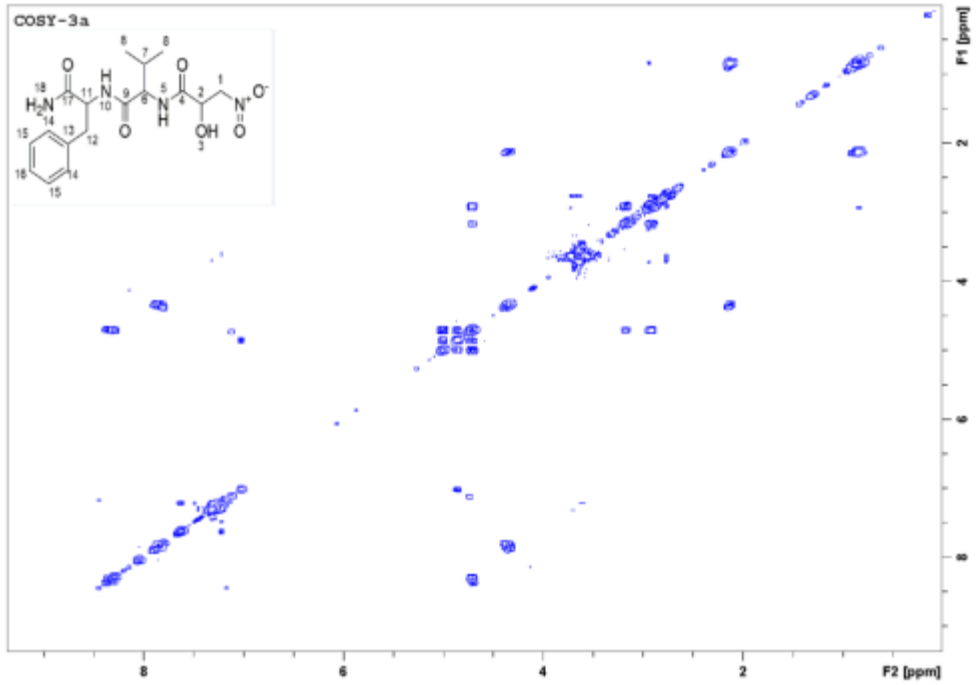

Chemoselective nature of bioconjugation with nitro-derivatives.

Reaction of hindered nitro derivatives with peptide aldehyde.

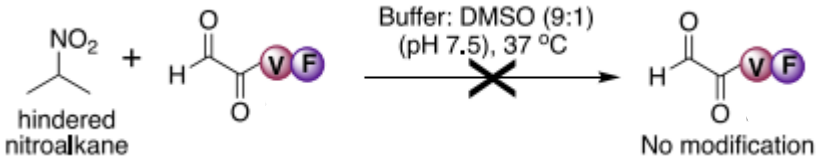

To a solution of peptide aldehyde CHO-VF (7.1 mM) in phosphate buffer (pH 7.5, 50 mM): DMSO (9:1) (0.44 mL) was added hindered nitroalkane (5 equiv.). The reaction mixture was stirred at 37 °C for 16 h. The reaction was analyzed by injecting samples in HPLC and MS. The formation of any nitro-peptide bioconjugate was not observed.

Reaction of nitro derivatives with peptide.

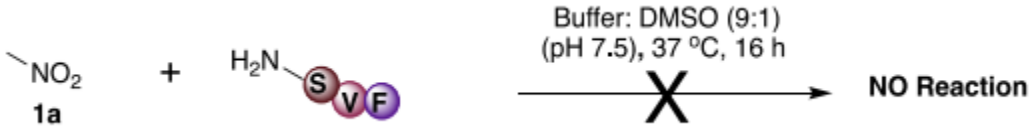

To a solution of peptide SVF (7.1 mM) in phosphate buffer (pH 7.5, 50 mM): DMSO (9:1) (0.44 mL) was added nitromethane (**3.1a**, 5 equiv.). The reaction mixture was stirred at 37 °C for 16 h. The reaction was analyzed by injecting samples in HPLC and MS. The formation of any nitro-peptide bioconjugate was not observed.

Stability studies of nitro-peptide conjugate 3.3b under different pH conditions. Nitropeptide conjugate **3.3b** (1 µM) was incubated in 10 mM phosphate buffer at different pH ranging from 3.5 to 10.5 at room temperature. The reaction was monitored by injecting the sample in HPLC after regular intervals of time 1 h, 10 h and 24 h. Small degradation of nitro-peptide conjugate **3.3b** was observed at high pH.

Procedure for the selective fluorination of nitro-peptide bioconjugate 3.3a.

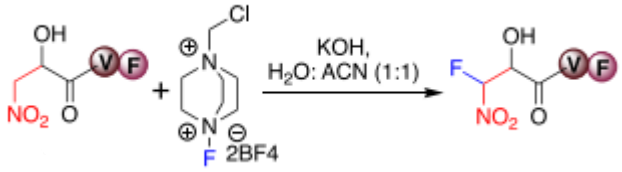

To a nitro-peptide conjugate **3.3a** (13 µM) in 1mL of water: ACN (1:1) was added selectfluor (1.5 equiv) and KOH (1.5 equiv). The reaction mixture was stirred at 37 °C for 16 h. The reaction was analyzed using MS and resulting flourinated nitro-peptide conjugate **3.4a** was purified by HPLC. The flourinated nitro-peptide conjugate **3.4a** was characterized by HSQC NMR, 19F-NMR and MS.

Characterization data of 3.4a.

HRMS of 3.4a

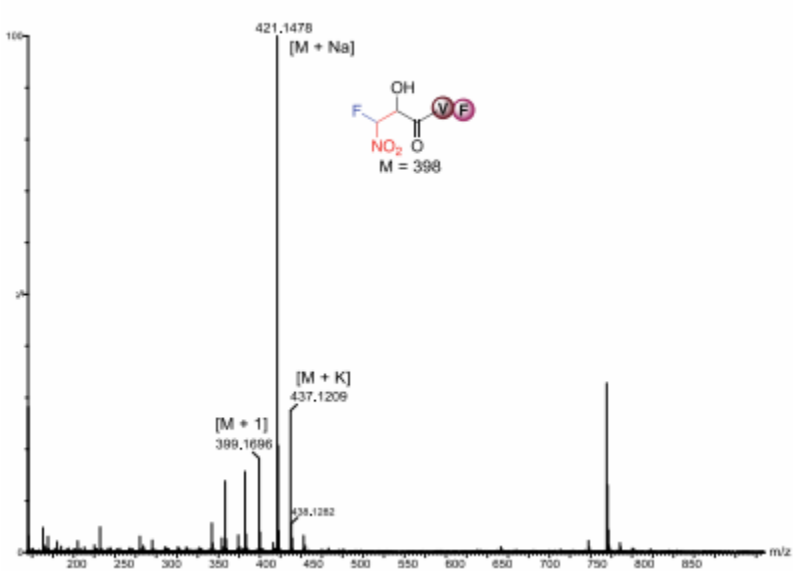

<u>^{19}F NMR of 3.4a</u>

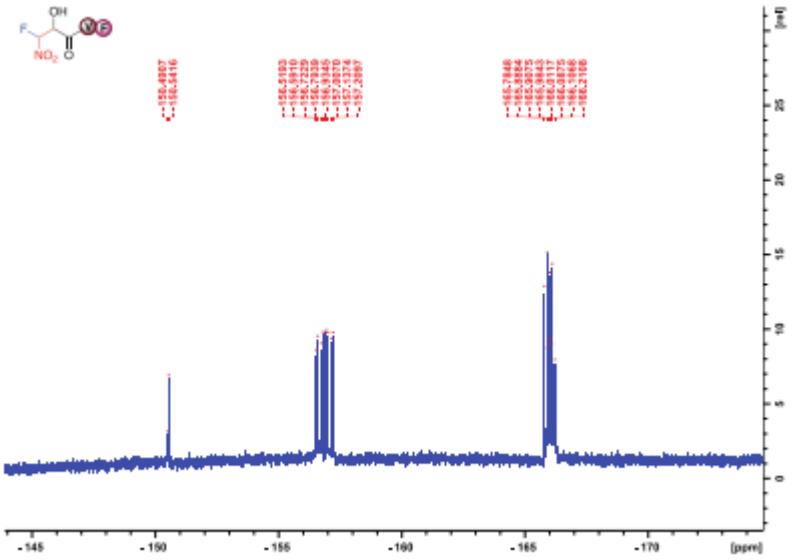

HSQC NMR of 3.4a

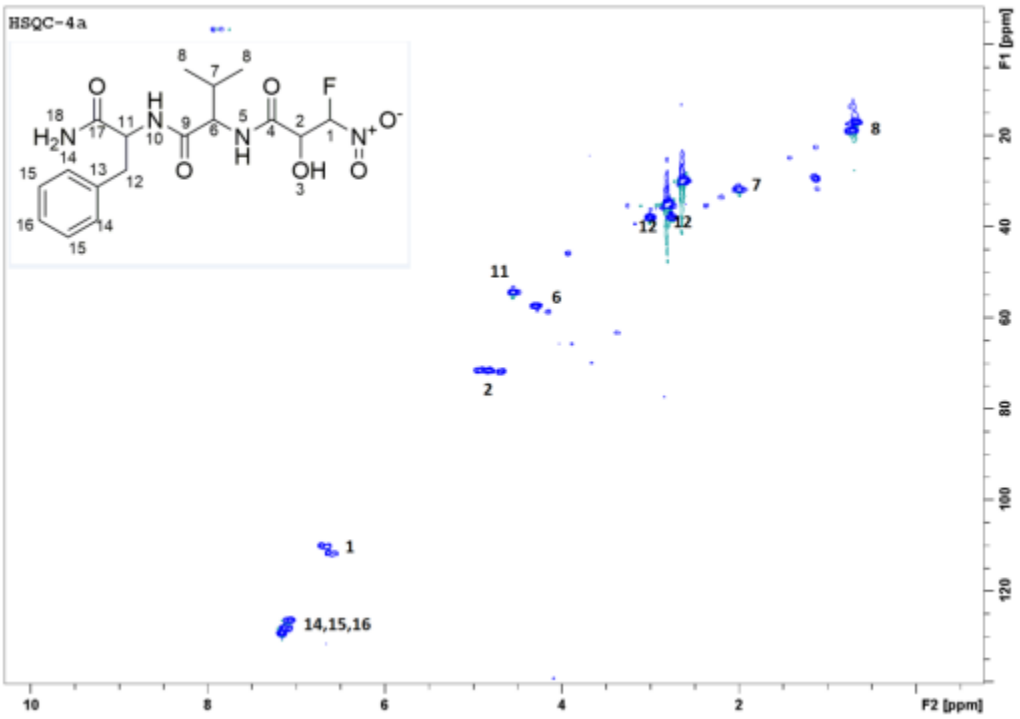

General procedure for the conjugation of nitro derivatives on peptide aldehyde.

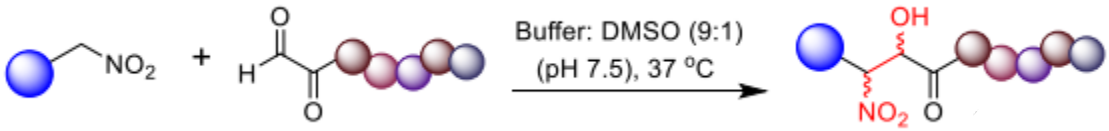

To a solution of peptide aldehydes (**3.2**, 7.1 mM) in phosphate buffer (pH 7.5, 50 mM): DMSO (9:1) (0.44 mL) was added nitro derivatives (**3.1**, 5 equiv.). The reaction mixture was stirred at 37 °C for 30 min to 3 h and analyzed by LCMS. % conversion to the nitro-peptide adduct **3.3**

was determined by integrating the area of HPLC peaks. The nitro-peptide adducts **3.3** were purified by HPLC and characterized by MS and NMR.

Procedure for the conjugation of biotin-nitro derivative 3.1f on peptide aldehyde.

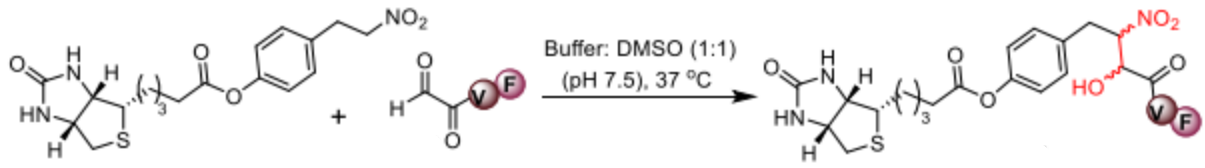

To a solution of peptide aldehyde CHO-VF (**3.2a**, 7.1 mM) in phosphate buffer (pH 7.5, 50 mM): DMSO (1:1) (0.44 mL) was added biotin-nitro derivative (**3.1f**, 5 equiv.). The high amounts of DMSO was added to solubilize the biotin-nitro derivative **3.1f**. The reaction mixture was stirred at 37 ^{o}C for 12 h and analyzed by LCMS. % conversion was determined by integrating the area of HPLC peaks. The nitropeptide adducts **3.3f** was purified by HPLC and characterized by MS.

Characterization of all nitro-peptide conjugates 3.3 (HPLC and HRMS traces)

HRMS of 3.3b

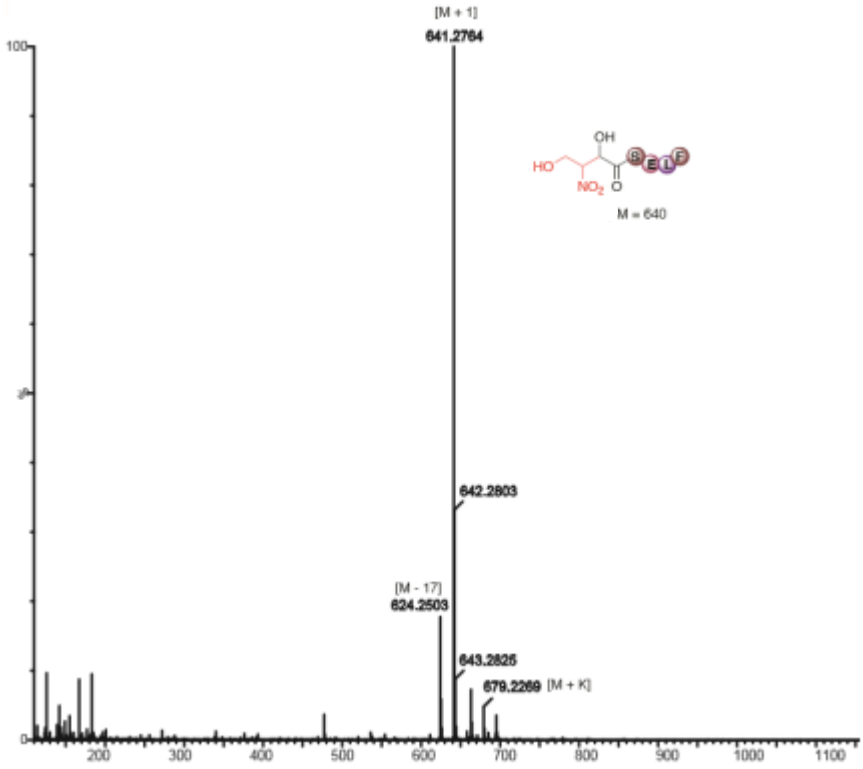

HRMS of 3.3d

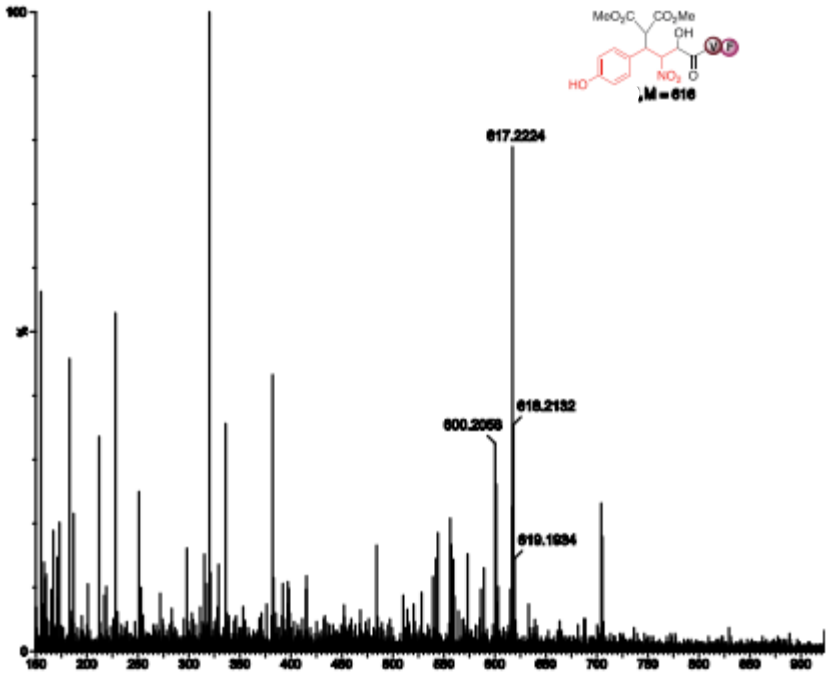
MeO2C
CO2Me
OH
HO
NO2
O
M = 616
617.2224
618.2132
600.2058
619.1934
100
%
0
160
200
250
300
350
400
450
500
550
600
650
700
750
800
850
900

HRMS of 3.3c

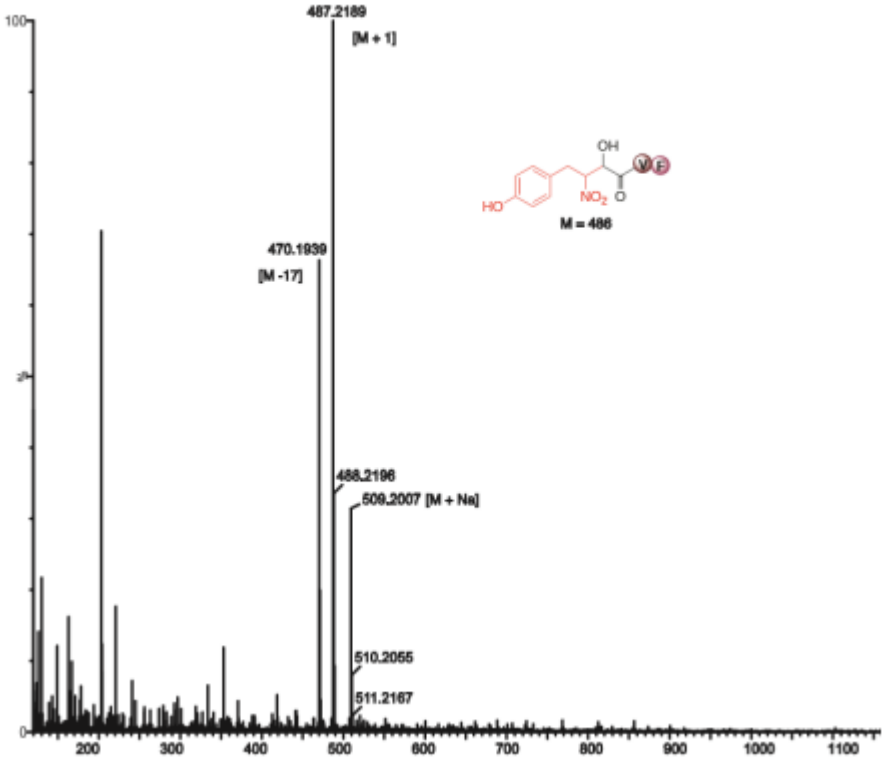
487.2189
[M + 1]
470.1939
[M -17]
488.2196
509.2007 [M + Na]
510.2055
511.2167
M = 486
100
%
0
200
300
400
500
600
700
800
900
1000
1100

HRMS of 3.3b”

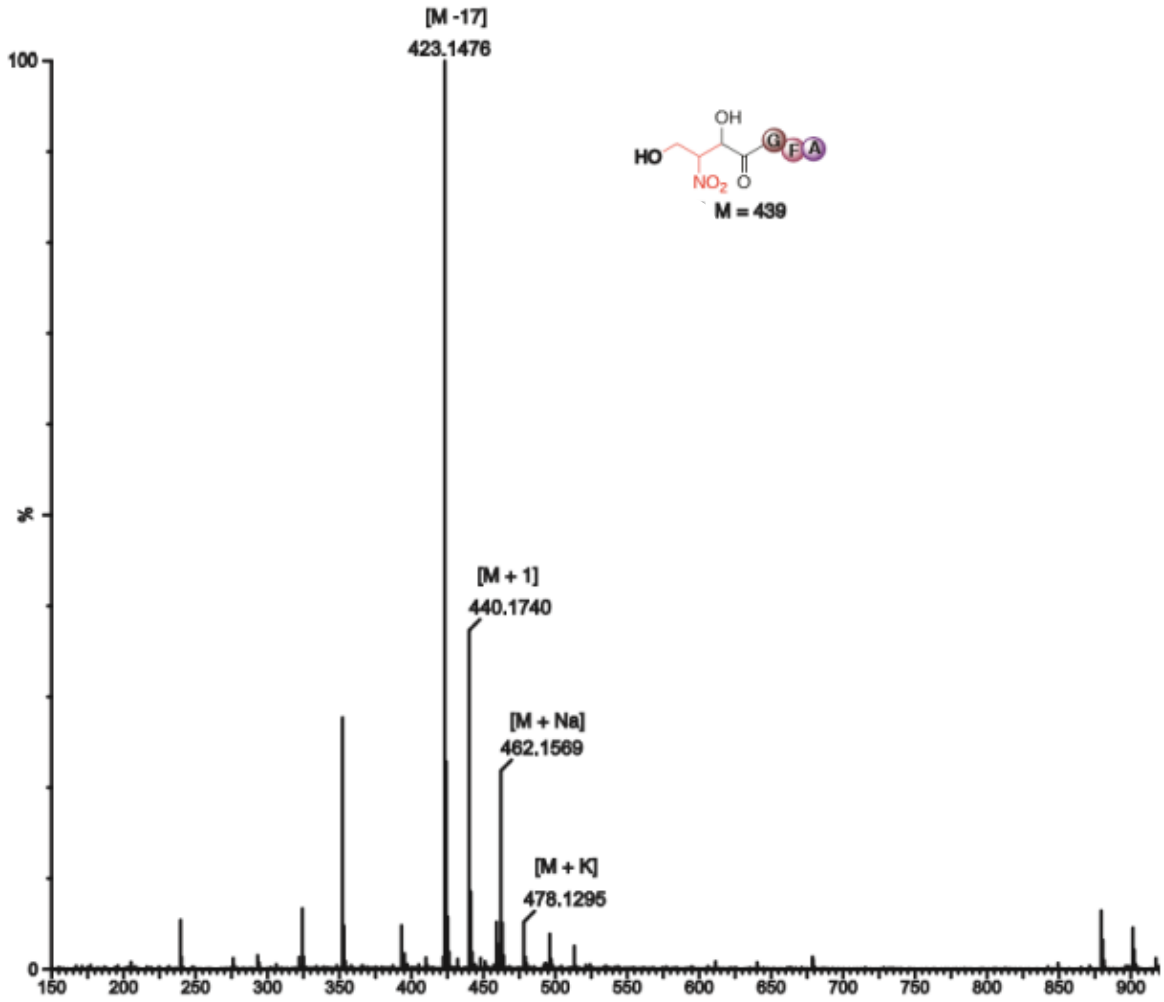
[M -17]
423.1476
100
%
0
OH
HO
NO2
O
G
F
A
M = 439
[M + 1]
440.1740
[M + Na]
462.1569
[M + K]
478.1295
150
200
250
300
350
400
450
500
550
600
650
700
750
800
850
900

HRMS of 3.3c'

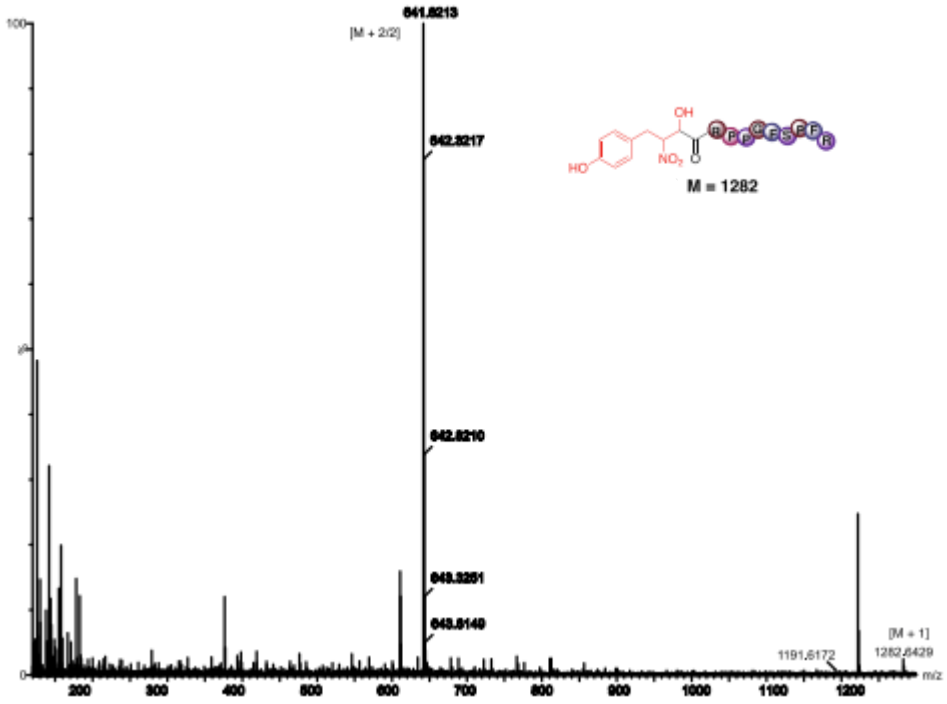
641.8213
[M + 2(2)]
642.8217
642.8210
643.8251
643.8149
1191.6172
[M + 1]
1282.6429
m/z
M = 1282

HRMS of 3d”

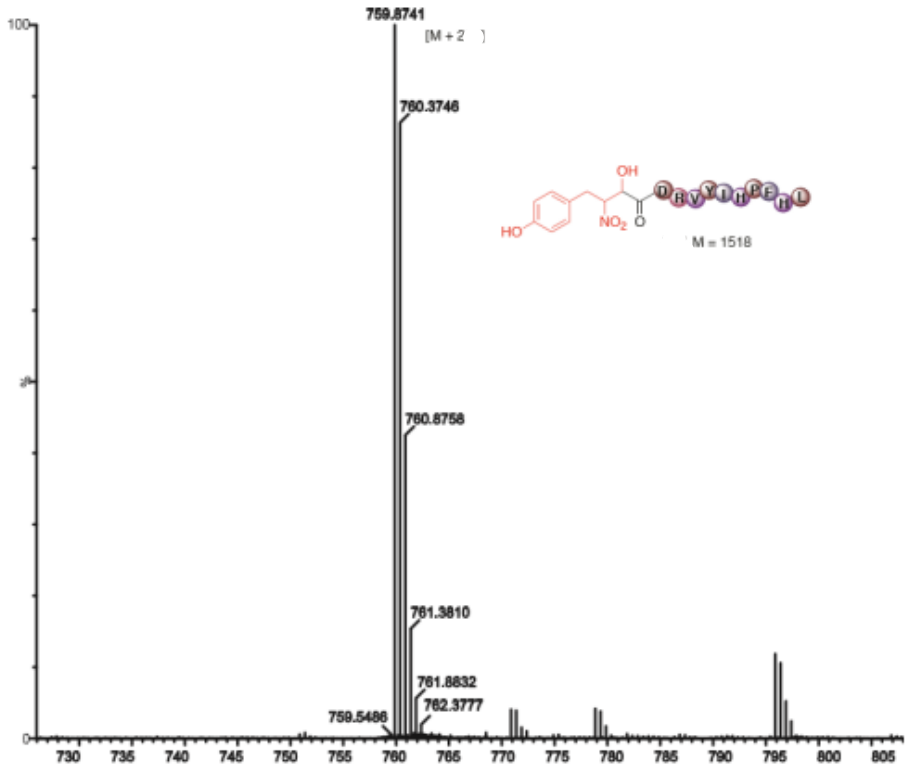
759.8741
[M + 2]
760.3746
760.8758
761.3810
761.8832
762.3777
759.5486
100
0
730
735
740
745
750
755
760
765
770
775
780
785
790
795
800
805
OH
HO
NO2
O
M = 1518

HRMS of 3.3f

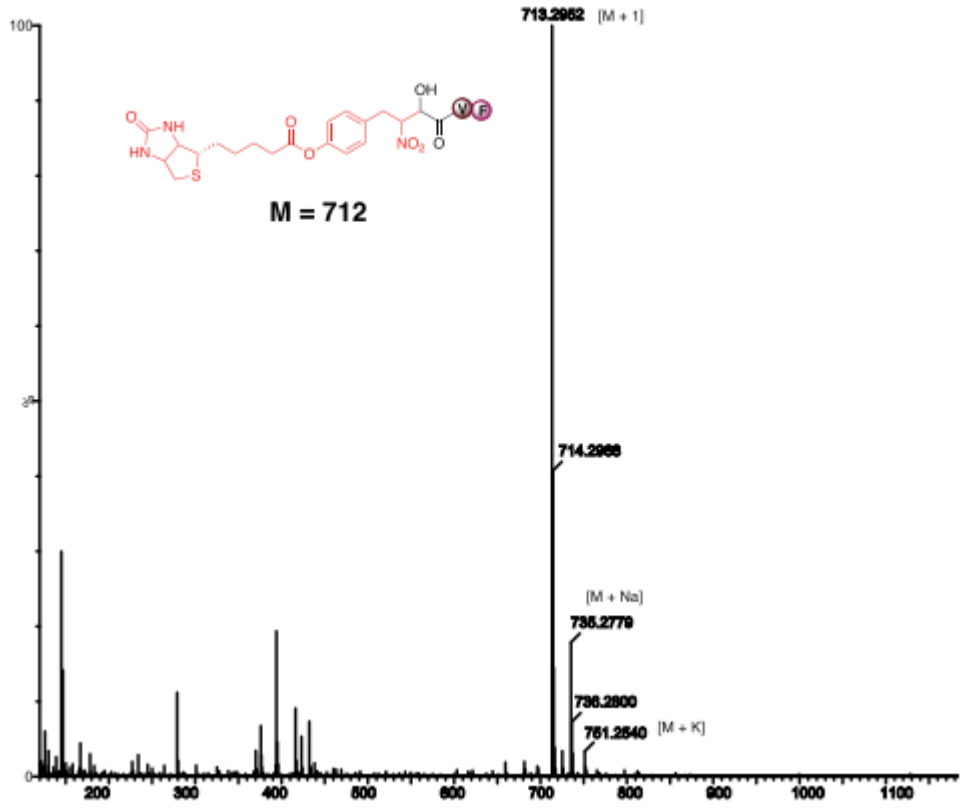
713.2952 [M + 1]
714.2988
[M + Na]
735.2779
736.2800
751.2540 [M + K]
M = 712
100
%
0
200
300
400
500
600
700
800
900
1000
1100

Characterization of nitro-peptide conjugate 3.3e (NMR): Based on 1D and 2D NMR data **3.3e** was found as mixture of diastereomers.

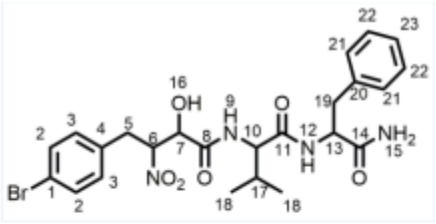

nitro-peptide conjugate (^{1}H NMR)

Atom No.	Chemical Shift[b] (ppm)	Integration	Atom No.	Chemical Shift[b] (ppm)	Integration
12	8.35-8.33	1H	6	5.32-5.24	1H
9	7.92-7.87	1H	7	4.75-4.66	1H
2	7.62-7.54	2H	13	4.75-4.66	1H
15	7.62-7.54	1H	10	4.43-4.30	1H
23	7.37-7.18	1H	5	3.45-3.31	1H
22	7.37-7.18	2H	19	3.20-3.13	1H
21	7.37-7.18	2H	5	3.02-2.97	1H
15	7.37-7.18	1H	19	2.96-2.92	1H
3	7.37-7.18	2H	17	2.20-2.10	1H
16	7.24-7.06	1H	18	0.92-0.82	6H

nitro-peptide conjugate (^{13}C NMR)

Atom No.	Chemical Shift[b] (ppm)	Atom No.	Chemical Shift[b] (ppm)
14	173.4	6	90.3
8	171.1	7	71.9
11	170.1	10	58.0
4	138.6	13	54.7
20	136.3	19	38.3
3	132.1	5	32.4
2	131.9	17	31.7
22	129.6	18	19.4
21	128.4		
23	126.7		
1	120.9		

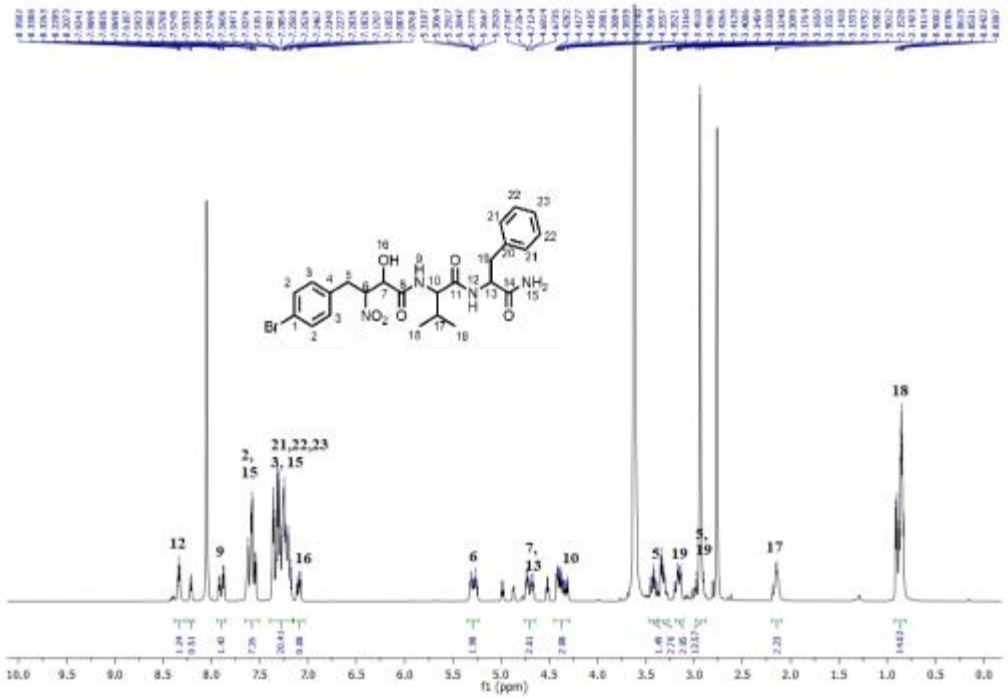
12
9
2, 15
21,22,23
3, 15
16
6
7, 13
10
5
19
5, 19
17
18
f1 (ppm)

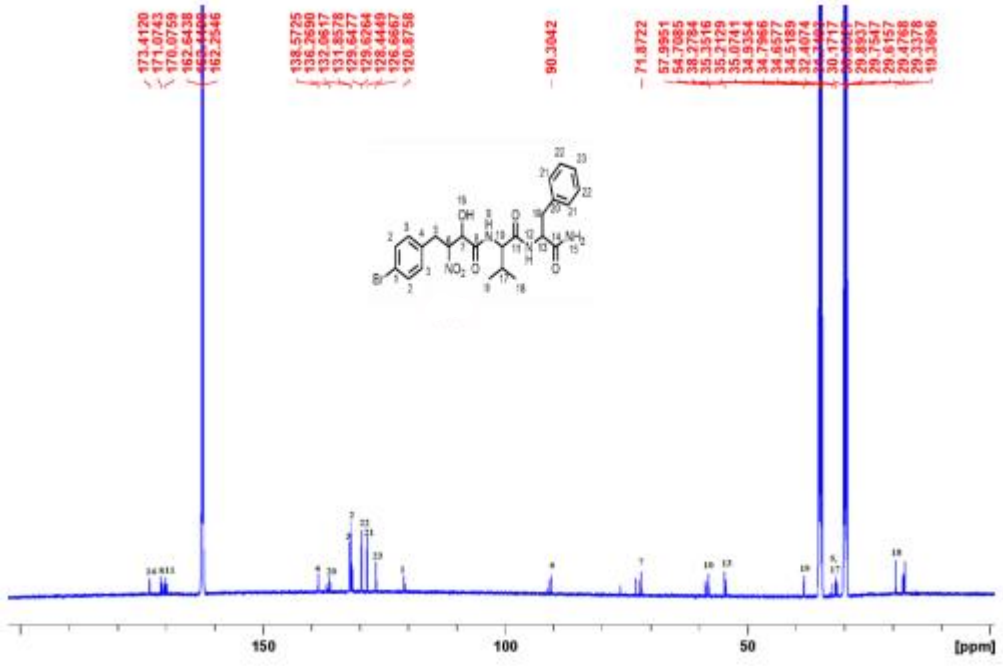
173.4120
171.0743
170.0759
162.6438
162.2546
138.5725
136.2680
132.8617
131.8578
129.6477
129.6264
128.4449
126.6667
120.8758
90.3042
71.8722
57.9951
54.7085
38.2784
35.3516
35.2129
35.0741
34.9354
34.7966
34.6577
34.5189
32.4074
30.1717
29.8937
29.7547
29.6157
29.4768
29.3378
19.3696
150
100
50
[ppm]

HSQC-

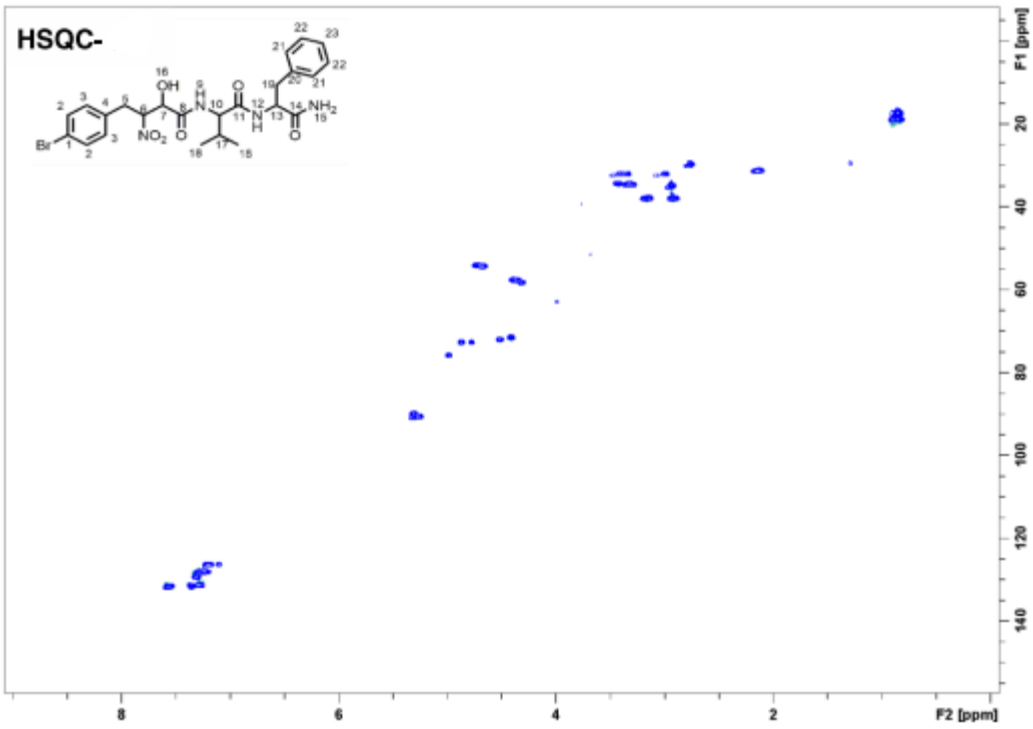

Cosy-

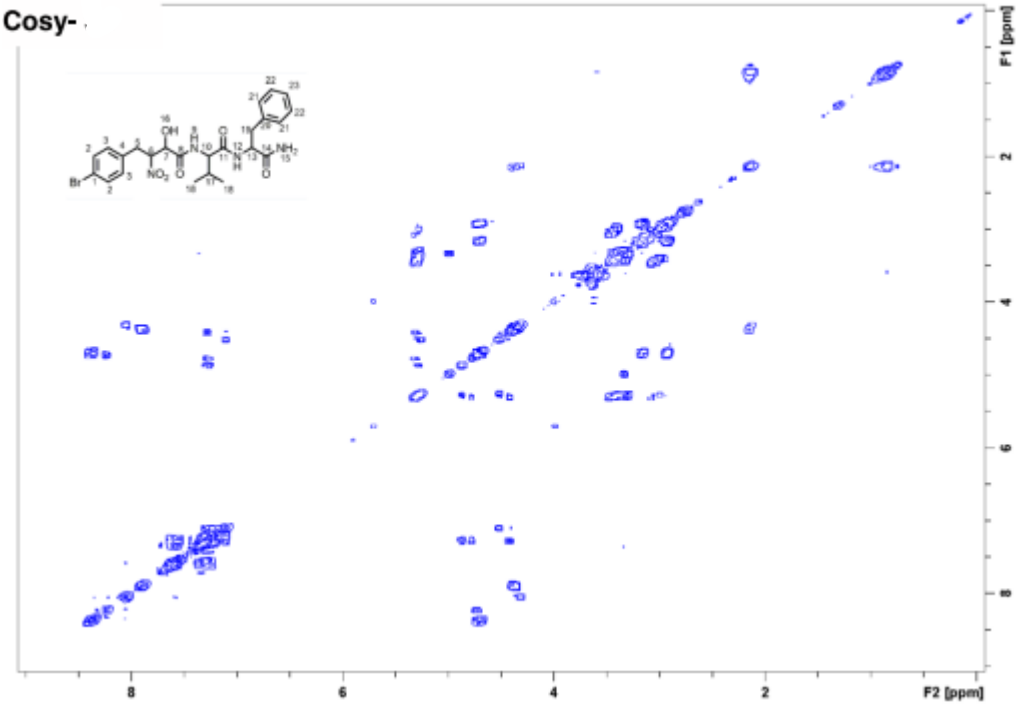

Synthesis of nitro derivatives (3.1c, 3.1e and 3.1j).

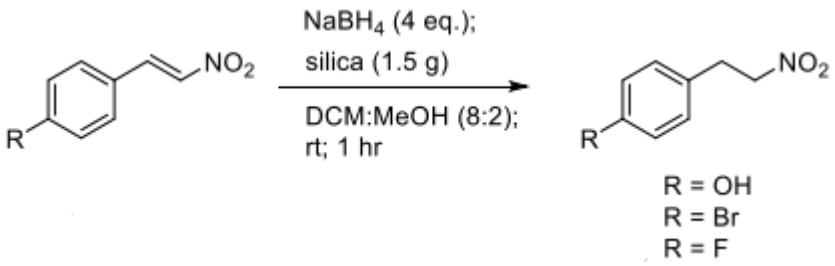

To a vigorously stirred mixture of **3.1A** (2.17 mmol) in DCM and MeOH (8:2) was added silica gel (100 mesh-1.5 g) at rt followed by addition of $NaBH_4$ (4 eq.) portion wise. The reaction mixture stirred at rt until the complete consumption of **3.1A** was observed as indicated by TLC. The reaction mixture quenched with 1N HCl and filtered. The silica was washed with DCM and the combined organic layers were dried over Na_2SO_4 and evaporated using rotary evaporator. Crude was purified over silica gel using ethylacetate and hexane solvent mixture as an eluent.

4-(2-Nitroethyl)phenol (3.1c): Yield 59 %. ^{1}H NMR (600 MHz, $CDCl_3$) δ 7.07 (d, J = 8.4 Hz, 2H), 6.79 (d, J = 8.5 Hz, 2H), 5.07 (s, 1H), 4.57 (t, J = 7.3 Hz, 2H), 3.24 (t, J = 7.3 Hz, 2H). ^{13}C NMR (151 MHz, $CDCl_3$) δ 155.1, 129.9, 127.5, 115.9, 76.8, 32.7.

1-Bromo-4-(2-nitroethyl)benzene (3.1e): Yield 80%. ^{1}H NMR (600 MHz, $CDCl_3$) δ 7.45 (d, J = 8.3 Hz, 2H), 7.09 (d, J = 8.2 Hz, 2H), 4.60 (t, J = 7.2 Hz, 2H), 3.27 (t, J = 7.2 Hz, 2H). ^{13}C NMR (151 MHz, $CDCl_3$) δ 134.7, 132.2, 130.4, 121.5, 76.1, 32.8.

1-Fluoro-4-(2-nitroethyl)benzene (3.1j): Yield 82% ^{1}H NMR (600 MHz, $CDCl_3$) δ 7.19 – 7.16 (m, 2H), 7.01 (t, J = 8.4 Hz, 2H), 4.59 (t, J = 7.2 Hz, 2H), 3.28 (t, J = 7.2 Hz, 2H). ^{13}C NMR (151 MHz, $CDCl_3$) δ 162.1 (d, J = 245.9 Hz), 131.4 (d, J = 3.2 Hz), 130.3 (d, J = 8.1 Hz), 115.9 (d, J = 21.5 Hz), 76.4, 32.6. ^{19}F NMR (235 MHz, $CDCl_3$) δ -115.1.

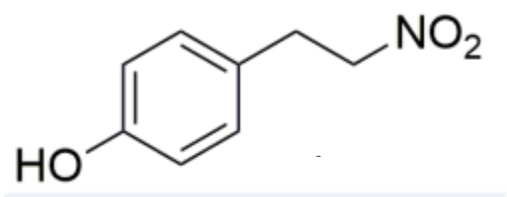
NO2
HO

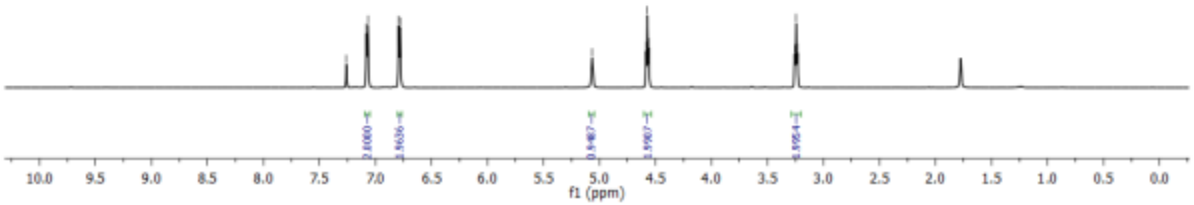
10.0
9.5
9.0
8.5
8.0
7.5
7.0
6.5
6.0
5.5
5.0
4.5
4.0
3.5
3.0
2.5
2.0
1.5
1.0
0.5
0.0
f1 (ppm)

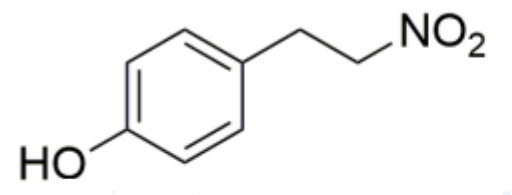
NO2
HO

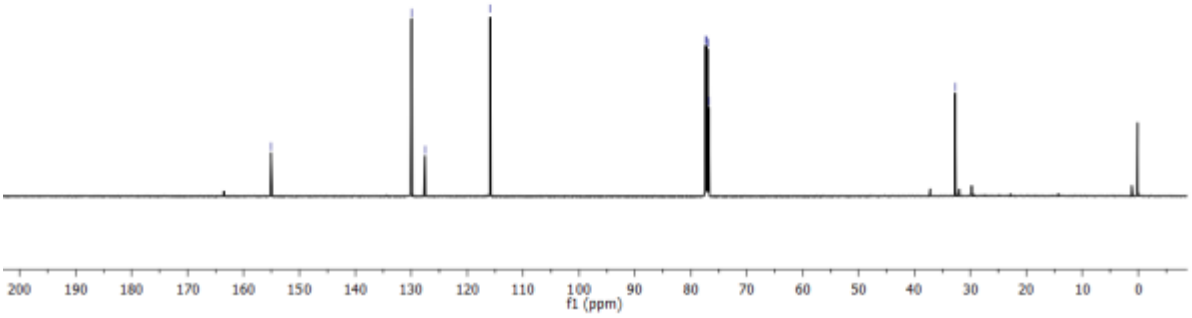
200
190
180
170
160
150
140
130
120
110
100
90
80
70
60
50
40
30
20
10
0
f1 (ppm)

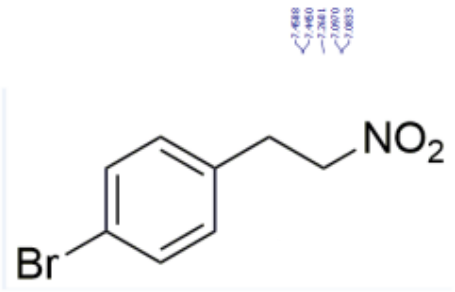
NO2
Br

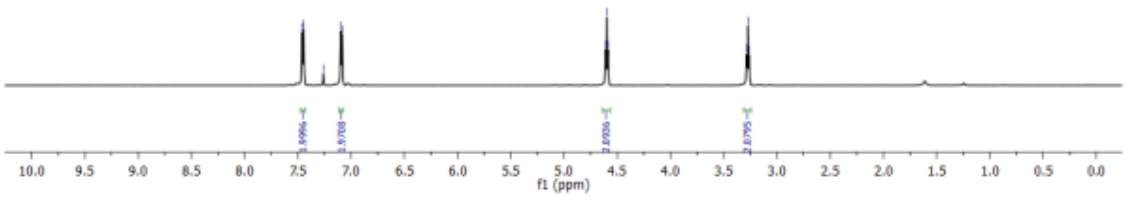
f1 (ppm)

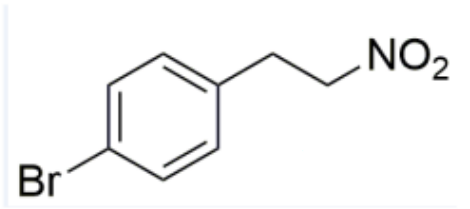
NO2
Br

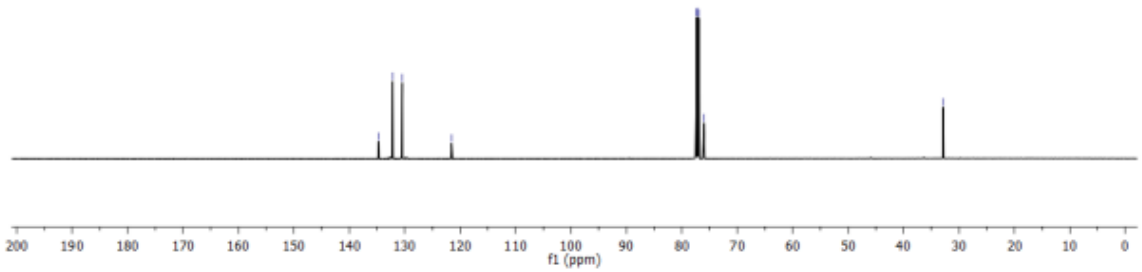
f1 (ppm)

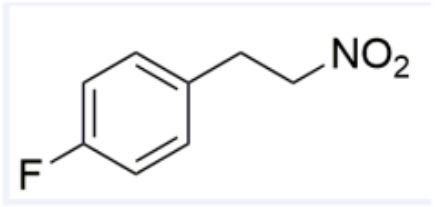
NO2
F

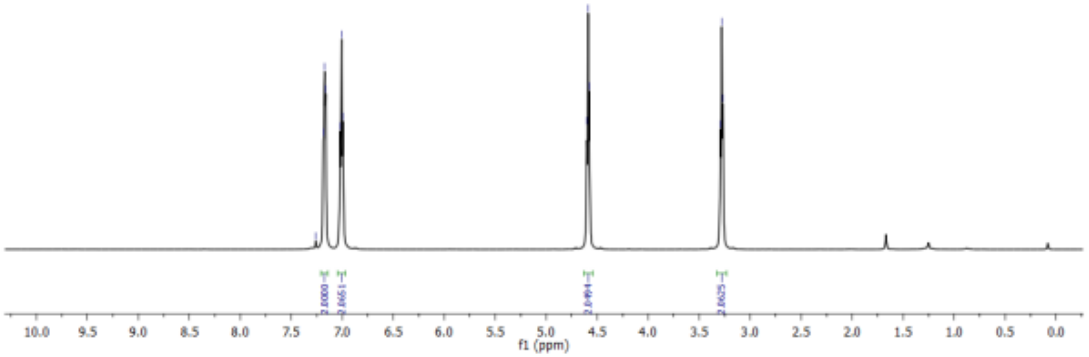
f1 (ppm)

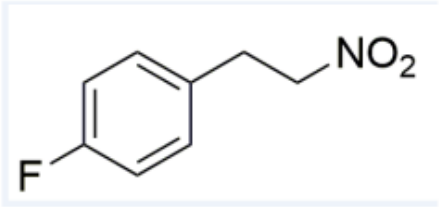
NO2
F

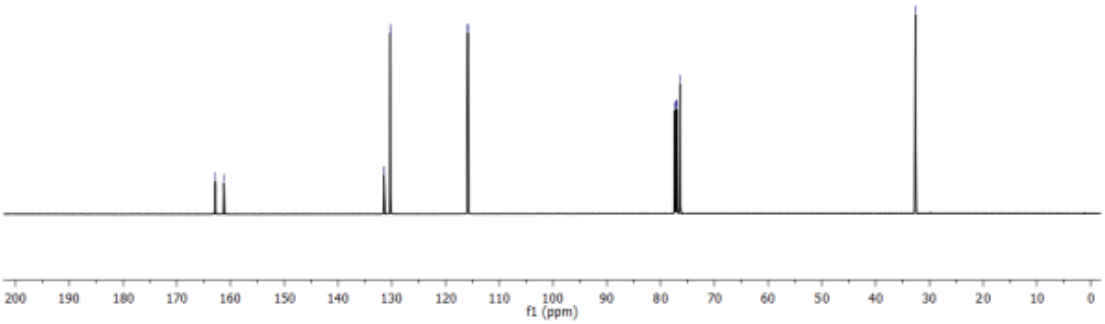
f1 (ppm)

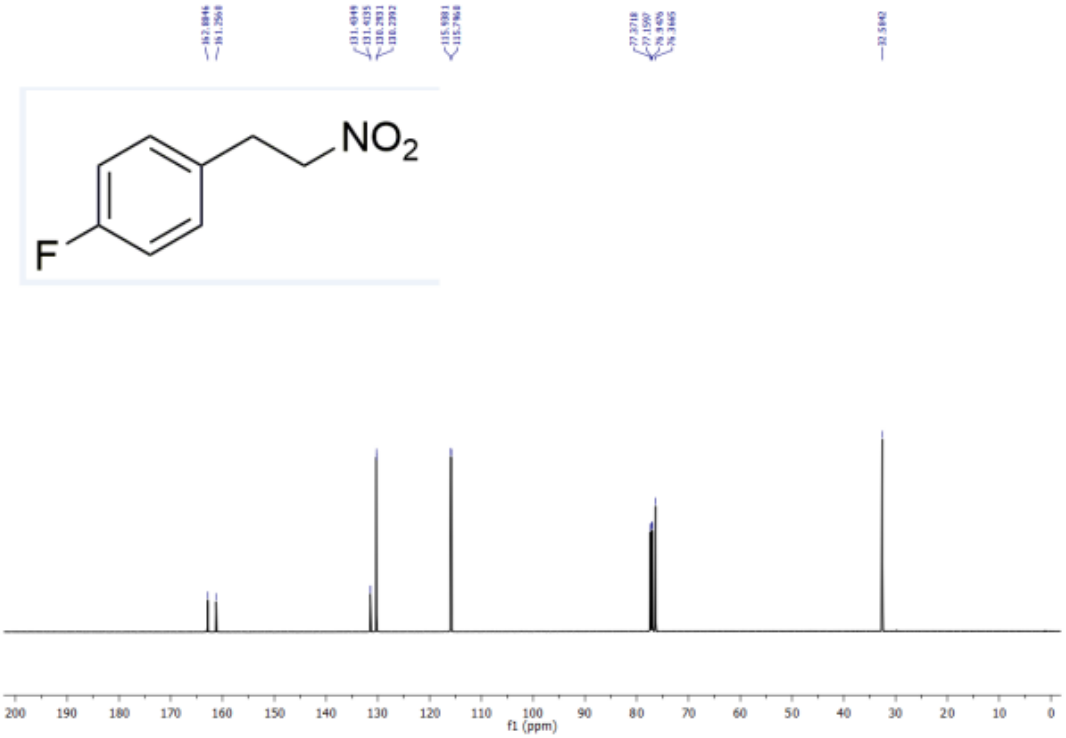

Synthesis of nitro derivative (3.1d).

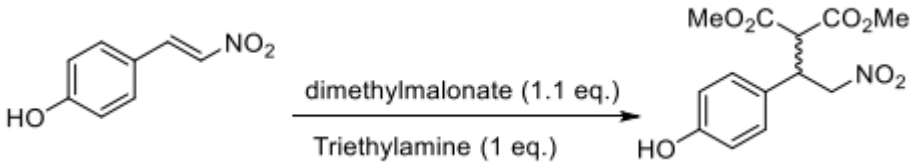

To a briefly vortexed mixture of **3.1A** (0.06 mmol) and dimethylmalonate (1.1 eq.) was added triethylamine and the reaction mixture was stirred at rt until the complete consumption of **3.1A** observed as indicated by TLC. Volatiles were removed under reduced pressure, and crude purified over silicagel using ethylacetate and hexane solvent mixture as an eluent.

Dimethyl 2-(1-(4-hydroxyphenyl)-2-nitroethyl)malonate (3.1d): Yield 60%. 1H NMR (400 MHz, CDCl3) δ 7.08 (d, J = 8.5 Hz, 2H), 6.73 (d, J = 8.4 Hz, 2H), 4.91 – 4.78 (m, 2H), 4.20 – 4.10

(m, 1H), 3.82 (d, J = 9.3 Hz, 1H), 3.76 (s, 3H), 3.57 (s, 3H). 13C NMR (101 MHz, CDCl3) δ 168.1, 167.6, 155.9, 129.3, 127.9, 116.1, 77.8, 55.0, 53.2, 53.1, 42.5.

NMR spectra of 3.1d

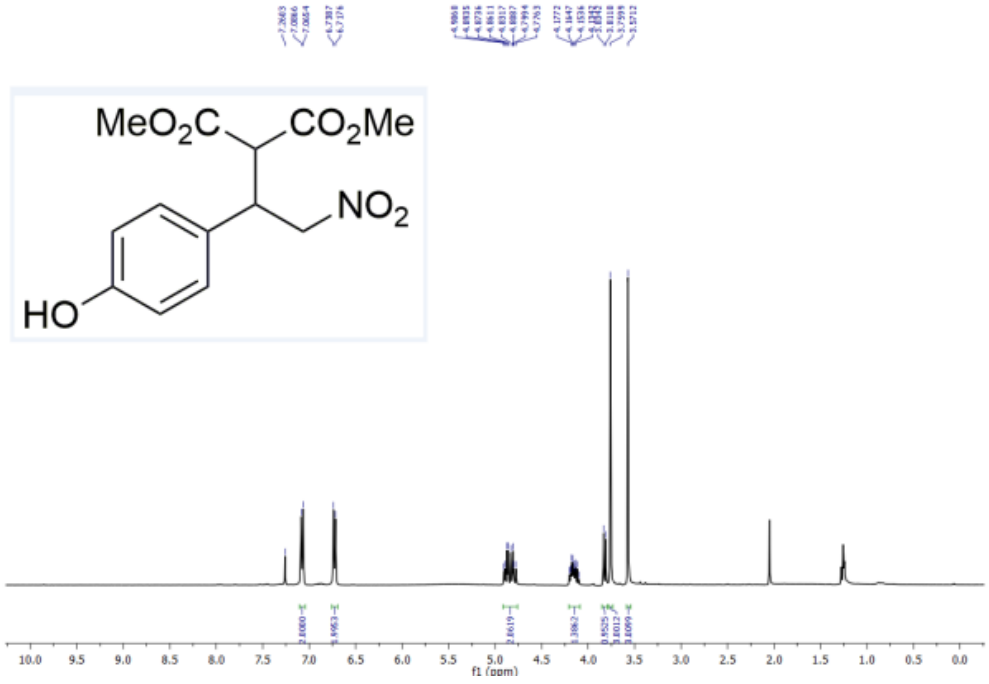

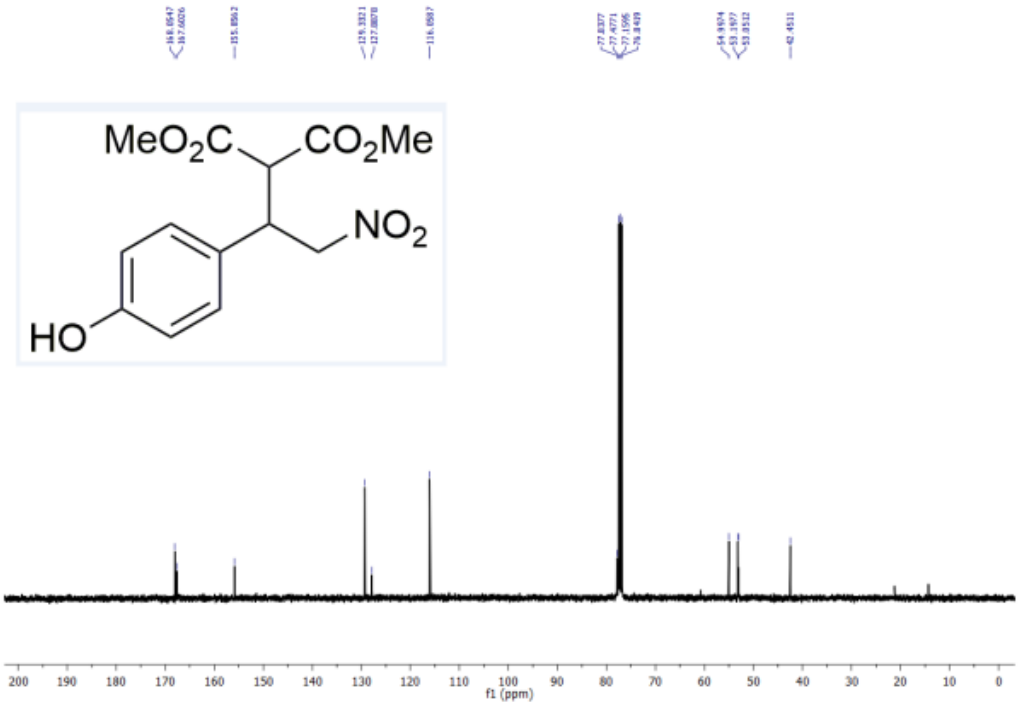

Synthesis of nitro derivative (3.1f).

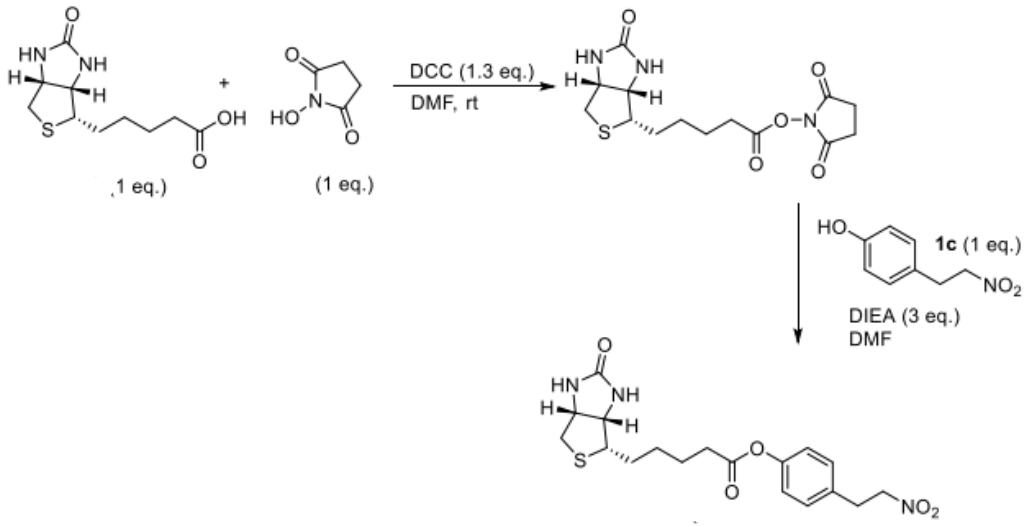

To a dissolved solution of d-Biotin (**3.1B**-0.82 mmol) and N-hydroxy succinimide (1 eq.) in DMF at 60 ^{o}C was added DCC (1.3 eq.) and the reaction mixture was stirred at rt overnight. The reaction mixture was filtered, and DMF was evaporated under reduced pressure. The crude was triturated with ether and the white solid was filtered and washed with ether to give Biotin-NHS ester as white

powder. To a solution of **3.1c** (0.06 mmol) and DIEA (3 eq.) in DMF, was added Biotin-NHS ester (1.5 eq.) the reaction mixture was stirred at rt overnight. The reaction mixture was filtered, and DMF was evaporated under reduced pressure. Crude was dissolved in water: ACN (1:1) and was purified using HPLC to get **3.1f** as off-white powder.

HRMS of 3.1f

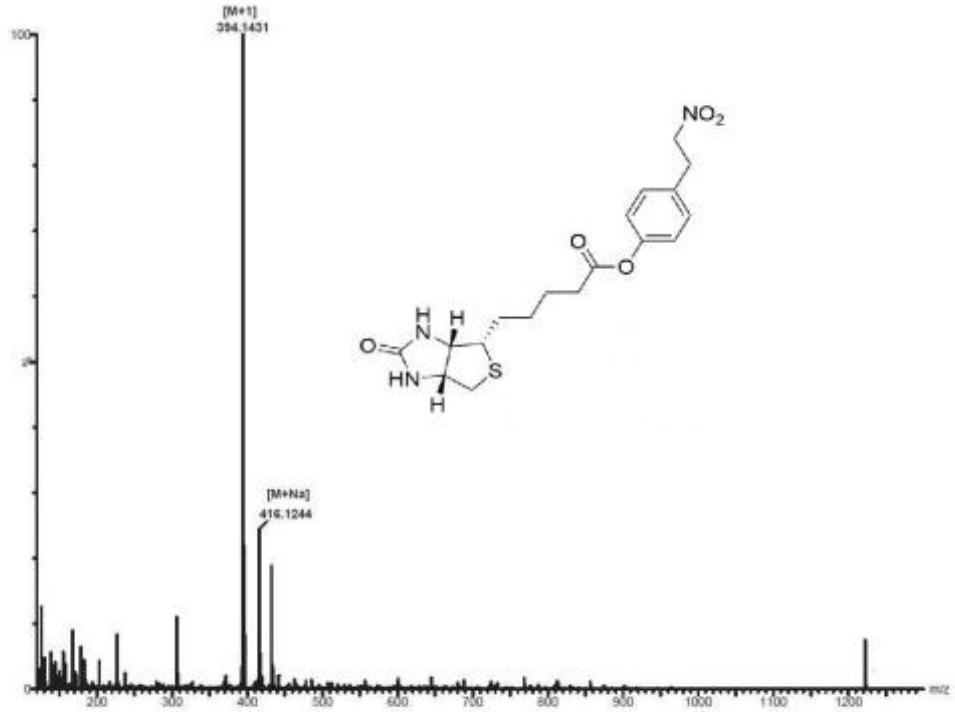

Synthesis of nitro derivative (**3.1h**)

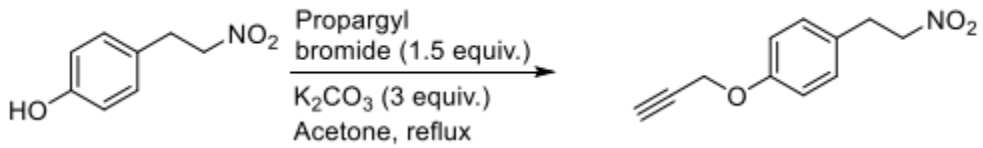

To a mixture of 4-(2-nitroethyl)phenol (1.5 mmol) and potassium carbonate (3 eq.) in acetone, propargyl bromide (1.5 eq.) was added and the reaction mixture was refluxed for 18 h. Acetone was removed under reduced pressure. Crude reaction mixture was extracted using ethylacetate and water followed by washing with brine. Combined organic layers were dried over Na_2SO_4, evaporated and crude material was purified over silicagel using ethylacetate and hexane solvent mixture as an eluent.

1-(2-Nitroethyl)-4-(prop-2-yn-1-yloxy)benzene (**3.1h**): Yield 20%. ^{1}H NMR (400 MHz, $CDCl_3$) δ 7.14 (d, J = 8.5 Hz, 2H), 6.94 (d, J = 8.6 Hz, 2H), 4.68 (d, J = 2.2 Hz, 2H), 4.58 (t, J = 7.4 Hz, 2H), 3.27 (t, J = 7.4 Hz, 2H), 2.52 (t, J = 2.2 Hz, 1H). ^{13}C NMR (101 MHz, $CDCl_3$) δ 157.0, 129.8, 128.7, 115.5, 78.6, 76.6, 75.8, 56.0, 32.8.

NMR spectra of 3.1h

Synthesis of nitro derivative (1i)

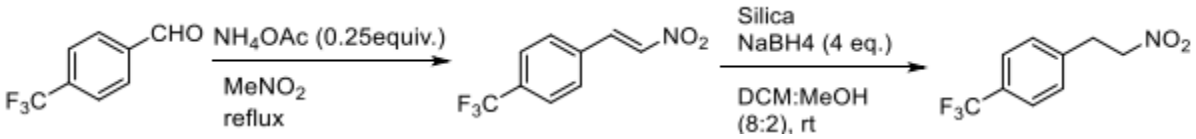

A solution of 4-trifluoromethylbenzaldehyde (1 mmol) and ammoniumacetate (0.25 eq.) in nitromethane was refluxed for 6h. Nitromethane was removed under reduced pressure. Crude reaction mixture was extracted using ethylacetate and water followed by washing with brine. Combined organic layers were dried over Na2SO4, evaporated and crude purified over silicagel using ethylacetate and hexane solvent mixture as an eluent to obtain nitrostyrene (**3.1D**) derivative in 83% yield. To a vigorously stirred mixture of nitrostyrene (**3.1D**-0.5 mmol) in DCM and MeOH (8:2) was added silica gel (100 mesh) at rt followed by portion wise addition of NaBH4 (4 eq.). The reaction mixture was stirred at rt until the complete consumption of nitrostyrene (**3.1D**) was observed as indicated by TLC. The reaction mixture was quenched with 1N HCl and filtered. The silica was washed with DCM. The organic layers were combined and dried over Na_2SO_4 followed by removal of solvent using rotary evaporator. The crude was purified over silica gel using

ethylacetate and hexane solvent mixture as an eluent to obtain **3.1i**. 1-(2-Nitroethyl)-4-(trifluoromethyl)benzene (**3.1i**): Yield 50%. ^{1}H NMR (600 MHz, $CDCl_3$) δ 7.59 (d, J = 7.8 Hz, 2H), 7.34 (d, J = 7.7 Hz, 2H), 4.65 (t, J = 7.1 Hz, 2H), 3.38 (t, J = 7.0 Hz, 2H). ^{13}C NMR (151 MHz, $CDCl_3$) δ 139.8, 129.8 (q, J = 32.6 Hz), 129.1, 126.0 (q, J = 3.6 Hz), 124.1 (q, J = 272.2 Hz), 75.8, 33.1. ^{19}F NMR (235 MHz, $CDCl_3$) δ -62.6.

NMR spectra of 3.1i

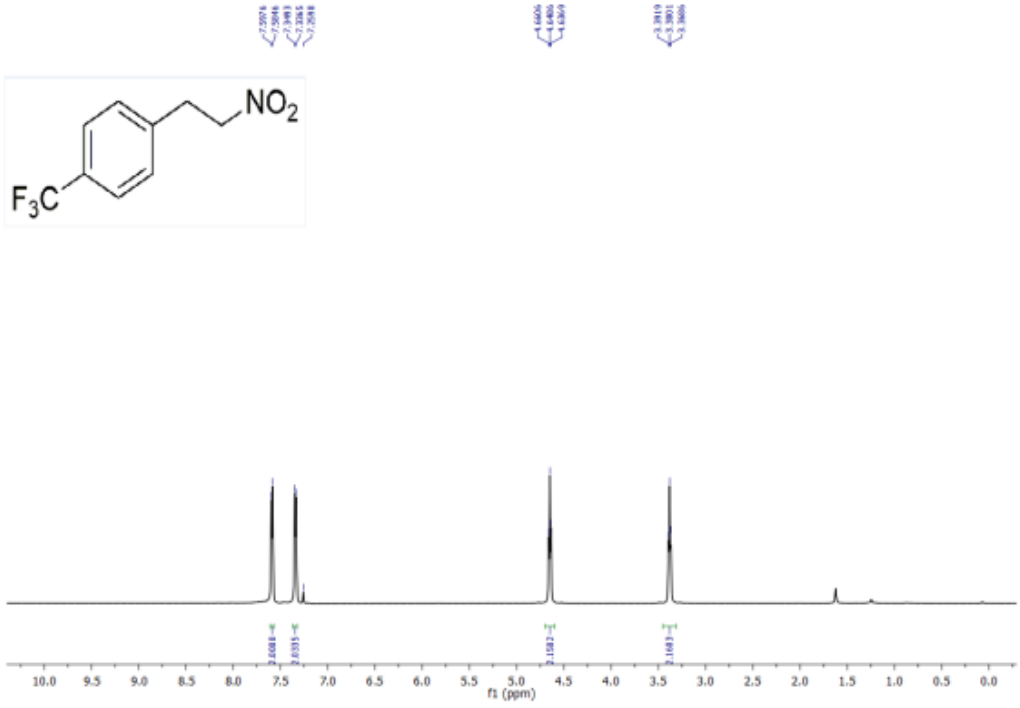

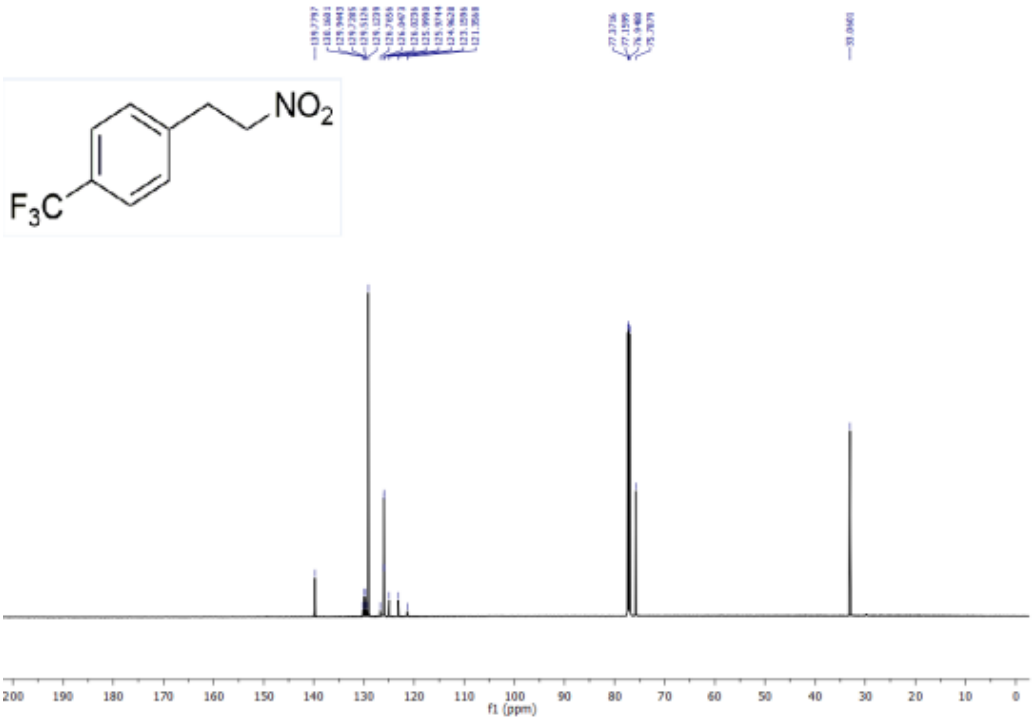

19F NMR spectra of 3.1i

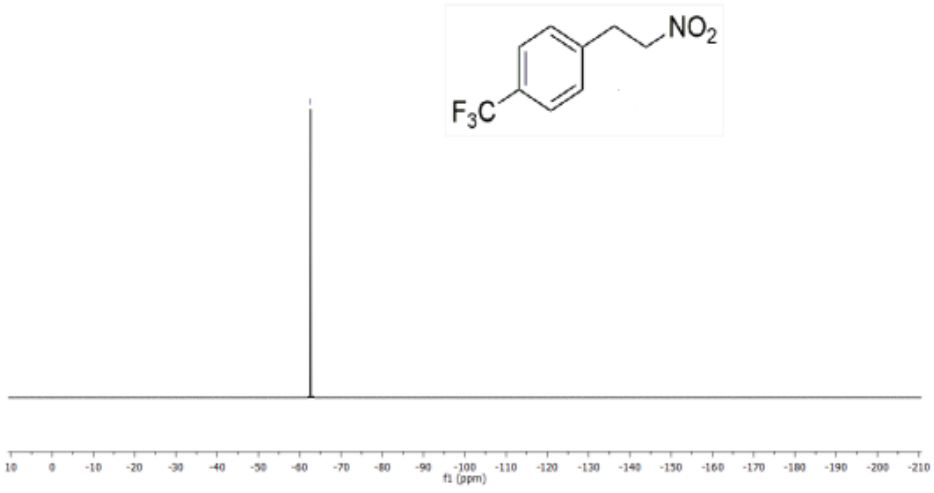

Synthesis of nitro derivative (3.1k).

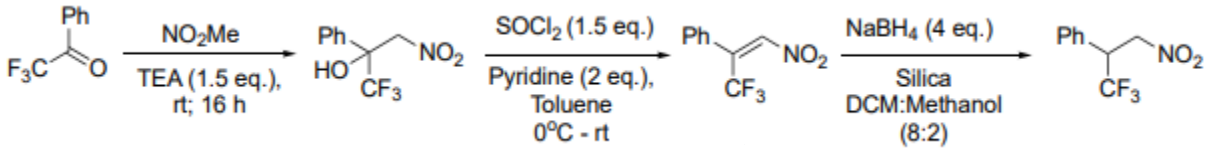

To a solution of **3.1E** (2.9 mmol) in nitromethane was added triethylamine (1.5 eq.) and the reaction mixture was stirred at rt for 16 h. Nitromethane was evaporated under reduced pressure and crude was extracted with 1 N HCl, water and brine. Combined organic layers were dried over Na_2SO_4, evaporated and crude was purified over silica gel using ethyl acetate and hexane solvent mixture as an eluent to obtain **3.1F** (yield 89%).

To a solution of **3.1F** (2.5 mmol) in toluene was added $SOCl_2$ (1.5 eq.) and pyridine (2 eq.) at 0 ^oC and the reaction mixture was stirred until the complete consumption of **3.1F** was observed as indicated by TLC. The reaction mixture was extracted using ethylacetate and water followed by washing with brine. The combined organic layers were dried over Na_2SO_4, evaporated and crude was purified over silica gel using ethylacetate and hexane solvent mixture as an eluent to obtain 3.1G (yield 44%).

To a vigorously stirred mixture of nitrostyrene (**3.1G**-0.46 mmol) in DCM and MeOH (8:2) was added silica gel (100 mesh) at rt followed by portion wise addition of $NaBH_4$ (4 eq.). The reaction mixture was stirred at rt until the complete consumption of nitrostyrene (**3.1G**) was observed as indicated by TLC. The reaction mixture was quenched with 1N HCl and filtered. The silica was washed with DCM and the combined organic layers were dried over Na_2SO_4 followed by removal of solvent using rotary evaporator. The crude was purified over silica gel using ethylacetate and hexane solvent mixture as an eluent to obtain **3.1k**.

(1,1,1-Trifluoro-3-nitropropan-2-yl)benzene (**3.1k**): Yield 59%. 1H NMR (400 MHz, CDCl3) δ 7.42 – 7.41 (m, 3H), 7.35 – 7.33 (m, 2H), 4.98 (dd, J = 13.7, 5.8 Hz, 1H), 4.84 (dd, J = 13.7, 8.9 Hz, 1H), 4.39 – 4.29 (m, 1H). 13C NMR (101 MHz, CDCl3) δ 130.2 (br), 129.7, 129.4, 128.9, 125.1(q, J = 281 Hz), 74.0, 48.2 (q, J = 28.8 Hz). 19F NMR (235 MHz, CDCl3) δ -68.98 (d, J = 8.8 Hz).

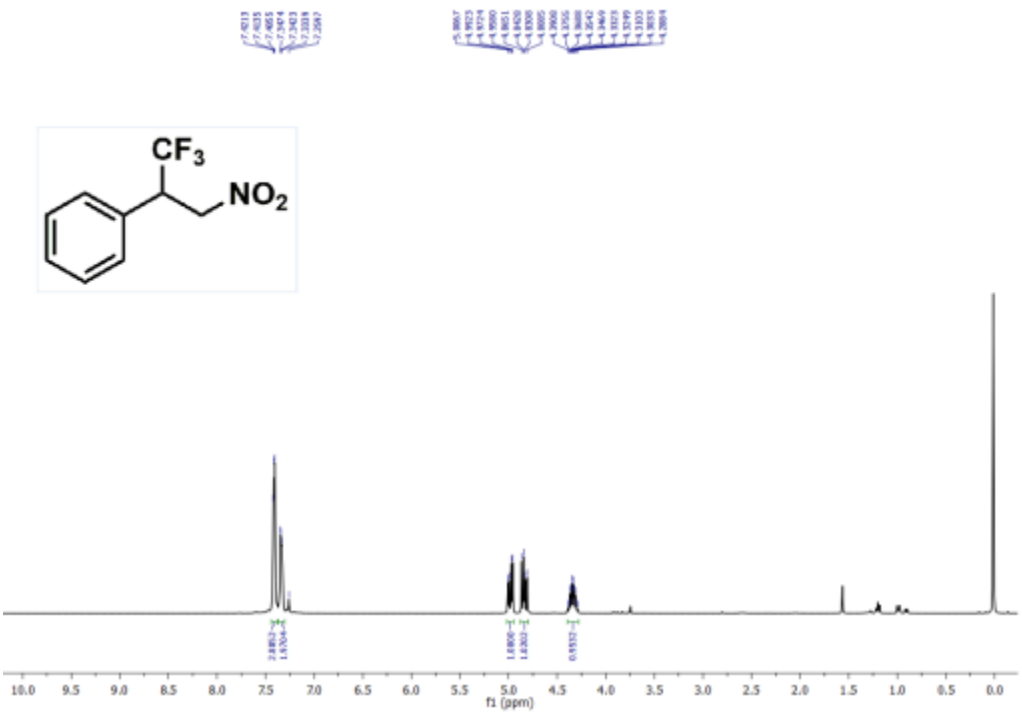

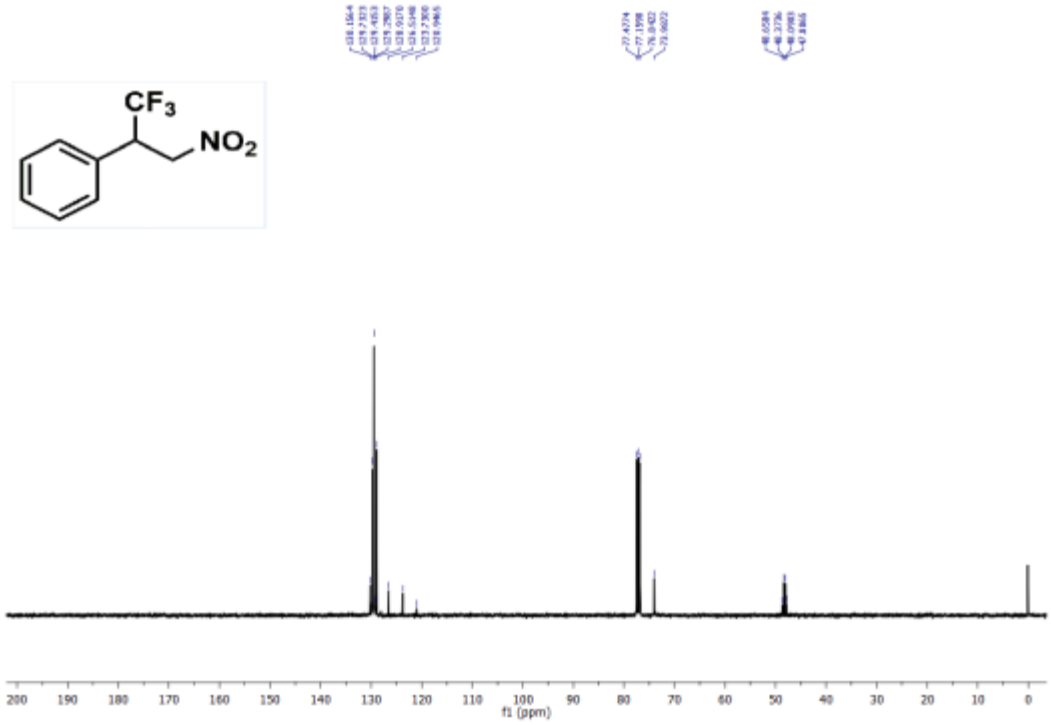

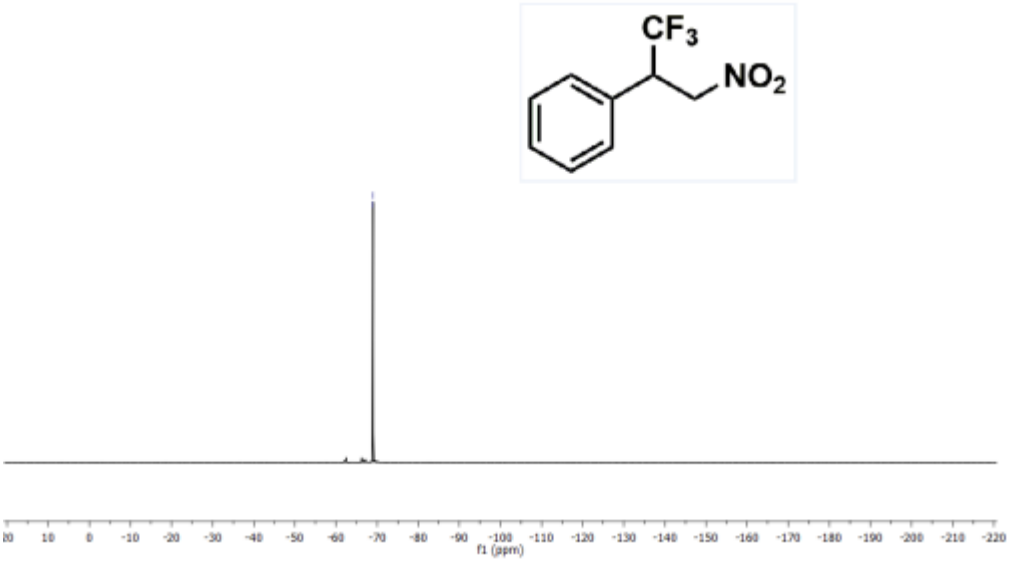

Synthesis of nitro derivative (3.1l)

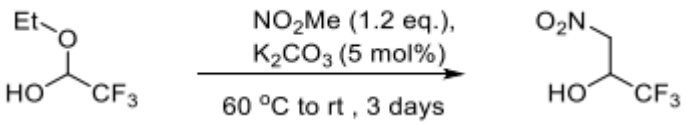

A mixture of 3.1H (3.47 mmol), nitromethane (1.2 eq.), and K_2CO_3 (5 mol%) was stirred at 60 ^oC to rt for 3 days. The reaction mixture was diluted with 1N HCl and extracted with diethylether thrice followed by washing with brine. Combined organic layers were dried over Na_2SO_4, evaporated by using rotary evaporator. The crude was purified over silica gel using ethyl acetate and hexane solvent mixture as an eluent to obtain 3.1l. 1,1,1-Trifluoro-3-nitropropan-2-ol (3.1l): Yield 72%. ^1H NMR (400 MHz, $CDCl_3$) δ 4.84 (bs, 1H), 4.69 – 4.56 (m, 2H), 4.28 (bs, 1H). ^{13}C NMR (101 MHz, $CDCl_3$) δ 123.3 (q, J = 282.9 Hz), 74.5, 67.8 (q, J = 33.2 Hz). ^{19}F NMR (235 MHz, $CDCl_3$) δ -78.23 (d, J = 6.5 Hz).

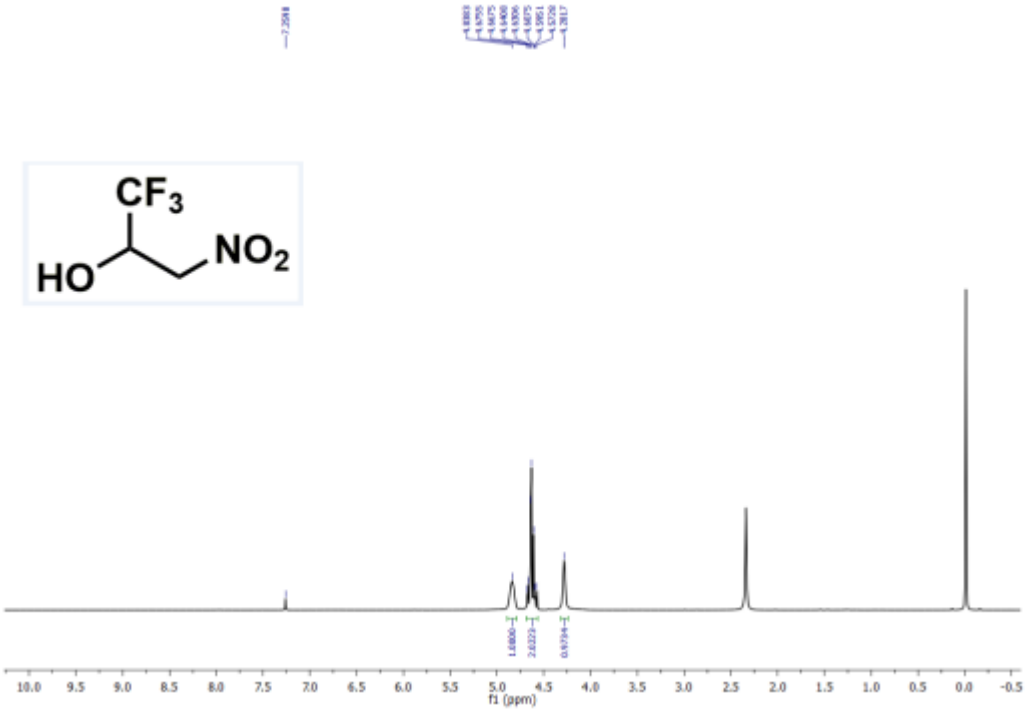

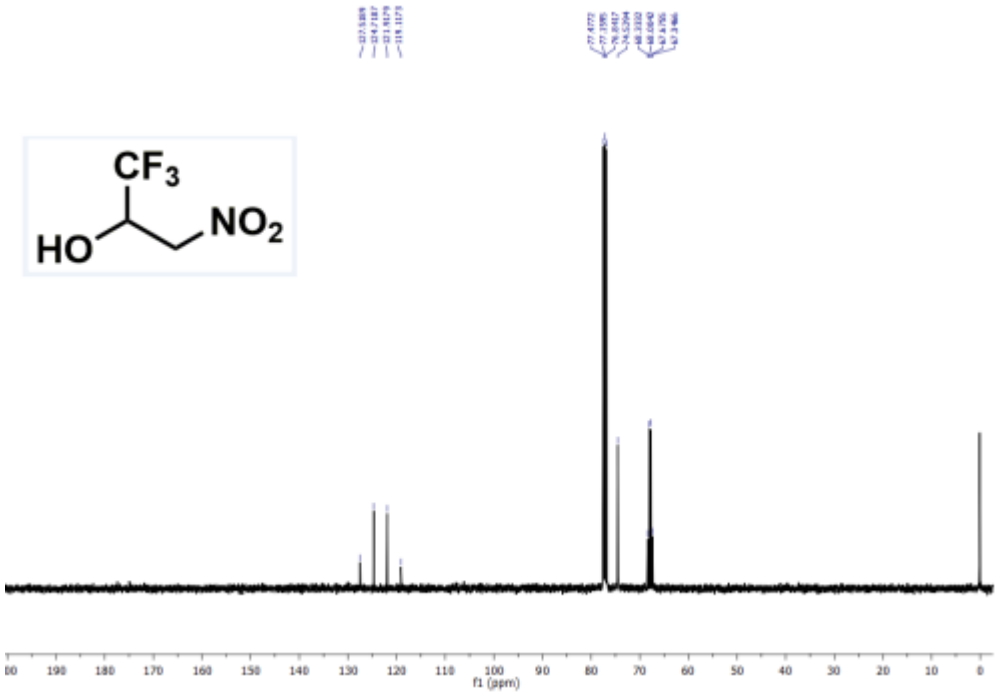

19F NMR spectra of 3.1l

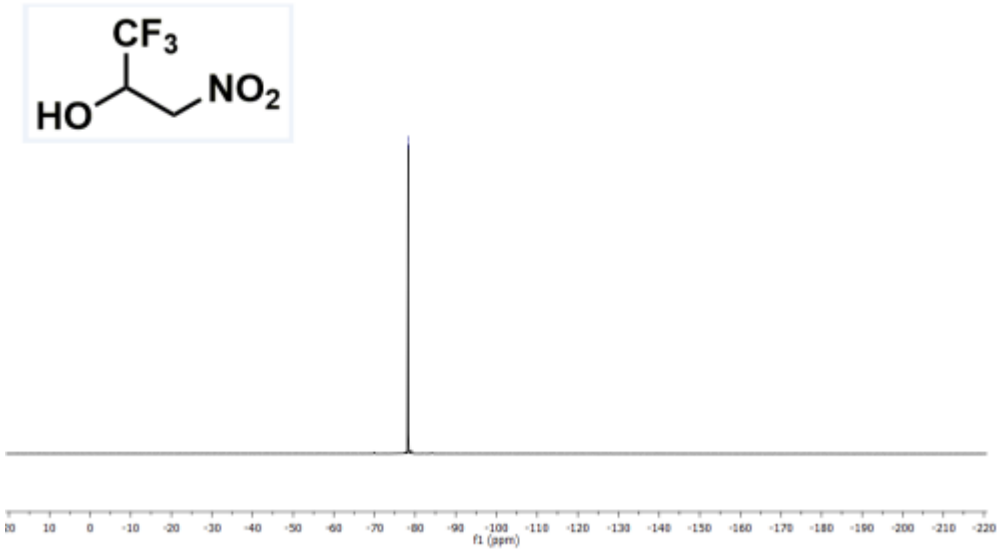

Synthesis of nitro derivative (3.1m and 3.1n)

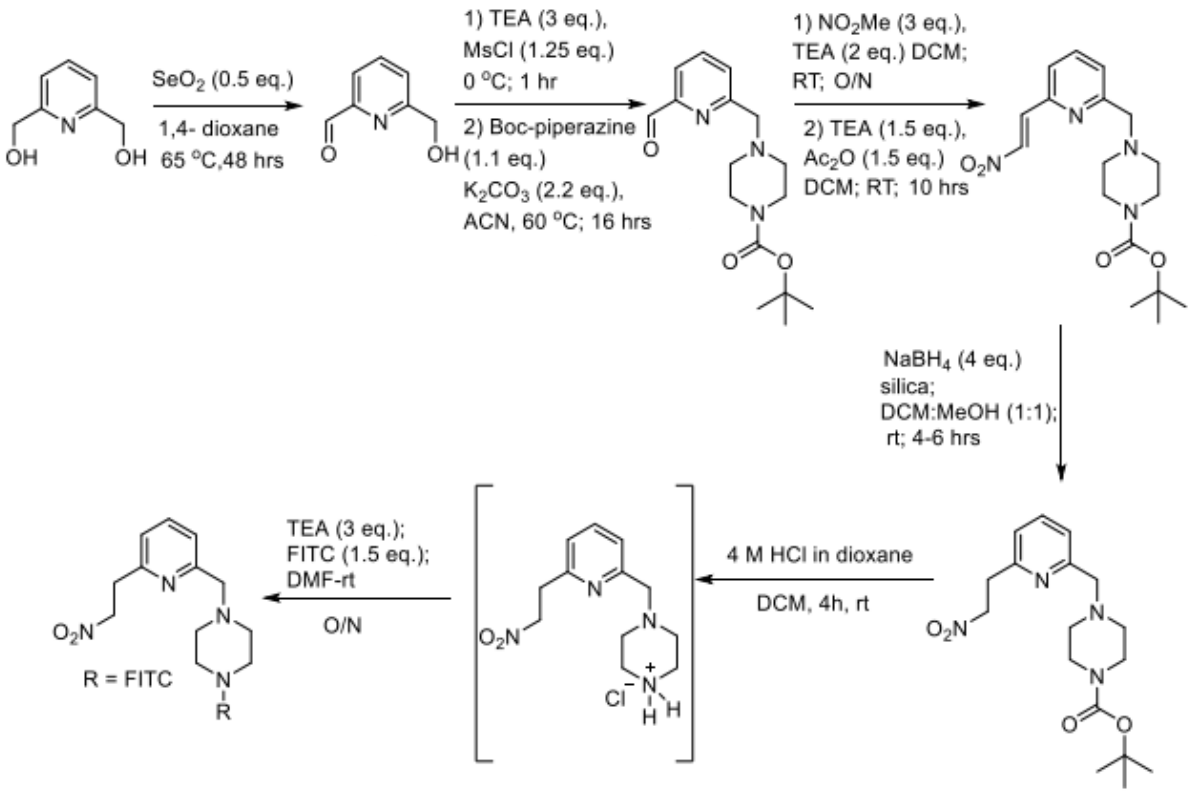

A mixture of 2,6-pyridinedimethanol (3.1I -7.19 mmol), and SeO2 (0.5 eq.) in 1,4-dioxane was stirred at 65 °C for 48 h. The reaction was cooled to room temperature and diluted with dichloromethane. The mixture was filtered through celite, and the filtrate was concentrated under reduced pressure. The resulting crude material was purified by column chromatography using 2.5% methanol in dichloromethane to afford 3.1J as an off-white solid with 71% yield. To a stirred solution of 6-(hydroxymethyl)-2-pyridinecarboxaldehyde (3.1J-4.7 mmol) and triethylamine (3 eq.) in dichloromethane was added methanesulfonylchloride (1.25 eq.) dropwise at 0 °C for 1 h. The reaction was quenched with saturated aqueous sodium bicarbonate. The aqueous layer was

separated and extracted three times with dichloromethane. The combined organic layers were dried over sodium sulfate, filtered and concentrated under reduced pressure to afford mesylate as a brown oil. To a vigorously stirred solution of mesylate (**3.1Ja**-2.55 mmol) and 1-boc-piperazine (1.1 eq.) in acetonitrile was added potassium carbonate (2.2 eq.). The resulting mixture was heated at 60 °C for 16 h. Volatiles removed under reduced pressure and the resulting crude was extracted with dichloromethane thrice and washed with brine. The aqueous layer was separated and extracted three times with dichloromethane. Combined organic layers were dried over Na_2SO_4, evaporated and the crude was purified over silica gel using ethyl acetate and hexane solvent mixture as an eluent to obtain 3.1K with 65% yield. To a solution of 3.1K (0.66 mmol) in dichloromethane was added nitromethane (3 eq.), and triethylamine (2 eq.) and the reaction mixture was stirred at rt overnight. Volatiles removed under reduced pressure. To a solution of crude reaction mixture (0.65 mmol) in dichloromethane was added triethylamine (1.5 eq.), and acetic anhydride (1.5 eq.) and the reaction mixture was stirred at rt for 10 h. Volatiles removed under reduced pressure and crude was purified over silicagel using ethylacetate and hexane solvent mixture as an eluent to obtain **3.1L** (65% yield). To a vigorously stirred mixture of nitrostyrene (3.1L-0.29 mmol) in DCM and MeOH (1:1) was added silica (100 mesh) at rt followed by portion wise addition of $NaBH_4$ (4 eq.). The reaction mixture was stirred at rt until the complete consumption of nitrostyrene (**3.1L**) was observed as indicated by TLC. The reaction mixture was quenched with 1N HCl and filtered. The silica was washed with DCM and the organic layer was separated and dried over Na_2SO_4. The combined organic layers were evaporated using rotary evaporator and crude was purified over silica gel using ethyl acetate and hexane solvent mixture as an eluent to obtain 3.1m (60% yield). To a stirred solution of 3.1m (0.17 mmol) in dichloromethane was added 4 M HCl in 1,4-dioxane (1 mL) for 4 h and the reaction mixture was

concentrated under reduced pressure. The resulting thick oil was repeatedly taken up in dichloromethane and concentrated under reduced pressure. The resulting crude reaction mixture was dried overnight under high vacuum. Dry crude mixture was treated with triethylamine (3 eq.), and FITC (1.5 eq.) in DMF at rt overnight. Volatiles lyophilized. Crude was dissolved in water: ACN (1:1) mixture and was purified using HPLC to obtain pure product 3.1n.

(6-Formylpyridin-2-yl)methyl methanesulfonate (3.1Ja): ^{1}H NMR (400 MHz, $CDCl_3$) δ 10.02 (s, 1H), 7.97 – 7.90 (m, 2H), 7.71 (dd, J = 6.7, 1.7 Hz, 1H), 5.40 (s, 2H), 3.13 (s, 3H). ^{13}C NMR (101 MHz, $CDCl_3$) δ 192.8, 154.7, 152.5, 138.4, 126.5, 121.6, 70.8, 38.1.

tert-Butyl 4-((6-formylpyridin-2-yl)methyl)piperazine-1-carboxylate (3.1K): ^{1}H NMR (400 MHz, CDCl3) δ 10.06 (s, 1H), 7.86 – 7.84 (m, 2H), 7.70 – 7.68 (m, 1H), 3.77 (s, 2H), 3.46 (t, J = 4.8 Hz, 4H), 2.48 (t, J = 4.8 Hz, 4H), 1.45 (s, 9H). ^{13}C NMR (101 MHz, CDCl3) δ 193.7, 159.6, 154.9, 152.5, 137.6, 127.5, 120.4, 79.8, 64.2, 53.2, 28.5.

tert-Butyl (E)-4-((6-(2-nitrovinyl)pyridin-2-yl)methyl)piperazine-1-carboxylate (3.1L): ^{1}H NMR (600 MHz, $CDCl_3$) δ 8.01 (d, J = 13.1 Hz, 1H), 7.91 (d, J = 13.1 Hz, 1H), 7.75 (t, J = 7.6 Hz, 1H), 7.55 (d, J = 7.8 Hz, 1H), 7.36 (d, J = 7.4 Hz, 1H), 3.69 (s, 2H), 3.45 (bs, 4H), 2.47 (bs, 4H), 1.44 (s, 9H). ^{13}C NMR (151 MHz, CDCl3) δ 159.8, 154.9, 148.7, 140.7, 137.7, 137.4, 125.4, 125.0, 79.9, 64.3, 53.1, 28.5.

tert-Butyl 4-((6-(2-nitroethyl)pyridin-2-yl)methyl)piperazine-1-carboxylate (3.1m): ^{1}H NMR (400 MHz, $CDCl_3$) δ 7.59 (t, J = 7.7 Hz, 1H), 7.29 (d, J = 7.7 Hz, 1H), 7.07 (d, J = 7.6 Hz, 1H), 4.86 (t, J = 6.7 Hz, 2H), 3.62 (s, 2H), 3.45-3.43 (m, 6H), 2.43 (bs, 4H), 1.45 (s, 9H). ^{13}C NMR (151 MHz, $CDCl_3$) δ 158.2, 155.2, 154.8, 137.3, 121.9, 121.7, 79.7, 73.9, 64.4, 53.0, 34.5, 28.5.

NMR data of intermediates for synthesis of 3.1m and 3.1n

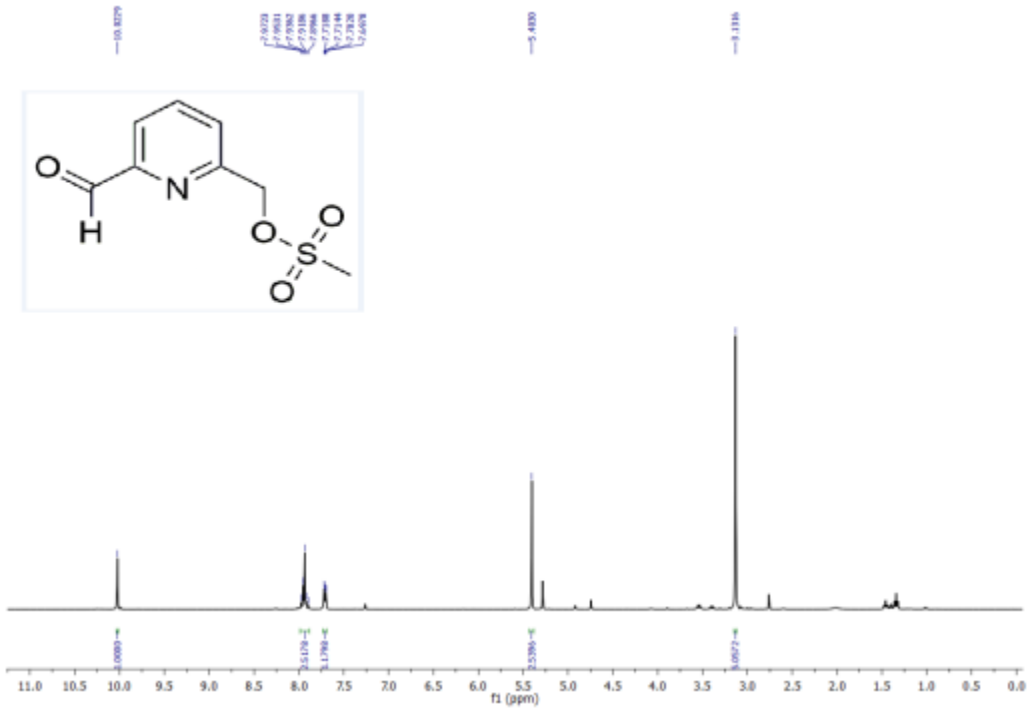

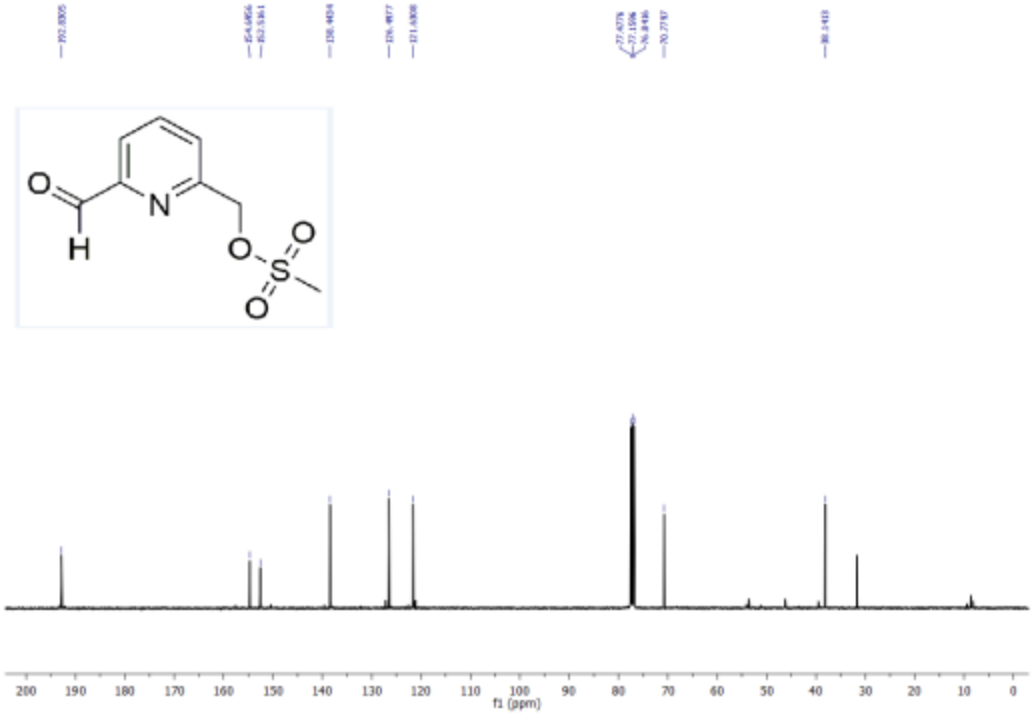
O
N
H
O
O
S
O
O
200 190 180 170 160 150 140 130 120 110 100 90 80 70 60 50 40 30 20 10 0
f1 (ppm)

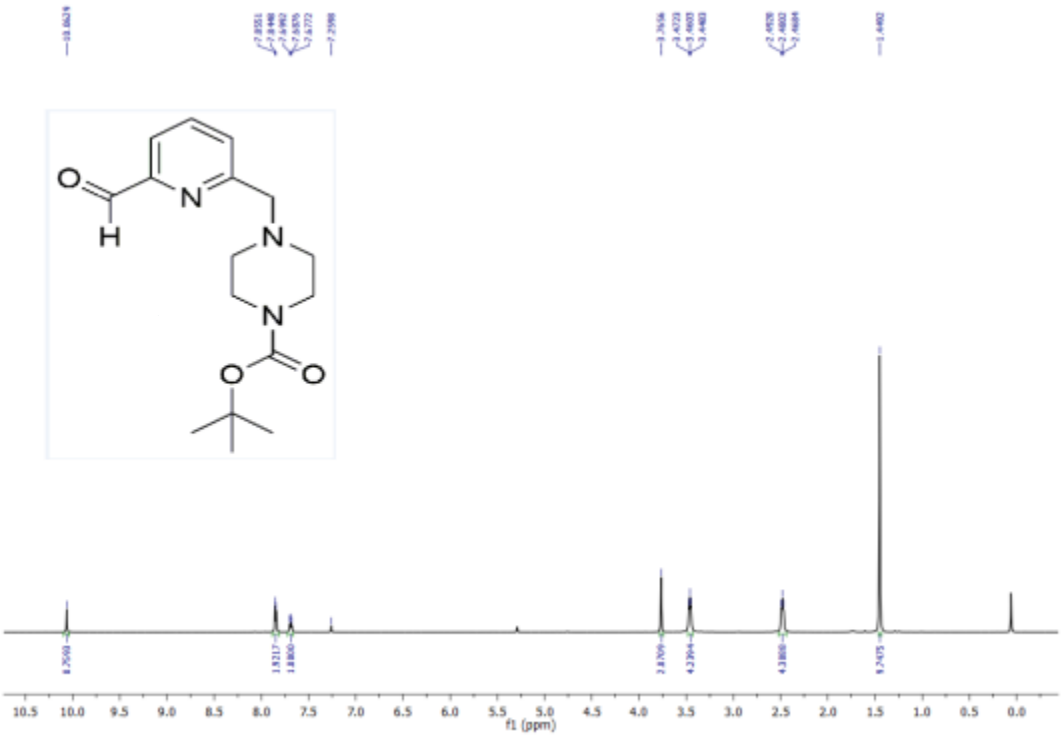
O
N
H
N
N
O
O
10.5 10.0 9.5 9.0 8.5 8.0 7.5 7.0 6.5 6.0 5.5 5.0 4.5 4.0 3.5 3.0 2.5 2.0 1.5 1.0 0.5 0.0
f1 (ppm)

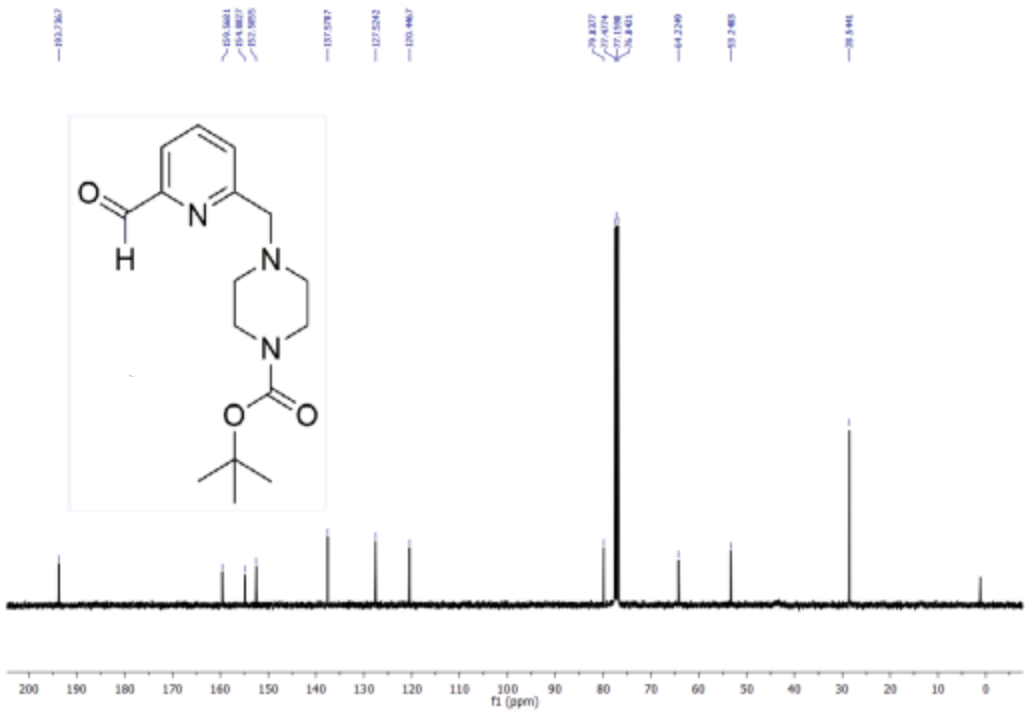
O
N
H
N
N
O
O
200 190 180 170 160 150 140 130 120 110 100 90 80 70 60 50 40 30 20 10 0
f1 (ppm)

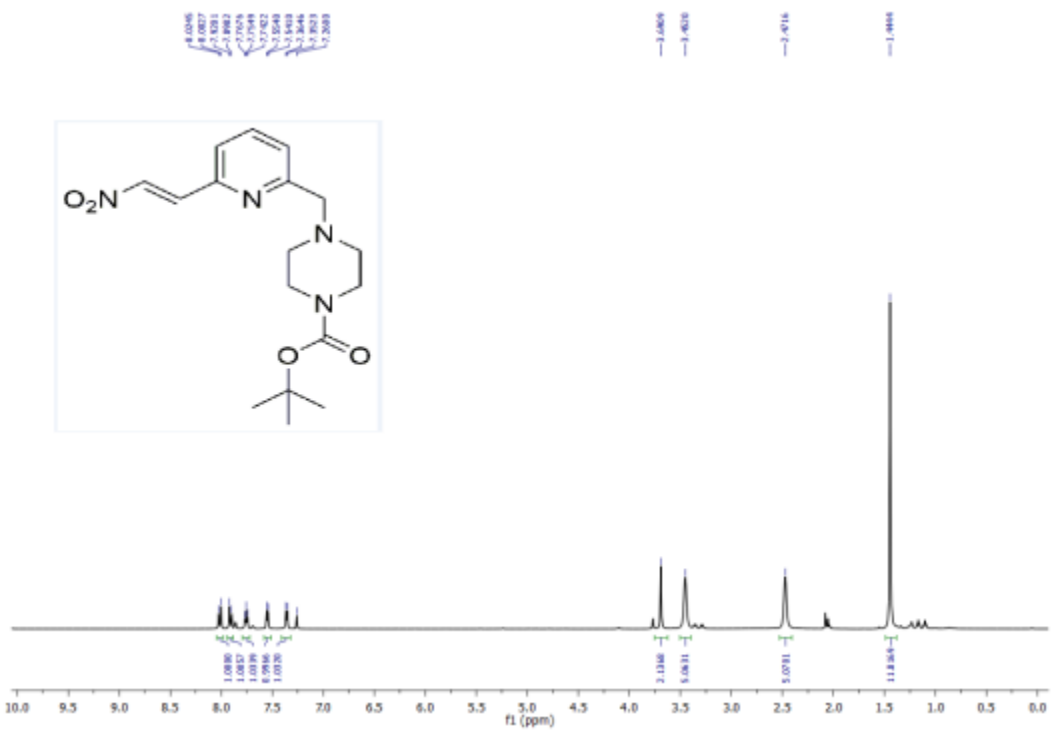
O2N
N
N
N
O
O
10.0 9.5 9.0 8.5 8.0 7.5 7.0 6.5 6.0 5.5 5.0 4.5 4.0 3.5 3.0 2.5 2.0 1.5 1.0 0.5 0.0
f1 (ppm)

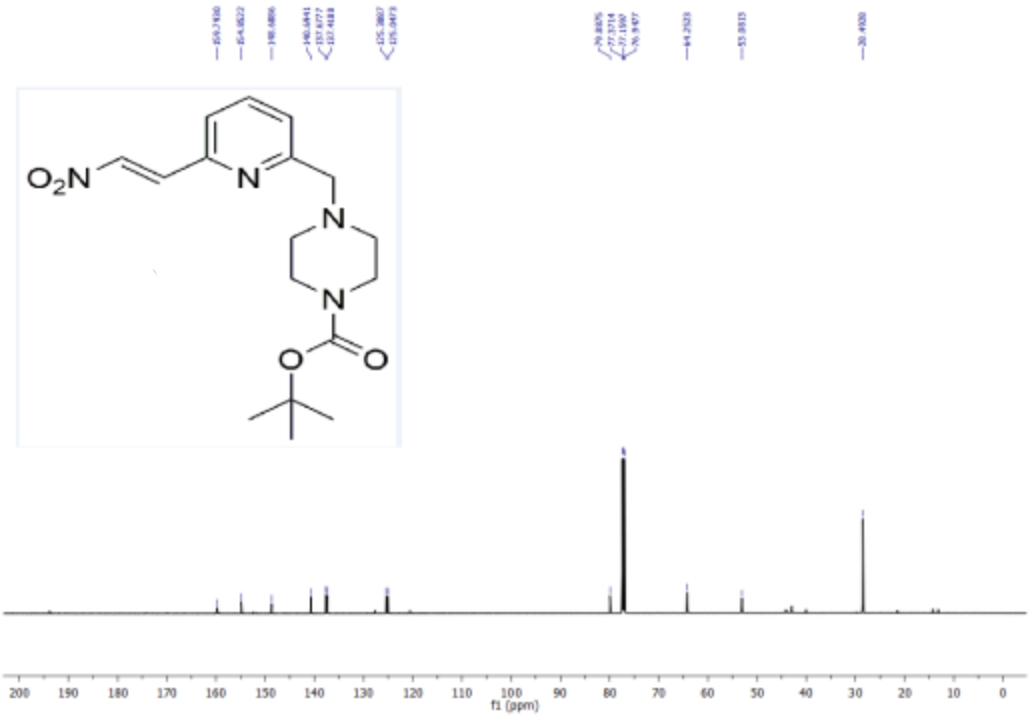

NMR spectra of 3.1m

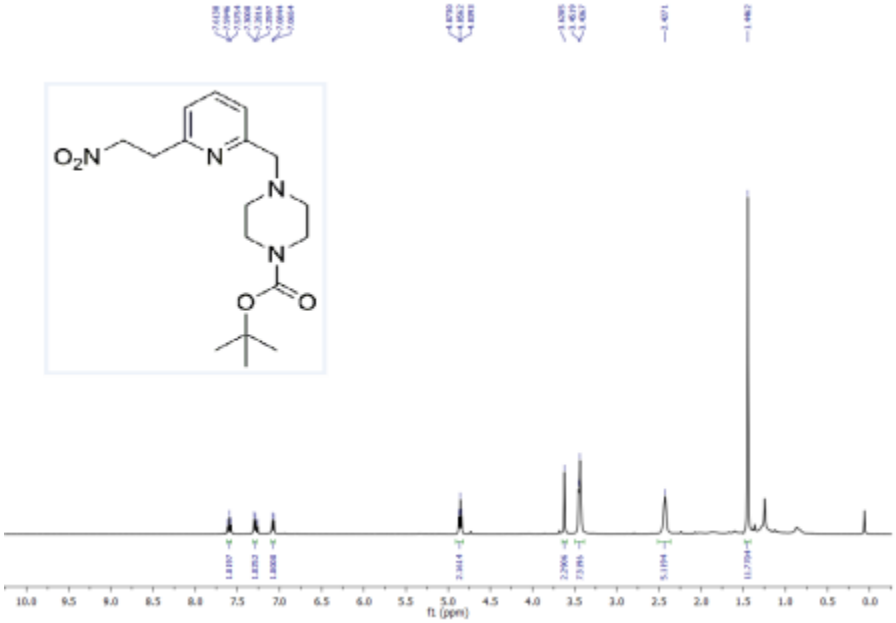

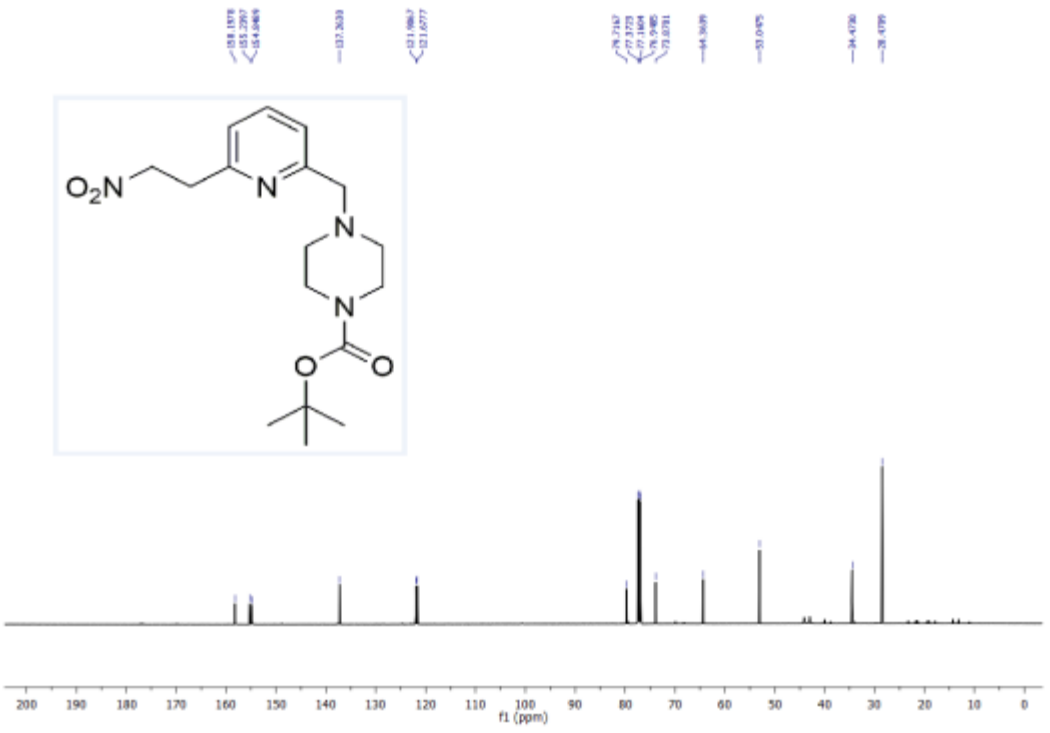
O2N
N
N
N
O
O
200
190
180
170
160
150
140
130
120
110
100
90
80
70
60
50
40
30
20
10
0
f1 (ppm)

HPLC and MS spectra of 3.1n

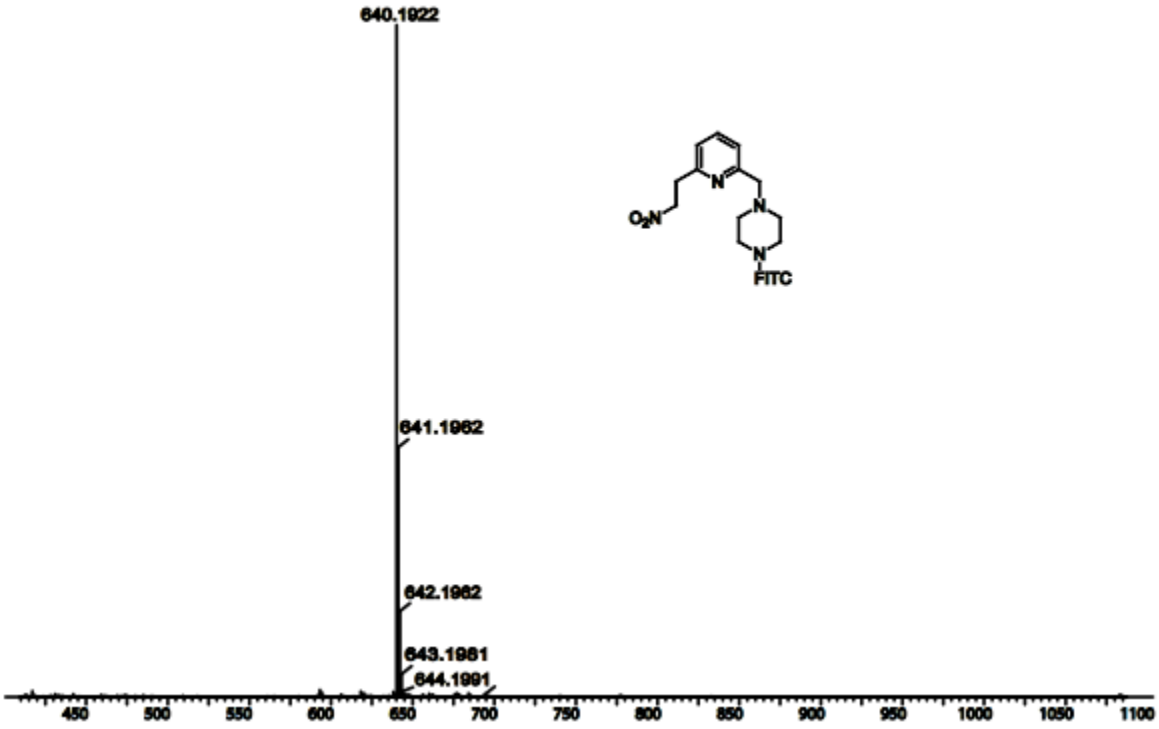

Synthesis of Ferrocenyl nitro derivative

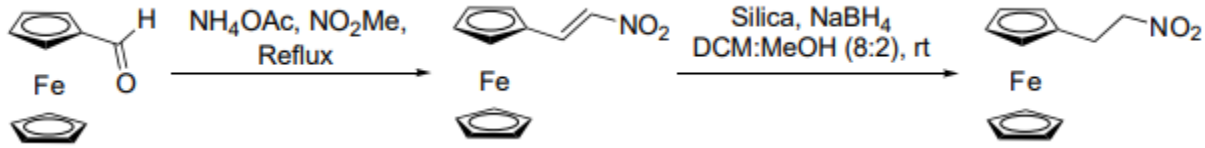

A solution of ferrocenecarboxaldehyde (1 mmol) and ammoniumacetate (0.25 eq.) in nitromethane was refluxed for 6 h. Nitromethane was removed under reduced pressure. Crude reaction mixture was extracted using ethylacetate and water followed by washing with brine. Combined organic layers were dried over Na_2SO_4, evaporated and crude was purified over silica gel using ethylacetate and hexane solvent mixture as an eluent to obtain ferrocene nitrostyrene derivative. To a vigorously stirred mixture of ferrocenenitrostyrene (0.7 mmol) in DCM and MeOH (8:2) was

added silica gel (100 mesh) at rt followed by addition of NaBH4 (4 eq.) portion wise. The reaction mixture stirred at rt until the complete consumption of ferrocenenitrostyrene was observed as indicated by TLC. The reaction mixture was quenched with 1N HCl and filtered. The silica was washed with DCM and the organic layer was separated and dried over Na_2SO_4. The combined organic layer was evaporated using rotary evaporator and crude was purified over silica gel using ethylacetate and hexane solvent mixture as an eluent to obtain pure 1o.

Ferrocenenitrostyrene intermediate. (2-Nitrovinyl-cyclopentadienyl)cyclopentadienyliron. Yield 69%. ^{1}H NMR (600 MHz, $CDCl_3$) δ 7.99 (d, J = 12.5 Hz, 1H), 7.27 (d, J = 12.3 Hz, 1H), 4.60 – 4.55 (m, 4H), 4.22 (s, 5H).

(2-Nitroethyl-cyclopentadienyl)cyclopentadienyliron (3.1o). Yield 56%. ^{1}H NMR (600 MHz, $CDCl_3$) δ 4.50 (t, J = 7.4 Hz, 2H), 4.18 – 4.10 (m, 9H), 3.06 (t, J = 7.4 Hz, 2H). ^{13}C NMR (151 MHz, $CDCl_3$) δ 82.5, 76.3, 68.8, 68.2, 68.1, 27.8.

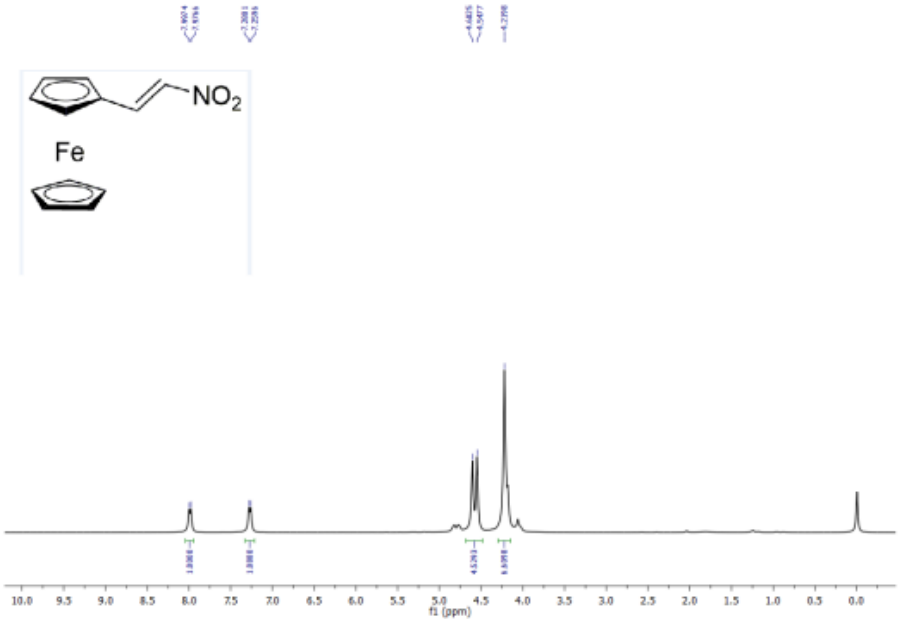

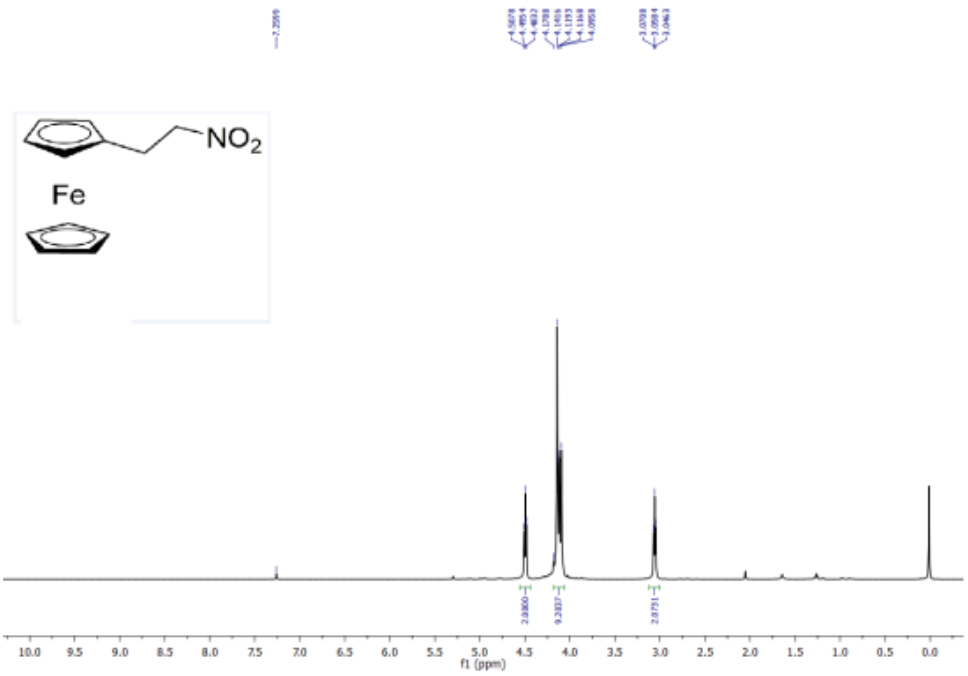
NO2
Fe
10.0 9.5 9.0 8.5 8.0 7.5 7.0 6.5 6.0 5.5 5.0 4.5 4.0 3.5 3.0 2.5 2.0 1.5 1.0 0.5 0.0
f1 (ppm)

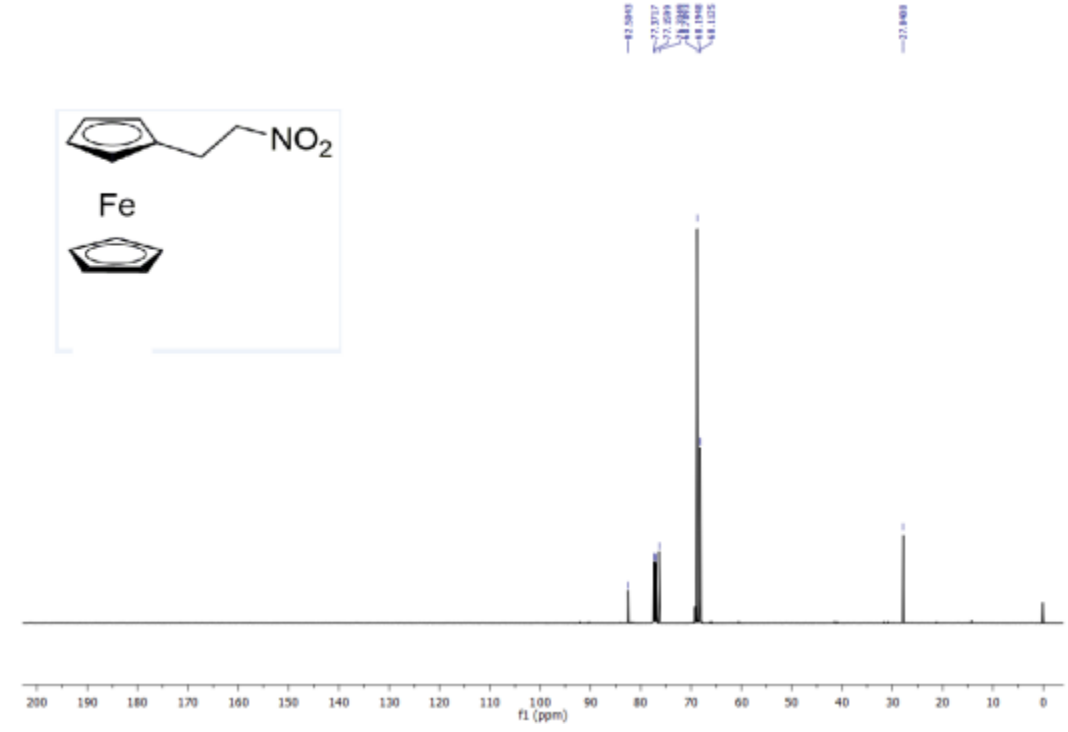
NO2
Fe
200 190 180 170 160 150 140 130 120 110 100 90 80 70 60 50 40 30 20 10 0
f1 (ppm)

Procedure for the kinetic studies for the synthesis of nitro-protein bioconjugate 3.6a by reaction of nitromethane 3.1a with myoglobin aldehyde 3.5.

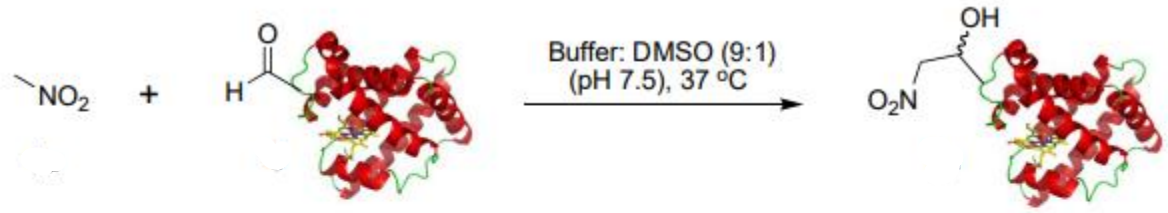

Time	% Conv.
30 min	65
60 min	80
120 min	95

To a solution of myoglobin aldehyde (**3.5**, 0.13 mM) in phosphate buffer (pH 7.5, 10 mM): DMSO (9:1) (0.44 mL) was added nitromethane (**3.1a**, 200 equiv.). The reaction mixture was incubated at 37 ^{o}C and monitored by injecting the sample in LCMS after regular intervals of time. % conversion to nitroprotein adduct **3.6a** was determined by comparing the intensity of LCMS peaks of starting myoglobin aldehyde **3.5** and nitro-protein adduct **3.6a**. The adduct **3.6a** was purified using molecular weight cut off and characterized by LCMS.

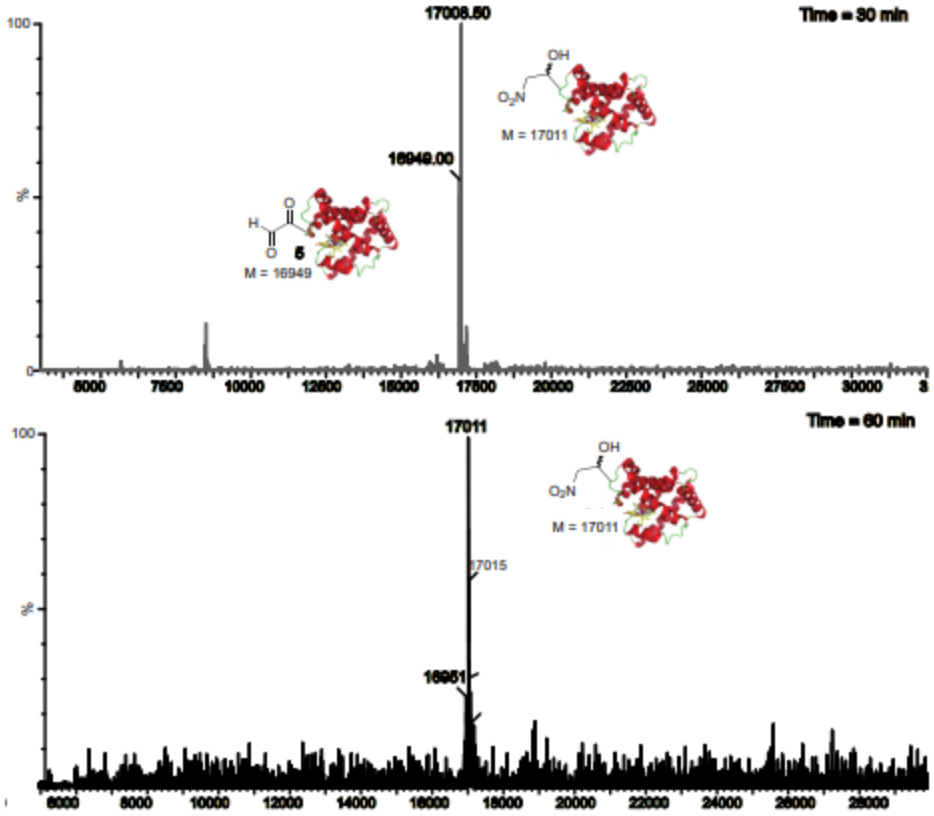

General procedure for the conjugation of nitro derivatives (3.1) on protein aldehydes (3.5).

To a solution of a protein aldehyde (**3.5**, 0.13 mM) in phosphate buffer (pH 7.5, 10 mM): DMSO (9:1) (0.44 mL) was added nitro derivative (**3.1**, 200 equiv.). The reaction mixture was incubated in shaker at 37 °C for 16 h and analyzed by LCMS. % conversion to nitro-protein bioconjugate **3.6** was determined by LCMS. The nitro-protein bioconjugates **3.6** were purified by molecular weight cut off or by HPLC and characterized by LCMS.

General procedure for the conjugation of biotin-nitro derivative 3.1f on myoglobin aldehyde 3.5.

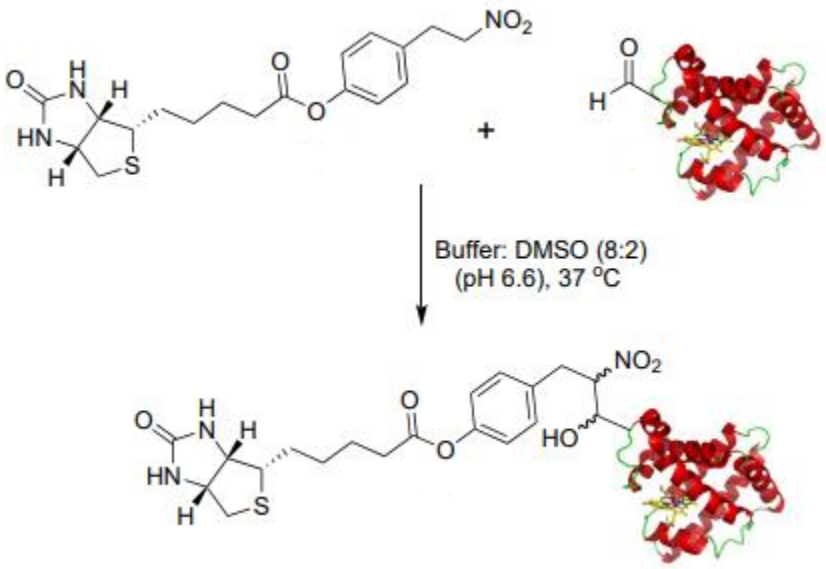

To a solution of protein aldehyde (**3.5**, 0.13 mM) in phosphate buffer (pH 6.6, 10 mM): DMSO (8:2) (0.5 mL) was added biotin-nitro derivative (**3.1f**, 200 equiv.). The high amounts of DMSO was added to solubilize the biotin-nitro derivative **3.1f**. Low pH (6.6) was used to increase the stability of the ester linkage of nitro-biotin derivative **3.1f**. The reaction mixture was incubated in shaker at 37 ^{o}C for 4 h and analyzed by LCMS. % conversion to nitro-protein bioconjugate 6f was determined by LCMS. The nitro-protein bioconjugates **3.6f** was purified by molecular weight cut off and characterized by LCMS.

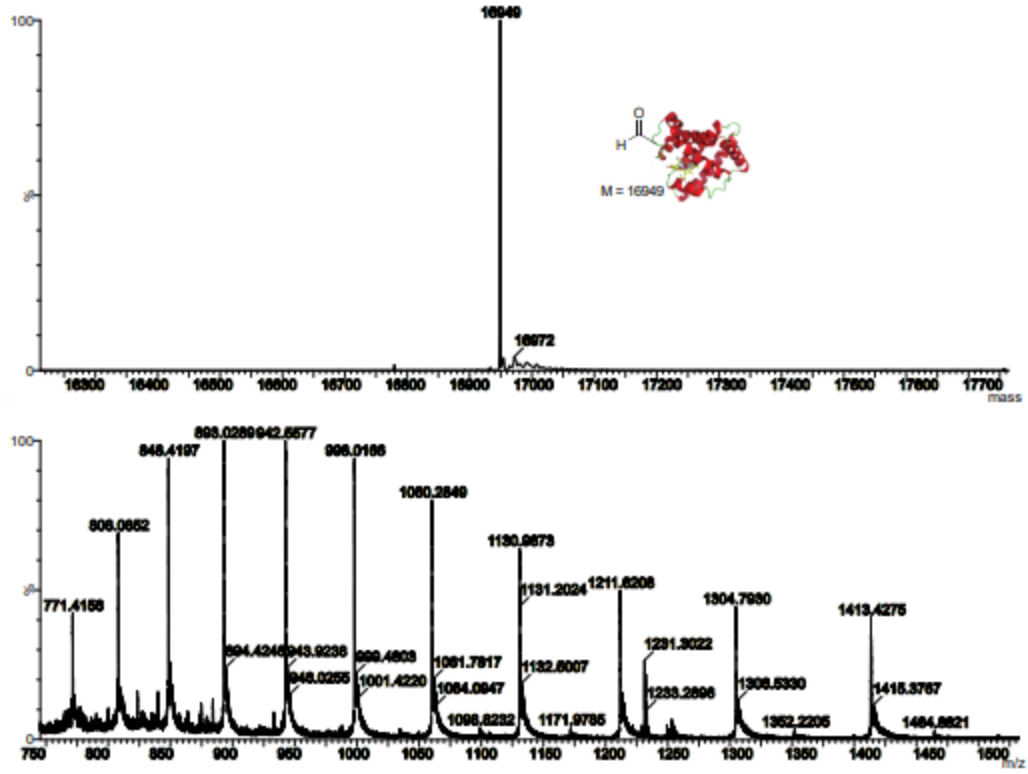
16949
16972
M = 16949
mass
848.4197
806.0652
771.4158
1130.9673
1131.2024
1211.6208
1304.7930
1413.4275
1231.3022
1233.2896
1308.5330
1415.3767
1352.2205
1484.8821
1171.9785
m/z

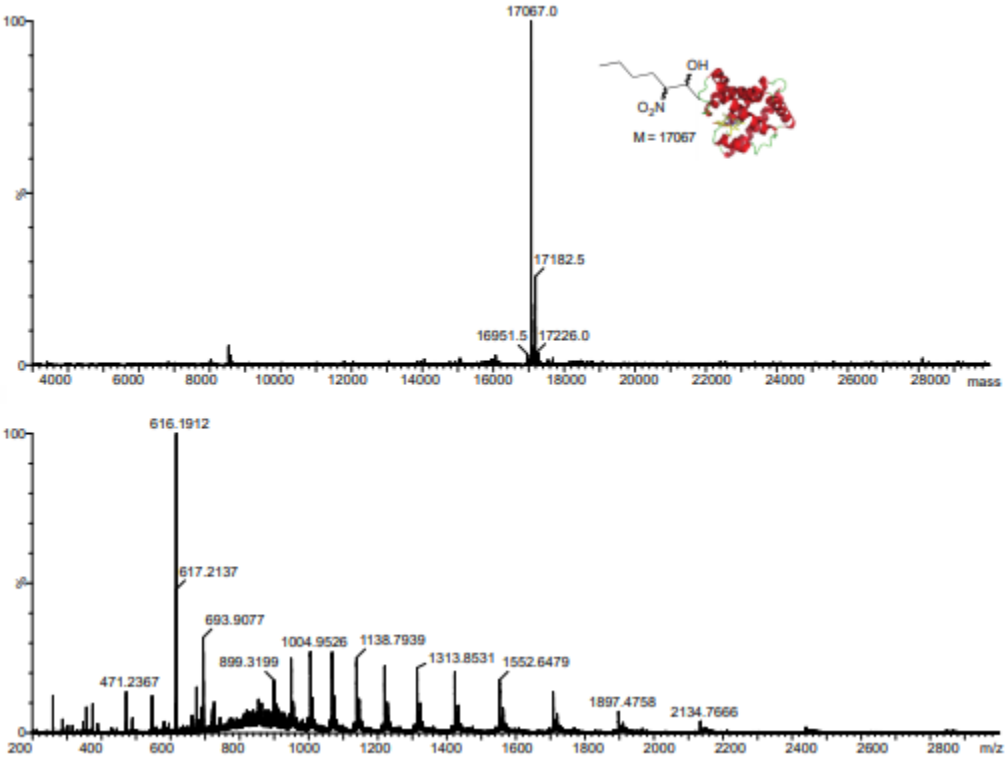
17067.0
17182.5
16951.5
17226.0
M = 17067
mass
616.1912
617.2137
693.9077
1004.9526
1138.7939
899.3199
1313.8531
1552.6479
471.2367
1897.4758
2134.7666
m/z

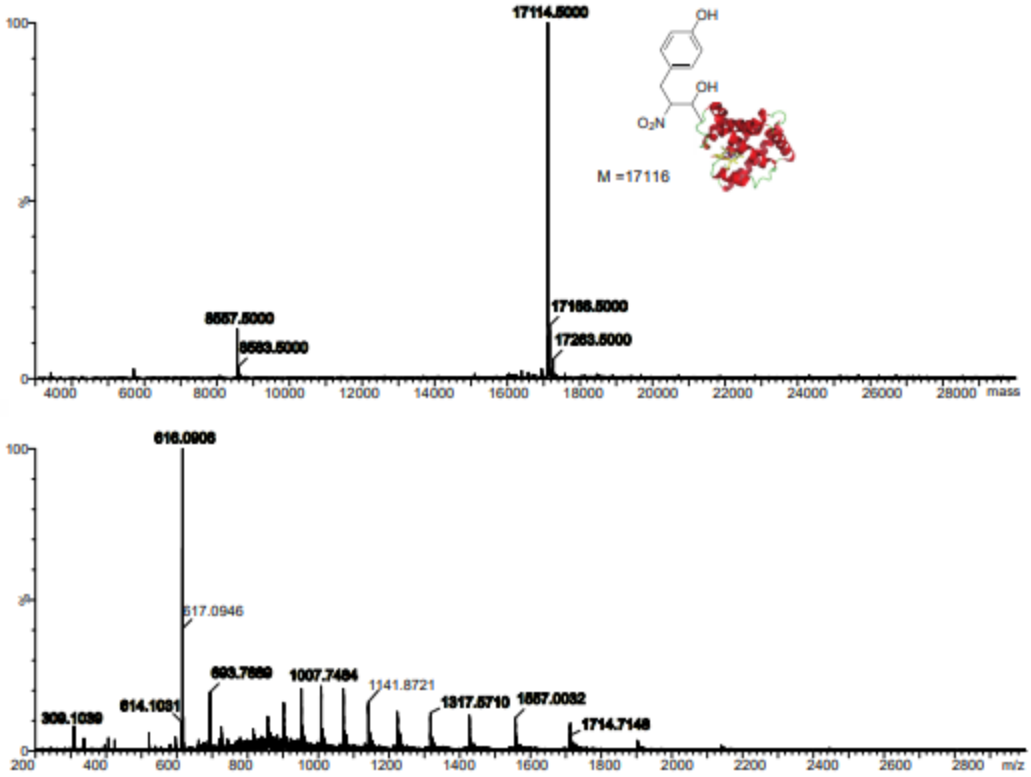
17114.5000
OH
OH
O2N
M =17116
8557.5000
8583.5000
17166.5000
17263.5000
mass
616.0906
617.0946
693.7689
1007.7484
1141.8721
614.1031
1317.5710
1557.0032
309.1039
1714.7148
m/z

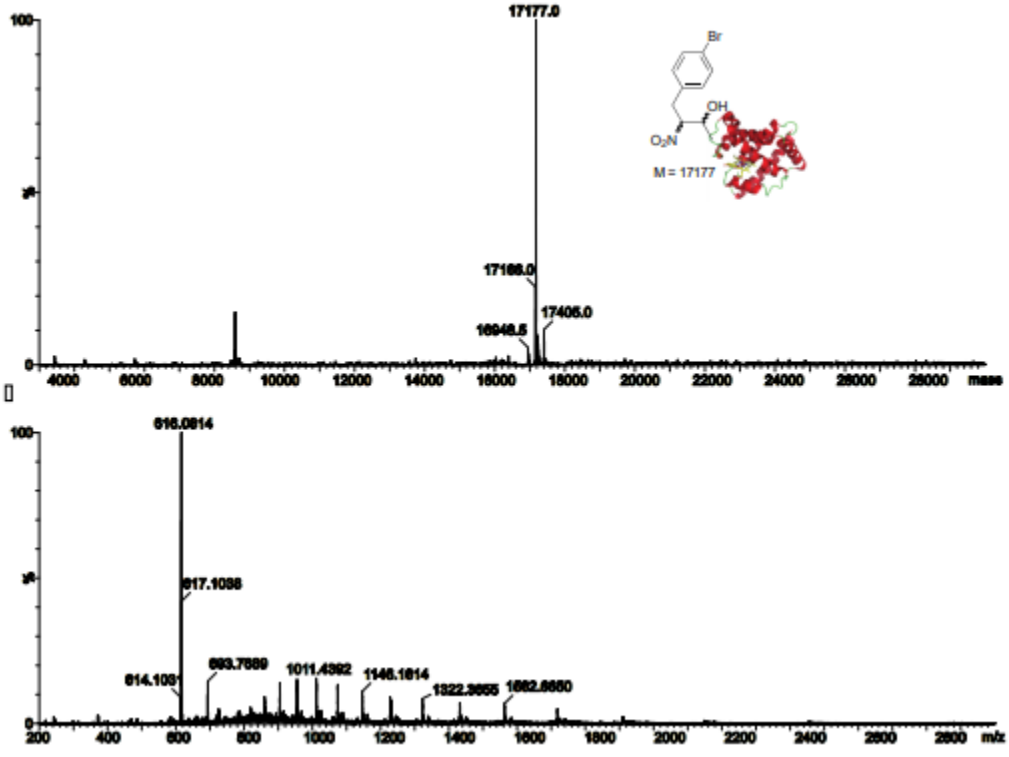
17177.0
Br
OH
O2N
M = 17177
17166.0
17405.0
16948.5
mass
616.0814
617.1038
693.7689
1011.4392
614.1031
1146.1614
1322.3655
1562.8660
m/z

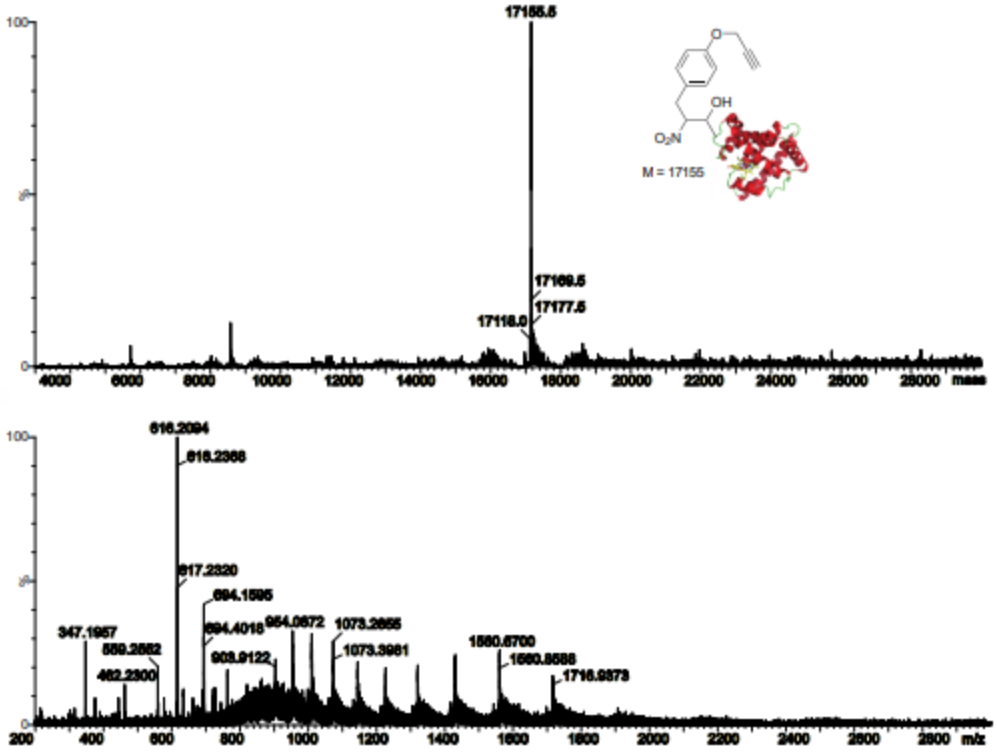
17155.5
17169.5
17177.5
17116.0
M = 17155
mass
616.2094
616.2366
617.2320
694.1595
347.1957
559.2552
462.2300
694.4018
954.0872
1073.2655
903.9122
1073.3981
1580.6700
1580.8588
1716.9873
m/z

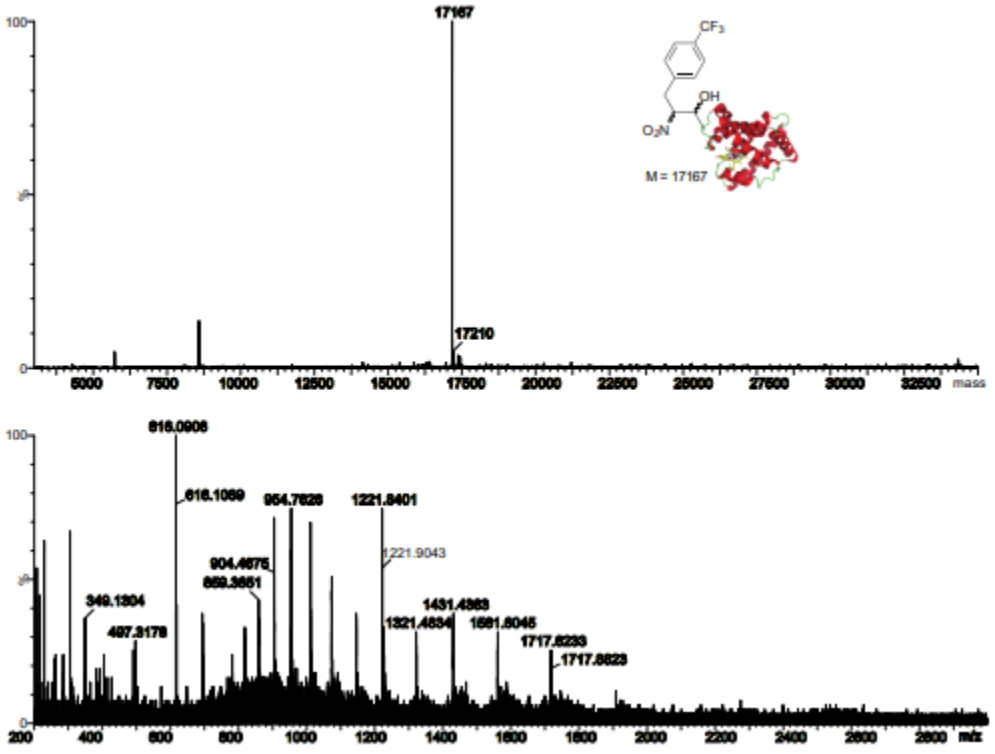
17167
17210
M = 17167
mass
616.0906
616.1069
954.7628
1221.8401
1221.9043
904.4875
859.3651
349.1304
497.3178
1431.4563
1321.4834
1581.6045
1717.6233
1717.6823
m/z

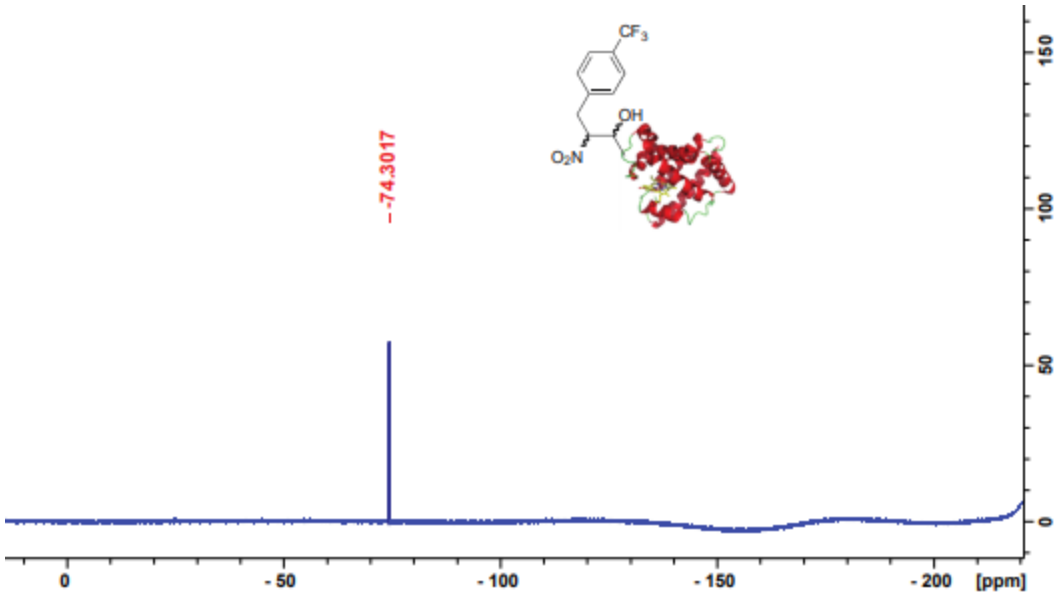
-74.3017
CF3
OH
O2N
150
100
50
0
0
- 50
- 100
- 150
- 200
[ppm]

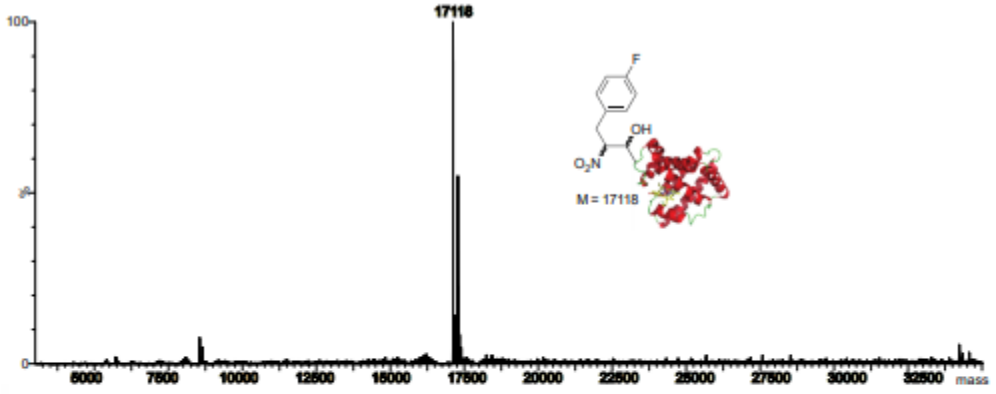
17118
F
OH
O2N
M = 17118
100
%
0
6000
7500
10000
12500
15000
17500
20000
22500
25000
27500
30000
32500
mass

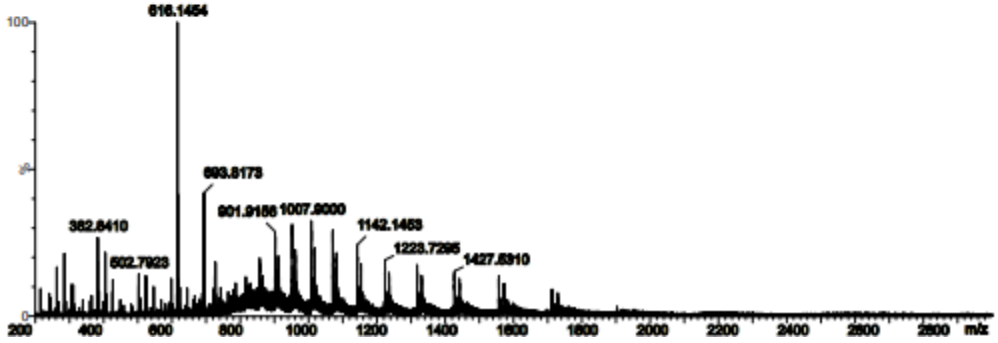
616.1454
693.8173
382.8410
602.7923
901.9186
1007.9000
1142.1463
1223.7295
1427.8310
100
%
0
200
400
600
800
1000
1200
1400
1600
1800
2000
2200
2400
2600
2800
m/z

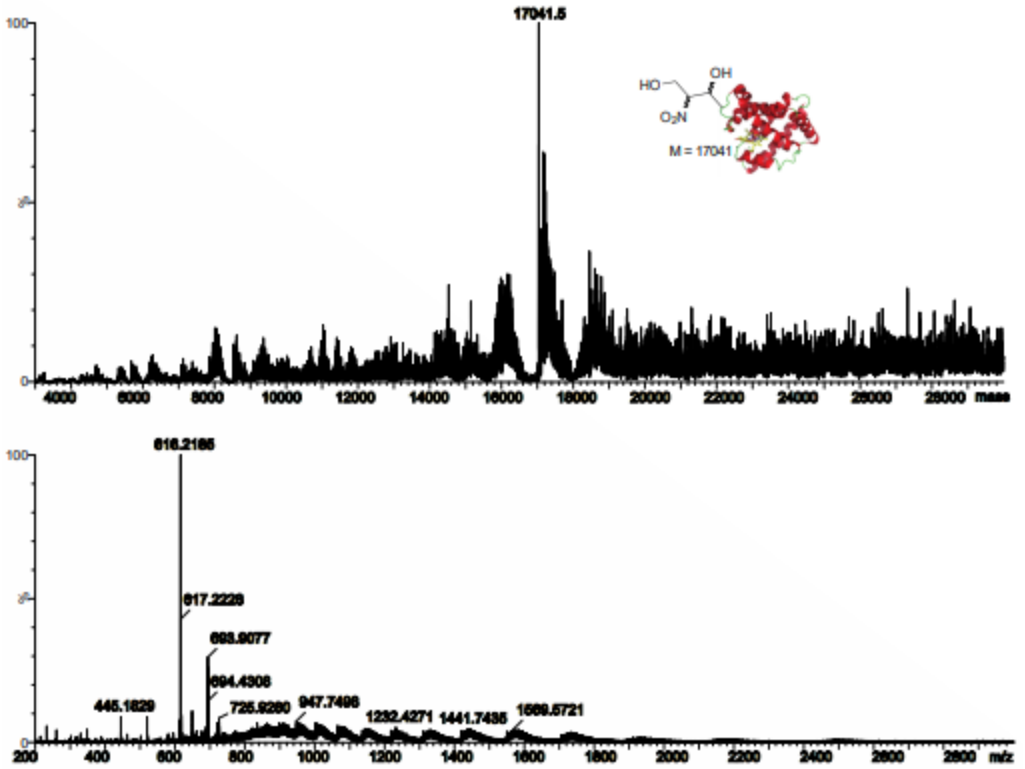
17041.5
HO
OH
O2N
M = 17041
100
%
0
4000
6000
8000
10000
12000
14000
16000
18000
20000
22000
24000
26000
28000
mass
616.2186
617.2228
693.9077
694.4308
445.1629
726.9280
947.7496
1232.4271
1441.7436
1569.5721
200
400
600
800
1000
1200
1400
1600
1800
2000
2200
2400
2600
2800
m/z

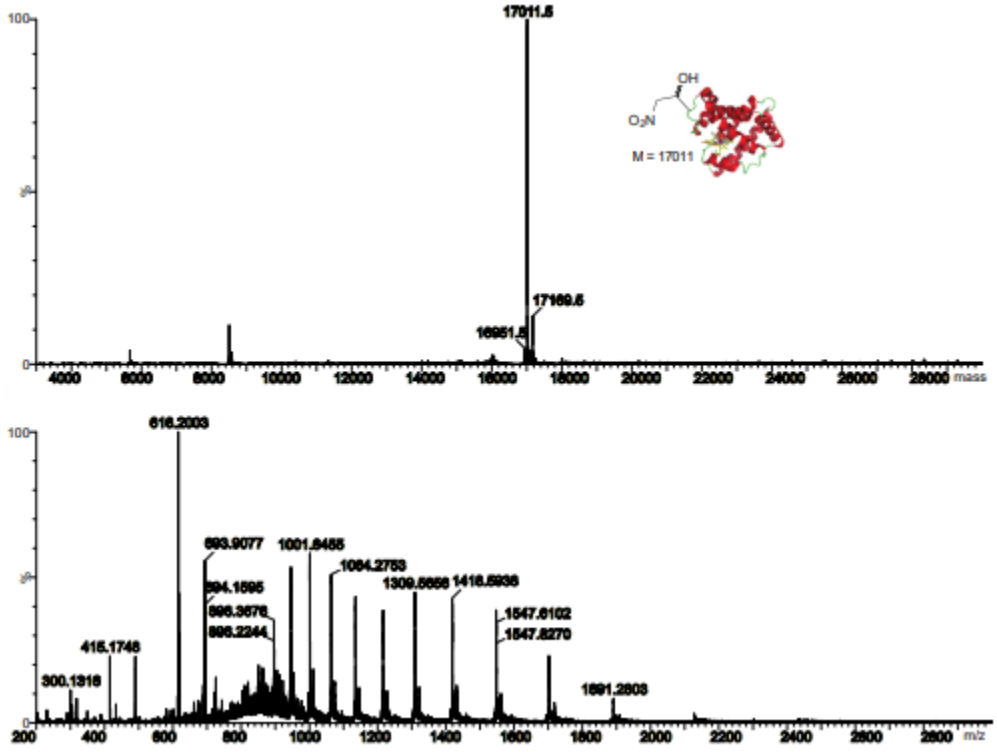
17011.5
OH
O2N
M = 17011
100
%
0
17169.6
16951.5
4000
6000
8000
10000
12000
14000
16000
18000
20000
22000
24000
26000
28000
mass
616.2003
693.9077
1001.8455
1084.2753
1309.6668
1416.6936
694.1595
696.3678
696.2344
1547.6102
1547.8279
415.1746
300.1318
1691.2803
200
400
600
800
1000
1200
1400
1600
1800
2000
2200
2400
2600
2800
m/z

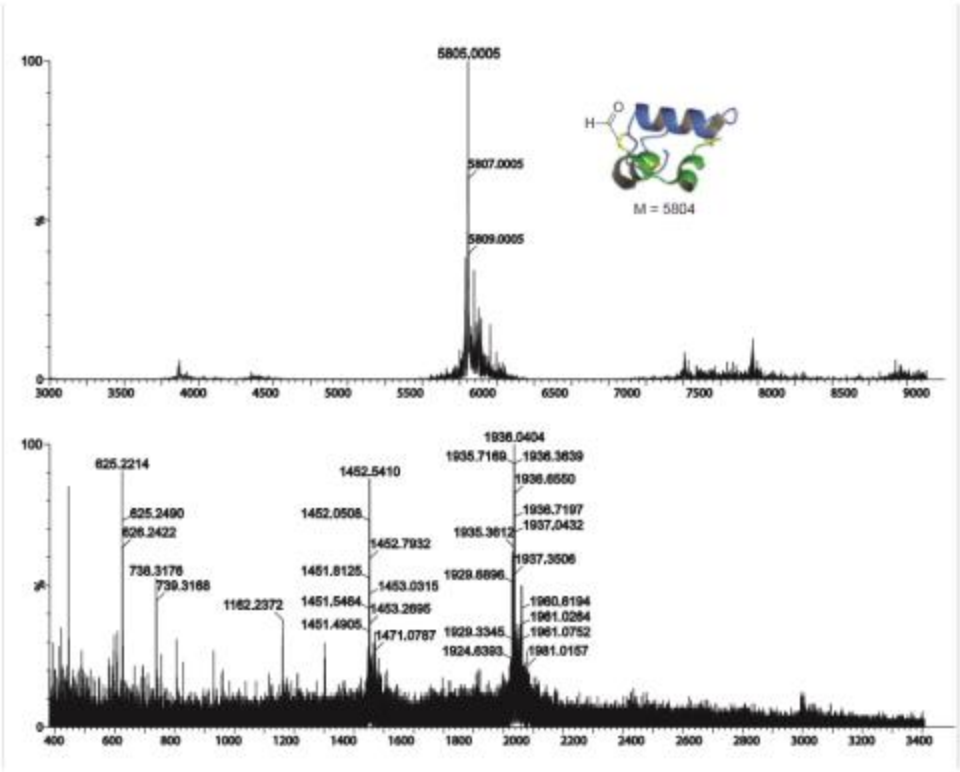
5805.0005
5807.0005
5809.0005
M = 5804
625.2214
625.2490
626.2422
738.3176
739.3188
1162.2372
1452.5410
1452.0508
1452.7932
1451.8125
1453.0315
1451.5464
1453.2696
1451.4905
1471.0787
1936.0404
1935.7169
1936.3639
1936.6550
1936.7197
1937.0432
1935.3612
1937.3506
1929.6896
1960.8194
1961.0264
1961.0752
1929.3345
1924.6393
1981.0157

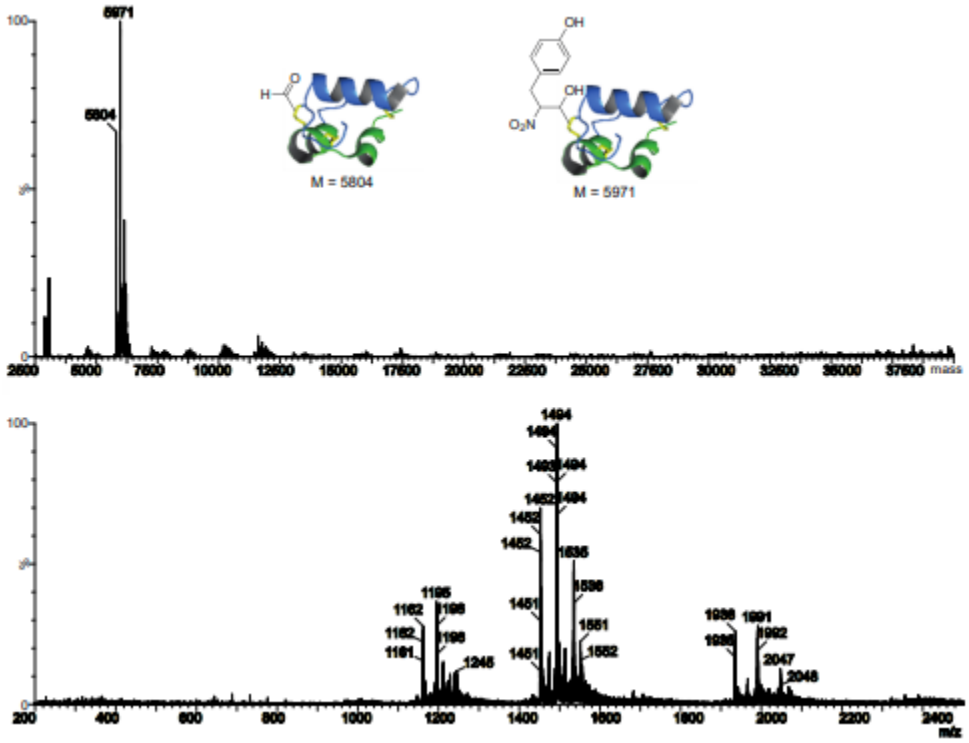
5971
5804
M = 5804
M = 5971
mass
m/z

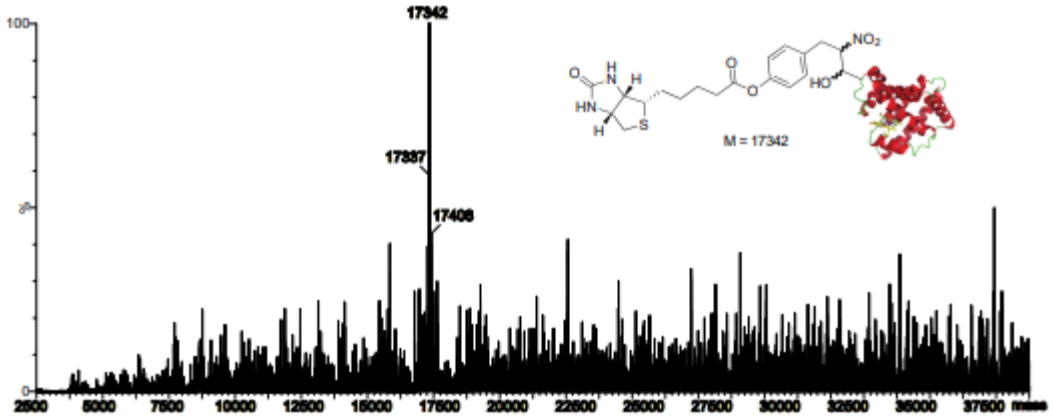
17342
17337
17408
M = 17342
mass

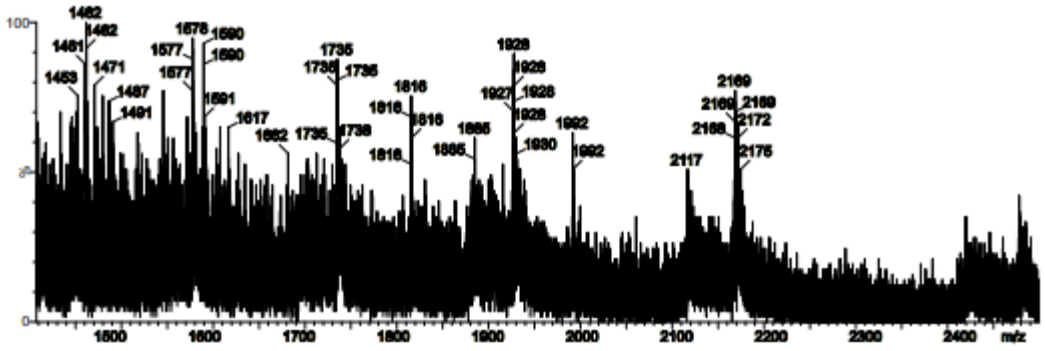
m/z

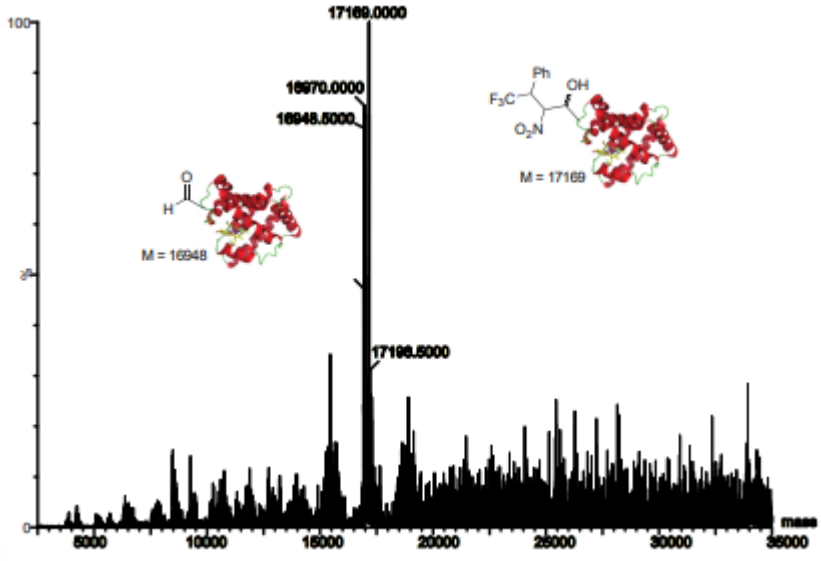
17169.0000
16970.0000
16948.5000
17196.5000
M = 16948
M = 17169
mass

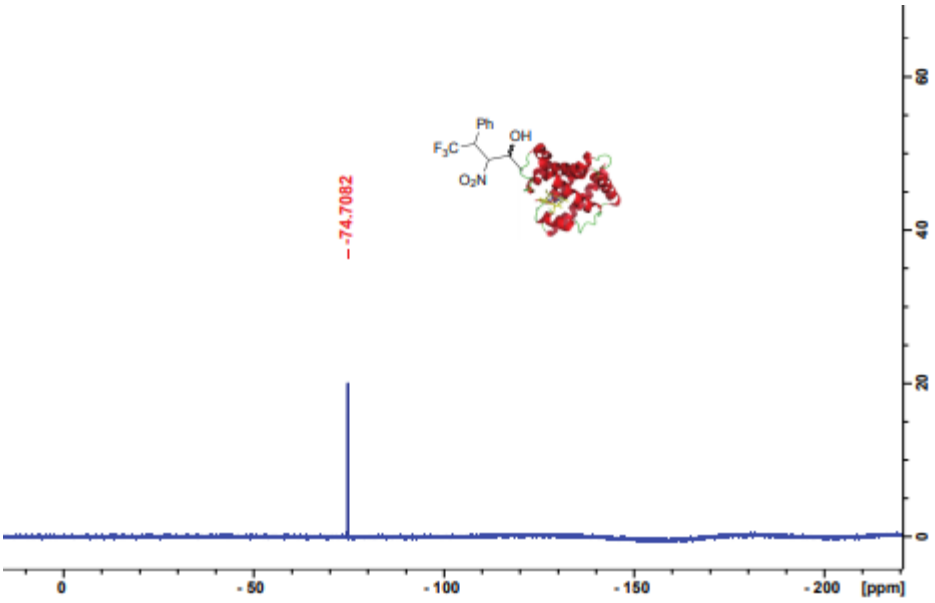
Ph
OH
F3C
O2N
-74.7082
60
40
20
0
0
-50
-100
-150
-200
[ppm]

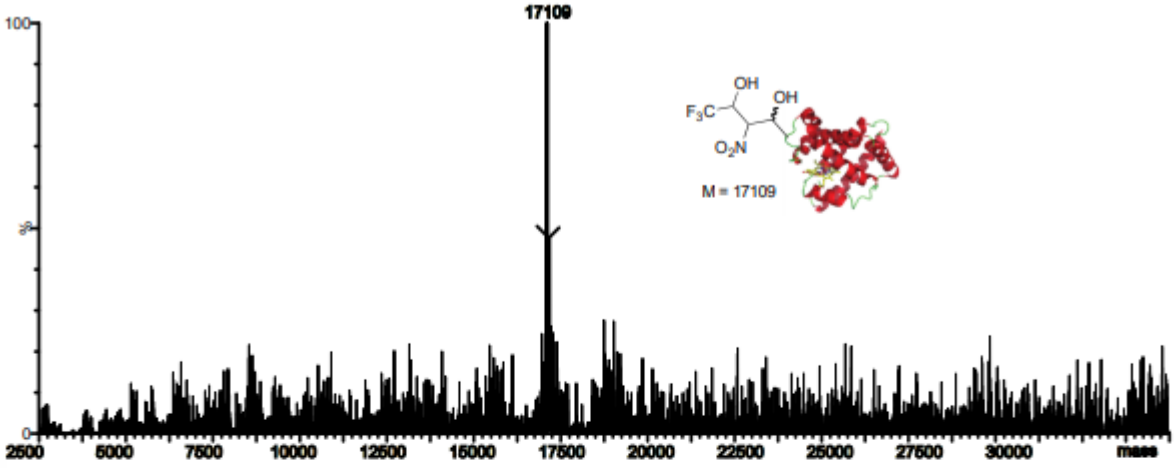
17109
100
%
0
2500
5000
7500
10000
12500
15000
17500
20000
22500
25000
27500
30000
mass
OH
OH
F3C
O2N
M = 17109

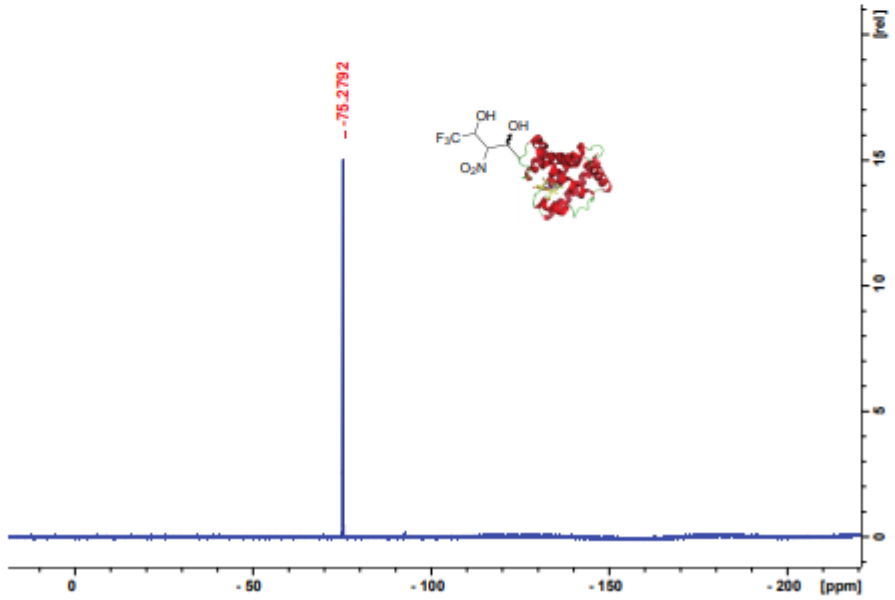
-75.2792
OH
OH
F3C
O2N
[rel]
15
10
5
0
0
- 50
- 100
- 150
- 200
[ppm]

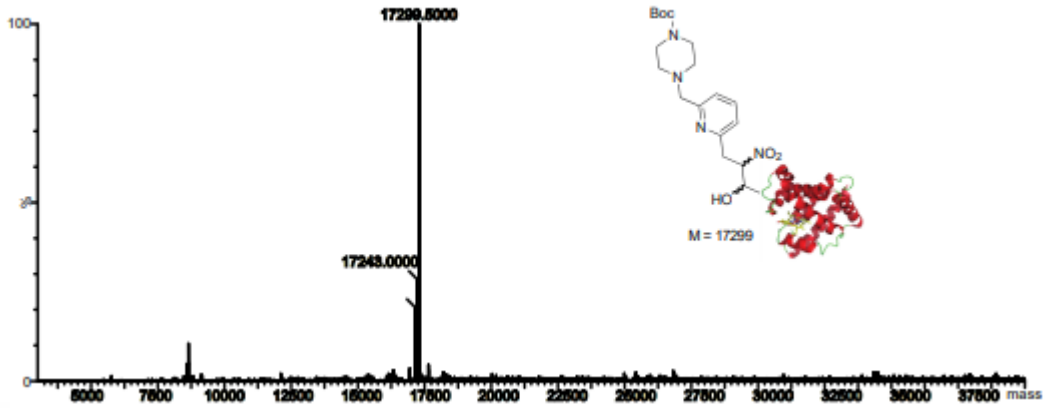
17299.5000
17243.0000
100
%
0
5000
7500
10000
12500
15000
17500
20000
22500
25000
27500
30000
32500
35000
37500
mass
Boc
N
N
N
NO2
HO
M = 17299

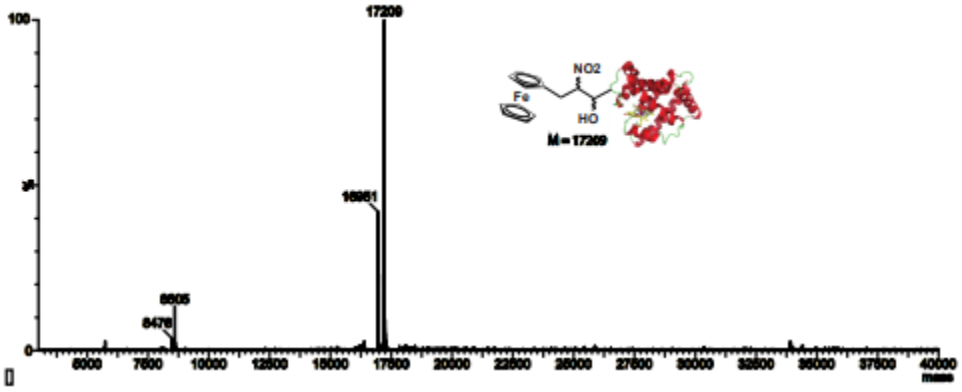

Low equivalents reactions with proteins. Procedure for reaction of nitro derivative **3.1** with myoglobin aldehyde **3.5**. To a solution of myoglobin aldehyde (**3.5,** 0.13 mM) in phosphate buffer (pH 7.5, 10 mM): DMSO (9:1) (0.44 mL) was added nitroderivative (**3.1**, 5 equiv.). The reaction mixture was incubated in shaker at 37 ^{o}C for 12-16 h. The reaction mixture was purified by molecular weight cut off and analyzed by LCMS.

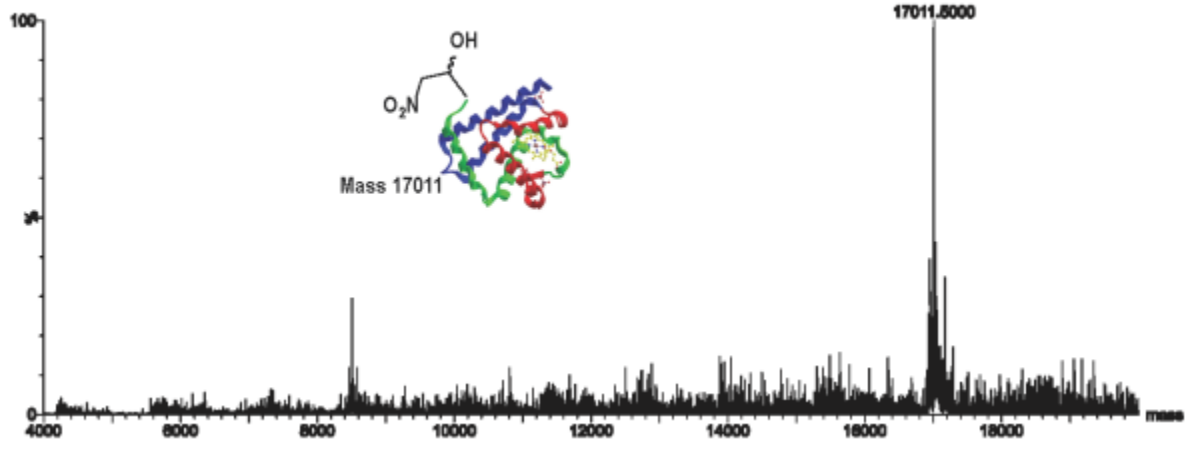

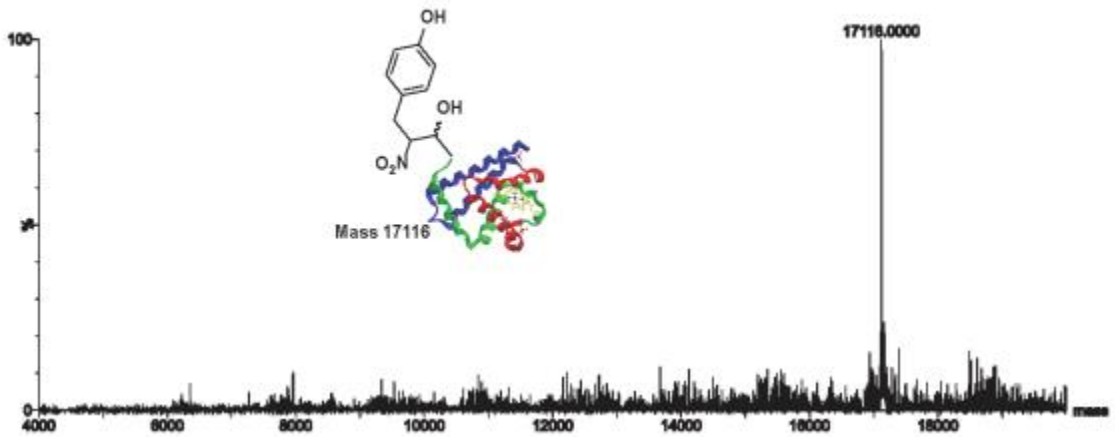

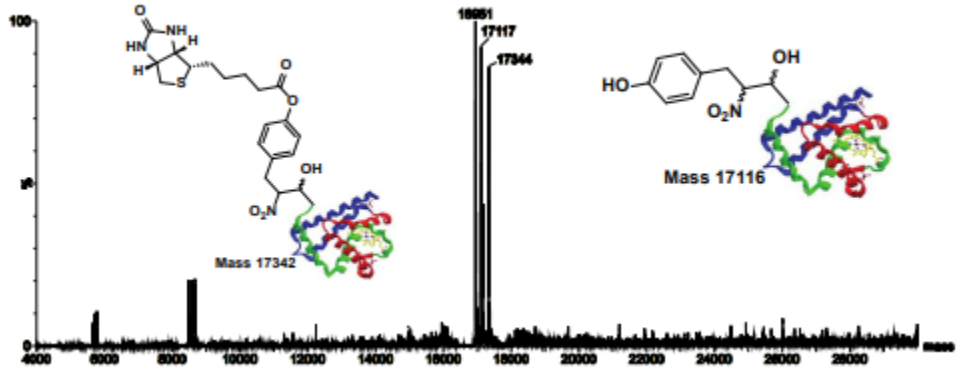

UV data of nitro-ferrocene derivative, myoglobin and ferrocene-myoglobin conjugate.

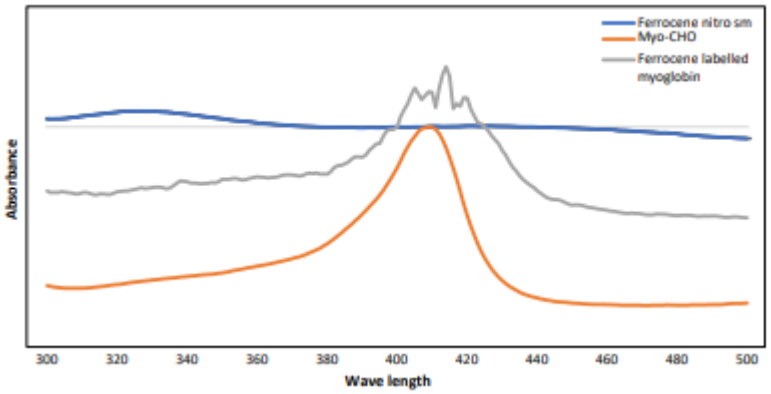

Control reactions with proteins.

Reaction of dye-nitro derivative 3.1n with myoglobin.

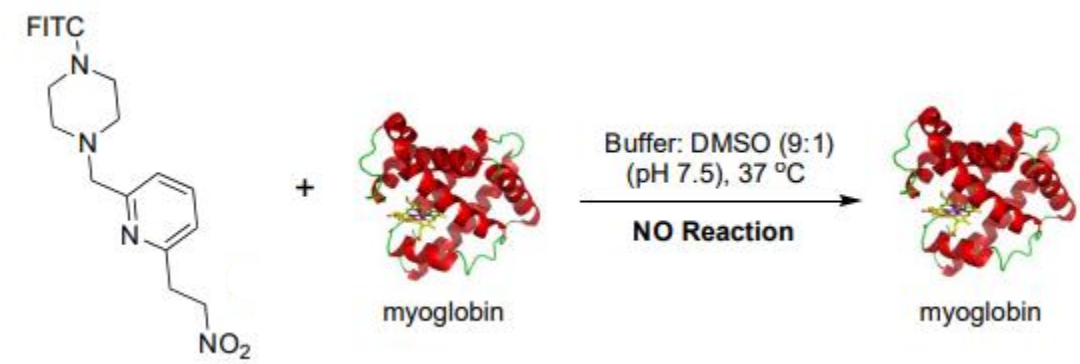

To a solution of myoglobin (0.13 mM) in phosphate buffer (pH 7.5, 10 mM): DMSO (9:1) (0.44 mL) was added nitroderivative (**3.1n**, 200 equiv.). The reaction mixture was incubated in shaker at 37 °C for 16 h. The reaction mixture was purified by molecular weight cut off and analyzed by LCMS. The formation of any nitro-protein bioconjugate was not observed. This showed high chemoselectivity of nitro derivatives for aldehydes.

Reaction of nitroalkanes with a protein ketone.

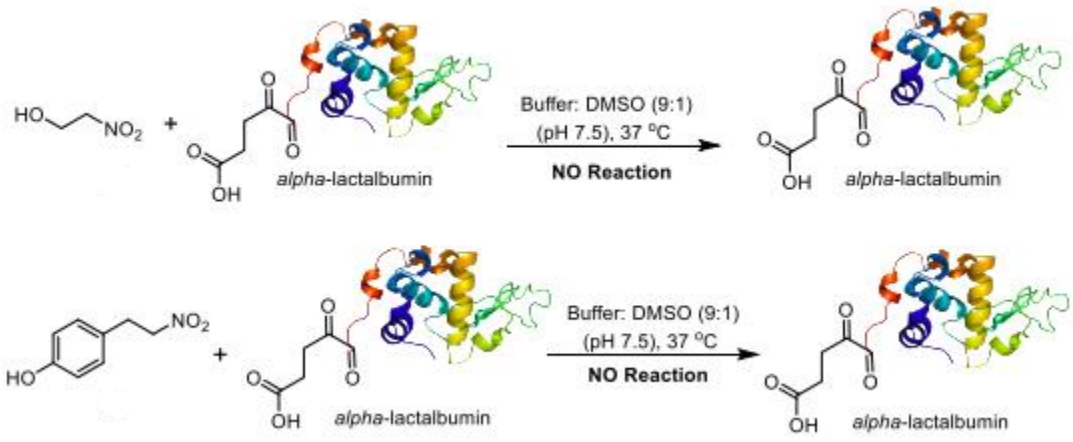

To a solution of alpha-lactalbumin ketone (0.13 mM) in phosphate buffer (pH 7.5, 50 mM): DMSO (9:1) (0.44 mL) was added nitro derivatives (**3.1b** and **3.1c**, 200 equiv.). The reaction mixtures

were incubated in shaker at 37 ^{o}C for 16 h. The reaction mixtures were purified by molecular weight cut off and characterized by LCMS. The formation of any nitro-protein bioconjugates were not observed. This showed high chemoselectivity of nitro derivatives for aldehydes.

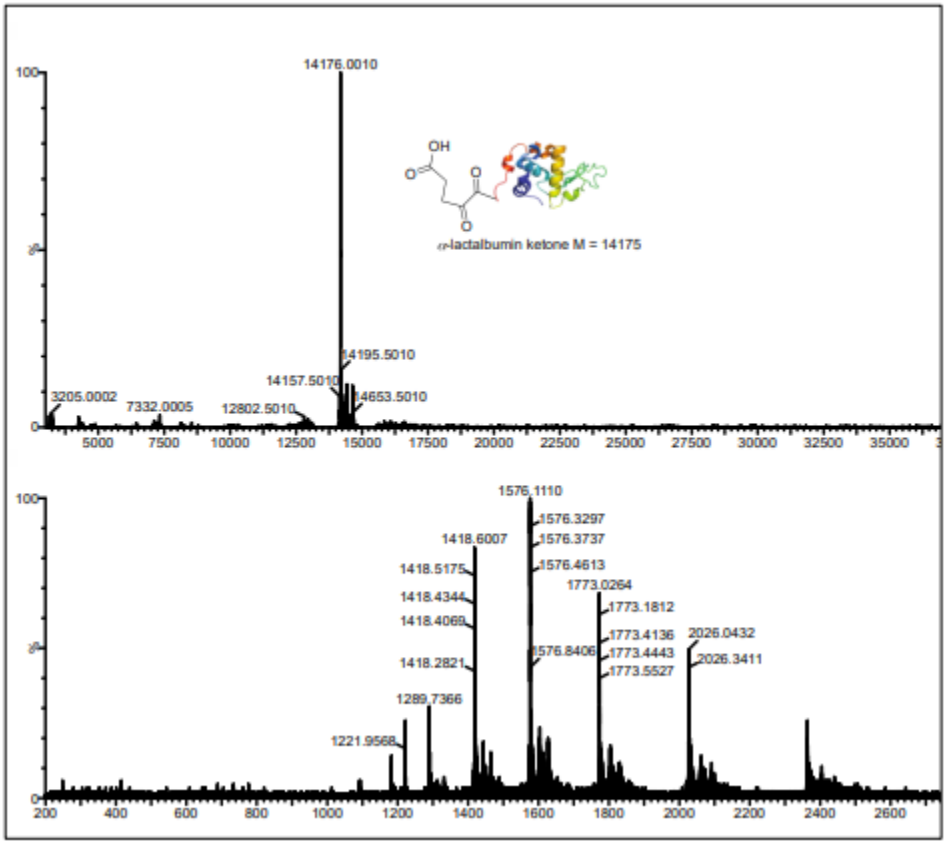

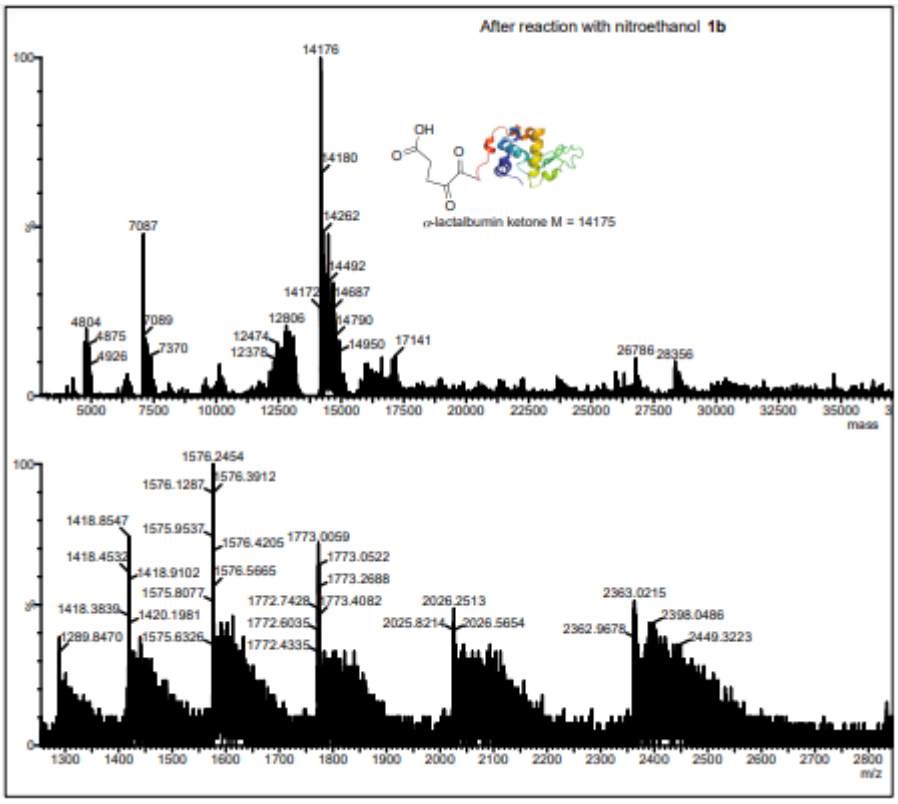
After reaction with nitroethanol 1b
α-lactalbumin ketone M = 14175
mass
m/z

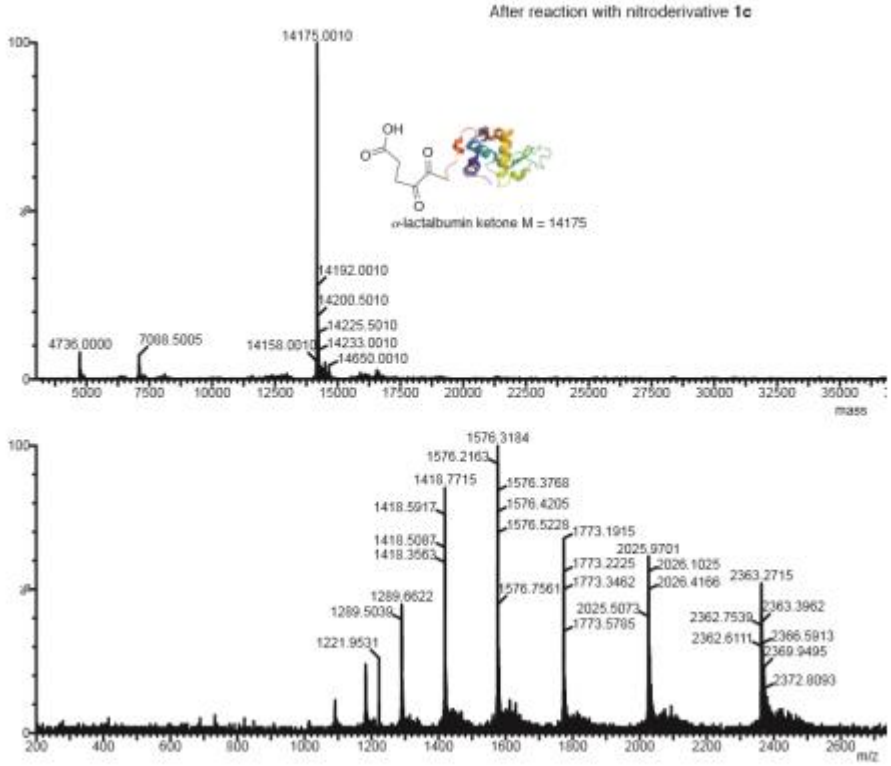
After reaction with nitroderivative 1c
α-lactalbumin ketone M = 14175
mass
m/z

Bromine characterization of Nitro-protein bioconjugate.

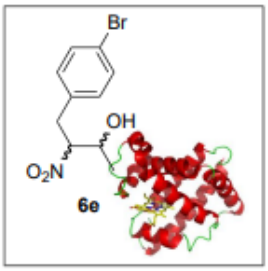

Bromo derivatives of nitroalkanes were synthesized for easy characterization of modified proteins since bromine atom gives a unique signature in a mass spectrometer. Notably, the presence of a bromine atom on the labeled residue would enable rapid detection of the exogenous adduct through inspection of the MS isotopic distribution of the peptide. To confirm our hypothesis, bromo-nitro-myoglobin was synthesized and was then analyzed using LC-MS. The LCMS data corresponding to the two expected adducts 17177 (bearing ^{79}Br) and 17179 (bearing ^{81}Br) were identified. The 0.1 to 0.2 mass difference peaks are matching for the deconvolution of 17177 and 17179.

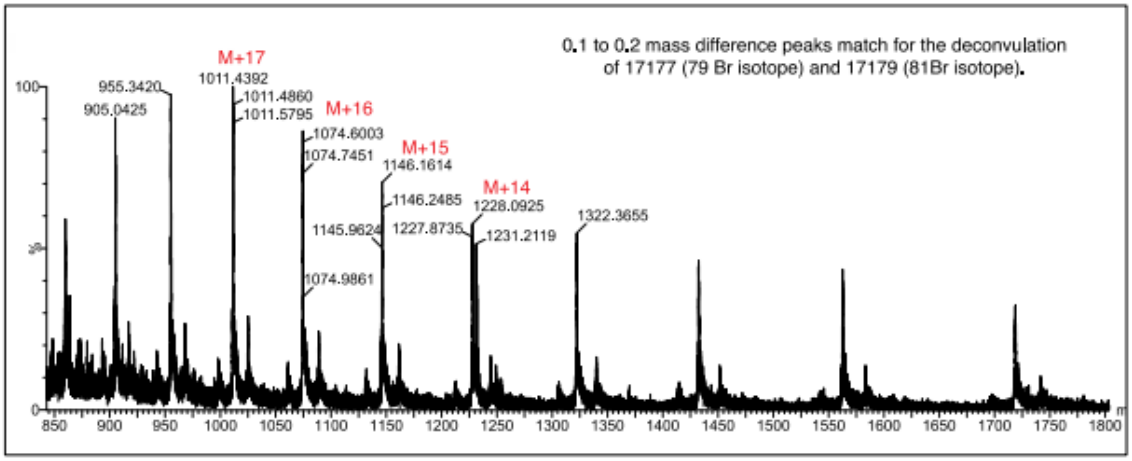

Characterization of dye-nitro-functionalized myoglobin.

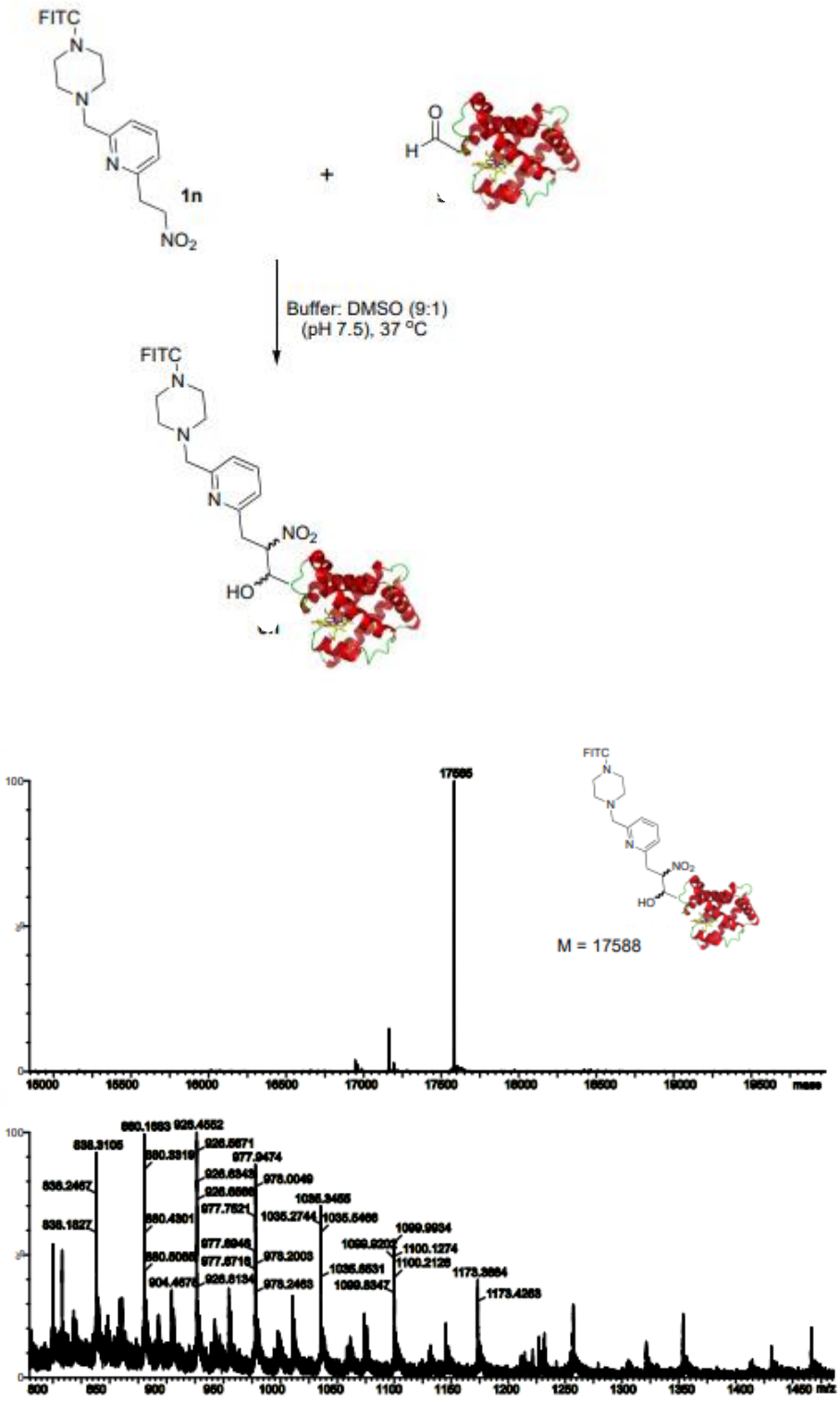

MS/MS studies of nitro-protein conjugate with nitroalkyl group for fingerprinting pattern.

Protein digestion. To a mixture of 4 mg of protein conjugate, dissolved in 400 uL of Tris urea buffer [pH = 7.8, 6M Urea and 0.1 M Tris], was added 400 uL of tBuOH and the reaction mixture was shaken for 3 h at 37 ^{o}C. Reaction mass diluted 10 times with water. 50 ul of 1millimolar HCl, 50 ul of 0.1 M tris buffer [pH = 7], 50ul of 0.01M CaCl2, enzyme (1:20 ratio of protein) was added to reaction mass and stirred at 37 ^{o}C for 18 h. Reaction mixture freezed at -78 ^{o}C and lyophilized to remove volatiles completely.

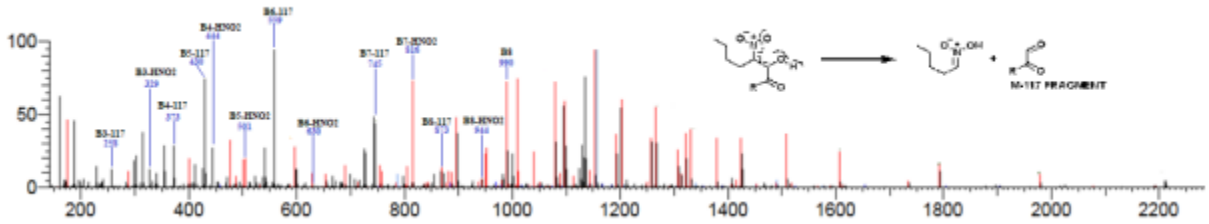

Digestion protocol (CNBr) Protein (0.1 um) was dissolved in 2 ml of 0.1 N HCl and 200 equiv. of CNBr was added to reaction mixture. The reaction mixture was stirred at rt for 24 h and then lyophilized to remove volatiles.

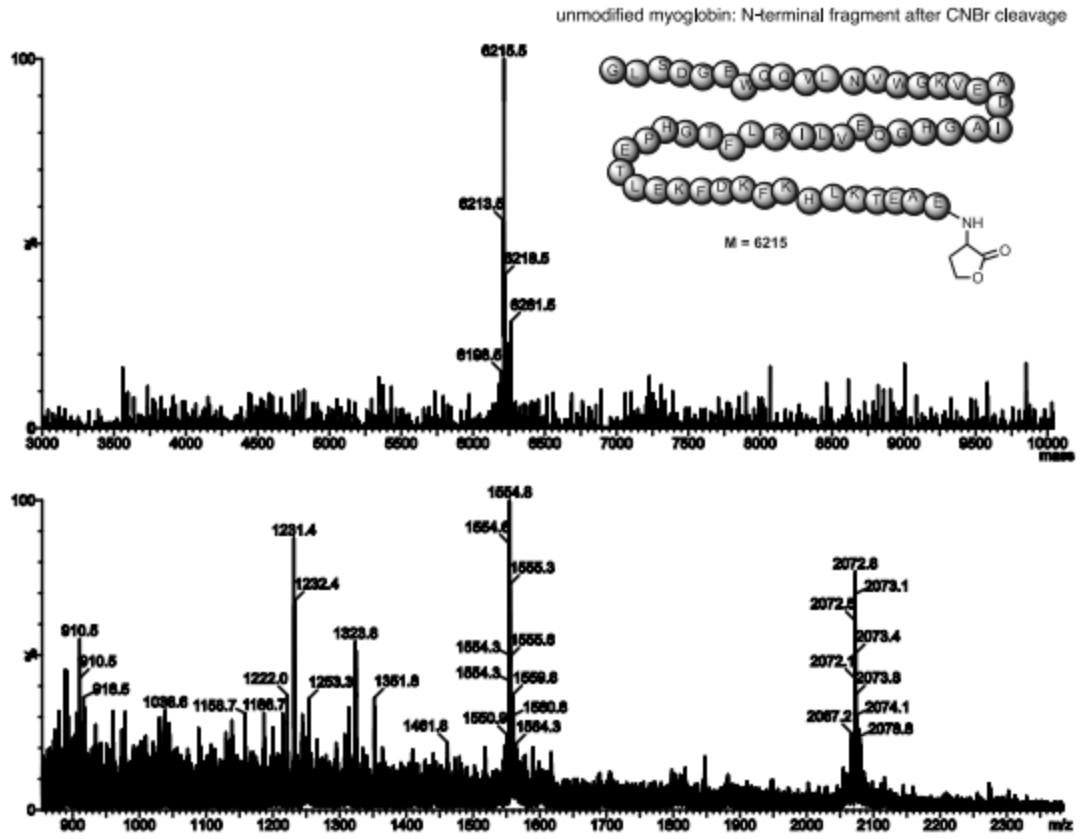
unmodified myoglobin: N-terminal fragment after CNBr cleavage
M = 6215
NH
O
O
6215.5
6213.5
6218.5
6281.5
6198.5
%
mass
1554.8
1231.4
1232.4
1555.3
2072.8
2073.1
910.5
910.5
916.5
1323.8
1554.3
1555.8
2073.4
1222.0
1253.3
1351.8
1554.3
1559.8
2073.8
1038.8
1158.7
1186.7
1560.8
2074.1
1461.8
1550.5
1564.3
2078.8
m/z

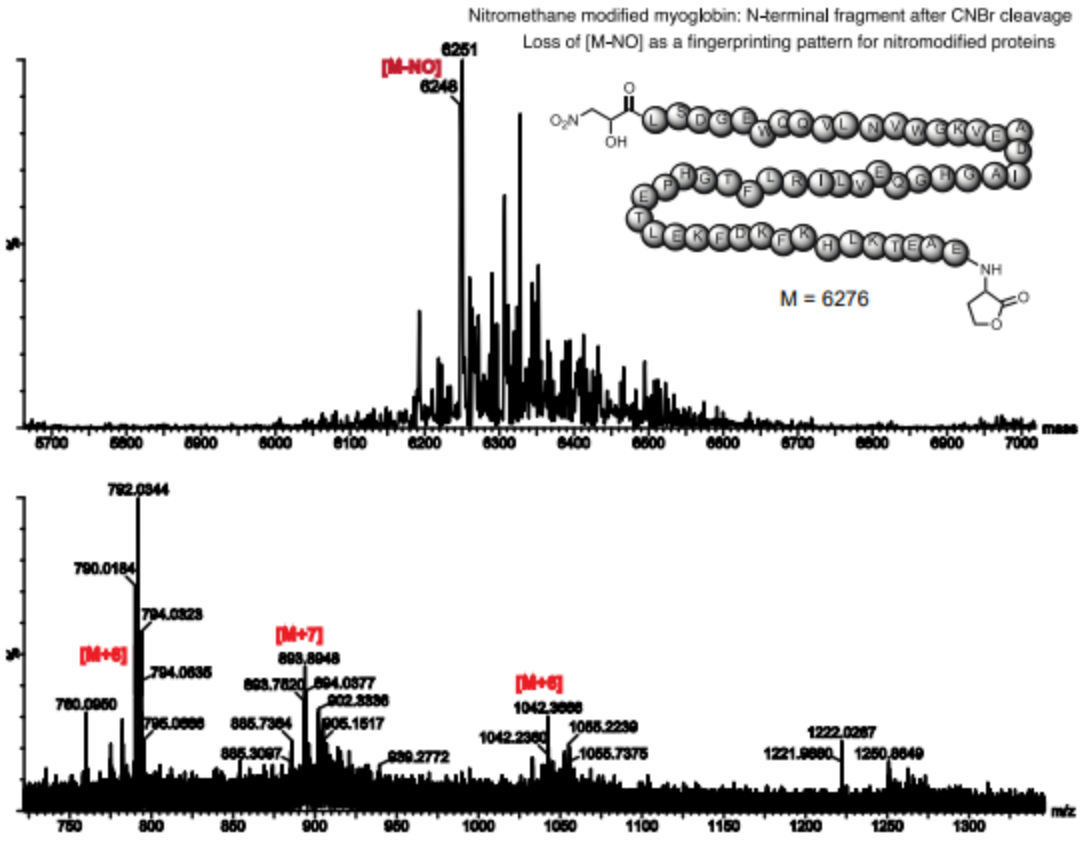

Determination of the secondary structure of the modified nitro-myoglobin bioconjugates 3.6e and 3.6n. To obtain insight into whether the secondary and tertiary structure of the protein remained intact after the modification by nitroalkane derivatives, we carried out UV studies on bromo derivative (3.6e) and dye-derivative of nitroalkane-modified myoglobin (3.6n). We dissolved functionalized (3.6e and 3.6n) and un-functionalized myoglobin in phosphate buffer (10 mM, pH 7.5) and recorded the UV. Compared to the native myoglobin, we did not observe any change in the UV absorbance pattern of the modified myoglobin. The absorbance at 408 nm is due to the heme group present inside the myoglobin. No change in the absorbance showed that the heme group remained intact which further indicated that the secondary and tertiary structure of a protein is unaffected due to the modification under the reaction conditions.

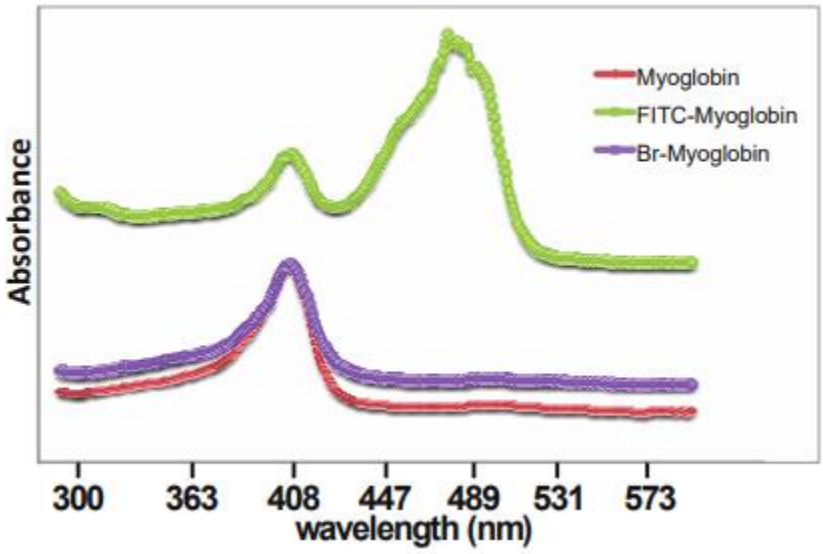

Activity assay of the modified nitro-myoglobin bioconjugate 3.6a. Enzymatic assay of myoglobin activity before and after the labeling was checked by oxidation of o-phenylenediamine with hydrogen peroxide. Oxidation of o-phenylenediamine to 2,3-diaminophenazine was monitored at 426 nm (A426) using nanodrop. Citric acid-Na_2HPO_4 buffer (pH 5.6) was prepared by mixing of 0.1 M citric acid and 0.2 M Na_2HPO_4. All solutions were made in aqueous buffer. The myoglobin, nitromethane labeled myoglobin, o-phenylenediamine, and hydrogen peroxide (30 %) solutions were used for the assay. Conditions used for the assay: 1. o-phenylenediamine (1 mM) and H2O2 (1 mM) in absence of myoglobin 2. o-phenylenediamine (1 mM), H2O2 (1 mM) and myoglobin (1 × 10-4mM) 3. o-phenylenediamine (1 mM), H_2O_2 (1 mM) and labeled myoglobin (1 × 10-4mM).

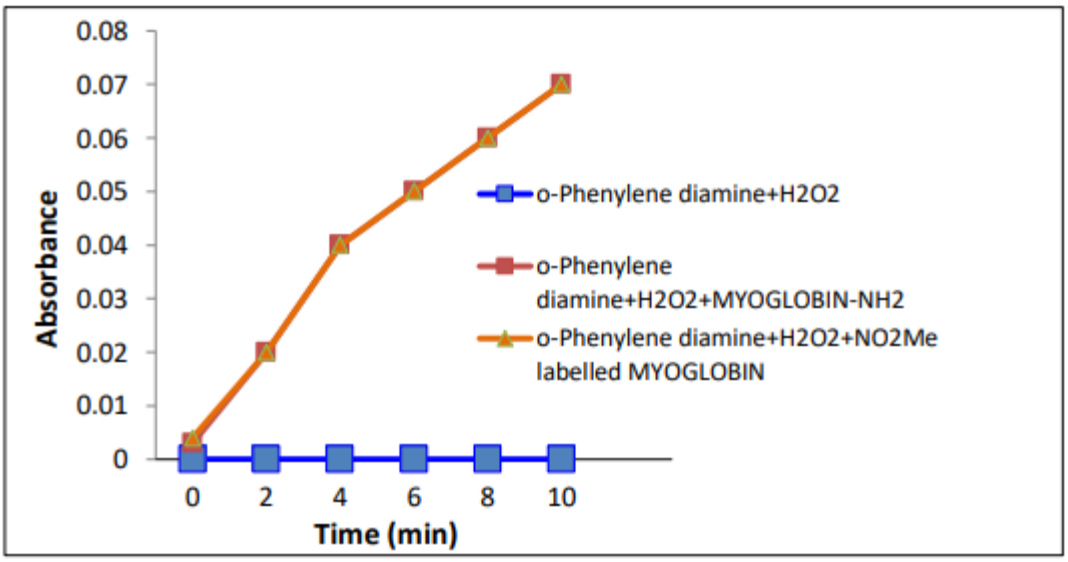

General procedure for late stage diversification of peptide by nitromethane.

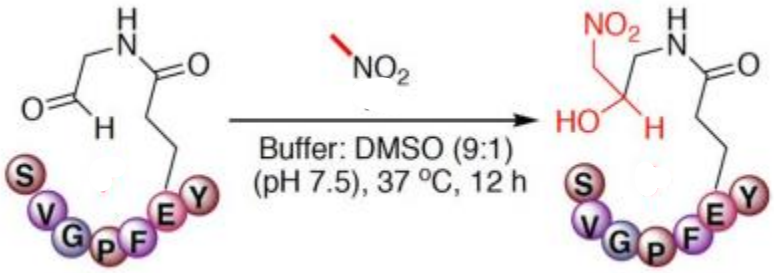

To a solution of peptide aldehyde (**3.7**, 7.1 mM) in phosphate buffer (pH 7.5, 50 mM): DMSO (9:1) (0.44 mL) was added nitromethane (**3.1a**, 5 equiv.). The reaction mixture was stirred at 37 ^{o}C for 12 h and analyzed by LCMS. % conversion to the nitro-peptide adduct **3.8** was determined by integrating the area of HPLC peaks. The nitro-peptide adduct **3.8** was purified by HPLC and characterized by LCMS (60% conversion).

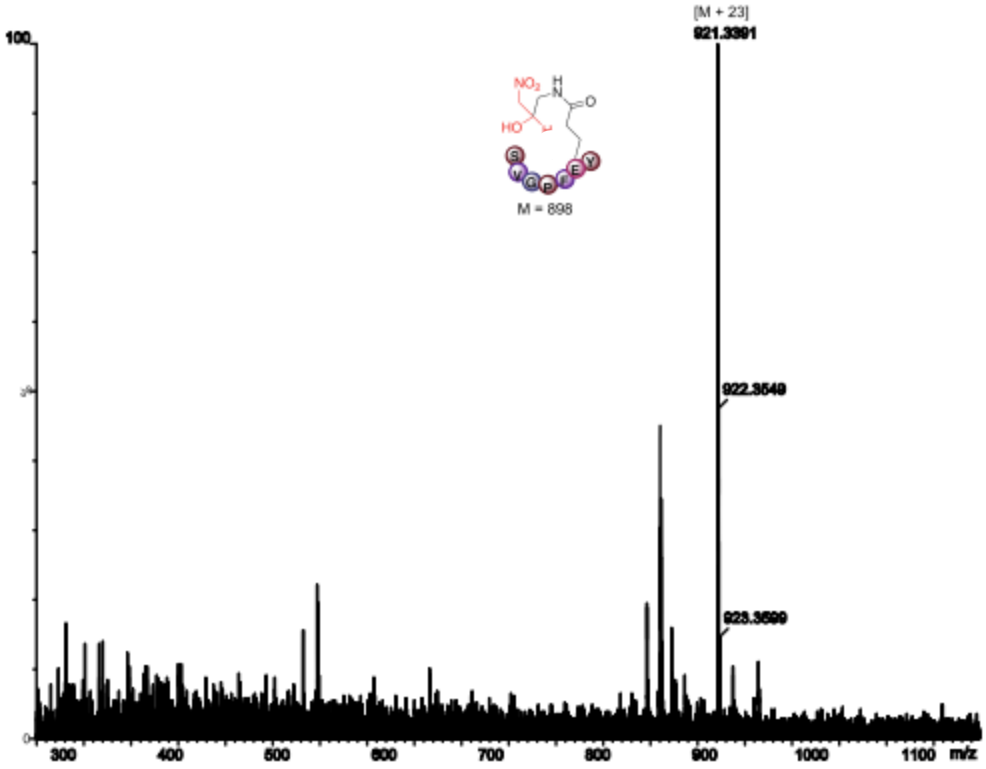

General procedure for synthesis of dinitrohexane 3.9.

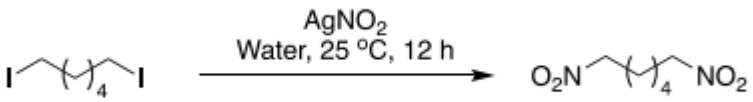

To a solution of 1,6 diiodohexane (0.6 mmol) in water was added silver nitrate (4 equiv.) and reaction was stirred at room temperature for 12 h under dark. The reaction mixture filtered, extracted with ethylacetate and dried over MgSO4. Solvent was removed under vacuum. The crude reaction mixture was purified by column chromatgraphy to obtain desired product 3.9.

NMR data and spectra of 3.9: Yield 77% ^{1}H NMR (600 MHz, CDCl3) δ 4.39 (t, J = 6.8 Hz, 2H), 2.03- 2.02 (m, 2H), 1.46 (s, 2H). ^{13}C NMR (151 MHz, $CDCl_3$) δ 75.5, 27.1, 25.7.

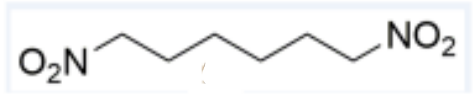

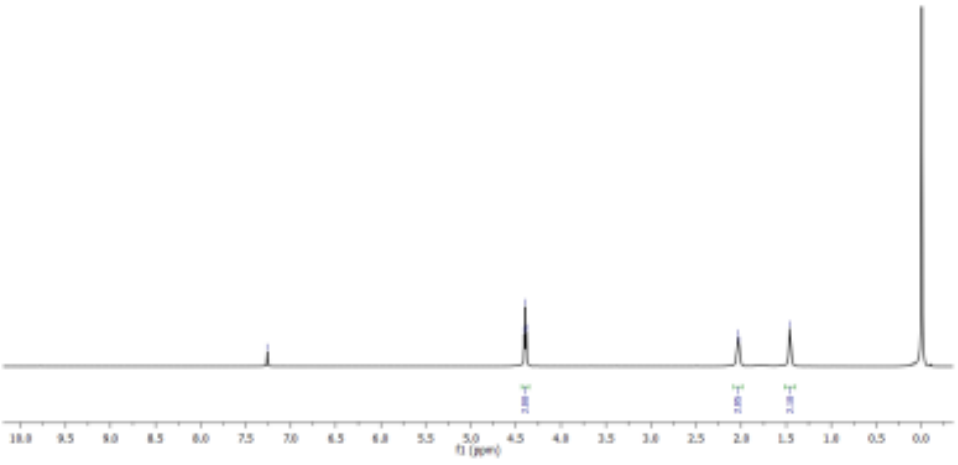

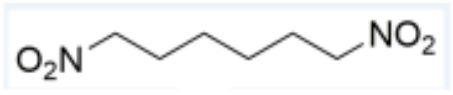

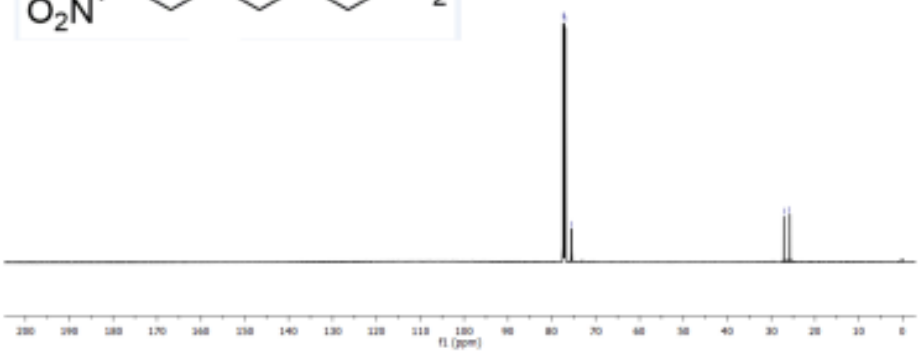

General procedure for the stapling of dialdehdye peptide 3.10 by dinitrohexane 3.9.

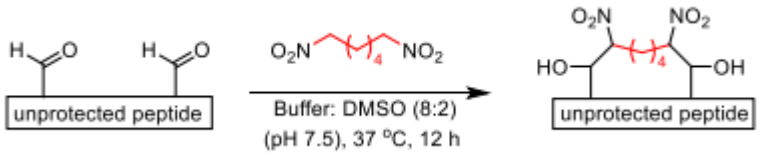

To a solution of peptide dialdehyde (**3.10**, 7.1 mM) in phosphate buffer (pH 7.5, 50 mM): DMSO (8:2) (0.5 mL) was added dinitrohexane **(3.9**, 3 equiv.) portion wise. The reaction mixture was stirred at 37 ^{o}C for 12 h and analyzed by LCMS. % conversion to the stapled nitro-peptide **3.11** was determined by integrating the area of HPLC peaks. The stapled nitro-peptide **3.11** was purified by HPLC and characterized by LCMS. % conversion (87%-98%).

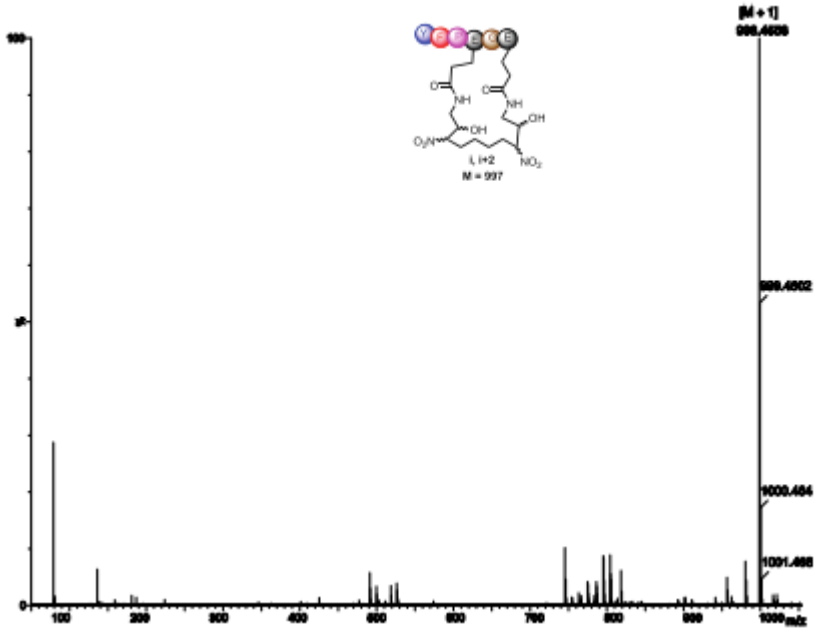

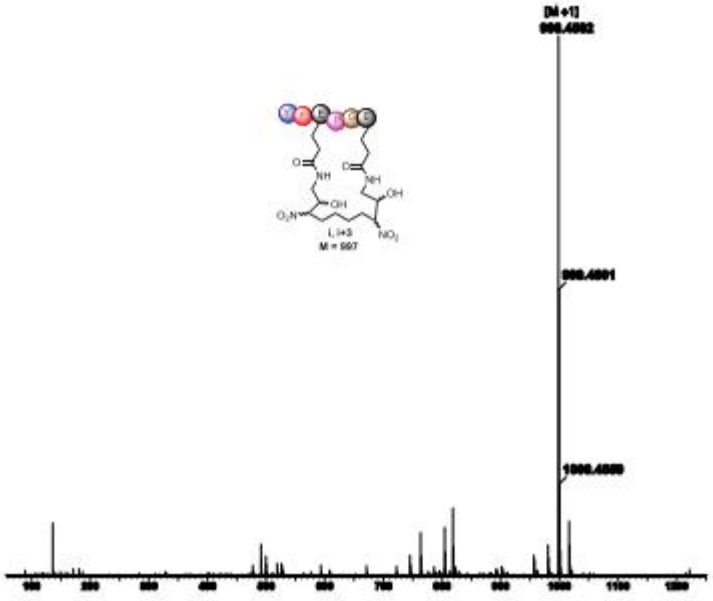
[M+1]
998.4892
998.4891
1000.4999

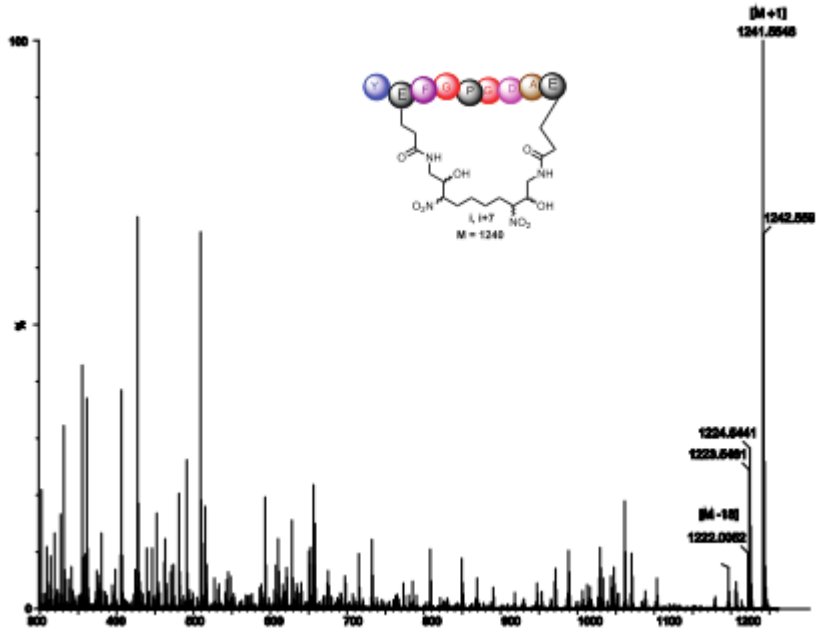
[M+1]
1241.5548
1242.558
1234.6441
1223.5491
[M-18]
1222.0062
100
%
0
800
400
600
900
700
800
900
1000
1100
1200

[i] Zhao, Y.; Truhlar, D.G. The M06 suite of density functionals for main group thermochemistry, thermochemical kinetics, noncovalent interactions, excited states, and transition elements: two new functionals and systematic testing of four M06-class functionals and 12 other functionals. *Theor. Chem. Acc*. **2008**, *120*, 215−41

[ii] Ahlrichs, R.; Weigend, F. Balanced basis sets of split valence, triple zeta valence and quadruple zeta valence quality for H to Rn: Design and assessment of accuracy. *Phys. Chem. Chem. Phys*. **2005**, *7*, 3297−305

[iii] Marenich, A. V.; Cramer, C. J.; Truhlar, D. G. Universal solvation model based on solute electron density and on a continuum model of the solvent defined by the bulk dielectric constant and atomic surface tensions. *J. Phys. Chem. B*, **2009**, *113*, 6378−6396.

[iv] a) Lee, C.; Yang, W.; Parr, R. G. Development of the Colle-Salvetti correlation-energy formula into a functional of the electron density. *Phys. Rev. B: Condens. Matter Mater. Phys.* **1988**, *37*, 785; b) Becke, A. D. Density-functional thermochemistry. III. The role of exact exchange. *J. Chem. Phys.* **1993**, *98* , 5648−5652.

[v] Grimme, S. Semiempirical GGA-type density functional constructed with a long-range dispersion correction. *J. Comput. Chem*. **2006**, *27*, 1787−1799.

[vi]Zhao, Y.; Truhlar, D.G. The M06 suite of density functionals for main group thermochemistry, thermochemical kinetics, noncovalent interactions, excited states, and transition elements: two new functionals and systematic testing of four M06-class functionals and 12 other functionals. *Theor. Chem. Acc*. **2008**, *120*, 215−41

[vii] Chai, J.D.; Head-Gordon, M. Long-range corrected hybrid density functionals with damped atom-atom dispersion corrections. *Phys. Chem. Chem. Phys*. **2008**, *10*, 6615−20

[viii] Scalmani, G.; Frisch, M. J. Continuous surface charge polarizable continuum models of solvation. I. General formalism. *J. Chem. Phys.* **2010**, *132*, 114110

[ix] Cossi, M.; Rega, N.; Scalmani, G.; Barone, V. Energies, structures, and electronic properties of molecules in solution with the C-PCM solvation model. *J. Comp. Chem.* **2003**, *24*, 669−81